Washington University in St. Louis
Washington University Open Scholarship

Arts & Sciences Electronic Theses and Dissertations

Arts & Sciences

5-2-2024

# Anodic Cyclizations to Form Alkaloid Ring Systems and the Role of the Second Oxidation Step

Zachary Tyler Medcalf
*Washington University in St. Louis*

Follow this and additional works at: https://openscholarship.wustl.edu/art_sci_etds

## Recommended Citation

Medcalf, Zachary Tyler, "Anodic Cyclizations to Form Alkaloid Ring Systems and the Role of the Second Oxidation Step" (2024). *Arts & Sciences Electronic Theses and Dissertations*. 3048.
https://openscholarship.wustl.edu/art_sci_etds/3048

This Dissertation is brought to you for free and open access by the Arts & Sciences at Washington University Open Scholarship. It has been accepted for inclusion in Arts & Sciences Electronic Theses and Dissertations by an authorized administrator of Washington University Open Scholarship. For more information, please contact digital@wumail.wustl.edu.

WASHINGTON UNIVERSITY IN ST. LOUIS

Department of Chemistry

Dissertation Examination Committee:
Timothy Wencewicz, Chair
Jonathan Barnes
Vladimir Birman
Chang Ji
Kevin Moeller

# Anodic Cyclizations to Form Alkaloid Ring Systems and the Role of the Second Oxidation Step

by
Zachary Medcalf

A dissertation presented to
Washington University in St. Louis
in partial fulfillment of the
requirements for the degree
of Doctor of Philosophy

May 2024
St. Louis, Missouri

© 2024, Zachary Medcalf

# Table of Contents

# List of Figures

# List of Tables

# List of Schemes

# Acknowledgments

I would like to thank everyone in the lab, past and present, along with Dr. Moeller for their support and guidance throughout graduate school. I would like to thank my brother for getting me interested in Organic chemistry when I was an undergraduate student. I would also like to thank my parents for their support along with my girlfriend for helping me relax throughout my time in graduate school. I would also like to thank my dog Emmett for always putting a smile on my face regardless of the day I had. I would also like to thank the NSF and the CSOE for their financial support.

Zachary Medcalf

*Washington University in St. Louis*

*May 2024*

ABSTRACT OF THE DISSERTATION

Anodic Cyclizations to Form Alkaloid Ring Systems and the Role of the Second Oxidation Step

by

Zachary Medcalf

Doctor of Philosophy in Chemistry

Washington University in St. Louis, 2024

Professor Kevin D. Moeller

Abstract: In chapter 1 we will explore the essential background on electrochemistry and anodic cyclization reactions, laying the foundation for understanding the subsequent chapters. In chapter 2, we will explore the mechanistic model established for anodic olefin coupling reactions and the importance of the second oxidation step in the success of these reactions. We showed how a fast second oxidation step can be used to push an anodic cyclization down a kinetic pathway. We will also explore how this step impacts the generation of product in photoelectron-transfer initiated radical cation reactions. It is evident that a fast second oxidation step alone is insufficient to guide a reaction with a slow cyclization to the desired product. The decomposition of the initial radical cation takes place first. Therefore, when planning a cyclization reaction, both steps must be considered and employed to devise a successful process. In chapter 3, we will be examining how a fast second electron oxidation can be used to channel a reaction down a new synthetic pathway. We will examine one such application that reverses the normal reactivity of an imine group to make cyclic proline derivatives. Through including a chiral imine, we showed that we can induce asymmetry into an anodic cyclization. In chapter 4, we will briefly outline the history of our efforts to perform a tandem anodic cyclization along with our most recent efforts to carry

out this transformation. This latest effort utilized a fast second oxidation step to drive the first cyclization down a kinetic pathway, ensuring the first ring generated stayed shut. This bought time for the subsequent cyclization to take place and allowed us to successfully perform a tandem cyclization on a model substrate. Efforts to extend this idea to using an imine as a relay group in these transformations proved unsuccessful. We will also explore cyclizations that utilized an acetylene trapping group. By adding a TMS group the acetylene we were able to successfully channel it down a cationic pathway to an allene product. In chapter 5, we will be exploring anodic cyclizations to make a key nitrogen-carbon bond in the alkaloid backbone of the chrysosporazine family of natural products. We will explore how lowering the pKa of N-H of the amide by converting it into a thioamide allowed for deprotonation of this coupling partner so that it could be selectively oxidized to a radical that then triggered the subsequent cyclizations. The cyclizations leading to five-membered rings used ferrocene as the oxidative mediator. However, in the six-membered ring example that directly targeted the chrysosporazine ring skeleton the oxidative mediator was changed to copper acetate. This modification enabled the six-membered ring cyclization to occur with yields comparable to those of the five-membered ring cyclizations. At the end of this chapter, I propose further experiments that need to be carried out in order to successfully synthesize the chrysosporazine family of natural products.

# Chapter 1: Introduction

This chapter provides the essential background on electrochemistry and anodic cyclization reactions, laying the foundation for understanding the subsequent chapters. Electrochemical oxidation serves as a powerful tool for removing electrons and leading to umpolung reactions that reverse the polarity of known functional groups. The reaction lead to the generation of reactive radical cation intermediates, and enable the development of unique pathways to synthetic targets of interest.[1–19] The research in this thesis examines intramolecular trapping of radicals and radical cations by electron-rich olefins, reactions that allow for the coupling of two nucleophilic groups

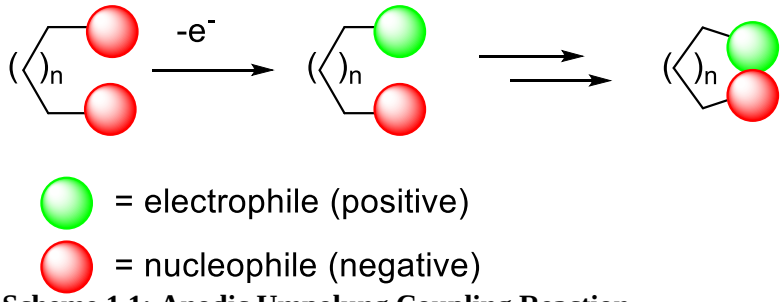


**Scheme 1.1: Anodic Umpolung Coupling Reaction**

to form a cyclic product (Scheme 1.1).

## 1.1 Anodic Cyclization Reactions

Anodic olefin coupling reactions follow the mechanism shown in Scheme 1.2.[20] First, the substrate is oxidized at the anode to form radical cation **1**. The mechanistic scheme excludes the initial oxidation step since the oxidations are usually run using constant-current and simply involve the loss of an electron to the anode.[21] Radical cation **1** can then cyclize reversibly or irreversibly ($k_1/k_{-1}$) to form the cyclic radical cation **2**. The cyclized radical cation then undergoes a second oxidation step, forming di-cation **3**. The reversibility of this cyclization depends on the rate of the second

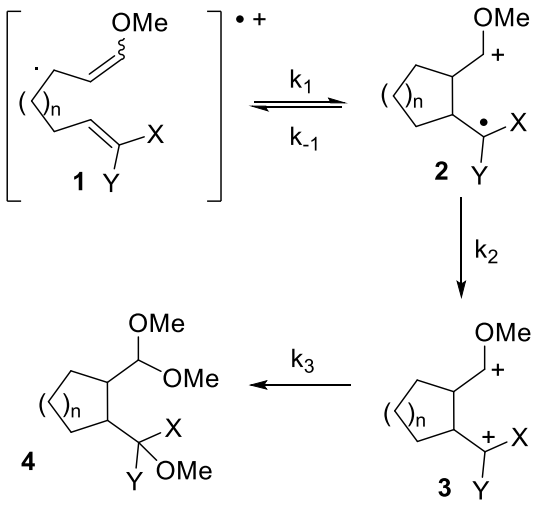


**Scheme 1.2: Mechanistic Model for an Anodic Cyclization**

oxidation step, where it can be either reversible ($k_{-1}>k_2$) or irreversible ($k_2 > k_{-1}$).[22] Following the second oxidation step, the final product **4** is formed through methanol trapping of the cations or a combination of methanol trapping and elimination (as observed in cases utilizing an allylsilane trapping group). The steps occurring after the second oxidation step are denoted as $k_3$. In the process of this reaction, a new bond and ring are formed, while preserving the functional group used to initiate reaction. When an enol ether (an aldehyde equivalent) is used to initiate the reaction, an acetal is formed (another aldehyde equivalent) following the cyclization, etc. Consequently, these reactions can preserve or enhance the overall functionality of the molecule during the course of a transformation. Additionally, these reactions can be achieved under neutral conditions with high selectivity by controlling the either the potential at the working electrode or the current. The control of the potential at the working electrode either with the use of a reference electrode or a constant current electrolysis allows for a systematic study of the intermediates involved in the cyclization. [20,23]

Intramolecular anodic coupling reactions are compatible with a wide array of nucleophilic functional groups. The initial oxidation in these reactions has involved enol ethers,[24–34] ketene acetals,[24,35–43] electron-rich aryl rings,[26] and amides (forming amidyl radicals[44] and N-acyliminium

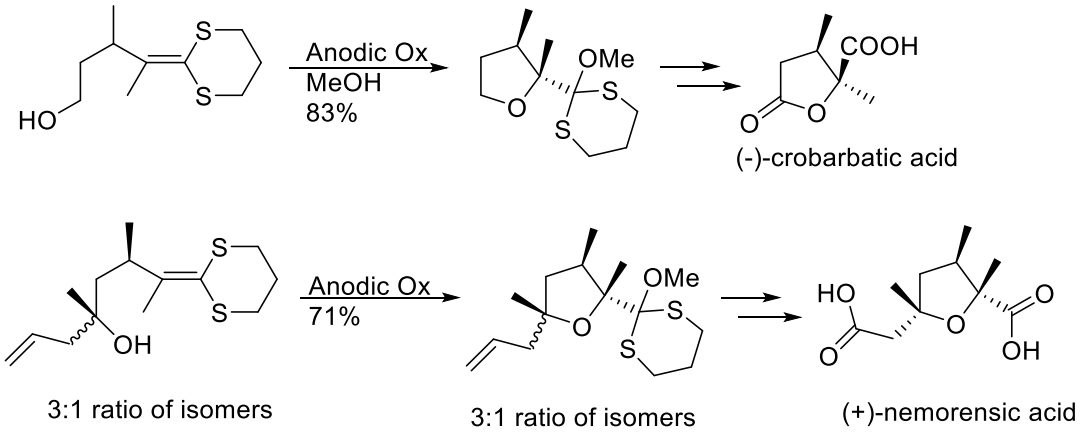


**Scheme 1.3: Anodic Olefin Coupling Reactions Making C-O Bonds in Total Synthesis**

ions[45,46]). Once oxidized, these reactive intermediates produced can be coupling with various trapping groups, selected according to the desired products one aims to generate. To form C-O bonds, amides[39], carboxylic acids[47], and primary alcohols[22,24,27,29,40,48] can serve as trapping partners. To form C-N bonds, imines[49], amines[50], and sulfonamides[22,48,51,52] can serve as trapping partners. To form C-C bonds, allyl silanes[32,37,38], enol ethers[26,28,30,31,38,43], di- and tri- substituted olefins[30,31], heterocycles[20,35,36], and electron-rich aromatic rings[26] can all act as trapping partners.

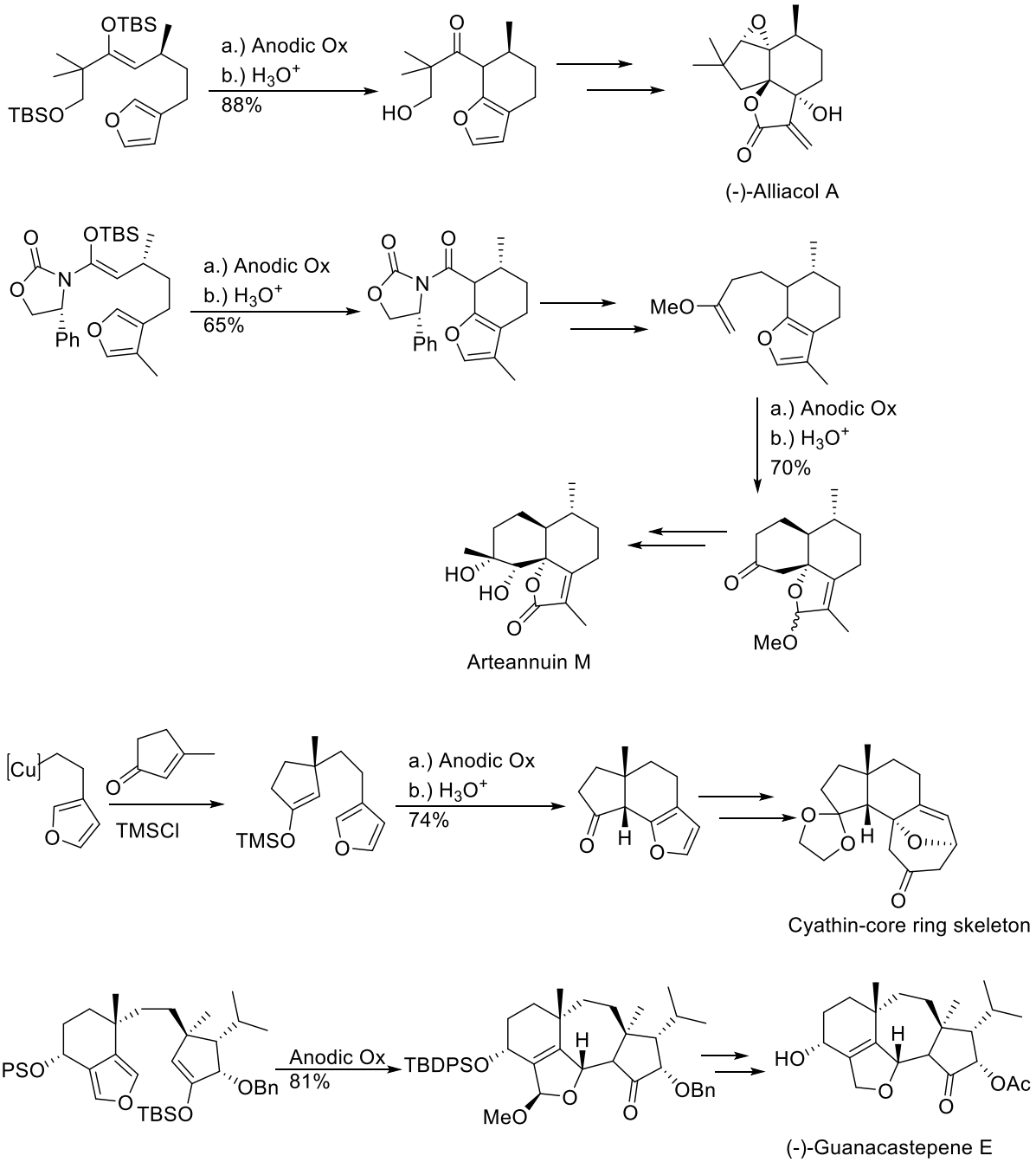


**Scheme 1.4: Anodic Olefin Coupling Reactions Making C-C Bonds in Total Synthesis**

These features of the anodic cyclization reactions suggest significant potential for their use in synthesizing complex molecules, an ongoing theme in the Moeller group among others. During

these studies, a number of total syntheses have utilized an anodic cyclization to form C-O, C-C bonds, and C-N bonds. Anodic coupling reactions to form C-O bonds have been employed in the synthesis of (-)-Crobarbatic Acid[40], (+)-Nemorensic Acid[24], and a series of C-Glycoside derivatives[53–55](Scheme 1.3). Examples of C-C bond forming reactions include Alliacol A,[56] Arteannuin M,[36] the Cyathin-core ring skeleton,[57] and Guanacastepene[25](scheme 1.4). The synthesis of Guanacastepene depicted in scheme 1.4 is notable because it showcases that an anodic olefin coupling reaction can be employed not only in the early stages of a synthesis, but also at a later stage with complicated substrates. For making C-N bonds, a series of peptidomimetics and amino acid derivatives have been synthesized.[47]

**Figure 1.2: ElectraSyn 2.0 from IKA**

## 1.2 Anodic Cyclization Reactions

We will now turn our attention towards examining how these reactions are performed. A typical setup for an electrolysis consists of an electrolysis cell and a DC power supply. The cell contains the electroactive substrate, electrolyte, solvent, and at two electrodes (an anode and a cathode).

### 1.2.1 Reaction Experimental Apparatus

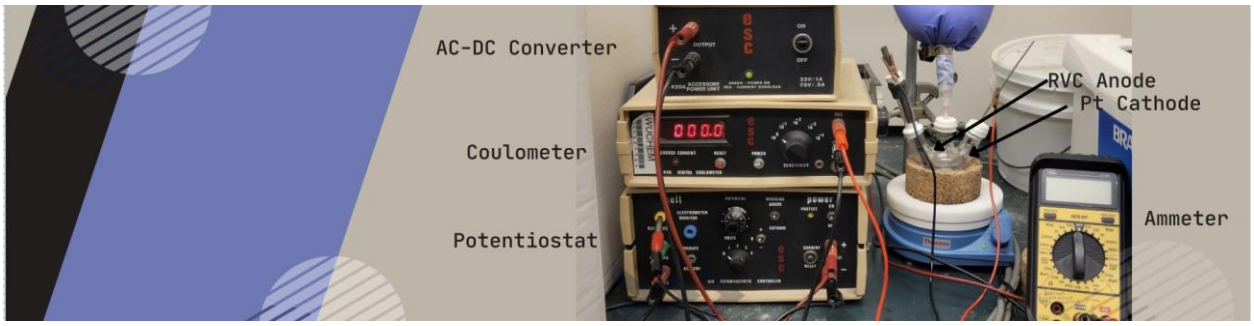


**Figure 1.1: Power Source Commonly Used in the Moeller Group**

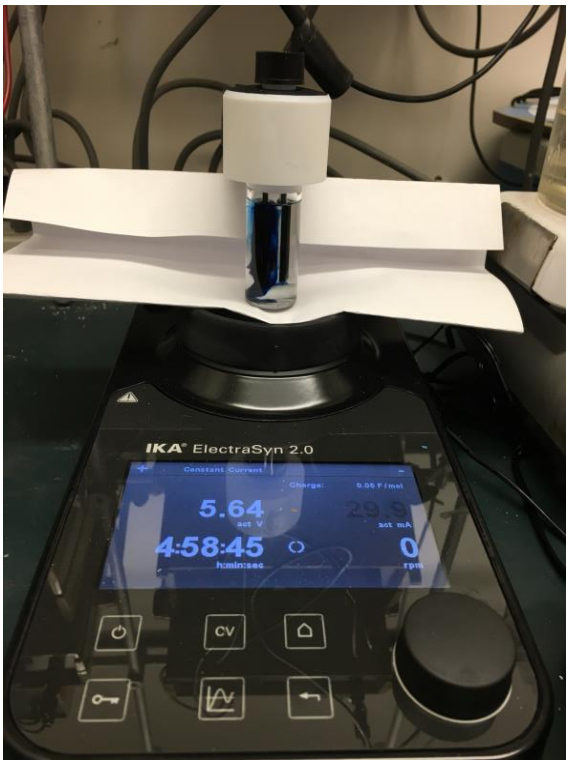


Two types of cells are employed in an electrolysis. The first is a divided cell, which has two chambers separated by a semi-permeable membrane. This design is used when products generated at the counter-electrode could disrupt the reaction at the electrode of interest. The undivided cell, which can be a three-neck round-bottom flask or a vial, is the preferred electrolysis cell utilized most often in the Moeller group because of its simplicity and its availability to any synthetic chemistry group. Two carbon rods, serving as electrodes, are then inserted in the flask (using either a hole in a rubber stopper or a thermometer adapter. The electrodes are then connected to a direct current (DC) power source. This is the setup used for most of the reactions discussed in this thesis.

The two half reactions (oxidation of the substrate at the anode and reduction of methanol at the cathode) automatically occurs when a constant current (see below) is applied to the reaction. Therefore, the key is the DC power supply utilized to apply this current. Shown in Figure 1.1 is

the power supply typically used in the Moeller group. This setup includes an AC/DC converter, a potentiostat that controls the current flowing through the electrochemical cell, an ammeter that monitors this current, and a coulometer used to measure the amount of electric charge that is passed through the cell over the course of the reaction. Additionally, the Moeller group has shown that a lantern battery or a photovoltaic can be used as a simple power source for an electrolysis reaction.[58,59] In fact, any source of current can be used. Figure 1.2 shows a more modern commercial setup from IKA, which is designed to offer a compact and versatile power supply suitable for a wide variety of electrochemical applications and experiments.

## 1.2.2 Constant Potential and Constant Current Electrolysis

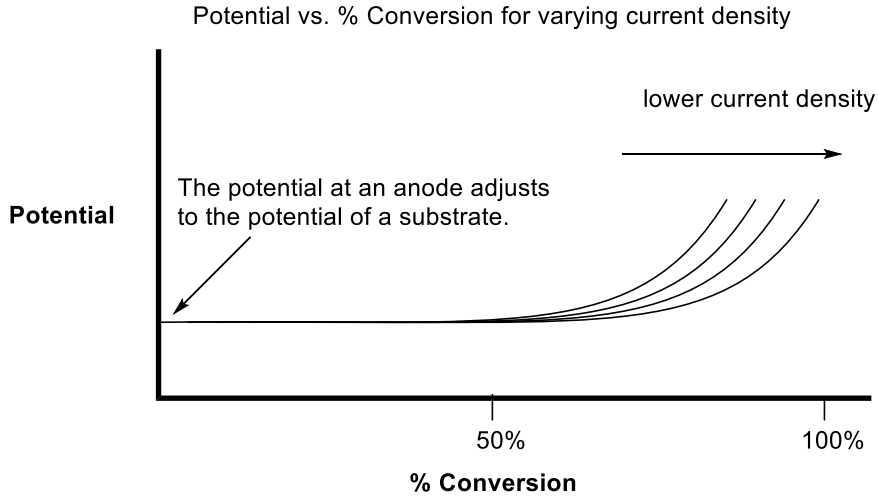


**Figure 1.3: Constant Current Electrolysis**

There are two major approaches to regulate the flow of current through the cell: a constant potential electrolysis or a constant current electrolysis. In constant potential electrolysis, the potential of the working electrode remains constant relative to a reference electrode throughout the reaction. This method enables selective oxidation of specific functional groups in the presence of multiple electroactive species, due to precise potential control. Typically, this method offers superior selectivity compared to constant current electrolysis. However, as the substrate is consumed, the resistance across the cell increases, causing a drop in current. Consequently, with decreasing

current, it takes longer to oxidize the substrate. Therefore, the time needed for the substrate to be completely consumed in a constant potential electrolysis is typically much longer compared to a constant current reaction.

All the anodic cyclizations studied in this thesis utilized the latter method, constant current electrolysis. In these experiments, the current flowing through the cell remains constant, and the working potential at the electrodes is allowed to float. As a result, the working potential at each electrode adjusts automatically to match the oxidation potential of the substrate at the anode and the reduction potential of the substrate at the cathode. This is depicted in Figure 1.3, which illustrates the working potential at the anode during a constant current electrolysis. In this reaction, the potential gradually rises until it matches with the potential associated with the most readily oxidizable group in solution. Once reached, the potential remains stable at that level until the oxidation of the substrate nears completion. After the first substrate is consumed, the electrode potential increases until another electroactive species of solvent can be oxidized. In the majority of the electrolysis reactions we studied, the resulting products were either electrochemically inactive or had potentials much higher than the starting material. Therefore, selectivity was not a concern, and the constant current method was chosen for its simplicity and the relative short time required to complete the reaction.

### 1.2.3 The Influence of Substrate Concentration

Radical cations are extremely reactive intermediates, and their concentration at the surface of an electrode and within the reaction environment surrounding the electrode can significantly influence the subsequent reactions. When considering the concentration of these intermediates, we must take into account various factors such as electrode materials, the electrode surface double

layers, substrate, and electrolyte. Polymerization reactions can occur if the concentration of radical cations is too high. Consequently, the choice of electrode surface becomes crucial. For instance, consider the reaction depicted in Scheme 1.5 where the outcome was affected by the type of the anode material employed.[34] Two potential reasons account for this difference. The first reason is because the reticulated vitreous carbon anode (RVC) has a high surface area which significantly

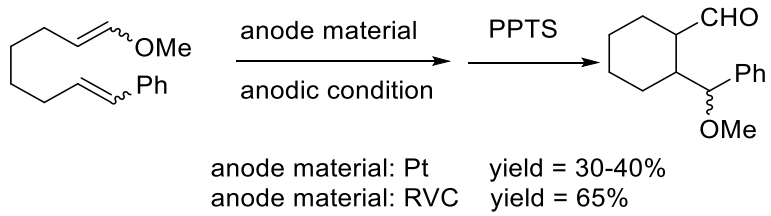


**Scheme 1.5: Influence of Anode Material on Anodic Cyclization**

decreases the concentration of the radical cation at the anodes surface. When two reactions are conducted at the same current, they will result in different current densities (representing the effective concentration of the oxidant) depending on the surface area of the anode used. A high surface area corresponds to a low concentration of the oxidant, a reduced concentration of the radical cation, and more of the intramolecular reaction. The second reason is that RVC anodes favor two-electron oxidations over Pt electrodes that can undergo surface fouling during the course of the reaction.[34] In several reactions, we have observed that the rate of the second oxidation step in an electrolysis can greatly influence the reaction's success, a matter we will delve into in later chapters in this thesis.[60] In the above reaction, it is likely that the RVC electrode plays both roles in optimizing the yield.

Another factor that plays a role in an electrochemical reaction is the formation of the "double layer" involving the electrolyte. Figure 1.4 depicts a model of the double layer formed around the anode in the solution. When potential is applied in the reaction, the anode acquires a positive

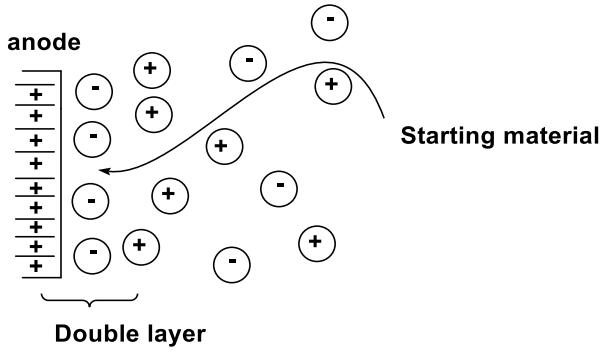


charge. This positive charge attracts negative ions from the solution, forming a tightly packed

**Figure 1.4: Electrochemical Double Layer**

negatively charged layer. This layer, in turn, attracts cations, forming a second layer of ions. As the distance from the electrode increases, the strength of the electric field diminishes, causing the layers to become more diffuse. The electrochemical double layer comprises the compact inner layer and the diffuse layer. The starting material needs to navigate through this double layer and reach the electrode surface to undergo oxidation and form the charged intermediate. This is crucial because double layers can serve to exclude methanol from trapping a reactive intermediate too rapidly and to regulate the substrate concentration, thereby forming the radical cation, based on its solubility in the generated double layer. The polarity of the electrolyte influences what molecules can reach the electrode surface. A highly polar electrolyte, like lithium perchlorate, facilitates the approach of polar substrates and methanol solvent more readily compared to a nonpolar electrolyte, such as tetraethylammonium tosylate. In contrast, a nonpolar electrolyte permits nonpolar substrates to approach the electrode while excluding methanol. This greasier electrolyte "buys" time for the intramolecular cyclization by excluding methanol from the double layer.

Therefore, consideration should be given to the factors influencing the double layer when optimizing reaction conditions.

## 1.3 Mechanism Related Topics in Anodic Olefin Coupling Reactions

In Chapter 2 of this thesis, we will explore the mechanism of the anodic cyclization reaction in more detail. Specifically, we will emphasize the significance of the polarity of the generated radical cation in influencing the rate of the initial cyclization. Additionally, we will examine the importance of the second oxidation step for the success of these reactions. The subjects covered in the sections that follow are somewhat independent of each other, but they are all related to anodic cyclizations we will discuss in future chapters.

### 1.3.1 Curtin-Hammett Controlled Reactions

When a substrate undergoes oxidation at the anode, the exact location of the generated radical cation may not always be evident. In cases where the substrate contains multiple electron-rich functional groups, intramolecular electron-transfer reactions can take place, resulting in a

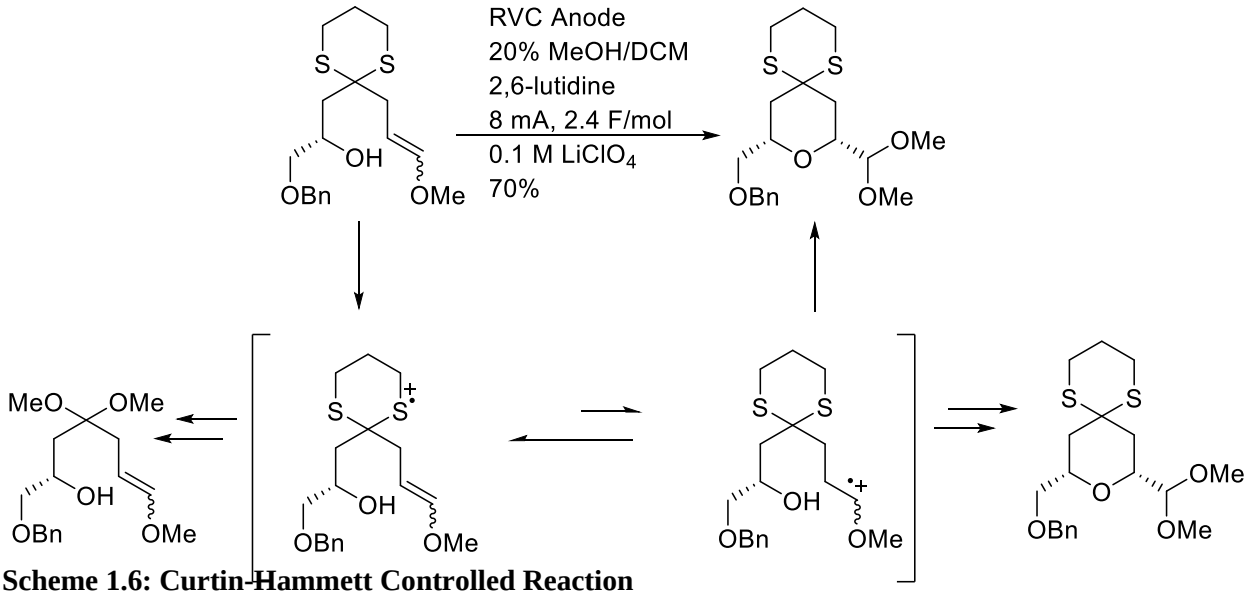


**Scheme 1.6: Curtin-Hammett Controlled Reaction**

reversible, intramolecular electron-transfer reaction. In these scenarios, the product resulting from oxidation follows the Curtin-Hammett Principle. An instance of this is depicted in Scheme 1.6.[35]In this reaction, the enol ether has a higher oxidation potential ($E_{p/2}$ = +1.4 V vs Ag/AgCl) than the dithioketene acetal ($E_{p/2}$ = +1.1 V vs Ag/AgCl). Therefore, the initial oxidation at the anode occurs at the sulfur atoms, resulting in a sulfur-based radical cation. Next, an intramolecular electron transfer reaction occurs leading to an enol ether derived radical cation that is trapped by the alcohol, a reaction that is known to be very fast.[22] This fast cyclization shifts the equilibrium towards the desired product, exemplifying the Curtin-Hammett principle in action. The energy barrier for cyclization is much lower than that for methanol trapping of the sulfur-based radical cation. Therefore, the product is determined by the rapid cyclization reaction. In the case when the alcohol was protected with a silane, the only product formed was the trapping of the sulfur-based radical cation by methanol.[35]

## 1.3.2 Substrate Selectivity and Steady State Kinetics

In section 1.2.2, we talked about constant potential vs constant current electrolysis reactions. Typically, under constant current conditions, the oxidation potential at the electrode surface

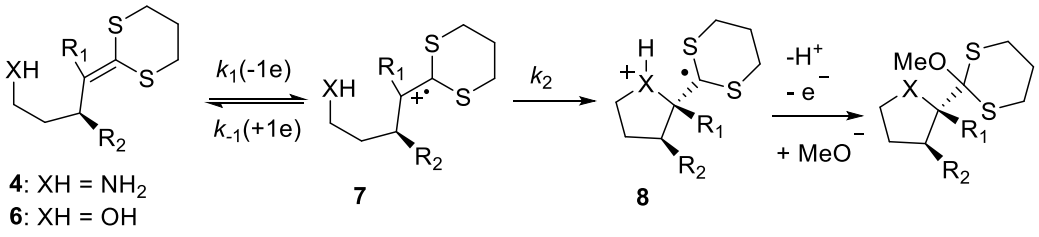


if "steady state", then... $[\mathbf{7}] = \frac{k_1[\mathbf{4} \text{ or } \mathbf{6}]}{(k_{-1} + k_2)}$ (1)

...and the Nernst Equation becomes:

$$E_{obsv} = E^o - (RT/(nF))\ln\left(\frac{[\mathbf{4} \text{ or } \mathbf{6}]}{[\mathbf{7}]}\right)$$

$$E_{obsv} = E^o - (RT/(nF))\ln\left(\frac{(k_{-1} + k_2)}{k_1}\right) \quad (2)$$

**Scheme 1.7: Relationship of Observed Oxidation Potential and Cyclization Rates**

remains at the level of the substrate with the lowest oxidation potential. It increases only after this substrate is consumed, thus preserving substrate selectivity throughout the reaction. However, it is important to recognize that the oxidation potential of the substrate is not solely determined by the functional group being oxidized; it is also influenced by the rate of the following transformation, as depicted in Scheme 1.7. The Nernst equation demonstrates how the oxidation potential of a molecule reflects the equilibrium established between the substrate and the radical cation intermediate at the electrode surface. Any process that removes the radical cation from the electrode surface, such as a fast cyclization reaction, shifts the equilibrium towards the radical cation, thus reducing the oxidation potential. This can be seen in the equation if one assumes the reaction shown displays steady state kinetics. In this case, the concentration of the radical cation **7** can be derived using steady state kinetics resulting in equation (1). When we then plug this value for **7** into the Nernst equation, the result is equation (2) which describes the relationship between the observed oxidation potential and the rate of cyclization. In equation (2), $E^o$ is positive and $RT/nF$ is positive and constant. Therefore, as $k_2$ gets larger (indicating a faster cyclization), $E_{obsv}$ decreases. This effect is clearly seen, as illustrated in Scheme 1.7. The oxidation potential of an isolated dithioketene acetal is *Ep/2* = +1.06 V vs Ag/AgCl. The measured oxidation potential of **6** with an alcohol trapping group is *Ep/2* = +0.95 V vs Ag/AgCl. While the oxidation potential of **4** with an amine trapping group is *Ep/2* = +0.60 V vs Ag/AgCl.[50] The decrease in potential indicates the difference in cyclization rates, suggesting that the amine-based cyclization happens more rapidly than the alcohol-based cyclization, an observation completely consistent with the ability of the amine to serve as a nucleophile.

## 1.4 Conclusion

With the following background on electrochemistry outlined in this chapter, we have established a foundation for comprehending anodic olefin coupling reactions moving forward. This sets the stage for conducting the structure/activity studies detailed in the remainder of this thesis; studies that leverage the benefits of constant current electrolysis and the ability to conduct oxidations on a variety of substrates under the same or very similar reaction conditions.

## References

(1) B. Sperry, J.; L. Wright, D. The Application of Cathodic Reductions and Anodic Oxidations in the Synthesis of Complex Molecules. *Chem. Soc. Rev.* **2006**, *35* (7), 605–621. https://doi.org/10.1039/B512308A.

(2) Yoshida, J.; Kataoka, K.; Horcajada, R.; Nagaki, A. Modern Strategies in Electroorganic Synthesis. *Chem. Rev.* **2008**, *108* (7), 2265–2299. https://doi.org/10.1021/cr0680843.

(3) A. Frontana-Uribe, B.; Daniel Little, R.; G. Ibanez, J.; Palma, A.; Vasquez-Medrano, R. Organic Electrosynthesis: A Promising Green Methodology in Organic Chemistry. *Green Chem.* **2010**, *12* (12), 2099–2119. https://doi.org/10.1039/C0GC00382D.

(4) Francke, R.; Daniel Little, R. Redox Catalysis in Organic Electrosynthesis: Basic Principles and Recent Developments. *Chem. Soc. Rev.* **2014**, *43* (8), 2492–2521. https://doi.org/10.1039/C3CS60464K.

(5) Yan, M.; Kawamata, Y.; Baran, P. S. Synthetic Organic Electrochemical Methods Since 2000: On the Verge of a Renaissance. *Chem. Rev.* **2017**, *117* (21), 13230–13319. https://doi.org/10.1021/acs.chemrev.7b00397.

(6) Nutting, J. E.; Rafiee, M.; Stahl, S. S. Tetramethylpiperidine N-Oxyl (TEMPO), Phthalimide N-Oxyl (PINO), and Related N-Oxyl Species: Electrochemical Properties and Their Use in Electrocatalytic Reactions. *Chem. Rev.* **2018**, *118* (9), 4834–4885. https://doi.org/10.1021/acs.chemrev.7b00763.

(7) Mitsudo, K.; Kurimoto, Y.; Yoshioka, K.; Suga, S. Miniaturization and Combinatorial Approach in Organic Electrochemistry. *Chem. Rev.* **2018**, *118* (12), 5985–5999. https://doi.org/10.1021/acs.chemrev.7b00532.

(8) Sauermann, N.; Meyer, T. H.; Qiu, Y.; Ackermann, L. Electrocatalytic C–H Activation. *ACS Catal.* **2018**, *8* (8), 7086–7103. https://doi.org/10.1021/acscatal.8b01682.

(9) Sauer, G. S.; Lin, S. An Electrocatalytic Approach to the Radical Difunctionalization of Alkenes. *ACS Catal.* **2018**, *8* (6), 5175–5187. https://doi.org/10.1021/acscatal.8b01069.

(10) Möhle, S.; Zirbes, M.; Rodrigo, E.; Gieshoff, T.; Wiebe, A.; Waldvogel, S. R. Modern Electrochemical Aspects for the Synthesis of Value-Added Organic Products. *Angew. Chem. Int. Ed.* **2018**, *57* (21), 6018–6041. https://doi.org/10.1002/anie.201712732.

(11) Elsherbini, M.; Wirth, T. Electroorganic Synthesis under Flow Conditions. *Acc. Chem. Res.* **2019**, *52* (12), 3287–3296. https://doi.org/10.1021/acs.accounts.9b00497.

(12) Xiong, P.; Xu, H.-C. Chemistry with Electrochemically Generated N-Centered Radicals. *Acc. Chem. Res.* **2019**, *52* (12), 3339–3350. https://doi.org/10.1021/acs.accounts.9b00472.

(13) Hilt, G. Basic Strategies and Types of Applications in Organic Electrochemistry. *ChemElectroChem* **2020**, *7* (2), 395–405. https://doi.org/10.1002/celc.201901799.

(14) Li, H.; Xue, Y.-F.; Ge, Q.; Liu, M.; Cong, H.; Tao, Z. Chiral Electroorganic Chemistry: An Interdisciplinary Research across Electrocatalysis and Asymmetric Synthesis. *Mol. Catal.* **2021**, *499*, 111296. https://doi.org/10.1016/j.mcat.2020.111296.

(15) Beil, S. B.; Pollok, D.; Waldvogel, S. R. Reproducibility in Electroorganic Synthesis—Myths and Misunderstandings. *Angew. Chem. Int. Ed.* **2021**, *60* (27), 14750–14759. https://doi.org/10.1002/anie.202014544.

(16) Marken, F.; Cresswell, A. J.; Bull, S. D. Recent Advances in Paired Electrosynthesis. *Chem. Rec.* **2021**, *21* (9), 2585–2600. https://doi.org/10.1002/tcr.202100047.

(17) Dörr, M.; Hielscher, M. M.; Proppe, J.; Waldvogel, S. R. Electrosynthetic Screening and Modern Optimization Strategies for Electrosynthesis of Highly Value-Added Products. *ChemElectroChem* **2021**, *8* (14), 2621–2629. https://doi.org/10.1002/celc.202100318.

(18) Okada, Y.; Chiba, K. Redox-Tag Processes: Intramolecular Electron Transfer and Its Broad Relationship to Redox Reactions in General. *Chem. Rev.* **2018**, *118* (9), 4592–4630. https://doi.org/10.1021/acs.chemrev.7b00400.

(19) Hammerich, O.; Speiser, B. *Organic Electrochemistry: Revised and Expanded*; CRC Press, 2015.

(20) Feng, R.; Smith, J. A.; Moeller, K. D. Anodic Cyclization Reactions and the Mechanistic Strategies That Enable Optimization. *Acc. Chem. Res.* **2017**, *50* (9), 2346–2352. https://doi.org/10.1021/acs.accounts.7b00287.

(21) Moeller, K. D. Synthetic Applications of Anodic Electrochemistry. *Tetrahedron* **2000**, *56* (49), 9527–9554. https://doi.org/10.1016/S0040-4020(00)00840-1.

(22) Campbell, J. M.; Xu, H.-C.; Moeller, K. D. Investigating the Reactivity of Radical Cations: Experimental and Computational Insights into the Reactions of Radical Cations with Alcohol and p-Toluene Sulfonamide Nucleophiles. *J. Am. Chem. Soc.* **2012**, *134* (44), 18338–18344. https://doi.org/10.1021/ja307046j.

(23) Moeller, K. D. Using Physical Organic Chemistry To Shape the Course of Electrochemical Reactions. *Chem. Rev.* **2018**, *118* (9), 4817–4833. https://doi.org/10.1021/acs.chemrev.7b00656.

(24) Liu, B.; Duan, S.; Sutterer, A. C.; Moeller, K. D. Oxidative Cyclization Based on Reversing the Polarity of Enol Ethers and Ketene Dithioacetals. Construction of a

Tetrahydrofuran Ring and Application to the Synthesis of (+)-Nemorensic Acid. *J. Am. Chem. Soc.* **2002**, *124* (34), 10101–10111. https://doi.org/10.1021/ja026739l.

(25) Miller, A. K.; Hughes, C. C.; Kennedy-Smith, J. J.; Gradl, S. N.; Trauner, D. Total Synthesis of (−)-Heptemerone B and (−)-Guanacastepene E. *J. Am. Chem. Soc.* **2006**, *128* (51), 17057–17062. https://doi.org/10.1021/ja0660507.

(26) New, D. G.; Tesfai, Z.; Moeller, K. D. Intramolecular Anodic Olefin Coupling Reactions and the Use of Electron-Rich Aryl Rings1. *J. Org. Chem.* **1996**, *61* (5), 1578–1598. https://doi.org/10.1021/jo9518359.

(27) Duan, S.; Moeller, K. D. Anodic Coupling Reactions: Probing the Stereochemistry of Tetrahydrofuran Formation. A Short, Convenient Synthesis of Linalool Oxide. *Org. Lett.* **2001**, *3* (17), 2685–2688. https://doi.org/10.1021/ol0162670.

(28) Reddy, S. H. K.; Moeller, K. D. Intramolecular Anodic Olefin Coupling Reactions: The Construction of Bridged Bicyclic Ring Skeletons. *Tetrahedron Lett.* **1998**, *39* (44), 8027–8030. https://doi.org/10.1016/S0040-4039(98)01793-6.

(29) Sutterer, A.; Moeller, K. D. Reversing the Polarity of Enol Ethers: An Anodic Route to Tetrahydrofuran and Tetrahydropyran Rings. *J. Am. Chem. Soc.* **2000**, *122* (23), 5636–5637. https://doi.org/10.1021/ja001063k.

(30) Moeller, K. D.; Marzabadi, M. R.; New, D. G.; Chiang, M. Y.; Keith, S. Oxidative Organic Electrochemistry: A Novel Intramolecular Coupling of Electron-Rich Olefins. *J. Am. Chem. Soc.* **1990**, *112* (16), 6123–6124. https://doi.org/10.1021/ja00172a035.

(31) Moeller, K. D.; Tinao, L. V. Intramolecular Anodic Olefin Coupling Reactions: The Use of Bis Enol Ether Substrates. *J. Am. Chem. Soc.* **1992**, *114* (3), 1033–1041. https://doi.org/10.1021/ja00029a036.

(32) Frey, D. A.; Krishna Reddy, S. H.; Moeller, K. D. Intramolecular Anodic Olefin Coupling Reactions: The Use of Allylsilane Coupling Partners with Allylic Alkoxy Groups. *J. Org. Chem.* **1999**, *64* (8), 2805–2813. https://doi.org/10.1021/jo982280v.

(33) Hudson, C. M.; Moeller, K. D. Intramolecular Anodic Olefin Coupling Reactions and the Use of Vinylsilanes. *J. Am. Chem. Soc.* **1994**, *116* (8), 3347–3356. https://doi.org/10.1021/ja00087a021.

(34) Hudson, C. M.; Marzabadi, M. R.; Moeller, K. D.; New, D. G. Intramolecular Anodic Olefin Coupling Reactions: A Useful Method for Carbon-Carbon Bond Formation. *J. Am. Chem. Soc.* **1991**, *113* (19), 7372–7385. https://doi.org/10.1021/ja00019a038.

(35) Redden, A.; Moeller, K. D. Anodic Coupling Reactions: Exploring the Generality of Curtin−Hammett Controlled Reactions. *Org. Lett.* **2011**, *13* (7), 1678–1681. https://doi.org/10.1021/ol200182f.

(36) Wu, H.; Moeller, K. D. Anodic Coupling Reactions: A Sequential Cyclization Route to the Arteannuin Ring Skeleton. *Org. Lett.* **2007**, *9* (22), 4599–4602. https://doi.org/10.1021/ol702118n.

(37) Huang, Y.; Moeller, K. D. Anodic Coupling Reactions: The Use of N,O-Ketene Acetal Coupling Partners. *Org. Lett.* **2004**, *6* (23), 4199–4202. https://doi.org/10.1021/ol048450+.

(38) Huang, Y.; Moeller, K. D. Anodic Cyclization Reactions: Probing the Chemistry of N,O-Ketene Acetal Derived Radical Cations. *Tetrahedron* **2006**, *62* (27), 6536–6550. https://doi.org/10.1016/j.tet.2006.04.009.

(39) Brandt, J. D.; Moeller, K. D. Oxidative Cyclization Reactions: Amide Trapping Groups and the Synthesis of Furanones. *Org. Lett.* **2005**, *7* (16), 3553–3556. https://doi.org/10.1021/ol051296m.

(40) Xu, H.-C.; Brandt, J. D.; Moeller, K. D. Anodic Cyclization Reactions and the Synthesis of (−)-Crobarbatic Acid. *Tetrahedron Lett.* **2008**, *49* (24), 3868–3871. https://doi.org/10.1016/j.tetlet.2008.04.075.

(41) Duan, S.; Moeller, K. D. Anodic Cyclization Reactions: Capitalizing on an Intramolecular Electron Transfer to Trigger the Synthesis of a Key Tetrahydropyran Building Block. *J. Am. Chem. Soc.* **2002**, *124* (32), 9368–9369. https://doi.org/10.1021/ja027227+.

(42) Sun, Y.; Liu, B.; Kao, J.; d'Avignon, D. A.; Moeller, K. D. Anodic Cyclization Reactions: Reversing the Polarity of Ketene Dithioacetal Groups. *Org. Lett.* **2001**, *3* (11), 1729–1732. https://doi.org/10.1021/ol015925d.

(43) Sun, Y.; Moeller, K. D. Anodic Olefin Coupling Reactions Involving Ketene Dithioacetals: Evidence for a 'Radical-Type' Cyclization. *Tetrahedron Lett.* **2002**, *43* (40), 7159–7161. https://doi.org/10.1016/S0040-4039(02)01663-5.

(44) Xu, H.-C.; Campbell, J. M.; Moeller, K. D. Cyclization Reactions of Anode-Generated Amidyl Radicals. *J. Org. Chem.* **2014**, *79* (1), 379–391. https://doi.org/10.1021/jo402623r.

(45) Sun, H.; Martin, C.; Kesselring, D.; Keller, R.; Moeller, K. D. Building Functionalized Peptidomimetics: Use of Electroauxiliaries for Introducing N-Acyliminium Ions into Peptides. *J. Am. Chem. Soc.* **2006**, *128* (42), 13761–13771. https://doi.org/10.1021/ja064737l.

(46) Sun, H.; Moeller, K. D. Silyl-Substituted Amino Acids: New Routes to the Construction of Selectively Functionalized Peptidomimetics. *Org. Lett.* **2002**, *4* (9), 1547–1550. https://doi.org/10.1021/ol025776e.

(47) Xu, H. Intramolecular Anodic Olefin Coupling Reactions: Synthesis Of Nitrogen- And Oxygen-Heterocycles. *Theses Diss. ETDs* **2010**. https://doi.org/10.7936/K7S75DCK.

(48) Xu, H.-C.; Moeller, K. D. Intramolecular Anodic Olefin Coupling Reactions: Using Competition Studies to Probe the Mechanism of Oxidative Cyclization Reactions. *Org. Lett.* **2010**, *12* (8), 1720–1723. https://doi.org/10.1021/ol100317t.

(49) Medcalf, Z.; Redd, E. G.; Oh, J.; Ji, C.; Moeller, K. D. Anodic Cyclizations and Umpolung Reactions Involving Imines. *Org. Lett.* **2023**, *25* (22), 4135–4139. https://doi.org/10.1021/acs.orglett.3c01399.

(50) Xu, H.-C.; Moeller, K. D. Intramolecular Anodic Olefin Coupling Reactions: Use of the Reaction Rate To Control Substrate/Product Selectivity. *Angew. Chem.* **2010**, *122* (43), 8176–8179. https://doi.org/10.1002/ange.201003924.

(51) Xu, H.-C.; Moeller, K. D. Intramolecular Anodic Olefin Coupling Reactions and the Synthesis of Cyclic Amines. *J. Am. Chem. Soc.* **2010**, *132* (8), 2839–2844. https://doi.org/10.1021/ja910586v.

(52) Xu, H.-C.; Moeller, K. D. Intramolecular Anodic Olefin Coupling Reactions: The Use of a Nitrogen Trapping Group. *J. Am. Chem. Soc.* **2008**, *130* (41), 13542–13543. https://doi.org/10.1021/ja806259z.

(53) Smith, J. A.; Moeller, K. D. Oxidative Cyclizations, the Synthesis of Aryl-Substituted C-Glycosides, and the Role of the Second Electron Transfer Step. *Org. Lett.* **2013**, *15* (22), 5818–5821. https://doi.org/10.1021/ol402826z.

(54) Krueger, R.; Feng, E.; Barzova, P.; Lieberman, N.; Lin, S.; Moeller, K. D. Anodic Cyclizations, Densely Functionalized Synthetic Building Blocks, and the Importance of Recent Mechanistic Observations. *J. Org. Chem.* **2024**, *89* (3), 1927–1940. https://doi.org/10.1021/acs.joc.3c02659.

(55) Xu, G.; Moeller, K. D. Anodic Coupling Reactions and the Synthesis of C-Glycosides. *Org. Lett.* **2010**, *12* (11), 2590–2593. https://doi.org/10.1021/ol100800u.

(56) Mihelcic, J.; Moeller, K. D. Oxidative Cyclizations: The Asymmetric Synthesis of (−)-Alliacol A. *J. Am. Chem. Soc.* **2004**, *126* (29), 9106–9111. https://doi.org/10.1021/ja048085h.

(57) Wright, D. L.; Whitehead, C. R.; Sessions, E. H.; Ghiviriga, I.; Frey, D. A. Studies on Inducers of Nerve Growth Factor: Synthesis of the Cyathin Core. *Org. Lett.* **1999**, *1* (10), 1535–1538. https://doi.org/10.1021/ol991032y.

(58) Frey, D. A.; Wu, N.; Moeller, K. D. Anodic Electrochemistry and the Use of a 6-Volt Lantern Battery: A Simple Method for Attempting Electrochemically Based Synthetic Transformations. *Tetrahedron Lett.* **1996**, *37* (46), 8317–8320. https://doi.org/10.1016/0040-4039(96)01946-6.

(59) H. Nguyen, B.; Redden, A.; D. Moeller, K. Sunlight, Electrochemistry, and Sustainable Oxidation Reactions. *Green Chem.* **2014**, *16* (1), 69–72. https://doi.org/10.1039/C3GC41650J.

(60) Medcalf, Z.; Moeller, K. D. Anodic Olefin Coupling Reactions: Elucidating Radical Cation Mechanisms and the Interplay between Cyclization and Second Oxidation Steps. *Chem. Rec.* **2021**, *21* (9), 2442–2452. https://doi.org/10.1002/tcr.202100118.

# Chapter 2: Anodic Olefin Coupling Reactions: Elucidating Radical Cation Mechanisms and the Interplay between Cyclization and Second Oxidation Steps

In this chapter, we will explore the mechanistic model established for anodic olefin coupling reactions, along with our recent contributions to that model. The chapter is based on two papers we published that highlight the importance of both the initial cyclization and the second oxidation step for the success of an anodic cyclization.[1,2] As depicted in Scheme 2.1, the reactions involve three steps, namely $k_1/k_{-1}$, $k_2$, and $k_3$. We will be focusing most on the second oxidation step, however a brief summary will be given for the importance of the initial cyclization. (Sections of this chapter were taken from our papers: Medcalf, Z.; Moeller, K. D. Anodic Olefin Coupling Reactions: Elucidating Radical Cation Mechanisms and the Interplay between Cyclization and Second Oxidation Steps. *Chem. Rec.* **2021**, *21* (9), 2442–2452. https://doi.org/10.1002/tcr.202100118 and Graaf, M. D.; Gonzalez, L.; Medcalf, Z.; Moeller, K. D. Using a Combination of Electrochemical and Photoelectron Transfer Reactions to Gain New Insights into Oxidative Cyclization Reactions. *J. Electrochem. Soc.* **2020**, *167* (15), 155520. https://doi.org/10.1149/1945-7111/abbe5c).

## 2.1 Anodic Cyclization Reaction Mechanism Structure

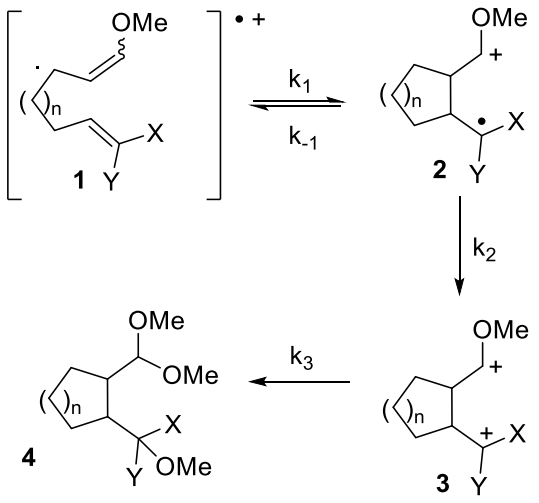


**Scheme 2.1: Anodic Cyclization Reaction Mechanism Model**

As described in Chapter 1, anodic coupling reactions generally follow the mechanistic paradigm shown in Scheme 2.1. Generally, the anodic oxidation of a substrate results in the formation of radical cation**1**, which can then undergo a reversible or irreversible cyclization reaction ($k_1/k_{-1}$). This cyclized radical cation then undergoes a second oxidation, forming di-cation **3**. Depending on the speed of this second oxidation step this cyclization can be reversible ($k_2 > k_{-1}$) or irreversible ($k_{-1} > k_2$).[3] After the second oxidation step, the final product **4** is made by methanol trapping of the cations or a combination of methanol trapping and an elimination (as seen in cases using an allylsilane trapping group). These steps which occur after the second oxidation step are designated as $k_3$.

The key for a successful anodic cyclization is both a fast initial cyclization, a rapid second oxidation step, and a $k_3$ that leads to a stable product.[2]

## 2.1.1 The Initial Cyclization

For years, the mechanistic studies done focused on the initial cyclization that transformed the initial radical cation **1** into the cyclic radical cation **2**. The reactions worked or failed based upon

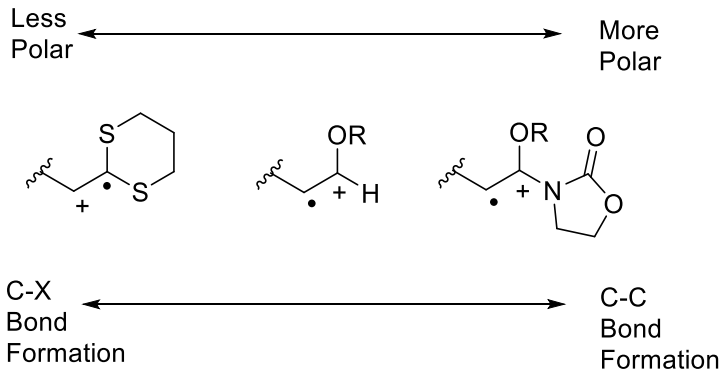


**Scheme 2.2: Anodic Cyclizations Depend on the Nature of the Radical Cation**

how fast the initial cyclization occurred relative to other side reactions. We found that the success of these reactions was dependent on the nature of the radical cation generated. As depicted in Scheme 2.2, more polar radical cations, such as those generated from an N,O-ketene acetal, prefer to make carbon-carbon bonds; whereas less polar radical cations, like those generated from a ketene dithioacetal prefer to make carbon-heteroatom bonds.[4,5] Reactions which made carbon-carbon bonds were best described as reversible radical type reactions.[6,7] Generally speaking, reactions that failed could be dealt with by buying time for the cyclization reaction to occur. If the reactions result in the solvent trapping of the radical cation, the reactive intermediate can be protected by using non-nucleophilic cosolvents and greasier electrolytes. These electrolytes would exclude methanol, utilized for trapping cations in the final product, from the electrode surface.[8,9] If the reactions were slow to cyclize, resulting in elimination reactions involving the initial radical cation **1,** as seen in Scheme 2.1, the radical cation could be pushed down a radical pathway. This would allow more time for the slower cyclization to take place, thereby preventing the elimination reaction from occurring.[10]

In many of these studies, the events that happened after the cyclization reaction were overlooked. This included a loss of a second electron, followed by a loss of a proton, a silyl group, or methanol trapping to afford the final product. The timing of these steps remained unknown, but they were generally considered unimportant.

## 2.1.2 The Second Oxidation Step

Following the cyclization, the next step is the removal of the second electron from the cyclized radical cation intermediate **2** to form the dication **3,** as depicted in Scheme 2.1, with the rate of this second oxidation step influencing kinetic vs thermodynamic control in these reactions.[3] Additionally, a fast second oxidation step ($k_2$) appears to be essential for anodic carbon-carbon bond forming reactions even if a fast cyclization occurs.[1] In this chapter, we will explore several examples highlighting the significance of the second oxidation step for the success of anodic cyclization reactions.

**Scheme 2.3: Allyl Silanes and the Need for an RVC Anode**

### Early Results

The first indication of the importance of the second oxidation step can be seen in Scheme 2.3. In this study, an allyl silane was used to trap an enol ether derived radical cation.[11] Originally, a platinum anode was used due to its stability. The allylsilane served as the terminating group to channel the reaction towards an olefin. While the reaction worked, the isolated yield of the product **6** was low. Additionally, the oxidation still resulted in a mixture of products. Of note, one of these side products was a vinylsilane which posed a concern. The purpose of using an allylsilane as a trapping group was to give the cation generated a favorable elimination pathway (Scheme 2.4).

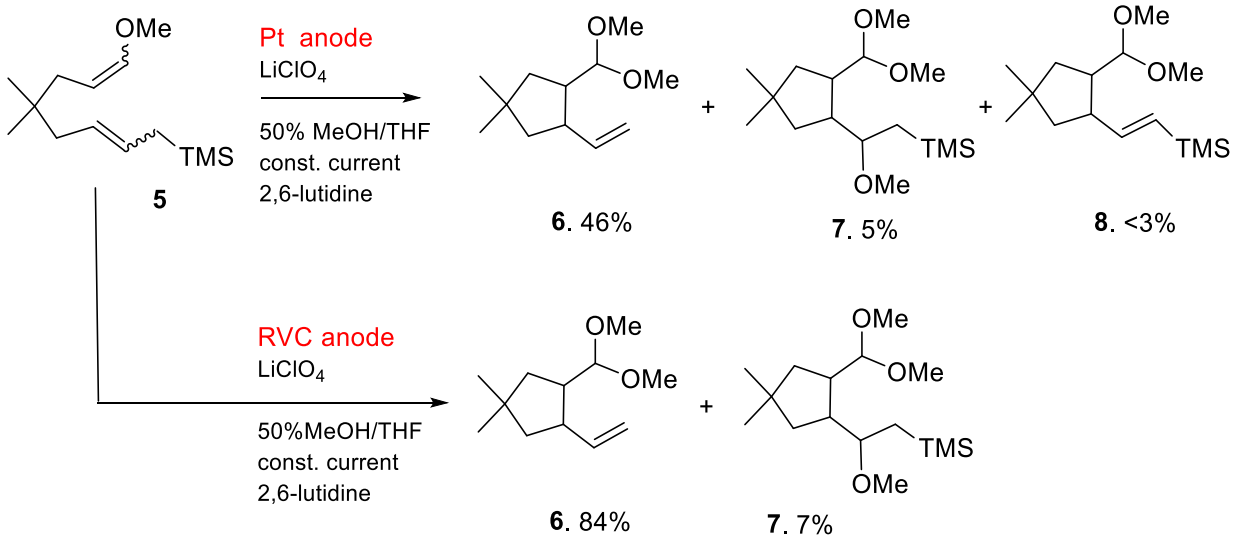


The presence of the vinylsilane product was not consistent with the cation being present; rather, its formation was consistent with a radical intermediate and the elimination of a hydrogen atom instead of the silane. It remained uncertain whether the trace amount of vinylsilane resulted from

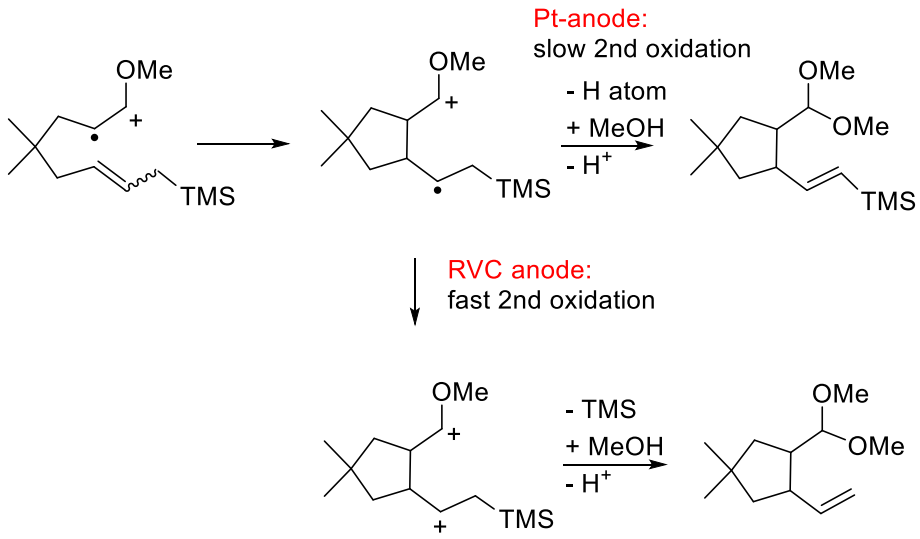


**Scheme 2.4: Suggested Mechanism for the Formation of the Vinylsilane**

a minor product from a major pathway or a major product from a minor pathway. However, if it

originated from a major pathway, then it was indicative that the second oxidation step did not occur readily.

At that time, a literature search indicated that Pt-anodes favored on electron oxidation pathways, while C-anodes favored two-electron oxidation pathways.[12] This observation stemmed from the fact that the Pt-anode would corrode during the course of the reaction, which hindered further oxidation reactions. On the other hand, carbon anodes do not corrode to the same extent and they also have a higher surface area. Due to this, the anode for the oxidative cyclization was switched to reticulated vitreous carbon (RVC) to maximize the available surface area (Scheme 2.3). As a result of this change, the yield rose to 84% of the desired olefinic product. Facilitating the second oxidation step proved crucial for the success of this reaction.

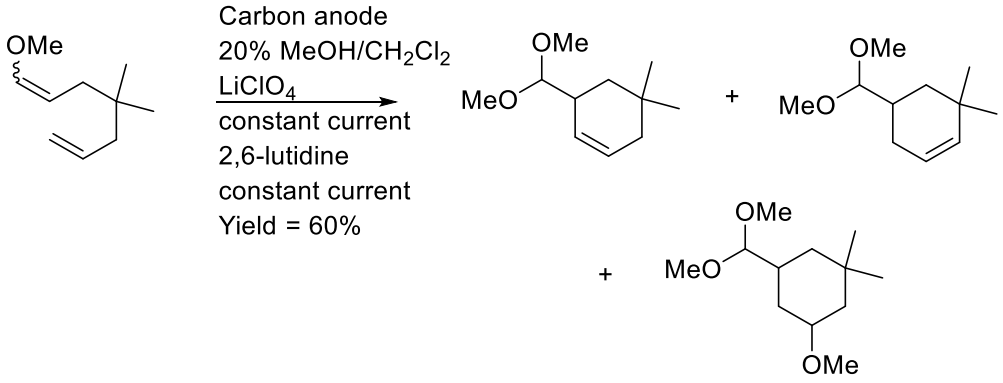


**Scheme 2.5: Initial cyclizations with a mono-substituted olefin led to only six-membered ring products**

The second example of a reaction that benefited from an efficient second oxidation step, was found when extending an anodic cyclization to include the use of vinylsilane trapping groups.[6] Once again, this chemistry stemmed from efforts to control the terminal stages of an anodic cyclization. As seen in Scheme 2.3, this allylsilane trapped reaction suggested a radical-like nature of the

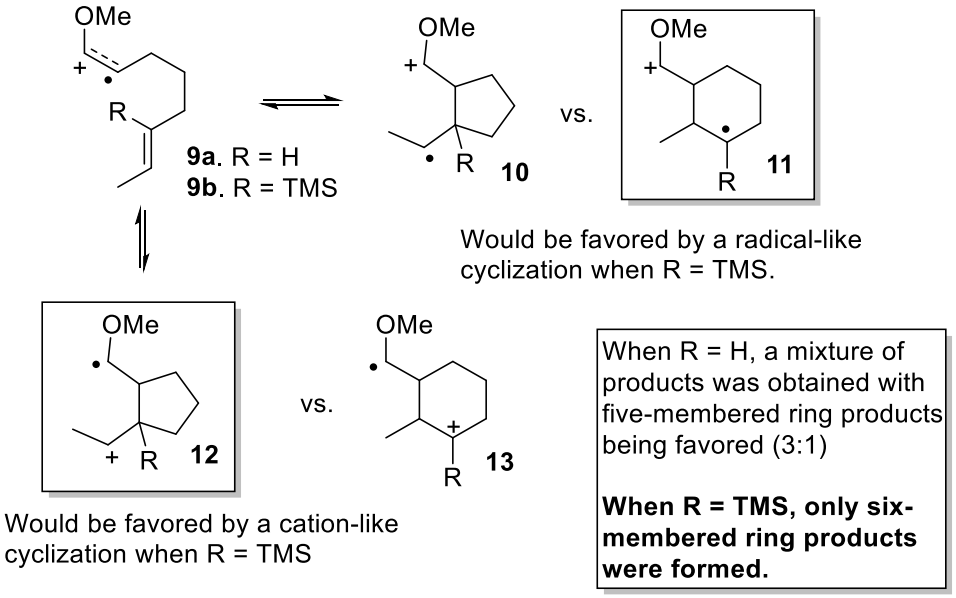


**Scheme 2.6: Vinylsilanes and Probing Radical vs. Cation Pathways**

intermediate formed at the terminating end of the cyclization. Early anodic cyclizations were found to generate 6-endo products instead of 5-exo products. This led to the conclusion that these reactions were "cation-like" cyclizations (Scheme 2.5).[6,13] Due to this discrepancy, the chemistry shown in Scheme 2.6 was carried out. Silyl groups are known to stabilize radical intermediates situated alpha to the silicon group and cations located beta to the silicon group.[14] Keeping this in consideration, substrates **9a** and **9b** were specifically designed. When substrate **9a** was oxidized, it resulted in a mixture of five- and six-membered ring products, in a 3:1 ratio favoring the five-membered ring. When a silyl group was added as seen in **9b**, two different scenarios could arise depending on if the reaction led to a "radical-like" or "cation-like" intermediate on the terminating end of the cyclization. If the former was true, then the reaction would lead to a six-membered ring

product (**11**). However, if the latter was found true, then the reaction would lead to a five-membered ring product (**12**). When **9b** was oxidized it yielded exclusively six-membered ring products, indicating a "radical-like" cyclization.

The use of a vinylsilane trapping group, along with evidence supporting a "radical-like" cyclization, prompted the design of substrate **14** in Scheme 2.7.[6] This reaction was conceptualized

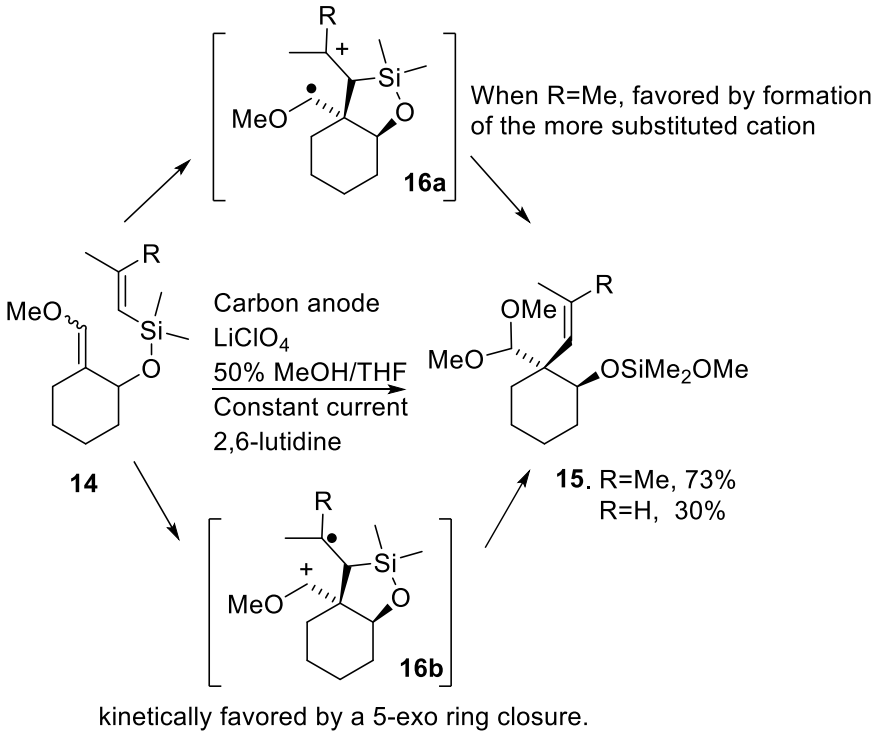


based on an empirical observation made after a number of the earliest anodic olefin coupling

**Scheme 2.7: Silicon Tethers Resulting in The Formation Of A Quaternary Carbon**

reactions had been studied by the Moeller group. In these studies, these reactions worked best when one would predict a kinetic radical pathway would lead to the same product as a kinetic cationic pathway. In this instance, the introduction of a silicon tether facilitated the creation of a quaternary carbon. The trapping group employed in this reaction was a trisubstituted olefin. If one

would disregard the silyl group in the tether, a 5-exo process would be favored by both cationic and radical processes. When the experiment was conducted, this thought process held true and the reaction led to a 73% yield of the quaternary carbon product. This result was reliant on a trisubstituted olefin. If a disubstituted olefin was used instead then the yield dropped significantly to 30% and led to a mixture of products. The reason for this was because the cyclization was a reversible radical type reaction. If a trisubstituted olefin was used, then the favored product would lead to a radical that would be readily oxidized into a cation (**16**). However, if a disubstituted olefin was used instead the radical generated after the cyclization would undergo a slower oxidation and lead to a mixture of products. This outcome provided another instance of an anodic olefin coupling reaction that relied on an efficient second oxidation step to achieve synthetically useful yields of product.

**A Critical Competition Study**

In the competition study seen in Scheme 2.8, a cyclization between an electron-rich olefin under basic conditions was examined to determine whether the reaction proceeded through an initially formed nitrogen radical or a radical cation of the olefin.[3] The objective was to see if the two intermediates (**18** and **19**) in Scheme 2.8 could equilibrate by a potential intramolecular electron transfer reaction. If this intramolecular electron transfer did not happen, then the oxidation would result in only the nitrogen-centered radical **18** and the cyclization would only result in product **20**. Without the electron transfer occurring, there would be no opportunity for the alcohol trapping product to occur, therefore **21** would not be made. However, in the case that the electron transfer did take place, then both intermediates (**18** and **19**) would be generated. Therefore, both nucleophiles could trap, and both products would be observed.

When this experiment was carried out, the oxidation of **17** led to both **20** and **21**, which meant the intramolecular electron transfer reaction occurred. The specific product formed could be influenced by the reaction conditions used. If a higher current and lower temperatures were used

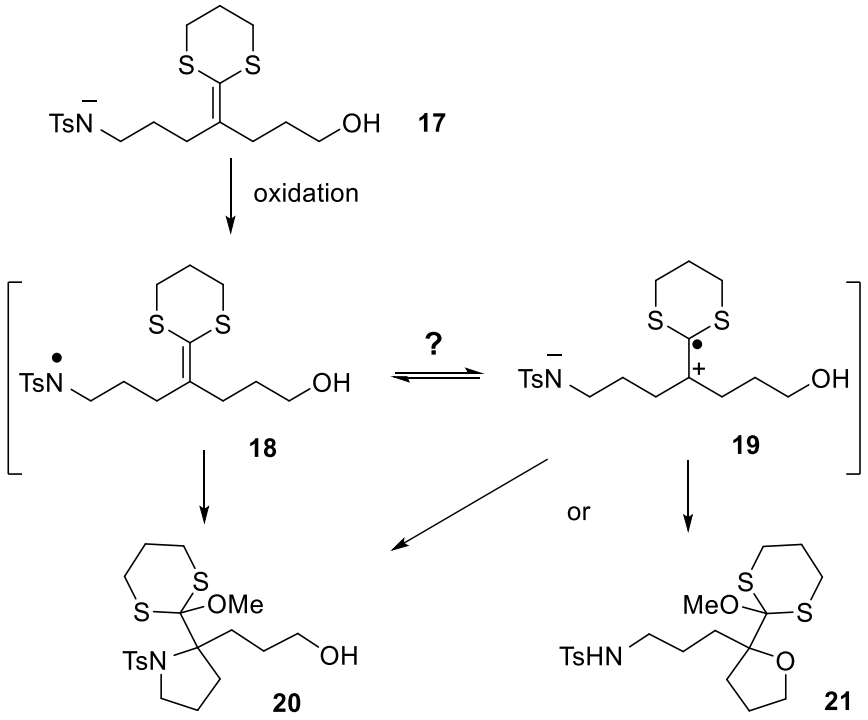


**Scheme 2.8: A Competition Study Resulting in the Formation of Kinetic or Thermodynamic Products Based on the Oxidation Rate**

then the alcohol trapping product **21** would be formed preferentially. However, if a lower current and higher temperatures were used, then the sulfonamide trapping product **20** would be observed. The explanation for these results, as seen in Scheme 2.9, was that the alcohol product was the kinetic trapping product. This product was favored by using lower temperatures along with a higher current flow, which would slow the reverse reaction and accelerate the second oxidation step. After the second electron was removed, the generated dication could not adopt an acyclic form, which would place the two positive charges next to each other. However, if the temperature

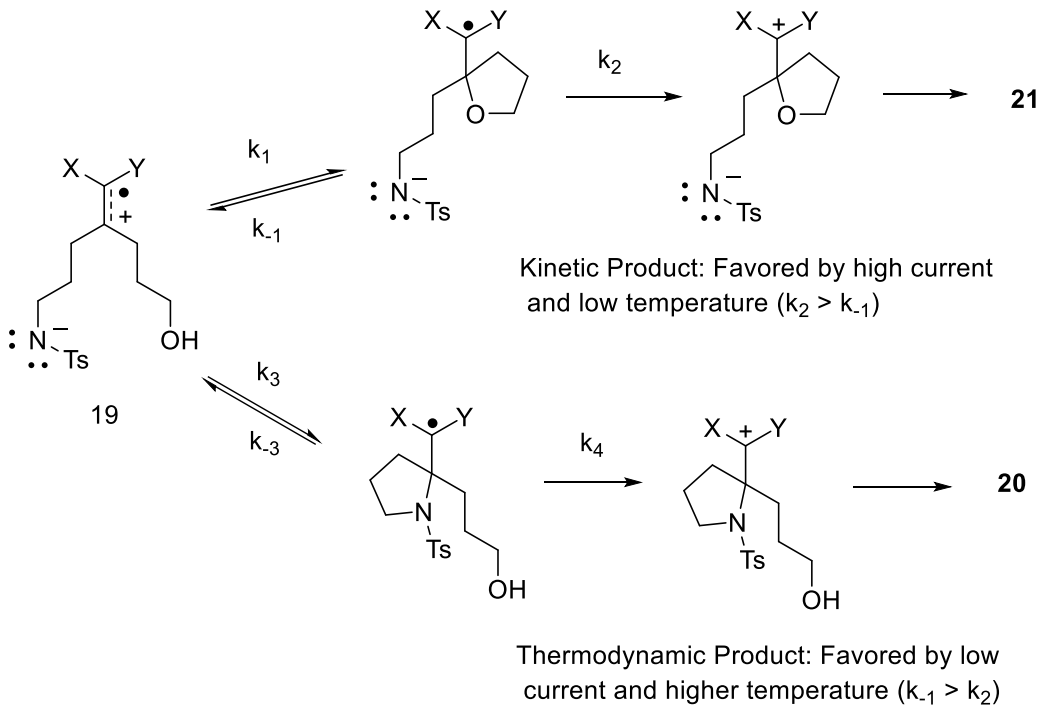


**Scheme 2.9: Mechanistic Rational to Explain the Competition Study**

was raised and a lower current density was used then the reverse reaction would be accelerated and the second oxidation step would be slowed. This would allow the initial cyclization to reverse, resulting in the formation of the more stable thermodynamic product, **20**. The competition study revealed that the rate of the second oxidation step played a crucial role in determining the generated product, indicating that the reaction was not solely governed by the kinetics of the cyclization reaction.

**Synthetic Ramifications**

The significance of a fast second oxidation step can be seen in the synthesis of C-glycosides, as illustrated in Table 2.1.[15] The substrate for this reaction was made using a Wittig reaction on a sugar to install the styrene group. From there, the styrene group was oxidized to generate a radical cation which would then be trapped by the alcohol to make a ring and form the C-glycoside. The data for four examples utilizing various phenyl rings is shown in Table 2.1. In the first case, a styrene group (**22a**) was oxidized. While the reaction was clean since only starting material and product was found, the yield of the product was low (entry 1). The reason for this result remained

**Table 2.1: The Impact of the Second Oxidation Step and the Formation of C-Glycosides**

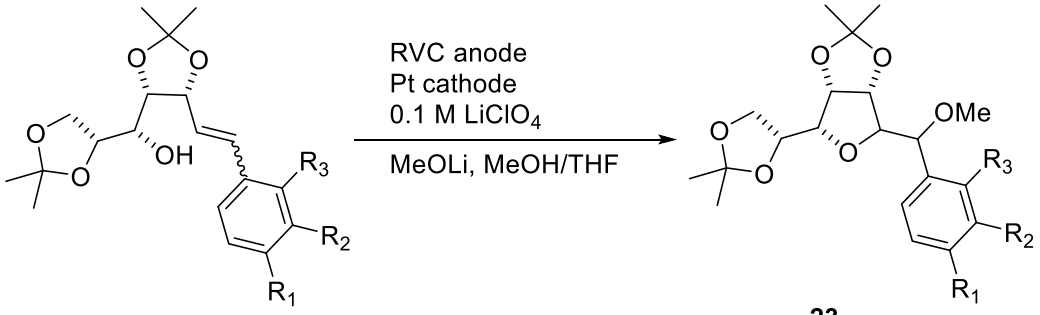


**22**. a. $R_1 = R_2 = R_3 = H$
b. $R_1 = OMe$, $R_2 = H$, $R_3 = H$
c. $R_1 = H$, $R_2 = OMe$, $R_3 = H$
d. $R_1 = H$, $R_2 = H$, $R_3 = OMe$

**23**

| Entry | Substrate | $E_{p/2}$ | F/mole | %yield |
|---|---|---|---|---|
| 1 | 22a | 1.34V | 2.2 | 22(60)[a,b,c] |
| 2 | 22b | 1.16V | 2.2 | 84 |
| 3 | 22c | 1.20V | 2.2 | 48(27)[b] |
| 4 | 22d | 1.17V | 2.2 | 70(17) |

[a] The yield of the recovered starting material. [b] The yield with 10F/mol was 74% with 5% recovered starting material. [c] The yield with 1 M $LiClO_4$ was 65% with 18% recovered starting material.

unclear due to the following factors: first, the substrate had a reasonable oxidation potential, which

was significantly lower than other groups present in the reaction; second, it was unclear how the current could be consumed without converting the starting material into the desired product or a side product.

While the yield for the reaction could be increased if more current was passed through the solution, the reaction required 10 F/mole of charge to convert the starting material to product. Upon examining the mechanism of the reaction as shown in Scheme 2.10, a possible explanation arose. Once the cyclization occurred, it would lead to a stable benzylic radical (**25**). If this radical is not oxidized quickly, then the intermediate could migrate to the cathode where it could be re-reduced, which would consume current and result in the starting material being regenerated. If more electrolyte was added to solution, a modification which would slow down the migration of **25** from the anode to the cathode, then the current efficiency of the reaction would be improved. As observed in entry 1c in Table 2.1, this change resulted in a 65% yield of product, along with 18% recovered starting material.

Additional support for the involvement of the second oxidation step in the mechanism was obtained by introducing substituents to the aryl ring. The yield of C-glycoside formation could be improved by adding an electron-donating group to the aryl ring. However, this would only be effective if the position of the donor group allowed an interaction with the benzylic radical, thereby increasing the rate of the second oxidation step (see entries 2-4 in Table 2.1). In each instance, adding a methoxy group to the aryl ring resulted in an approximately equal decrease in oxidation potential of the substrate (+1.2V vs Ag/AgCl). This indicates the rate of oxidation and the following cyclization were approximately equal for all three substrates (see 1.3.2 for explanation).[15] However, the location of the methoxy group on the aryl ring played an important role in the success of the reaction. For instance, when the methoxy group was placed at the meta position on the aryl ring — a location where it could readily donate electron-density to the benzylic radical — the second oxidation step would not occur readily. Conversely, if the methoxy group

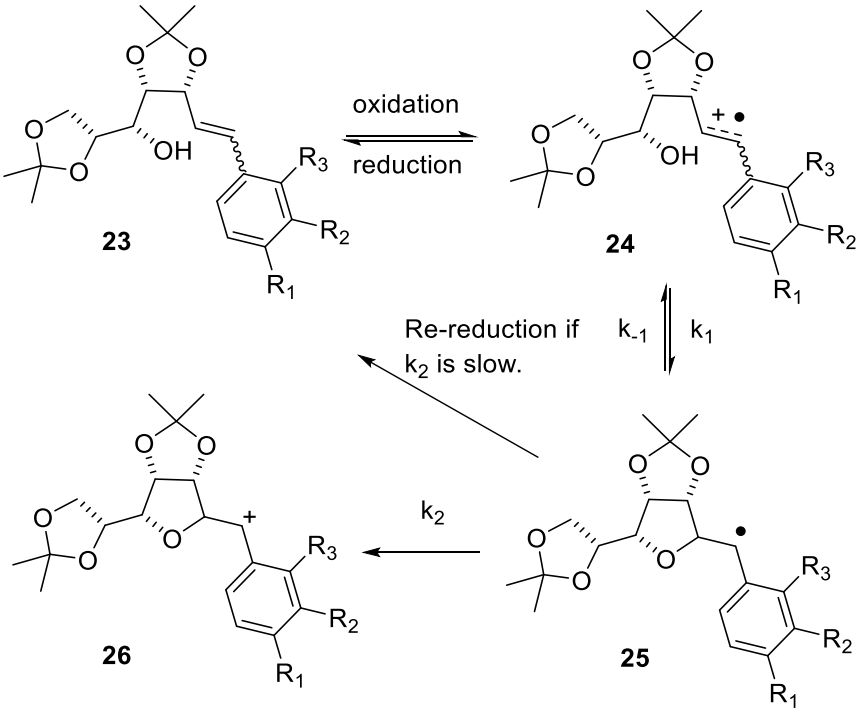


**Scheme 2.10: Mechanism of C-Glycoside Formation**

was placed at the ortho or para position then the cyclization was more efficient. It became evident

that the methoxy group had to be placed so that it could donate electron density to the benzylic radical and accelerate the second oxidation step leading to a higher yield of cyclized product (Scheme 2.10).

Similar observations arose while investigating the anodic coupling of carboxylic acids to styrene groups (Table 2.2).[16] In these cases, a comparison was made between the substrate that could cyclize (n=1) and the substrate that could not cyclize (n=3). This allowed the study of the Nernstian shift in potential associated with the cyclization reaction,[16] indicating that the initial cyclization step was rapid and occurred at or near the electrode surface. In the substrates examined, they also varied in the presence and positioning of electron donating (OMe) groups on the aryl ring, with three of these substrates featured in Table 2.2. The CV data for all three substrates showed a decrease in potential for the cyclization substrate (n=1) when compared to the isolated styrene functional group (n=3), signifying a fast initial cyclization. Once again, only the substrate bearing the para-methoxy substituent led to a high yield of product. The most plausible explanation for this was that the 4-methoxy functional group increased the rate of the second oxidation step of radical **28**. When the two other substrates, the one lacking the donor group and the one with the methoxy group positioned meta to the radical in **28**, were oxidized the lower yield of product was attributed to a slower second oxidation step. This occurred because the 4-methoxy functional group increased the rate of the second oxidation step of radical **28**. When a substrate lacking the donor group and a substrate with the methoxy group positioned

**Table 2.2: Anodic Coupling of Carboxylic Acids and Styrenes**

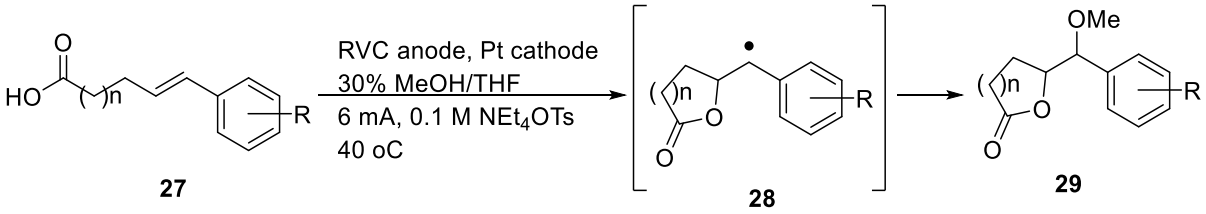


27 28 29

| R | n | $E_{p/2}$ | F/mole | %yield |
|---|---|---|---|---|
| H | 1 | 1.52V | 10 | 33 |
| H | 3 | 1.73 | NA | NA |
| 4-OMe | 1 | 1.31V | 2 | 76 |
| 4-OMe | 3 | 1.42V | NA | NA |
| 3-OMe | 1 | 1.42V | 2 | 23 |
| 3-OMe | 3 | 1.50V | NA | NA |

[a] Cyclic voltammetry data were obtained relative to a Ag/AgCl reference electrode with a sweep rate of 50 mv/s

meta to the radical in **28** were oxidized, the lower yield of product was attributed to a slower second oxidation step.

## 2.2 Using A Combination Of Electrochemical And Photoelectron Transfer Reactions To Gain New Insights Into The Role Of The Second Oxidation Step In Anodic Cyclizations

### 2.2.1 Introduction to Photochemistry

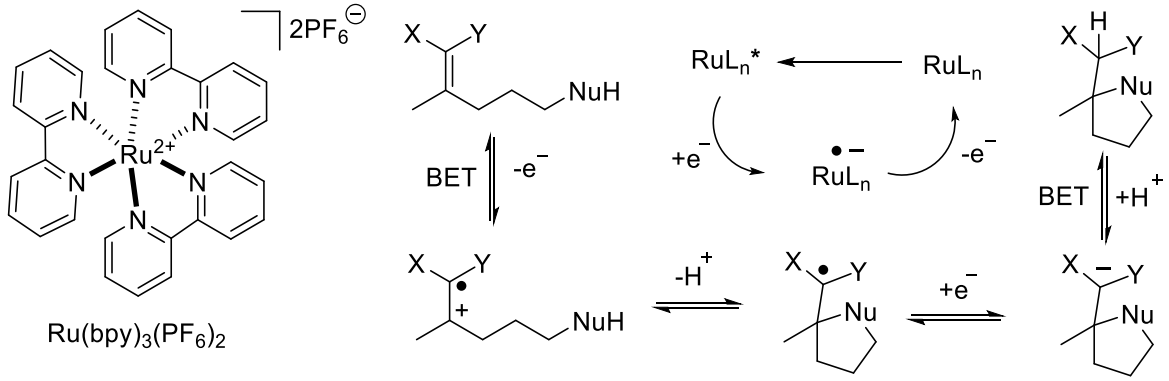


**Scheme 2.11: Scheme 2.11: General Scheme of Photochemical Reaction**

Photoelectron transfer reactions offer a valuable approach for exploring novel methods that entail radical cation and radical anion reaction pathways. The reactions we are interested in are oxidative photochemical reactions which proceed via a radical cation mechanism facilitated by an excited state photocatalyst.[17,18] In the reactions we are conducting, the catalyst is tris(2,2′-bipyridine)ruthenium(II) hexafluorophosphate. The general scheme for these photoredox reactions is outlined in Scheme 2.. The proposed mechanism for the photoelectron transfer reaction begins with a photocatalyst excited by 450nm wavelength light, typically in the LED range. In its excited state, the catalyst oxidizes the substrate, forming a radical cation – radical anion pair. The radical cation undergoes a cyclization akin to the initial step in the electrochemical mechanism. Once cyclized, instead of undergoing a second oxidation step leading to a dication, the photocatalyst returns an electron to the radical through a Back-Electron-Transfer (BET). This process

regenerates the ground state catalyst and gives an anionic intermediate. The anionic intermediate is then protonated to give cyclized product with the photocatalyst being free to repeat the cycle. This reaction is complementary to the electrochemical cyclizations talked about previously; however, it is redox-neutral, in contrast to the two-electron processes carried out electrochemically. From here on in this chapter we will discuss the application of photoredox catalysis towards our understanding of electrochemical cyclizations and the importance of a fast second oxidation step.

## 2.2.2 Electrochemical And Photoelectron-transfer Reactions

Having

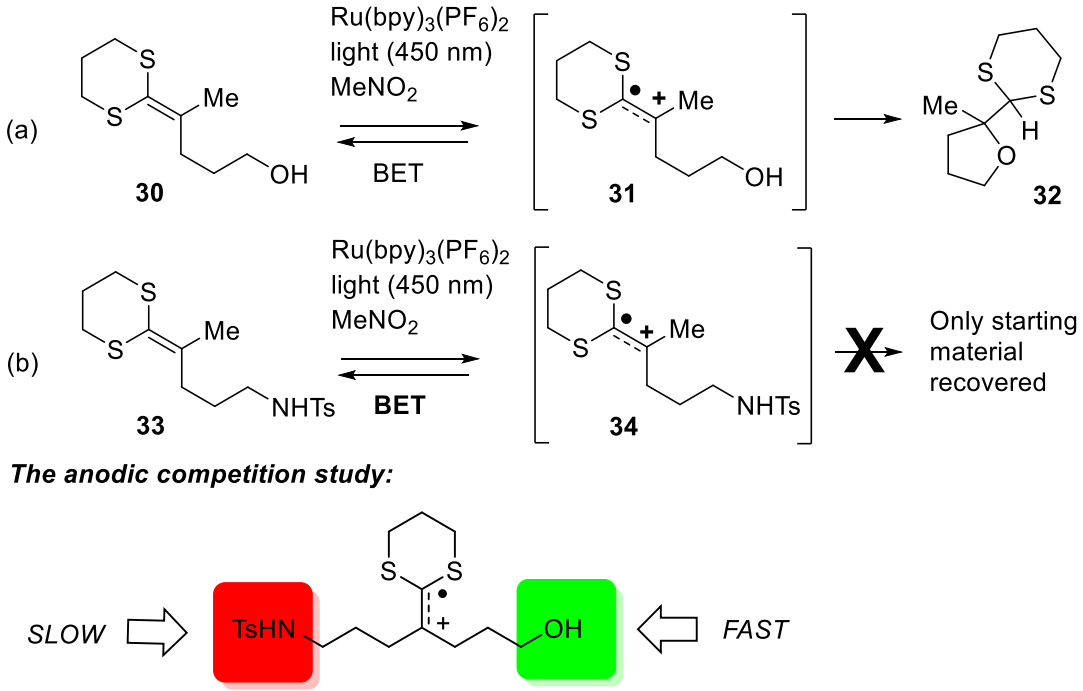


**Scheme 2.12: Gaining Insights into Photochemically Induced Radical Cation Cyclizations Through the Use of Electrochemical Data**

thoroughly investigated electrochemically generated radical cation-based cyclizations, we were curious if the lessons we learned might also be applicable to analogous reactions generated through visible light-based photoelectron-transfer methods. We were interested in understanding how the relative cyclizations rate data obtained from electrochemical competition studies could enable us to predict if photochemical reactions would be successful. The first exploration into this inquiry

involving the trapping ability of an alcohol and a sulfonamide for a dithioketene acetal based radical cation (Scheme 2.12) showed promise.[1] Our initial efforts to conduct the photochemical reactions could be explained using the competition study outlined above in Scheme 2.8. Remember that the electrochemical competition studies examined the relative rates of trapping reactions involving a radical cation derived from a ketene dithioacetal and either an alcohol or sulfonamide nucleophile. When kinetic conditions were used, only the faster alcohol trapping product was found, and no sulfonamide product was observed.

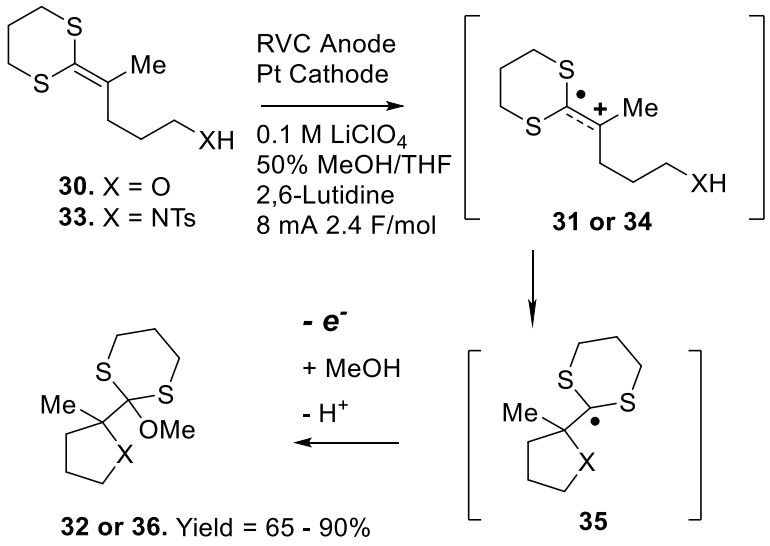


**Scheme 2.13: Complimentary Electrolysis Reaction**

With this knowledge in place, we examined the two photochemical reactions shown in Scheme 2.12. In the first case, an alcohol nucleophile was used to trap the radical cation generated. As anticipated, the faster alcohol-based cyclization led to an 83% isolated yield of product in the absence of air. This reaction clearly demonstrated the complementary nature of the process compared to the corresponding electrolysis reaction depicted in Scheme 2.13. The nature of the two processes differed in the fact that the electrolysis proceeded through a net two electron oxidation while the photochemical transformation was redox neutral. In the electrochemical

reaction, radical **35** is oxidized to a cation which is then trapped by methanol solvent. Conversely, in the photoelectron transfer process, a back electron transfer occurs from the radical anion of the photocatalyst to radical **35**, generating an anion that is then protonated. Attempts to perform the photoelectron-transfer reaction in a way that would facilitate a two-electron oxidation process by introducing oxygen to the reaction resulted in a decreased yield of the cyclized product **32** to 67%, with no observable two-electron oxidation product. This suggested that the back electron-transfer reaction occurred too rapidly in comparison to the oxidation of radical **35** by oxygen.

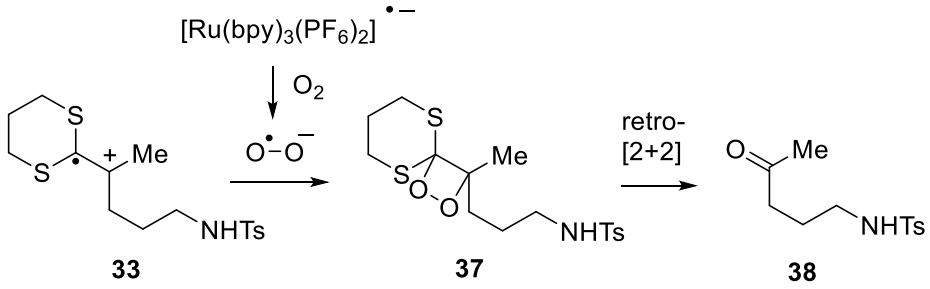


While both the electrochemical and photochemical reactions involving an alcohol trapping group were successful, the same can not be said for the reactions utilizing a sulfonamide. In this instance, the photoelectron-transfer reaction, in the absence of oxygen, resulted in the recovery of starting material **33** (Scheme 2.14) When oxygen was added into the reaction, it led to the formation of a ketone which arose from cleavage of the olefin in the starting material. A proposed mechanism for this ketone product is shown in Scheme 2.14. In this scheme, the formation of the ketone is attributed to the trapping of the olefinic radical cation by oxygen before the cyclization can occur.

**Scheme 2.14: Mechanism of Ketone Formation**

Once oxygen traps, a retro [2+2] cycloaddition reaction occurs to yield the ketone. It is important to note that there is currently no experimental evidence to support this mechanism. However, this hypothesis aligns with the observed product and previous instance of photocatalyzed alkene

cleavage reactions in the presence of oxygen.[19,20] In comparison, the equivalent electrolysis using a sulfonamide proceeded smoothly leading to cyclic product **36** (Scheme 2.13). No challenges in the cyclization were noted use the identical reaction conditions that were employed for oxidizing the substrate utilizing an alcohol trapping group.

These findings align with the data acquired from the electrochemical competition study in Scheme 2.8. In this study, the alcohol trapping of the radical cation is faster than the corresponding reaction with a sulfonamide nucleophile.[3] When the two nucleophiles competed for a central radical cation under kinetic condition, only alcohol trapping product was observed. This difference in rate proved critical for the success or failure of the photochemical reactions. In the faster alcohol-based cyclization, the trapping of the radical cation by the alcohol outcompeted both the back electron transfer from the radical anion of the photoredox catalyst and the trapping by oxygen. As a result, cyclized product was made in both the presence and absence of oxygen. Conversely, with the sulfonamide nucleophile, the cyclization reaction occurred too slowly. In the absence of oxygen, the back electron transfer occurred before the cyclization so only recovered starting material was found. While in the presence of oxygen, the slower cyclization led to oxygen trapping the radical cation leading to a ketone product being formed.

These findings also implied that the electrochemical competition study could function as a predictive tool for determining the success of a photoelectron-transfer-based cyclization. Cyclization reactions slower than the sulfonamide-based trapping reaction would not occur

readily. While cyclizations that occur faster than an alcohol trapping reaction were expected to proceed well under photoelectron-transfer conditions.

The focus shifted to the formation of carbon-carbon bonds, exploring whether the electrochemical competition studies could predict previously unexplored photo-electron transfer reactions. As demonstrated in the competition study outlined in Scheme 2.15, reactions using an allylsilane were

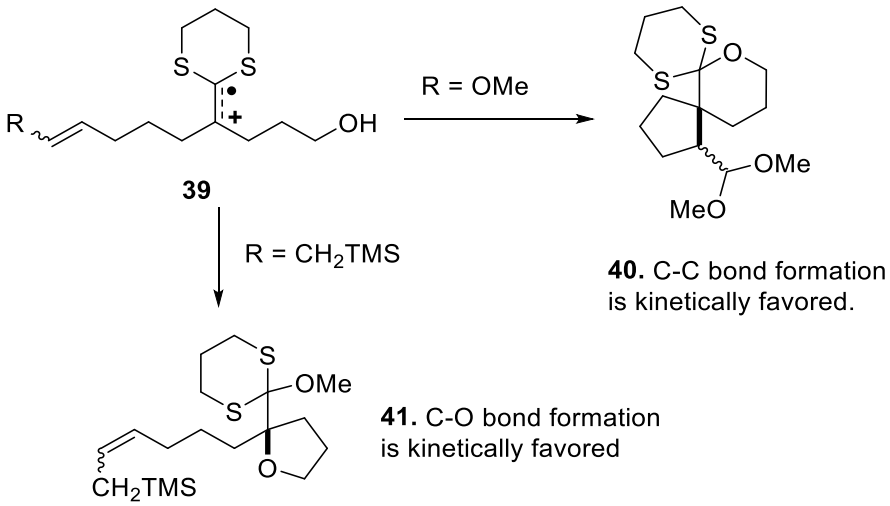


slower than the sulfonamide trapping reaction, while reactions using an enol ether trapping group were faster than the alcohol-based reaction.[21] In every case, the enol ether outcompeted the alcohol for the central radical cation. This outcome was expected, as enol ether trapping groups are one of the best trapping groups found to date. They function as both effective radical acceptors and nucleophiles for cations. As a result, anodic olefin coupling reactions utilizing an enol ether cyclize efficiently with both polar radical cations, promoting C-C bond formation, and non-polar radical cations, which facilitate heteroatom formation.[4,5] In contrast, allylsilanes are less effective as

**Scheme 2.15: Competition Studies Investigating the Formation of Carbon-Carbon Bonds**

trapping groups and do not cyclize well with non-polar radical cations. In the current case, the allylsilane did not compete with the alcohol and in all cases studied the only trapping product observed was the alcohol.

Therefore, it was anticipated that a photoelectron-transfer-based cyclization with an allyl silane would not lead to product, whereas one employing an enol ether trapping group should be successful.

With this consideration, substrate 42 was synthesized and oxidized using both electrochemistry and photochemistry (Scheme 2.16). Both reactions resulted in complete consumption of the starting material, an observation that supported a rapid cyclization (absence of back electron-transfer for the photoelectron-transfer induced reaction). However, only the anodic cyclization yielded the desired cyclic product (**43**), with an approximately 70% yield based on proton NMR

***An anodic competition study:***

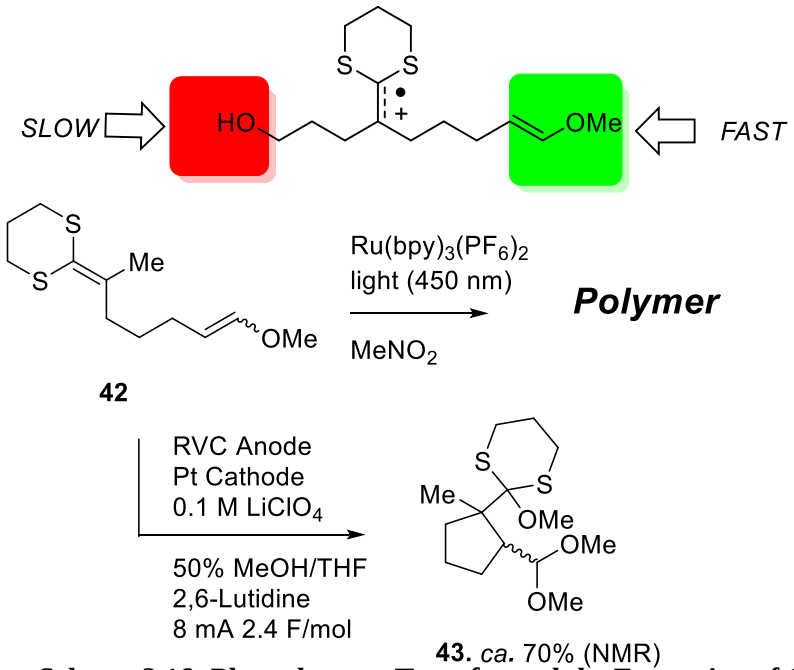


**Scheme 2.16: Photoelectron-Transfer and the Formation of C-C Bonds**

analysis against an internal standard. Although the product from electrolysis was challenging to isolate due to its instability and the volatility of the methyl ester derived from hydrolysis of the ortho-ester in product **43**, the reported NMR yield aligns with previous cyclization reactions using anodic coupling of a ketene dithioacetal-derived radical cation and an enol ether to form a quaternary carbon.[21] The electrochemical cyclization conditions were deliberately kept identical to those used in earlier competition experiments for a direct comparison. The structure of the cyclic product was confirmed through 2D-NMR analysis.

No cyclized product was found in the photoelectron-transfer reaction; instead, only polymer products were obtained. Notably, the proton NMR of the crude product from this reaction showed no evidence of the ketene dithioacetal or enol ether functional groups present in the starting materials, indicating that both olefins were consumed during the reaction. The observation that a failed oxidative cyclization resulted in polymer formation while consuming both the initiating and trapping groups is noteworthy. In anodic cyclization reactions, this aligns with a fast cyclization, a slow second oxidation step, and polymerization of the cyclized radical cation[22]. In the current scenario, this observation suggests that the photoelectron transfer reaction proceeded through the cyclization step successfully (as both olefins were consumed), and a slow cyclization would have led to a back electron transfer from the radical anion of the photocatalyst, resulting in recovered starting material, as seen with the sulfonamide substrate in Scheme 2.12. This data was consistent with the photoelectron transfer reaction being a one electron process and hence not able to remove the second electron. The result was a failure to obtain the desired product from the initial cyclic intermediate.

This chemistry indicated that for radical cation cyclization reactions utilizing even the very best trapping group to date (the enol ether) a fast second oxidation step is crucial for product generation. This conclusion was not apparent earlier due to the second oxidation step occurring rapidly in the electrolysis. However, comparing this data to a recognized one-electron process reveals the significance of the second oxidation step in the overall reaction. This scenario highlights the mechanistic insight that can be gained by investigating new radical cation reactions employing both one-electron and two-electron oxidation methods.

## 2.3 The First Cyclization Step and A Caution

The conclusions drawn in the previous section posed a significant question regarding several earlier findings. For instance, in the setup of the competition studies in Scheme 2.15, it was stated that the enol ether stands out as the most effective trapping group due to its ability to trap both radicals and cations, while the allylsilane was deemed less effective in trapping radical cations. The suggestion was that the distinction between the two groups lay in their ability to trap the radical cation. However, could it be that the disparity between the reactions is less about the initial cyclization and more about the loss of the second electron occurring faster when the enol ether is used?

### 2.3.1 A Fast Cyclization And A Fast Second Oxidation Step Are Crucial For The Success Of Anodic Cyclizations

The first insight into this question arose while examining the oxidation of substrate **44** which utilized a furan trapping group (Scheme 2.17). Furans are recognized as one of the most effective radical cation trapping groups studied to date.[22] Once they trap, they generate a radical intermediate that is stabilized by an oxygen atom (akin to the enol ether) and undergo a second oxidation step

readily. Despite this fact, the anodic oxidation and photoelectron-transfer reactions with substrate **44** failed to yield the cyclic product efficiently. The anodic oxidation reaction suggested a struggle to cyclize consistent with a non-polar radical cation forming carbon-carbon bonds. However, similar cyclization reactions between a polar enol ether radical cation and a furan ring have proceeded in high yield.[22] It seems the aromatic furan ring in substrate **44** did not function as an effective nucleophile for the non-polar radical cation. Indicating that a more radical-like pathway with a polar radical cation would be needed for the success of this reaction. Optimization of the reaction yield to 31% involved increasing the current to 60 mA, but the overall impact on the

**Scheme 2.17: Electrolysis with a Furan Trapping Group**

reaction, despite accelerating the oxidation of radical intermediate **45**, was negligible. This observation suggested that a fast second oxidation step alone could not drive a suboptimal cyclization toward the desired product.

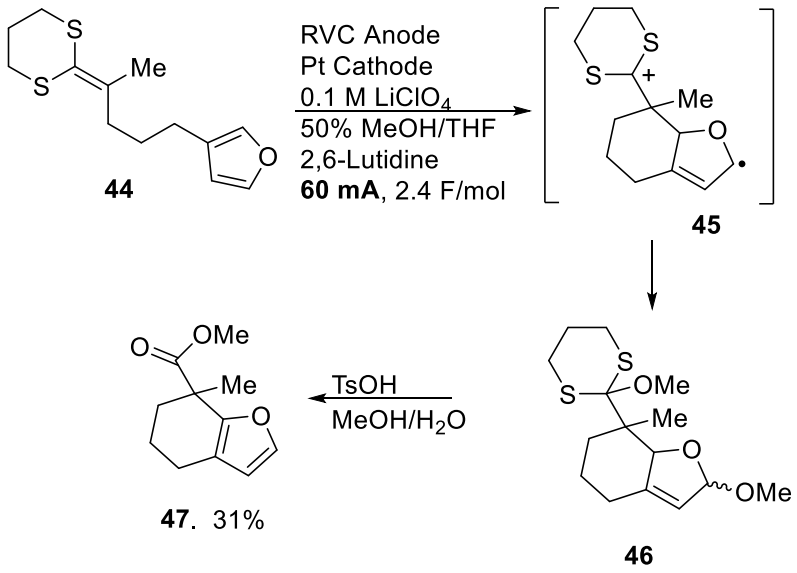

The same conclusion was drawn from a more direct comparison between cyclizations involving different radical cations but using the same electron-rich styrene trapping group (Scheme 2.18). In this experiment, the nature of the radical cation generated differed. The dithioketene acetal generated a less polar radical cation, which favors heteroatom formation, while a more polar enol ether-derived radical cation prefers carbon-carbon bond formation. Both radical cations were trapped with a 4-methoxystyrene functional group known to facilitate the second oxidation step of an oxidative cyclization reaction (see Table 2.1 and Table 2.2). The reaction initiated by the oxidation of the ketene dithioacetal resulted in a low yield of cyclized product, marked by impurities and the inability to isolate a completely pure product. In contrast, the reaction initiated by the oxidation of the enol ether was considerably cleaner, yielding a 65% isolated yield of pure cyclized product. Although the oxidation of **50** was clean in terms of starting material consumption and product generation, further optimization of the yield was limited by the sterically hindered dimethoxy acetal, which underwent rapid hydrolysis. The difference between the two processes can be attributed to the cyclization step leading to the cyclic radical intermediate, considering the

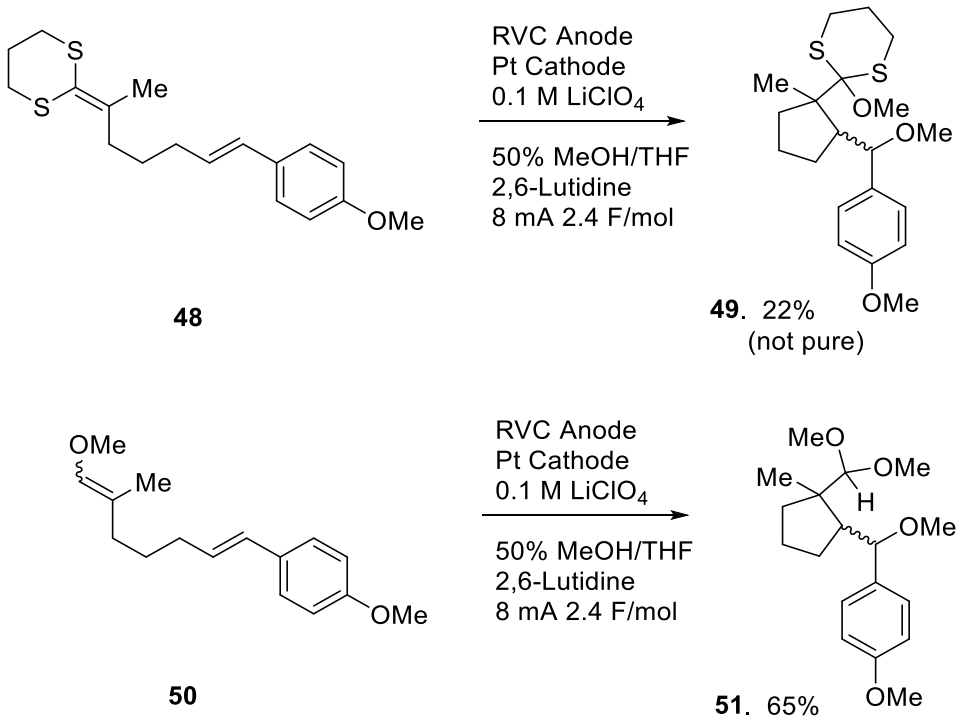


minimal difference in the second oxidation step for both reactions (Scheme 2 19). Two key

**Scheme 2.18: Electron-Rich Styrene Trapping of a Radical Cation**

takeaways from the chemistry depicted in Scheme 2.16 - Scheme 2 19 are noteworthy. Firstly, the enol ether remains the most effective radical cation trapping group, standing out as a unique case capable of trapping both non-polar and polar radical cations well. Secondly, although a rapid second oxidation step is crucial for the success of an oxidative cyclization, it alone is insufficient to overcome a slow cyclization. Earlier findings regarding the polarity of a radical cation intermediate and the selectivity/efficiency of cyclization reactions concerning heteroatom nucleophiles and C-C bond formation remain accurate. The best cyclizations integrate an effective trapping reaction with a quick second oxidation step (Scheme 2.18).

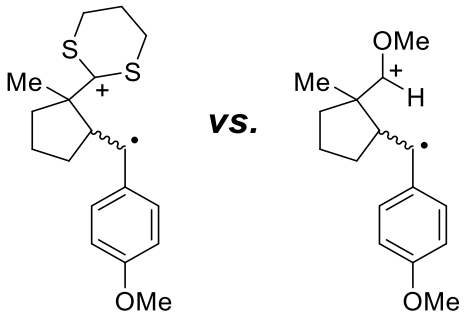


**Scheme 2 19: Cyclic Intermediates Generated**

## 2.4 The First Cyclization Step And A Caution

In many cases, the rate of the second oxidation step in an anodic cyclization proves crucial for product formation. This step is critical for generating both carbon-carbon and carbon-heteroatom bonds. Additionally, it can determine whether a reaction is under thermodynamic or kinetic control. It also impacts the generation of product in photoelectron-transfer initiated radical cation reactions. The initial cyclization plays a key role in the success of these reactions too. Presently, it is evident that a fast second oxidation step alone is insufficient to guide a reaction with a slow cyclization to the desired product; the decomposition of the initial radical cation takes place first. Therefore, when planning a cyclization reaction, both steps must be considered and employed to devise a successful process.

## 2.5 Experimental Section

### 2.5.1 General Information

All glassware was flame dried prior to use and all reactions conducted under argon atmosphere unless otherwise noted. All reactants were purchased from commercial suppliers and used without further purification except where otherwise noted. Solvents were bought in anhydrous form and some were also distilled before use. Tetrahydrofuran was distilled over sodium and benzophenone. Dichloromethane was distilled from calcium hydride.

Flash chromatography was carried out by using silica gel (230-400 mesh) purchased from Sorbent Technologies, Inc. All proton and carbon-13 nuclear magnetic resonance ($^{1}H$ and $^{13}C$ NMR) spectra were recorded by a Agilent DD2 500 MHz, or a Varian Mercury Plus 300 MHz in a deuterated chloroform ($CDCl_3$) solvent with tetramethylsilane (TMS) as an internal standard unless otherwise noted. Infrared (IR) spectra were recorded by a Bruker Optics Alpha FT-IR instrument. High-resolution mass spectra (HRMS) were obtained using electrospray ionization (ESI) with Q-TOF (quadrupole time of flight) detection.

## 2.5.2 Synthesis and Electrolysis of 42

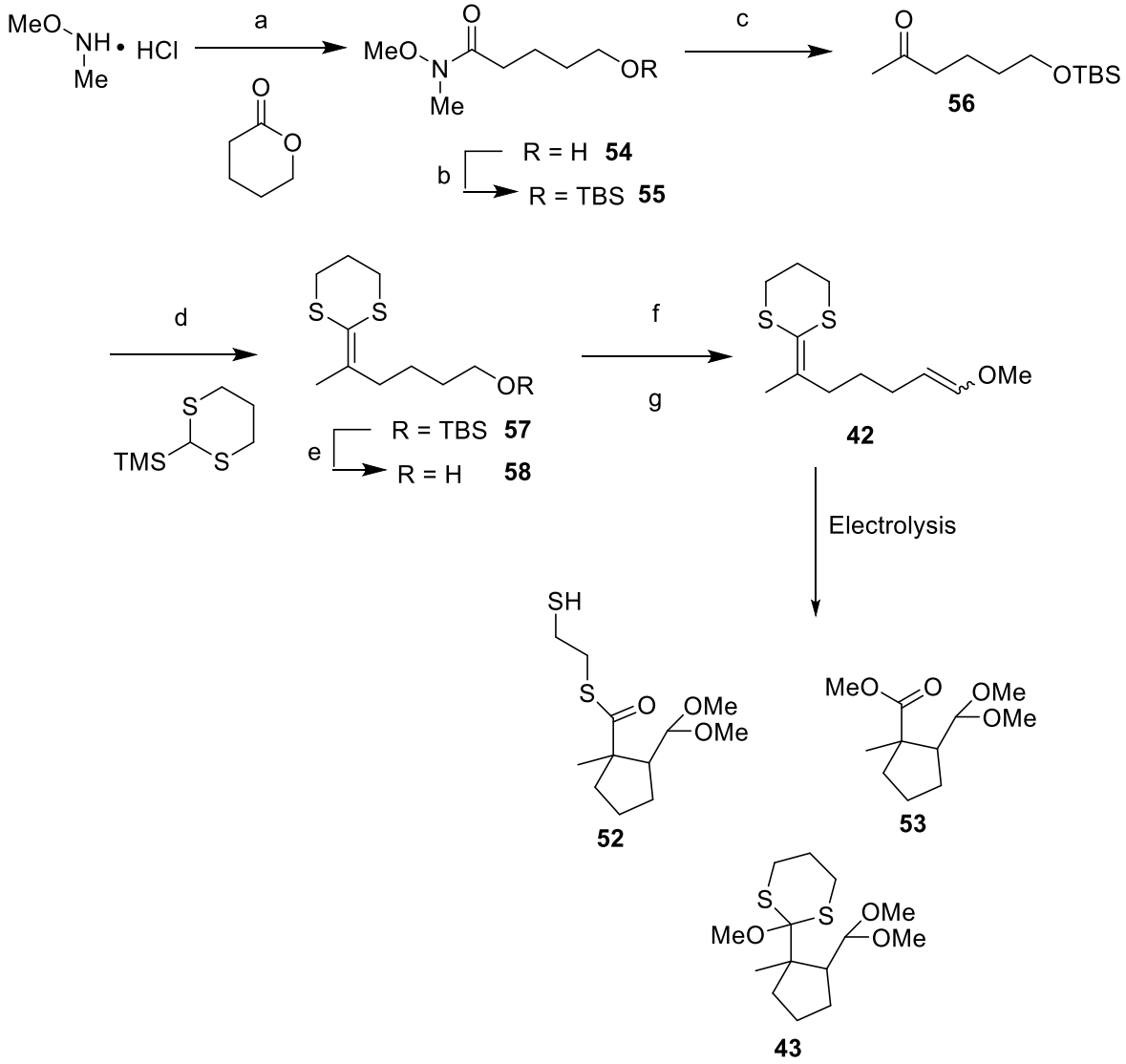


a) DIBAL, δ-Valerolactone b)Imidazole, TBSCl, c) Methyl Lithium, d) 2-trimethylsilyl-1,3-dithiane, n-butyl lithium, e) TBAF, f) oxalyl chloride, dimethyl sulfoxide, g) (methoxymethyl)triphenyl phosphonium chloride, n-butyl lithium

Electrolysis Conditions: Pt cathode, RVC anode, 0.1 M $LiClO_4$, 2,6-lutidine, 1:1 MeOH:THF, 6 mA, 2.1 F/mole

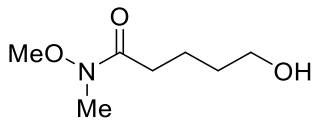


**Synthesis of 54.** 5.000 grams N,O-Dimethylhydroxylamine hydrochloride salt (1 equivalent, 51.26mmol) was submerged in benzene in a 100 mL round bottom flask. The benzene was then evaporated off using a rotary evaporator. The flask containing the salt was flushed with argon. 15mL of tetrahydrofuran was added to suspend the amine salt. The suspension was then stirred in a dry ice/acetone bath for 15 minutes. Now, 52.00mL diisobutyl aluminum hydride (1.0 M, 1 equivalent) was added to the suspension dropwise to prevent the quick evolution of hydrogen gas. The reaction flask was then taken from the dry ice/acetone bath and stirred at room temperature for 1 hour to give a clear, light yellow solution. The reaction flask was returned to the dry ice/acetone bath to cool for 15 minutes before 2.34 mL valerolactone (0.5 equivalents, 24.7mmol) was added. The reaction was stirred in a dry ice/acetone bath for 30 minutes. The flask was then removed from the dry ice/acetone bath and allowed to stir at room temperature for 3 hours. After completion, the flask was placed in a dry ice/acetone bath again, diluted with hexane under an open atmosphere, and quenched with a saturated solution of sodium potassium tartrate (10mL). The quenched reaction was stirred overnight at room temperature. After being allowed to stir at room temperature overnight, there were two distinct layers: a clear upper layer and a cloudy bottom layer. The top layer was decanted off 3 times. The organic layers were combined, dried over magnesium sulfate, and concentrated down on a rotary evaporator to yield product **54** (3.550g, 87% yield) as a yellow oil.

IR (neat, $cm^{-1}$) 3384 (broad), 2939, 1640, 1072, and 1003

$^{1}$H NMR (300 MHz, $CDCl_3$) δ 3.674 (s, 3.0H), 3.63 (t, 1.74H, J = 6.2 Hz), 3.17 (s, 2.32H), 2.46 (t, 2H, J = 7.0 Hz) 1.73 (m, 2H), 1.61 (m, 2H)

$^{13}$ C NMR (126 MHz, $CDCl_3$) δ 177.2, 64.35, 63.75, 34.82, 32.17, 30.20, 23.20

HRMS (ESI/TOF-Q) m/z: [M+Na]+ Calcd for $C_7H_{15}NO_3$ $[M+Na]^+$ 161.10; found 162.11.

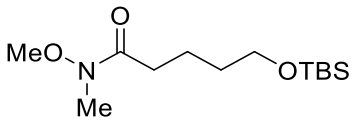


**Synthesis of 55.** 3.750g Imidazole (2.5 equivalents, 55.1 mmol) was weighed into a flame-dried round bottom flask. This flask was then flushed with argon. Tetrahydrofuran (10 mL) was added to the flask to suspend the imidazole. The suspension was stirred in an ice bath for 15 minutes to chill. In a separate flask, 3.550g **54** (1 equivalent, 22.0 mmol) was dissolved in 5 mL tetrahydrofuran, which was then transferred over to the stirring imidazole solution. 3.653g Tert-butyl silyl chloride (1.1 equivalents, 24.2 mmol) was placed in a separate flask. This flask was then flushed with argon. Tetrahydrofuran (4 mL) was added to this flask to dissolve the silyl chloride. The tert-butyl silyl chloride solution was then transferred dropwise to the stirring solution. Upon addition, a cloudy white precipitate formed. The reaction was allowed to stir and warm up to room temperature for 6 hours before being diluted with hexane. Water was then added to quench the reaction and to dissolve the white precipitate. The solution was allowed to stir for 30 minutes to give 2 layers: a clear top layer and a cloudy bottom layer. The top layer was decanted off 3 times, dried over magnesium sulfate, and concentrated with the use of a rotary evaporator. The crude oil was then treated with hexane to crash out any remaining imidazole. **55** was concentrated back down with the use of a rotary evaporator to yield 5.352g (88%) as a yellow oil.

IR (neat, $cm^{-1}$) 2938, 2857, 1640, 1098

$^{1}H$ NMR (300 MHz, $CDCl_3$) δ 3.66 (s, 3H), 3.62 (t, 2H, J = 6.4 Hz ), 3.17 (s, 3H), 2.44 (t, 2H, J = 7.4 Hz), 1.66 (m, 2H), 1.56 (m, 2 H)

$^{13}$ C NMR (126 MHz, $CDCl_3$) δ 177.2, 65.50, 63.80, 35.10, 28.60, 23.71, 20.90, -2.68

HRMS (ESI/TOF-Q) m/z: [M+Na]+ Calcd for $C_{13}H_{29}NO_3Si$ 275.46; found 276.20.

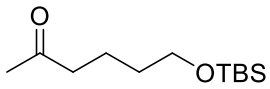


**Synthesis of 56**. A round bottom flask was flame dried and flushed with argon. 3.196g of **55** (1 equivalent, 13.9 mmol) was dissolved with 15 mL tetrahydrofuran and added to the round bottom flask. This solution was then stirred in an ice bath for 30 minutes. Then 12.1 mL (27.8 mmol, 2.00 equivalents) of methyl lithium (1.6 M in Diethyl Ether) was added dropwise to the stirring solution. The reaction stirred for 3 hours in an ice bath. After 3 hours, the reaction was quenched with water and diluted with hexane to give two clear layers. The top layer was decanted off 3 times. The organic layers were combined, dried over magnesium sulfate, and concentrated in vacuo to yield 2.432 g (91%) of **56**.

IR (neat, $cm^{-1}$) 2923, 2854, 1720, 1462, 1101, 837

$^{1}H$ NMR (300 MHz, $CDCl_3$) δ 3.43 (t, 2H, J = 6.6 Hz), 2.44 (t, 2H, J = 7.4 Hz), 2.13 (s, 3H), 1.64 (m, 2H), 1.52 (m, 2H, J = 7.2 Hz)  0.88 (s, 9H), 0.04 (s, 6H)

$^{13}$ C NMR (126 MHz, $CDCl_3$) δ 211.27, 65.26, 46.00, 34.76, 32.30, 28.60, 22.80, 20.90,

-2.76

HRMS (ESI/TOF-Q) m/z: [M+Na]+ Calcd for $C_{12}H_{26}O_2Si$ 253.1594; found 253.1598.

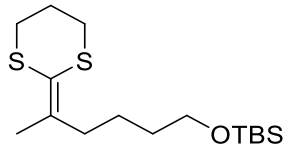


**Synthesis of 57**. A round bottom flask was flame dried and flushed with argon. Next, 1.96mL 2-(trimethylsilyl)-1,3-dithiane (1.2 equivalent, 10.3mmol ) was added to the flask which was then dissolved in tetrahydrofuran (10mL). This solution was then stirred in dry ice/acetone bath for 30 minutes. The stirring solution was then treated with 3.81mL n-butyl lithium (1.1 equivalent, 2.5M in hexanes, 9.53mmol). The reaction stirred for 1 hour before being removed from the dry ice/acetone bath. The flask was then stirred at room temperature for 30 minutes. While the dithiane solution was stirring at room temperature, 1.992g of **56** (1 equivalent, 8.65 mmol) was dissolved in 5 mL of tetrahydrofuran. The stirring dithiane solution was then cooled in a dry ice/acetone bath for 15 minutes. The methyl ketone solution was then added to the dithiane solution dropwise. The reaction was then allowed to warm up and react overnight. Upon completion, the reaction was quenched with water and diluted with hexane. The top layer was decanted off 3 times. The organic layers were combined, dried over magnesium sulfate, and concentrated using a rotary evaporator to yield 2.559 g of **57**. Ketene dithio acetal **57** was carried forward to the next step without further purification

IR (neat, $cm^{-1}$) 2928, 2855, 1462, 1254, 1098, 836, 775

$^1H$ NMR (300 MHz, $CDCl_3$) δ 3.61 (t, 2H, J = 6.3 Hz), 2.84 (m, 4H, J = 6.0 Hz), 2.36 (t, 2H, J = 7.1 Hz) 2.11 (t, 2H, J = 6.1 Hz), 1.90 (s, 3H), 1.53 (m, 2H), 1.26 (m, 2H), 0.9 (s, 9H), 0.16 (s, 6H)

HRMS (ESI/TOF-Q) m/z: [M+Na]+ Calcd for $C_{16}H_{32}OS_2Si$ 355.1556; found 355.1562.

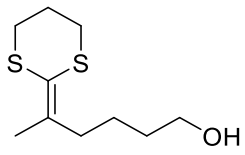


**Synthesis of 58.** A round bottom flask was flame-dried and flushed with argon. Next, 1.509g of the ketene dithio acetal **57** (1 equivalent, 4.5 mmol) was added to the flask, dissolved in 8mL of tetrahydrofuran, and set to stir at room temperature. Next, 5.4mL of tetrabutylammonium fluoride (1M in hexane, 1.2 equivalents, 5.4 mmol) was added to the stirring solution at room temperature. The reaction was monitored by thin-layer chromatography (1:1 Diethyl Ether: Hexane). At completion, reaction was diluted with diethyl ether and quenched with water. The top layer was then decanted off 3 times. The organic layers were combined, dried over magnesium sulfate and concentrated in vacuo to yield a crude oil. The crude material was then further purified by column chromatography (1:1 Diethyl Ether: Hexane) to yield 0.5167g (52%) of **58**.

IR (neat, $cm^{-1}$) 3320 (broad), 2929, 1421, 127,4, 1057, 910, 816

$^1$H NMR (500 MHz, $CDCl_3$) δ 3.65 (t, 2H, J = 6.3 Hz), 2.86 (m, 4H), 2.38 (t, 2H, J = 7.1 Hz), 1.91 (s, 3H), 1.56 (m, 2H), 1.48 (m, 2H)

$^{13}$ C NMR (126 MHz, $CDCl_3$) δ 143.10, 121.97, 65.35, 38.10, 34.92, 32.96, 32.82, 27.65, 26.69, 22.79

HRMS (ESI/TOF-Q) m/z: [M+Na]+ Calcd for $C_{10}H_{18}OS_2$ 241.0691; found 241.0698.

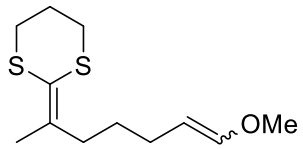


**Synthesis of 42.** 1.207g of triphenyl phosphine (4 equivalents, 3.52 mmol) were submerged in benzene in a round bottom flask. The benzene was then evaporated off using a rotary evaporator. The flask was then flushed with argon. Tetrahydrofuran (6mL) was added to the flask. The mixture was then stirred in a dry ice/acetone bath for 30 minutes. While stirring in a dry ice acetone bath, 1.4mL of n-Butyl lithium (4 equivalents, 2.5 M in Hexane, 3.52 mmol) was added dropwise to the stirring solution. The reaction flask was then removed from the dry ice/acetone bath and stirred at room temperature for 30 minutes to give a deep red solution.

In a separate flask flushed with argon, 0.15mL dimethyl sulfoxide (2.4 equivalents, 2.11 mmol) was dissolved in 5mL tetrahydrofuran and set to stir at room temperature. Next, 0.09mL oxalyl chloride (freshly distilled) (1.2 equivalents, 1.06 mmol) was transferred to the DMSO solution. This solution was then set to stir in a dry ice/acetone bath for 15 minutes. Now, 0.1922g 58 (1 equivalent, 0.88 mmol) was dissolved in 2 mL tetrahydrofuran which was then added to the dimethyl sulfoxide/oxalyl chloride reaction flask. Next, 0.59mL triethylamine (4.8 equivalents, 4.22 mmol) was added after 5 minutes. The reaction was then stirred at room temperature for 3 hours to give a solution with a white precipitate. The reaction was then diluted with hexane and filtered. The filtered liquid was collected and concentrated down to approximately 10 mL in a pear-shaped flask. This material was then transferred to the stirring phosphine solution. The reaction was then allowed to stir at room temperature overnight. After reacting overnight, the reaction was diluted with hexane. The resulting solution was then filtered through a cold silica plug to collect the majority of the triphenyl phosphine oxide material. The crude material was then

purified via column chromatography 100 % hexane to 1:99 Diethyl Ether: Hexane, to yield (0.051g, 23%) of 42 as a mixture of isomers (0.55:0.45 trans:cis)

IR (neat, $cm^{-1}$) 2927, 2852, 1655, 1456, 1275, 1208, 1133, 1109, 934

$^{1}H$ NMR (500 MHz, $CDCl_3$) δ 6.29 (d, 1H, J = 12.6 Hz), 5.87 (d, 1H, J = 6.3 Hz), 4.72 (dt, 1H, J = 12.6 Hz, 7.2 Hz), 4.34 (dt, 1H, J = 6.3Hz), 3.57 (s, 1.18H), 3.50 (s, 1.97H), 2.85 (m, 4H), 2.35 (m, 2H), 2.16-2.02 (m, 3H), 1.95-1.89 (m+s, 4H), 1.43(m, 2H)

$^{13}$ C NMR (126 MHz, $CDCl_3$) δ 149.88, 148.88, 143.66, 143.30, 121.73, 121.53, 109.16, 105.38, 62.12, 58.54, 38.34, 38.05, 32.97, 32.96, 32.88, 32.85, 30.72, 30.16, 27.74, 27.70,

32.96, 32.88, 32.85, 31.67, 30.72, 30.16, 27.74, 27.70, 26.42, 22.90, 22.84, 26.42, 22.90, 22.84

HRMS (ESI/TOF-Q) m/z: [M+Na]+ Calcd for $C_{12}H_{20}OS_2$ 267.0848; found 267.0850.

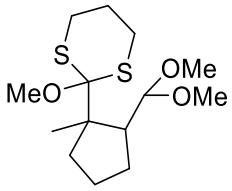


**43**

To a flame-dried three-neck flask, 0.0244 g (1 equivalent, 0.1mmol) of substrate **42** were added. Next, 3.3 mL of 1:1 THF:MeOH were added. Now, 0.0351g (0.33mmol, 0.1M) of $LiClO_4$ were added to the 3-neck round bottom flask. To this solution, 0.01 mL (0.1mmol, 1 equivalent) 2,6-lutidine was added via syringe. The solution was then sonicated for 1 minute and stirred in ice bath for 10 minutes. A platinum cathode and reticulated vitreous carbon anode were then connected to the reaction flask. A potentiostat was set to 6 mAmp and connected to the reaction flask at the electrodes. The electrolysis was ran until 57.89 C had passed (2.1 F/mole), and was monitored via

thin layer chromatography. On completion, the solution was diluted with hexane and quenched with 1mL of water. The aqueous layer was extracted three times with hexane. The organic layers were combined, dried over magnesium sulfate and concentrated with the use of a rotary evaporator. Initially, a mixture of three main products was obtained. The products were unstable to hydrolysis, and if the ortho ester in the initial product hydrolyzed all of the way to the methyl ester the resulting product proved to be volatile. The products after partial separation could be characterized by 2D-NMR (NOESY and COSY) to ensure that they were the expected cyclized molecules. The data is provided below. The yield of the reaction was determined by NMR with the use of 1,3,5-trimethoxybenzene as an internal standard. Using this method, it was determined that an approximately 70% yield of cyclized product was obtained from the reaction; a value that was consistent with related cyclizations that also coupled a ketene dithioacetal derived radical cation and an enol ether at a RVC anode to form a quaternary carbon. The purification of the mixture of products was completed on a column using 5-10% $Et_2O$ in hexane. Two fractions were taken for the partially separated products. The two sets of 2D-NMR data presented below are the result of these two fractions.

$^1$H NMR for the crude mixture of products following separation from the electrolysis mixture

(300 MHz, $CDCl_3$) δ 4.95(broad s, 1H), 4.49 (s, 1H), 3.54 (s, 3H), 3.36 (s, 3H), 3.33(s, 3H), 2.97 (m, 2H), 2.75 (m, 2H), 2.22(m, 2H), 1.97 (m, 2H), 1.84 (m, 2H), 1.67 (m, 2H), 1.52 (m, 2H), 1.38 (m, 2H), 1.26 (s, 3H) 1.18(s, 3H).

See below for the 2D-NMR data (NOESY and COSY).

## 2.5.3 $^{1}H$ and $^{13}C$ NMR Spectra

### Compound 54

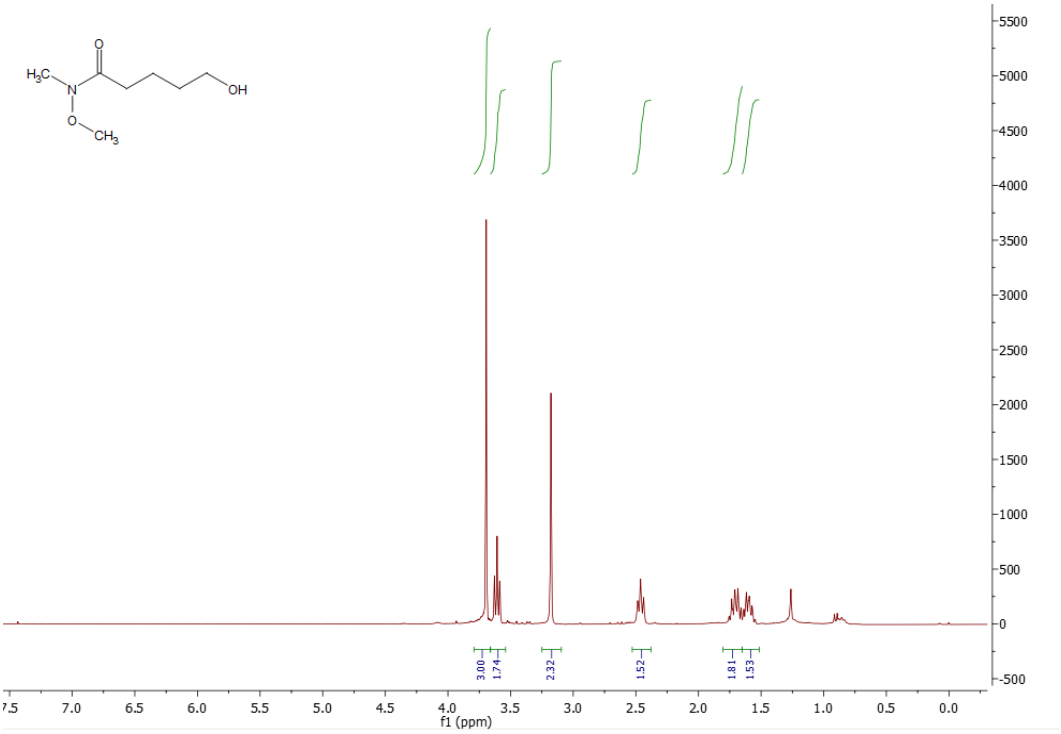

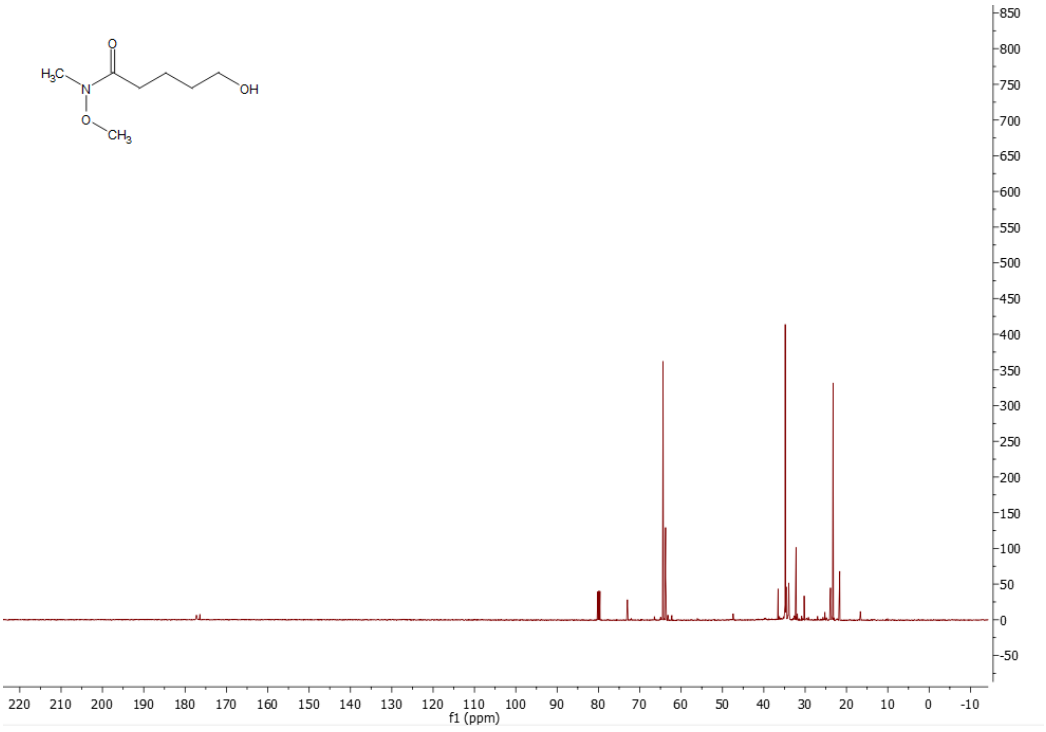
O
H3C
N
O
CH3
OH
850
800
750
700
650
600
550
500
450
400
350
300
250
200
150
100
50
0
-50
220 210 200 190 180 170 160 150 140 130 120 110 100 90 80 70 60 50 40 30 20 10 0 -10
f1 (ppm)

**Compound 55**

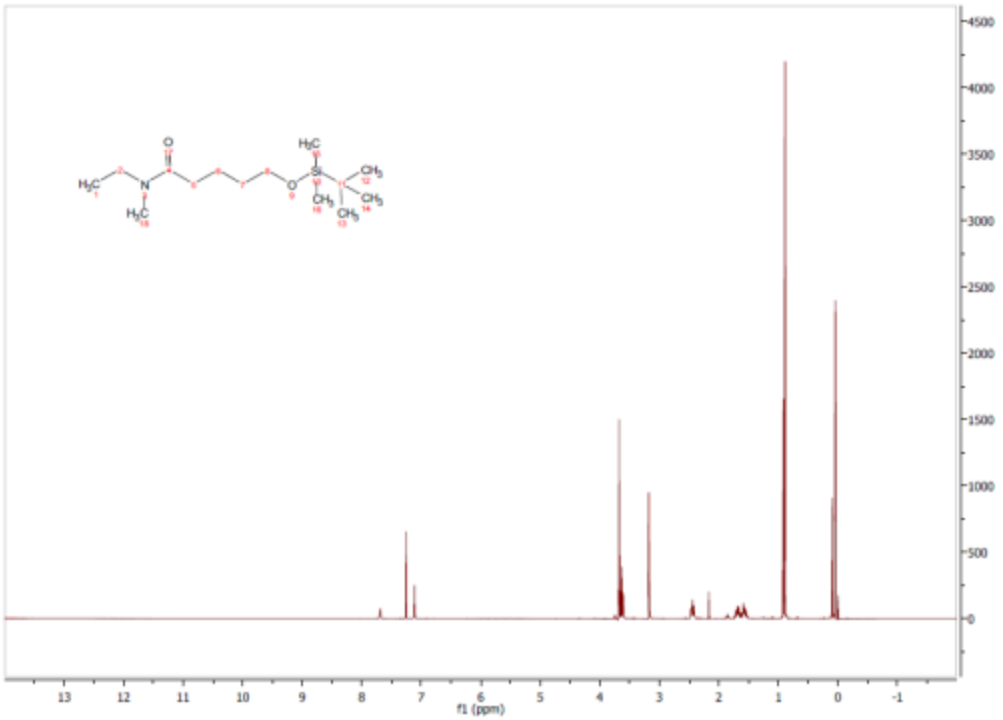


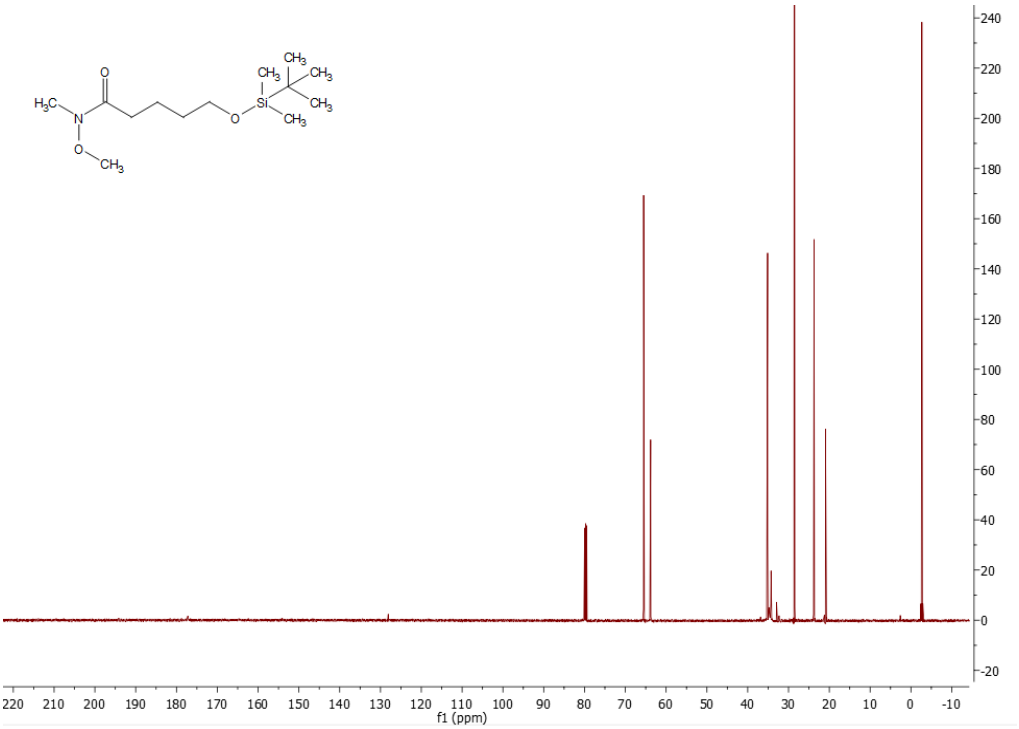

**Compound 56**

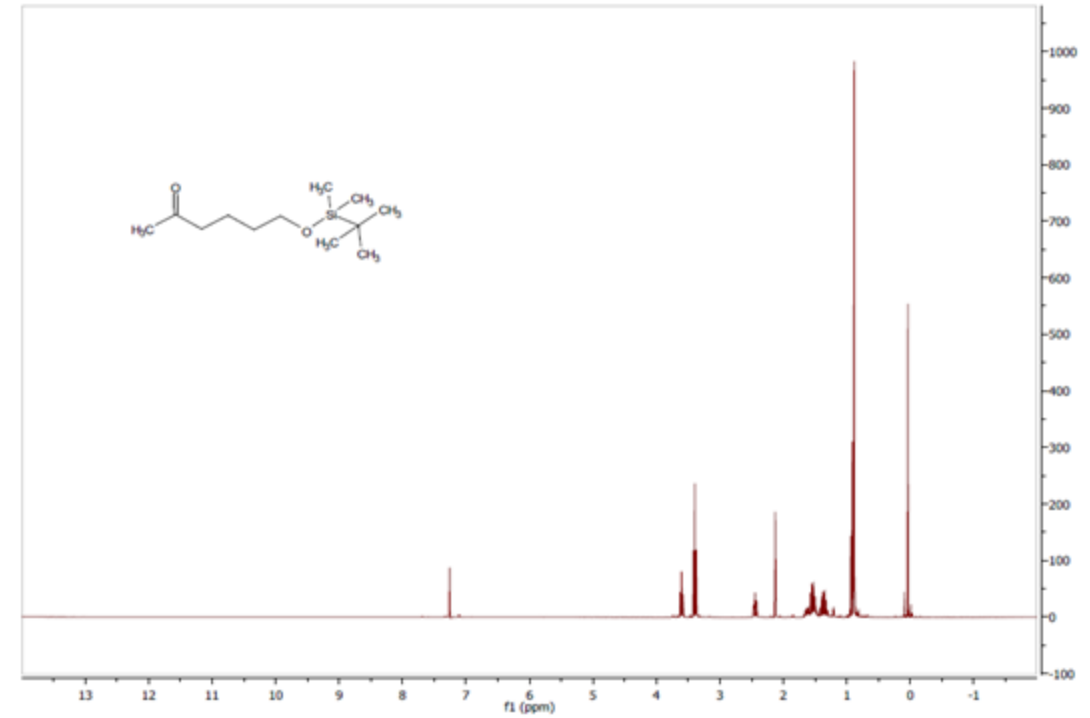


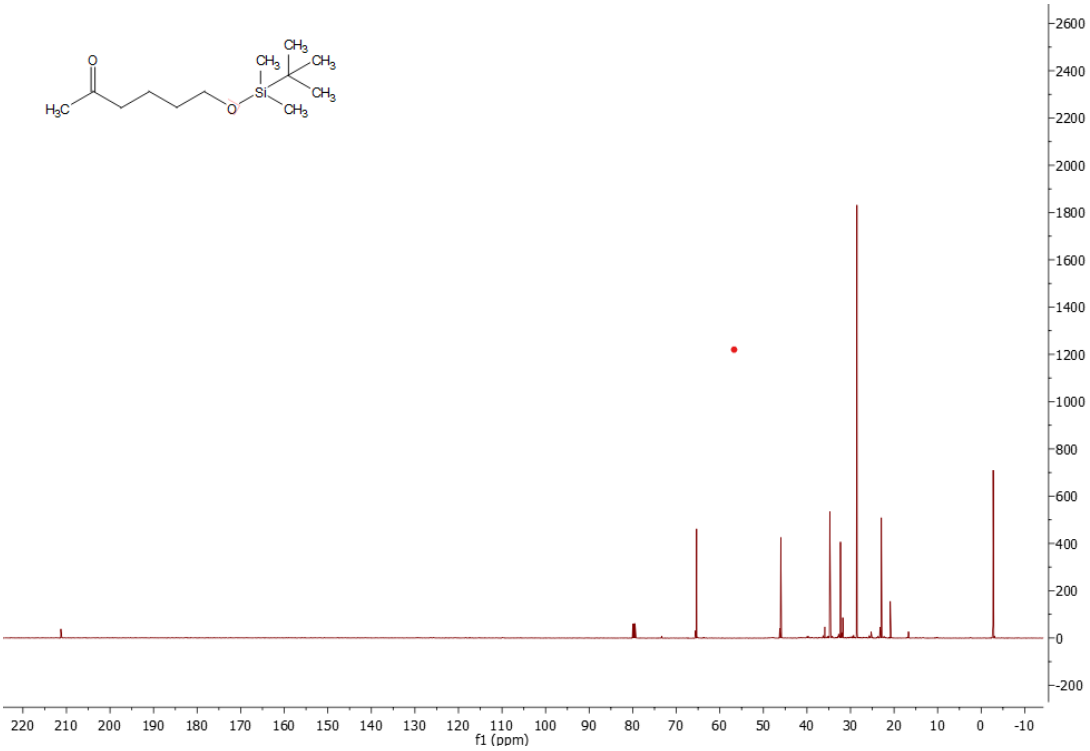

**Compound 57**

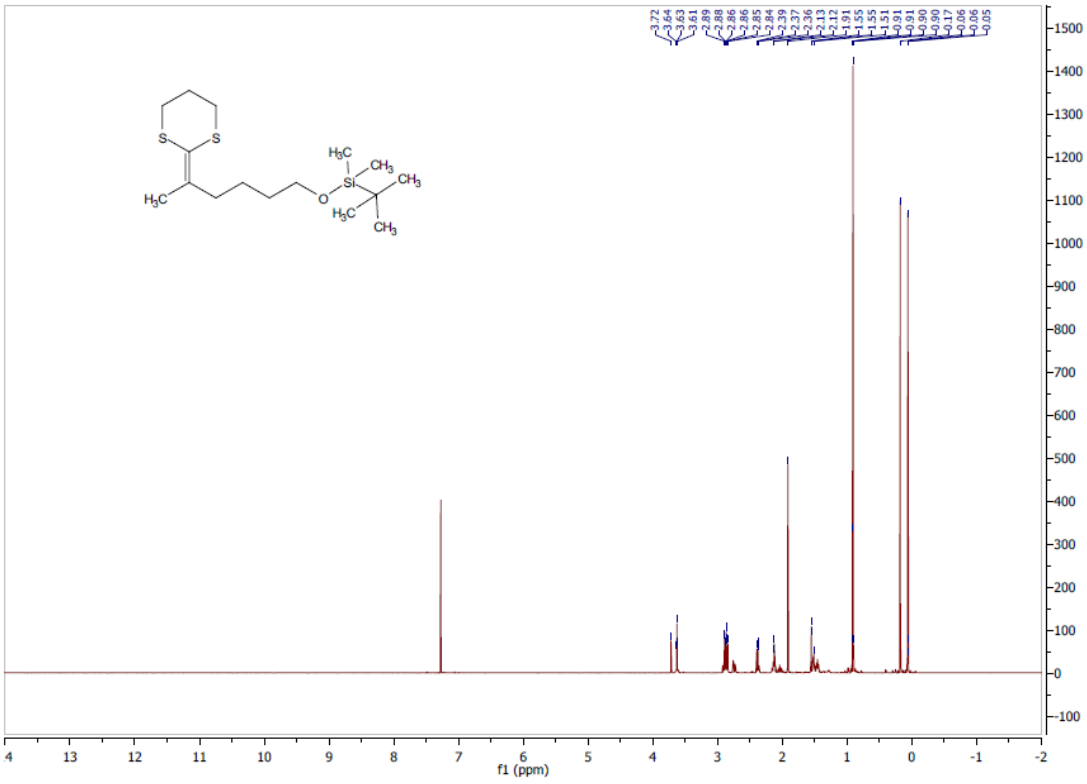
3.72
3.64
3.63
3.61
2.89
2.88
2.86
2.86
2.85
2.84
2.39
2.37
2.36
2.13
2.12
1.91
1.55
1.55
1.51
0.91
0.91
0.90
0.90
0.17
0.06
0.06
0.05
S
S
H3C
O
Si
H3C
CH3
CH3
H3C
CH3
f1 (ppm)

**Compound 58**

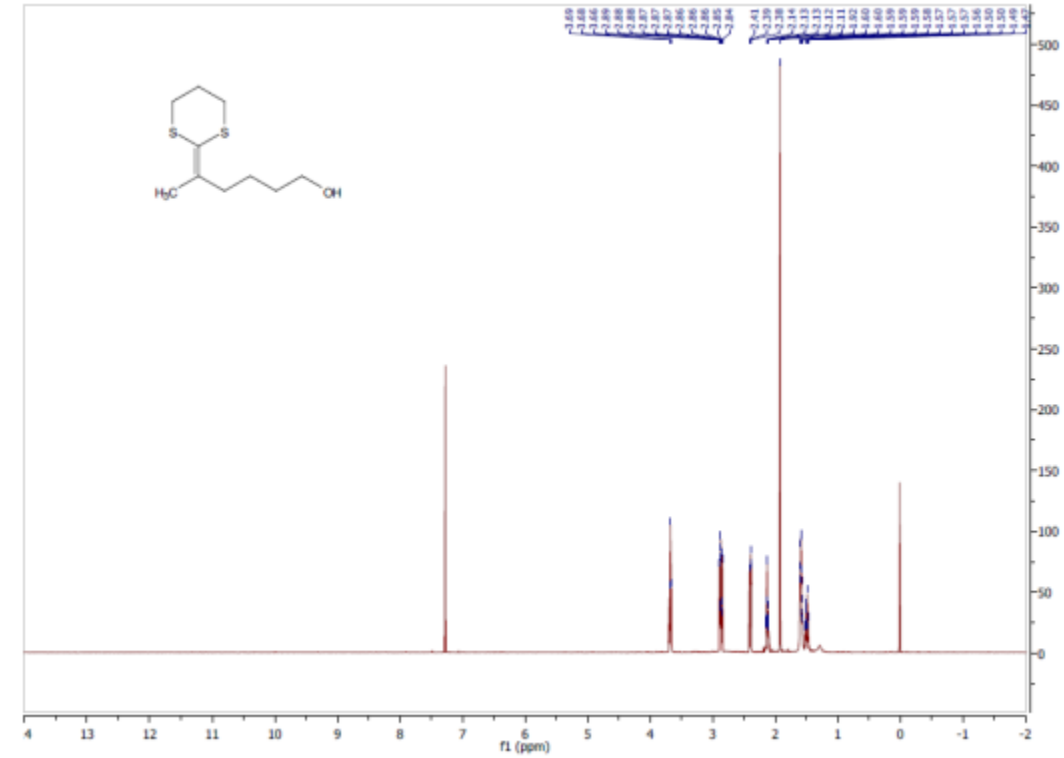


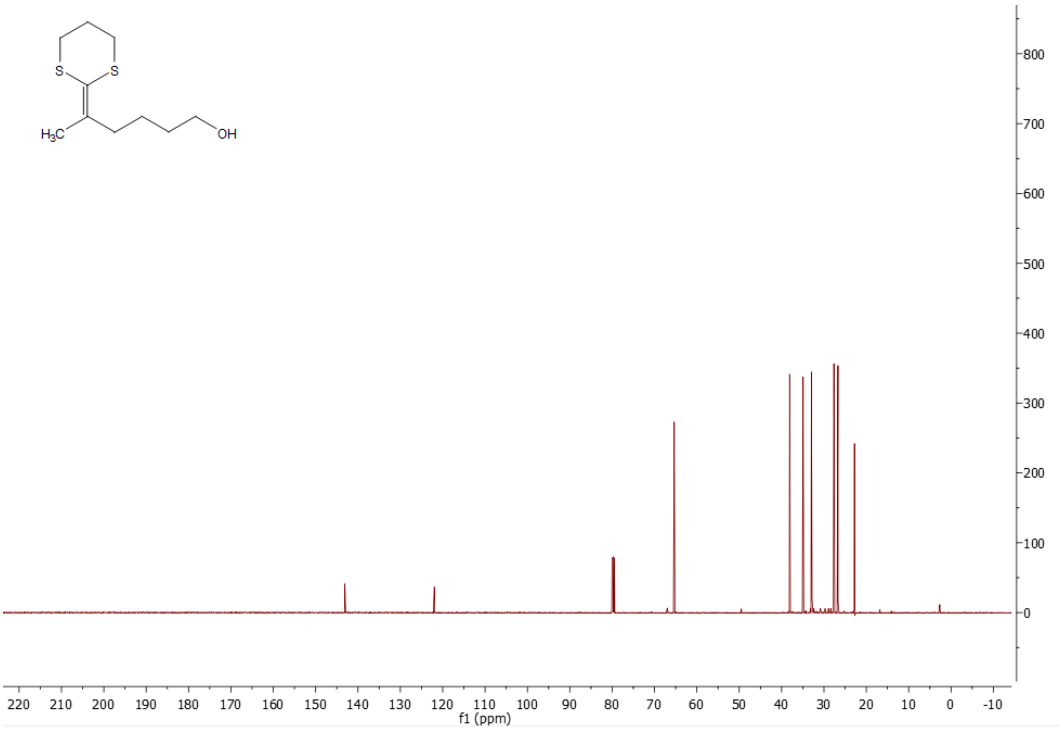

**Compound 42**

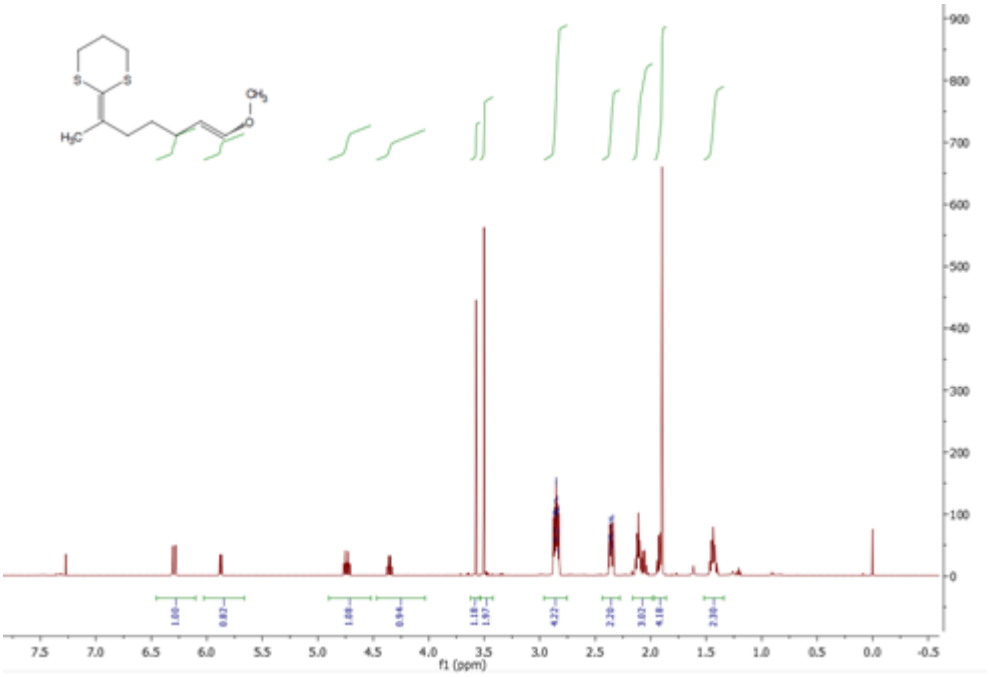
S
S
H3C
O
CH3
900
800
700
600
500
400
300
200
100
0
1.00
0.82
1.00
0.94
1.18
1.97
4.23
2.26
3.02
4.18
2.30
7.5
7.0
6.5
6.0
5.5
5.0
4.5
4.0
3.5
3.0
2.5
2.0
1.5
1.0
0.5
0.0
-0.5
f1 (ppm)

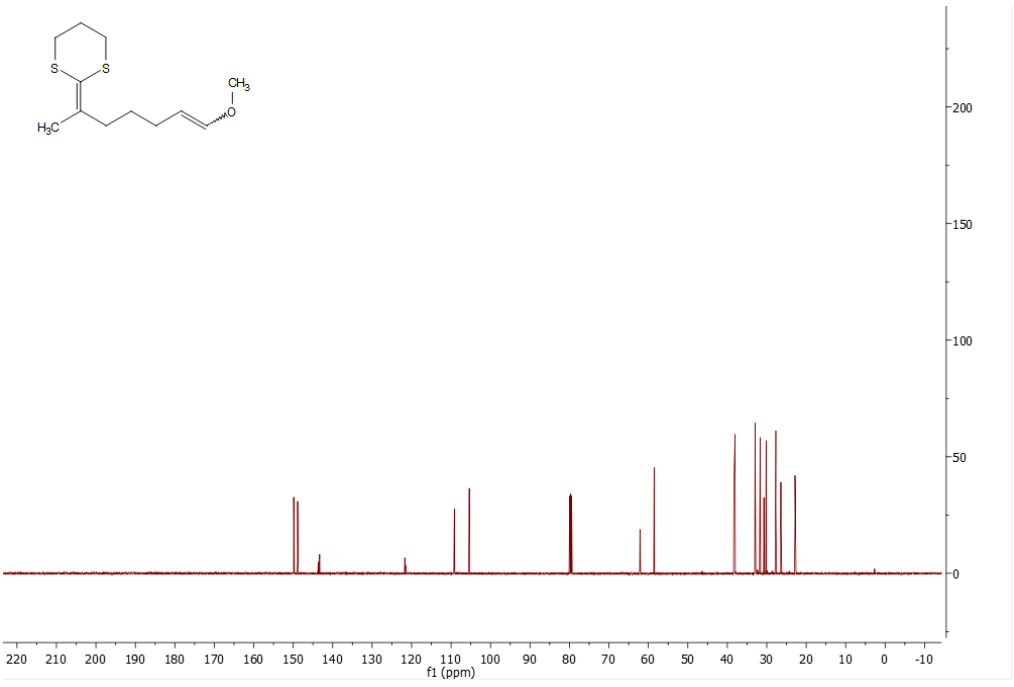
S
S
H3C
O
CH3
200
150
100
50
0
220
210
200
190
180
170
160
150
140
130
120
110
100
90
80
70
60
50
40
30
20
10
0
-10
f1 (ppm)

**Compound 43**

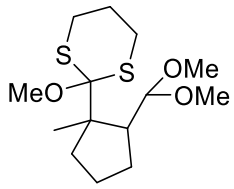


**43**

/

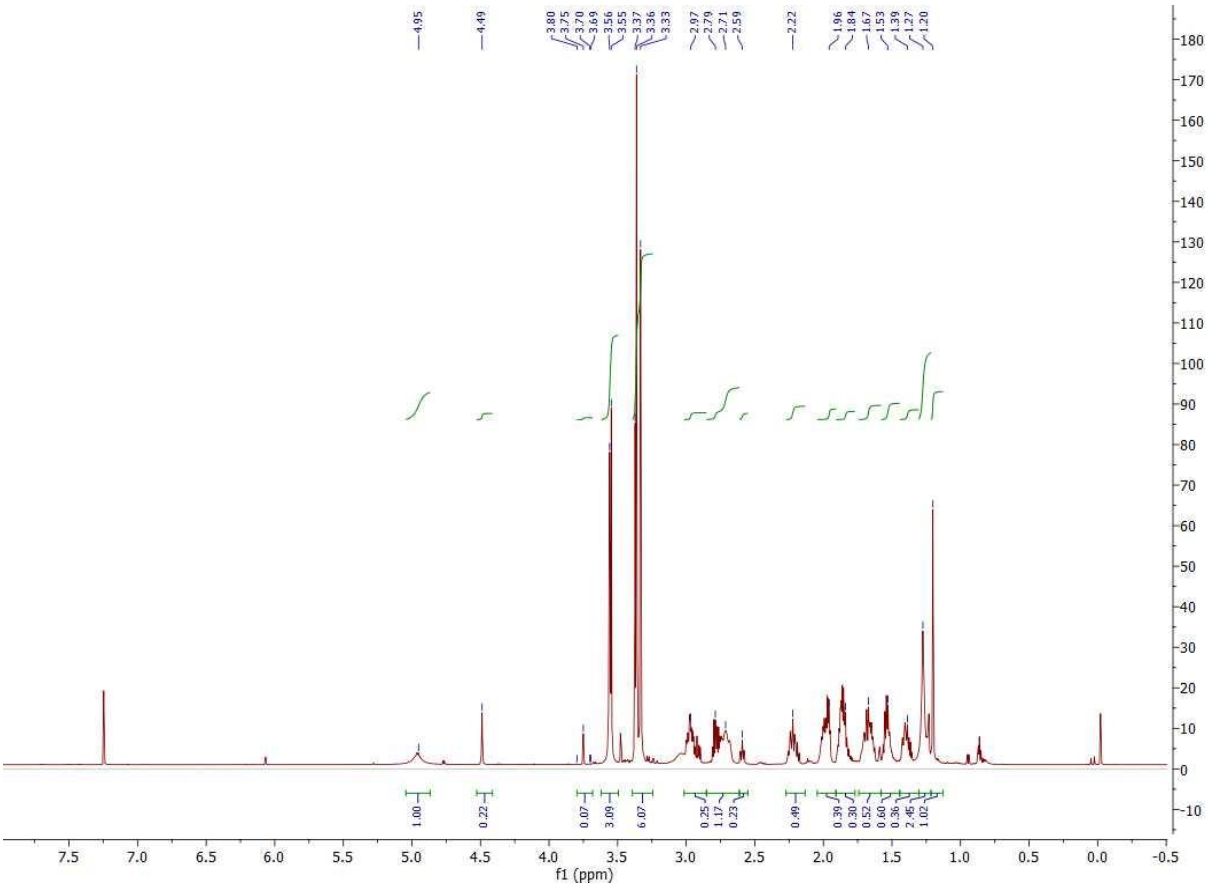

**Compound 52 and 53**

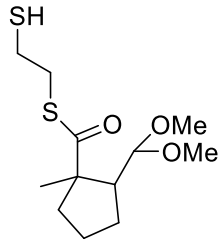


**52**

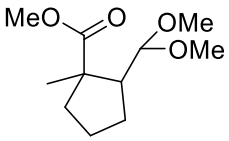


**53**

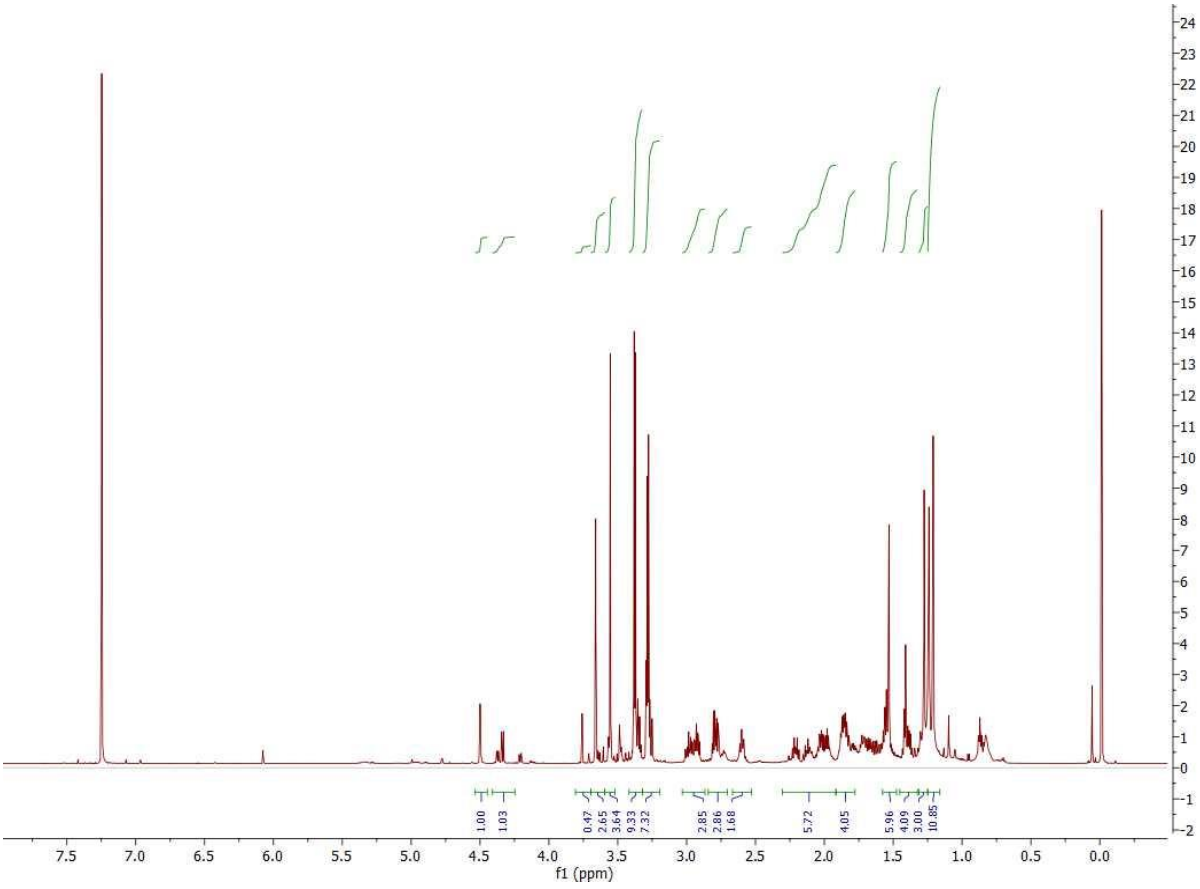

### 2.5.3 NOESY and COSY

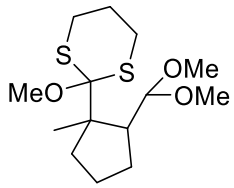


**43**

NOESY(yellow) and COSY(blue) of compound **43**.

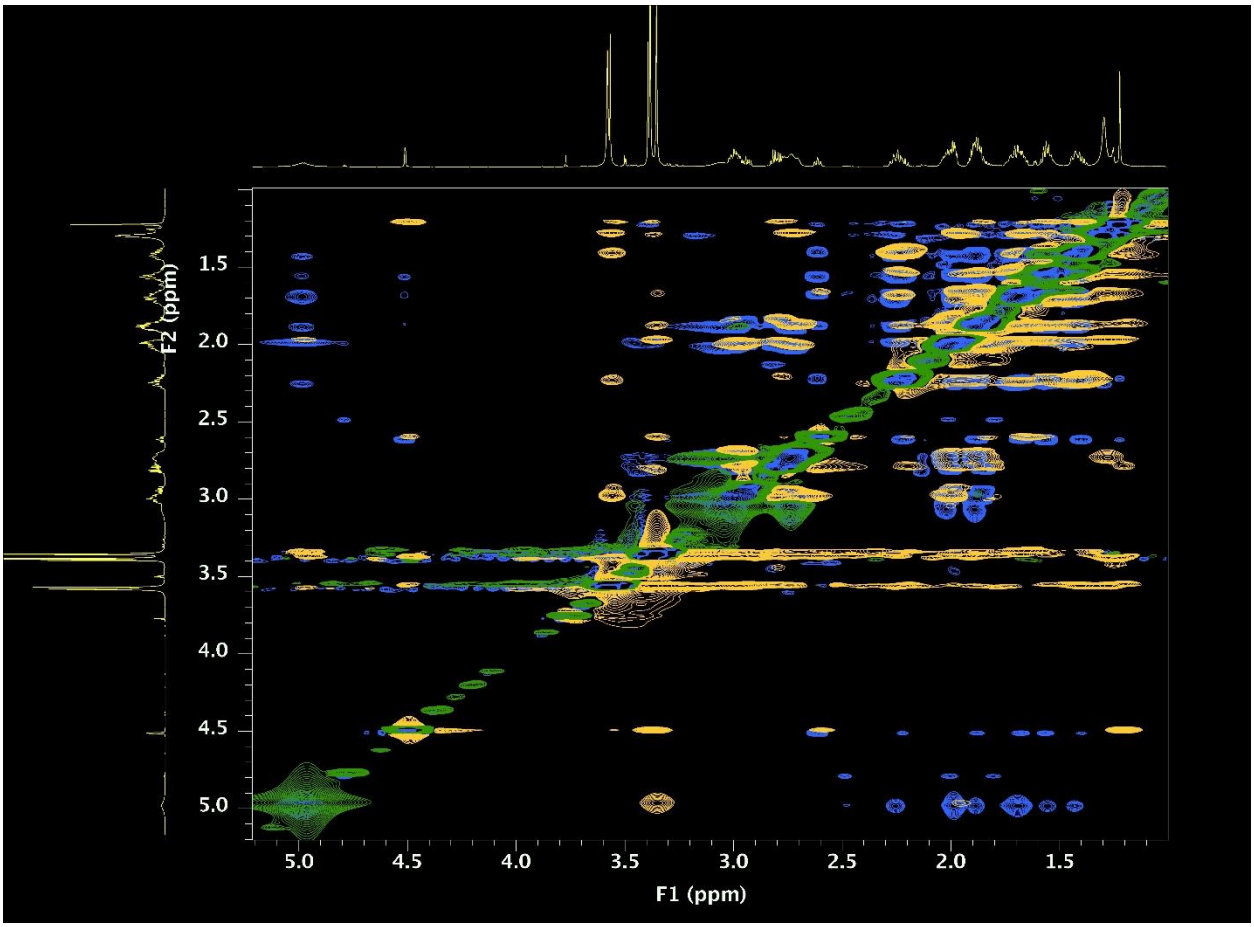

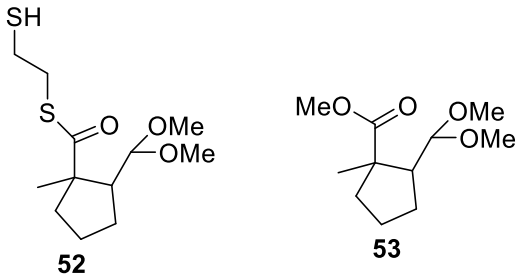


**52**




**53**

NOESY(yellow) and COSY(blue) of compounds **52** and **53**.

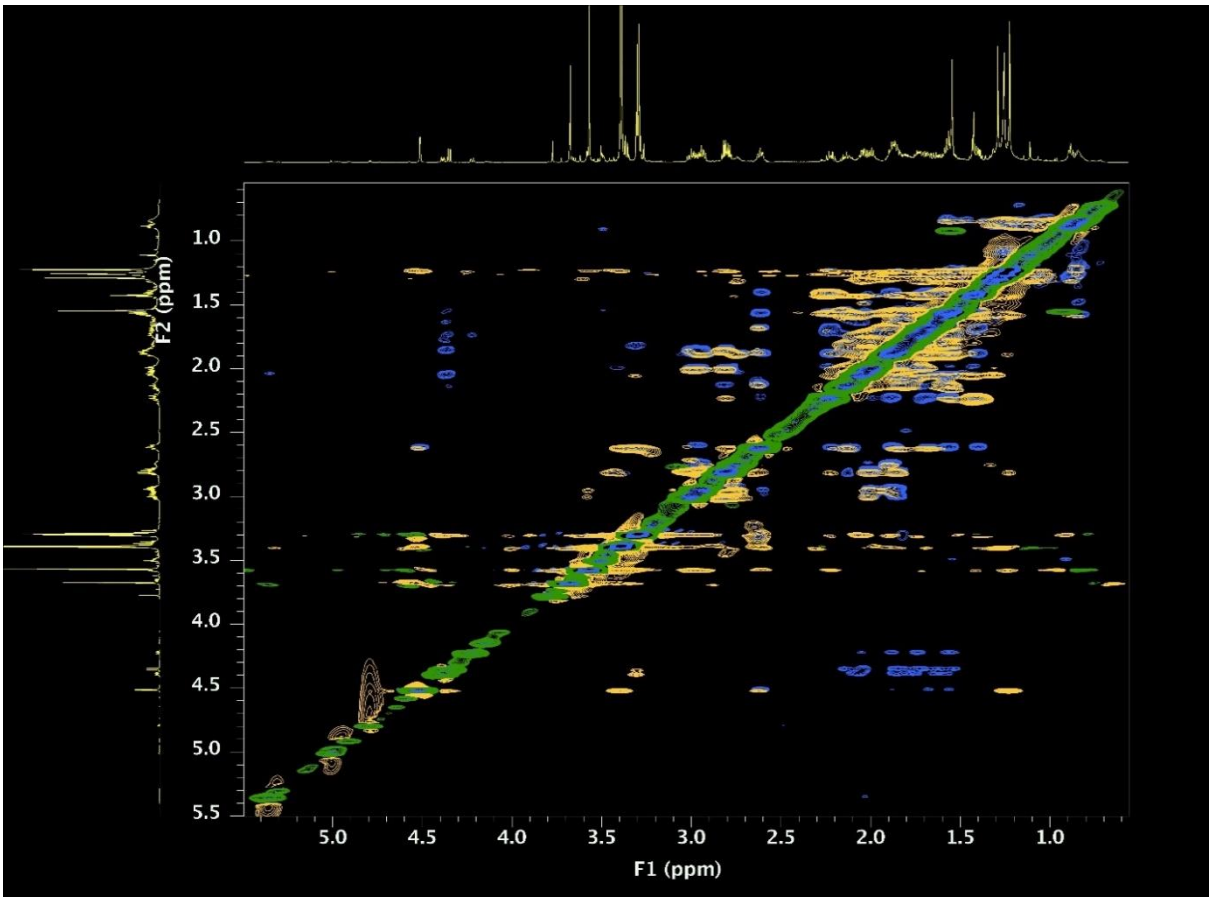

## References


(1) Graaf, M. D.; Gonzalez, L.; Medcalf, Z.; Moeller, K. D. Using a Combination of Electrochemical and Photoelectron Transfer Reactions to Gain New Insights into Oxidative Cyclization Reactions. *J. Electrochem. Soc.* **2020**, *167* (15), 155520. https://doi.org/10.1149/1945-7111/abbe5c.

(2) Medcalf, Z.; Moeller, K. D. Anodic Olefin Coupling Reactions: Elucidating Radical Cation Mechanisms and the Interplay between Cyclization and Second Oxidation Steps. *Chem. Rec.* **2021**, *21* (9), 2442–2452. https://doi.org/10.1002/tcr.202100118.

(3) Campbell, J. M.; Xu, H.-C.; Moeller, K. D. Investigating the Reactivity of Radical Cations: Experimental and Computational Insights into the Reactions of Radical Cations with Alcohol and p-Toluene Sulfonamide Nucleophiles. *J. Am. Chem. Soc.* **2012**, *134* (44), 18338–18344. https://doi.org/10.1021/ja307046j.

(4) Tang, F.; Moeller, K. D. Intramolecular Anodic Olefin Coupling Reactions: The Effect of Polarization on Carbon−Carbon Bond Formation. *J. Am. Chem. Soc.* **2007**, *129* (41), 12414–12415. https://doi.org/10.1021/ja076172e.

(5) Tang, F.; Moeller, K. D. Anodic Oxidations and Polarity: Exploring the Chemistry of Olefinic Radical Cations. *Tetrahedron* **2009**, *65* (52), 10863–10875. https://doi.org/10.1016/j.tet.2009.09.028.

(6) Hudson, C. M.; Moeller, K. D. Intramolecular Anodic Olefin Coupling Reactions and the Use of Vinylsilanes. *J. Am. Chem. Soc.* **1994**, *116* (8), 3347–3356. https://doi.org/10.1021/ja00087a021.

(7) Sun, Y.; Moeller, K. D. Anodic Olefin Coupling Reactions Involving Ketene Dithioacetals: Evidence for a 'Radical-Type' Cyclization. *Tetrahedron Lett.* **2002**, *43* (40), 7159–7161. https://doi.org/10.1016/S0040-4039(02)01663-5.

(8) Frey, D. A.; Krishna Reddy, S. H.; Moeller, K. D. Intramolecular Anodic Olefin Coupling Reactions: The Use of Allylsilane Coupling Partners with Allylic Alkoxy Groups. *J. Org. Chem.* **1999**, *64* (8), 2805–2813. https://doi.org/10.1021/jo982280v.

(9) Redden, A.; Moeller, K. D. Anodic Coupling Reactions: Exploring the Generality of Curtin−Hammett Controlled Reactions. *Org. Lett.* **2011**, *13* (7), 1678–1681. https://doi.org/10.1021/ol200182f.

(10) Redden, A.; Perkins, R. J.; Moeller, K. D. Oxidative Cyclization Reactions: Controlling the Course of a Radical Cation-Derived Reaction with the Use of a Second Nucleophile. *Angew. Chem.* **2013**, *125* (49), 13103–13106. https://doi.org/10.1002/ange.201308739.

(11) Hudson, C. M.; Marzabadi, M. R.; Moeller, K. D.; New, D. G. Intramolecular Anodic Olefin Coupling Reactions: A Useful Method for Carbon-Carbon Bond Formation. *J. Am. Chem. Soc.* **1991**, *113* (19), 7372–7385. https://doi.org/10.1021/ja00019a038.

(12) Brennan, M. P. J.; Brettle, R. Anodic Oxidation. Part XI. Carbon Anodes in Electrosyntheses Based on Carboxylate Ions. *J. Chem. Soc. Perkin 1* **1973**, No. 0, 257–261. https://doi.org/10.1039/P19730000257.

(13) Shono, T.; Nishiguchi, I.; Kashimura, S.; Okawa, M. Electroorganic Chemistry. XXXIV. Novel Intramolecular Cyclization through Anodic Oxidation of Enol Acetates. *Bull. Chem. Soc. Jpn.* **1978**, *51* (7), 2181–2182. https://doi.org/10.1246/bcsj.51.2181.

(14) Miura, K.; Oshima, K.; Utimoto, K. Stabilizing Effect of Trialkylsilyl Group on Carbon Radical: Radical Induced Ring Opening of 1-Trialkylsilyl-2-Vinylcyclopropanes. *Tetrahedron Lett.* **1989**, *30* (33), 4413–4416. https://doi.org/10.1016/S0040-4039(00)99375-4.

(15) Smith, J. A.; Moeller, K. D. Oxidative Cyclizations, the Synthesis of Aryl-Substituted C-Glycosides, and the Role of the Second Electron Transfer Step. *Org. Lett.* **2013**, *15* (22), 5818–5821. https://doi.org/10.1021/ol402826z.
(16) Perkins, R. J.; Xu, H.-C.; Campbell, J. M.; Moeller, K. D. Anodic Coupling of Carboxylic Acids to Electron-Rich Double Bonds: A Surprising Non-Kolbe Pathway to Lactones. *Beilstein J. Org. Chem.* **2013**, *9* (1), 1630–1636. https://doi.org/10.3762/bjoc.9.186.
(17) Schultz, D. M.; Yoon, T. P. Solar Synthesis: Prospects in Visible Light Photocatalysis. *Science* **2014**, *343* (6174), 1239176. https://doi.org/10.1126/science.1239176.
(18) Narayanam, J. M. R.; Stephenson, C. R. J. Visible Light Photoredox Catalysis: Applications in Organic Synthesis. *Chem. Soc. Rev.* **2010**, *40* (1), 102–113. https://doi.org/10.1039/B913880N.
(19) Fox, M. A.; Chen, C. C. Mechanistic Features of the Semiconductor Photocatalyzed Olefin-to-Carbonyl Oxidative Cleavage. *J. Am. Chem. Soc.* **1981**, *103* (22), 6757–6759. https://doi.org/10.1021/ja00412a044.
(20) Eriksen, J.; Foote, C. S. Electron-Transfer Photooxygenation. 5. Oxidation of Phenyl-Substituted Alkenes Sensitized by Cyanoanthracenes. *J. Am. Chem. Soc.* **1980**, *102* (19), 6083–6088. https://doi.org/10.1021/ja00539a018.
(21) Campbell, J. M.; Smith, J. A.; Gonzalez, L.; Moeller, K. D. Competition Studies and the Relative Reactivity of Enol Ether and Allylsilane Coupling Partners toward Ketene Dithioacetal Derived Radical Cations. *Tetrahedron Lett.* **2015**, *56* (23), 3595–3599. https://doi.org/10.1016/j.tetlet.2015.01.144.
(22) New, D. G.; Tesfai, Z.; Moeller, K. D. Intramolecular Anodic Olefin Coupling Reactions and the Use of Electron-Rich Aryl Rings1. *J. Org. Chem.* **1996**, *61* (5), 1578–1598. https://doi.org/10.1021/jo9518359.

# Chapter 3: Anodic Cyclizations and Umpolung Reactions Involving Imines

While in the last chapter we focused on the role of the second oxidation step for the success of an anodic cyclization. In this chapter we will be examining how a fast second electron oxidation can be used to channel a reaction down a new synthetic pathway. Herein we describe one such application that reverses the normal reactivity of an imine group and sets the stage for the asymmetric synthesis of cyclic amines using an anodic cyclization.[1]

(Sections of this chapter were taken from our paper: Medcalf, Z.; Redd, E. G.; Oh, J.; Ji, C.; Moeller, K. D. Anodic Cyclizations and Umpolung Reactions Involving Imines. *Org. Lett.* **2023**, *25* (22), 4135–4139. https://doi.org/10.1021/acs.orglett.3c01399.)

## 3.1 Introduction

As described in chapters 2 and 3, anodic olefin coupling reactions follow the general mechanism shown in Scheme 3.1.[2] The reactions convert normally nucleophilic electron-rich olefins into reactive intermediates. These intermediates then react with nucleophiles and offer numerous possibilities to construct new bonds and rings systems in novel ways. Furthermore, the study of anodic olefin coupling reactions has allowed for a more in-depth look at how electrochemical reactions can be conducted and the factors that are important for their success.[2,3]

Anodic reactions belonging to this category are controlled not only by the initial oxidation and cyclization steps in the mechanism, but also the removal of a second electron from the molecule, occurring downstream of those events ($k_2$ in Scheme 3.1).[4] Even anodic cyclizations using the best radical cation trapping groups, require a fast second oxidation step. Take for example the chemistry shown in Scheme 3.2, that was discussed in more detail in chapter 2.[5] The chemistry shown highlights a radical cation-initiated reaction that was initiated by oxidation of a dithioketene acetal and terminated by trapping the radical cation with an enol ether. The enol ether was selected because it is the best radical cation trapping group that we have studied. In the experiment shown,

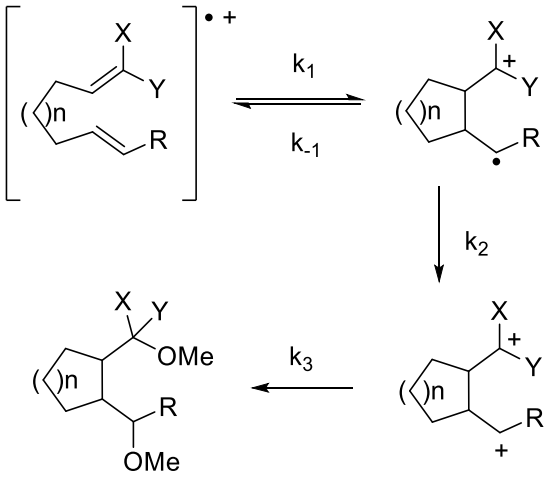


**Scheme 3.1: Anodic Cyclization Reaction Mechanism Model**

the desired cyclization reaction was triggered with both a photoelectron transfer reaction and an anodic cyclization.[6–11] In both cases, the starting material was consumed, resulting in the generation of a radical cation and the initiation of a cyclization. However, only the electrochemical reaction led to product, while the photoelectron transfer-initiated reaction led primarily to polymer formation. The difference between the two methods was the ability of the electrolysis reaction to rapidly remove a second electron from intermediate **2** following the cyclization. This oxidation drove the reaction to completion. In contrast, the one-electron photoelectron transfer reaction could not efficiently accomplish the oxidation of intermediate **2**, resulting in the polymerization of the

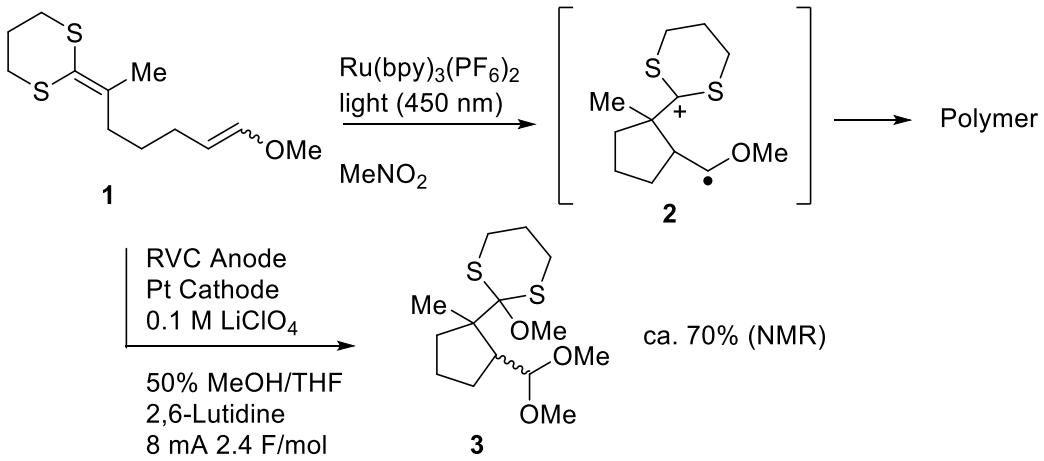


**Scheme 3.2: The Need For The Removal Of A Second Electron**

cyclic radical. This result was consistent with a variety of cyclization reactions that all exhibited the same behavior.[2,4] In each case, a slow second oxidation step led to the formation of polymers and reaction mixtures instead of a high yield of the desired cyclized product.

It is tempting to suggest that the importance of the second oxidation step in an anodic cyclization reaction can be used as a design element for introducing new types of selectivity into the reactions. Consider the proposed anodic cyclization shown in Scheme 3.3. In this process, an electron-rich olefin would undergo oxidation, and the resultant radical cation intermediate would be trapped by an imine. Typically, cyclization reactions involving electron-rich olefins and imines are accomplished by treatment of the substrate with acid. The acid protonates the nitrogen generating an iminium ion that is then attacked by the nucleophilic olefin at the carbon of the imine. With the substrate shown in Scheme 3.3, such a transformation would result in the formation of six-membered ring product **5**. As an alternative, the proposed oxidative cyclization would potentially afford a complementary mode of addition to the imine. The oxidation would generate radical cation intermediate **6**, which would then add to the imine in one of two possible ways. A cyclization leading to the formation of the six-membered ring intermediate **7,** consistent with a "normal addition" to the imine, would result in the production of a six-membered ring product. However,

in this case the addition would result in a N-centered radical. This N-centered radical would be more difficult to oxidize than an alternative benzylic radical (**8a**) that would be derived from a cyclization leading to a five-membered ring. In this case, the oxidation of **8a** would product stable iminium ion **8b**. Considering the reversibility of radical cation-derived cyclizations and the role the second oxidation plays in product determination for such transformations,[2–4] one would expect Curtin-Hammett control of the reaction. In this scenario, the faster oxidation of **8a** would drive the reaction to the formation of the five-membered ring product. The oxidation of **8a** to iminium ion

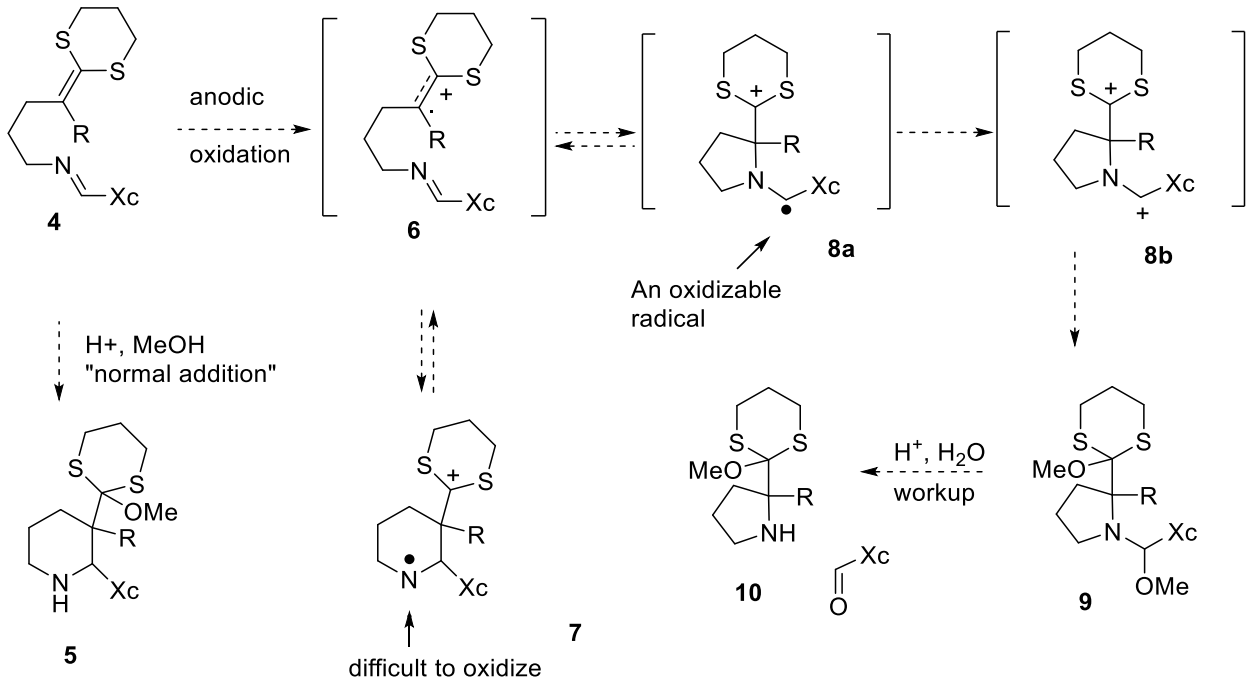


**Scheme 3.3: Using A Second Oxidation Step To Change The Course Of A Reaction**

**8b** would result in methanol trapping to form **9**. Product **9**, upon the addition of water during the workup, would hydrolyze to yield the cyclic substituted proline derivative **10** and the aldehyde.

Reactions of this type are particularly attractive because the starting imine can be rapidly synthesized in one step from the primary amine used in prior C-N anodic bond forming reactions.[12] This provides an opportunity to introduce an auxiliary into the reaction, capable of influencing the

course of the cyclization reaction and potentially introducing selectivity into the product in a way not attainable in amine-based cyclizations. Additionally, once the reaction was complete, the auxiliary would be recovered. However, such a proposal requires that the second oxidation step in the mechanism can be used to drive the reaction in a manner that reverses the "normal" addition of a nucleophile to an imine. Is this true? As reported below, the answer to this question is yes.

## 3.2 Results and Discussion

The investigation into the proposed anodic cyclization reactions began with the synthesis of an initial set of substrates. These substrates were designed to explore the compatibility of the chemistry with imines having different electronic properties. To this end, the imines were generated by condensing an amine substrate with either benzaldehyde or an electron-rich or electron-poor benzaldehyde derivative. For the derivatives, the substituents were strategically positioned at the para position of the aromatic ring to maximize their influence on the second

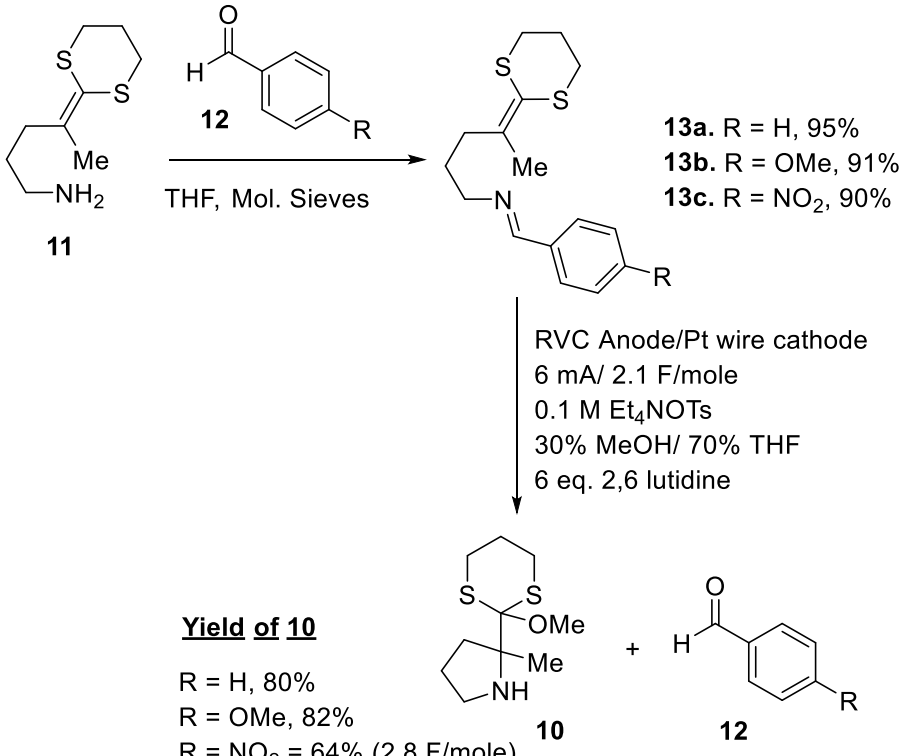


**Scheme 3.4: A Test With An Initial Set Of Substrates**

oxidation step of the reaction (Scheme 3.4). The anodic cyclization of all three arylimine substrates proceeded nicely using electrolysis conditions that are commonly used for a variety of anodic cyclization reactions. Such reactions benefit from high surface area carbon electrodes which facilitate the rapid removal of the second electron.[13] Additionally, MeOH/THF electrolyte solutions with tetraethylammonium tosylate as the electrolyte reduce the amount of methanol at the anode surface. This reduction in methanol at the anode surface buys time for the cyclization reaction. The reactions also benefit from the use of low current densities, which help maintain a minimal concentration of the highly reactive radical cation. This prevents dimerization and polymerization reactions that can arise from the radical cation intermediate. A base (2,6-lutidine) was used as a proton scavenger to prevent methanolysis of the acid-labile ketene dithioacetal at the surface of the anode. For these reactions, the use of LiOMe in pure methanol solvent that was employed for the anodic cyclization of amine **11** was avoided. This was done to allow more time for the cyclization in case the reaction with the imine was slower.

The oxidation of both the substrate with the simple benzaldehyde-derived imine and the substrate derived from the 4-methoxybenzaldehyde proceeded to the product in high yield while consuming on the theoretical amount of current. In both cases, the second oxidation step involving intermediate **8** following the cyclization was expected to be fast. However, when an electron-poor aryl ring was used (**13c**), the anodic cyclization reaction led to a lower yield and a decrease in the overall current efficiency of the process. The need for more current was consistent with earlier cyclization reactions where a slower second oxidation step was encountered.[4] In an undivided cell, a slow second oxidation of the cyclic intermediate can lead to re-reduction, substrate reformation, and a reduction in current efficiency. In such cases, employing a divided cell enhances the current

efficiency of the reaction, even if the yield of product is not improved due to polymerization pathways.[4] While the drop in current efficiency in the present case was not as large as in previous cases, this was not a surprise since the neighboring amine lone pair in intermediate **8** would ensure a successful second oxidation step to make the iminium ion needed to form the cyclization product **9** in spite of the electron-poor aryl ring.

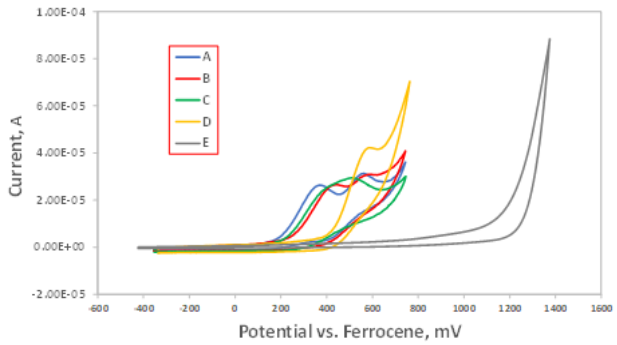


**Figure 3.1: Cyclic voltammograms of (A) 2.2 mM N-[(4-methoxyphenyl)methylene]-4-(1,3-dithian-2-ylidene)-1-pentanamine 13b, (B) 2.2 mM N-(phenylmethylene)-4-(1,3-dithian-2-ylidene)-1-pentanamine 13a, (C) 2.2 mM N-[(4-nitrophenyl)methylene]-4-(1,3-dithian-2-y//lidene)-1-pentanamine 13c, (D) a substrate having only a ketene dithioacetal, 3.2 mM 5-(tert-butyldimethylsilyloxy)-2-(1,3-dithian-2-ylidene)pentane, and (E) a substrate having only a benzaldehyde derived imine, 2.8 mM N-(phenylmethylene)-1-pentanamine at glassy carbon electrode with a scan rate of 25 mV $s^{-1}$ in 30% MeOH/70% THF containing 0.1 M $Et_4NOTs$.**

Cyclic voltammetry data confirmed that the difference between the cyclizations was due to the second oxidation step and not the cyclization reaction itself. In Figure 3.1, the cyclic voltammetry data is presented for a substrate having an isolated dithioketene acetal moiety (D), a substrate having only an imine derived from benzaldehye and a primary amine (E), and the three cyclization substrates 13a-c (A-C). Each of the electrolysis substrates has an oxidation potential that was approximately equal and significantly less positive than either of the isolated functional groups.

These observations were consistent with an oxidation of the ketene dithioacetal group with a similar Nernstian shift occurring for all three cyclization substrates.[12] This suggested that the cyclizations were all fast, occurred at or near the electrode surface, and proceeded at roughly the same rate. Therefore, the difference observed for the substrate with the p-nitro group did not stem from the rate of the cyclization reaction, but rather the presence of the nitro-group slowing the reaction "downstream" of that cyclization. This suggestion was most consistent with the presence of the nitro-group slowing the second oxidation step in the mechanism involving intermediate **8**.

The rate of the cyclization reactions also indicated that the earlier precautions of using less methanol and a weaker base to "buy time" for the cyclizations, was not necessary. In fact, when substrate **11** was oxidized using the same conditions as the previous amine cyclizations (LiOMe base instead of 2,6-lutidine and pure methanol solvent),[12] the reaction resulted in a nearly identical yield of product (80%).

Similar to the earlier amine cyclization, the use of a less electron-rich olefin was incompatible with the reactions due to the low oxidation potential associated with the cyclic amine product. In those cases, the Nernstian shift associated with the substrate was not sufficient to drop the oxidation potential of the substrate below that of the product (ca. + 0.89 V vs. ferrocene).[12] When a methoxy enol ether substrate with an oxidation potential approximately 300 mV higher than that of the ketene dithioacetal was used as a substrate the for cyclization, the reaction resulted in a large number of products, presumably from over-oxidation of the product.

With the initial experiment in place, the scope of the imines that can be used was examined (Figure 3.2). For each of these reactions, the cyclic ketene dithioacetal was chosen due to its stability, ease of synthesis, and known compatibility with the cyclizations. Since the use of the imine did not appear to significantly alter the anodic cyclization compared to the previous amine cyclizations, and the aldehyde component of the imine is not incorporated into the product, the goal of the study was not to explore the nature of the products that could be made, but rather to identify types of

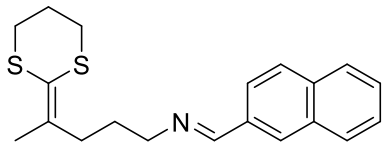

**13.** Cyclization Yield of **10** = 71%

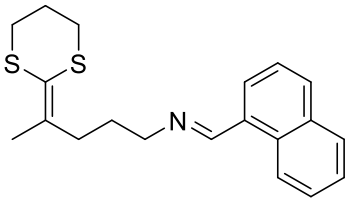

**14.** Cyclization Yield of **10** = 60%

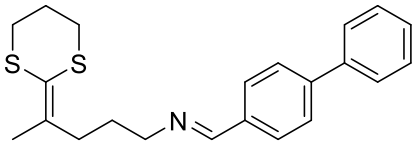

**15.** Cyclization Yield of **10** = 53%

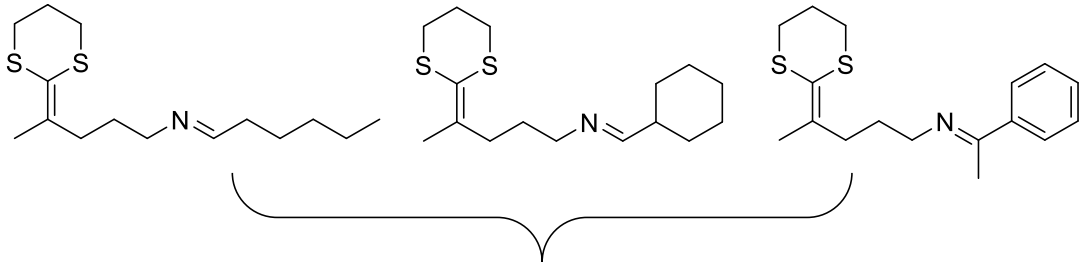

Cyclization Yield = 0% due to the instability of the imines

**Figure 3.2: Varying The Structure Of The Imine**

auxiliaries that could be used to influence future reactions. With this in mind, two factors governed the substrate selection: first, the potential use of a chiral auxiliary to control the absolute stereochemistry of the products generated, and second, the recent observation that electrochemical reactions involving substrates with aryl rings can be confined to the surface of an electrode.[14] Both

developments presented new opportunities to introduce selectivity into an anodic cyclization reaction.

The oxidations were all run using the conditions outlined in Scheme 3.4. Two conclusions were quickly reached. First, the reactions tolerated the incorporation of more conjugated aryl rings such as naphthalene rings even when the imine was more hindered (**14**), as well as the use of a biphenyl ring (**15**). In this way, the reaction proved compatible with the types of aryl rings that are found in chiral auxiliaries,[15–17] used to optimize guest-host interactions,[18] and known to have affinity towards aryl-ring based anodic surfaces.[14] Second, the use of simple alkyl imines and imines derived from ketones were unsuccessful due to the inherent instability of these imines in the

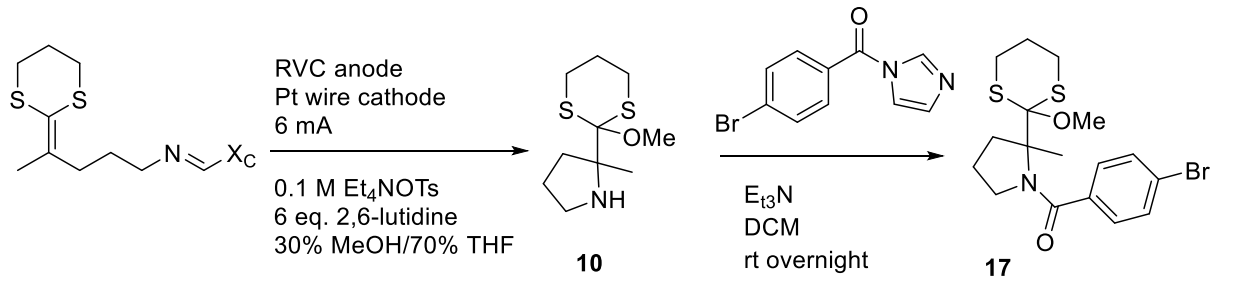


**16a.** Imine derived from (1R)-(-)-Myrtenal
(cyclization yield = 18%)

$X_C$ =

**17**: % ee
From **16a**: 50%
From **16b**: 30%
From **16c**: -30% (opposite enantiomer)

**16b.** Imine derived from 10R-Binapthaldehyde
(cyclization yield (NMR) = 16%)

$X_C$ =

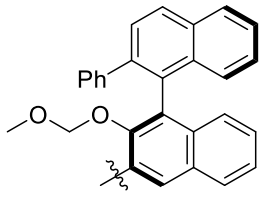

**16c.** Imine derived from 10S-Binapthaldehyde
(cyclization yield (NMR) = 45%)

$X_C$ =

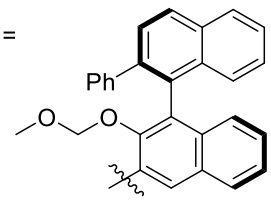

**Scheme 3.5: Reactions Using Chiral Imines**

electrolysis reaction. While it may be possible to alter the electrolysis in a manner that enables the

use of these more sensitive substrates, it is evident that at the present, the use of imines derived from aryl aldehydes provide the best path forward for introducing new types of selectivity into anodic cyclization reactions.

In an exploratory study, the reaction was shown to be compatible with the use of chiral imines (Scheme 3.5).[19] To this end, three substrates (**16a-c**) were synthesized and oxidized. Following the cyclization, the product amine was converted into an amide for HPLC analysis on a chiral column. Each of the chiral imines used did influence the absolute stereochemistry of the reaction, with the myrtenal-based imine resulting in a 50% e.e. of the major product and the binapthaldehyde imines leading to a 30% e.e. of the major product. As expected, the two different enantiomers of binapthaldehyde produced the opposite enantiomer of the product obtained. While the yields for the cyclizations were low, they were not further optimized at this point due to the level of asymmetric induction obtained. Typically, such lower yields reflect the imine not being stable to the reaction conditions. While such scenarios can frequently be optimized, this would be ideally done after screening for a more optimal chiral auxiliary.

Lastly, we demonstrated that the reaction could be run on a larger scale than that used to pioneer the initial cyclization reactions (Scheme 3.6). For simplicity, the scaled reaction was run using methanol with lithium methoxide serving as both the base to neutralize the acid generated at the anode and as the electrolyte needed for the reaction. While the yield of the process was lower than the optimized conditions used for the pioneering reactions, the ability to avoid the use of an external electrolyte and 2,6-lutidine as an additive made up for this difference. When the reaction was scaled up and conducted without the addition of an external electrolyte, it led to increased

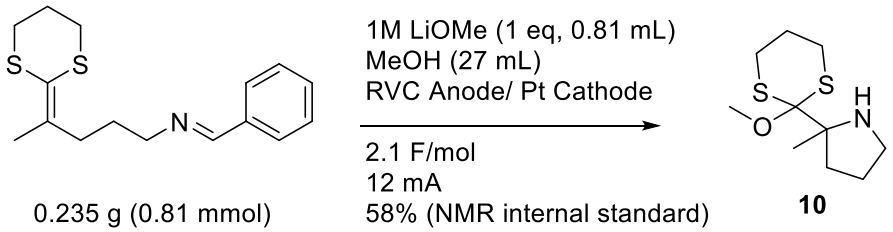


**Scheme 3.6: Reaction On A 235 mg Scale**

polymerization of the radical cation. This resulted in a messier reaction, making the isolation of amine **10** more difficult. Consequently, we used NMR analysis to get an accurate yield of the cyclization.

## 3.3 Conclusions

We have discovered that the second oxidation step in an anodic cyclization can act as a driving force to provide products that originate from a reversal of the normal addition of a nucleophilic olefin to an imine. This presents an opportunity to temporarily place an aryl ring into a reaction that affords a cyclic amino acid derivative. Efforts to utilize that aryl ring to introduce new types of selectivity into anodic cyclization reactions are underway.

## 3.4 Experimental Section

### 3.4.1 General Information

NMR spectra were acquired on either a Varian Mercury 300, Agilent DD2 500 MHz, or Bruker Avance 400 NMR spectrometer at either 300, 400, or 500 MHz for 1H or 75, 101 or 126 MHz for 13C{1H} unless otherwise noted. Chemical shifts (δ) are reported in ppm relative to tetramethylsilane (0 ppm) for 1H and 13C{1H}. Mass spectra were recorded on either a Thermo LTQ-Orbitrap spectrometer under positive ion mode or a Maxis 4G ESI-QTOF spectrometer with flow rate of 3 μL/min. Reactions were run under either an argon or nitrogen atmosphere unless otherwise noted. Tetrahydrofuran was purchased from Sigma-Aldrich Corporation and

distilled from sodium benzophenone ketyl under argon atmosphere prior to use. Triethylamine and dichloromethane reaction solvent were purchased from Sigma-Aldrich Corporation and distilled from calcium hydride under argon atmosphere prior to use. Flash column chromatography was performed on 60 Å silica gel purchased from Sorbent Technologies. Thin layer chromatography was performed on Analtec UNIPLATE™ and visualized by ultraviolet irradiation, ceric ammonium molybdate, phosphomolybdic acid, or 2,4-dinitrophenylhydrazine. Carbonyldiimidazole was purchased from Chem-Impex Int'l Inc. While 4-bromo-2-methylbenzoic acid was purchased from Matrix Scientific. Both were used as received. All other starting materials and reagents were purchased from Sigma-Aldrich Corporation and used as received. Electrolysis reactions were conducted using a model 630 coulometer, a model 410 potentiostatic controller, and a model 420A power supply purchased from the Electrosynthesis Company, Inc. (now Electroytica). Carbon rods were also purchased from the Electrolytica Company. Reticulated vitreous carbon (RVC) electrodes were purchased from ERG Aerospace Corp. CV studies were conducting using a 3-mm-diameter glassy carbon working electrode with a scan rate of 25 mV s–1 in 30% MeOH/70% THF containing 0.1 M Et4NOTs. A platinum wire was employed as the auxiliary electrode. The reference electrode was Ag/AgCl and 2 mM of ferrocene was also added to the solutions. All CV potentials are quoted with respect to ferrocene.

### 3.4.2 Synthesis and Electrolysis of Imines

Scheme to synthesize **11**

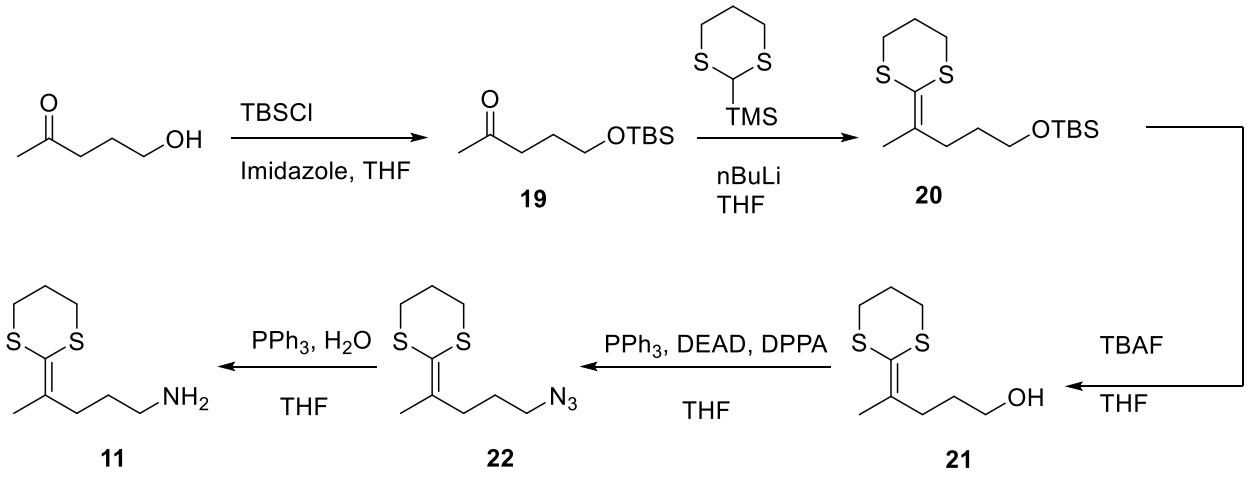


**Synthesis of 5-(tert-butyldimethylsilyloxy)-2-pentanone (19)**

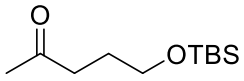

**19**

To a round bottom flask containing 5 g (73.4 mmol, 2.5 eq.) imidazole in 40 mL dry THF stirred under argon atmosphere at 0 °C was added 3 g (29.4 mmol, 1 eq., in 20 mL THF) 5-hydroxy-2-pentanone. Subsequently, 4.87 g (32.3 mmol, 1.1 eq.) TBSCl in 20 mL THF solution was added dropwise. After stirring overnight at room temperature, the solution was quenched with water and extracted with diethyl ether. The organic layer was dried over anhydrous magnesium sulfate and concentrated at reduced pressure. The crude product was purified by flash column chromatograph (silica gel, 10% ether/90% hexane) to afford a colorless oil (5.10 g, 80%). In case the side product TBSOH is present, it can be removed under vacuum overnight.

$^{1}$H NMR (300 MHz, $CDCl_3$) δ 3.61 (t, J = 6.1Hz, 2H), 2.51 (t, J = 7.2Hz, 2H), 2.15 (s, 3H), 1.83-1.74 (m, 2H), 0.89 (s, 9H), 0.04 (s, 6H).

$^{13}$C NMR (126 MHz, $CDCl_3$) δ 208.6, 61.9, 39.8, 29.7, 26.6, 25.7, 18.0, -5.6.

**Synthesis of 4-(1,3-dithian-2-ylidene)-1-pentanol (21)**

Scheme to synthesize **21**

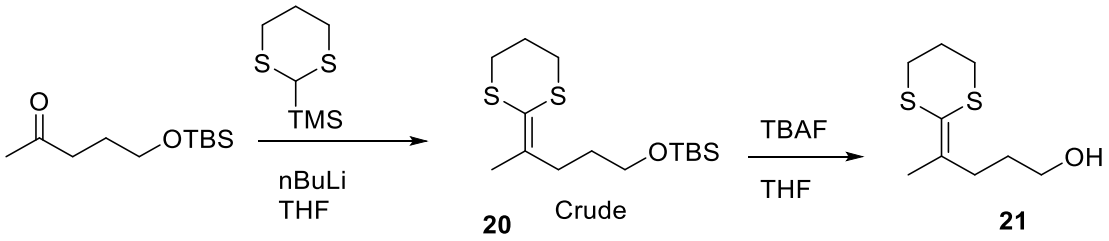


*n*-BuLi (1.6 M in hexanes, 4.7 mL, 7.5 mmol) was added to a solution of 2-(trimethylsilyl)-1,3-dithiane (1.45 g, 7.5 mmol) in dry THF (25 mL) at −78 °C under argon atmosphere. The reaction was stirred at −78 °C for 0.5 h and room temperature for another 0.5 h. The solution was cooled to −78 °C, to which was added 0.81 g (3.75 mmol) 5-(*tert*-butyldimethylsilyloxy)-2-pentanone. The reaction was gradually warmed to room temperature and stirred overnight. Brine was added and extraction was carried out twice with ether. The combined organic layers were dried over anhydrous $MgSO_4$ and the solvent was evaporated under reduced pressure to afford crude compound **20** (5-(*tert*-butyldimethylsilyloxy)-2-(1,3-dithian-2-ylidene)pentane).

To a solution of crude compound **20** (1.93 g) in dry THF (20 mL) under argon atmosphere was added tetrabutylammonium fluoride (TBAF, 1.0 M in THF, 10 mL) and stirred overnight. The reaction was cooled to 0 °C and quenched with saturated $NaHCO_3$ solution (30 mL). The aqueous layer was separated from the organic phase and extracted twice with ether and once with dichloromethane. The combined organic phases were dried over anhydrous $MgSO_4$ and the solvent was evaporated under reduced pressure. The crude product was purified by flash column chromatograph (silica gel, 50% ether/50% hexane) to afford a pale yellow oil **21** (0.67 g, 87%).

$^1$H NMR (300 MHz, $CDCl_3$) δ 3.62 (q, $J$ = 6.1 Hz, 2H), 2.88-2.85 (m, 4H), 2.44 (t, 7.3 Hz, 2H), 2.15-2.10 (m, 2H), 1.91 (s, 3H), 1.88 (t, 1H), 1.72-1.63 (m, 2H).

$^{13}$C NMR (126 MHz, $CDCl_3$) δ 139.5, 119.6, 61.8, 31.7, 30.5, 30.3, 30.2, 24.8, 20.1.

**Synthesis of 2-(5-azidopentan-2-ylidene)-1,3-dithiane (22)**

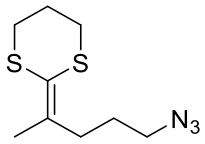

**22**

Diethyl azodicarboxylate (DEAD, 40% wt. in toluene, 0.53 g, 1.2 mmol) was added to a solution containing 0.221 g (1.08 mmol) 4-(1,3-dithian-2-ylidene)-1-pentanol and 0.315 g (1.2 mmol) triphenylphosphine ($Ph_3P$) in dry THF (20 mL), followed by addition of 0.3300 g (1.2 mmol) diphenylphosphoryl azide (DPPA). The reaction was stirred overnight at room temperature and the solvent was removed under reduced pressure. The crude azide was purified by flash column chromatograph (silica gel, ether:hexane=1:10) to give 0.1500 g colorless oil (64%).

$^1$H NMR (500 MHz, $CDCl_3$) δ 3.27 (t, *J* = 6.9 Hz, 2H), 2.89-2.85 (m, 4H), 2.43 (t, J =7.5 Hz, 2H), 2.14-2.09 (m, 2H), 1.91 (s, 3H), 1.73-1.67 (m, 2H).

$^{13}$C NMR (126 MHz, $CDCl_3$) δ 138.4, 121.0, 51.3, 33.2, 30.4, 30.3, 27.3, 25.1, 20.4

**Synthesis of 4-(1,3-dithian-2-ylidene)pentan-1-amine (11)**

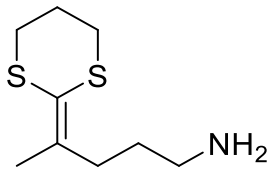

**11**

0.15 g (0.65 mmol) azide was dissolved in THF (15 mL). 0.43 g (1.63 mmol) $Ph_3P$ and 0.06 mL (3.3 mmol) water were added. After the reaction was brought to reflux for 5 h, the solvent was removed under reduced pressure and the crude product was purified by flash column chromatograph (silica gel, MeOH:$CH_2Cl_2$:$Et_3N$=4:1:0.1) to give 0.125 g (57%) pale yellow oil.

$^1$H NMR (500 MHz, $CDCl_3$) δ 2.88-2.84 (m, 4H), 2.69 (t, *J* = 6.9 Hz, 2H), 2.40 (t, J =7.5 Hz, 2H), 2.14-2.09 (m, 2H), 1.91 (s, 3H), 1.72 (s, 1H), 1.59-1.53 (m, 2H).

$^{13}$C NMR (126 MHz, $CDCl_3$) δ 140.0, 119.5, 41.6, 33.0, 31.6, 30.3, 30.1, 25.0, 20.1.

**Synthesis of N-(phenylmethylene)-4-(1,3-dithian-2-ylidene)-1-pentanamine (13a)**

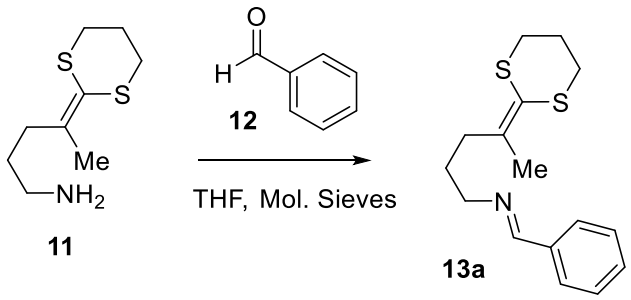


To a THF (15 mL, no inhibitor) solution containing 0.25 g (1.23 mmol) 4-(1,3-dithian-2-ylidene)-1-pentanamine was added 0.13 g (1.23 mmol) freshly distilled benzaldehyde. After the addition of activated molecular sieves, the reaction was stirred overnight. The solution was then filtered through celite and washed with methanol. The solvents were removed under reduced pressure to afford 0.339 g (95%) viscous yellow oil.

$^{1}$H NMR (500 MHz, $CDCl_3$) δ 8.29 (s, 1H), 7.73-7.71 (m, 2H), 7.41-7.39 (m, 3H), 3.60 (t, J = 6.9 Hz, 2H), 2.87-2.82 (m, 4H), 2.44 (t, J =7.6 Hz, 2H), 2.13-2.08 (m, 2H), 1.93 (s, 3H), 1.85-1.79 (m, 2H).

$^{13}$C NMR (126 MHz, $CDCl_3$) δ 161.2, 140.2, 136.5, 130.6, 128.7, 128.2, 119.7, 61.4, 33.9, 30.4, 30.3, 29.2, 25.1, 20.3.

ESI HRMS *m*/*z* ($M+H^+$) calculated 292.1188, observed 292.1191

**Electrolysis of N-(phenylmethylene)-4-(1,3-dithian-2-ylidene)-1-pentanamine (13a)**

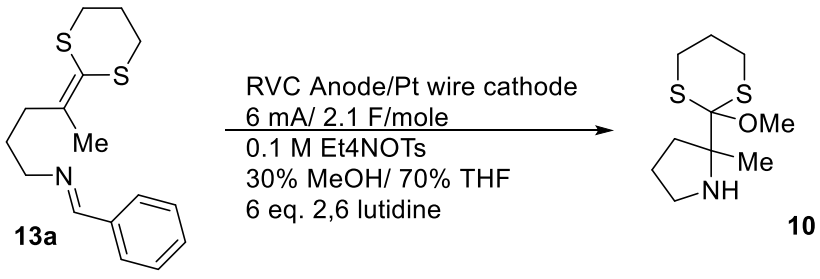

0.0791 g (0.272 mmol) *N*-(phenylmethylene)-4-(1,3-dithian-2-ylidene)-1-pentanamine was dissolved in 20 mL of 30% MeOH/70% THF in a 25-mL three-neck round bottom flask at room temperature. The electrolyte $Et_4NOTs$ (0.1 M, 0.60 g) and 6 equivalent 2,6-lutidine (0.175 g) were added to the solution. The electrolysis was carried out with reticulated vitreous carbon (RVC, 100 PPI) anode and platinum wire cathode at constant current of 6 mA with stirring until 2.1 F/mol of charge was passed. Ether was added and the solution was washed with brine twice. The organic layer was dried over anhydrous $MgSO_4$ and the solvent was removed under reduced pressure. The residue was purified by a silica gel column (slurry packed with 1% $Et_3N$ in ether, eluted with 20% MeOH/80% ether) to give 0.051 g (80%) 2-(2-methoxy-1,3-dithian-2-yl)-2-methylpyrrolidine.

$^1H$ NMR (500 MHz, $CDCl_3$) δ 3.58 (s, 3H), 3.08-2.96 (m, 4H), 2.84-2.75 (m, 2H), 2.33-2.27 (m, 1H), 2.07-2.00 (m, 1H), 1.91-1.70 (m, 4H), 1.64-1.59 (m, 1H), 1.37 (s, 3H).

$^{13}C$ NMR (126 MHz, $CDCl_3$) δ 101.9, 71.8, 53.4, 47.4, 36.3, 27.6, 27.5, 26.0, 24.3, 23.7.

**Synthesis of N-[(4-nitrophenyl)methylene]-4-(1,3-dithian-2-ylidene)-1-pentanamine (13c)**

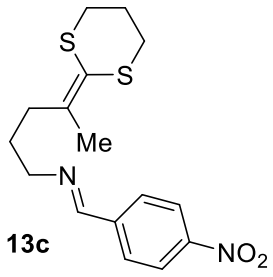


**13c**

The synthesis was carried out according to procedures in Step 5. 0.292 g (1.43 mmol) 4-(1,3-dithian-2-ylidene)-1-pentanamine and 0.217 g (1.43 mmol) 4-nitrobenzaldehyde were used to give 0.432 g product (90%, purity is 93%) as yellow solid.

$^{1}$H NMR (500 MHz, $CDCl_3$) δ 8.37 (s, 1H), 8.27 (d, J = 8.4 Hz, 2H), 7.90 (d, J = 8.4 Hz, 2H), 3.66 (t, J = 7.0 Hz, 2H), 2.88-2.83 (m, 4H), 2.46 (t, J = 7.2 Hz, 2H), 2.13-2.09 (m, 2H), 1.94 (s, 3H), 1.88-1.82 (m, 2H).

$^{13}$C NMR (126 MHz, $CDCl_3$) δ 158.9, 149.0, 142.0, 139.6, 128.8, 124.0, 120.0, 61.5, 33.7, 30.4, 30.2, 29.0, 25.1, 20.3.

ESI HRMS *m*/*z* ($M+H^+$) calculated 337.1039, observed 337.1040.

**Electrolysis of N-[(4-nitrophenyl)methylene]-4-(1,3-dithian-2-ylidene)-1-pentanamine (13c)**

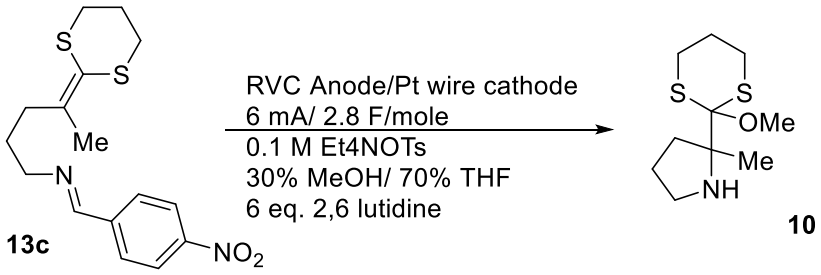


The electrolysis of *N*-[(4-nitrophenyl)methylene]-4-(1,3-dithian-2-ylidene)-1-pentanamine (0.0690 g, 93% purity) was carried out under similar conditions as specified in Step 6 with 2.8 F/mol of charge passed to consume all the starting material. The crude product was purified by a silica gel column (slurry packed with 1% $Et_3N$ in ether, eluted with hexanes (6) : ether (3) : MeOH (1) : $Et_3N$ (0.2)) to give 0.0300 g (64% yield) 2-(2-methoxy-1,3-dithian-2-yl)-2-methylpyrrolidine.

**Synthesis of N-[(4-methoxyphenyl)methylene]-4-(1,3-dithian-2-ylidene)-1-pentanamine (13b)**

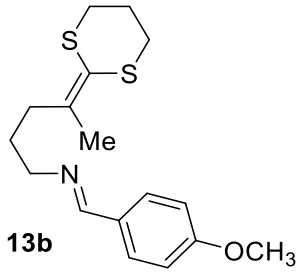


**13b**

The synthesis was carried out according to procedures in Step 5. 0.1054 g (0.52 mmol) 4-(1,3-dithian-2-ylidene)-1-pentanamine and 0.072 g (0.52 mmol) 4-methoxybenzaldehyde were used to give 0.153 g product (91%, purity is 93%) as yellow oil.

$^{1}$H NMR (500 MHz, $CDCl_3$) δ 8.21 (s, 1H), 7.67 (d, J = 8.8 Hz, 2H), 6.92 (d, J = 8.8 Hz, 2H), 3.84 (s, 3H), 3.56 (t, J = 6.7 Hz, 2H), 2.87-2.82 (m, 4H), 2.43 (t, J = 7.7 Hz, 2H), 2.13-2.08 (m, 2H), 1.93 (s, 3H), 1.83-1.77 (m, 2H).

$^{13}$C NMR (126 MHz, $CDCl_3$) δ 161.6, 160.5, 140.3, 129.7, 129.5, 119.6, 114.1, 61.3, 55.5, 33.9, 30.4, 30.3, 29.3, 25.1, 20.3.

ESI HRMS *m/z* ($M+H^+$) calculated 322.1294, observed 322.1298.

**Electrolysis of N-[(4-methoxyphenyl)methylene]-4-(1,3-dithian-2-ylidene)-1-pentanamine (13b)**

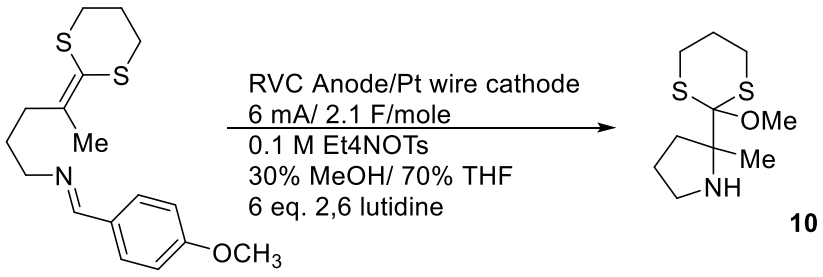


**10**

The electrolysis of *N*-[(4-methoxyphenyl)methylene]-4-(1,3-dithian-2-ylidene)-1-pentanamine (0.0628 g, 93% purity) was carried out under similar conditions as specified in Step 6 with 2.1 F/mol of charge passed. The crude product was purified by a silica gel column (slurry packed

with 1% $Et_3N$ in ether, eluted with hexanes (6) : ether (3) : MeOH (1) : $Et_3N$ (0.2)) to give 0.0348 g (82%) 2-(2-methoxy-1,3-dithian-2-yl)-2-methylpyrrolidine.

**Synthesis of N-(2-naphthalenylmethylene)-4-(1,3-dithian-2-ylidene)-1-pentanamine (14)**

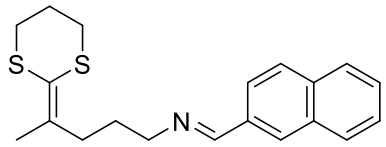

**14**

The synthesis was carried out according to similar procedures in Step 5. 0.2321 g (1.14 mmol) 4-(1,3-dithian-2-ylidene)-1-pentanamine and 0.1782 g (1.14 mmol) 2-naphthaldehyde were used to give 0.3295 g product (85%, purity is 95%, FW 341.53) as yellow oil.

$^1H$ NMR (400 MHz, $CDCl_3$) δ 8.44 (s, 1H), 8.03 (s, 1H), 7.98 (d, 1H), 7.90-7.84 (m, 3H), 7.52-7.50 (m, 2H), 3.66 (t, J = 7.1 Hz, 2H), 2.88-2.83 (m, 4H), 2.47 (t, J = 7.5 Hz, 2H), 2.14-2.08 (m, 2H), 1.95 (s, 3H), 1.90-1.83 (m, 2H).

$^{13}C$ NMR (101MHz, $CDCl_3$) δ 161.2, 140.0, 134.7, 134.1, 133.1, 129.7, 128.6, 128.4, 127.9, 127.0, 126.4, 123.9, 119.7, 61.4, 33.8, 30.3, 30.2, 29.2, 25.0, 20.2.

ESI HRMS *m*/*z* ($M+H^+$) calculated 342.1345, observed 342.1335.

**Electrolysis of N-(2-naphthalenylmethylene)-4-(1,3-dithian-2-ylidene)-1-pentanamine**

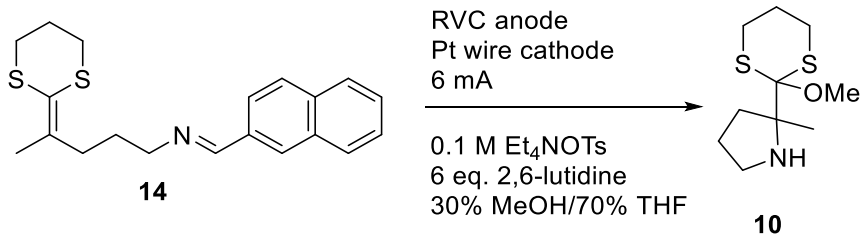


**14** **10**

The electrolysis of *N*-(2-naphthalenylmethylene)-4-(1,3-dithian-2-ylidene)-1-pentanamine (0.0718 g, 95% purity) was carried out under similar conditions as specified in Step 6 with 2.1 F/mol of charge passed. The crude product was purified by a silica gel column (slurry packed with 1% $Et_3N$ in ether, eluted with hexanes (6) : ether (3) : MeOH (1) : $Et_3N$ (0.2)) to give 0.0331 g (71%) 2-(2-methoxy-1,3-dithian-2-yl)-2-methylpyrrolidine.

**Synthesis of N-(4-phenylbenzylidene)-4-(1,3-dithian-2-ylidene)-1-pentanamine (16)**

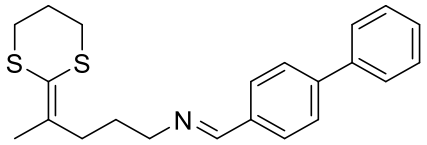


**16**

The synthesis was carried out according to similar procedures in Step 5. 0.0380 g (0.187 mmol) 4-(1,3-dithian-2-ylidene)-1-pentanamine and 0.0341 g (0.187 mmol) 4-biphenylcarboxaldehyde were used to give 0.0718 g product (97%, purity is 93%, FW 367.57) as yellow oil.

$^1$H NMR (400 MHz, $CDCl_3$) δ 8.33 (s, 1H), 7.80 (d, 2H), 7.65-7.61 (m, 4H), 7.45 (t, 2H), 7.35 (t, 1H), 3.63 (t, J = 6.8 Hz, 2H), 2.88-2.83 (m, 4H), 2.46 (t, J = 7.9 Hz, 2H), 2.14-2.08 (m, 2H), 1.94 (s, 3H), 1.87-1.80 (m, 2H).

$^{13}$C NMR (101 MHz, $CDCl_3$) δ 161.1, 143.6, 140.8, 140.4, 135.7, 129.2, 128.9, 128.0, 127.6, 127.5, 120.0, 61.7, 34.1, 30.6, 30.5, 29.5, 25.3, 20.5.

ESI HRMS *m*/*z* ($M+H^+$) calculated 368.1501, observed 368.1492.

**Electrolysis of N-(4-phenylbenzylidene)-4-(1,3-dithian-2-ylidene)-1-pentanamine**

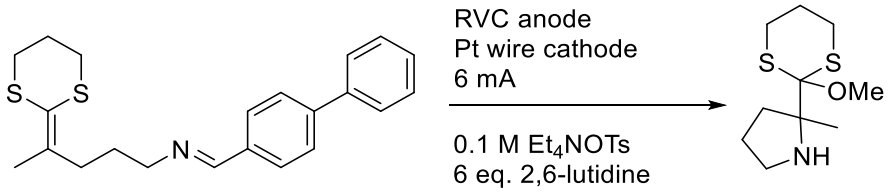


**10**

The electrolysis of *N*-(4-phenylbenzylidene)-4-(1,3-dithian-2-ylidene)-1-pentanamine (0.0702 g, 93% purity) was carried out under similar conditions as specified in Step 6 with 2.1 F/mol of charge passed. The crude product was purified by a silica gel column (slurry packed with 1% $Et_3N$ in ether, eluted with hexanes (6) : ether (3) : MeOH (1) : $Et_3N$ (0.2)) to give 0.0220 g (53%) 2-(2-methoxy-1,3-dithian-2-yl)-2-methylpyrrolidine (FW 233.39).

**Synthesis of N-(1-naphthalenylmethylene)-4-(1,3-dithian-2-ylidene)-1-pentanamine (15)**

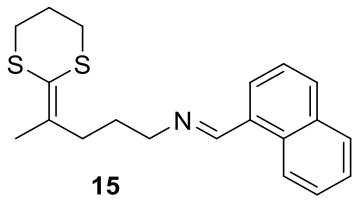

**15**

The synthesis was carried out according to similar procedures in Step 5. 0.091 g (0.447 mmol) 4-(1,3-dithian-2-ylidene)-1-pentanamine and 0.071 g (0.455 mmol) 1-naphthaldehyde were used to give 0.1435 g product (92%, purity is 92%, FW 341.53) as pale-yellow oil.

$^1$H NMR (400 MHz, $CDCl_3$) δ 8.95 (s, 1H), 8.91 (d, 1H), 7.91-7.87 (m, 3H), 7.60-7.55 (m, 1H), 7.53-7.49 (m, 2H), 3.71 (t, J = 7.1 Hz, 2H), 2.88-2.82 (m, 4H), 2.52 (t, J = 7.6 Hz, 2H), 2.13-2.07 (m, 2H), 1.96 (s, 3H), 1.95-1.87 (m, 2H).

$^{13}$C NMR (101 MHz, $CDCl_3$) δ 161.0, 140.4, 134.2, 132.2, 131.6, 131.1, 128.90, 128.87, 127.3, 126.3, 125.6, 124.8, 120.0, 62.5, 34.2, 30.6, 30.5, 29.6, 25.3, 20.6.

ESI HRMS *m*/*z* ($M+H^+$) calculated 342.1345, observed 342.1328.

**Electrolysis of N-(1-naphthalenylmethylene)-4-(1,3-dithian-2-ylidene)-1-pentanamine**

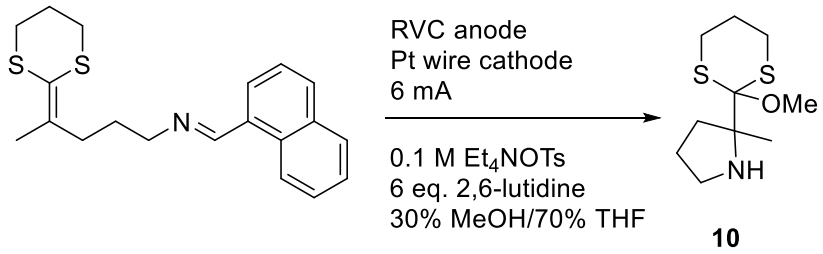


**10**

The electrolysis of *N*-(1-naphthalenylmethylene)-4-(1,3-dithian-2-ylidene)-1-pentanamine (0.0756 g, 92% purity) was carried out under similar conditions as specified in Step 6 with 2.1 F/mol of charge passed. The crude product was purified by a silica gel column (slurry packed with 1% $Et_3N$ in ether, eluted with hexanes (6) : ether (3) : MeOH (1) : $Et_3N$ (0.2)) to give 0.0284 g (60%) 2-(2-methoxy-1,3-dithian-2-yl)-2-methylpyrrolidine.

## 3.4.3 Summary of Initial Reactions and Mechanisms

### Synthesis of Substrates

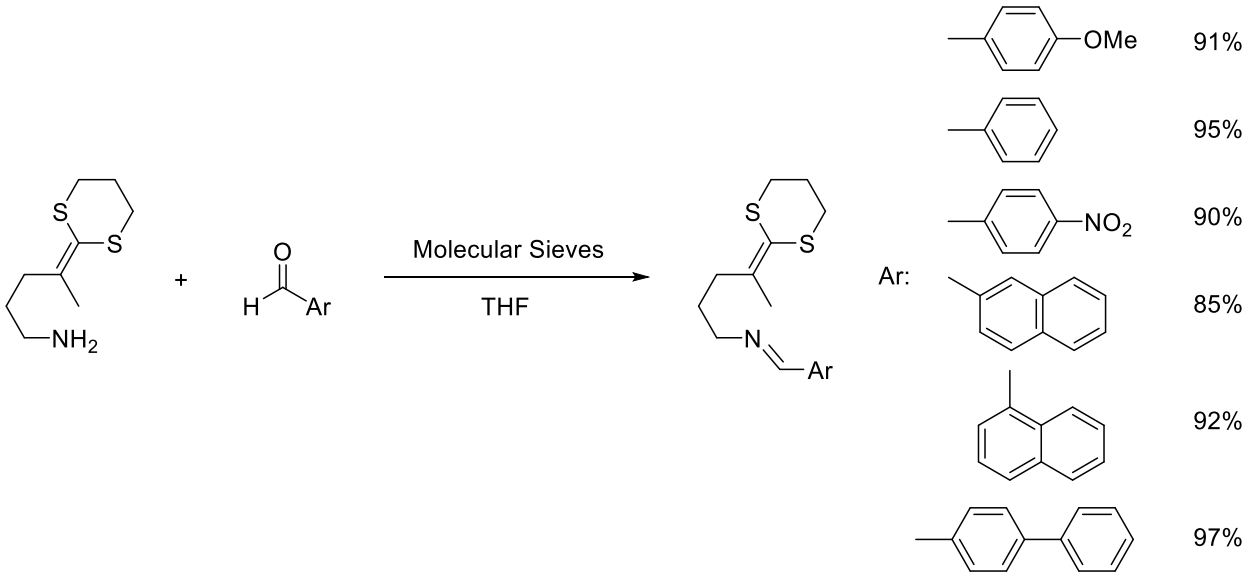


### Initial Cyclizations

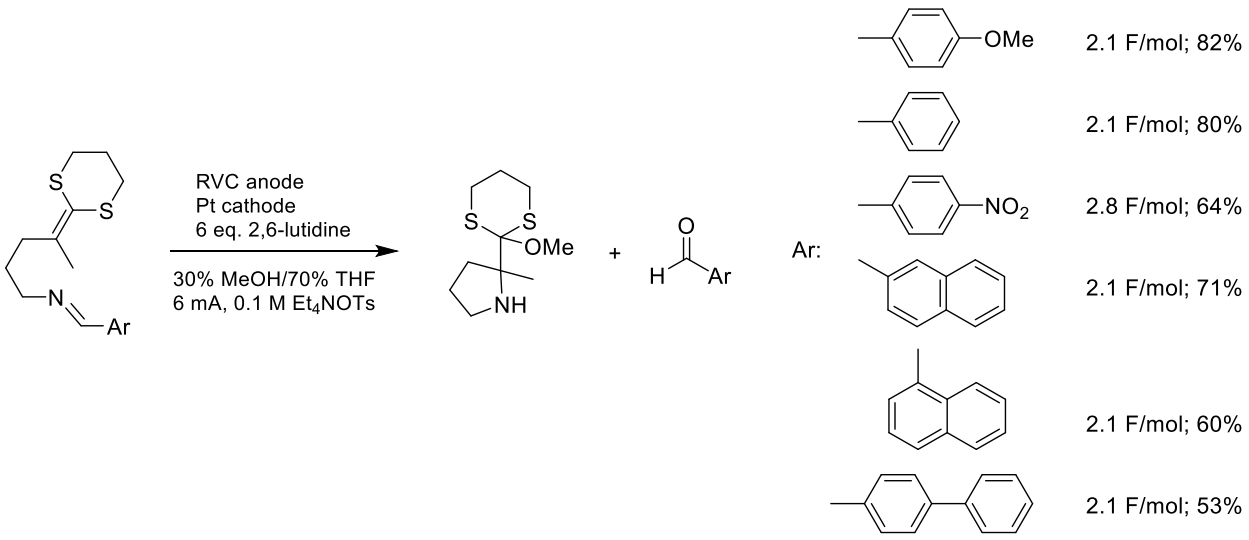

## Mechanistic Considerations

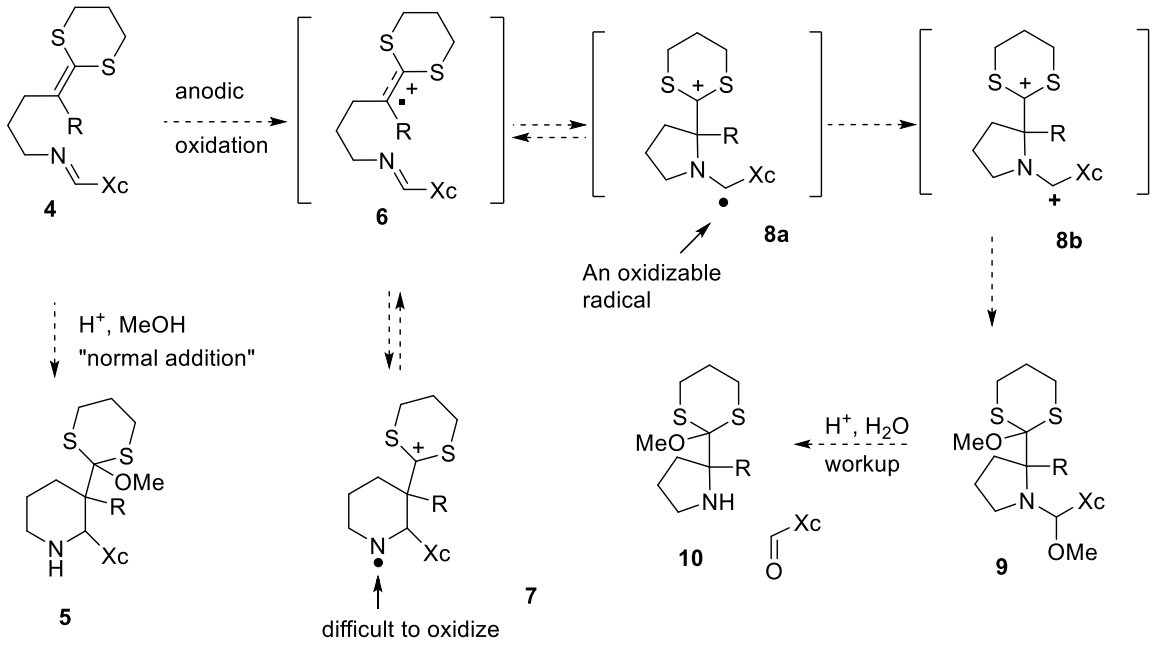

## 3.4.4 Synthesis and Electrolysis of Substrates with Chiral Auxiliaries, and HPLC Data

**The Synthesis of Substrate 17a:**

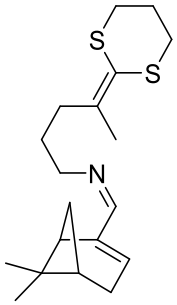

**17a**

Using the general procedure outlined above, 0.057 g of 4-(1,3-dithian-2-ylidene)-1-pentanamine and 0.043 g of (1*R*)-(-)-myrtenal were combined to afford 0.086 g of the chiral imine electrolysis substrate **17a** (92% yield, 92% purity) as yellow oil.

$^{1}$H NMR (500 MHz, $CDCl_3$) δ 7.81 (s, 1H), 5.98 (s, 1H), 3.47-3.39 (m, 2H), 2.96 (t, J = 5.6Hz, 1H), 2.87-2.82 (m, 4H), 2.48-2.41 (m, 3H), 2.35 (t, J = 7.9 Hz, 2H), 2.14-2.08 (m, 3H), 1.90 (s, 3H), 1.76-1.66 (m, 2H), 1.33 (s, 3H), 1.12 (d, J = 9Hz, 1H), 0.79 (s, 3H).

$^{13}$C NMR (126 MHz, $CDCl_3$) δ 162.1, 148.3, 140.2, 133.8, 119.4, 61.0, 41.0, 40.1, 37.6, 33.7, 32.3, 31.3, 30.3, 30.2, 29.3, 25.9, 25.0, 20.9, 20.2.

ESI HRMS *m*/*z* ($M+H^+$) calculated 336.1814, observed 336.1818.

**The Electrolysis of 17a:**

The electrolysis of *imine* **17a** (0.067 g) was carried out in the manner described above for in the general procedure for the preparative electrolysis reaction. In this case, 2.1 F/mol of charge was passed to afford approximately .008 g of the desired cyclic product (18% yield). The reaction did afford a complex mixture of products in a manner similar to the alkylimine substrates that were not stable to the electrolysis conditions. The % e.e. of the cyclic product generated was

determined with the use of a chiral HPLC column after protecting the secondary amine as the 4-bromobenzyl amide. HPLC analyses were performed on a Shimadzu LC system using 2% isopropanol in hexane and a Chiralcel OD-H analytical chiral stationary phase column (4.6 × 250 mm, Chiral Technologies, Inc.) with a UV detector at 254 nm with a flow rate of 1.0 mL/min. The benzyl amide **18** was made by the following procedure:

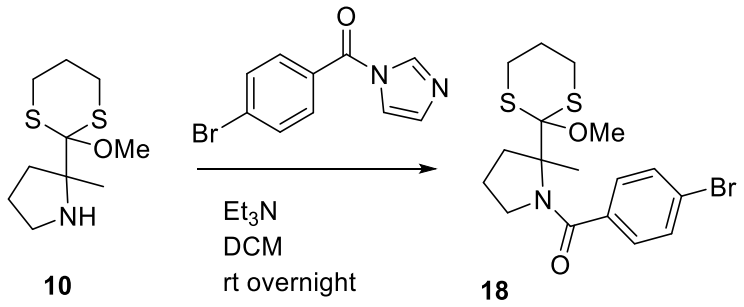


0.005g of cyclic amine **10** (1.0 eq, 0.0214mmol) in 0.5mL DCM was added to 0.0054g (4-bromophenyl)(1*H*-imidzol-1-yl)methanone (1.0 eq, 0.0214mmol) and stirred at rt. Next, 3.6μL of Triethylamine (1.2 eq 0.0257mmol) was added. The reaction was allowed to stir overnight. After stirring overnight, the reaction was diluted with diethyl ether and washed with brine. The layers were separated. The aqueous layer was extracted 2x with diethyl ether. The organic layers were combined, dried over $MgSO_4$ and concentrated in vacuo to give 0.0073g of protected cyclic amide **18** (82%).

$^1$H NMR (500 $^1$H NMR (500 MHz, $CDCl_3$) δ 7.94 (d, *J* = 8.2 Hz, 2H), 7.50 (d, *J* = 8.1 Hz, 2H), 3.57 (s, 3H), 3.25-3.17 (m, 1H), 3.15-3.06 (m, 1H), 3.04-2.94 (m, 2H), 2.88-2.76 (m, 2H), 2.37-2.27 (m, 1H), 2.07-1.96 (m, 1H), 1.92-1.79 (m, 2H), 1.73-1.62 (m, 1H), 1.5 (s, 3H).

$^{13}$C NMR (126 MHz, $CDCl_3$) δ 170.9, 132.2, 131.1, 126.0, 121.3, 100.6, 74.6, 52.9, 46.8, 35.2, 29.7, 28.0, 23.17.

The data obtained for the amide derivative is shown below. The % e.e. was determined by comparison to the HPLC trace obtained for the racemic product.

*HPLC trace for the racemic material:*

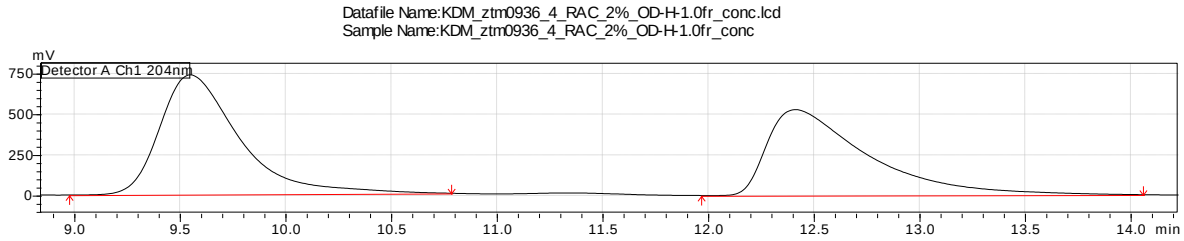


| Peak# | Ret. Time | Area | Height | Area% |
|---|---|---|---|---|
| 1 | 9.55 | 19160140 | 735186 | 52.531 |
| 2 | 12.414 | 17313910 | 527112 | 47.469 |
| Total | | 36474050 | 1262298 | 100 |

*HPLC for the product derived from oxidation of **17a***:

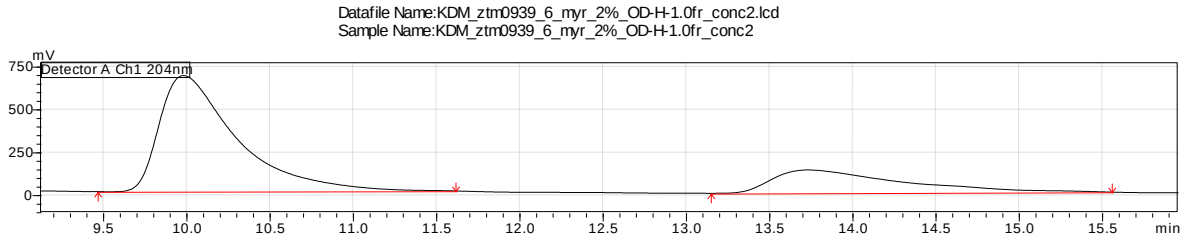


| Peak# | Ret. Time | Area | Height | Area% |
|---|---|---|---|---|
| 1 | 9.984 | 21658857 | 676419 | 75.219 |
| 2 | 13.734 | 7135436 | 134194 | 24.781 |
| Total | | 28794293 | 810613 | 100 |

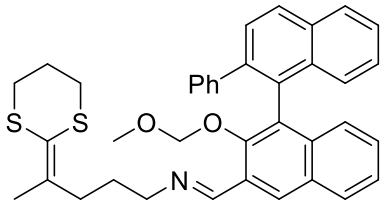


**The Synthesis of Substrate 17b: The 10*R*-imine ($C_{38}H_{37}O_2S_2N$)[1]**

Using the general procedure outlined above, 38 mg 4-(1,3-dithian-2-ylidene)-1-pentanamine and 77 mg 10***R*** were combined to afford 0.104 g product (93% yield, 91% purity) as white solid.

$^{1}$H NMR (500 MHz, $CDCl_3$) δ 8.61 (s, 1H), 8.47 (s, 1H), 8.03 (d, J = 8.5 Hz, 1H), 7.95 (d, J= 8.3 Hz, 1H), 7.91 (d, J = 8.2 Hz, 1H), 7.67 (d, J = 8.5 Hz, 1H), 7.47 (ddd, J = 8.1, 6.5, 1.4 Hz, 1H), 7.38 (ddd, J = 8.1, 6.6, 1.4 Hz, 1H), 7.30-7.22 (m, 4H), 7.12-7.09 (m, 2H), 7.04-7.01 (m, 3H), 4.57 (d, J = 5.5Hz, 1H), 4.33 (d, J = 5.4 Hz, 1H), 3.66-3.58 (m, 2H), 2.87-2.80 (m, 4H), 2.77 (s, 3H), 2.48-2.41 (m, 2H), 2.11-2.06 (m, 2H), 1.94 (s, 3H), 1.87-1.81 (m, 2H).

$^{13}$C NMR (126 MHz, $CDCl_3$) δ 158.2, 151.7, 141.7, 140.6, 139.9, 135.7, 133.4, 132.6, 131.0, 130.2, 129.2, 129.1, 128.7, 128.6, 128.5, 128.4, 128.3, 128.1, 128.0, 127.5, 127.4, 126.9, 126.5, 126.2, 125.8, 125.2, 119.7, 99.1, 61.7, 56.6, 33.8, 30.2, 30.1, 29.2, 25.0, 20.2.

ESI HRMS *m*/*z* ($M+H^+$) calculated 604.2339, observed 604.2330.

**The Electrolysis of 17b:**

The electrolysis of *imine* **17b** (0.102 g) was carried out in the manner described above for in the general procedure for the preparative electrolysis reaction. In this case, 2.1 F/mol of charge passed to give product 2-(2-methoxy-1,3-dithian-2-yl)-2-methylpyrrolidine in a 16% yield as determined by proton NMR. Once again, the reaction led to a complex mixture of products out of which the desired cyclic product was identified since it is the same product generated from each of the imine cyclizations. For the electrolysis of **17b**, the % e.e. of the cyclic product generated was determined with the use of a chiral HPLC column after protecting the secondary amine as the 4-bromobenzyl amide. The benzyl amide was prepared and the analysis performed as outlined for **17a**. The data obtained for this study is shown below. The % e.e. was determined by comparison to the HPLC trace obtained for the racemic product shown above.

*HPLC for the product derived from the oxidation of **17b***:

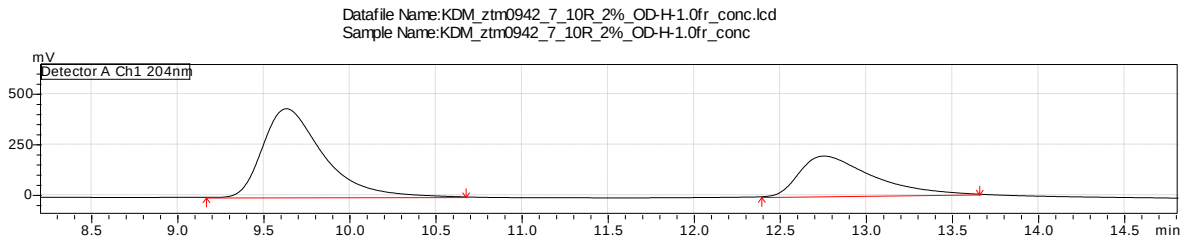


| Peak # | Ret. Time | Area | Height | Area% |
|---|---|---|---|---|
| 1 | 9.634 | 10630876 | 437573 | 64.929 |
| 2 | 12.756 | 5742144 | 197838 | 35.071 |
| Total | | 16373021 | 635410 | 100 |

**The Synthesis of Substrate 17c: The 10*S*-imine ($C_{38}H_{37}O_2S_2N$)[1]**

Using the general procedure outlined above, 39 mg 4-(1,3-dithian-2-ylidene)-1-pentanamine and 80 mg 10***S*** were used to give 0.108 g product (93% yield, 93% purity) as white solid.

$^1$H NMR (500 MHz, $CDCl_3$) δ 8.60 (s, 1H), 8.47 (s, 1H), 8.03 (d, J = 8.5 Hz, 1H), 7.95 (d, J = 8.3 Hz, 1H), 7.91 (d, J= 8.2 Hz, 1H), 7.67 (d, J = 8.5 Hz, 1H), 7.47 (ddd, J = 8.1, 6.5, 1.3 Hz, 1H), 7.38 (ddd, J = 8.1, 6.5, 1.3 Hz, 1H), 7.31-7.22 (m, 4H), 7.11-7.10 (m, 2H), 7.05-7.02 (m, 3H), 4.56 (d, J = 5.5 Hz, 1H), 4.33 (d, J = 5.5 Hz, 1H), 3.67-3.58 (m, 2H), 2.88-2.80 (m, 4H), 2.78 (s, 3H), 2.47-2.41 (m, 2H), 2.12-2.07 (m, 2H), 1.94 (s, 3H), 1.87-1.81 (m, 2H).

$^{13}$C NMR (126 MHz, $CDCl_3$) δ 158.2, 151.7, 141.7, 140.6, 139.9, 135.7, 133.4, 132.6, 131.0, 130.3, 129.2, 129.1, 128.7, 128.6, 128.5, 128.4, 128.3, 128.1, 128.0, 127.5, 127.4, 126.9, 126.6, 126.2, 125.8, 125.2, 119.7, 99.1, 61.7, 56.6, 33.8, 30.3, 30.1, 29.2, 25.0, 20.2.

ESI HRMS *m*/*z* ($M+H^+$) calculated 604.2339, observed 604.2331.

**The Electrolysis of 17c:**

The electrolysis of *imine* **17c** (0.107 g) was carried out in the manner described above for in the general procedure for the preparative electrolysis reaction. In this case, 2.1 F/mol of charge passed to give product 2-(2-methoxy-1,3-dithian-2-yl)-2-methylpyrrolidine in a 45% yield as

determined by proton NMR. Once again, the reaction led to a complex mixture of products out of which the desired cyclic product was identified since it is the same product generated from each of the imine cyclizations. For the electrolysis of **17c**, the % e.e. of the cyclic product generated was determined with the use of a chiral HPLC column after protecting the secondary amine as the 4-bromobenzyl amide. The benzyl amide was prepared and the analysis performed as outlined for **17a**. The data obtained for this study is shown below. The % e.e. was determined by comparison to the HPLC trace obtained for the racemic product shown above.

*HPLC for the product derived from the oxidation of **17c***:

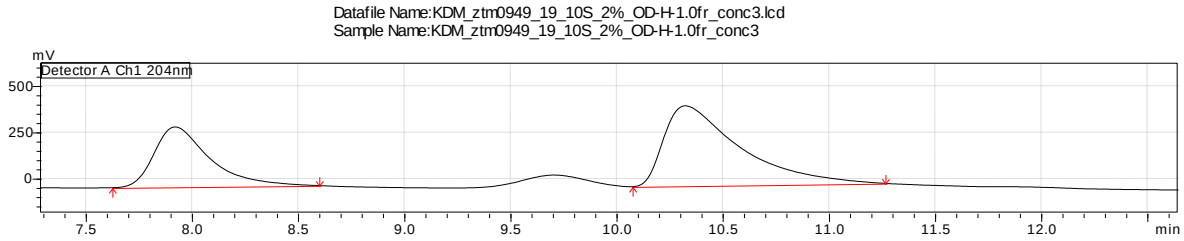


| Peak# | Ret. Time | Area | Height | Area% |
|---|---|---|---|---|
| 1 | 7.922 | 5902015 | 324478 | 35.453 |
| 2 | 10.326 | 1075511 | 433186 | 64.547 |
| Total | | 16647526 | 757664 | 100 |

## 3.4.5 $^{1}$H and $^{13}$C NMR Spectra

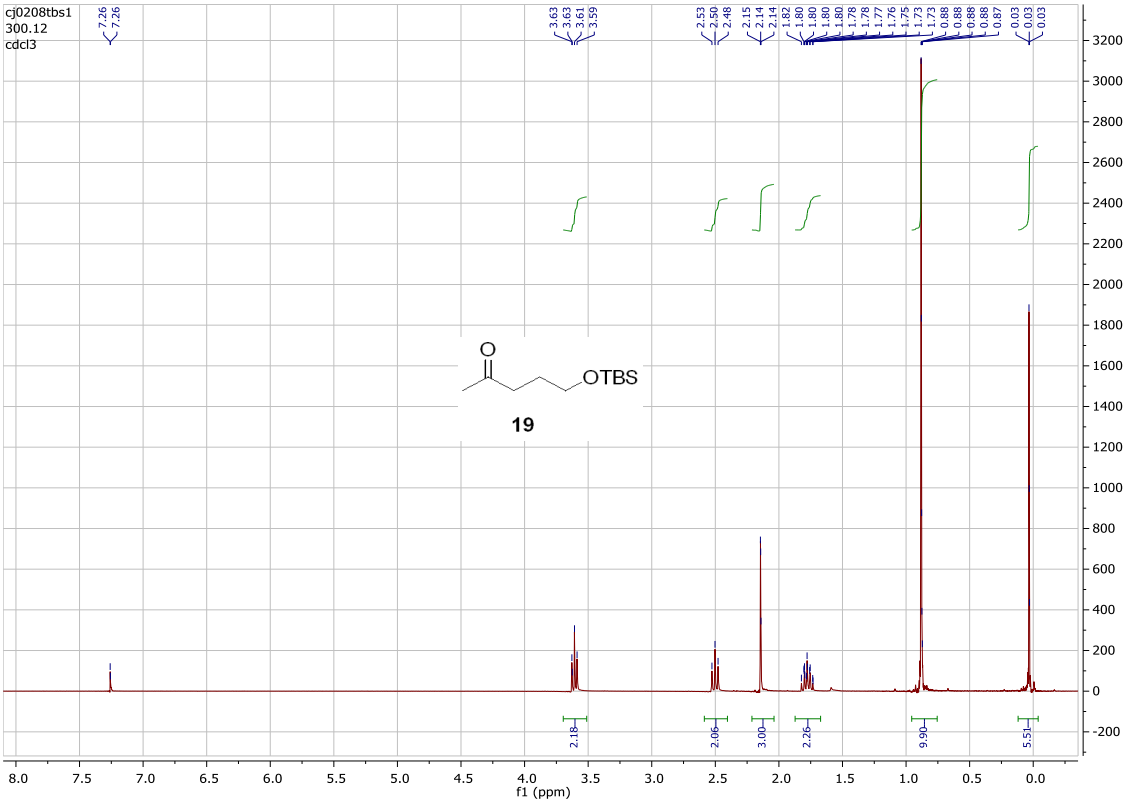


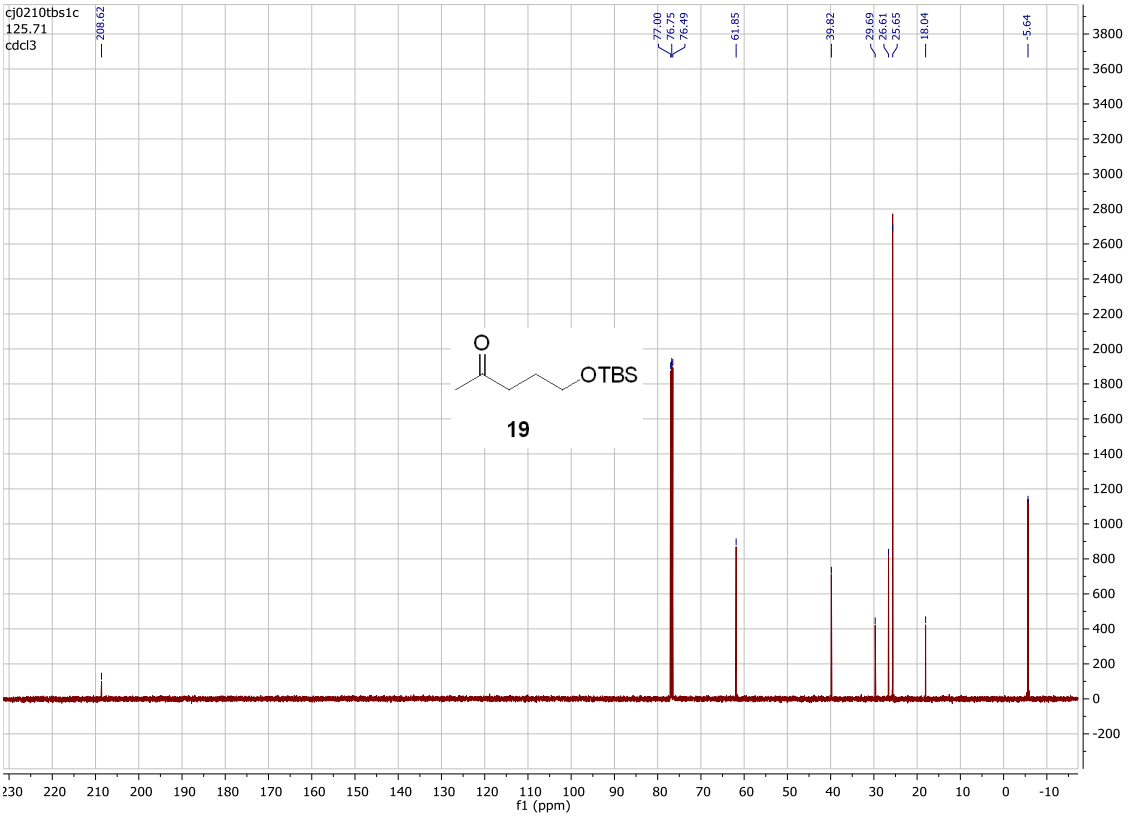

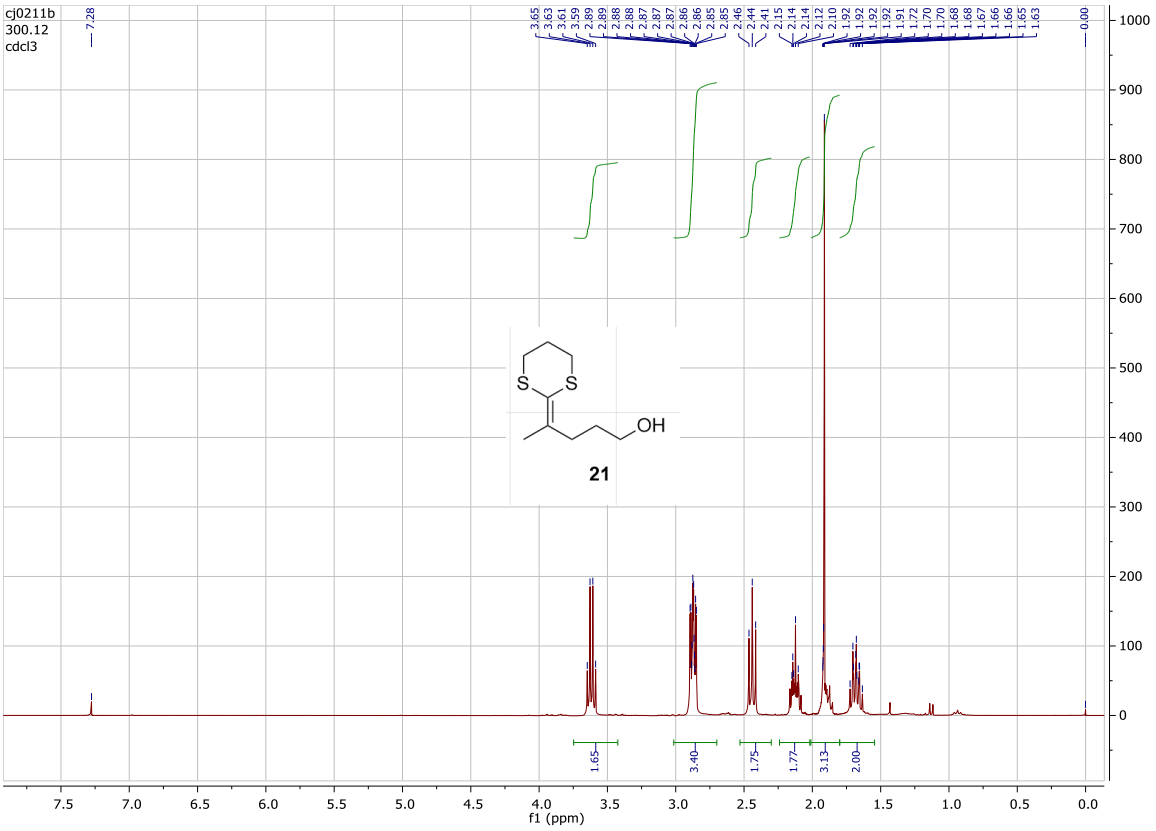
cj0211b
300.12
cdcl3
7.28
0.00
S
S
OH
21
1.65
3.40
1.75
1.77
3.13
2.00
f1 (ppm)

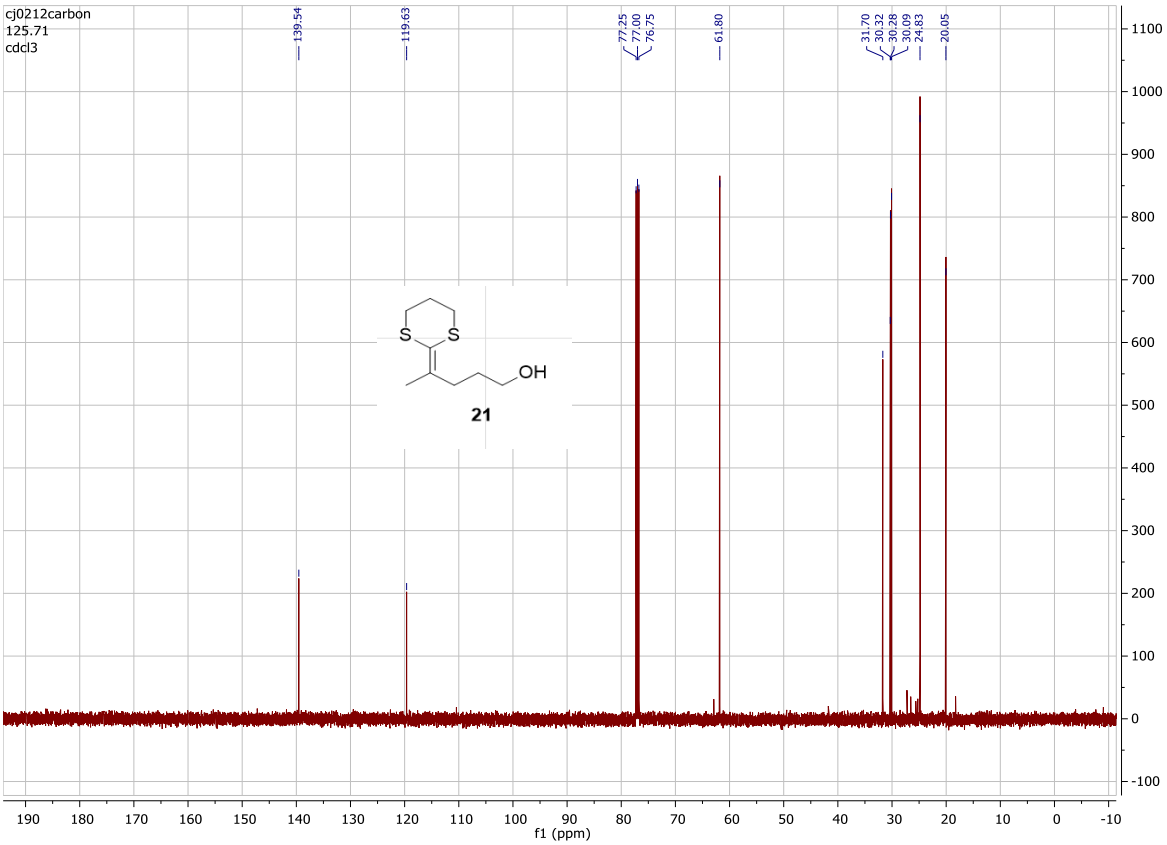
cj0212carbon
125.71
cdcl3
139.54
119.63
77.25
77.00
76.75
61.80
31.70
30.32
30.28
30.09
24.83
20.05
S
S
OH
21
f1 (ppm)

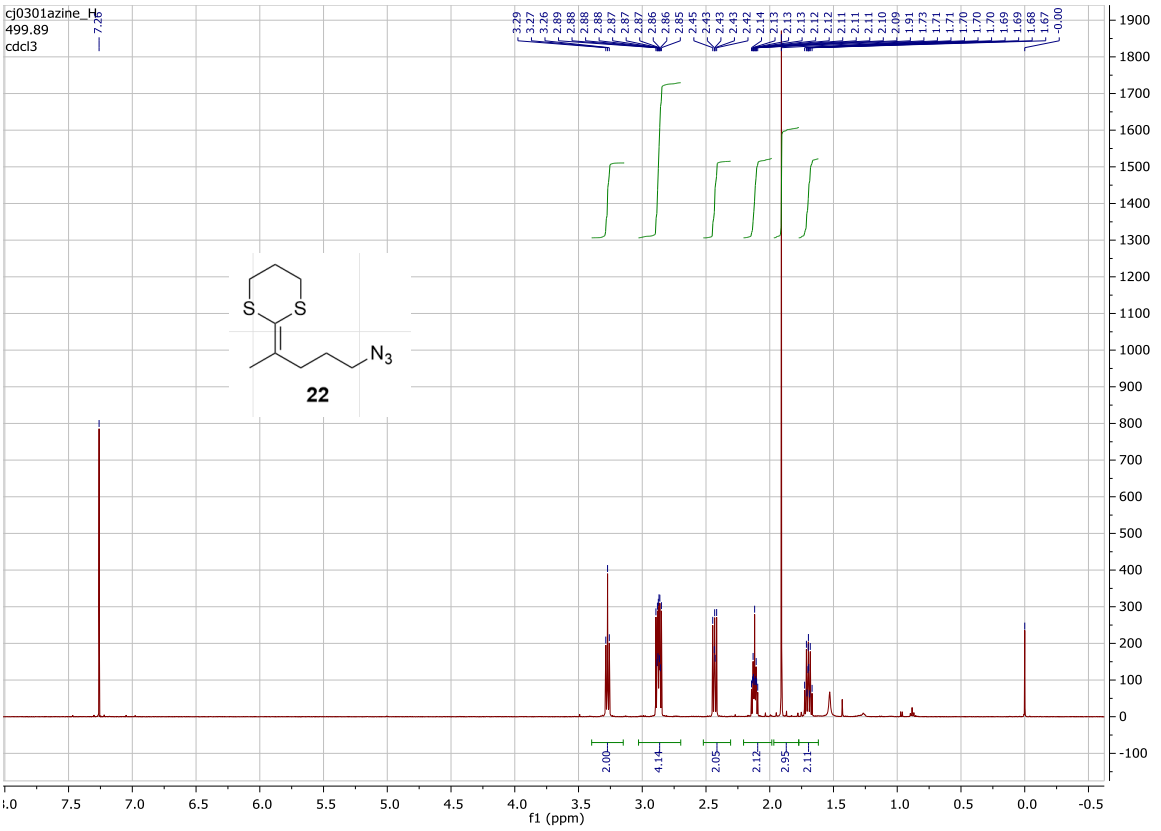
cj0301azine_H
499.89
cdcl3
22
f1 (ppm)

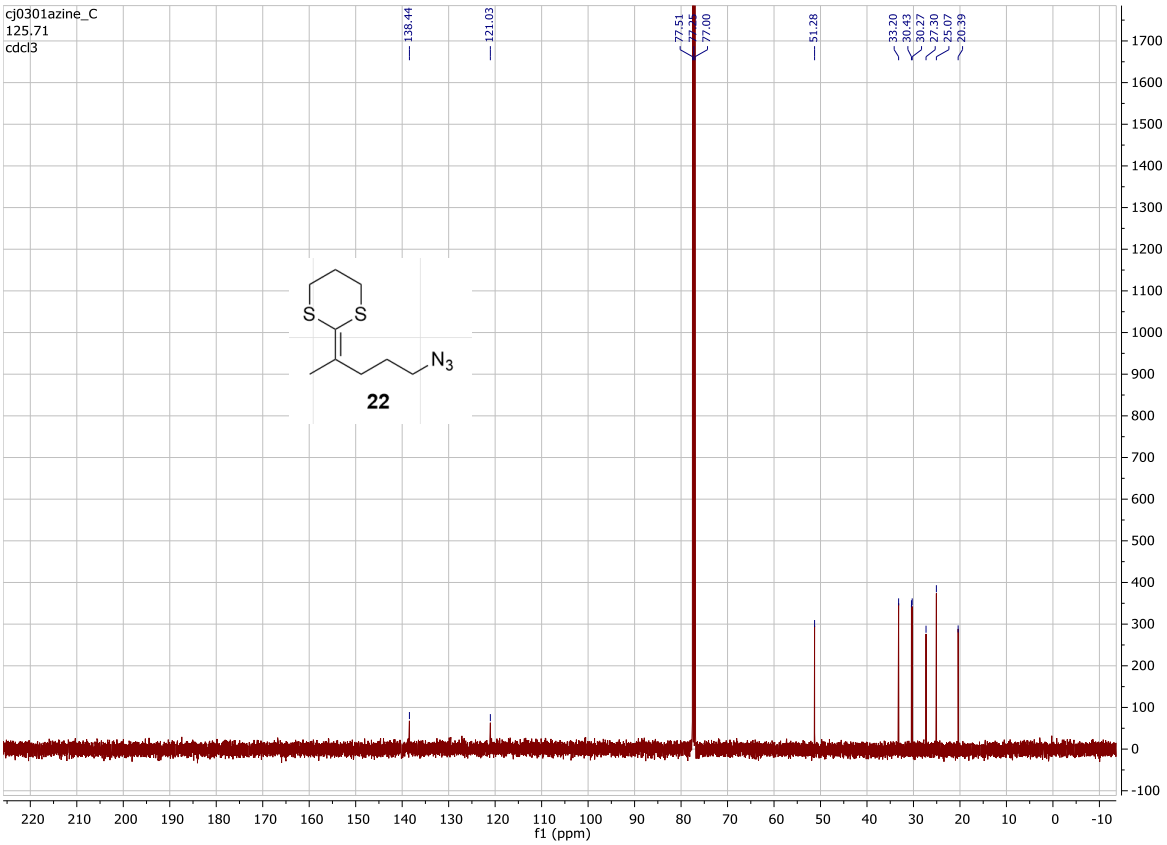
cj0301azine_C
125.71
cdcl3
22
f1 (ppm)

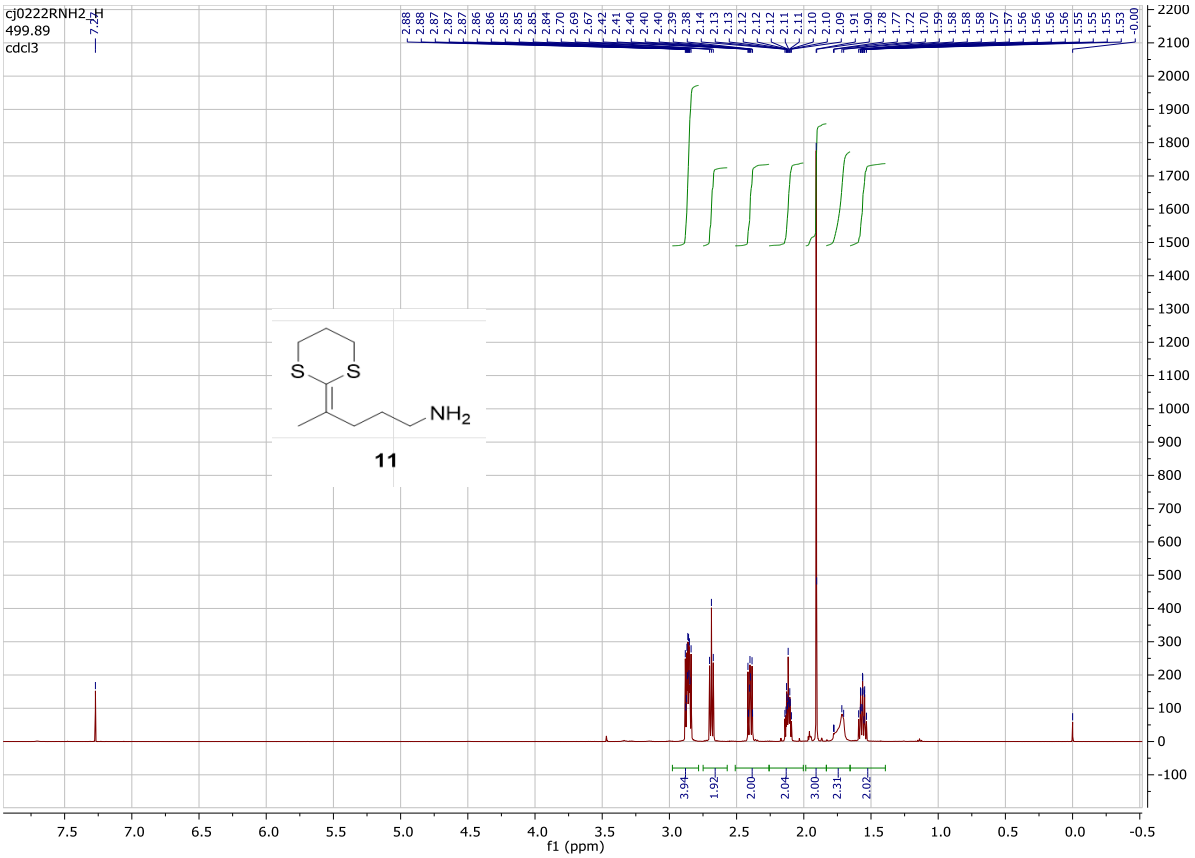
cj0222RNH2_H
499.89
cdcl3
7.27
S
S
NH2
11
3.94
1.92
2.00
2.04
3.00
2.31
2.02
f1 (ppm)

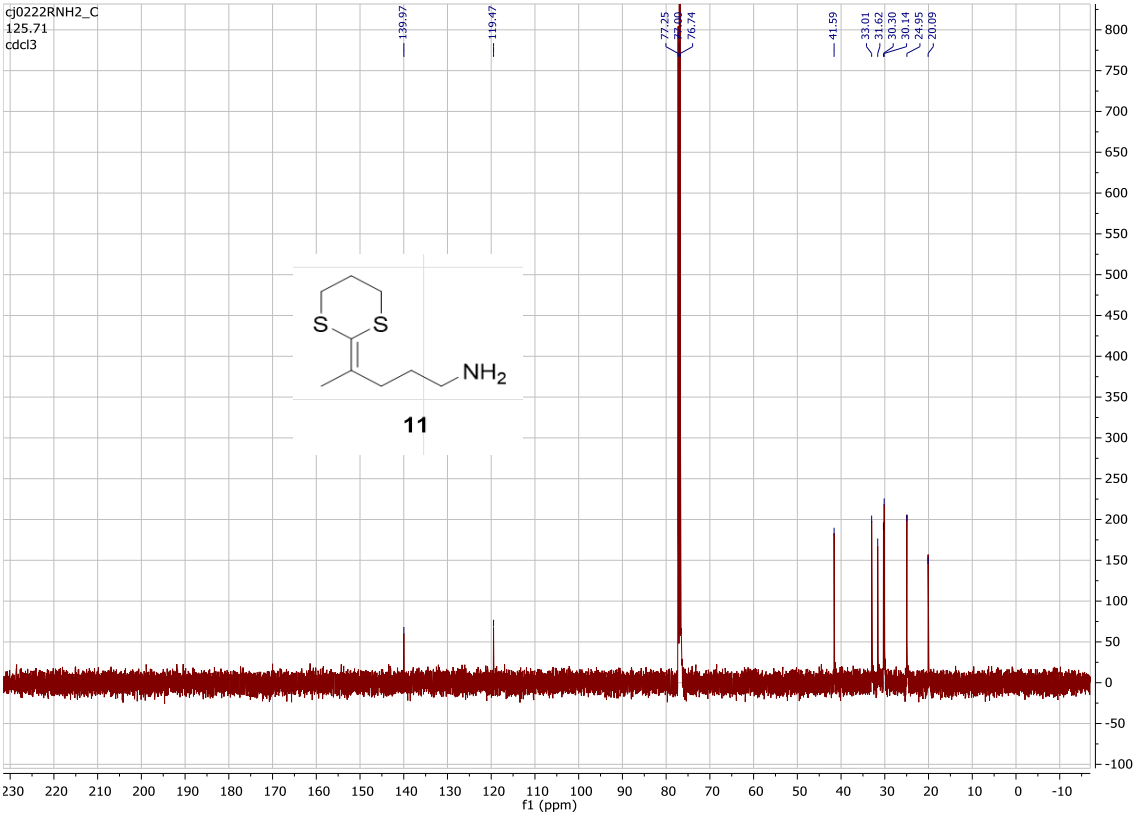
cj0222RNH2_C
125.71
cdcl3
139.97
119.47
77.25
77.00
76.74
41.59
33.01
31.62
30.30
30.14
24.95
20.09
S
S
NH2
11
f1 (ppm)

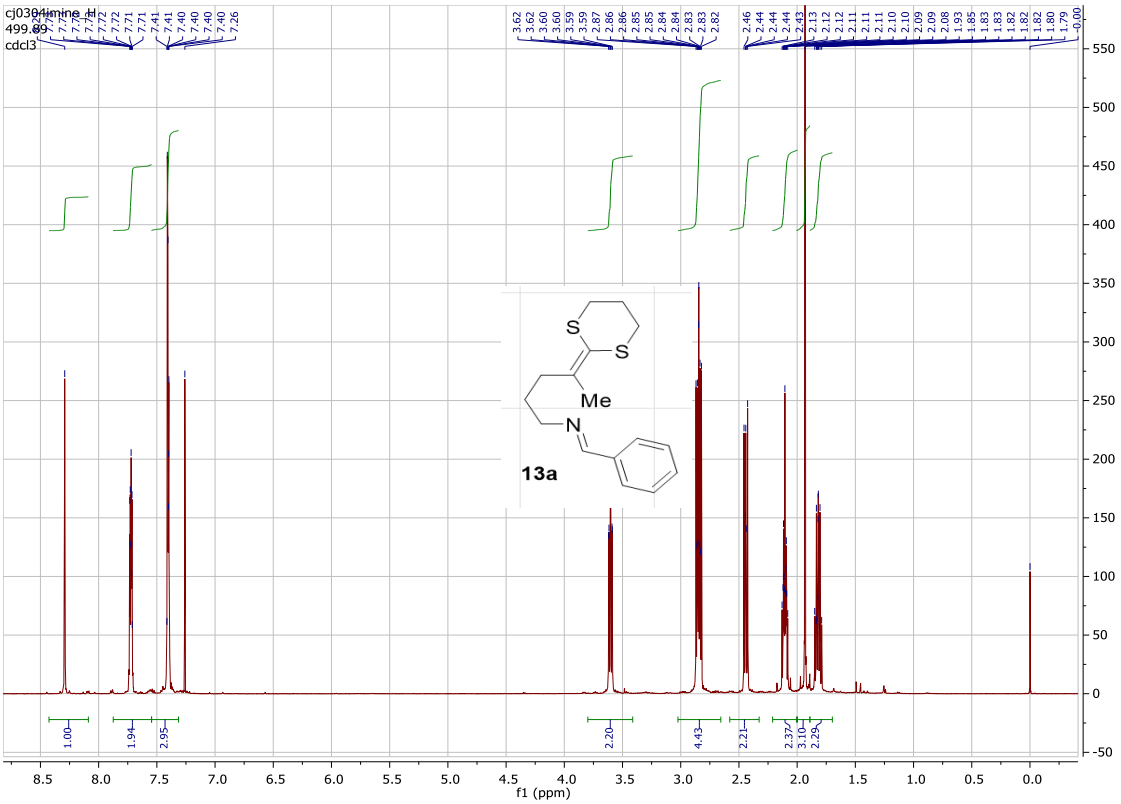
cj0304imine_H
499.89
cdcl3
13a
f1 (ppm)

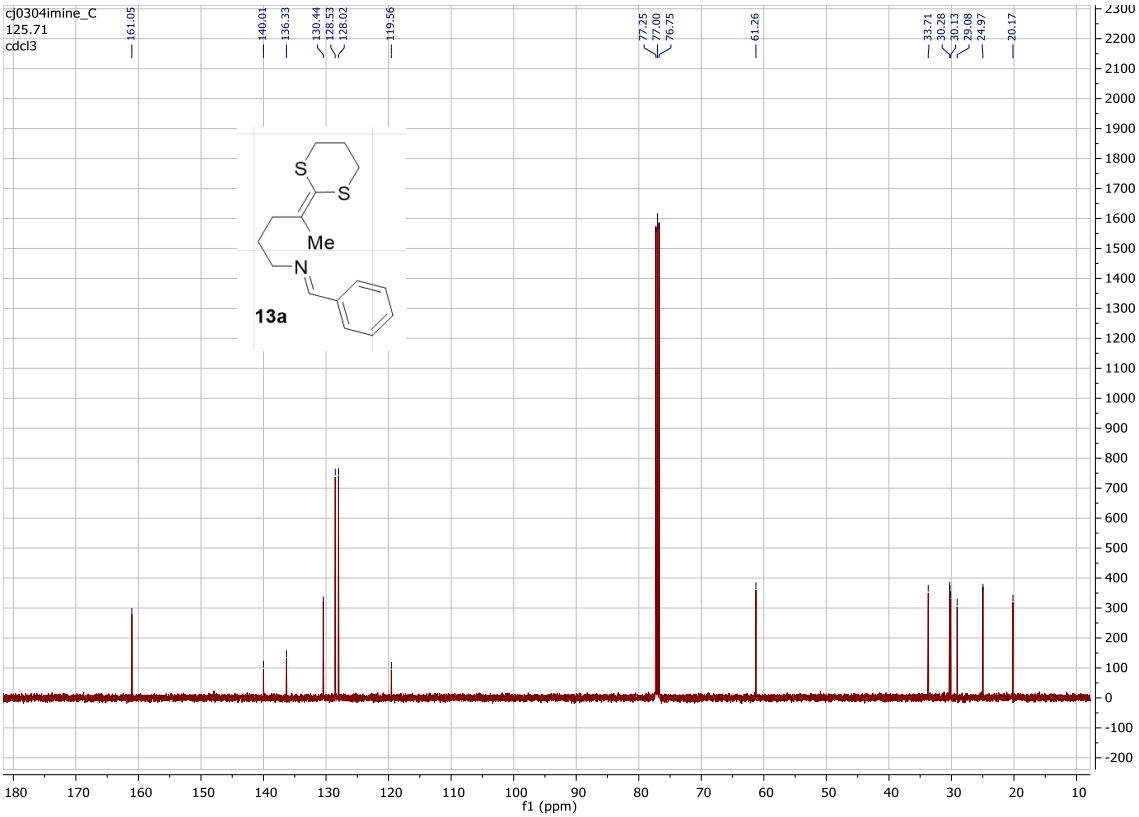
cj0304imine_C
125.71
cdcl3
13a
f1 (ppm)

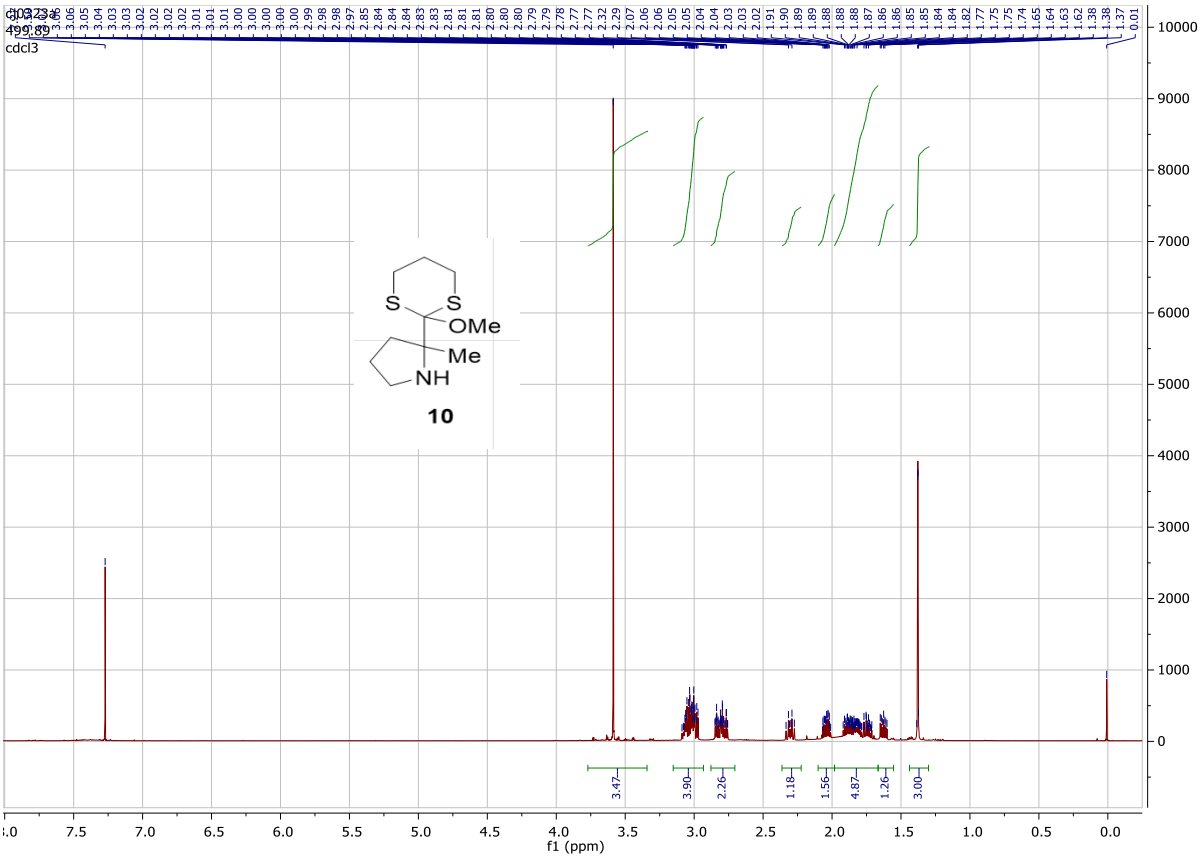
cdcl3
S
S
OMe
Me
NH
10
f1 (ppm)

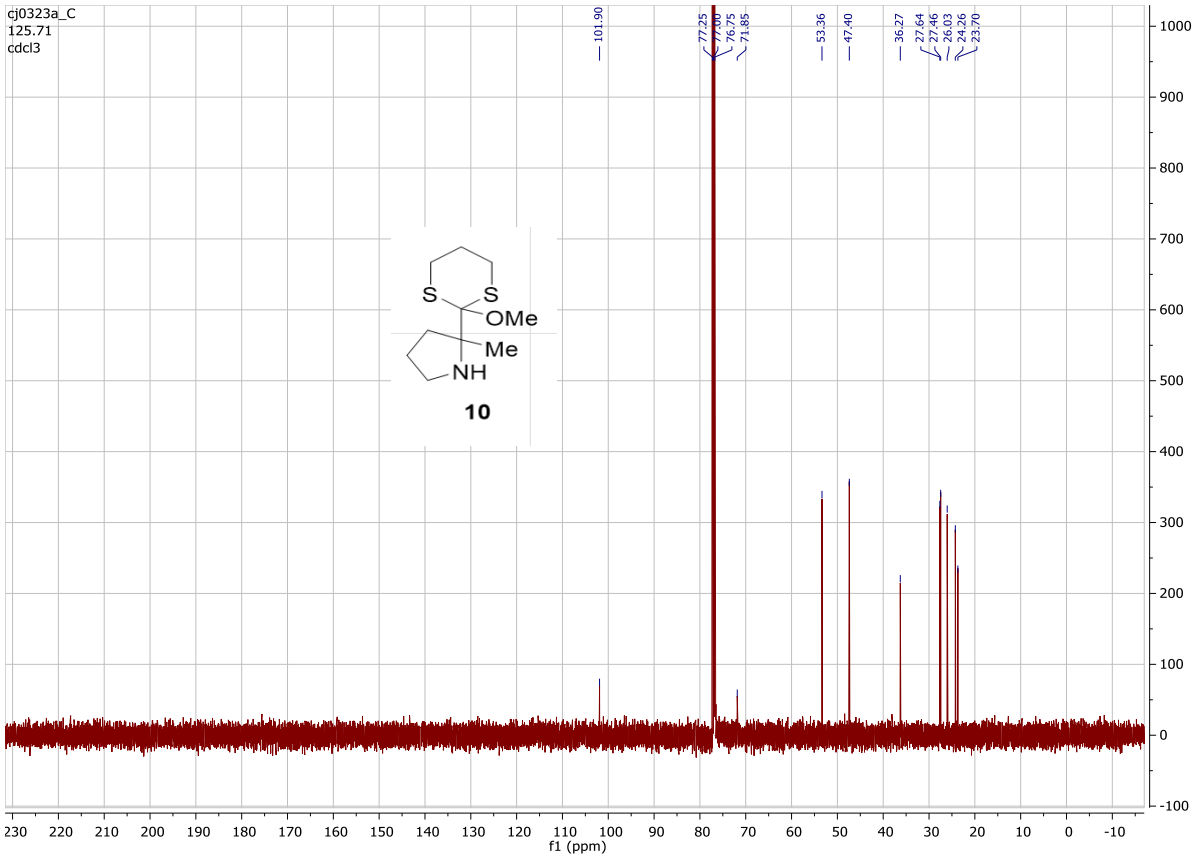
cj0323a_C
125.71
cdcl3
101.90
77.25
77.00
76.75
71.85
53.36
47.40
36.27
27.64
27.46
26.03
24.26
23.70
S
S
OMe
Me
NH
10
f1 (ppm)

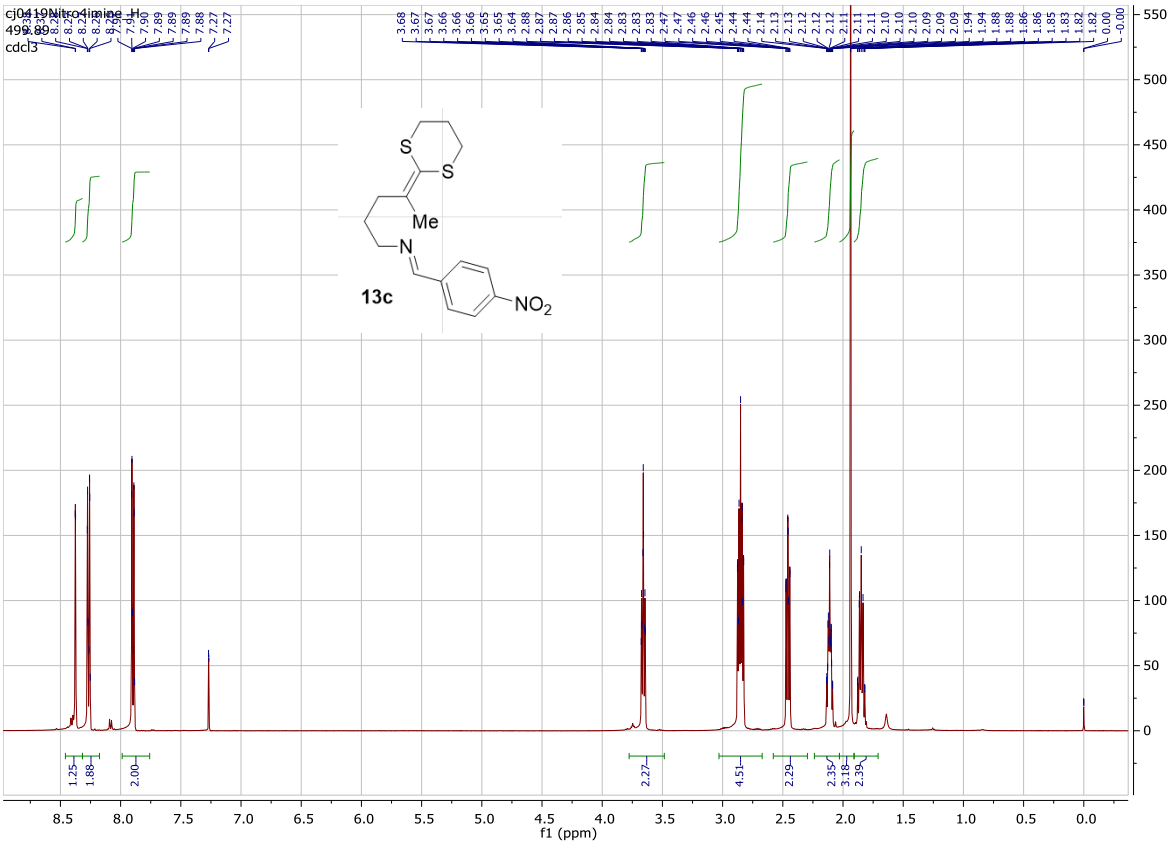
cj0419Nitro4imine_H
499.89
cdcl3
S
S
Me
N
13c
NO2
f1 (ppm)

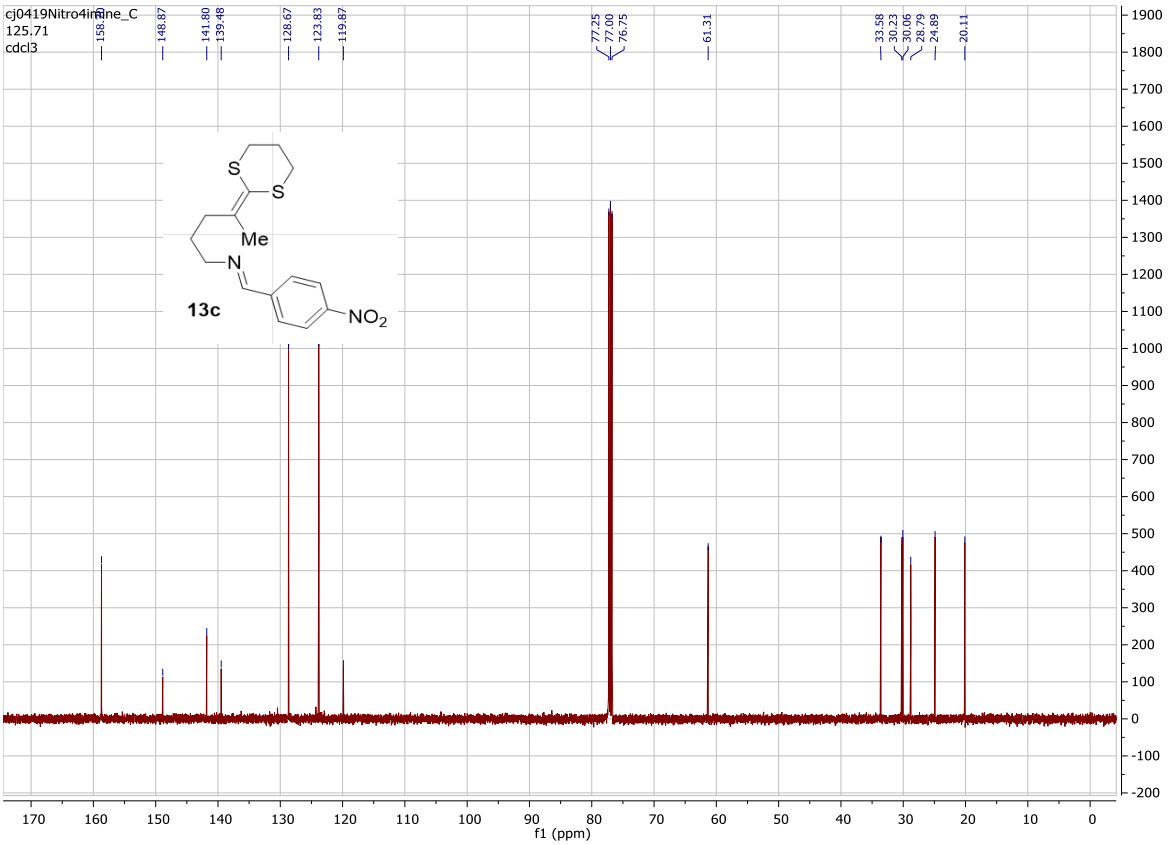
cj0419Nitro4imine_C
125.71
cdcl3
S
S
Me
N
13c
NO2
f1 (ppm)

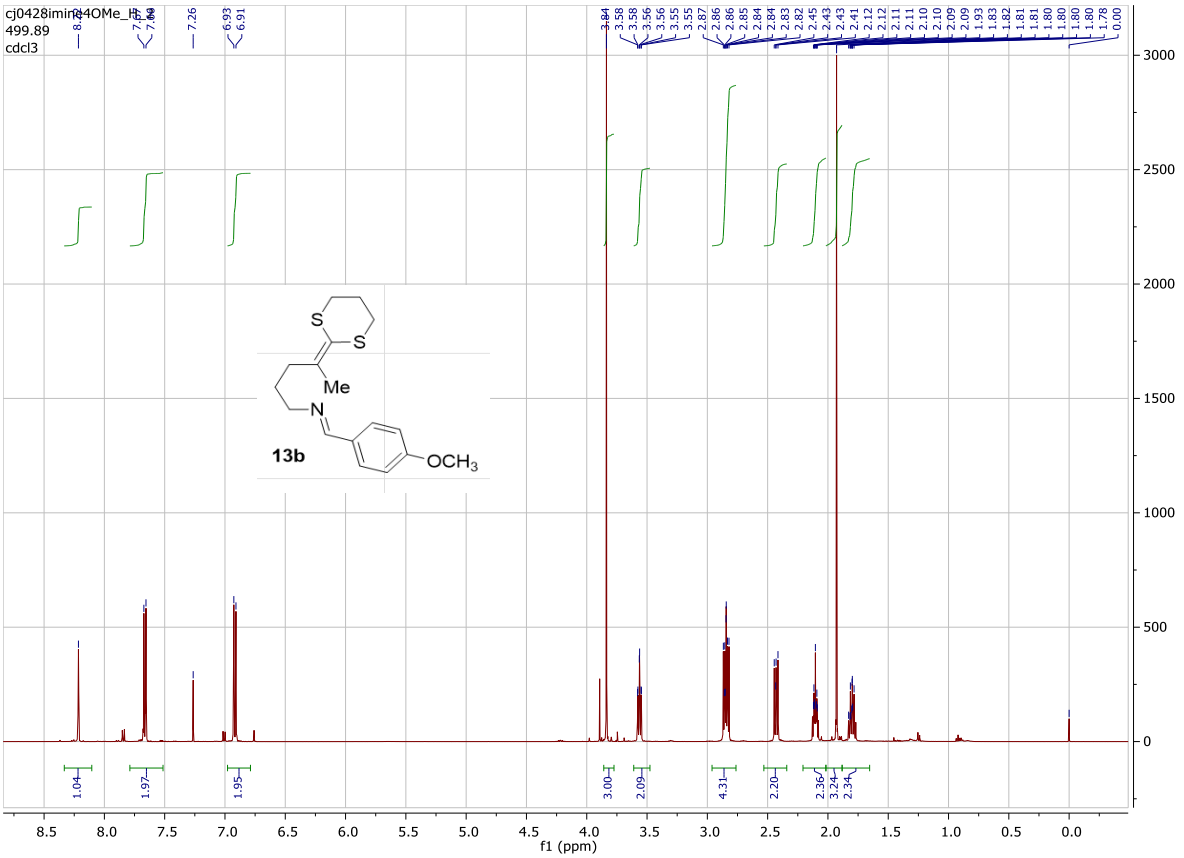
499.89
cdcl3
13b
Me
N
S
S
OCH3
f1 (ppm)

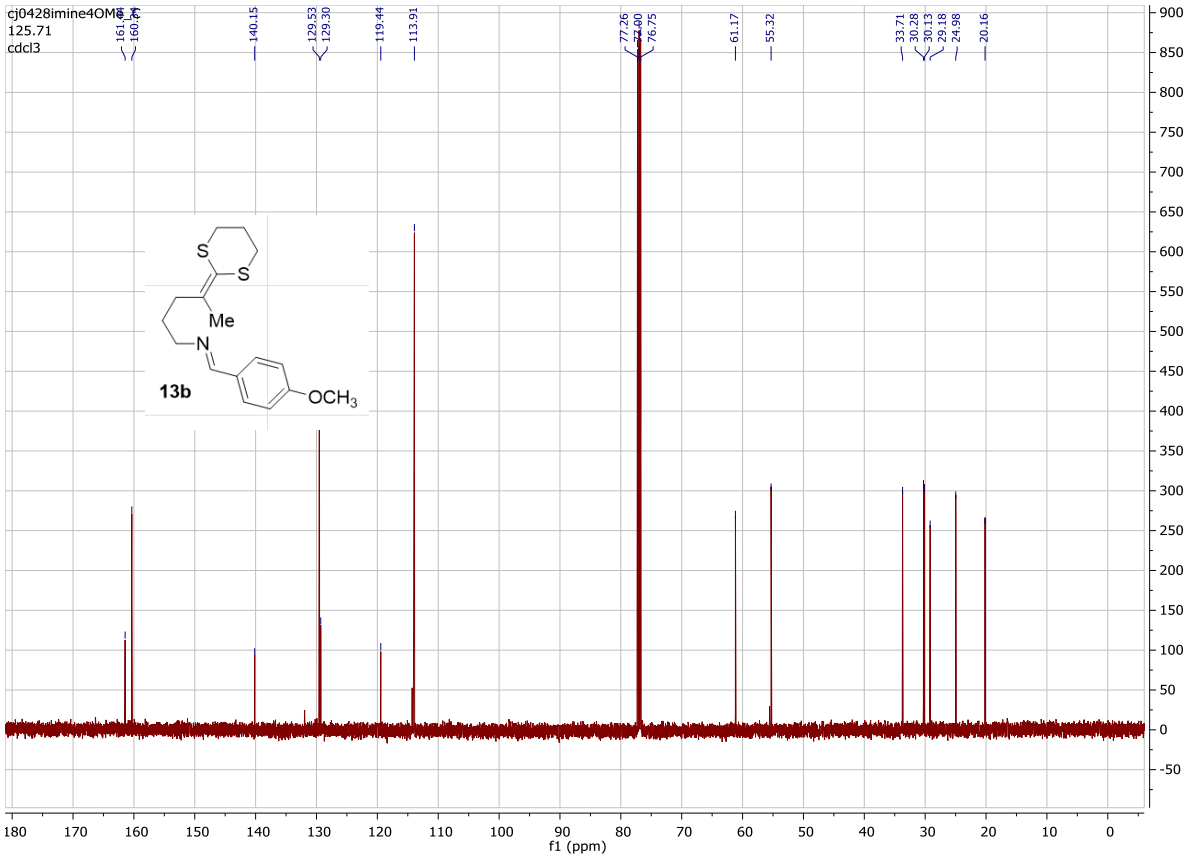
cj0428imine4OMe_C
125.71
cdcl3
161.47
160.17
140.15
129.53
129.30
119.44
113.91
77.26
77.00
76.75
61.17
55.32
33.71
30.28
30.13
29.18
24.98
20.16
S
S
Me
N
OCH3
13b
f1 (ppm)

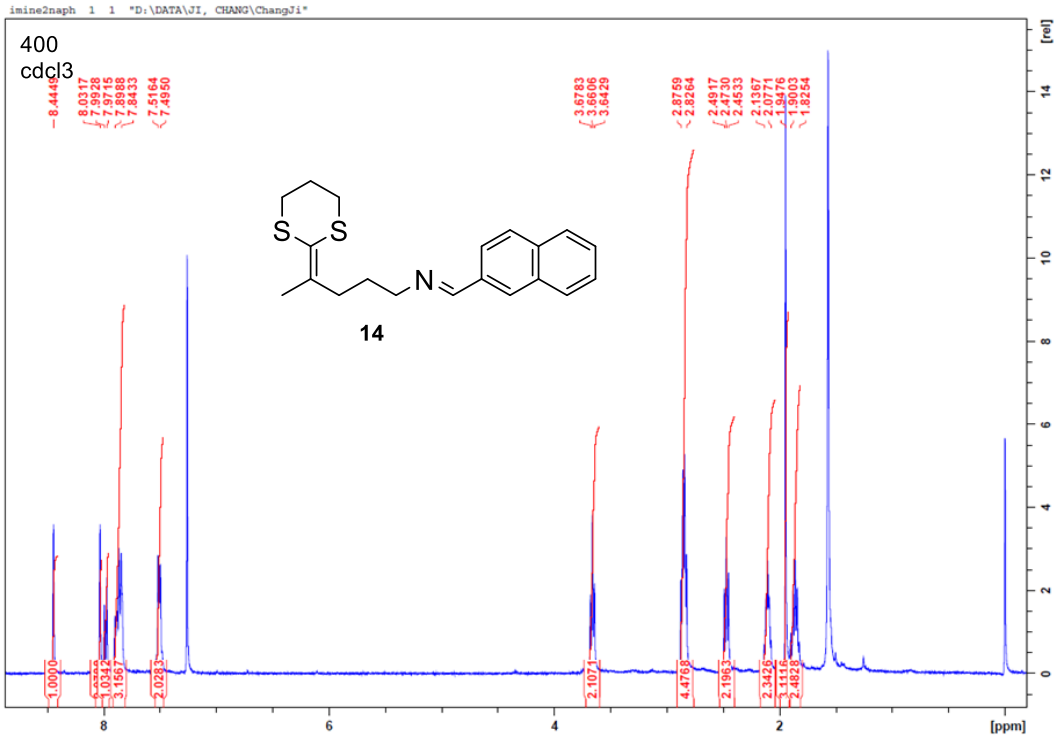
imine2naph 1 1 "D:\DATA\JI, CHANG\ChangJi"
400
cdcl3
8.4482
8.0317
7.9928
7.9715
7.8988
7.8433
7.5164
7.4950
3.6783
3.6606
3.6429
2.8759
2.8264
2.4917
2.4730
2.4533
2.1367
2.0771
1.9476
1.9003
1.8254
S
S
N
14
[ppm]
[rel]

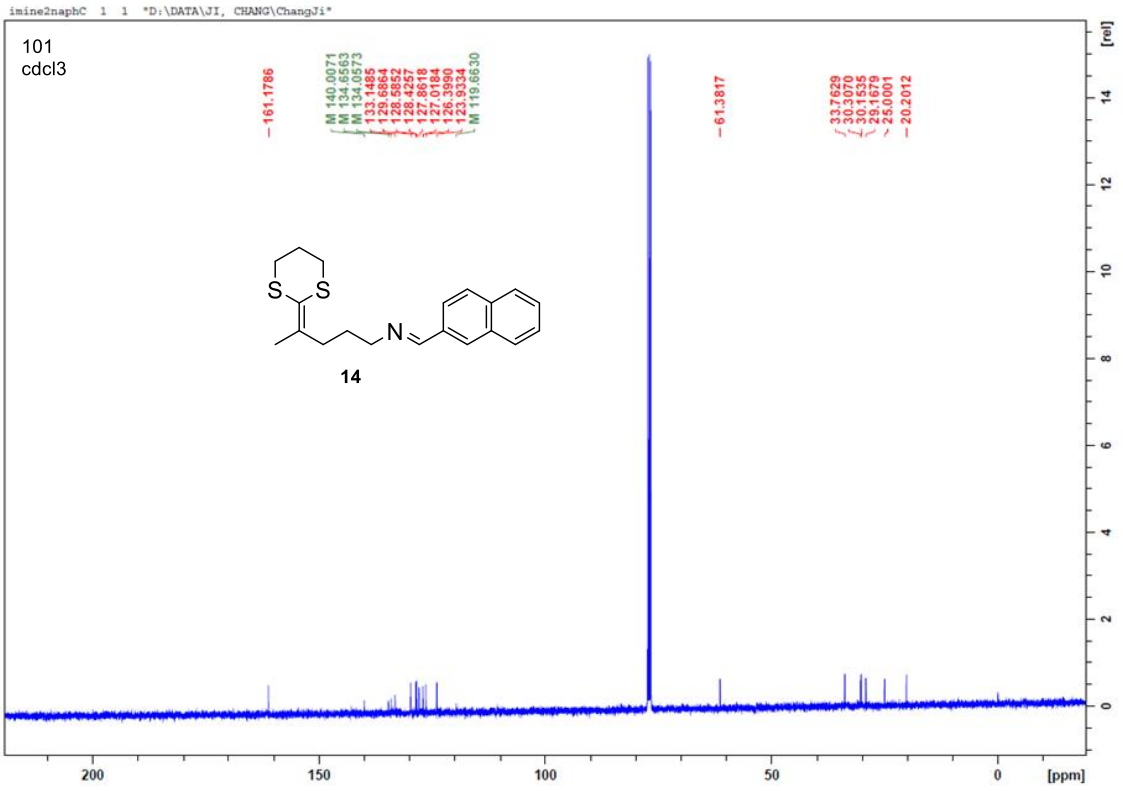
imine2naphC 1 1 "D:\DATA\JI, CHANG\ChangJi"
101
cdcl3
161.1786
M 140.0071
M 134.6563
M 134.0573
133.1485
129.6865
128.5852
128.4257
127.8618
127.0184
126.3990
123.9334
M 119.6630
61.3817
33.7629
30.3070
30.1525
29.1579
25.0001
20.2012
14
[rel]
[ppm]

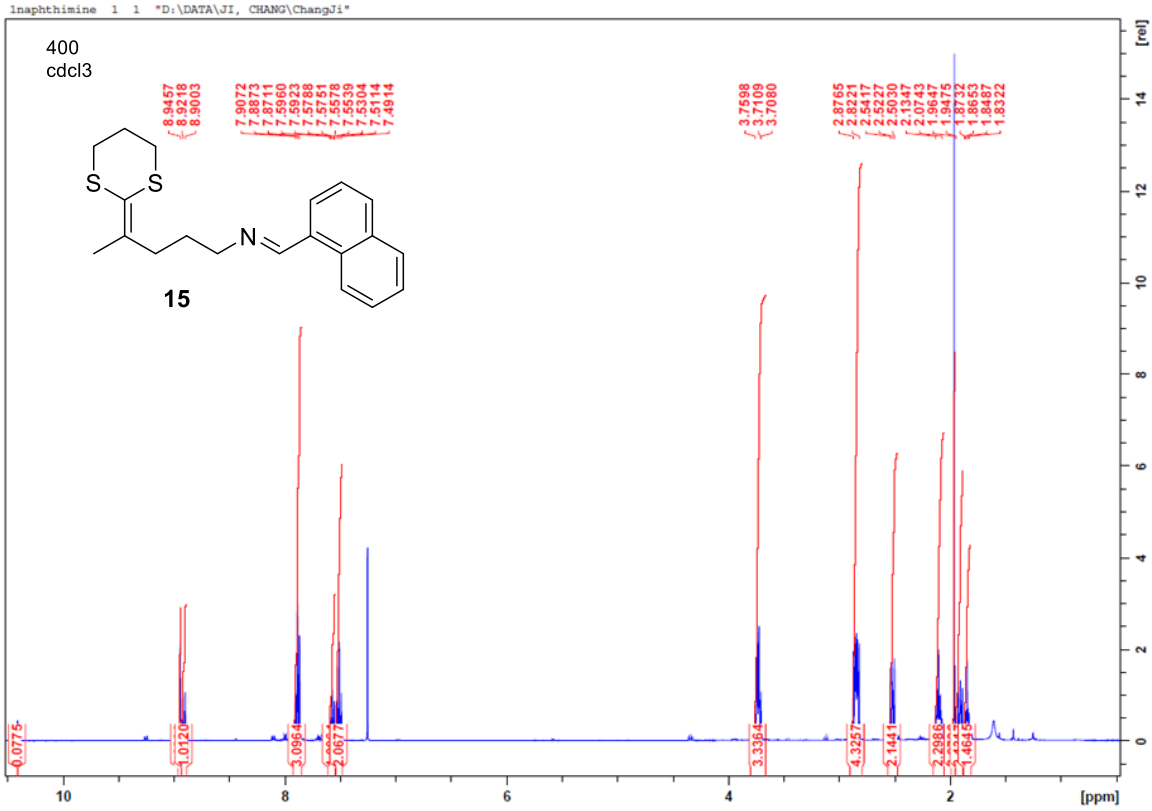
1naphthimine 1 1 "D:\DATA\JI, CHANG\ChangJi"
400
cdcl3
8.9457
8.9218
8.9003
7.9072
7.8873
7.8711
7.5960
7.5923
7.5788
7.5751
7.5578
7.5539
7.5304
7.5114
7.4914
3.7598
3.7109
3.7080
2.8765
2.8221
2.5417
2.5227
2.5030
2.1347
2.0743
1.9647
1.9475
1.8732
1.8553
1.8437
1.8322
15
0.0775
1.0120
3.0964
2.0677
3.3364
4.3257
2.1441
2.2986
1.4645
[rel]
[ppm]

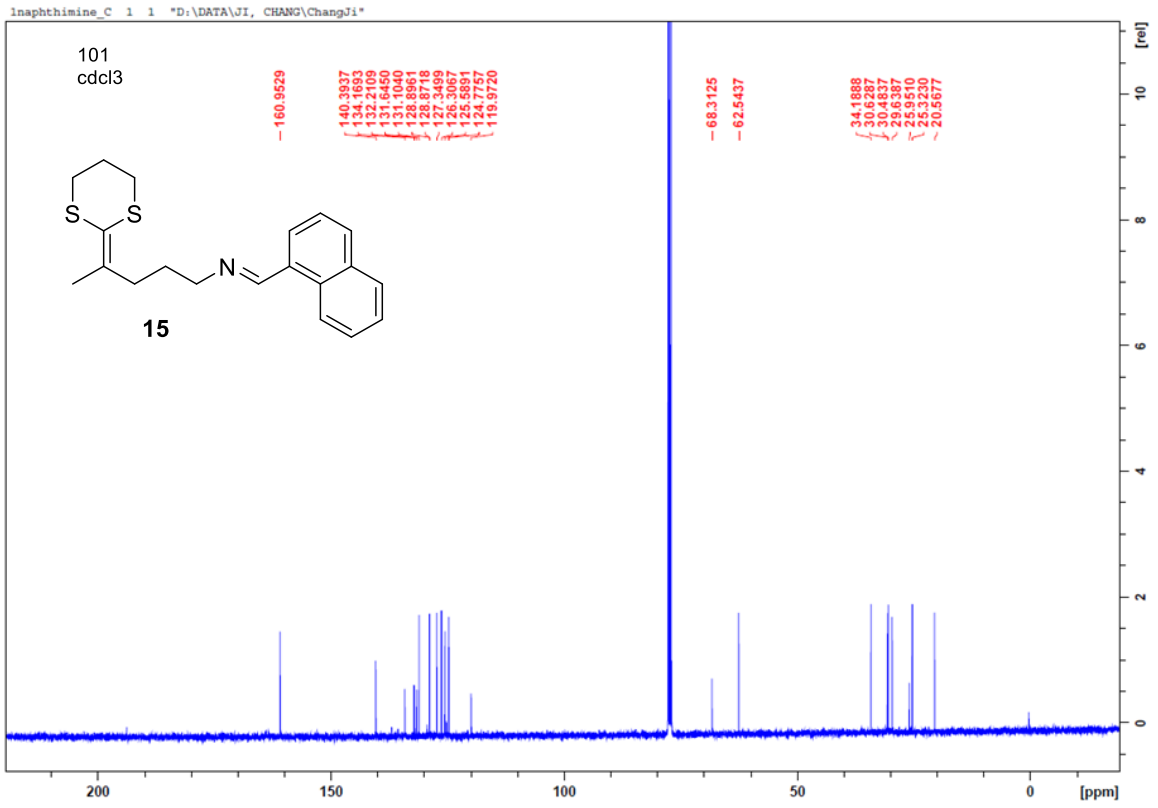
1naphthimine_C 1 1 "D:\DATA\JI, CHANG\ChangJi"
101
cdcl3
160.9529
140.3937
134.1693
132.2109
131.6450
131.1040
128.8961
128.8718
127.3499
126.3067
125.5891
124.7757
119.9720
68.3125
62.5437
34.1888
30.6287
29.4537
29.1387
25.9510
25.3230
20.5677
S
S
N
15
[rel]
[ppm]

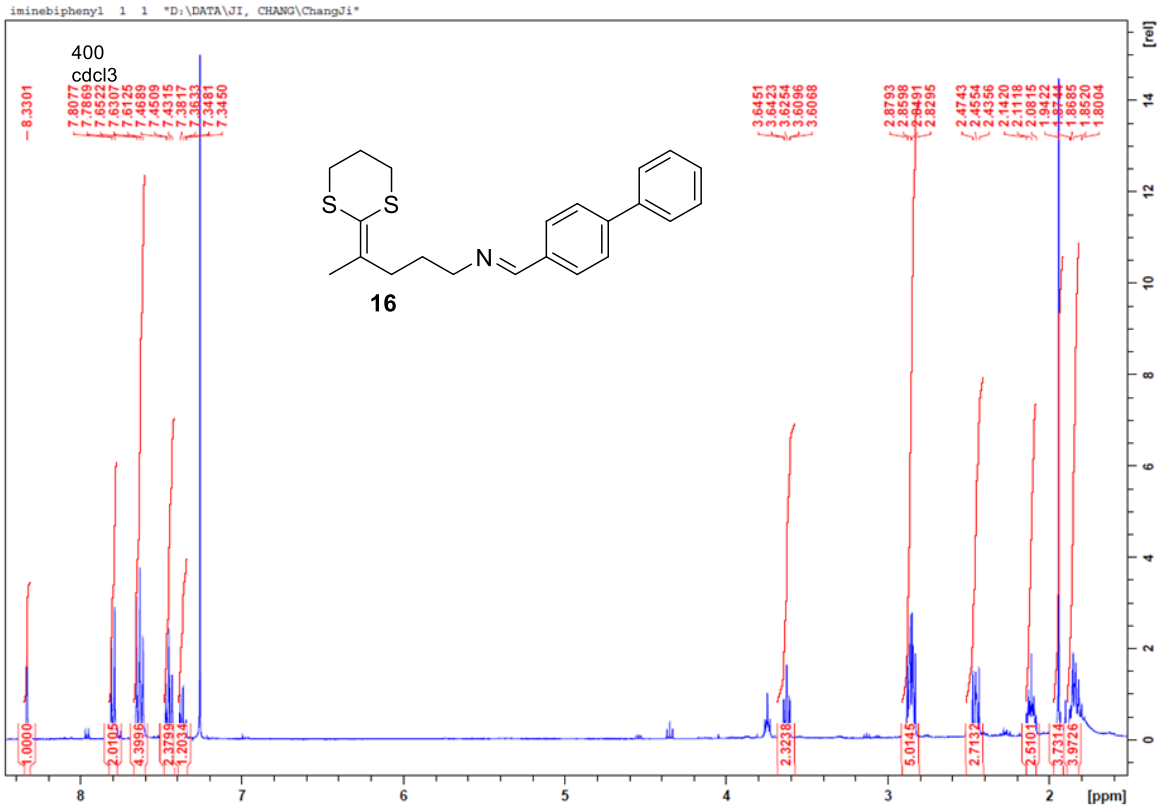
iminebiphenyl 1 1 "D:\DATA\JI, CHANG\ChangJi"
400
cdcl3
8.3301
7.8077
7.7869
7.6522
7.6307
7.6125
7.4689
7.4509
7.4315
7.3817
7.3633
7.3481
7.3450
3.6451
3.6423
3.6254
3.6096
3.6068
2.8793
2.8598
2.8491
2.8295
2.4743
2.4554
2.4356
2.1420
2.1118
2.0815
1.8744
1.8685
1.8520
1.8004
S
S
N
16
1.0000
2.0105
4.3996
2.3799
1.2034
2.3238
5.0145
2.7132
2.5101
3.7314
3.9726
[rel]
[ppm]

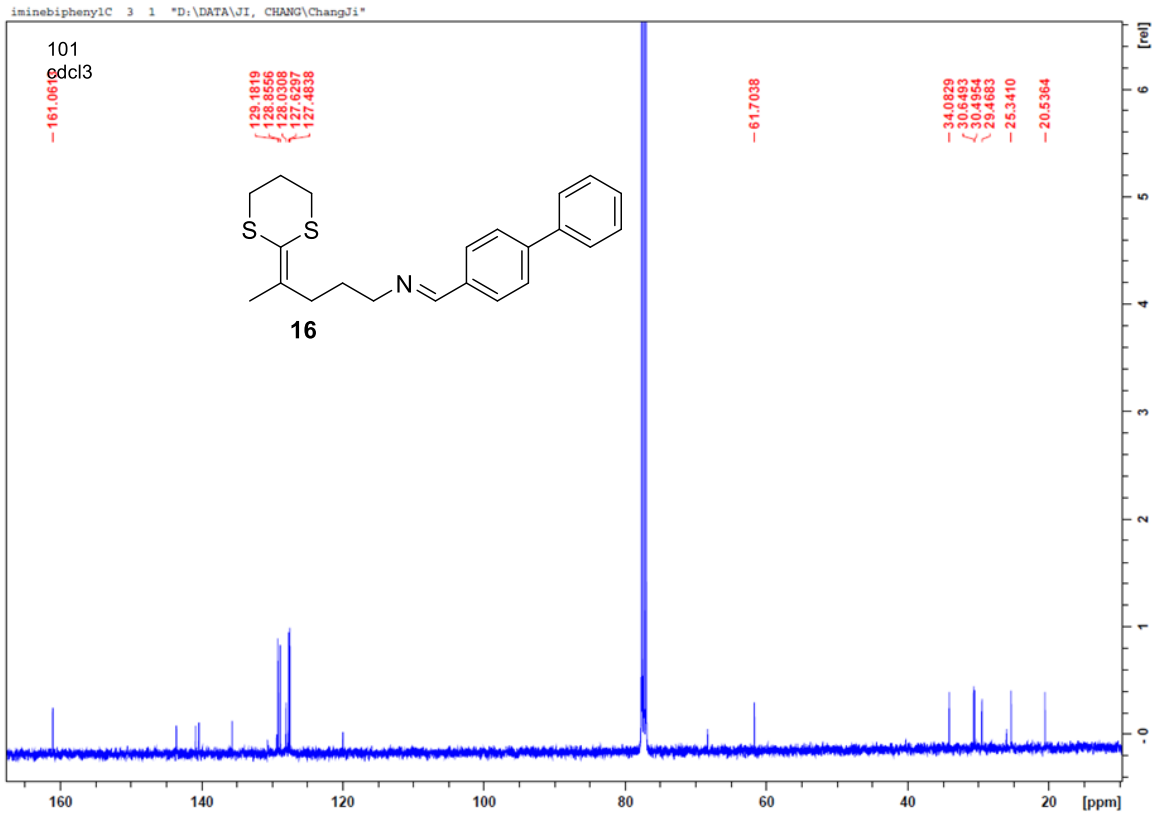
iminebiphenylC 3 1 "D:\DATA\JI, CHANG\ChangJi"
101
cdcl3
161.0616
129.1819
128.8556
128.0308
127.6297
127.4838
61.7038
34.0829
30.6493
30.4984
29.4683
25.3410
20.5364
S
S
N
16
[rel]
[ppm]

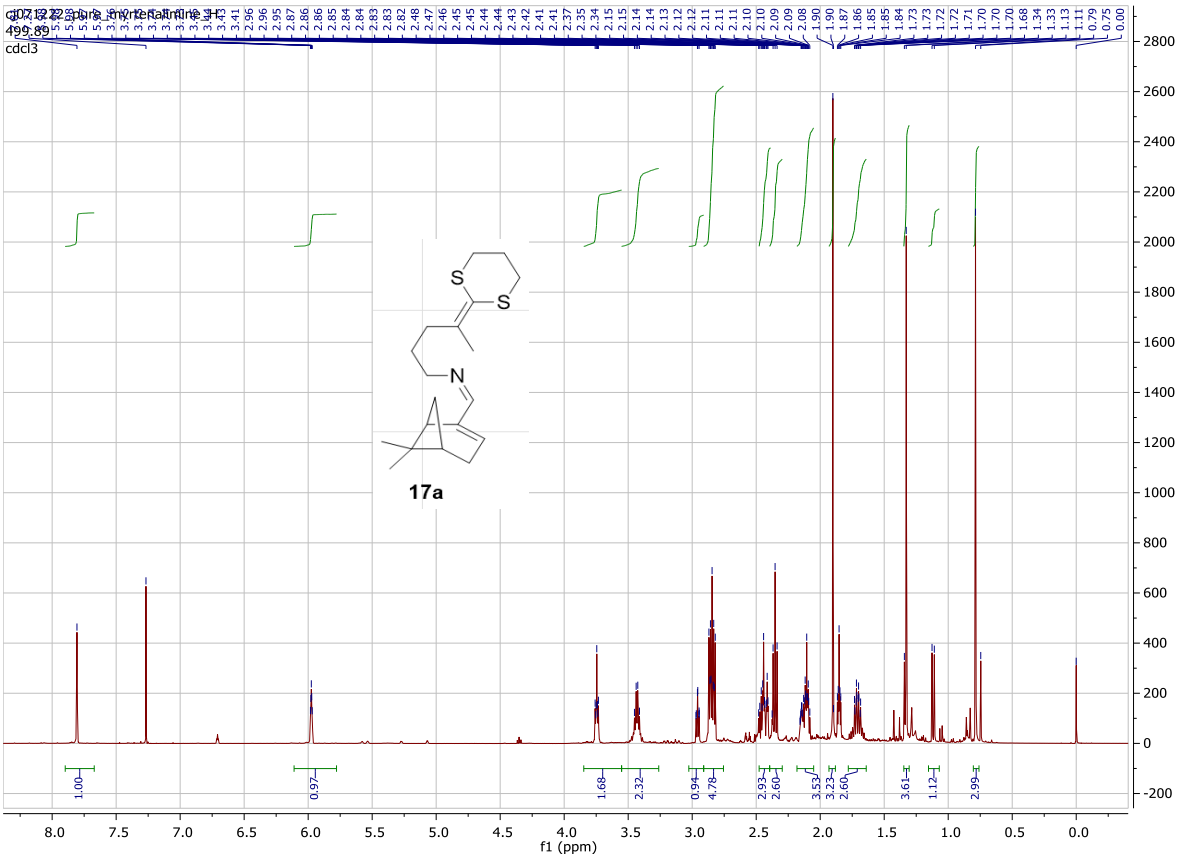
cdcl3
S
S
N
17a
f1 (ppm)

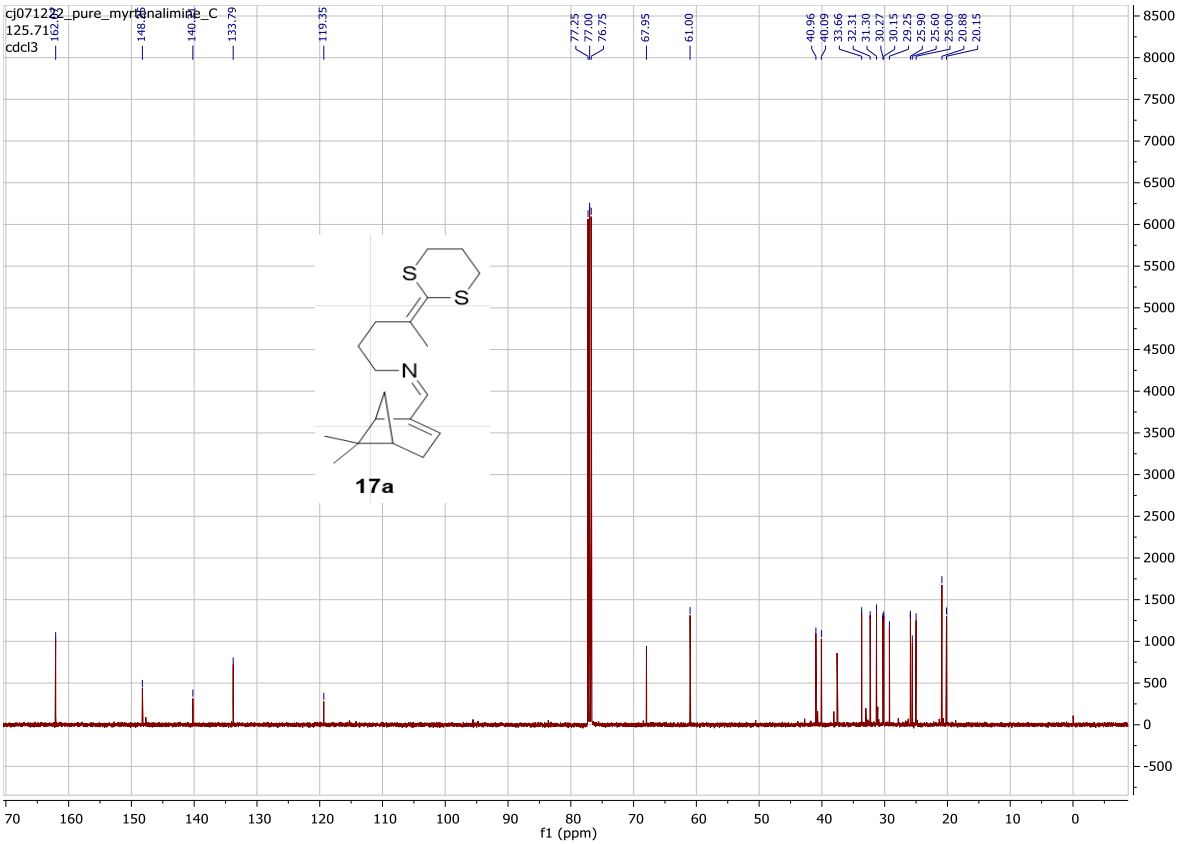
cj071222_pure_myrtenalimine_C
125.71
cdcl3
162.
148.
140.
133.79
119.35
77.25
77.00
76.75
67.95
61.00
40.96
40.09
33.66
32.31
31.30
30.27
30.15
29.25
25.90
25.60
25.00
20.88
20.15
S
S
N
17a
f1 (ppm)

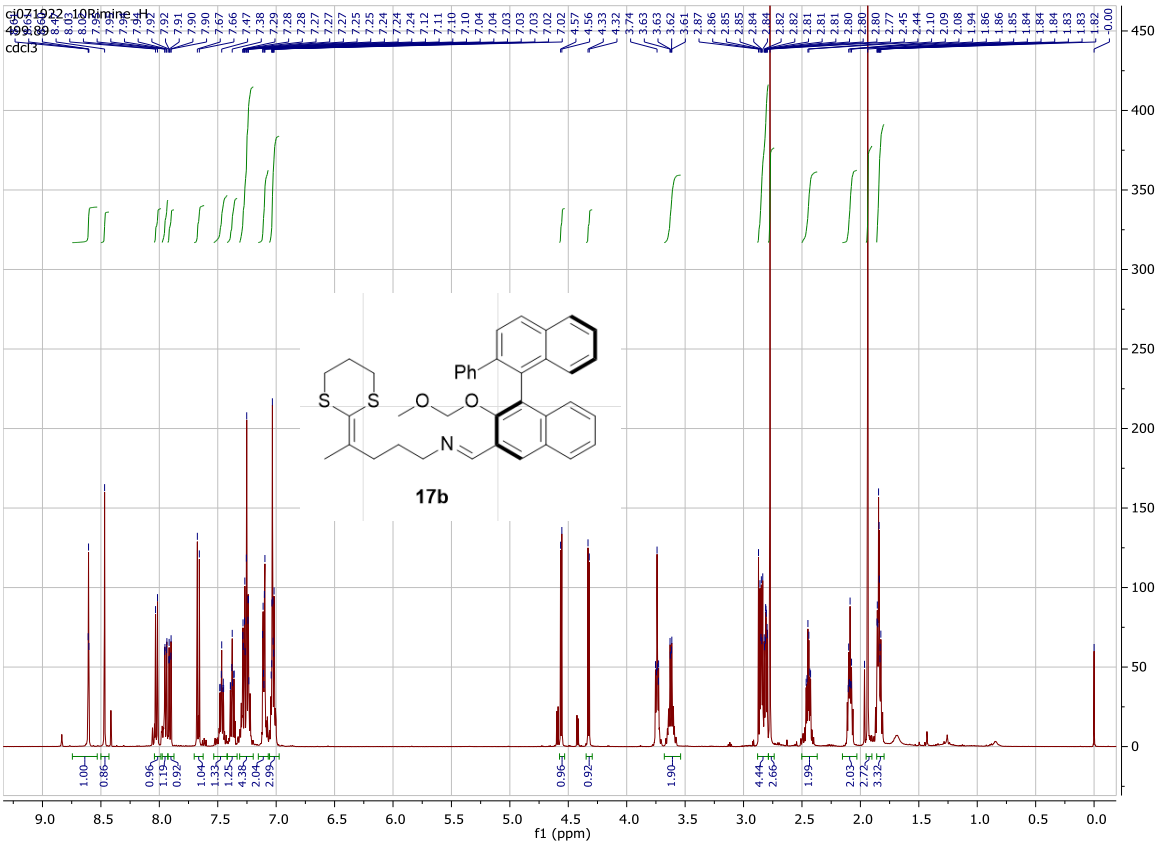
cj071922_10Rimine_H
499.89
cdcl3
Ph
S
S
O
O
N
17b
f1 (ppm)

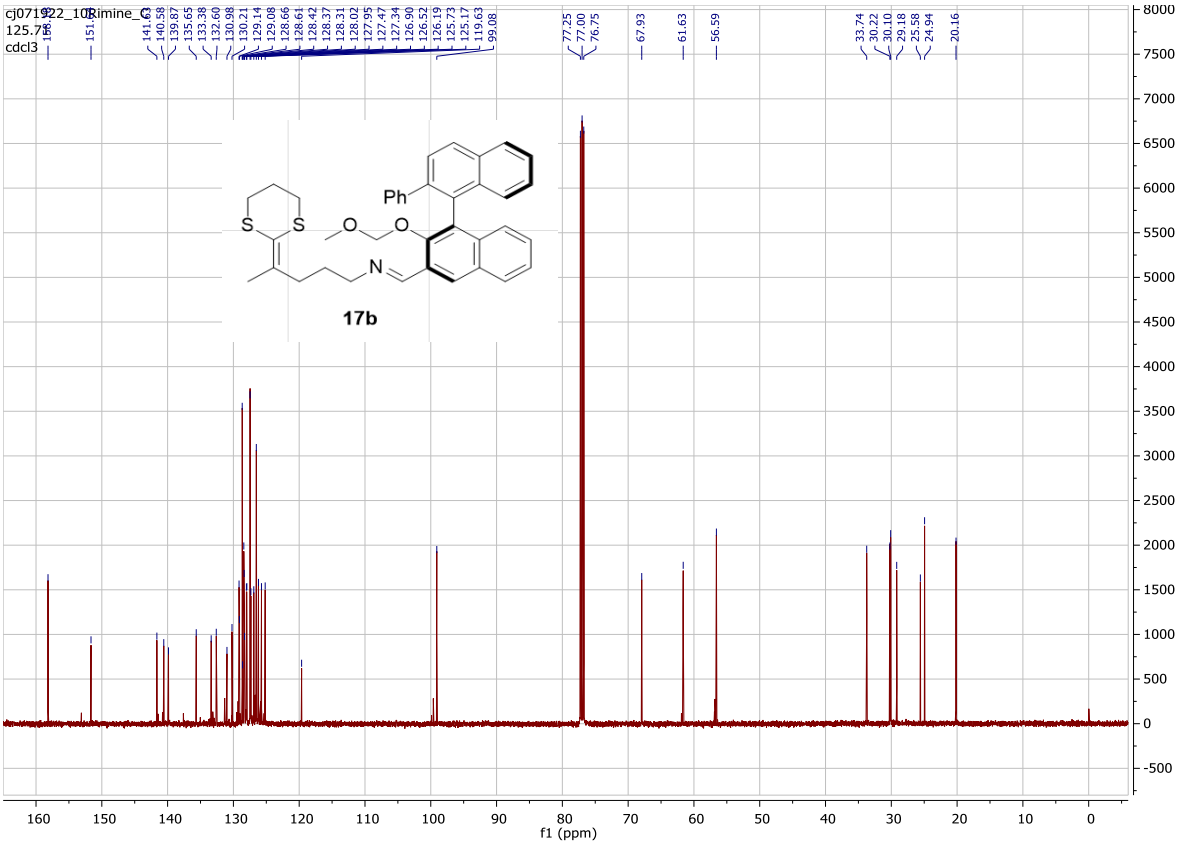
cj071922_10Simine_C
125.75
cdcl3
Ph
S
S
O
O
N
17b
f1 (ppm)

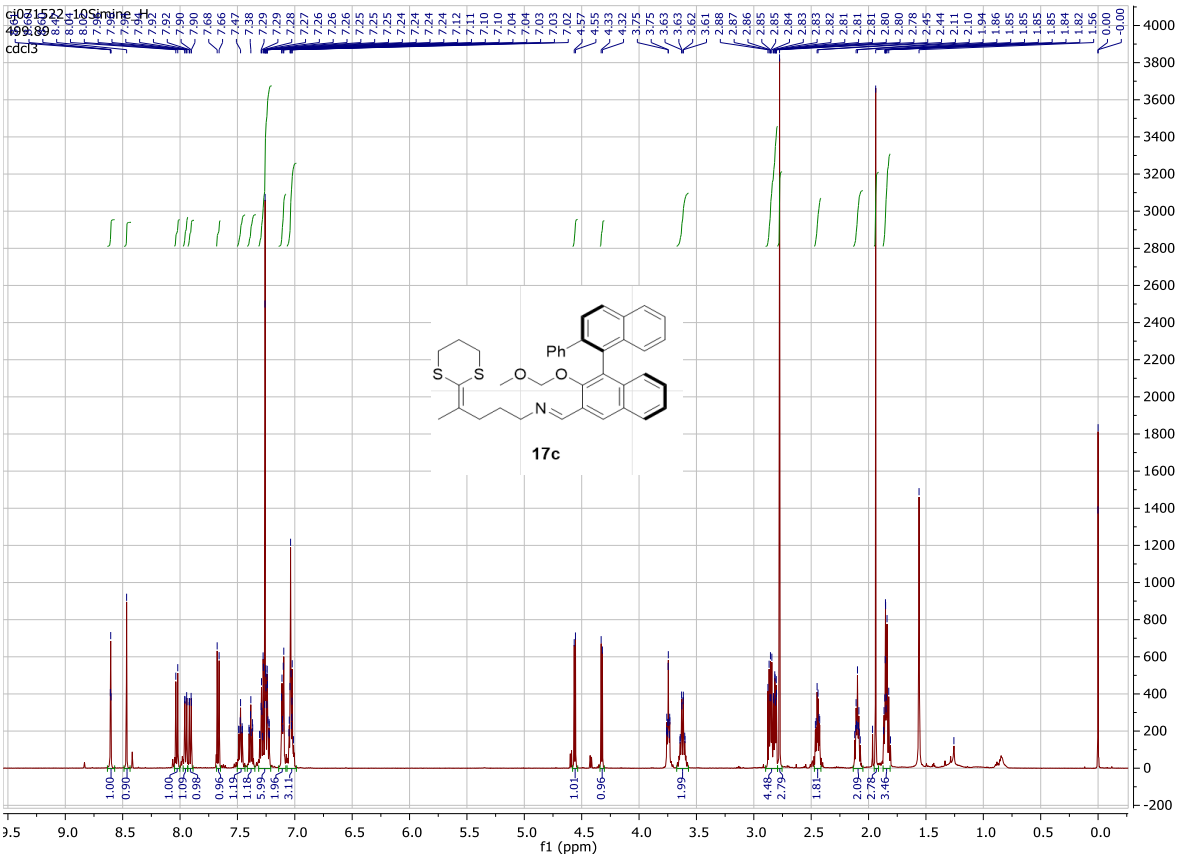
cj071522_10Simine_H
499.89
cdcl3
Ph
S
S
O
O
N
17c
f1 (ppm)

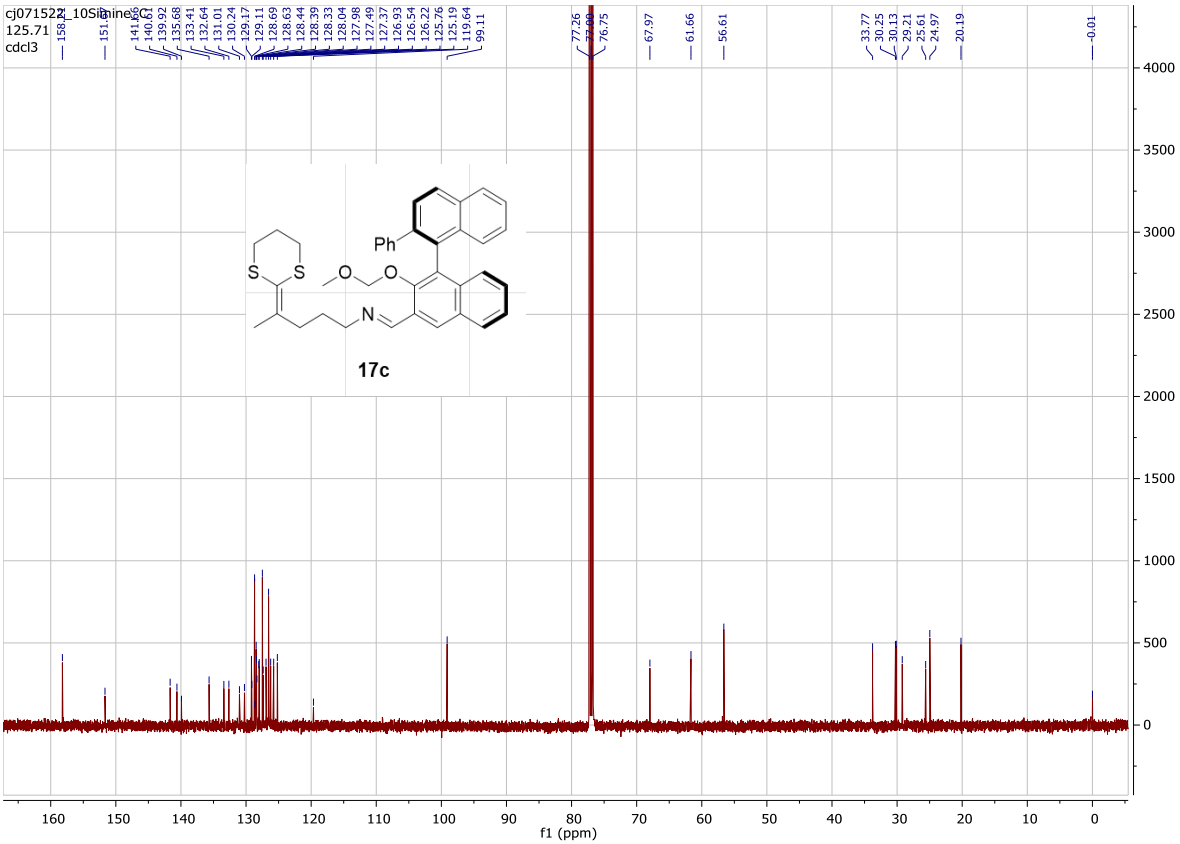
cj071522_10Simine2C
125.71
cdcl3
158.
151.
141.26
140.61
139.92
135.68
133.41
132.64
131.01
130.24
129.17
129.11
128.69
128.65
128.44
128.39
128.33
128.04
127.98
127.49
127.37
126.93
126.54
126.22
125.76
125.19
119.64
99.11
77.26
77.00
76.75
67.97
61.66
56.61
33.77
30.25
30.13
29.21
25.61
24.97
20.19
-0.01
Ph
S
S
O
O
N
17c
4000
3500
3000
2500
2000
1500
1000
500
0
160
150
140
130
120
110
100
90
80
70
60
50
40
30
20
10
0
f1 (ppm)

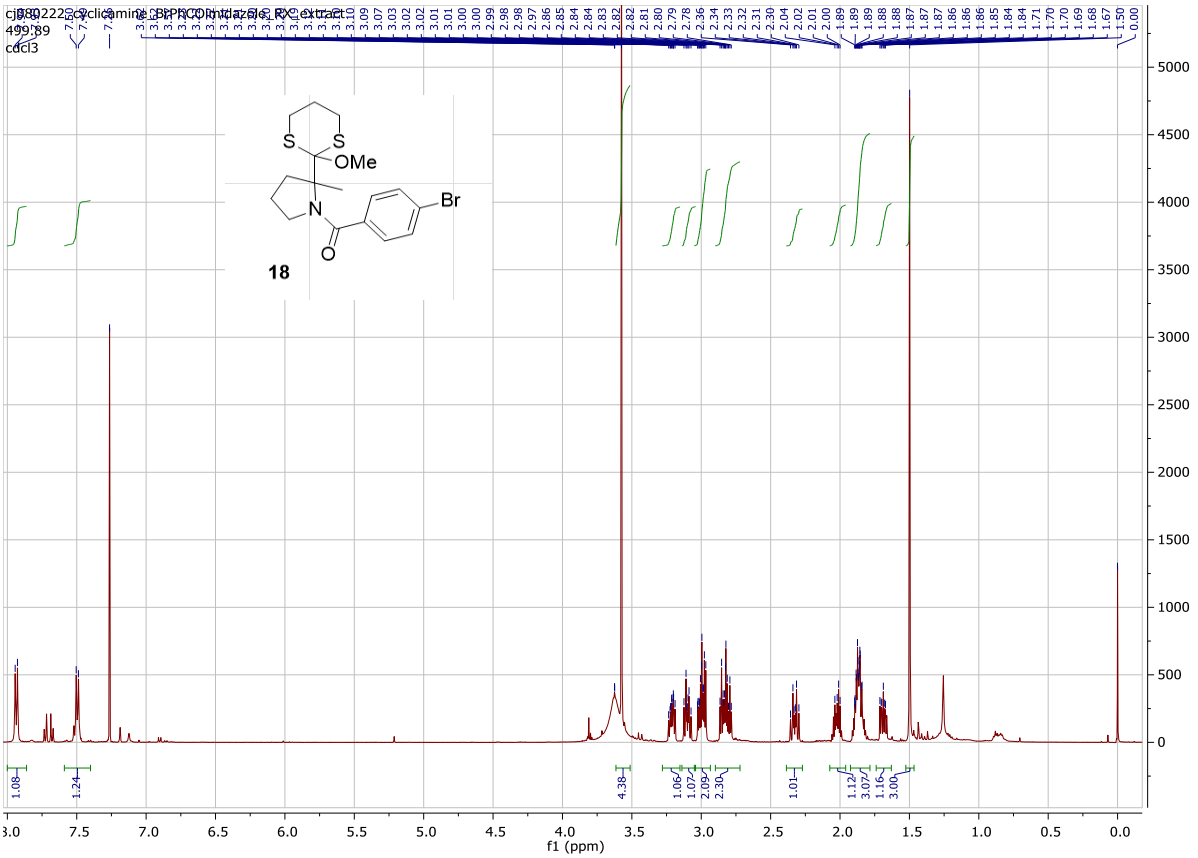
499.89
cdcl3
S
S
OMe
N
Br
O
18
f1 (ppm)

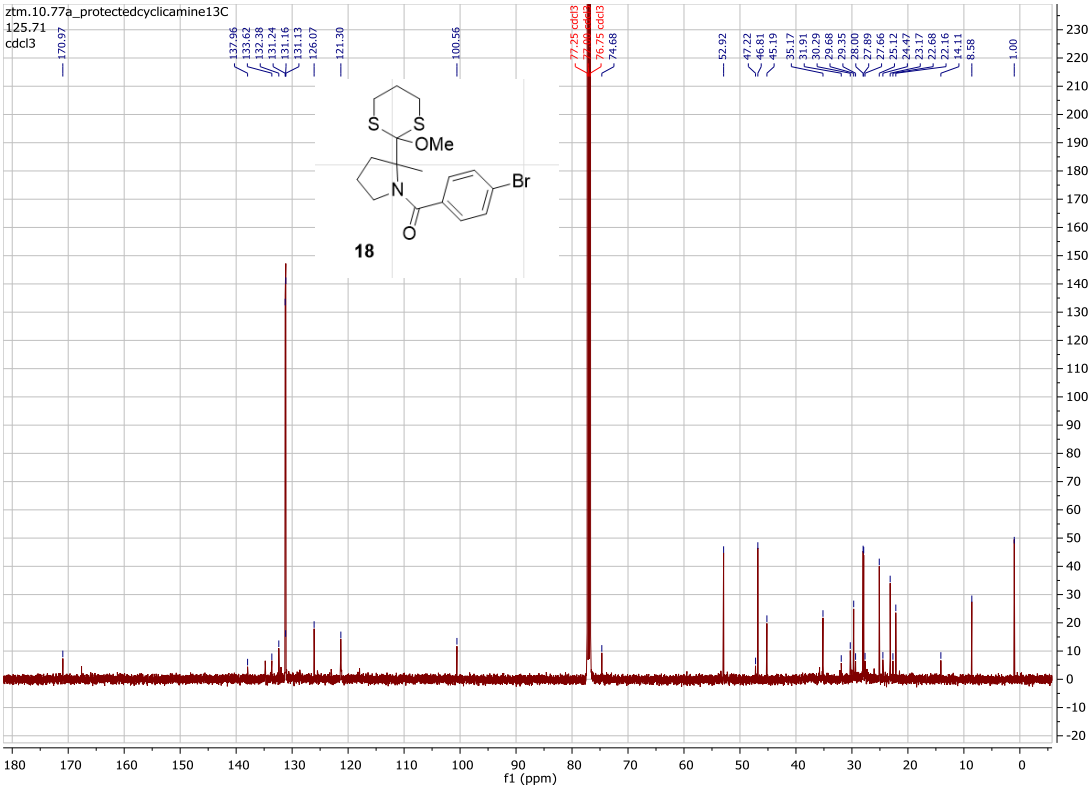
125.71
cdcl3
S
S
OMe
N
Br
O
18
f1 (ppm)

## References


(1) Medcalf, Z.; Redd, E. G.; Oh, J.; Ji, C.; Moeller, K. D. Anodic Cyclizations and Umpolung Reactions Involving Imines. *Org. Lett.* **2023**, *25* (22), 4135–4139. https://doi.org/10.1021/acs.orglett.3c01399.

(2) Feng, R.; Smith, J. A.; Moeller, K. D. Anodic Cyclization Reactions and the Mechanistic Strategies That Enable Optimization. *Acc. Chem. Res.* **2017**, *50* (9), 2346–2352. https://doi.org/10.1021/acs.accounts.7b00287.

(3) Moeller, K. D. Using Physical Organic Chemistry To Shape the Course of Electrochemical Reactions. *Chem. Rev.* **2018**, *118* (9), 4817–4833. https://doi.org/10.1021/acs.chemrev.7b00656.

(4) Medcalf, Z.; Moeller, K. D. Anodic Olefin Coupling Reactions: Elucidating Radical Cation Mechanisms and the Interplay between Cyclization and Second Oxidation Steps. *Chem. Rec.* **2021**, *21* (9), 2442–2452. https://doi.org/10.1002/tcr.202100118.

(5) Graaf, M. D.; Gonzalez, L.; Medcalf, Z.; Moeller, K. D. Using a Combination of Electrochemical and Photoelectron Transfer Reactions to Gain New Insights into Oxidative Cyclization Reactions. *J. Electrochem. Soc.* **2020**, *167* (15), 155520. https://doi.org/10.1149/1945-7111/abbe5c.

(6) Pagire, S. K.; Föll, T.; Reiser, O. Shining Visible Light on Vinyl Halides: Expanding the Horizons of Photocatalysis. *Acc. Chem. Res.* **2020**, *53* (4), 782–791. https://doi.org/10.1021/acs.accounts.9b00615.

(7) Chen, B.; Wu, L.-Z.; Tung, C.-H. Photocatalytic Activation of Less Reactive Bonds and Their Functionalization via Hydrogen-Evolution Cross-Couplings. *Acc. Chem. Res.* **2018**, *51* (10), 2512–2523. https://doi.org/10.1021/acs.accounts.8b00267.

(8) Yi, H.; Zhang, G.; Wang, H.; Huang, Z.; Wang, J.; Singh, A. K.; Lei, A. Recent Advances in Radical C–H Activation/Radical Cross-Coupling. *Chem. Rev.* **2017**, *117* (13), 9016–9085. https://doi.org/10.1021/acs.chemrev.6b00620.

(9) Morris, S. A.; Wang, J.; Zheng, N. The Prowess of Photogenerated Amine Radical Cations in Cascade Reactions: From Carbocycles to Heterocycles. *Acc. Chem. Res.* **2016**, *49* (9), 1957–1968. https://doi.org/10.1021/acs.accounts.6b00263.

(10) Hu, J.; Wang, J.; Nguyen, T. H.; Zheng, N. The Chemistry of Amine Radical Cations Produced by Visible Light Photoredox Catalysis. *Beilstein J. Org. Chem.* **2013**, *9*, 1977–2001. https://doi.org/10.3762/bjoc.9.234.

(11) Yoon, T. P. Visible Light Photocatalysis: The Development of Photocatalytic Radical Ion Cycloadditions. *ACS Catal.* **2013**, *3* (5), 895–902. https://doi.org/10.1021/cs400088e.

(12) Xu, H.-C.; Moeller, K. D. Intramolecular Anodic Olefin Coupling Reactions: Use of the Reaction Rate To Control Substrate/Product Selectivity. *Angew. Chem.* **2010**, *122* (43), 8176–8179. https://doi.org/10.1002/ange.201003924.

(13) Hudson, C. M.; Marzabadi, M. R.; Moeller, K. D.; New, D. G. Intramolecular Anodic Olefin Coupling Reactions: A Useful Method for Carbon-Carbon Bond Formation. *J. Am. Chem. Soc.* **1991**, *113* (19), 7372–7385. https://doi.org/10.1021/ja00019a038.

(14) Feng, E.; Jing, Q.; Moeller, K. D. Lessons from an Array: Using an Electrode Surface to Control the Selectivity of a Solution-Phase Chemical Reaction. *Angew. Chem.* **2022**, *134* (10), e202116351. https://doi.org/10.1002/ange.202116351.

(15) Wen, W.; Luo, M.-J.; Yuan, Y.; Liu, J.-H.; Wu, Z.-L.; Cai, T.; Wu, Z.-W.; Ouyang, Q.; Guo, Q.-X. Diastereodivergent Chiral Aldehyde Catalysis for Asymmetric 1,6-Conjugated

Addition and Mannich Reactions. *Nat. Commun.* **2020**, *11* (1), 5372. https://doi.org/10.1038/s41467-020-19245-3.
(16) Hu, D.; Yang, L.; Wan, J.-P. Biaryl and Atropisomeric Biaryl Aldehyde Synthesis by One-Step, Metal-Free Benzannulation of Aryl Enals and Propiolates. *Green Chem.* **2020**, *22* (20), 6773–6777. https://doi.org/10.1039/D0GC02806A.
(17) Shao, Y.-D.; Han, D.-D.; Dong, M.-M.; Yang, X.-R.; Cheng, D.-J. A One-Pot Stepwise Approach to Axially Chiral Quinoline-3-Carbaldehydes Enabled by Iminium–Allenamine Cascade Catalysis. *Org. Chem. Front.* **2021**, *8* (3), 605–612. https://doi.org/10.1039/D0QO01339K.
(18) Larose, J. H.; Werner, T. C. Binding of 2-Acetylnaphthalene to γ-Cyclodextrin: Stoichiometry of the Dimer Complex. *Appl. Spectrosc.* **2000**, *54* (2), 284–286. https://doi.org/10.1366/0003702001949221.
(19) For the synthesis of 10R and 10S-binapthaldehyde, please see: Sasaki, H.; Irie, R.; Hamada, T.; Suzuki, K.; Katsuki, T. Rational Design of Mn-Salen Catalyst (2): Highly Enantioselective Epoxidation of Conjugated Cis Olefins. *Tetrahedron* **1994**, *50* (41), 11827–11838. https://doi.org/10.1016/S0040-4020(01)89298-X.

# Chapter 4: Anodic Tandem Cyclization Using A Fast Second Oxidation Step

Having shown that the rate of the second oxidation step in an anodic cyclization proves crucial for product formation and that a fast second oxidation step can drive cyclizations down an irreversible kinetic pathway,[1] we wondered if we could apply this towards another problematic transformation. Specifically, the initiation of oxidative tandem cyclization reactions that form multiple bonds at one time. With the discoveries outlined in Chapter 2, the question arose: can we drive a tandem cyclization to completion by using the fast second oxidation. In this chapter, we will briefly outline the history of our efforts to perform a tandem anodic cyclization along with our most recent efforts to carry out this transformation.

## 4.1 Brief Background on Radical Based Cyclizations

As described in previous chapters, anodic coupling reactions generally follow the mechanistic paradigm shown in scheme 4.1.[2] From a synthetic perspective, these oxidative cyclizations are of interest because most radical-initiated cyclization reactions are either reductive or redox-neutral in nature.[3–11] Tributyltin hydride is commonly employed as the radical initiator in these cyclizations, as depicted in scheme 4.2.[5–7] As seen in case one, the reaction is a reductive cyclization catalyzed by tributyl tin hydride. The halide atom is first removed by the tin radical, resulting in an alkyl

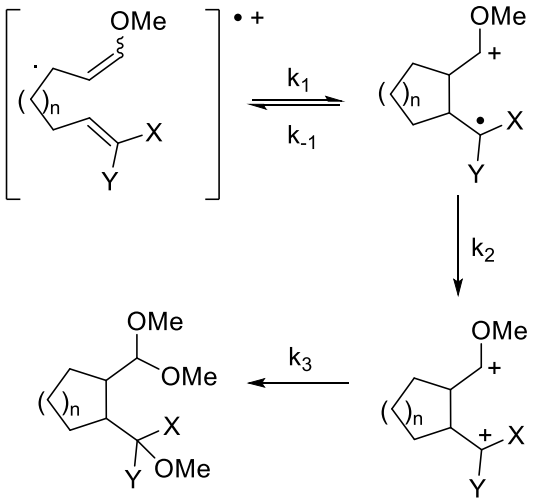


**Scheme 4.1: Anodic Cyclization Reaction Mechanism Model**

radical that undergoes a 5-exo cyclization onto the olefin. These reactions are terminated by the removal of a hydride from tributyltin hydride, leading to the formation of a

terminal alkyl group and a tin radical, which then initiates another reaction. This reaction converts a halogen into a hydrogen, resulting in an overall reduction in functionality. The terminating step can be adjusted so that the overall reaction becomes redox-neutral, as seen in cases two and three. These reactions may include atom-transfer reactions, often employing catalytic $Bu_3SnSnBu_3$ as a radical initiator[8] (as seen in case two), persistent radical reactions[9–11], or oxidative workups of tributyltin hydride reactions (as observed in case three). The overall transformation from starting

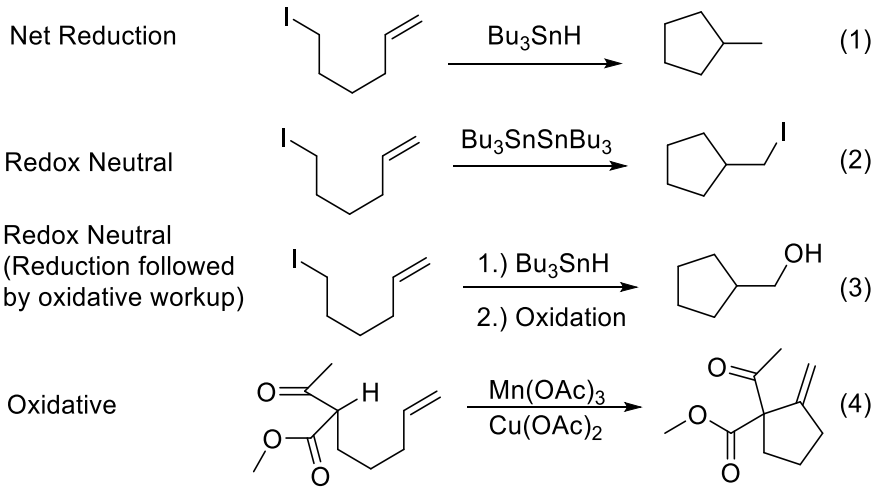


material to product is redox-neutral since the oxidation state of the starting material is equal to that of the product. The approaches demonstrated in cases one through three have been extended to tandem cyclizations to form multiple rings. Additional reductive cyclizations have been performed utilizing the radical anion of a carbonyl derivative generated by $SmI_2$ to undergo a conjugative addition to an α-β unsaturated carbonyl derivative. However, these reactions are limited in terms of the substrates that can be used.[12,13] More unconventional systems can engage in reductive or neutral cyclizations employing cobalt $V_{B12}$ crown complexes[14] with aromatic rings and titanocene complexes[15] with epoxides and conjugated carbonyls.

Cyclizations that are net oxidative (as in case four) have been carried out using Manganese(III)-based one-electron oxidants.[16–22] These reactions involve the formation of a Mn-enolate from the starting substrate. However, they come with several limitations, including the requirement for β-keto esters or benzylic substrates to enhance the acidity of the alpha proton, the utilization of stoichiometric Mn(II), the need for a stoichiometric co-oxidant to afford the final product, the use of acetic acid or protic solvents, and are limited by the range of functional groups that can withstand the reaction conditions. Oxidative radical-type cyclizations originating from silyl enol

ethers have been initiated using ceric ammonium nitrate. However, these are limited to the use of aromatic substrate and styrene derivatives.[23,24] DDQ has been demonstrated to catalyze oxidative cyclizations; however, these reactions are limited to the use of oxidation sites at the benzylic position.[25,26]

Each of these chemical oxidations have significant drawbacks. They all require stoichiometric metals, which contribute to the waste stream. In the case with $Mn(OAc)_3$ as the oxidant, the regiochemistry of the terminating step depends on the presence of an equivalent of copper(II)

**Scheme 4.2: General Overview of Radical Cyclizations**

acetate as a co-oxidant, resulting in an olefin at the terminal end. [16–22] This scenario requires additional manipulations to the product if an oxygen-based functional group is desired at the terminal position. Consequently, state-of-the-art oxidative cyclizations produce a significant quantity of potentially hazardous metallic waste and frequently demand additional post-cyclization transformations to provide a means for advancing the product toward a desired final target. This significantly increases the number of steps involved in the overall total synthesis. Another significant limitation is that the reactions are limited by the oxidation potential of the starting material. To explore a wide range of reactions with varying oxidation potentials, it requires the use of multiple chemical oxidants. Despite these limitations, these oxidative reactions have been employed in numerous total syntheses.[27–29]

Developing a general method that avoids the challenges linked with chemical oxidants would be beneficial. An electrochemical approach, as depicted in scheme 4.1, seems ideal for this endeavor.[2] Electrochemistry uses $2H^+$ as the stochiometric oxidant, and channels the waste product to hydrogen gas. It allows for the utilization of neutral conditions and is compatible with substrates possessing a wide range of oxidation potentials.

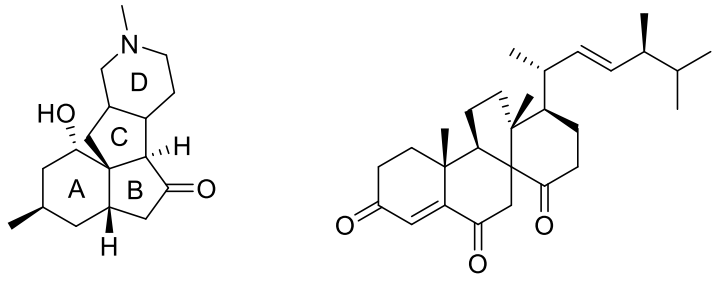


(+)-Paniculatine Dankasterone

**Figure 4.1: Structure of Paniculatine and Dankasterone**

## 4.2 Tandem Cyclizations Found in Literature

Tandem cyclizations have long been recognized as an effective strategy for synthesizing multiple ring structures efficiently.[30] Considering the role an oxidative cyclization reaction might play in this approach is intriguing since these reactions enhance the overall functionality of a molecule while forming new bonds. With this consideration, the molecules paniculatine and dankasterone were chosen as targets to explore the synthetic potential of oxidative tandem cyclizations. Both

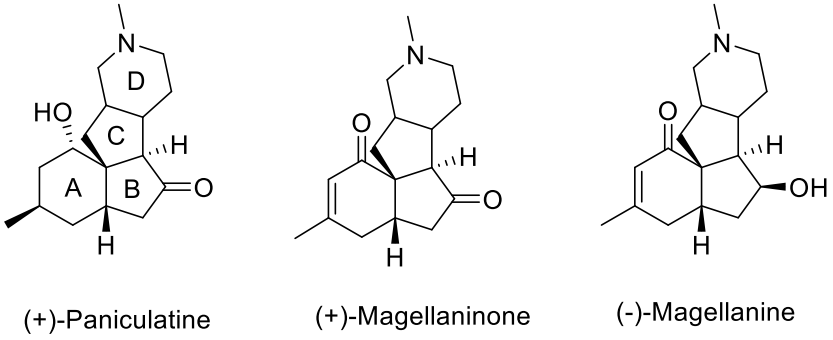


(+)-Paniculatine (+)-Magellaninone (-)-Magellanine

**Figure 4.2: Lycopodium Alkaloids**

compounds are structurally interesting natural products known for their significant biological activity.[30,31]

### 4.2.1 Paniculatine

Paniculatine was chosen as a target due to a previous synthesis, which provided us an opportunity to highlight the significance of employing an oxidative method in tandem cyclization reactions. Paniculatine, along with magellaninone and magellanine, are members of a class of *Lycopodium*

alkaloids characterized by a tetracyclic framework (Figure 4.2). Synthesizing this ring system has long been a demanding task for researchers, thus prompting numerous synthetic endeavors to construct this family of natural products.[30,32]

One such synthesis of Paniculatine was achieved by the Sha group by using a tandem radical cyclization (Scheme 4.3).[30] In order to prepare the substrate for the radical cyclization, the silyl

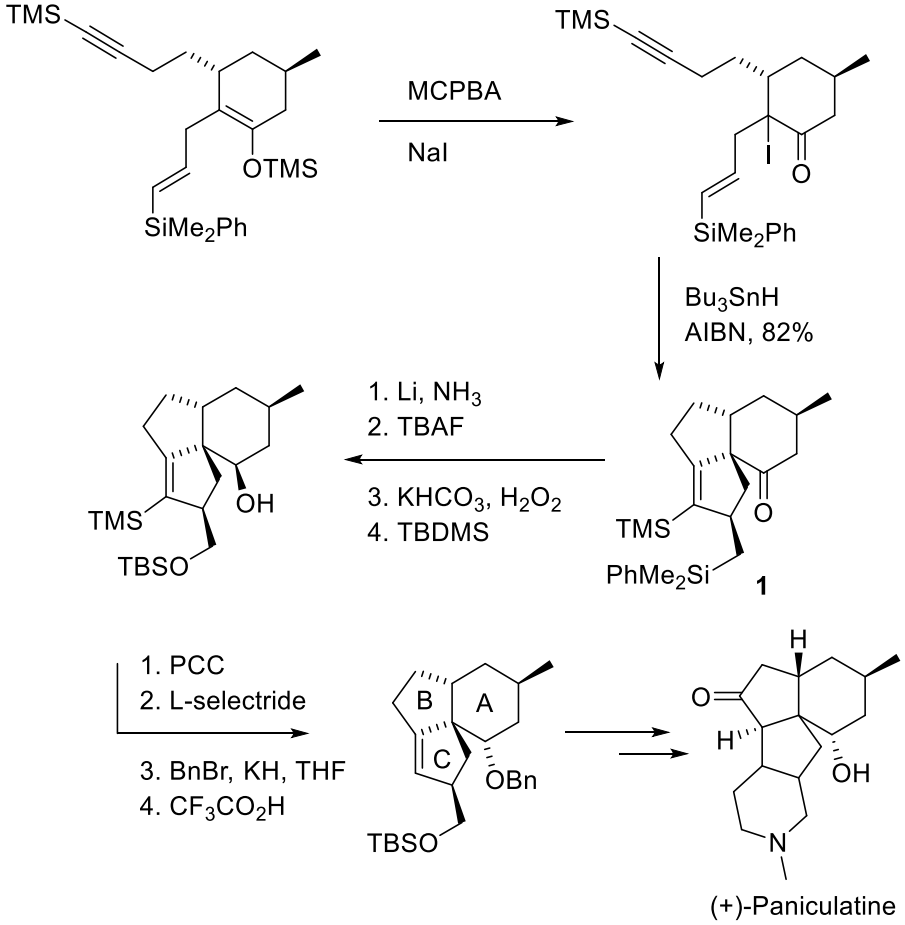


**Scheme 4.3: Sha's Synthesis of Paniculatine**

enol ether was oxidized with mCPBA and NaI to introduce a halogen at the alpha position of the ketone. Next, a tandem cyclization was initiated using tributyltin hydride and AIBN, leading to the formation of intermediate **1**. Because the key tandem radical cyclization in this scheme is a reductive process, the overall strategy necessitated an oxidation, reduction, oxidation approach, which involved the consumption of stoichiometric amounts of MCPBA, NaI, $Bu_3SnH$, TBAF,

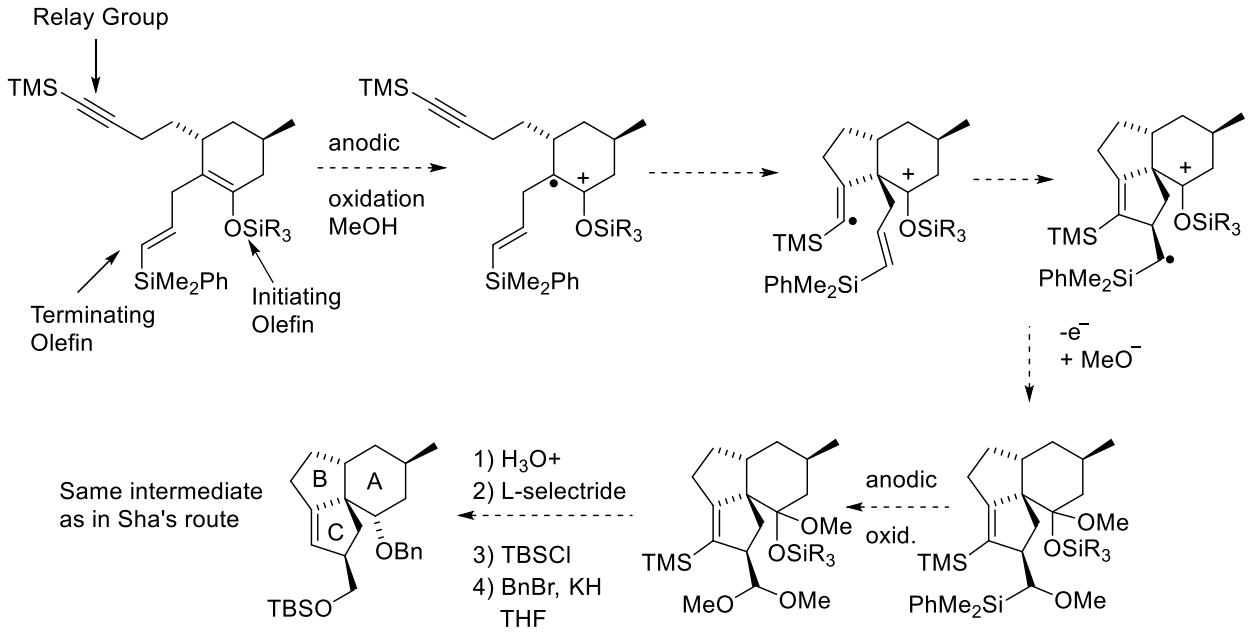


**Scheme 4.4: Synthesis of Paniculatine with an Anodic Cyclization**

$Li/NH_3$, $H_2O_2$, and PCC. In theory, by using an oxidative radical cyclization, as illustrated in Scheme 4.4, all the reagents listed above can be avoided, resulting in a significantly shortened synthesis. The key idea here is that the overall transformation is an oxidative process. Therefore, why not use an oxidative tandem cyclization in place of a reductive one? As seen in the depicted pathway above, an anodic oxidation would generate a radical cation from the silyl enol ether, which could then be trapped by the alkyne relay group to make the first ring. Next, the resulting vinyl radical would be trapped by the terminating olefin. The resulting radical would then undergo oxidation at the anode, with the resulting cation being captured by methanol. The alpha-methoxy silyl groups would then be oxidized at the anode in MeOH to form dimethoxy acetals, which can then be hydrolyzed to form the aldehyde. Further transformations would yield the same intermediate as in Sha's route.

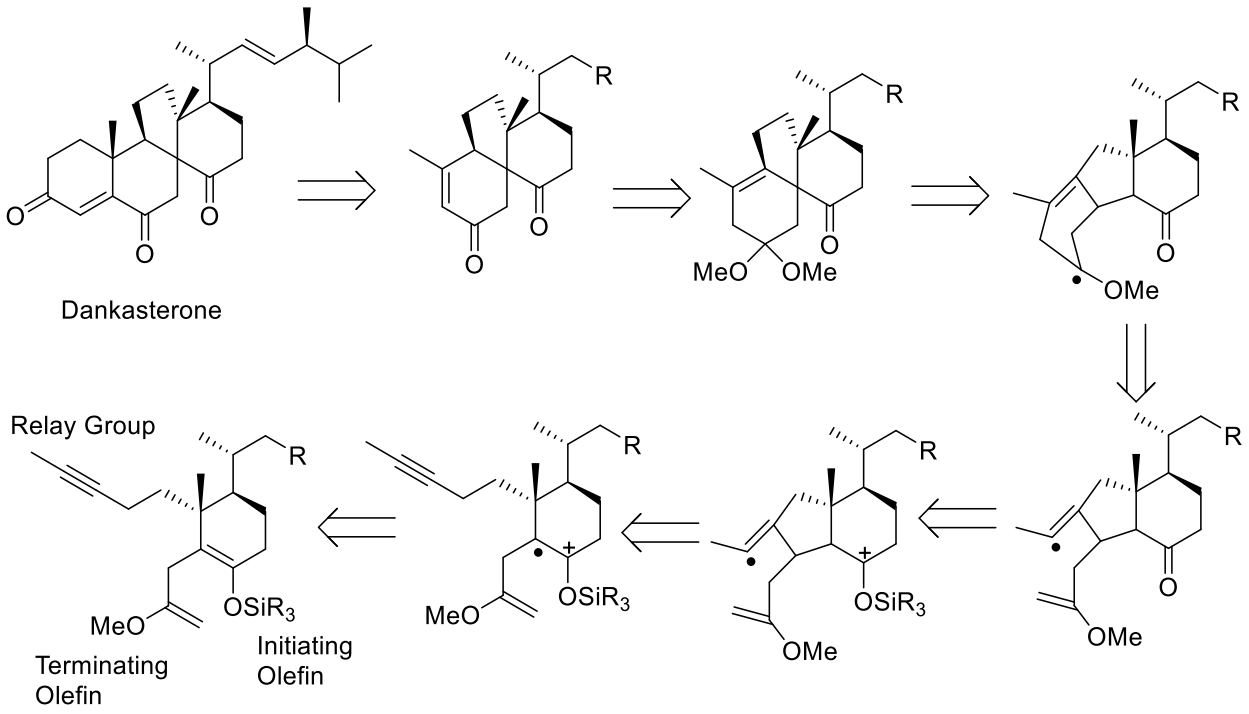


**Scheme 4.5: Retrosynthetic Analysis of Dankasterone Using an Anodic Tandem Cyclization**

## 4.2.2 Dankasterone

Dankasterone also features a tetracyclic ring system, suggesting the potential that this natural product could also be made with an oxidative tandem cyclization approach. This led to the design of the retrosynthetic analysis outlined in Scheme 4.5(Reference from Scates, B.A., Ph.D. Dissertation, Washington University in St. Louis, **2006**). In this scenario, the silyl enol ether would undergo oxidation to produce a radical cation, which would then initiate the tandem cyclization. The acetylene would function as the relay group in the tandem cyclization, and a methoxy vinyl ether would then act as the terminating group for the reaction.

The similarity between the proposed routes for Paniculatine and Dankasterone hinted at the potential of developing a general approach for an anodic tandem cyclization.

## 4.3 Preliminary Tests on Anodic Tandem Cyclization

Due to the promising synthetic potential offered by an anodic tandem cyclization, Bradley Scates, Laura Anderson, and Ruozhu Feng dedicated part of their doctoral studies to exploring the feasibility of this approach. However, they were unaware of the mechanistic insights outlined in Chapter 2. Therefore, we opted to take another, more informed look, at accomplishing this reaction. Before looking into my own contribution to that work, it is important to examine the attempts made by Bradley, Laura and Ruozhu.

### 4.3.1 Kolbe Electrolysis Route

The initial test was used in a route to synthesize Dankasterone. It employed a Kolbe electrolysis to produce the necessary radical to carry out the cyclization. Due to the synthesis of the substrate,

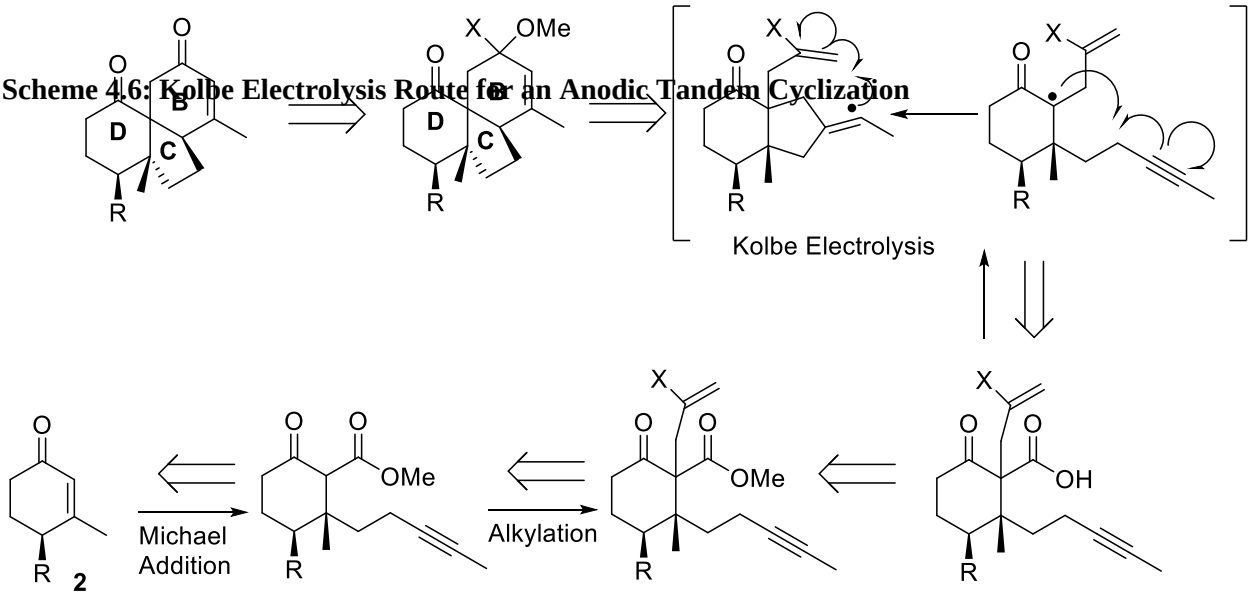


**Scheme 4.6: Kolbe Electrolysis Route for an Anodic Tandem Cyclization**

the required acid needed to carry out the Kolbe electrolysis was already present. (Scheme 4.6). (Reference from Scates, B.A., Ph.D. Dissertation, Washington University in St. Louis, **2006**).

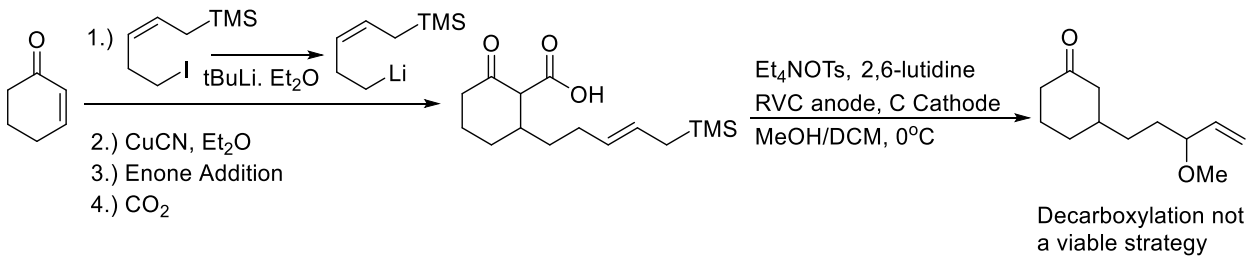


**Scheme 4.7: Kolbe Electrolysis Resulted in Decarboxylation**

The strategy involved incorporating a carboxyl group at the α-position of ketone **2** via a Michael reaction, followed by utilizing the resulting 1,3-dicarbonyl compound to add terminating olefin for the tandem cyclization. This approach circumvented issues related to alkylation and potential loss of regiospecificity inherent in the Michael reaction. Notably, a Michael-alkylation sequence starting from **2** would require the enolate to be remade, but by employing the Kolbe method to generate the radical, such issues were avoided. Consequently, the outcome remained a two-electron oxidative process, thus avoiding a reductive cyclization.

Regrettably, in practice, a non-oxidative decarboxylation could never be avoided. Upon

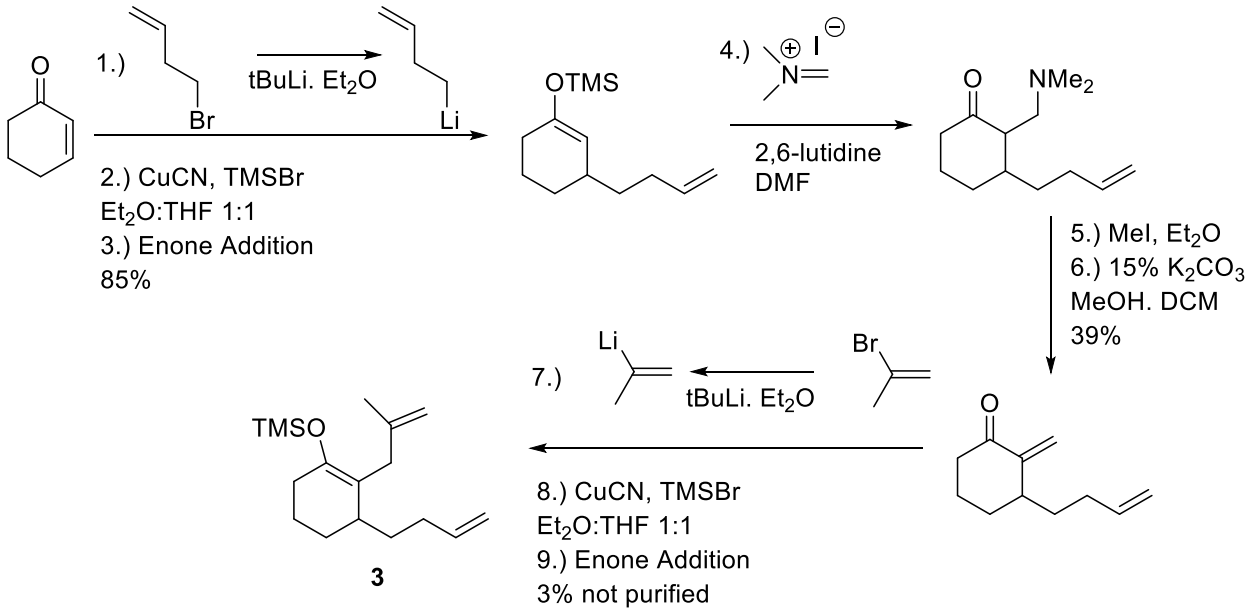


saponification of the ester, an immediate decarboxylation ensued post-alkylation. The quaternary

carbon was unstable. Even in instances where alkylation was avoided and a basic model system lacking the terminating olefin α to the carbonyl was exposed to electrolysis conditions (see Scheme 4.7), decarboxylation occurred prior to oxidation. As a result, the product arose from the oxidation of the allylsilane with no cyclization occurring.

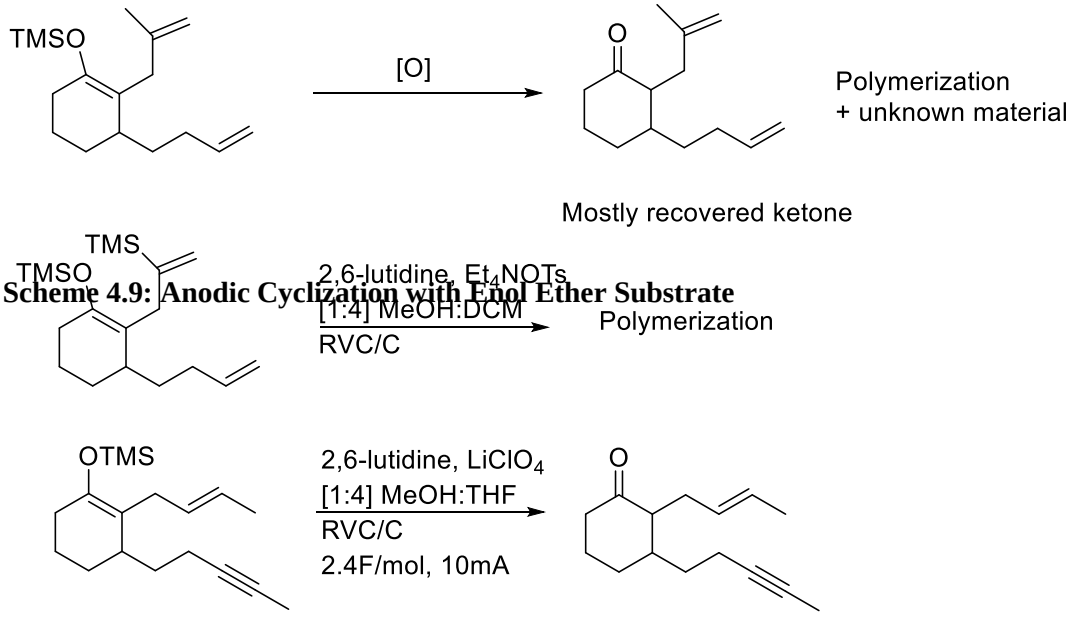


**Scheme 4.9: Anodic Cyclization with Enol Ether Substrate**

## 4.3.2 Double Michael Addition Route

Since the simple Kolbe approach failed, this led to a double Michael reaction route to make the desired substrate as seen in Scheme 4.8. (Reference from Anderson, L.A., Ph.D. Dissertation, Washington University in St. Louis, **2010**). In this approach, a monosubstituted olefin was employed as the relay group. While the terminating double bond was installed by a Mannich alkylation and elimination sequence, using Eschenmoser's salt, followed by the second Michael addition. The yield of the electrolysis substrate **3** was never achieved beyond 5%, and even that amount could not be purified. Attempts were made at the anodic cyclization, but due to the lack of clean starting material, little insight was gained. The electrolysis resulted in either product from straight hydrolysis or polymerized material, which may or may not have originated from the actual substrate. Consequently, the route was abandoned.

**Scheme 4.8: Synthesis of Enol Ether Substrate Using Double Michael Strategy**

### 4.3.3 Thiophene Route to make the Enol Ether Substrate Leading to the Radical Cation Pathway

The failure of the two substrates shown above led to another change in the route taken to synthesize the substrate (Scheme 4.10).

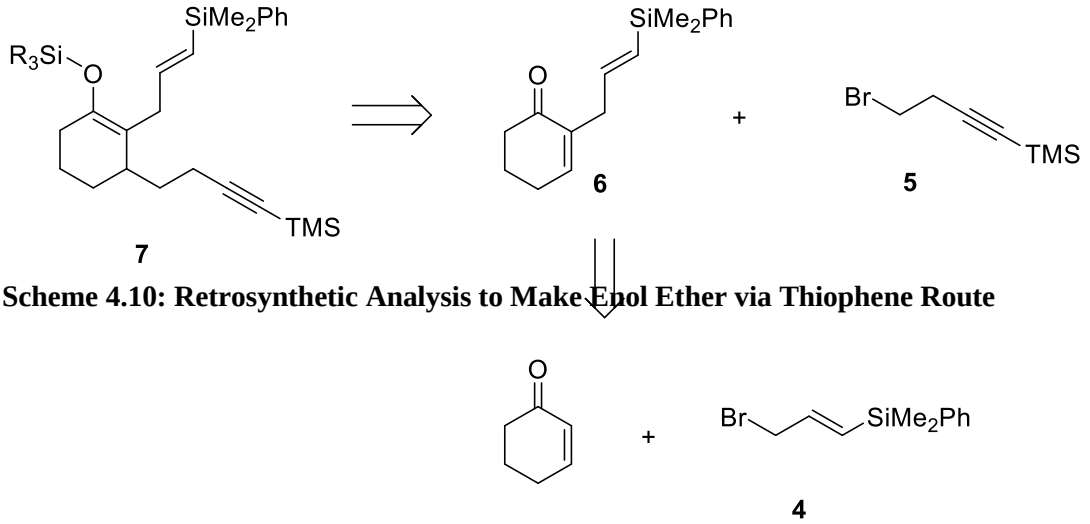


**Scheme 4.10: Retrosynthetic Analysis to Make Enol Ether via Thiophene Route**

In this approach, the two side chains were synthesized independently. Then the α-position alkyl side chain **4** was introduced, with a net retention of the double bond between C2-C3, using the established thiol-based strategy pioneered by Baraldi et al (Scheme 4.13).[33] These side chains were chosen to align with the previous synthesis of Paniculatine, as it was established that the radical-

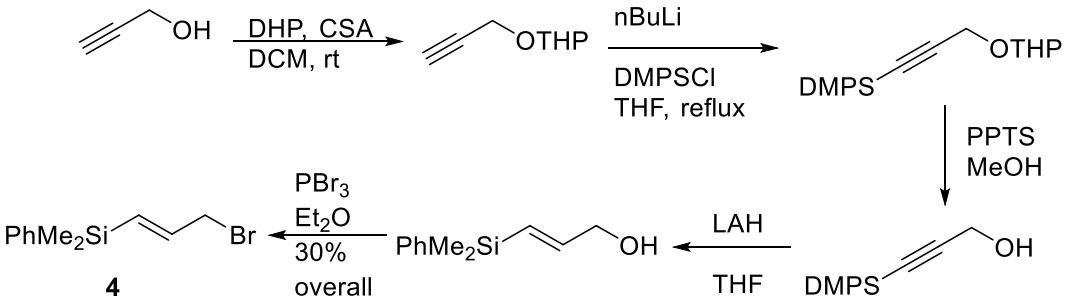


**Scheme 4.11: Synthesis of 4**

based reaction was compatible with those particular groups. Once the α-allylated enone **6**, was in hand intermediate **5** was added via a Michael addition to give the tandem cyclization substrate **32**.

The synthesis of compound 4 proceeded well. Following the pathway outlined in Scheme 4.11, compound **4** was achieved with a yield of 30% from the starting material. There was no need to purify the intermediates before obtaining the final bromide **4**.

The synthesis of intermediate **5** followed the route shown in Scheme 4.12. In this approach, the alcohol had to be purified before the Appel reaction was used to make the bromide **5**.

Having made the sidechains, intermediate **6** was synthesized following the route used by Baraldi and coworkers which started from the enone and a thiolated methylacetate.[33] From here a Michael reaction was used install the acetylene relay group at the β-position of the enone. In this reaction,

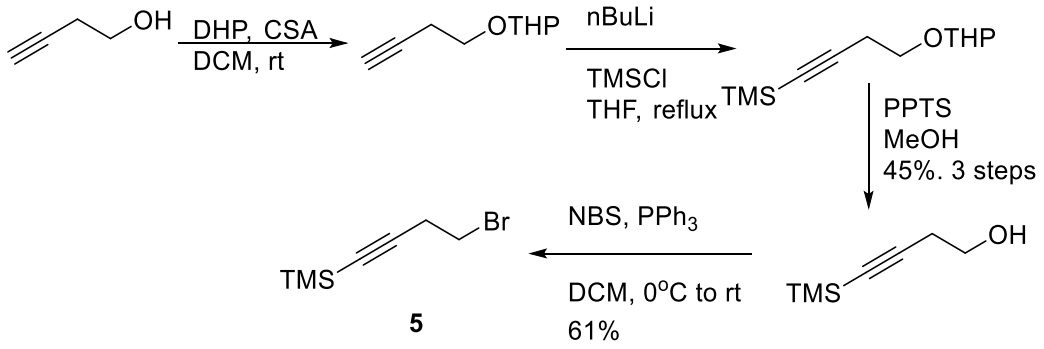


**Scheme 4.12: Synthesis of 5**

the Michael product **7a** with a TMS silyl trapping group could be isolated without purification, resulting in a mixture of the enol ether electrolysis substrate and the ketone arising from enol ether hydrolysis. Using a TBS trapping group enabled the isolation of pure silyl enol ether **7b**, although with a yield of only 17%, which was attributed to the decomposition of the enol ether during chromatography.

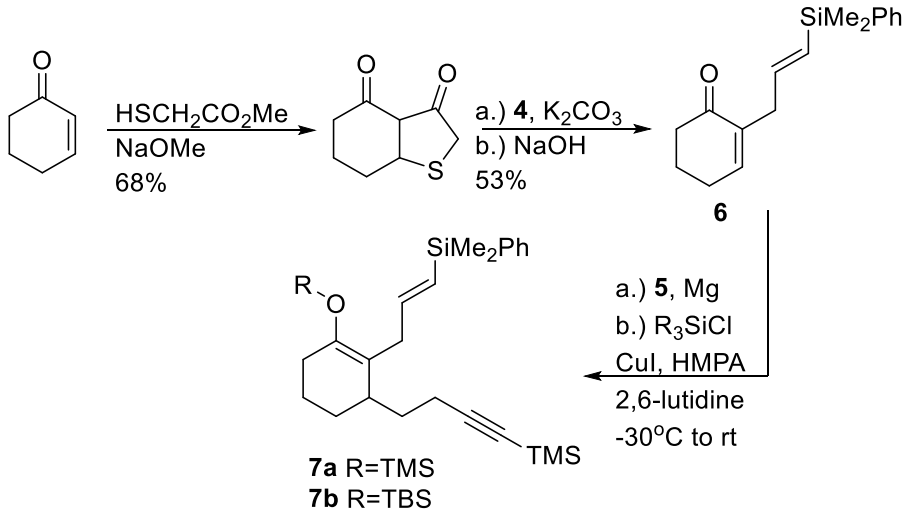


**Scheme 4.13: Synthesis of 7a and 7b**

**Electrolysis of Enol Ether Substrate**

Both types of silyl enol ether substrate underwent oxidation, even though the TMS substrate was contaminated with its hydrolysis product. Dr. Bradley Scates managed to identify approximately 10% yield of the desired product through NMR analysis of the crude reaction mixture. However, due to the complexity of the product mixture and the lack of complete characterization, this assignment remains tentative.

When Dr. Feng attempted to replicate this experiment and compound **7a** was oxidized, the yield of ketone derived from hydrolysis of the starting material was 18% (Scheme 4.14). The reaction mixture appeared messy, making it difficult to determine whether the issue stemmed from an unsuccessful oxidation or from the inadequate generation of high-quality substrate for the electrolysis. Dr. Feng tested various conditions differing from those outlined in Dr. Bradley Scates's thesis, including variations in electrolyte ($Bu_4NBF_4$) and temperature (0°C), yet still failed to produce any product. Regarding the TBS substrate**7b**, which is more stable than **7a**, the findings were more reliable because pure substrate could be isolated. However, the cyclization attempt was once again unsuccessful. The reaction yielded the ketone resulting from the hydrolysis of the silyl

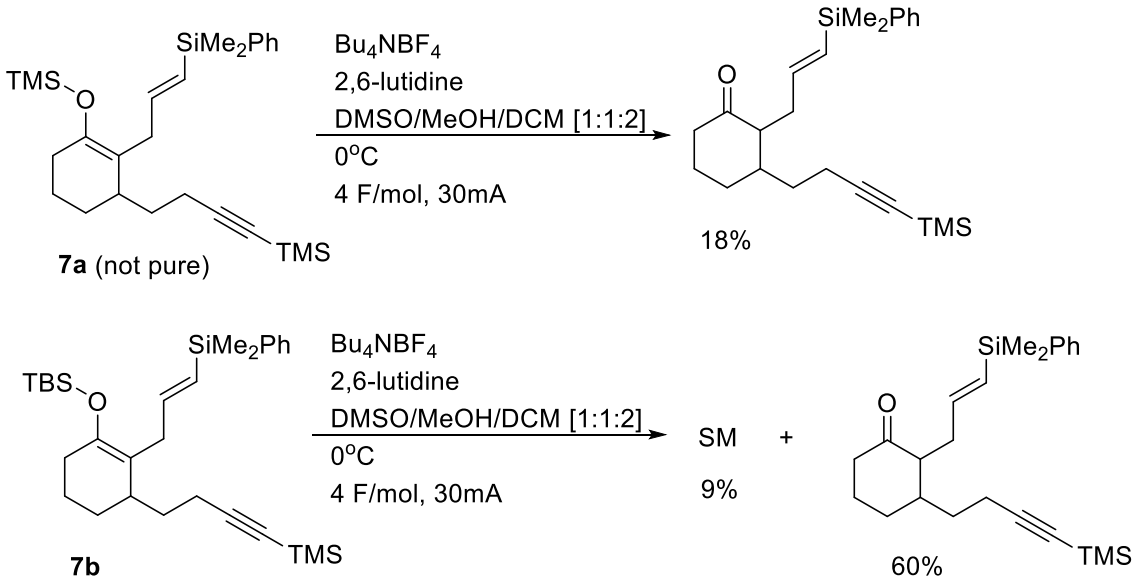


**Scheme 4.14: Electrolysis of Enol Ether Substrates 7a and 7b**

enol ether at a yield of 60%, along with 9% of the starting material recovered. The recovery of some starting material suggested that the TBS substrate was more resistant to the electrolysis conditions than the TMS substrate. (Reference from Feng, R., Ph.D. Dissertation, Washington University in St. Louis, **2018**).

Generally, TBS enol ethers are stable to electrolysis conditions. However, it is important to consider the that the hydrolysis product might originate from recovered starting material, and the recovery of starting material does not always mean the oxidation did not take place. A reversible cyclization that results in a stable radical cation can lead to the reduction of the radical cation at the cathode.[34] There were concerns that a reversible addition to make a 3-membered ring was interfering with the cyclization. If this situation occurs, then the reaction might be pushed to completion by enhancing the rate of the second oxidation step.

## 4.3.4 Alkynes as Olefin Coupling Partners

The suggestion that the addition of a radical cation to the acetylenes might be reversible was consistent with the coupling of a radical cation derived from an enol ether with a methyl acetylene. (Scheme 4.15). (Reference from Scates, B.A., Ph.D. Dissertation, Washington University in St. Louis, **2006**). In this study when R=H, the methoxy enol ether **8** underwent oxidation to generate

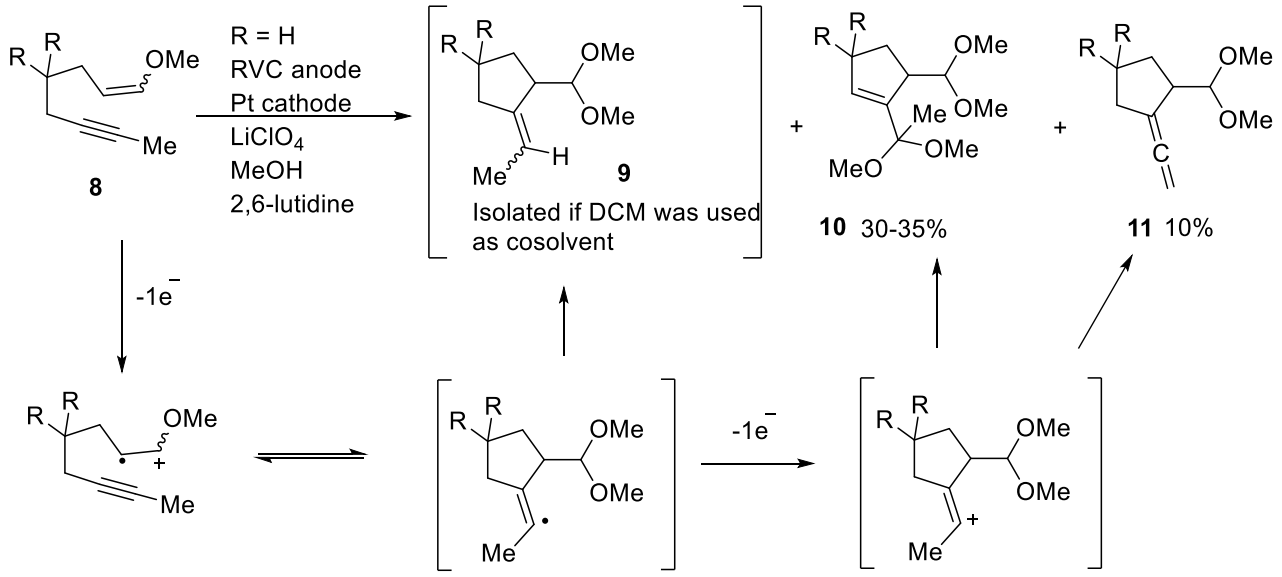


**Scheme 4.15: Anodic Cyclization of Enol Ether with Acetylene Trapping Group**

a radical cation. Although the mass balance was low in the subsequent reaction, all isolated products stemmed from the involvement of the alkyne in the reaction. One product resulted from the formation of a vinyl cation, which was then captured by methanol and oxidized to produce an

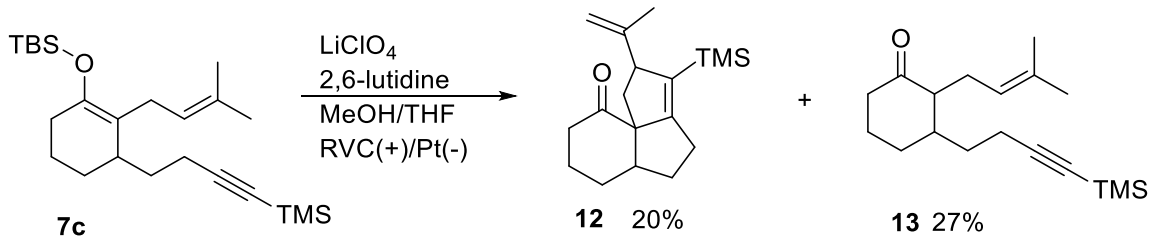


**Scheme 4.16: Substrate using Trisubstituted Alkene Trapping Group**

unsaturated acetal **10**. Another product arose from the elimination of a proton from the vinyl cation,

yielding allene **11**. In a mechanistic study, the introduction of dichloromethane to the reaction resulted in a hydrogen abstraction product **9**, which indicated the formation of a vinyl radical intermediate. Efforts to accelerate the rate of the cyclization with geminal substituents[35] (R = $CO_2Et$), resulted in the recovery of the starting material. In every instance, the reaction failed to yield a product, indicating decomposition of the enol ether radical cation before cyclization. This occurred despite the passage of a stoichiometric amount of current through the reaction and the enol ether being the functional group with the lowest oxidation potential in solution. This observation is significant because we know oxidation of an enol ether with a slow cyclization forms elimination reactions along with solvent trapping of the enol ether radical cation.[36] The absence of these products aligns better with the scenario where the enol ether undergoes oxidation, followed by the stabilization of the radical cation through an intramolecular trapping reaction. Next, a reversible cyclization occurs, resulting in the reduction of the radical cation at the cathode. This stabilization step is necessary because the enol ether radical cation on its own cannot persist in methanol solvent long enough to reach the cathode. During the time that these initial reactions were done, we did not know the solutions to this issue, such as using higher electrolyte concentrations or accelerating the second oxidation step. However, it was clear that the reaction resulted in a vinyl radical which presented a potential solution to drive the reaction to completion: accelerating the trapping of the vinyl radical. At the time, it was concluded that the vinyl silane trapping group in substrate **7b** might not be efficient for this purpose. Therefore, a more effective trisubstituted olefin **7c** was employed as the final radical trapping group (Scheme 4.16) (Reference from Scates, B.A., Ph.D. Dissertation, Washington University in St. Louis, **2006**). The outcome of this reaction was somewhat successful. The tandem cyclization yielded the desired product **12** with a 20% yield, alongside a 27% yield of a ketone derived from the methanolysis or hydrolysis of the

initial enol ether **13**. As mentioned earlier, the TBS enol ether has proven stable under the electrolysis conditions, leading to the speculation that the presence of this secondary product might stem from the hydrolysis of recovered starting material—a possibility consistent with a reversible cyclization followed by the reduction of the radical cation back to starting material. This outcome suggests that the reaction holds promise for improvement.

### 4.3.5 Alcohol Substrate Leading to Radical Pathway

Although the chemistry seemed feasible, the challenges encountered in synthesizing the substrates and the subsequent lack of success prompted the Moeller group to shift focus to other projects. As a result, this project remained inactive for several years until Dr. Feng resumed the project. Nevertheless, it was disconcerting that the Sha chemistry had successfully facilitated a tandem cyclization reaction from comparable substrates using the reductive radical approach. We started to speculate whether the issue with the previous attempts stemmed from the nature of the reactive intermediate. It's possible that the radical cation, with its tendency for reversible reactions, might not be the most suitable intermediate. Perhaps the reactions would be more effective with an oxidative radical-type approach, where the crucial intermediate for the tandem cyclization mirrors that of the Sha chemistry (Section 4.2.1).

**Background for Channeling Reaction Down a Radical Pathway**

Recall that while radical cations can undergo radical-like cyclizations,[37] they do possess significant cationic character. The presence of this cationic character is what causes the troublesome elimination reaction. Therefore, efforts were then undertaken to slow down this problematic elimination reaction. Alison Redden and Robert Perkins devised a method to limit

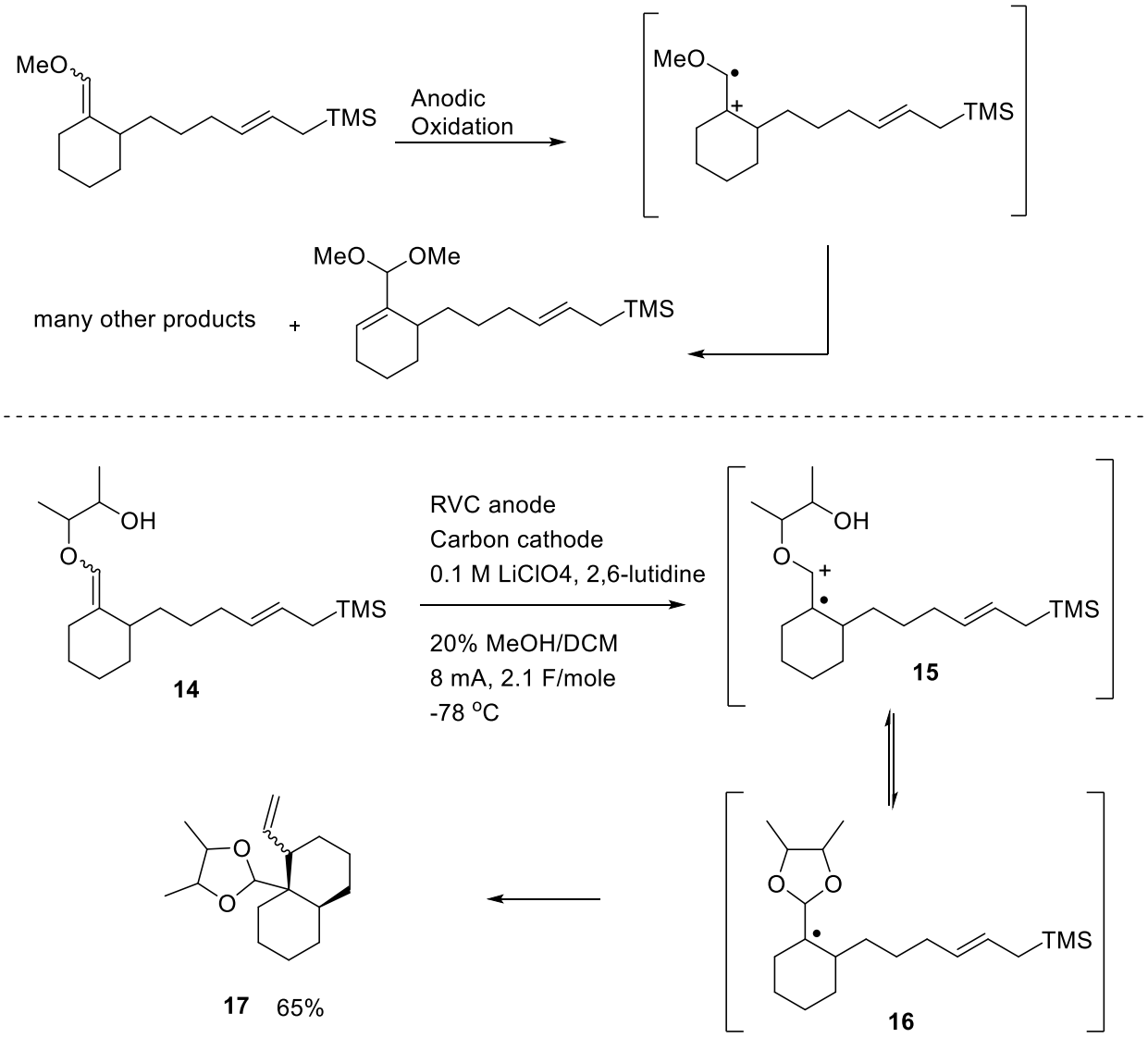


this cationic character and redirect the anodic oxidation reaction along an oxidative radical pathway.[36] Their approach was illustrated in the context of creating six-membered rings and

**Scheme 4.17: Channeling Reaction Down a Radical Pathway**

quaternary carbons using an allylsilane trapping group (Scheme 4.17). The first reaction in Scheme 4.17 was included as a background. In this reaction, the oxidation produced a radical cation from the enol ether. However, the cyclization was too slow, resulting in the elimination of a proton from the radical cation and polymerization reactions. To tackle this problem, the substrate (**14**) underwent modification by replacing the simple enol ether with a glycol-based enediol ether

containing a free hydroxy group. This alteration introduced a second nucleophile in the substrate (**15**), which had the capability to promptly trap the radical cation intermediate. This modification aimed to eliminate the side reaction of proton elimination arising from the cationic character of the intermediate. It left behind a radical intermediate still capable of undergoing the desired cyclization.

The concept was initially tested at room temperature. The reaction yielded a low product yield (10-25%), with most of the products stemming from the decomposition of the radical cation. However, ongoing research within the group revealed that the trapping of a radical cation by an alcohol was reversible and exothermic.[38] If the alcohol trapping of intermediate **15** is reversible, then some cationic character would persist, allowing for the possibility of a competing elimination reaction. However, given that the alcohol trapping is exothermic,[38] lowering the temperature would favor the formation of the cyclized product. Consequently, the oxidative cyclization was repeated at -78°C. Under these conditions, the isolated yield of the cyclized product increased to 65%. It is evident that an allylsilane could serve as a trapping group to achieve the simultaneous formation of a six-membered ring and a quaternary carbon, provided the reaction followed an oxidative radical pathway and avoided the formation of a persistent radical cation intermediate.[36]

The success of this reaction, achieved by directing the reaction along an oxidative radical pathway, suggested the potential for this approach to "buy time" for another, slower cyclization process, specifically a tandem anodic cyclization.

**Synthesis of an Enediol Based Tandem Cyclization Substrate**

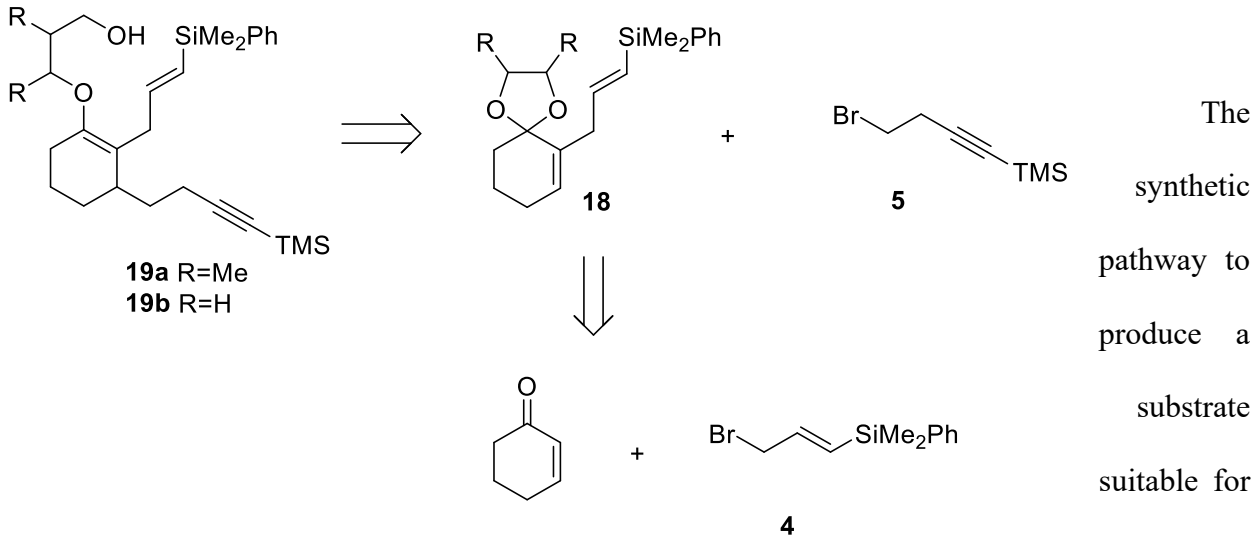


**Scheme 4.18: Retrosynthetic Analysis of Ene Diol 19**

The synthetic pathway to produce a substrate suitable for an oxidative radical cyclization was established by adjusting the method used to create the silyl enol ether substrate **7**. The retrosynthetic analysis is presented in scheme 4.18. The primary change involved incorporating a cyclic ketal **18** into the substrate for the Michael reaction. The approach initially involved introducing an α-side chain **4** to produce intermediate **6** (Scheme 4.13). The cyclic acetal was then installed to form **18** (scheme 4.19).

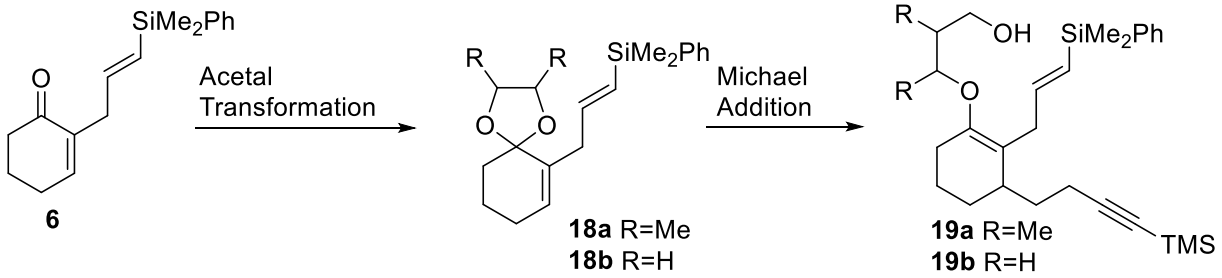


**Scheme 4. 19: Approach to Synthesize Ene Diol Substrate 19a/19b**

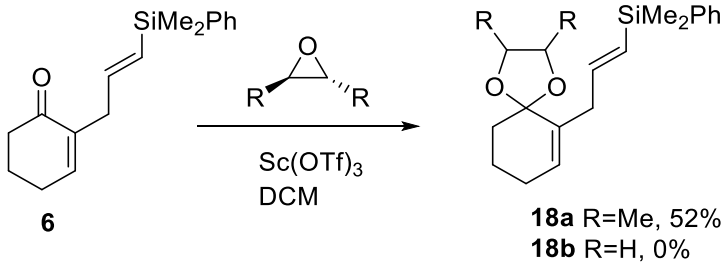


**Scheme 4.20: Formation of Ketal 18**

For a more detailed look at the synthesis of the following ene diol substrate see: Feng, R., Ph.D. Dissertation, Washington University in St. Louis, **2018**. In summary, ketalization of compound **6** with various Lewis acids and ethylene glycol were unsuccessful. After the failure of the condensation-type approaches, an attempt was made to change the mechanism of the transformation. In the example seen in Scheme 4.20, the carbonyl served as a nucleophile to open an epoxide, following the protocol established by William J. Scott.[39] When R=Me the reaction proceeded at a 52% yield of ketal **18a**. However, when an unsubstituted ethylene oxide was used the reaction did not occur (Scheme 4.20).

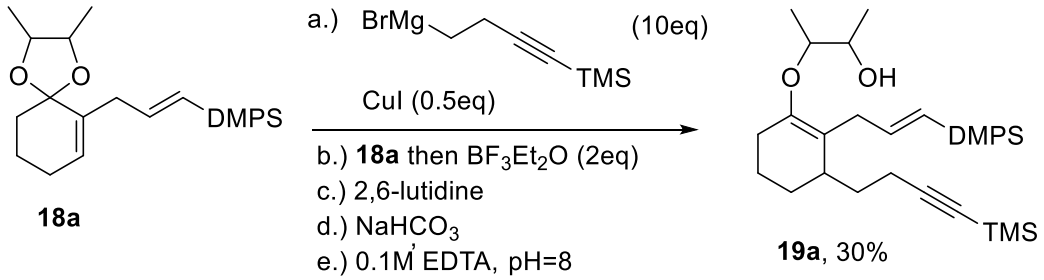


While not overly high yielding, Dr. Feng refrained from further optimization because the goal was

**Scheme 4.21: Michael-type Addition Reaction**

to test if the following oxidative cyclization was going to work before investing additional effort into optimizing the Michael reaction. Therefore, Dr. Feng utilized a similar approach to generate a series of electrolysis substrates, which we will now examine the electrolysis results of.

**Electrolysis of Enediol Based Tandem Cyclization Substrate**

The first electrochemical reaction was done on substrate **19a** at room temperature (Scheme 4.22). As seen in the scheme, the reaction was extremely messy as indicated by the TLC shown. The left lane corresponds to the reaction spot, while the right lane represents the starting material. The top spot in the right lane was generated due to instability during column chromatography. (Feng, R., Ph.D. Dissertation, Washington University in St. Louis, **2018**). It was clear that employing the oxidative radical pathway would not automatically replicate the reaction carried out by Sha. However, the source of the problem in the reaction was unclear. At the time, we were not certain if the problem was rooted in the initial cyclization, or did it occur downstream, involving either the intermediate produced from the first cyclization, the intermediate from the second cyclization,

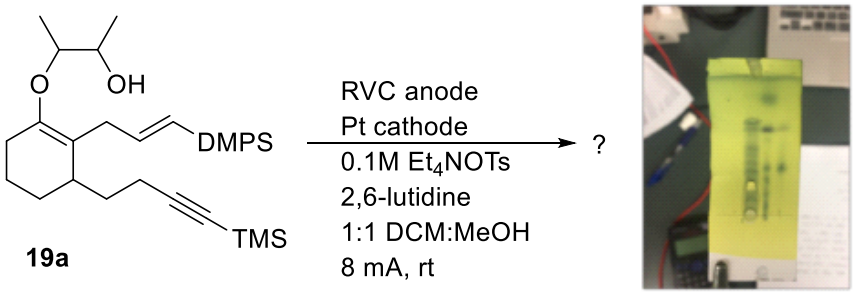


**Scheme 4.22: Initial Tandem Cyclization Test on 19a**

the second oxidation step, or perhaps a combination of these factors?

The next substrate we will examine had one change. Which stemmed from uncertainty regarding the behavior of the vinylsilane as a terminating olefin in the oxidative cyclization. Therefore, the next substrate (**20**), featured a trisubstituted olefin as the terminating group (scheme 4.23). Trisubstituted olefins have proven effective as trapping groups in anodic coupling reactions.[40]

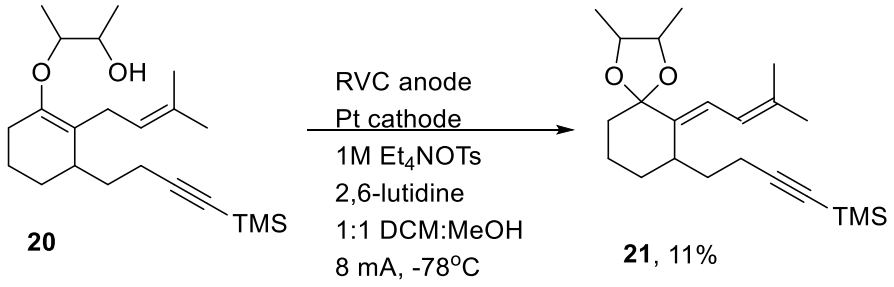


**Scheme 4.23: Electrolysis of 20 Leading to Elimination Product**

However, as seen in Scheme 4.23, the following change did not improve the reaction. Interestingly, when the reaction was carried out at -78°C with a high concentration of a greasier electrolyte such as $Et_4NOTs$, a change made to buy time for the cyclization to occur. The idea was to create a more distinct double layer that would eliminate methanol solvent and provide additional time for the desired tandem intramolecular reactions. The outcome was a cleaner reaction, from which the elimination product **21** could be isolated at an 11% yield.

The retrieval of this product was interesting as it offered some clues regarding a possible explanation for the challenges encountered in this reaction. Scheme 4.24 highlights how this elimination product could be formed. Once the desired radical **22** is formed it can cyclize in two ways: either through a reversible cyclization with the acetylene (pathway a) or through a potentially rapid reversible three-membered ring cyclization with the trisubstituted olefin (pathway b). If it cyclized via pathway a, then the vinylic radical would undergo a slow second oxidation step leading to a reversible cyclization. However, if it cyclized via pathway b, then the tertiary radical would undergo a rapid second oxidation step, pushing it down an irreversible pathway. The generated tertiary cation would then rearrange. From here a few possibilities could occur. Namely, a proton could be removed forming the diene **21**. Alternatively, polymerization reactions or methanol trapping may occur. The ensuing diene might readily engage in subsequent oxidation reactions, causing a loss of mass balance and resulting in the observed methoxylated products. It

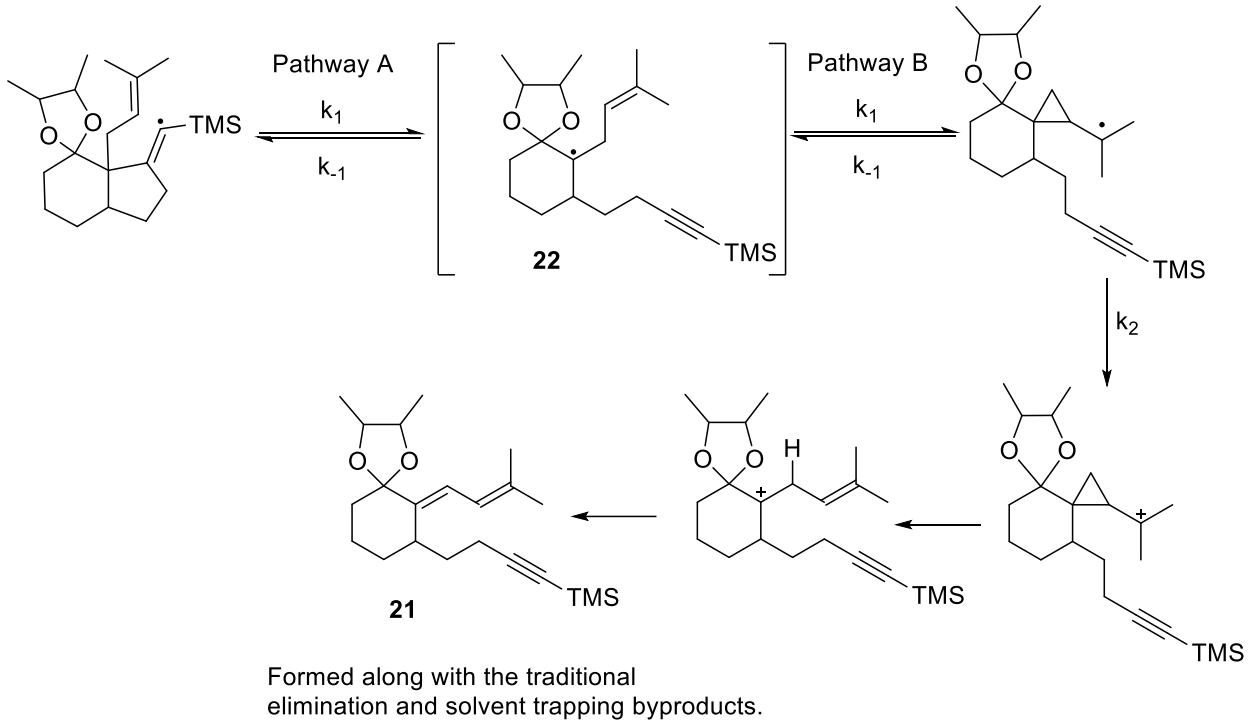


**Scheme 4.24: Possible Pathway for Making Diene**

became apparent that the trisubstituted olefin on the sidechain linked to the radical intermediate posed a challenge for the reaction. Even if the reaction was channeled down a radical pathway it still found a way to undergo a fast second oxidation step which drove it down an irreversible pathway. With this knowledge and the discoveries outlined in Chapter 2, we set out to determine if we could drive a tandem cyclization to completion by using a fast second oxidation step to drive it down a kinetic pathway involving the acetylene relay.

## 4.4 Using a Fast Second Oxidation Step to Drive an Anodic Tandem Cyclization to Completion

With the following background into previous forays into tandem anodic cyclizations in place. We will examine my efforts on this project to use a fast second oxidation step to drive these tandem cyclizations to completion by pushing them down a kinetic pathway.

## 4.4.1 Model Substrate for Anodic Tandem Cyclization

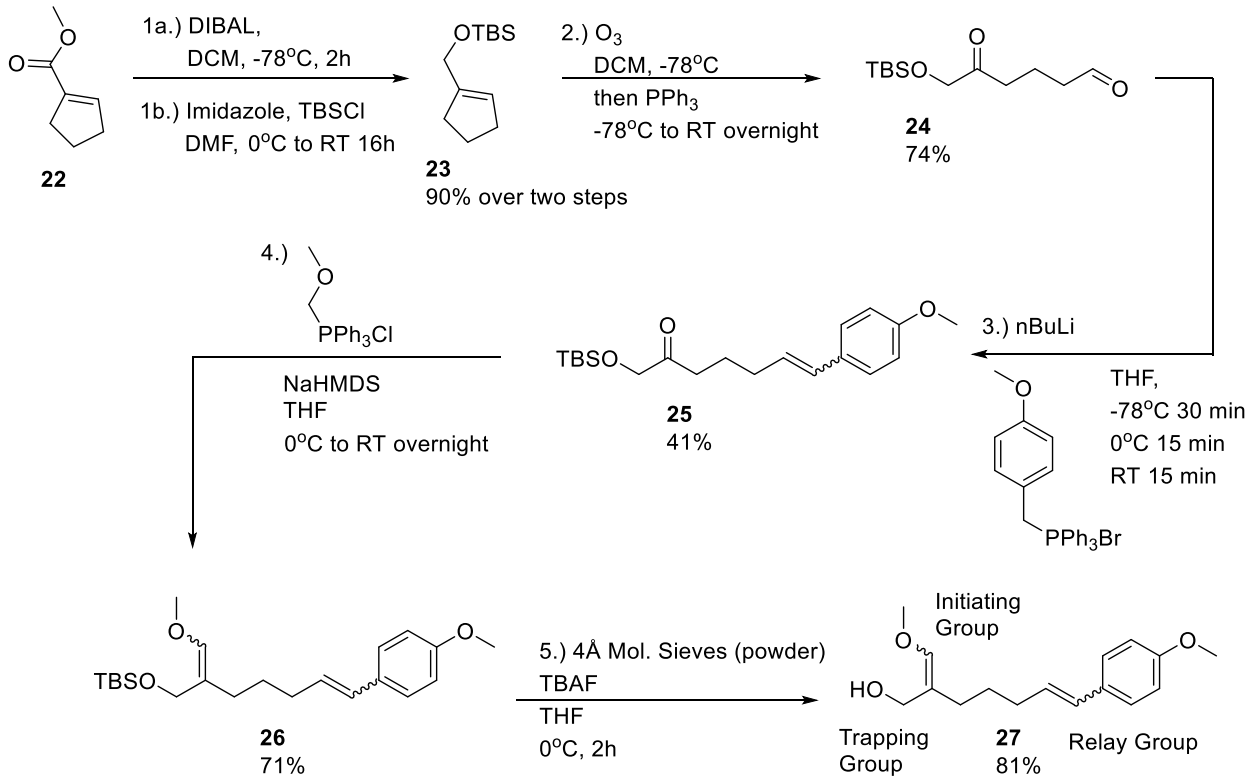


**Scheme 4.25: Synthesis of Model Substrate for Anodic Tandem Cyclization**

As mentioned previously we wondered if we could use a fast second oxidation step to accomplish a tandem anodic cyclization. With this in mind, the following model substrate (Scheme 4.25) was made. Two details of the following substrate were important when it was designed: first, it would utilize an enol ether initiating group that generates a radical cation which likes to make carbon-carbon bonds.[41,42] Second, it utilized a parathoxy styrene group known to facilitate the rate of the second oxidation step.[34,43] The synthesis of the model substrate started with the reduction of the methyl ester **22** by DIBAL. The alcohol was carried forward crude to the TBS protection. The yield of the following TBS protected alcohol was 90% over two steps. From here, the alkene was subjected to an ozonolysis followed by a reductive workup with triphenylphosphine to yield the following dione in a 74% yield. Next, a Wittig reaction was used to install the parathoxy styrene group onto the aldehyde leading to olefin **25** in a 41% yield. Now, another Wittig reaction was

utilized to install the enol ether onto the ketone in a 71% yield. Finally, a deprotection of the TBS group accomplished with TBAF in the presence of 4Å molecular sieves at 0ºC led to the following alcohol in an 81% yield. The substrate **26** was particularly sensitive to hydrolysis leading to protonation of the enol ether so molecular sieves were added to the reaction to protect the substrate from water present in TBAF.

**Electrolysis of Model Substrate**

With the substrate in hand, we performed the following electrolysis (scheme 4.26). Once the enol ether was oxidized to generate a radical cation it would cyclize onto the paramethoxy styrene relay group. This would lead to a benzylic radical which would undergo a rapid second oxidation step driving the reaction down a kinetic pathway leading to a benzylic cation. From here, two possibilities could occur depending upon the stereochemistry of the initial cyclization. If the first ring generated was trans, the alcohol trapping group could not reach the benzylic cation. Therefore, methanol would trap the cations and only monocyclized substrate **28** would be generated. However, if the initial cyclization was cis, the alcohol trapping group could reach the benzylic cation and the tandem cyclization product **29** would occur. In practice, the ratio of trans to cis cyclized product was 1.3:1, with the yield for the monocyclized compound **28** yielding 33% and the yield for the tandem cyclization compound **29** at 25% as determined by NMR analysis. For the cis product from the first cyclization, only the tandem cyclization was observed. The overall mechanistic design worked. Yet while the tandem cyclization was accomplished by using a fast second oxidation step to drive the initial cyclization down an irreversible pathway there was still a major issue with the mock substrate. Namely, the stereochemistry of the initial cyclization determined if the second cyclization occurred. In the case of the cis cyclized product, it can and does undergo a second cyclization. This could not occur if the first cyclization occurred in a trans

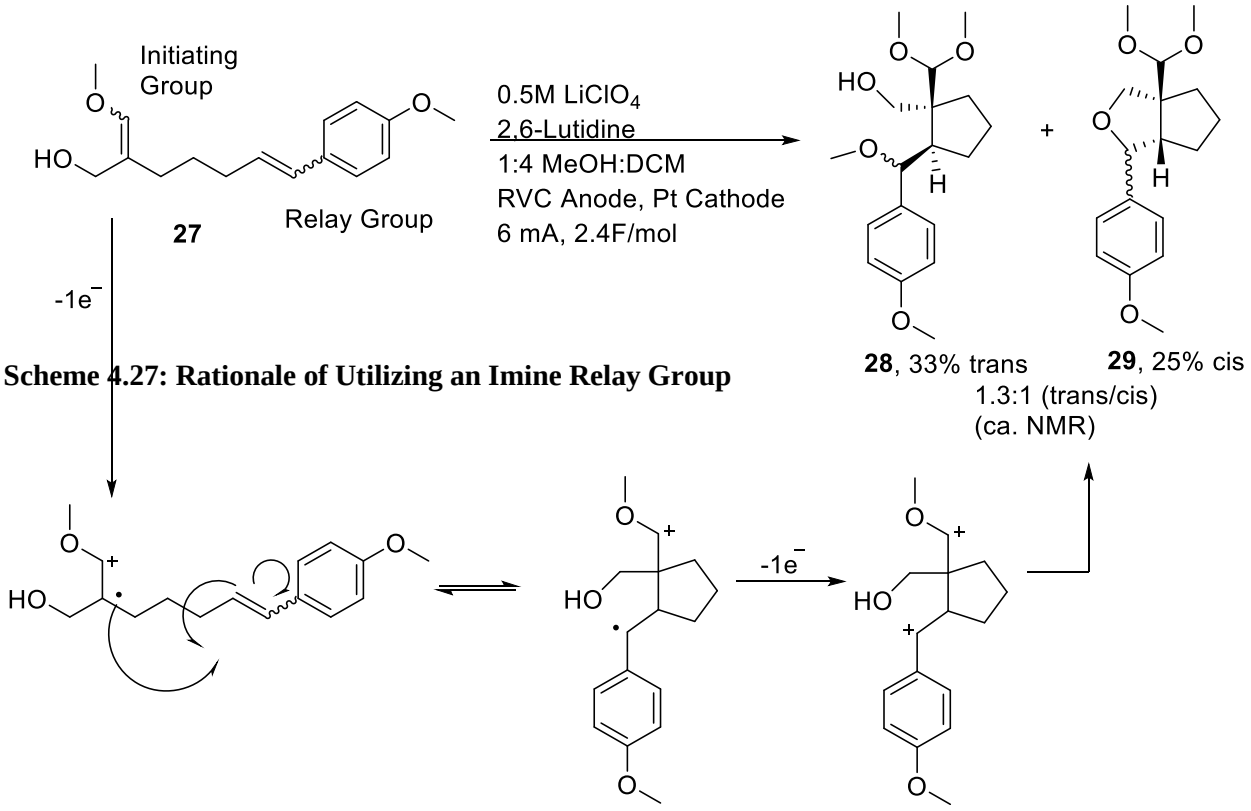


**Scheme 4.27: Rationale of Utilizing an Imine Relay Group**

**Scheme 4.26: Electrolysis of Model Substrate**

manner. There are two possible relay groups we could use to circumvent this issue: first, with the success of imines to generate cyclic proline derivatives[44] we could extend this idea to incorporate a tandem cyclization. Second, we could utilize an acetylene relay group as attempted by Bradley Scates, Laura Anderson, and Ruozhu Feng. Both routes would eliminate the issue of stereochemistry interfering with the tandem cyclization occurring.

## 4.4.2 Using an Imine as a Relay Group for an Anodic Tandem Cyclization

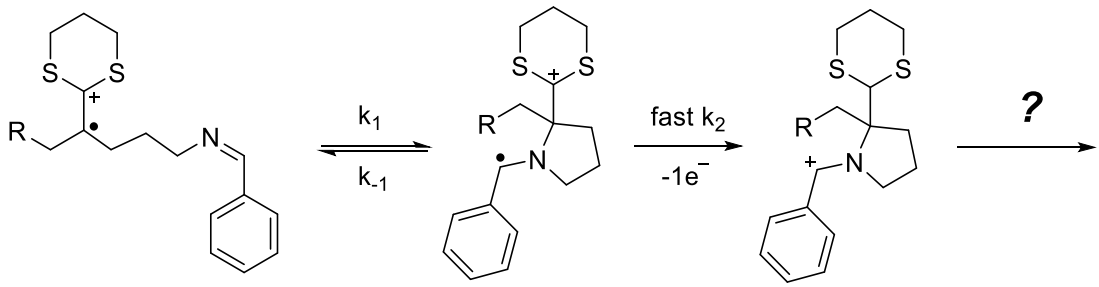


As described in chapter 3, we know that

imines are compatible with anodic cyclizations. They serve as excellent trapping groups for radical cations derived from dithioketene acetals. We also know that these cyclizations occur quickly and at or near the electrode surface. Additionally, these reactions undergo a fast second oxidation step resulting in a high yield of the cyclic proline derivative product.[44] The general idea of using an imine as a relay group to accomplish a tandem cyclization can be seen in Scheme 4.27. If an imine would be utilized as a relay group it would eliminate the issue of the stereochemistry of the initial cyclization interfering with the subsequent cyclization.

**Synthesis of First-Generation Tandem Cyclization Substrate Using an Imine**

The synthesis of the following imine substrate **37** (scheme 4.28) began with first synthesizing the Weinreb amide **30** from δ-valerolactone, a methoxy amine nucleophile, and diisobutylammonium hydride as reagent to activate the amine. This yielded the Weinreb amide **30** in 87%. The alcohol was then TBS protected to give **31** in 88% yield. Next, the weinreb amide was converted to ketone **32** in 88% yield. Next, the weinreb amide was converted to ketone **32** in an 83%with phenyl lithium and as $ZnBr_2$ as the lewis acid. The ketone was then subjected to a Peterson olefination in order to install the dithioketene acetal functional group. This was carried forward crude to the TBS deprotection, accomplished with TBAF to yield the free alcohol in 63% over two steps. Now, a Mitsunobu azidation was used to convert the alcohol into an azide in a 59% yield. This azide was then reduced to a primary amine in a 87% yield by using typical Staudinger reduction conditions. Finally, the amine was converted into an imine by condensing it onto para-anisaldehyde in the presence of 4Å molecular sieves to absorb the water generated during the reaction. This yielded imine **37** in a 95% yield.

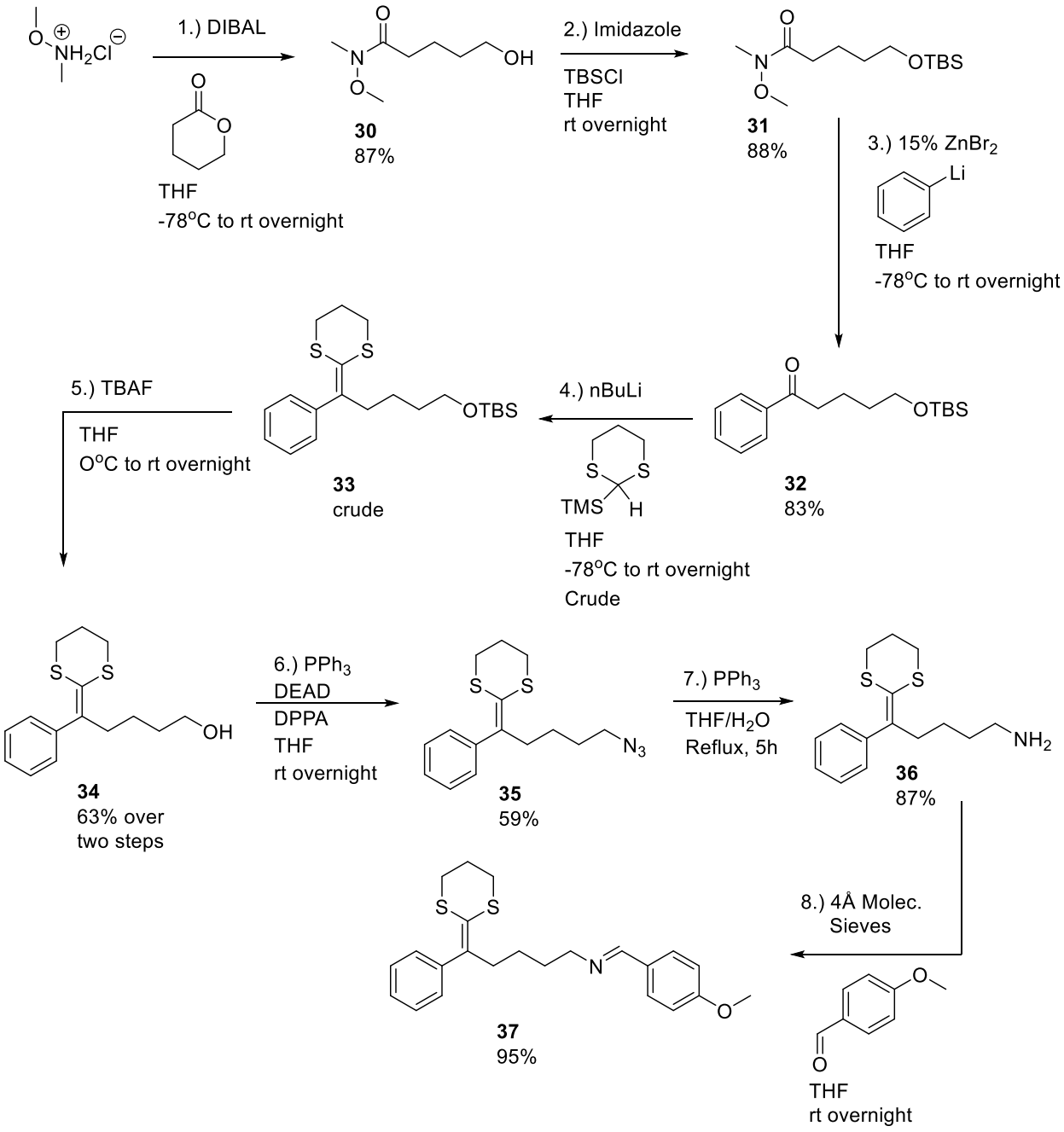


**Scheme 4.28: Synthesis of Imine Tandem Cyclization Substrate 37**

**Scheme 4.29: Electrolysis of 37**

**Electrolysis of First-Generation Tandem Cyclization Substrate Using an Imine**

With compound **37** in hand, we performed the following electrolysis (Scheme 4.29), utilizing the conditions shown to accomplish the imine cyclizations shown in Chapter 3. We envisioned this reaction first undergoing an oxidation at the dithioketene acetal which will generate a radical cation which will be trapped by the imine relay group. This benzylic radical would undergo a fast second oxidation step generating a benzylic cation. From here, we had hoped that the phenyl ring would trap the benzylic cation. Finally, the removal of a proton on the phenyl ring would return aromaticity to the product. However, in practice it led to a low mass balance for the reaction with no recovered starting material nor any discernable product. In fact, the only thing isolated after

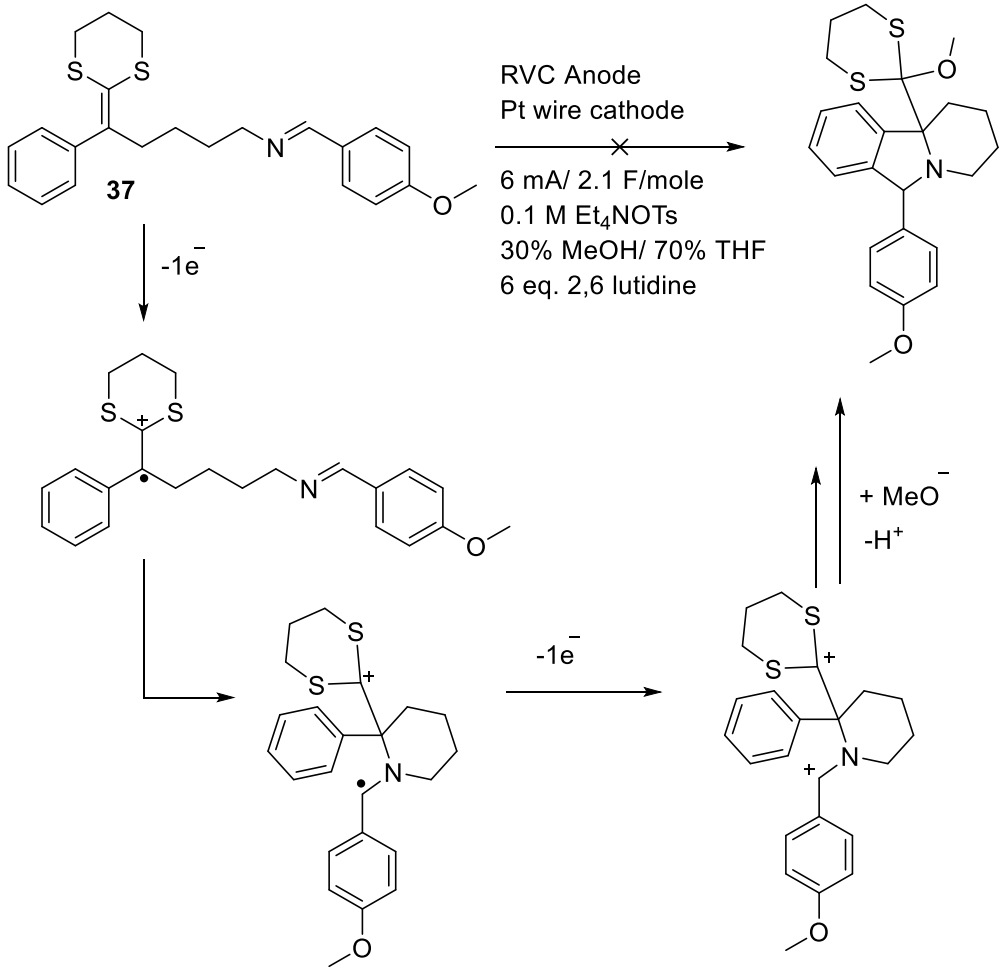


column chromatography was polymethoxylated polymer. There are two potential issues that could lead to these observations: first, the phenyl ring is directly conjugated to the dithioketene acetal

which could prove problematic in the reaction. Such a substrate had not been examined previously. Second, the initial cyclization onto the imine was a six-membered ring not a five-membered ring. Perhaps the imine cyclization is only compatible with a five-membered ring transformation.

**Synthesis of Second-Generation Tandem Cyclization Substrate Using an Imine**

The second-generation substrate that utilized an imine, was constructed to answer the above problems noted about the first-generation substrate. Specifically, we wanted to see if the tandem cyclization would be compatible with an aromatic ring conjugated to the dithioketene acetal and if the reaction would work if a five-membered ring cyclization onto the imine was employed. The route to the following substrate is shown in Scheme 4.30 The route taken was akin to the one shown in scheme 4.28 with two minor changes. The synthesis started with making the Weinreb amide **38** from γ-butyrolactone, a methoxy amine nucleophile, and diisobutylammonium hydride as reagent to activate the amine. This intermediate was carried forward crude to TBS protection of the alcohol leading to **39** in a 68% yield over two steps. Next, the weinreb amide was converted to ketone **40** in an 84% with 3-methoxyphenylmagnesium

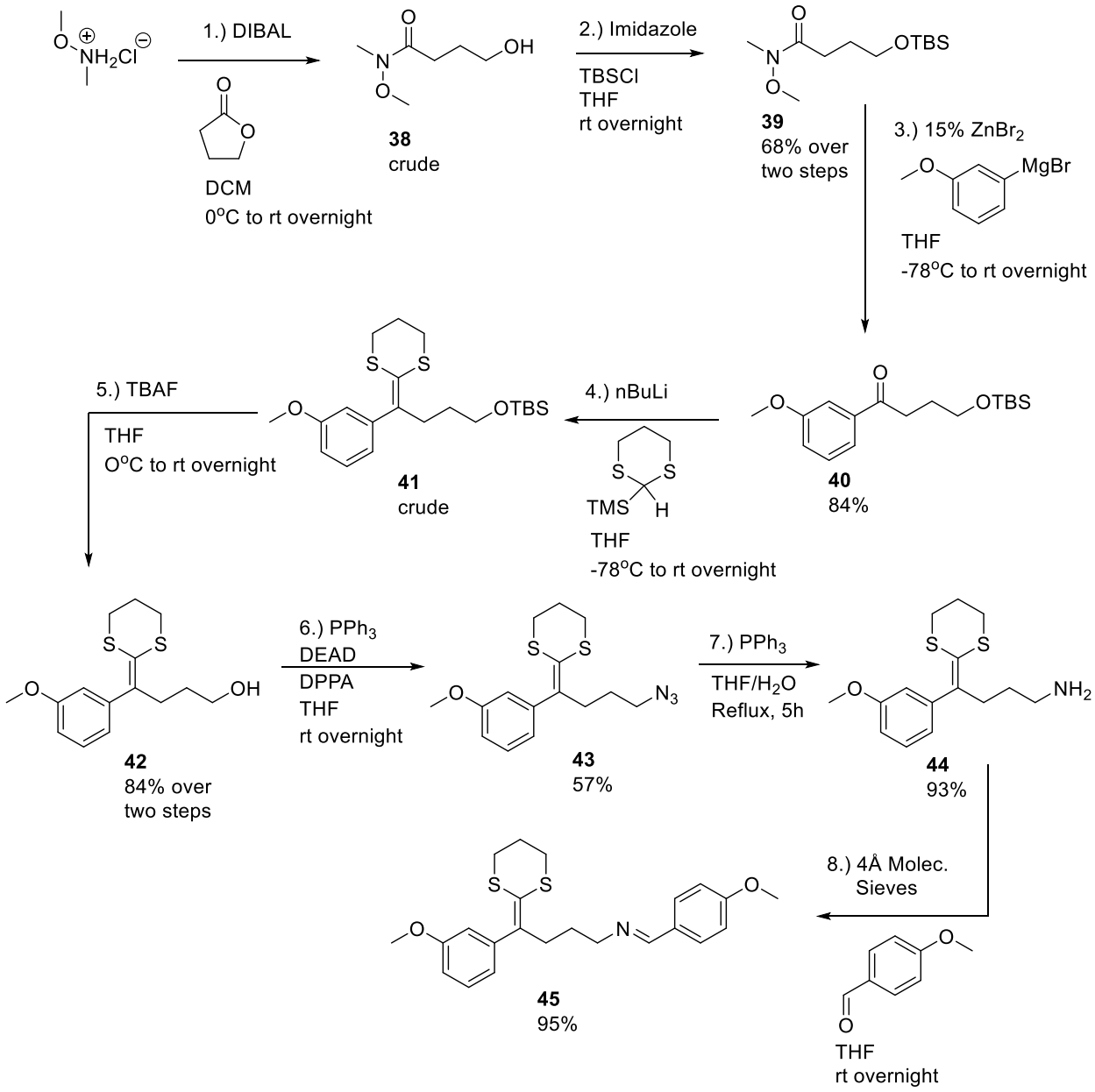


**Scheme 4.30: Synthesis of Second-Generation Substrate**

bromide and $ZnBr_2$ as the lewis acid. The ketone was then subjected to a Peterson olefination in order to install the dithioketene acetal functional group. This was carried forward crude to the TBS deprotection, accomplished with TBAF to yield the free alcohol in 84% over two steps. Now, a Mitsunobu azidation was used to convert the alcohol into an azide in a 57% yield. This azide was then reduced to a primary amine in a 93% yield by using typical Staudinger reduction conditions. Finally, the amine was converted into an imine by condensing it onto para-anisaldehyde in the presence of 4Å

molecular sieves to absorb the water generated during the reaction. This yielded imine **45** in a 95% yield.

**Electrolysis of Second-Generation Tandem Cyclization Substrate Using an Imine**

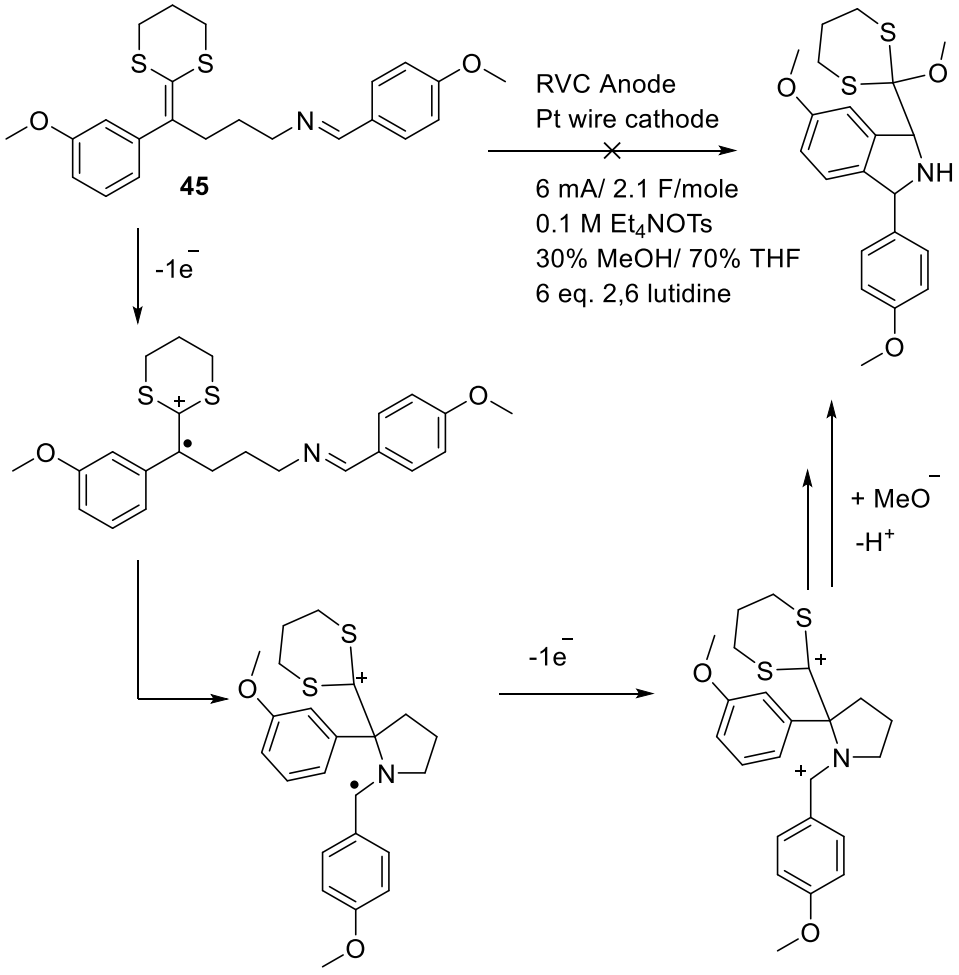


**Scheme 4.31: Electrolysis of 45**

Having compound **45** in hand, we conducted the electrolysis (Scheme 4.31) employing the conditions previously used for the imine cyclizations detailed in Chapter 3. Once oxidized, we thought the dithioketene acetal derived radical cation would cyclize which onto the imine relay group. This benzylic radical would undergo a fast second oxidation step generating a benzylic cation. Now, we had envisioned that the 3-methoxy substituted phenyl ring would be a better

trapping group for the benzylic cation. Once it cyclized a second time, the removal of a proton on the phenyl ring would return aromaticity to the product. In practice, the outcome was again a low mass balance for the reaction, yielding neither recovered starting material nor any discernible product. After column chromatography, only polymethoxylated product was found. A

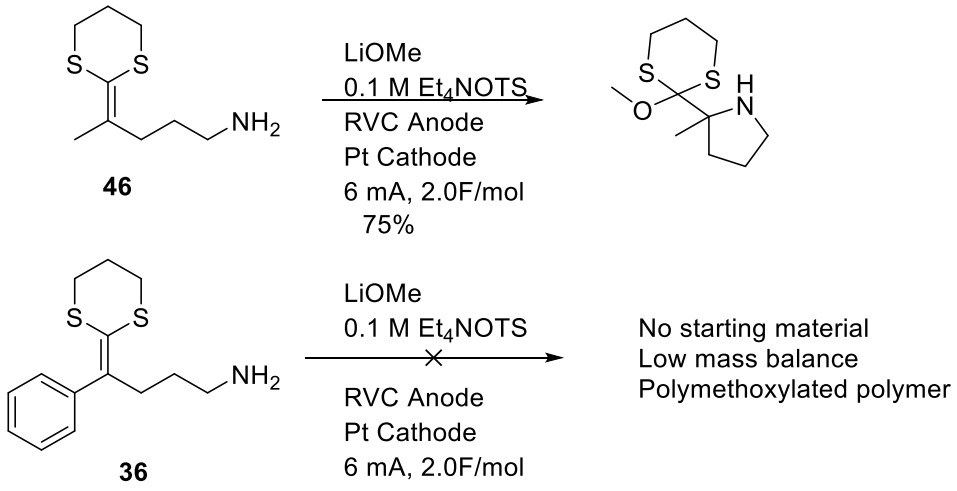


**Scheme 4.32: Electrolysis Examining if Phenyl Ring is Interfering with the Reaction**

potential reason for the failure in this reaction is that the phenyl ring was still directly conjugated to the dithioketene acetal, a scenario that has not been proven to be compatible with this reaction. To test this hypothesis, the reaction shown in scheme 4.32 was carried out. As shown in a previous study, the Moeller group has shown that amine **46** can be directly coupled to a dithioketene acetal in an electrolysis if LiOMe is used.[45] Utilizing the exact conditions described therein, we performed the following electrolysis of **36** to see if the phenyl ring interfered with the reaction. It did in fact interfere with the reaction, again leading to no discernable product with a low mass balance and no recovery of starting material.

**Synthesis of Third-Generation Tandem Cyclization Substrate Using an Imine**

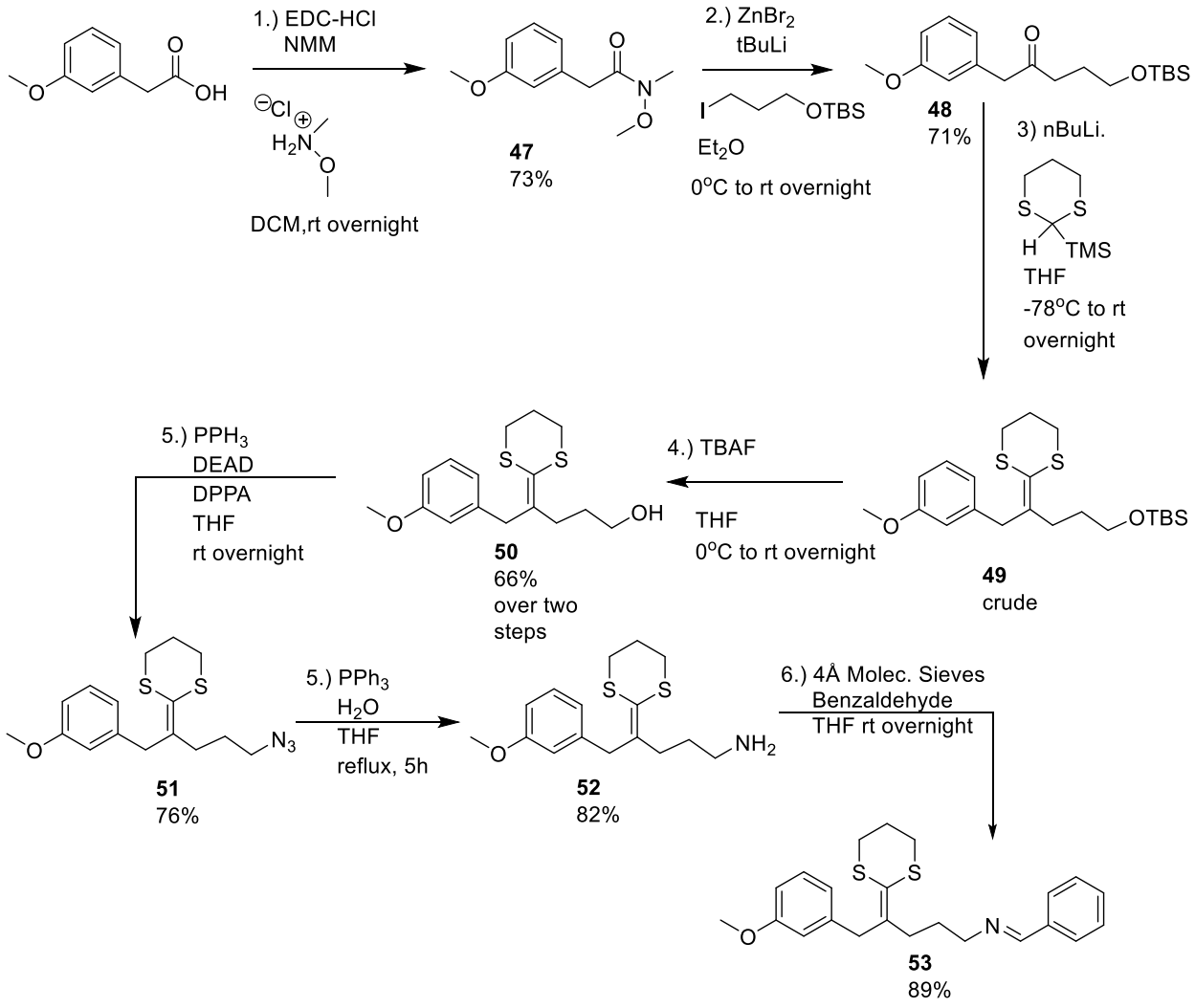


**Scheme 4.33: Synthesis of Third-Generation Imine Substrate**

With the phenyl group being conjugated to the dithioketene acetal clearly being an issue with the cyclization, we shifted our attention towards a third-generation substrate that incorporated a methylene unit between the aromatic ring and the dithioketene acetal. The route to generate said substrate is seen in scheme 4.33. The route started by coupling N,O-dimethylhydroxylamine hydrochloride to 3-methoxyphenyl acetic acid with the use of the peptide coupling agent EDC. This yielded the Weinreb amide **47** in 73% yield. The Weinreb amide was converted to the ketone **48** in a 71% yield. Now, a Peterson olefination was employed to install the dithioketene acetal.

This compound was carried forward crude to the TBS deprotection to yield alcohol **50** in 66% over two steps. Next, the alcohol was converted to the azide **51**with a Mitsunobu azidation. From here, typical Staudinger reduction conditions were used to give amine **52** in an 82% yield. Finally, the amine was coupled to benzaldehyde in the presence of 4Å molecular sieves to give imine **53**.

**Electrolysis of Third-Generation Tandem Cyclization Substrate Using an Imine**

Having obtained the imine, we oxidized it following the conditions outlined in Scheme 4.34. Although the reaction yielded the monocyclized product **54** in 34% yield, no tandem cyclized product was observed. To see if the reason for this was a slow second cyclization of the phenyl

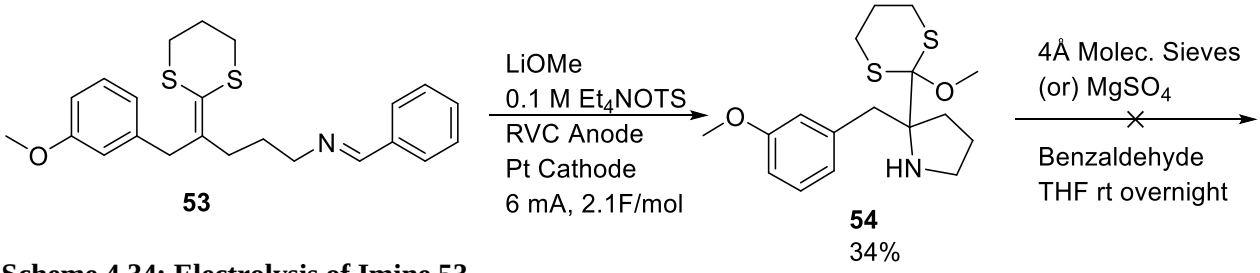


**Scheme 4.34: Electrolysis of Imine 53**

ring onto the benzylic cation following the initial cyclization, we attempted to condense the cyclic amine onto benzaldehyde using 4Å molecular sieves or $MgSO_4$ as the water scavenger. In either case the reaction yielded only recovered cyclic amine and benzaldehyde. At this point, since no discernable tandem cyclized product from an anodic cyclization using an imine relay group was found, we shifted our focus to utilizing an acetylene to accomplish this transformation.

## 4.4.3 Using an Acetylene as a Relay Group for an Anodic Tandem Cyclization

Acetylenes can serve as trapping groups for anodic cyclizations as previously seen in Scheme 4.15. However, they lead to three different products. One product resulted from the formation of a vinyl cation, which was then captured by methanol and oxidized to produce an unsaturated acetal **10**. Another product arose from the elimination of a proton from the vinyl cation, yielding allene **11**.

In a mechanistic study, the introduction of dichloromethane to the reaction resulted in a hydrogen abstraction product **9**, which indicated the formation of a vinyl radical intermediate. The formation of this final product from a vinylic radical is significant. Considering the insights from Chapter 2 regarding the importance of the second oxidation step, we now have a potential solution to achieve a successful cyclization using an acetylene trapping group. This involves accelerating the second oxidation step of the vinylic radical to drive the reaction toward completion along a kinetic pathway.

**Synthesis of Acetylene Substrate Designed to Increase the Rate of the Second Oxidation Step**

Before embarking on a tandem cyclization using an acetylene as a relay group, we deemed it crucial to test whether we could drive a monocyclization with an acetylene down an irreversible pathway. We wondered if we could channel this cyclization to a vinylic cation and convert it into the allene product. With this in mind, the following acetylene substrate was synthesized (Scheme 4.35). The rationale behind adding the silyl group is because we know that silyl groups stabilize ß-cations.[46] This should help with the second oxidation step and should give the allene product if

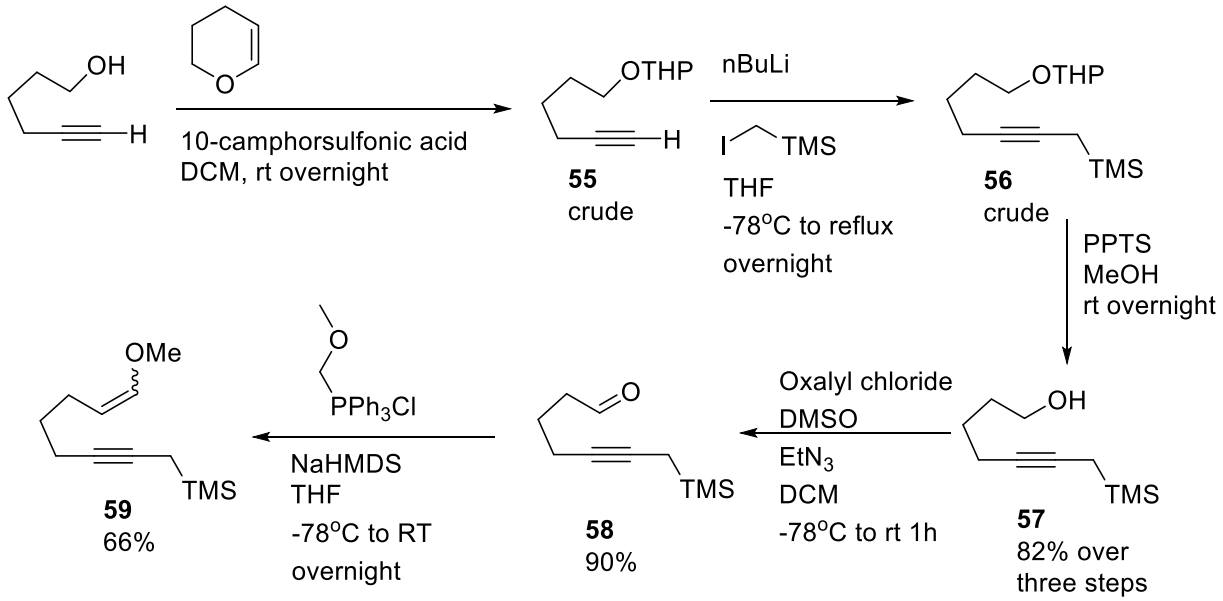


**Scheme 4.35: Synthesis of Acetylene Substrate 59**

a vinylic cation is formed. The synthesis started by THP protecting 5-hexyn-1-ol with dihydropyran catalyzed by 10-camphorsulfonic acid to give **55** which was carried forward crude. Now, the alkyne was alkylated with (iodomethyl)trimethylsilane. Next, the THP group was removed with PPTS in methanol stirring overnight to give alcohol **57** in 82% over three steps. The alcohol was then converted into an aldehyde in 90% yield with the use of the Swern oxidation.

**Table 4.1: Electrolysis of Acetylene to Give Allene 60**

Finally, a Wittig reaction was used to install the enol ether in a 66% yield.

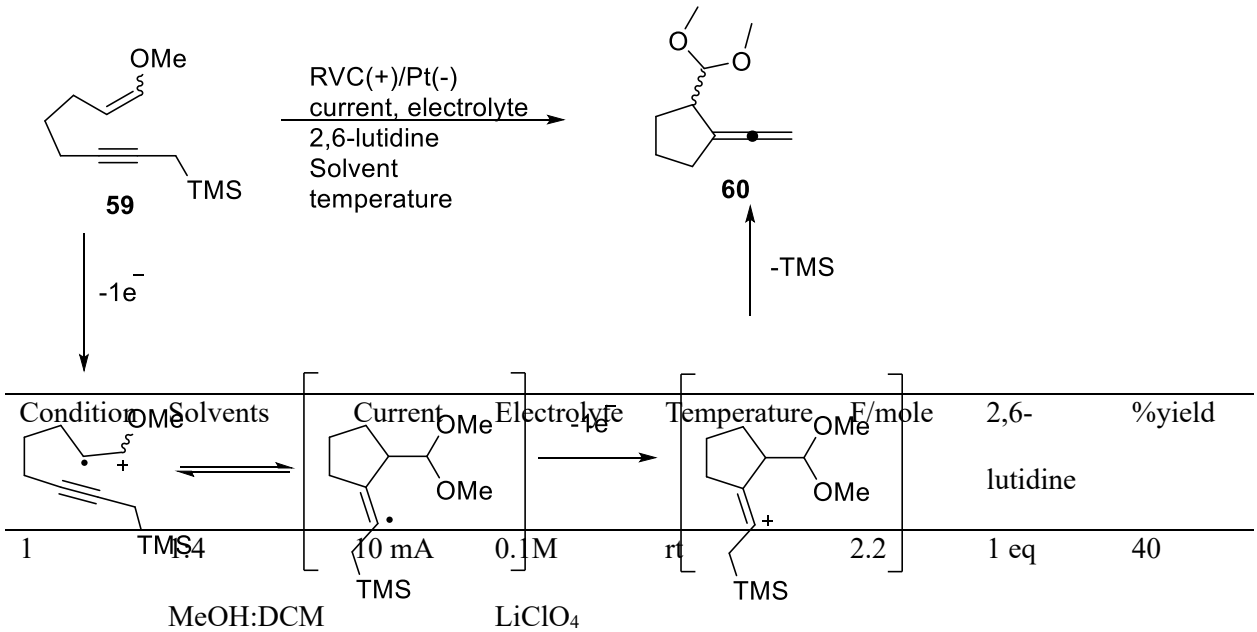


| Condition | Solvents | Current | Electrolyte | Temperature | F/mole | 2,6-lutidine | %yield |
|---|---|---|---|---|---|---|---|
| 1 | 1:4 MeOH:DCM | 10 mA | 0.1M $LiClO_4$ | rt | 2.2 | 1 eq | 40 |
| 2 | 1:4 MeOH:DCM | 12 mA | 0.1M $LiClO_4$ | rt | 2.2 | 1 eq | 30 |
| 3 | 1:4 MeOH:DCM | 10 mA | 0.2M $LiClO_4$ | rt | 2.2 | 1 eq | 33 |
| 4 | 1:4 MeOH:THF | 10 mA | 0.1M $LiClO_4$ | rt | 2.2 | 1 eq | 33 |
| 5 | 1:4 MeOH:DCM | 10 mA | 0.1M $Et_4NOTs$ | 0ºC | 2.2 | 1 eq | 28 |
| 6 | 1:4 MeOH:DCM | 10 mA | 0.1M $Bu_4NBF_4$ | rt | 2.2 | 1 eq | 51 |

| Condition | Solvents | Current | Electrolyte | Temperature | F/mole | 2,6-lutidine | %yield |
|---|---|---|---|---|---|---|---|
| 7 | 1:4 MeOH:DCM | 10 mA | 0.2M $Bu_4NBF_4$ | 0°C | 2.2 | 1 eq | 52 |

**Electrolysis of Acetylene Substrate**

As seen in table 4.1, when substrate **59** was oxidized it successfully formed the allene product **60**. Once, the enol ether was oxidized it would generate a radical cation. The radical would be trapped by the acetylene giving a vinylic radical. From here, a second oxidation step occurred giving a vinylic cation which would be stabilized by the ß-silyl group. Finally, the silyl group would be cleaved to give the cyclic allene. The formation of this allene would serve as a identifiable marker for how well the second oxidation step was occuring. The highest yield for this cyclization came from condition 7 in which the electrolyte was $Bu_4NBF_4$.This led to a 52% yield of allene **60** via NMR analysis This electrolyte places fluoride anions into solution which likely assists with the cleavage of the silyl group. Additionally, the reaction was carried out at 0°C since lower temperatures favor the formation of kinetic products.

## 4.5 Conclusion

We were able to successfully perform a tandem cyclization on a mock substrate (Scheme 4.26) by utilizing a fast second oxidation step to drive the first ring generated down an irreversible pathway. Unfortunately, that substrate had a stereochemistry problem. If the first ring generated was trans, the alcohol trapping group could not reach the benzylic cation. However, if the first ring cyclized in a cis fashion then the tandem cyclized product was seen. To solve this issue of stereochemistry we pursued two methods to eliminate this possibility. The first method involved utilizing an imine

as the relay group. In the three substrates pursued using an imine relay group no discernible tandem cyclized product was identified. The second method examined if we could push a cyclization using an acetylene down a kinetic pathway leading to an allene intermediate. While this monocyclization was successful, my efforts began to be focused on the chemistry shown in chapter 5. Specifically, we were interested in making a nitrogen-carbon bond between an amide and an electron-rich styrene trapping group anodically. The success of this reaction prompted my attention to shift to this topic. If efforts to perform a successful anodic tandem cyclization were to be pursued in the future, it will be necessary to identify a substrate that resolves the stereochemistry issue observed in the mock substrate while also utilizing a fast second oxidation step. Another avenue to explore would be to mediate the radical reaction with a transition metal as shown in Chapter 5.

# Experimental Section

## 4.6.1 General Experimental

NMR spectra were acquired on either a Varian Mercury 300 or Agilent DD2 500 MHz, spectrometer at either 300, or 500 MHz for 1H or 75 or 126 MHz for 13C{1H} unless otherwise noted. Chemical shifts (δ) are reported in ppm relative to tetramethylsilane (0 ppm) for 1H and 13C{1H}. Mass spectra were recorded on either a Thermo LTQ-Orbitrap spectrometer under positive ion mode or a Maxis 4G ESI-QTOF spectrometer with flow rate of 3 μL/min. Reactions were run under either an argon or nitrogen atmosphere unless otherwise noted. Flasks were flame-dried under vacuum unless otherwise noted. Tetrahydrofuran was purchased from Sigma-Aldrich Corporation and distilled from sodium benzophenone ketyl under argon atmosphere prior to use. Triethylamine and dichloromethane reaction solvent were purchased from Sigma-Aldrich Corporation and distilled from calcium hydride under argon atmosphere prior to use. Flash column chromatography was performed on 60 Å silica gel purchased from Sorbent Technologies. Thin layer chromatography was performed on Analtec UNIPLATE™ and visualized by ultraviolet irradiation, ceric ammonium molybdate, phosphomolybdic acid, or 2,4-dinitrophenylhydrazine.. All other starting materials and reagents were purchased from Sigma-Aldrich Corporation and used as received. Electrolysis reactions were conducted using a model 630 coulometer, a model 410 potentiostatic controller, and a model 420A power supply purchased from the Electrosynthesis Company, Inc. (now Electroytica). Carbon rods were also purchased from the Electrolytica Company. Reticulated vitreous carbon (RVC) electrodes were purchased from ERG Aerospace Corp.

## 4.6.2 Synthesis and Electrolysis of Compounds

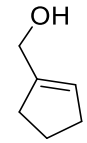


**22a**

First, the reaction was placed under a nitrogen atmosphere. Next, (1.7mL, 13.9 mmol) of Methyl 1-cyclopentene-1-carboxylate was added to a round-bottom flask. Now, 44 mL of DCM was added and the flask was placed in a dry ice acetone bath. Now, (31mL, 31 mmol) of DIBAL-H was added dropwise. The reaction was allowed to stir for 2h at -78ºC. The reaction was quenched with a saturated solution Rochelle's salt and stirred to rt for 1h. Reaction mixture was filtered through celite plug eluted with DCM. Reaction was concentrated in vacuo to yield 1.364g of **22a** which was carried forward crude and characterized after the subsequent step.

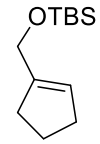


**23**

First, (1.416g, 20.8 mmol) of imidazole was added to a round-bottom flask. The reaction was placed under nitrogen and 10 mL DMF was added. The flask was then placed in an ice bath. Now, (1.364g, 13.9 mmol) of **22a** in 11 mL of DMF was added Next, (3.135g, 20.8 mmol) of TBSCl in 11 mL of DMF was added. The reaction was left to stir to room temp overnight. The reaction was brought to 0ºC and quenched with sat aq. $NH_4Cl$ solution. Aqueous layer extracted 3x with diethyl ether. Organic layers were combined and dried over $MgSO_4$ and concentrated in vacuo. The crude product was purified with column chromatography eluting with 1:4 to 1:1 DCM:Hexanes to yield 2.664g of **23** (90% over two steps).

$^{1}$H NMR ($CDCl_3$, 500 MHz): δ 5.51 (s, 1H), 4.14 (s, 2H), 2.35 – 2.13 (m, 4H), 1.85 (qd, *J* = 7.9, 6.8 Hz, 2H), 0.89 (s, 9H), 0.03 (s, 6H).

$^{13}$C NMR ($CDCl_3$, 125 MHz): δ 149.73, 129.83, 67.89, 37.92, 37.71, 37.22, 31.34, 28.95, 23.80, 19.51, 0.00.

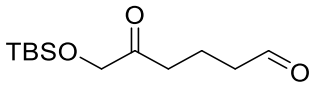


**24**

First, (2834g, 13.4 mmol) of olefin **23** in 54 mL of DCM was added to a round-bottom flask. The flask was placed in a dry ice acetone bath. Ozone was bubbled into solution until the reaction turned light blue and olefin was gone via TLC. Now, (6.997g, 26.8 mmol) of triphenyl phosphine was added and the reaction was allowed to stir to rt overnight. The reaction was concentrated in vacuo until it was 1/3$^{rd}$ of its original volume. The crude mixture was pushed through silica gel plug eluted with 1:1 diethyl ether:Hexanes and concentrated in vacuo. Crude product was then purified by column chromatography using 1:7 to 1:4 EA:Hexanes and flushed with 100% EA to yield 2.412g of **24** (74%).

$^{1}$H NMR ($CDCl_3$, 500 MHz): δ 9.64 (s, 1H), 4.08 (s, 2H), 2.48 (t, *J* = 7.1 Hz, 2H), 2.40 (td, *J* = 7.2, 1.4 Hz, 2H), 1.79 (p, *J* = 7.1 Hz, 2H), 0.84 (s, 9H), 0.01 (s, 6H).

$^{13}$C NMR ($CDCl_3$, 125 MHz): δ 214.96, 206.83, 74.72, 48.49, 42.52, 31.34, 23.81, 21.23, 0.00.

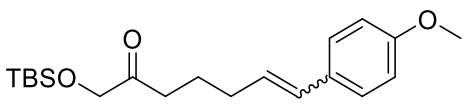


**25**

First, (5.217g, 11.3 mmol) of paramethoxy triphenylphosphonium bromide was added to a round-bottom flask. Now, 28 mL of THF was added. The reaction was placed under a nitrogen atmosphere. The flask was placed in a dry ice acetone bath. Now, (4.2 mL, 10.4 mmol) of nBuLi was added dropwise. The reaction was allowed to stir for 30 min at -78ºC for 30 minutes and for 15 minutes at room temperature. The flask was placed back in the dry ice acetone bath and (2.415g, 9.88 mmol) of **24** in 25 mL THF was added dropwise over 10 minutes. The reaction was stirred at -78ºC for 30 minutes, at 0ºC for 15 minutes, and room temp for 15 minutes. The reaction was brought back to 0ºC and quenched with sat aq $NH_4Cl$ solution and extracted 3x with diethyl ether. The organic layers were combined, dried over $MgSO_4$, and concentrated in vacuo The residue was diluted with hexanes and placed in freezer to crash out triphenylphosphine oxide. The reaction was filtered and concentrated in vacuo. The crude product was purified with column chromatography using 1:9 to 1:4 EA:Hexanes as the eluent to yield 1.412g (41%) of **25**.

$^1$H NMR ($CDCl_3$, 500 MHz): δ 7.16 (d, *J* = 8.7 Hz, 1.40H), 7.11 (d, *J* = 8.7 Hz, 0.6H), 6.78 (d, *J* = 8,8 Hz, 0.66H), 6.73 (d, *J* = 8.8 Hz, 1.35H), 6.29 (d, *J* = 11.6 Hz, 0.41H), 6.23 (d, *J* = 15.8 Hz, 0.72H), 5.92 (dt, *J* = 15.8, 7.0 Hz, 0.78H), 5.43 (dt, *J* = 11.6, 7.2 Hz, 0.41H), 4.06 (s, 1.14H), 4.03 (s, 10.55H), 3.67 (s, 1.01H), 3.66 (s, 1.81H), 2.41 (dt, *J* = 11.9, 7.3 Hz, 1.87H), 2.26 (qd, *J* = 7.4, 1.9 Hz, 0.98H), 2.12 (qd, *J* = 7.2, 1.4 Hz, 1.47H), 1.78 – 1.58 (m, 2.35H), 0.86 (s, 9H), 0.01 (s, 6H).

$^{13}$C NMR ($CDCl_3$, 125 MHz): δ 215.71, 164.32, 163.83, 135.89, 135.70, 135.64, 135.41, 134.67, 132.96, 132.56, 119.39, 119.37, 119.09, 74.77, 60.57, 43.06, 42.94, 37.95, 37.13, 33.47, 31.44, 31.30, 31.12, 28.95, 28.46, 28.19, 23.78, 19.67, 0.17, -0.00.

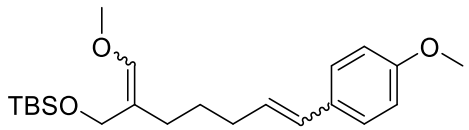


**26**

First, (4.182g, 12.2 mmol) of (Methoxymethyl)triphenylphosphonium chloride was added to a round-bottom flask. The reaction was placed under a nitrogen atmosphere. Now, 30 mL of THF was added and the flask was placed in an ice-bath. Next, (12.2 mL, 12.2 mmol) of NaHMDS was added dropwise. The reaction was allowed to stir for 30 minutes at 0ºC before (1.412g, 4.05 mmol) of **25** in 10 mL of THF was added over 10 minutes. The reaction was allowed to stir to room temperature overnight. The reaction was cooled to 0ºC, quenched with brine and extracted 3x with diethyl ether. The organic layers were combined, dried over $MgSO_4$, and concentrated in vacuo The residue was diluted with hexanes and placed in freezer to crash out triphenylphosphine oxide. The reaction was filtered and concentrated in vacuo. The crude product was purified with column chromatography using 1:19 to 1:9 EA:Hexanes as the eluent to yield 1.084g (71%) of **26**.

$^1$H NMR ($CDCl_3$, 500 MHz): δ 7.20 – 7.10 (m, 1.67H), 6.78 – 3.70 (m, 1.78H), 6.30 – 6.19 (m, 0.9H), 6.01 (m, 0.6H), 5.92 – 5.87 (m, 0.29H), 5.68 (s, 0.36H), 5.58 (m,0.42H), 4.22 (2s, , 1.16H), 3.95 (2s, 0.62H), 3.66 (2s, 2.80H), 3.64 (s, 0.67H), 3.44 (2s, 1.98H), 3.36 (s, 0.48H) 2.26 (m, 0.71H), 2.15 – 2.07 (m, 1.80H), 2.01 – 1.93 (m, 1.16H), 1.56 – 1.47 (m, 1.90H), 0.85 (s, 9H), 0.01 (s, 6H).

$^{13}$C NMR ($CDCl_3$, 125 MHz): δ 163.94, 163.89, 163.48, 163.44, 149.74, 148.44, 148.36, 142.64, 142.55, 139.07, 138.91, 135.20, 134.67, 133.94, 133.84, 133.78, 133.73, 132.24, 122.67, 122.59, 122.37, 119.14, 119.12, 118.80, 69.18, 64.61, 64.60, 64.54, 63.11, 63.08, 60.33, 60.30, 39.98,

38.34, 38.03, 36.92, 34.11, 34.03, 33.95, 33.88, 33.63, 33.44, 33.38, 33.11, 31.29, 31.22, 30.59, 30.43, 27.98, 23.67, 23.63, 19.45, 0.11, 0.00.

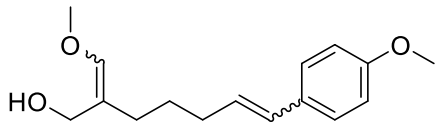

**27**

First (1.800g of powdered 4Å molecular sieves) was placed in a round-bottom flask. The flask was heated under vacuum to activate the sieves. The flask was placed under a nitrogen atmosphere. Now (0.3347g, 0.89 mmol) of tbs protected alcohol **26** in 9 mL of THF was added. The flask was placed in an ice-bath. Next, (2.7 mL, 2.7 mmol) of TBAF was added to the stirring flask. The reaction was allowed to stir at 0°C for 2h. The reaction was diluted with DCM and washed with di$H_2O$. The layers were separated, and the aqueous layer was extracted 2x with DCM. The organic layers were combined, dried over $MgSO_4$, and concentrated in vacuo The residue was purified by column chromatography using 1:9 to 3:7 to 1:1 EA:Hexanes with 1% thriethylamine as the eluent to yield 0.1888g (81%) of alcohol **27**.

$^1$H NMR ($CDCl_3$, 500 MHz): δ 7.29 – 7.16 (m, 2H), 6.88 – 6.76 (m, 1.92H), 6.37 – 6.25 (m, 0.98H), 6.16 – 5.97 (m, 0.98H), 5.84 (s, 0.45H), 5.74 (s, 0.18H), 5.64 – 5.45 (m, 0.31H), 4.17 (2s, 1.28H), 3.76 (3s, 2.91H), 3.54 (3s, 2.12H), 3.47 (s, 0.53H), 2.37 – 2.26 (m, 0.72H), 2.21 – 2.09 (m, 2.56H), 2.03 – 1.93 (m, 1.42H), 1.63 – 1.51 (m, 2.03H).

$^{13}$C NMR ($CDCl_3$, 125 MHz): δ 158.61, 158.53, 158.14, 158.08, 145.62, 144.61, 144.53, 129.91, 129.90, 129.42, 128.50, 128.39, 126.95, 117.51, 113.88, 113.85, 113.53, 63.57, 59.62, 59.55, 59.51, 58.91, 58.89, 55.21, 55.20, 55.17, 32.99, 32.55, 29.69, 29.58, 28.59, 28.15, 27.92, 27.79, 25.12.

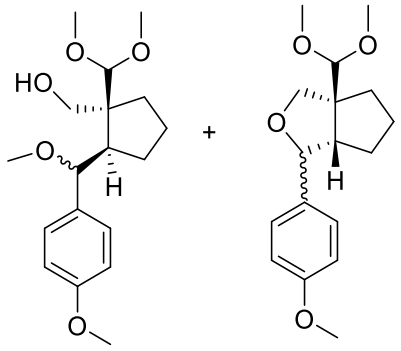

**28** **29**

1.3:1 (trans/cis)
(ca. NMR)

First, (0.7128g, 6.7 mmol) of $Et_4NOTs$ and 2.7 mL MeOH was added to a three-neck flask. The RVC anode and platinum wire cathode were prepared and fixed into thermometer adaptor and placed into a three-neck flask. The flask was placed under an Argon atmosphere. Next, (0.1052g, 0.4 mmol) substrate **27** in 10.6 mL of DCM was added along with (0.05mL, 0.4mmol) 2,6-lutidine. The reaction was sonicated for 15 minutes under argon to degas the solvent. The reaction was set at 6mA of current and the electrolysis was run until 92.9 C of charge had passed (2.4F/mol). Once complete, diethyl ether with 3 drops of triethylamine was added to the reaction. The organic layer was washed with di$H_2O$ and the layers were separated. The aqueous layer was extracted 2x with diethyl ether. The organic layers were combined, dried over $MgSO_4$, and concentrated in vacuo. The yield as determined by proton NMR with an internal standard was 33% for trans compound **28** and 25% for cis tandem cyclized compound **29**.

(**28**)$^1$H NMR ($CDCl_3$, 500 MHz): δ 7.20 (d, *J* = 8.3 Hz, 2H), 6.88 (d, *J* = 8.9 Hz, 2.41H), 4.62 (d, *J* = 10.5 Hz, 0.99H), 4.57 (s, 1.14H), 4.04 (d, *J* = 10.2 Hz, 1.14H), 3.81 (s, 3H), 3.69 (s, 3H), 3.54 (s, 3H), 3.32 (d, *J* = 10.5 Hz, 1.55H), 3.19 (s, 3H), 2.15 – 1.95 (m, 2H), 1.59 – 1.49 (m, 1.38H), 1.41 – 1.08 (m, 4.08H), 1.01 – 0.83 (m, 1.42H).

(**28**)$^{13}$C NMR ($CDCl_3$, 125 MHz): δ 159.28, 133.27, 128.29, 127.67, 113.72, 113.49, 108.28, 83.71, 70.16, 60.10, 56.86, 55.93, 55.57, 55.23, 54.38, 32.41, 30.40, 23.75.

(**29**)$^{1}$H NMR ($CDCl_3$, 500 MHz): δ 7.31 (d, *J* = 8.6 Hz, 1.75H), 6.88 (d, *J* = 8.7 Hz, 1.85H), 4.31 (d, *J* = 9.6 Hz, 1.01H), 4.27 (s, 0.94H), 4.21 (d, *J* = 8.2 Hz, 0.86H), 3.80 (s, 3H), 3.54 (2s, 5.39H), 3.54 (s, 3H), 3.40 (d, *J* = 9.5 Hz, 1.01H), 2.36 (m, 0.95H), 1.86 – 1.67 (m, 3.36H), 1.64 – 1.48 (m, 3.38H).

(**29**)$^{13}$C NMR ($CDCl_3$, 125 MHz): δ 159.08, 134.17, 127.46, 127.43, 113.79, 111.24, 87.75, 77.27, 77.02, 76.76, 75.92, 62.05, 58.50, 57.80, 55.96, 55.27, 31.60, 29.63, 24.71.

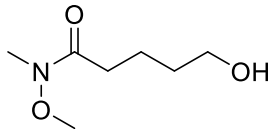


**30**

First, 5.000 grams N,O-Dimethylhydroxylamine hydrochloride salt (51.26mmol) was submerged in benzene in a round bottom flask. The benzene was then evaporated off using a rotary evaporator. The flask containing the salt was flushed with argon. 15mL of tetrahydrofuran was added to suspend the amine salt. The suspension was then stirred in a dry ice/acetone bath for 15 minutes. Now, 52.00mL diisobutyl aluminum hydride (52.0 mmol) was added to the suspension dropwise to prevent the quick evolution of hydrogen gas. The reaction flask was then taken from the dry ice/acetone bath and stirred at room temperature for 1 hour to give a clear, light yellow solution. The reaction flask was returned to the dry ice/acetone bath to cool for 15 minutes before 2.34 mL valerolactone (24.7 mmol) was added. The reaction was stirred in a dry ice/acetone bath for 30 minutes. The flask was then removed from the dry ice/acetone bath and allowed to stir at room temperature for 3 hours. After completion, the flask was placed in a dry ice/acetone bath again,

diluted with hexane under an open atmosphere, and quenched with a saturated solution of sodium potassium tartrate (10mL). The quenched reaction was stirred overnight at room temperature. After being allowed to stir at room temperature overnight, there were two distinct layers: a clear upper layer and a cloudy bottom layer. The top layer was decanted off 3 times. The organic layers were combined, dried over magnesium sulfate, and concentrated down on a rotary evaporator to yield product **30** (3.550g, 87% yield) as a yellow oil.

IR (neat, $cm^{-1}$) 3384 (broad), 2939, 1640, 1072, and 1003

$^{1}H$ NMR (300 MHz, $CDCl_3$) δ 3.674 (s, 3.0H), 3.63 (t, 1.74H, J = 6.2 Hz), 3.17 (s, 2.32H), 2.46 (t, 2H, J = 7.0 Hz) 1.73 (m, 2H), 1.61 (m, 2H)

$^{13}$ C NMR (126 MHz, $CDCl_3$) δ 177.2, 64.35, 63.75, 34.82, 32.17, 30.20, 23.20

HRMS (ESI/TOF-Q) m/z: [M+Na]+ Calcd for $C_7H_{15}NO_3$ $[M+Na]^+$ 161.10; found 162.11.

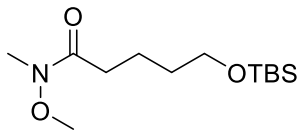


**31**

3.750g Imidazole (55.1 mmol) was weighed into a flame-dried round bottom flask. This flask was then flushed with argon. Tetrahydrofuran (10 mL) was added to the flask to suspend the imidazole. The suspension was stirred in an ice bath. In a separate flask, 3.550g **30** (22.0 mmol) was dissolved in 5 mL tetrahydrofuran, which was then transferred over to the stirring imidazole solution. 3.653g Tert-butyl silyl chloride (24.2 mmol) was placed in a separate flask. This flask was then flushed with argon. Tetrahydrofuran (4 mL) was added to this flask to dissolve the silyl chloride. The tert-butyl silyl chloride solution was then transferred dropwise to the stirring

solution. Upon addition, a cloudy white precipitate formed. The reaction was allowed to stir and warm up to room temperature for 6 hours before being diluted with hexane. Water was then added to quench the reaction and to dissolve the white precipitate. The solution was allowed to stir for 30 minutes to give 2 layers: a clear top layer and a cloudy bottom layer. The top layer was decanted off 3 times, dried over magnesium sulfate, and concentrated with the use of a rotary evaporator. The crude oil was then treated with hexane to crash out any remaining imidazole. **31** was concentrated back down with the use of a rotary evaporator to yield 5.352g (88%) as a yellow oil.

IR (neat, $cm^{-1}$) 2938, 2857, 1640, 1098

$^{1}H$ NMR (300 MHz, $CDCl_3$) δ 3.66 (s, 3H), 3.62 (t, 2H, J = 6.4 Hz ), 3.17 (s, 3H), 2.44 (t, 2H, J = 7.4 Hz), 1.66 (m, 2H), 1.56 (m, 2 H)

$^{13}$ C NMR (126 MHz, $CDCl_3$) δ 177.2, 65.50, 63.80, 35.10, 28.60, 23.71, 20.90, -2.68

HRMS (ESI/TOF-Q) m/z: [M+Na]+ Calcd for $C_{13}H_{29}NO_3Si$ 275.46; found 276.20.

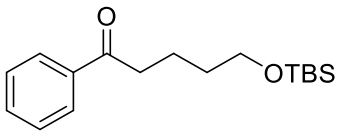


**32**

First, (0.2792g, 1.24 mmol) of $ZnBr_2$ was added to a round-bottom flask. The reaction was placed under Argon. Compound **31** (3.413g, 12.4 mmol) in 82 mL of THF was added. The flask was then placed in a dry ice acetone bath. Now, (21.5 mL, 40.9 mmol) of Phenyl Lithium was added dropwise over 15 minutes. The reaction was allowed to stir to room temperature overnight. The reaction was quenched at 0°C with sat aq $NH_4Cl$ and extracted with diethyl ether 2x. The organic

layers were combined, dried over $MgSO_4$, and concentrated in vacuo. The reaction was purified by column chromatography using 1:40 to 1:9 diethyl ether:Hexanes to yield (3.000g, 83%) of ketone **32**.

$^1$H NMR ($CDCl_3$, 500 MHz): δ 7.89 – 7.86 (m, 2H), 7.47 – 7.41 (m, 1.02H), 7.39 – 7.32 (m, 2H), 3.64 – 3.53 (m, 2H), 2.95 – 2.85 (m, 2H), 1.74 (pd, $J$ = 7.4, 2.0 Hz, 2H), 1.59 – 1.49 (m, 2H), 0.85 (s, 9H), 0.00 (s, 6H).

$^{13}$C NMR ($CDCl_3$, 125 MHz): δ 205.47, 205.44, 205.43, 142.25, 138.14, 138.13, 134.71, 133.79, 133.31, 120.76, 68.14, 43.55, 43.54, 37.60, 31.26, 26.14, 23.58, 0.00.

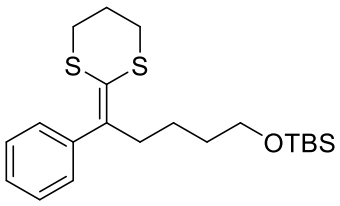


**33**

A round bottom flask was flame dried and flushed with argon. Next, 2.3mL 2-(trimethylsilyl)-1,3-dithiane (12.1 mmol) was added to the flask which was then dissolved in 30 mL of THF. This solution was then stirred in dry ice/acetone bath for 30 minutes. The stirring solution was then treated with 6.9 mL of nBuLi (11.1 mmol). The reaction stirred for 1 hour before being removed from the dry ice/acetone bath. The flask was then stirred at room temperature for 30 minutes. While the dithiane solution was stirring at room temperature, 2.962g of **32** (10.1 mmol) was dissolved in 26 mL of tetrahydrofuran. The stirring dithiane solution was then cooled in a dry ice/acetone bath for 15 minutes. The phenyl ketone solution was then added to the dithiane solution dropwise. The reaction was then allowed to warm up and react overnight. Upon completion, the reaction was quenched with water and extracted 3x with diethyl ether. The

organic layers were combined, dried over $MgSO_4$, and concentrated in vacuo to yield 3.987 g of **33** which was carried forward to the next step without further purification and analyzed after the next step.

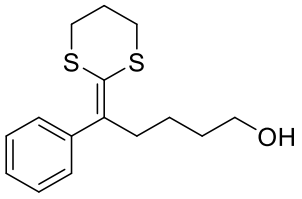


**34**

A round bottom flask was flame-dried and flushed with argon. Next, 3.987g of the ketene dithio acetal **33** (10.1 mmol) was added to the flask, dissolved in 34 mL of THF, and set to stir at 0°C. Next, 30 mL of tetrabutylammonium fluoride (30 mmol) was added to the stirring solution at 0°C. The reaction was allowed to stir to room temperature overnight. The reaction was brought to 0°C and quenched with sat aq $NaHCO_3$ and extracted 3x with diethyl ether. The organic layers were combined, dried over $MgSO_4$ and concentrated in vacuo to yield a crude oil. The crude material was then further purified by column chromatography (1:4 to 1:1 to 2:1 Diethyl Ether: Hexane) to yield 1.792g (63%) of **34** over two steps.

$^1$H NMR ($CDCl_3$, 500 MHz): δ 7.38 – 7.29 (m, 2H), 7.26 – 7.19 (m, 1H), 7.17 – 7.11 (m, 2H), 3.53 (t, *J* = 6.6 Hz, 2H), 2.96 – 2.91 (m, 2H), 2.80 – 2.70 (m, 2H), 2.69 – 2.61 (m, 2H), 2.11 – 2.04 (m, 2H), 1.51 (dt, *J* = 15.0, 6.7 Hz, 2H), 1.39 – 1.30 (m, 2H).

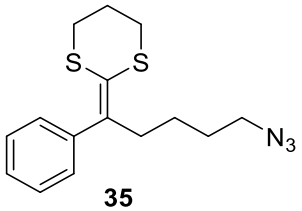


**35**

First, 0.1757 g (0.67 mmol) triphenylphosphine ($Ph_3P$) was added to a round-bottom flask. The flask was placed under an Argon atmosphere. Now, 0.1712 g of alcohol **34** (0.61 mmol) in 6.1 mL of THF was added and the reaction was stirred at room temperature. Now, Diethyl azodicarboxylate (DEAD, 40% wt. in toluene, 0.31 mL, 0.67 mmol) was added; followed by 0.14 mL (0.67 mmol) diphenylphosphoryl azide (DPPA). The reaction was stirred overnight at room temperature and the solvent was removed under reduced pressure. The crude azide was purified by column chromatograph using 1:9 diethyl ether:hexane as the eluent to give 0.0993 g of azide **35** (59%).

$^1$H NMR ($CDCl_3$, 500 MHz): δ 7.34 – 7.26 (m, 2H), 7.24 – 7.18 (m, 1H), 7.15 – 7.10 (m, 2H), 3.16 (t, *J* = 7.0 Hz, 2H), 2.96 – 2.84 (m, 2H), 2.77 – 2.59 (m, 2H), 2.17 – 1.93 (m, 2H), 1.53 (dt, *J* = 14.7, 7.1 Hz, 2H), 1.41 – 1.28 (m, 2H)

$^{13}$C NMR ($CDCl_3$, 125 MHz): δ 141.24, 141.07, 128.43, 128.00, 128.00, 126.99, 125.08, 51.08, 35.41, 29.73, 29.50, 28.18, 24.92, 24.29.

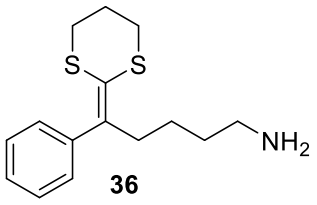


**36**

0.5723 g (1.9 mmol) azide **35** was dissolved in 13 mL of THF and added to a round-bottom flask. Next, (1.259g, 4.8 mmol) of triphenyl phosphine and 0.17 mL (9.5 mmol) water were added to the round-bottom flask. The flask was attached to a reflux condenser and placed under argon. After the reaction was brought to reflux for 5 h, the solvent was removed under reduced pressure and the crude product was purified by flash column chromatograph eluted with 1:19 to 1:9 MeOH:DCM with 1% $Et_3N$ to give 0.4504g (87%) of amine **36**.

$^{1}$H NMR ($CDCl_3$, 500 MHz): δ 7.40 – 7.22 (m, 3H), 7.19 – 7.11 (m, 2H), 3.04 – 2.86 (m, 2H), 2.85 – 2.70 (m, 2H), 2.70 – 2.53 (m, 4H), 2.16 – 2.02 (m, 2H), 1.76 (bs, 2H), 1.58 – 1.3 (m, 2H).

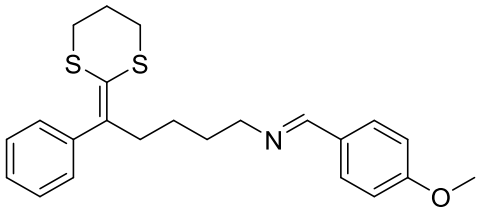

**37**

To a round bottom flask, was added molecular sieves which was placed under vacuum and heated to activate the sieves. Now, the flask was placed under argon. Next, (0.0841g, 0.3 mmol) of amine **36** in 5.5 mL THF was added to the flask. Finally, purified p-anisaldehyde (0.04 mL, 0.3 mmol) was added and the reaction was stirred overnight. The solution was then filtered through celite and washed with methanol. The solvents were removed under reduced pressure to afford 0.1137g (95%) of imine **37**.

$^{1}$H NMR ($CDCl_3$, 500 MHz): δ 8.13 (s, 1H), 7.83 (d, *J* = 8.7 Hz, 2H), 7.62 (d, *J* = 8.7 Hz, 2H), 7.31 (t, *J* = 7.4 Hz, 2H), 7.27 – 7.22 (m, 3H), 6.90 (d, *J* = 8.5 Hz, 2H), 3.82 (s, 3H), 3.52 (td, *J* = 6.9, 1.3 Hz, 2H), 2.97 – 2.89 (m, 2H), 2.80 – 2.60 (m, 4H), 2.15 – 2.02 (m, 2H), 1.68 (p, *J* = 7.1 Hz, 2H), 1.42 – 1.30 (m, 2H).

$^{13}$C NMR ($CDCl_3$, 125 MHz): δ 161.40, 160.14, 142.66, 141.45, 129.51, 129.30, 128.51, 128.01, 126.99, 124.19, 113.88, 61.21, 55.32, 35.93, 30.38, 29.96, 29.64, 25.49, 24.48

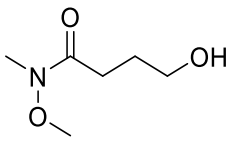

**38**

First, 3.500 grams N,O-Dimethylhydroxylamine hydrochloride salt (36 mmol) was submerged in benzene in a round bottom flask. The benzene was then evaporated off using a rotary evaporator. The flask containing the salt was flushed with argon. 20mL of DCM was added to suspend the amine salt. The suspension was then stirred in a dry ice/acetone bath. Now, 36.00mL diisobutyl aluminum hydride (36.0 mmol) was added to the suspension dropwise to prevent the quick evolution of hydrogen gas. The reaction flask was then taken from the dry ice/acetone bath and stirred at room temperature for 1 hour to give a clear, light yellow solution. The reaction flask was returned to the dry ice/acetone bath before 2.5 mL gamma-butyrolactone (33.0 mmol) was added in three portions over 15 minutes. The reaction was allowed to stir to rt overnight. After stirring overnight, the flask was placed back into a dry ice/acetone bath quenched with a saturated solution of sodium potassium tartrate. Flask was allowed to stir at room temperature until emulsion dissolved. (note: can add NaOH pellets to help break up emulsion). The filtrate was washed through a celite plug column with DCM. Organic layer was concentrated in vacuo to yield 3.928g of **38** (83%) which was used crude in the next step and characterized after the protection reaction.

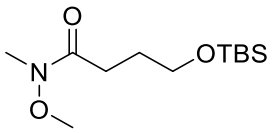


**39**

4.595g Imidazole (67.5 mmol) was weighed into a flame-dried round bottom flask. This flask was then flushed with argon. Next, 3.928g **38** (27.0 mmol) in 50 mL of DMF, was then transferred over to the imidazole solution. The flask was placed in an ice-bath. Now, 4.476g Tert-butyl silyl chloride (29.7 mmol) in 15 mL of DMF was added to the flask slowly. Upon complete addition, a cloudy white precipitate formed. The reaction was allowed to stir and warm up to room temperature overnight. The reaction was brought to 0$^{o}$C, quenched with brine and extracted 3x with EA. The

organic layers were combined, dried over $MgSO_4$ and concentrated in vacuo to yield a crude oil. The crude material was then further purified by column chromatography (1:4 to 1:1 EA: Hexane) to yield 5.013g (68%) of **39** over two steps.

$^1$H NMR ($CDCl_3$, 500 MHz): δ 3.63 (s, 3H), 3.61 (t, *J* = 6.0 Hz, 2H), 3.10 (s, 3H), 2.45 (t, *J* = 7.5 Hz, 2H), 1.77 (ddd, *J* = 13.5, 7.5, 6.1 Hz, 2H), 0.84 (s, 9H), -0.01 (s, 6H).

$^{13}$C NMR ($CDCl_3$, 125 MHz): δ 65.70, 64.53, 31.58, 31.13, 29.42, 29.33, 21.73, 21.59, -1.87.

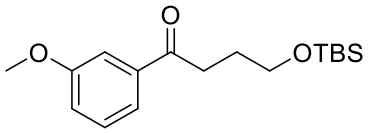


**40**

First, (0.6317 g, 2.81 mmol) of $ZnBr_2$ was added to a round-bottom flask. The reaction was placed under Argon. Compound **39** (5.013g, 18.7 mmol) in 75 mL of THF was added. The flask was then placed in a dry ice acetone bath. Now, (47 mL, 47 mmol) of 3-methoxyphenylmagnesium bromide was added dropwise over 15 minutes. The reaction was allowed to stir to room temperature overnight. The reaction was quenched at 0ºC with sat aq $NH_4Cl$ and extracted with diethyl ether 2x. The organic layers were combined, dried over $MgSO_4$, and concentrated in vacuo. The reaction was purified by column chromatography using 1:19 to 1:9 diethyl ether:Hexanes to yield (4.852g, 84%) of ketone **40**.

$^1$H NMR ($CDCl_3$, 500 MHz): δ 7.45 (d, *J* = 7.6 Hz, 1H), 7.40 (s, 1H), 7.23 (t, *J* = 7.9 Hz, 1H), 6.97 (dd, *J* = 8.2, 2.9 Hz, 1H), 3.70 (t, *J* = 2.9 Hz, 3H), 3.63 (dd, *J* = 7.1, 5.4 Hz, 2H), 2.94 (t, *J* = 7.2 Hz, 2H), 1.93 – 1.83 (m, 2H), 0.86 (s, 9H), 0.00 (s, 6H).

$^{13}$C NMR ($CDCl_3$, 125 MHz): δ 204.34, 165.20, 143.86, 134.79, 125.88, 124.35, 117.73, 67.53, 60.39, 40.12, 32.81, 31.31, 23.62, -0.00.

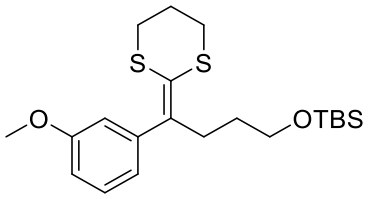


**41**

A round bottom flask was flame dried and flushed with argon. Next, 3.6mL 2-(trimethylsilyl)-1,3-dithiane (18.8 mmol) was added to the flask which was then dissolved in 47 mL of THF. This solution was then stirred in dry ice/acetone bath for 30 minutes. The stirring solution was then treated with 10.8 mL of nBuLi (17.3 mmol). The reaction stirred for 1 hour before being removed from the dry ice/acetone bath. The flask was then stirred at room temperature for 30 minutes. While the dithiane solution was stirring at room temperature, 4.852g of **40** (15.7 mmol) was dissolved in 39 mL of tetrahydrofuran. The stirring dithiane solution was then cooled in a dry ice/acetone bath for 15 minutes. The phenyl ketone solution was then added to the dithiane solution dropwise. The reaction was then allowed to warm up and react overnight. Upon completion, the reaction was quenched with water and extracted 3x with diethyl ether. The organic layers were combined, dried over $MgSO_4$, and concentrated in vacuo to yield 6.448 g of **41** which was carried forward to the next step without further purification and characterized after the deprotection reaction.

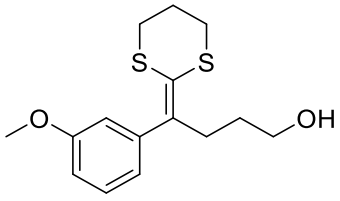


**42**

A round bottom flask was flame-dried and flushed with argon. Next, 6.448g of the ketene dithio acetal **41** (13.7 mmol) was added to the flask, dissolved in 52 mL of THF, and set to stir at 0ºC.

Next, 42 mL of tetrabutylammonium fluoride (42.0 mmol) was added to the stirring solution at 0ºC. The reaction was allowed to stir to room temperature overnight. The reaction was brought to 0ºC and quenched with sat aq $NaHCO_3$ and extracted 3x with diethyl ether. The organic layers were combined, dried over $MgSO_4$ and concentrated in vacuo to yield a crude oil. The crude material was then further purified by column chromatography (1:2 to 1:1 to 2:1 Diethyl Ether: Hexane) to yield 3.410 (84%) of **42** over two steps.

$^1$H NMR ($CDCl_3$, 500 MHz): δ 7.19 (t, *J* = 7.9 Hz, 1H), 6.79 – 6.69 (m, 2H), 6.68 (t, *J* = 2.0 Hz, 1H), 3.74 – 3.70 (m, 3H), 3.69 – 3.63 (m, 3H), 3.48 (t, *J* = 6.6 Hz, 2H), 3.26 (s, 1H), 2.90 (t, *J* = 6.3 Hz, 2H), 2.74 – 2.64 (m, 4H), 2.02 (t, *J* = 6.4 Hz, 2H), 1.78 (dd, *J* = 10.2, 3.3 Hz, 3H), 1.54 – 1.47 (m, 2H)

$^{13}$C NMR ($CDCl_3$, 125 MHz): δ 161.89, 145.22, 143.87, 131.64, 127.42, 123.56, 116.87, 114.99, 70.44, 64.39, 57.68, 35.22, 33.59, 32.41, 32.16, 28.22, 26.99.

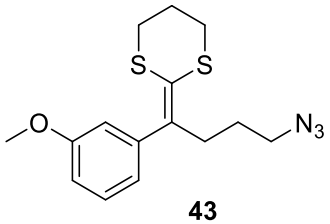


**43**

First, 1.660g (6.33 mmol) triphenylphosphine ($Ph_3P$) was added to a round-bottom flask. The flask was placed under an Argon atmosphere. Now, 1.705g of alcohol **42** (5.75 mmol) in 57 mL of THF was added and the reaction was stirred at room temperature. Now, Diethyl azodicarboxylate (DEAD, 40% wt. in toluene, 2.9 mL, 6.33 mmol) was added; followed by (1.4 mL 6.33mmol) diphenylphosphoryl azide (DPPA). The reaction was stirred overnight at room temperature and the solvent was removed under reduced pressure. The crude azide was purified

by column chromatograph using 1:19 to 1:9 diethyl ether:hexane as the eluent to give 1.046 g of azide **43** (57%).

$^{1}$H NMR ($CDCl_3$, 500 MHz): δ 7.29 – 7.24 (m, 1H), 6.86 – 6.66 (m, 3H), 3.80 (s, 3H), 3.24 (t, *J* = 6.9 Hz, 2H), 2.98 (dd, *J* = 7.0, 5.6 Hz, 2H), 2.87 – 2.64 (m, 4H), 2.18 – 2.03 (m, 2H), 1.74 – 1.49 (m, 2H).

$^{13}$C NMR ($CDCl_3$, 125 MHz): δ 159.38, 142.24, 139.99, 129.21, 125.92, 120.92, 114.24, 112.63, 55.19, 50.95, 33.20, 29.81, 29.70, 29.54, 27.21, 24.28.

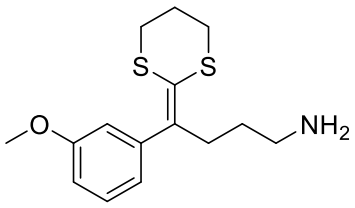


**44**

0.4622 g (1.44 mmol) azide **43** was dissolved in 10 mL of THF and added to a round-bottom flask. Next, (0.9442g, 3.60 mmol) of triphenyl phosphine and 0.13 mL (7.20 mmol) water were added to the round-bottom flask. The flask was attached to a reflux condenser and placed under argon. After the reaction was brought to reflux for 5 h, the solvent was removed under reduced pressure and the crude product was purified by flash column chromatograph eluted with 1:49 to 1:19 to 1:9 MeOH:DCM with 1% $Et_3N$ to give 0.4001g (93%) of amine **44**.

$^{1}$H NMR ($CDCl_3$, 500 MHz): δ 7.22 (m, 1H), 6.83 – 6.60 (m, 3H), 4.15 – 3.67 (bs + s, 5H), 2.93 (m, 2H), 2.84 – 2.54 (m, 4H), 2.08 (m, 2H), 1.49 (m, 2H).

$^{13}$C NMR ($CDCl_3$, 125 MHz): δ 159.27, 142.41, 140.88, 129.10, 125.12, 120.92, 114.19, 112.54, 55.17, 40.73, 33.25, 30.16, 29.84, 29.77, 29.75, 29.56, 29.49, 24.33.

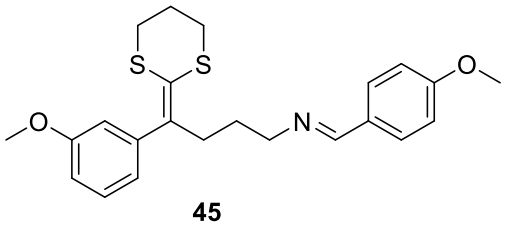

**45**

To a round bottom flask, was added molecular sieves which was placed under vacuum and heated to activate the sieves. Now, the flask was placed under argon. Next, (0.4001g, 1.4 mmol) of amine **44** in 25 mL THF was added to the flask. Finally, purified p-anisaldehyde (0.14 mL, 1.4 mmol) was added and the reaction was stirred overnight. The solution was then filtered through celite and washed with 1:9 methanol:DCM. The solvents were removed under reduced pressure to afford 0.4992g (95%) of imine **45**.

$^{1}$H NMR ($CDCl_3$, 500 MHz): δ 8.09 (s, 1H), 7.62 (d, *J* = 8.7 Hz, 2H), 7.34 – 7.11 (m, 1H), 6.89 (d, *J* = 8.8 Hz, 2H), 6.82 – 6.75 (m, 2H), 3.80 (s, 3H), 3.77 (s, 3H), 3.57 – 3.46 (m, 2H), 2.93 (t, *J* = 6.3 Hz, 2H), 2.82 – 2.66 (m, 4H), 2.14 – 2.00 (m, 2H), 1.77 – 1.63 (m, 2H).

$^{13}$C NMR ($CDCl_3$, 125 MHz): δ 164.58, 161.44, 159.27, 142.73, 141.65, 131.96, 129.94, 129.24, 129.03, 124.75, 121.05, 114.30, 114.22, 113.89, 112.53, 60.93, 55.57, 55.31, 55.14, 33.93, 29.91, 29.58, 29.36, 24.41.

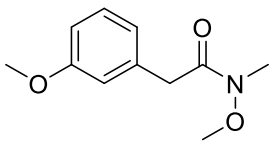

**47**

First, (3.124g, 18.8 mmol) of 3-Methoxyphenylacetic acid was added to a round bottom flask. Next, 50 mL of DCM was added, and the reaction was stirred at room temperature. Next, (4.305g, 22.5 mmol) of EDC/HCl was added to the flask. Now, (2.1 mL, 18.8 mmol) of NMM was added. Finally, (2.009g, 20.6 mmol) N,O-Dimethylhydroxylamine hydrochloride was placed in the flask.

The reaction was allowed to stir at room temperature overnight. The reaction was diluted with diethyl ether and washed with sat aq. $NaHCO_3$. The aqueous layer was extracted 3x with diethyl ether. The organic layers were combined, dried over $MgSO_4$, and concentrated in vacuo. The crude product was purified by column chromatography with 1:2 to 1:1 EA:Hexane as the eluent to yield 2.881g of weinreb amide (73%).

$^1H$ NMR ($CDCl_3$, 500 MHz): δ 7.22 – 7.10 (m, 1H), 6.83 (m, 2H), 6.74 (m, 1H), 3.73 – 3.63 (m, 5H), 3.52 (s, *J* = 6.7, 3.6 Hz, 3H), 3.10 (s, 3H).

$^{13}C$ NMR ($CDCl_3$, 125 MHz): δ 174.53, 162.23, 139.11, 131.86, 124.17, 117.51, 114.71, 114.69, 63.67, 57.49, 57.48, 41.74, 34.54.

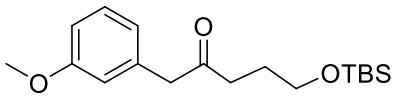


**48**

First, (0.4504g, 2.0 mmol) of $ZnBr_2$ was added to a round-bottom flask. The reaction was placed under Argon. Now, tert-butyl(3-iodopropoxy)dimethylsilane (3.931g, 13.1 mmol) in 30 mL of diethyl ether (dried overnight with molecular sieves) was added. The flask was then placed in a dry ice acetone bath. Now, (15.4 mL, 26.2 mmol) of tBuLi was added. The reaction was stirred at -78ºC for 1h and at 0ºC for 30 minutes. The flask was placed back in a dry ice acetone bath. Next, (1.925g, 9.2 mmol) of Weinreb amide **47** in 8 mL of diethyl ether was added to the stirring flask. The flask was then placed in an ice bath and allowed to warm to rt overnight. The reaction was quenched at 0ºC with sat aq $NH_4Cl$ and extracted with diethyl ether 2x. The organic layers were combined, dried over $MgSO_4$, and concentrated in vacuo. The reaction was purified by column chromatography using 1:14 to 1:9 to 1:6 EA:Hexanes to yield (2.092g, 71%) of ketone **48**.

$^{1}$H NMR ($CDCl_3$, 500 MHz): δ 7.16 (td, *J* = 7.7, 1.2 Hz, 1H), 6.78 – 6.68 (m, 3H), 3.70 (s,3H), 3.58 (s, 2H), 3.56 – 3.50 (m, 2H), 2.48 (td, *J* = 7.1, 1.2 Hz, 2H), 1.72 (dd, *J* = 7.3, 5.9 Hz, 2H), 0.87 (s, 9H), 0.00 (s, 6H).

$^{13}$C NMR ($CDCl_3$, 125 MHz): δ 209.90, 162.44, 138.54, 132.11, 124.24, 117.61, 114.90, 64.50, 57.41, 52.67, 40.56, 29.33, 28.53, 28.48, 20.77, -2.86.

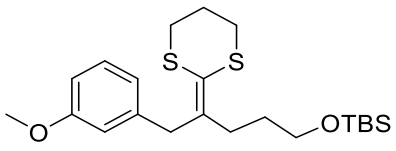


**49**

A round bottom flask was flame dried and flushed with argon. Next, 1.5mL of 2-(trimethylsilyl)-1,3-dithiane (7.90 mmol) was added to the flask which was then dissolved in 20 mL of THF. This solution was then stirred in dry ice/acetone bath for 30 minutes. The stirring solution was then treated with 4.6 mL of nBuLi (7.30 mmol). The reaction stirred for 1 hour before being removed from the dry ice/acetone bath. The flask was then stirred at room temperature for 30 minutes. While the dithiane solution was stirring at room temperature, 1.961g of **48** (6.08 mmol) was dissolved in 15 mL of tetrahydrofuran. The stirring dithiane solution was then cooled in a dry ice/acetone bath for 15 minutes. The ketone solution was then added to the dithiane solution dropwise. The reaction was then allowed to warm up and react overnight. Upon completion, the reaction was quenched with water and extracted 3x with diethyl ether. The organic layers were combined, dried over $MgSO_4$, and concentrated in vacuo to yield 2.514 g of **49** which was carried forward to the next step without further purification and was characterized after the deprotection of the TBS group.

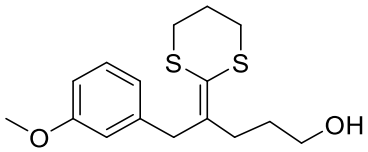


**50**

A round bottom flask was flame-dried and flushed with argon. Next, 2.514g of the ketene dithio acetal **49** (5.92 mmol) was added to the flask, dissolved in 20 mL of THF, and set to stir at 0ºC. Next, 17.8 mL of tetrabutylammonium fluoride (17.8 mmol) was added to the stirring solution at 0ºC. The reaction was allowed to stir to room temperature overnight. The reaction was brought to 0ºC and quenched with sat aq $NaHCO_3$ and extracted 3x with diethyl ether. The organic layers were combined, dried over $MgSO_4$ and concentrated in vacuo to yield a crude oil. The crude material was then further purified by column chromatography (1:19 to 1:9 to 1:4 to 1:1 Diethyl Ether: Hexane) to yield 1.210g (66%) of **50** over two steps.

$^1$H NMR ($CDCl_3$, 500 MHz): δ 7.31 – 7.06 (m, 1H), 6.73 (m, 4H), 3.76 (s, 3H), 3.69 (d, *J* = 3.3 Hz, 2H), 3.60 – 3.46 (m, 2H), 2.89 (m, 4H), 2.44 – 2.20 (m, 4H), 2.12 (m, 2H), 1.59 (m, 2H).

$^{13}$C NMR ($CDCl_3$, 125 MHz): δ 162.32, 144.41, 143.62, 132.00, 125.60, 123.73, 117.16, 113.99, 64.69, 57.80, 41.92, 33.43, 33.05, 32.91, 32.10, 27.46.

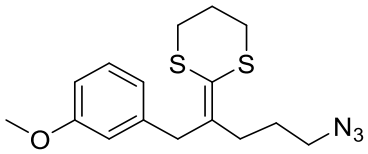


**51**

First, 0.6164g (2.35 mmol) triphenylphosphine ($Ph_3P$) was added to a round-bottom flask. The flask was placed under an Argon atmosphere. Now, 0.6647g of alcohol **50** (2.14 mmol) in 21.4 mL of THF was added and the reaction was stirred at room temperature. Now, Diethyl

azodicarboxylate (DEAD, 40% wt. in toluene, 1.1 mL, 2.35 mmol) was added; followed by (0.51 mL 2.35 mmol) diphenylphosphoryl azide (DPPA). The reaction was stirred overnight at room temperature and the solvent was removed under reduced pressure. The crude azide was purified by column chromatograph using 1:19 to 1:9 to 1:4 diethyl ether:hexane as the eluent to give 0.5464 g of azide **51** (76%).

$^{1}$H NMR ($CDCl_3$, 500 MHz): δ 7.41 – 7.28 (m, 1H), 7.28 – 7.03 (m, 1H), 6.87 – 6.68 (m, 2H), 3.76 (s, 3H), 3.68 (s, 2H), 3.18 (t, *J* = 6.9 Hz, 2H), 3.02 – 2.80 (m, 4H), 2.33 (dd, *J* = 8.8, 6.8 Hz, 2H), 2.22 – 1.94 (m, 2H), 1.78 – 1.47 (m, 2H).

$^{13}$C NMR ($CDCl_3$, 125 MHz): δ 162.42, 143.49, 142.91, 132.75, 132.08, 131.72, 130.91, 128.83, 128.82, 126.80, 123.72, 122.92, 122.88, 117.19, 114.08, 57.79, 53.80, 42.18, 33.30, 32.93, 32.77, 29.94, 27.40.

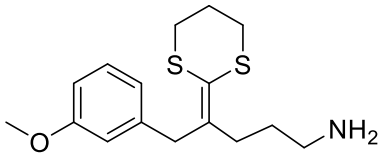


**52**

0.5464 g (1.63 mmol) azide **51** was dissolved in 11 mL of THF and added to a round-bottom flask. Next, (1.070g, 4.08 mmol) of triphenyl phosphine and 0.15 mL (8.15 mmol) water were added to the round-bottom flask. The flask was attached to a reflux condenser and placed under argon. After the reaction was brought to reflux for 5 h, the solvent was removed under reduced pressure and the crude product was purified by flash column chromatograph eluted with 1:9:0.2 to 1:4:0.1 MeOH:DCM:$Et_3N$ to give 0.4129g (82%) of amine **52**.

$^{1}$H NMR ($CDCl_3$, 500 MHz): δ 7.16 (t, *J* = 7.8 Hz, 1H), 6.83 – 6.58 (m, 3H), 3.75 (s, 3H), 3.69 (s, 2H), 2.88 (m, 4H), 2.63 (t, *J* = 7.0 Hz, 2H), 2.41 – 2.22 (m+bs, 4H), 2.11 (m, 2H), 1.51 (t, *J* = 7.6 Hz, 2H).

$^{13}$C NMR ($CDCl_3$, 125 MHz): δ 162.27, 144.28, 143.60, 134.67, 134.59, 131.91, 131.19, 131.09, 125.64, 123.64, 117.07, 113.89, 57.71, 44.24, 41.83, 34.11, 33.18, 32.98, 32.82, 27.45.

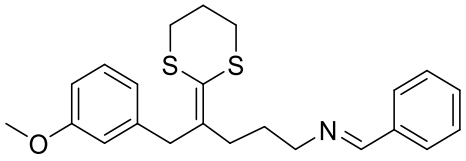


**53**

To a round bottom flask, was added molecular sieves which was placed under vacuum and heated to activate the sieves. Now, the flask was placed under argon. Next, (0.1042g, 0.337 mmol) of amine **52** in 4.2 mL THF was added to the flask. Finally, purified benzaldehyde (0.03 mL, 0.34 mmol) was added and the reaction was stirred overnight. The solution was then filtered through celite and washed with methanol. The solvents were removed under reduced pressure to afford 0.1193g (89%) of imine **53.**

$^{1}$H NMR ($CDCl_3$, 500 MHz): δ 8.23 (s, 1H), 7.81 – 7.59 (m, 2H), 7.39 (m, 3H), 7.14 (t, *J* = 7.8 Hz, 1H), 6.85 – 6.68 (m, 3H), 3.75 (s, 3H), 3.73 (s, 2H), 3.56 (m, 2H), 3.04 – 2.79 (m, 4H), 2.45 – 2.28 (m, 2H), 2.20 – 2.07 (m, 2H), 1.84 – 1.71 (m, 2H).

$^{13}$C NMR ($CDCl_3$, 125 MHz): δ 163.69, 162.31, 144.65, 143.75, 139.01, 133.10, 131.92, 131.20, 130.70, 125.58, 123.83, 117.12, 114.02, 63.99, 57.76, 41.93, 33.82, 33.03, 32.86, 31.89, 27.53.

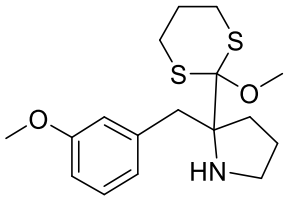


**54**

First, (0.2261g, 0.75 mmol) of $Et_4NOTs$ and (0.0893g, 0.23mmol) in 7.5 mL MeOH was added to a three-neck flask. The RVC anode and platinum wire cathode were prepared and fixed into thermometer adaptor and placed into a three-neck flask. The flask was placed under an Argon atmosphere. Next, (0.1052g, 0.4 mmol) substrate **53** in 10.6 mL of DCM was added along with (0.05mL, 0.4mmol) 2,6-lutidine. The reaction was sonicated for 15 minutes under argon to degas the solvent. The reaction was set at 6mA of current and the electrolysis was run until 45.5C of charge had passed (2.1F/mol). Once complete, diethyl ether was added to the reaction. The organic layer was washed with sat aq. $NaHCO_3$ and the layers were separated. The organic layers were combined, dried over $MgSO_4$, and concentrated in vacuo. The residue was purified by column chromatography with 1:9:0.1 to 1:4:0.05 EA:Hexanes:$Et_3N$ to yield 0.0266g cyclic amine **54** (34%).

$^1H$ NMR ($CDCl_3$, 500 MHz): δ 7.19 (t, $J$ = 7.8 Hz, 1.17H), 6.86 – 6.82 (m, 1.84H), 6.78 (m, 0.99H), 3.80 (s, 3H), 3.61 (s, 2H), 3.23 (s, 1H), 3.12 – 2.96 (m, 4.21H), 2.96 – 2.75 (m, 3.23H), 2.55 (m, 1.12H), 2.32 (m, 1.14H), 2.10 – 1.99 (m, 2.05H), 1.92 – 1.81 (m, 2.28H), 1.51 (m, 1.34H).

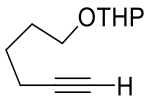


**55**

First, (0.046g, 0.2 mmol) of 10-camphorsulfonic acid was added to a round-bottom flask. The flask was purged with nitrogen and 10 mL of DCM was added. Now, (2.0mL, 22.0 mmol) of 3,4-

Dihydro-2*H*-pyran was added. Finally, (2.2mL, 20.0 mmol) of 5-Hexyn-1-ol was added dropwise over 10 minutes. The reaction was stirred at room temperature overnight. The reaction was washed with sat. aq. $NaHCO_3$ and extracted 3x with diethyl ether. The organic layers were combined, dried over $MgSO_4$ and concentrated in vacuo to yield 3.645g of **55** which was carried forward as crude and characterized after the next two steps.

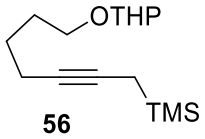


**56**

A round-bottom flask was connected to a reflux condenser and purged with nitrogen. Next, (3.645g, 20.0 mmol) of **55** in 36 mL of THF was added. The flask was placed in a dry ice acetone bath. Now, (13.2mL, 22.0 mmol) of nBuLi was added. The reaction was allowed to stir for 15 minutes at -78°C and 15 minutes at room temperature. Finally, (3.6mL, 24.0 mmol) of (Iodomethyl)trimethylsilane was added. The reaction was then refluxed overnight. The reaction was cooled to room temperature, diluted with water, and extracted 3x with diethyl ether. The organic layers were combined, dried over $MgSO_4$ and concentrated in vacuo to yield 5.369g of **56** which was used crude in the next step and fully characterized after deprotection of the THP group in the subsequent step.

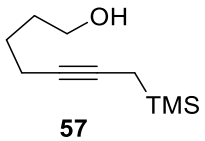


**57**

First, (5.369g, 20.0 mmol) of **56** in 100 mL of MeOH was added to a round-bottom flask. Now, (1.005g, 4.0 mmol) of PPTS was added to the flask. The reaction was allowed to stir at room temperature overnight open to the air. The reaction was quenched with sat. aq $NaHCO_3$ and the

reaction was concentrated in vacuo. The residue was diluted with di$H_2O$ and extracted 3x with DCM. The organic layers were combined, dried over $MgSO_4$ and concentrated in vacuo. The crude product was purified with column chromatography using 1:2 EA:Hexane as the eluent to yield 3.020g of alcohol **57** in 82% yield over three steps.

$^1$H NMR ($CDCl_3$, 500 MHz): δ 3.55 (t, *J* = 6.5 Hz, 2H), 3.25 (bs, 1H), 2.11 (m 2H), 1.58 (m, 2H), 1.52 – 1.41 (m, 2H), 1.34 (t, *J* = 2.7 Hz, 2H), 0.02 (s, 9H).

$^{13}$C NMR ($CDCl_3$, 125 MHz): δ 81.01, 80.07, 64.44, 64.42, 34.29, 28.26, 21.20, 9.38, 0.38.

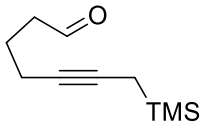


**58**

A round-bottom flask was purged with Argon. Next, (1.5mL, 18.0 mmol) of freshly distilled oxalyl chloride in 45 mL DCM was added to the flask. The flask was placed in a dry ice acetone bath. Now, (2.6mL, 36.0 mmol) of DMSO in 40 mL DCM was added. The reaction was stirred at -78°C for 2 minutes. Next, (3.020g, 16.4 mmol) of alcohol **57** in 33 mL DCM was added to the flask. The reaction was allowed to stir at -78°C for 45 minutes. Finally, (11.4mL, 82.0 mmol) of triethylamine was added. The reaction was allowed to stir at -78°C for 15 minutes and at room temperature for 1h. After 1h, the reaction was quenched with di$H_2O$. The layers were separated and the aqueous layer was extracted 3x with DCM. The organic layers were combined, dried over $MgSO_4$, and concentrated in vacuo. The crude product was purified with column chromatography using 1:19 to 1:9 Diethyl ether:Hexane as the eluent to yield 2.691g of aldehyde **58** in 90% yield.

$^1$H NMR ($CDCl_3$, 500 MHz): δ 9.66 (s, 1H), 2.44 (td, *J* = 7.2, 1.5 Hz, 2H), 2.10 (tt, *J* = 6.9, 2.6 Hz, 2H), 1.67 (p, *J* = 7.1 Hz, 2H), 1.31 (t, *J* = 2.8 Hz, 2H), -0.00 (s, 9H).

$^{13}$C NMR ($CDCl_3$, 125 MHz): δ 202.99, 80.59, 79.67, 45.09, 33.93, 24.97, 24.29, 20.66, 16.33, 9.07, 0.04.

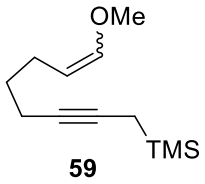


**59**

First, (10.147g, 29.6 mmol) of (Methoxymethyl)triphenylphosphonium chloride was added to a round-bottom flask. The reaction was placed under a Argon atmosphere. Now, 74 mL of THF was added and the flask was placed in a dry ice acetone bath. Next, (30mL, 30 mmol) of NaHMDS was added dropwise. The reaction was allowed to stir for 15 minutes at -78ºC and at room temperature for 30 minutes. The flask was returned to the dry ice acetone bath. Now, (2.691g, 14.8 mmol) of aldehyde **58** in 37 mL of THF was added. The reaction was allowed to stir to room temperature overnight. The reaction was cooled to 0ºC, quenched with brine and extracted 3x with diethyl ether. The organic layers were combined, dried over $MgSO_4$, and concentrated in vacuo The residue was diluted with hexanes and placed in freezer to crash out triphenylphosphine oxide. The reaction was filtered and concentrated in vacuo. The crude product was purified with column chromatography using 1:19 to 1:9 Diethyl Ether:Hexanes as the eluent to yield 2.056g (66%) of **59**.

$^{1}$H NMR ($CDCl_3$, 500 MHz): δ 6.21 (d, *J* = 12.6 Hz, 0.67H), 5.78 (d, *J* = 6.2 Hz, 0.21H), 4.59 (dt, *J* = 12.6, 7.4 Hz, 0.74 H), 4.23 (td, *J* = 7.4, 6.3 Hz, 0.22H), 3.46 (s, 0.69H), 3.39 (s, 2.23H), 2.29 – 2.00 (m, 2H), 1.96 – 1.90 (2.0H) 1.47 – 1.38 (m, 2H), 1.34 – 1.30 (m, 2.0H) 0.00 (s, 9H).

$^{13}$C NMR ($CDCl_3$, 125 MHz): δ 149.70, 149.70, 148.63, 108.16, 104.04, 80.59, 79.58, 79.57, 61.40, 57.77, 32.63, 32.62, 31.90, 28.92, 25.36, 20.72, 20.28, 9.10, 9.08, 0.03, 0.00.

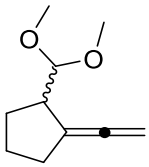

**60**

First, (0.5071g, 1.54 mmol) of $nBu_4NBF_4$ and 1.5 mL MeOH was added to a three-neck flask. The RVC anode and platinum wire cathode were prepared and fixed into thermometer adaptor and placed into a three-neck flask. The flask was placed under an Argon atmosphere. Next, (0.0485g, 0.23 mmol) substrate **59** in 6.2 mL of DCM was added along with (0.03 mL, 0.23 mmol) 2,6-lutidine. The reaction was sonicated for 15 minutes under argon to degas the solvent. The flask was placed in an ice-bath. The reaction was set at 10 mA of current and the electrolysis was run until 48.8 C of charge had passed (2.2 F/mol). Once complete, diethyl ether with 3 drops of triethylamine was added to the reaction. The organic layer was washed with di$H_2O$ and the layers were separated. The aqueous layer was extracted 3x with diethyl ether. The organic layers were combined, dried over $MgSO_4$, and concentrated in vacuo. The yield as determined by proton NMR with an internal standard was 52% for **60**.

$^1$H NMR ($CDCl_3$, 500 MHz): δ 4.79 – 4.58 (m, 2H), 4.26 (d, *J* = 6.3 Hz, 0.94H), 3.38 (s, 2.88H), 3.36 (s, 2.88H) 3.01 – 2.78 (m, 0.94H), 2.40 (ddt, *J* = 6.2, 4.5, 1.5 Hz, 2.16H), 1.96 – 1.49 (m, 5.27H).

$^{13}$C NMR ($CDCl_3$, 125 MHz): δ 203.16, 106.90, 102.85, 75.66, 65.86, 54.31, 54.00, 45.46, 31.73, 28.29, 25.66, 15.28.

## 4.6.3 $^{1}$H and $^{13}$C NMR Spectra

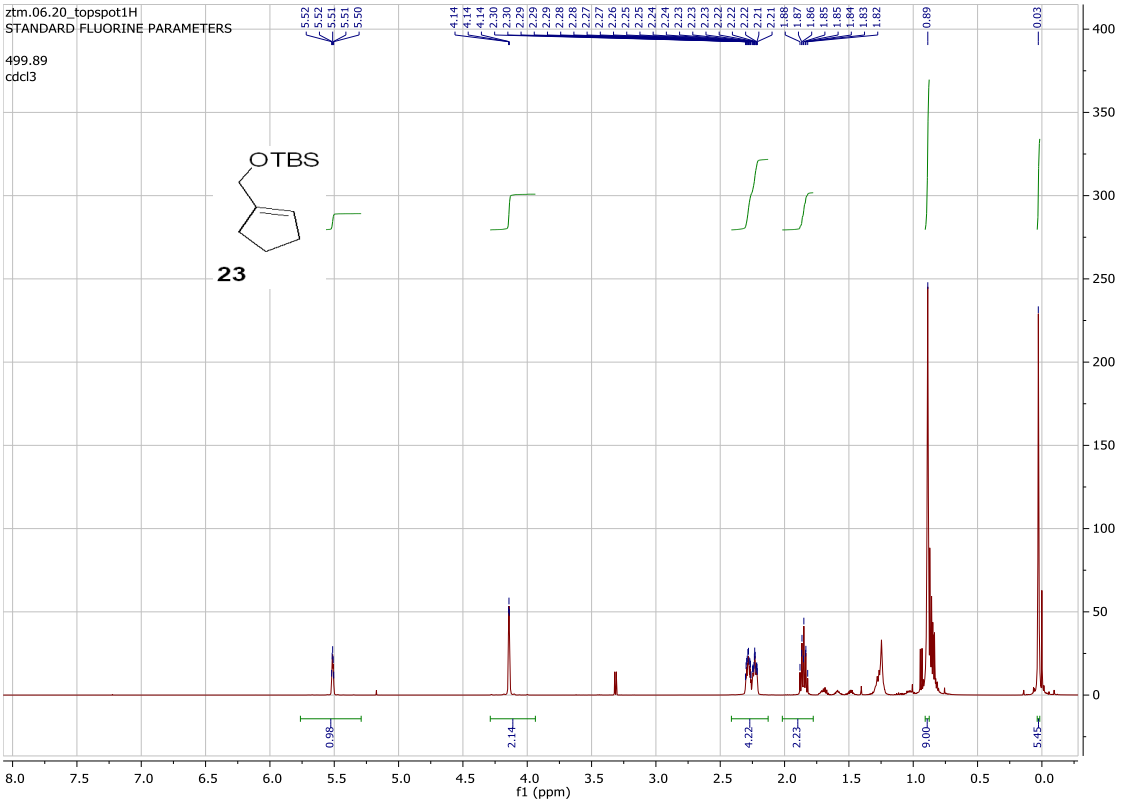


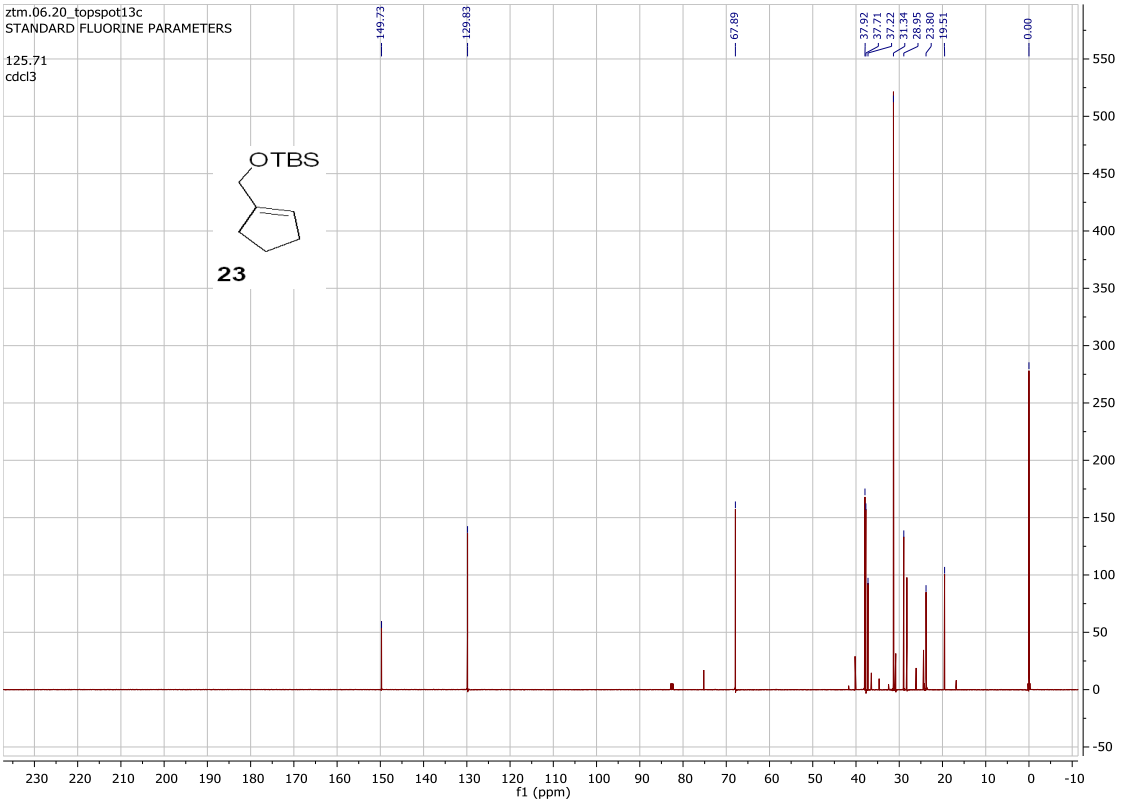

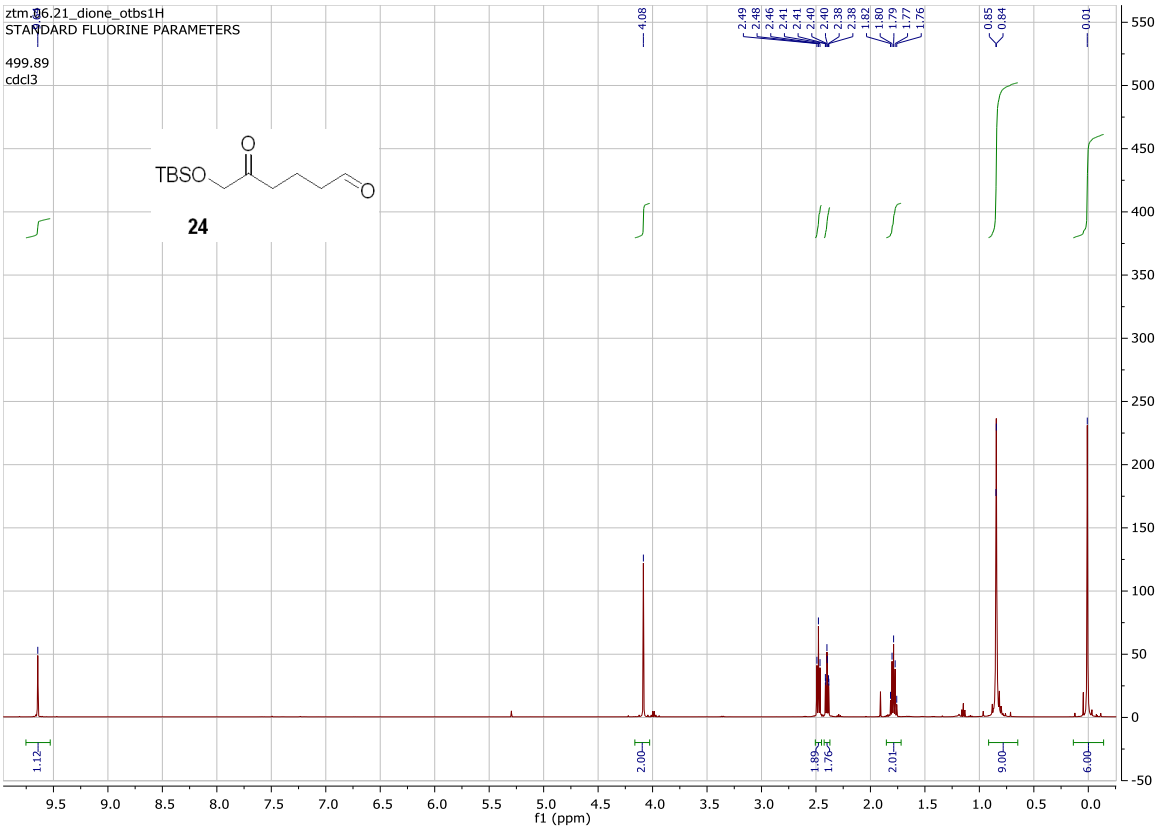
ztm.06.21_dione_otbs1H
STANDARD FLUORINE PARAMETERS
499.89
cdcl3
TBSO
O
O
24
f1 (ppm)

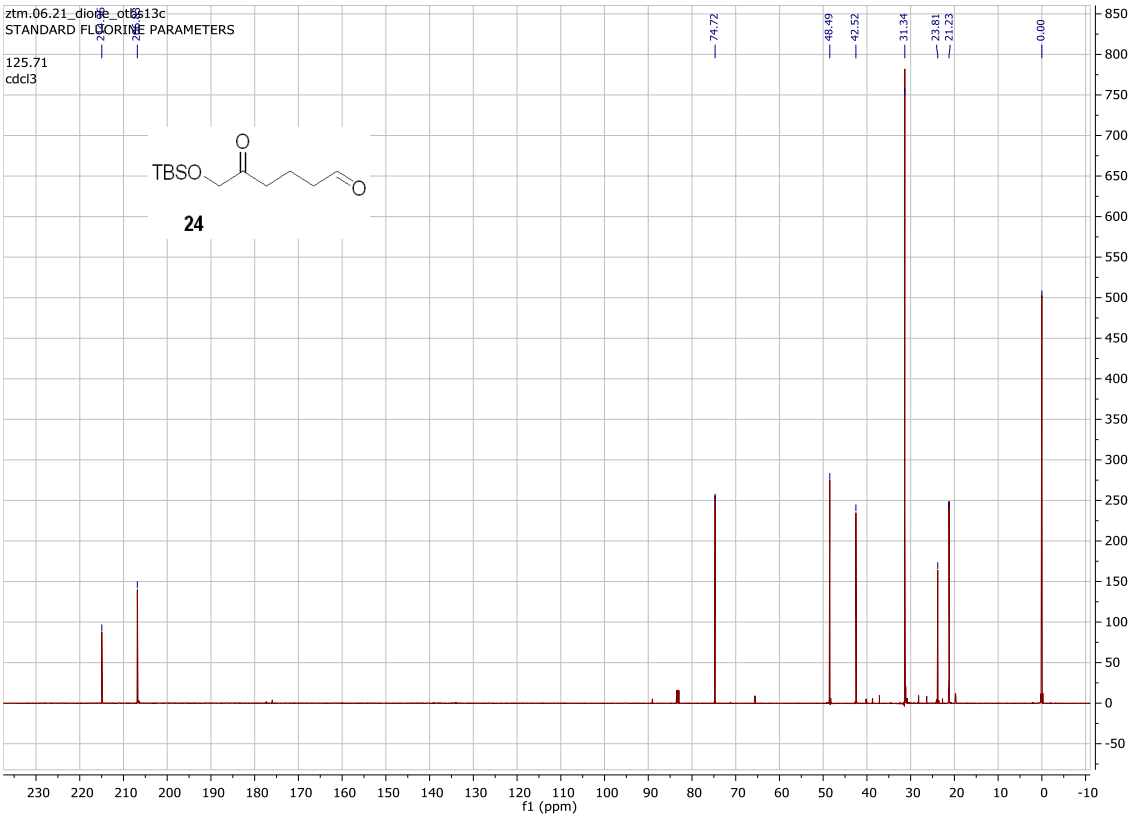
ztm.06.21_dione_otbs13c
STANDARD FLUORINE PARAMETERS
125.71
cdcl3
TBSO
O
O
24
f1 (ppm)

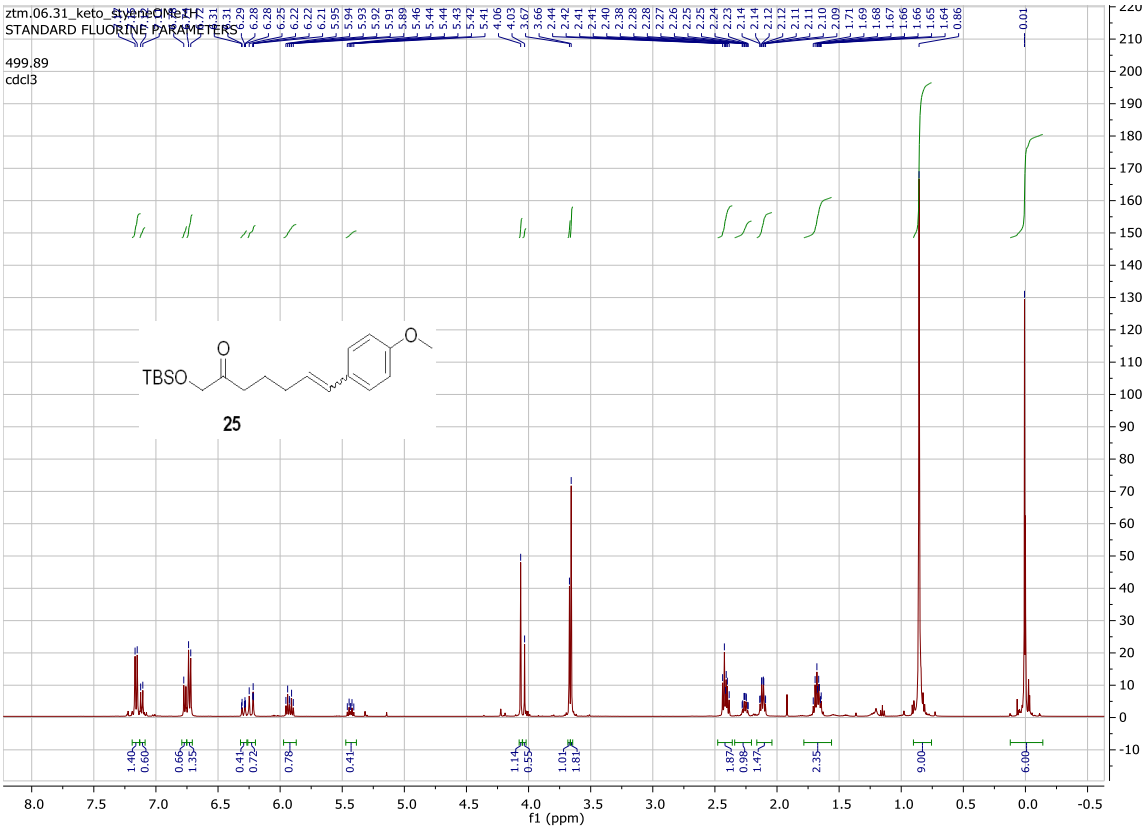
ztm.06.31_keto_styeneOMe1H
STANDARD FLUORINE PARAMETERS
499.89
cdcl3
TBSO
O
O
25
f1 (ppm)

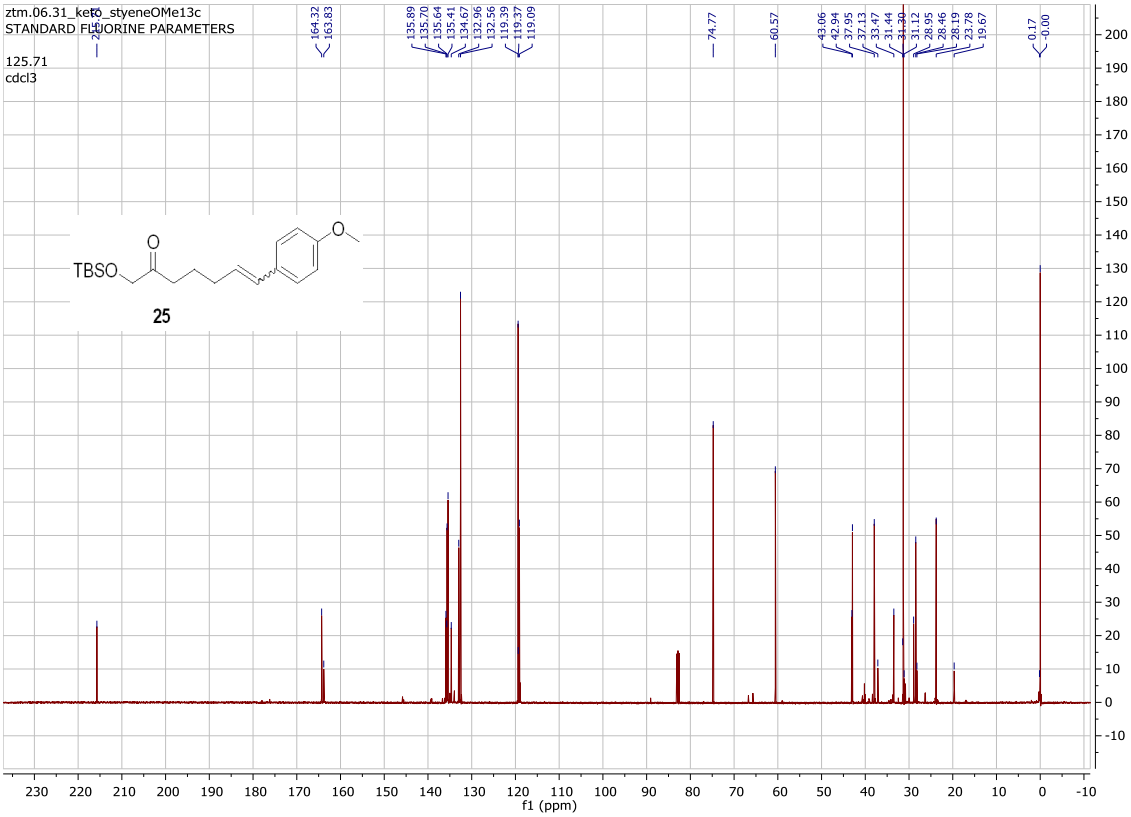
ztm.06.31_keto_styeneOMe13c
STANDARD FLUORINE PARAMETERS
125.71
cdcl3
TBSO
O
O
25
f1 (ppm)

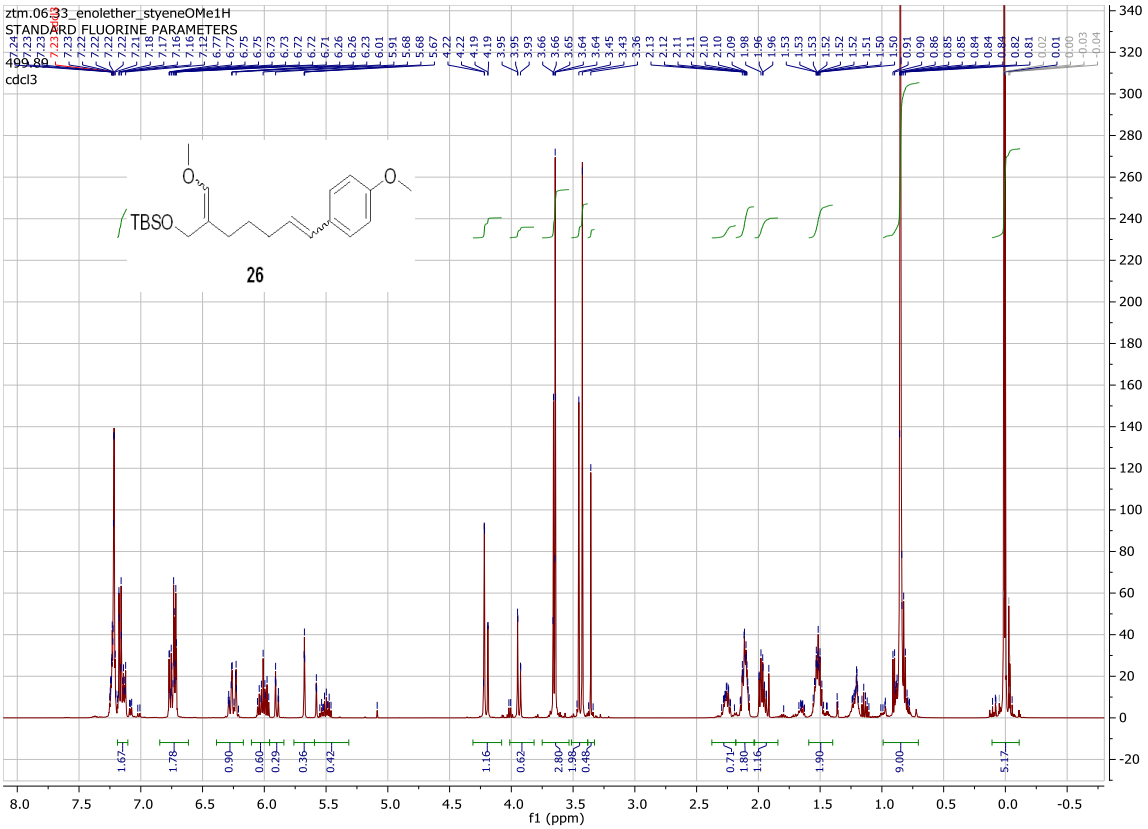
ztm.06.33_enolether_styeneOMe1H
STANDARD FLUORINE PARAMETERS
499.80
cdcl3
TBSO
O
O
26
f1 (ppm)

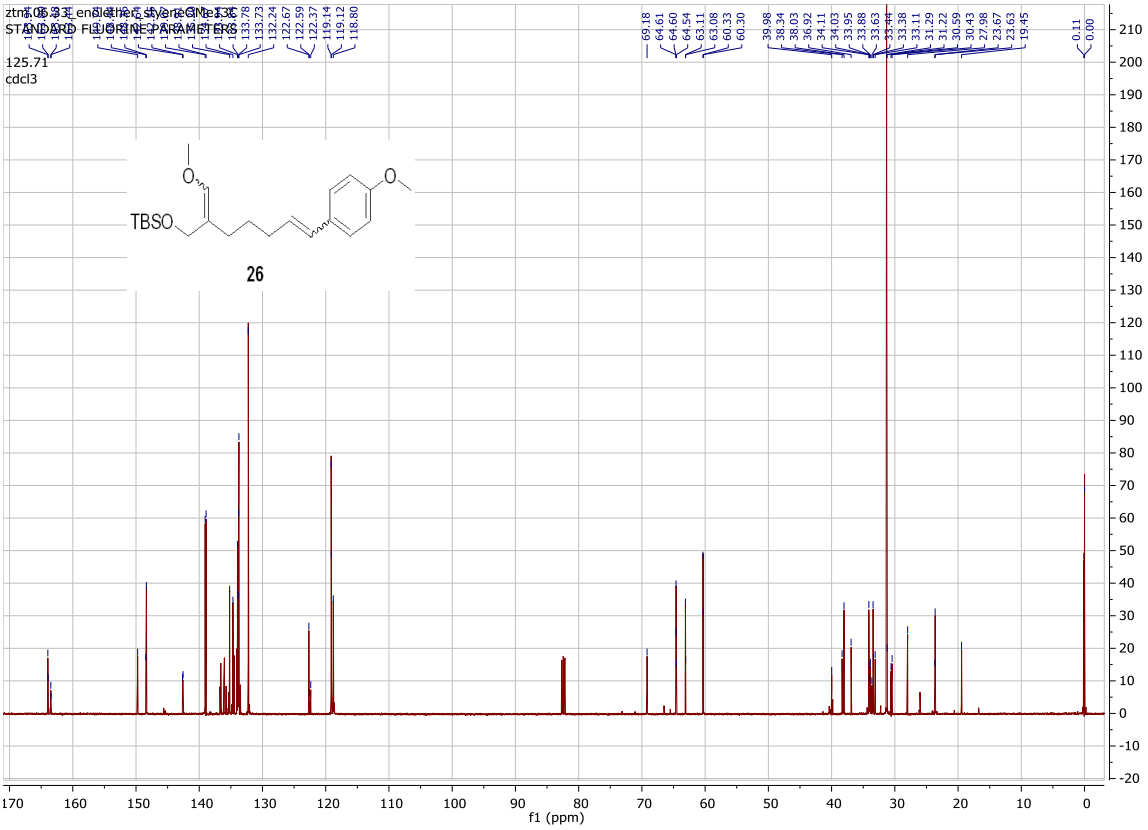
ztm.06.33_enolether_styeneOMe13C
STANDARD FLUORINE PARAMETERS
125.71
cdcl3
TBSO
O
O
26
f1 (ppm)

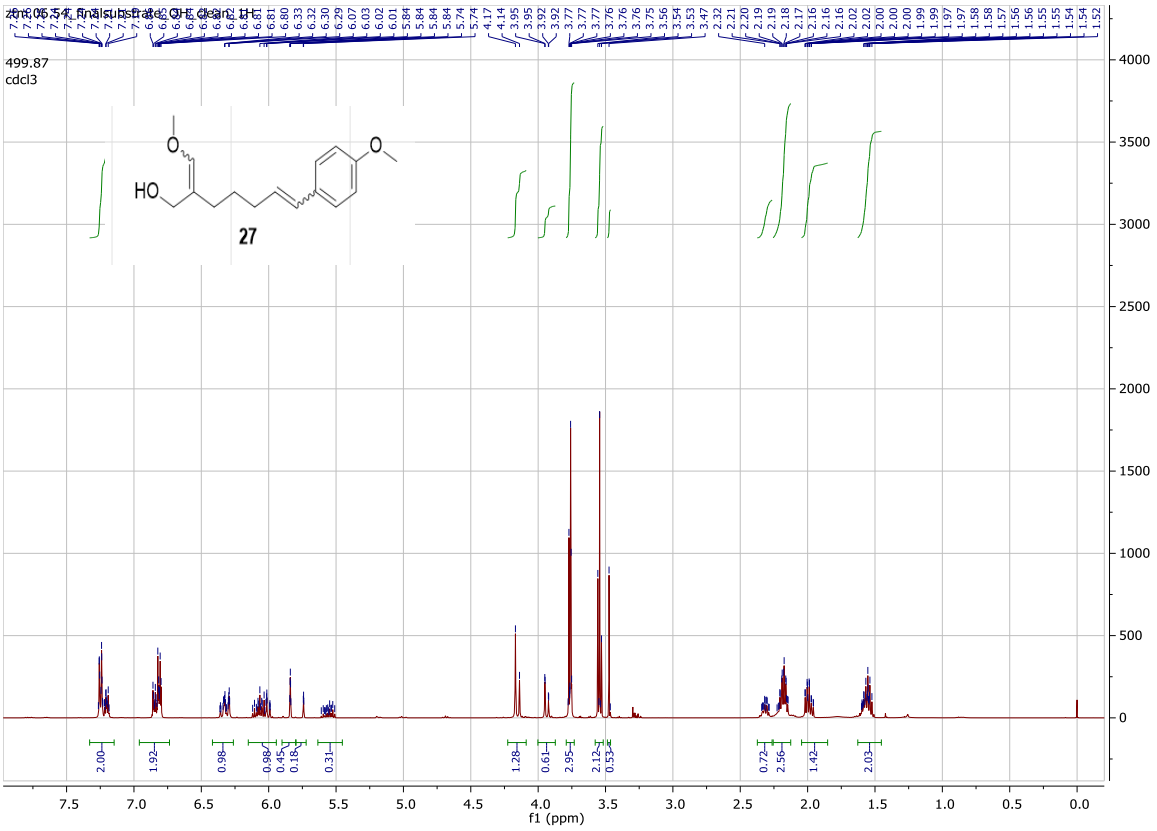
499.87
cdcl3
HO
O
O
27
f1 (ppm)

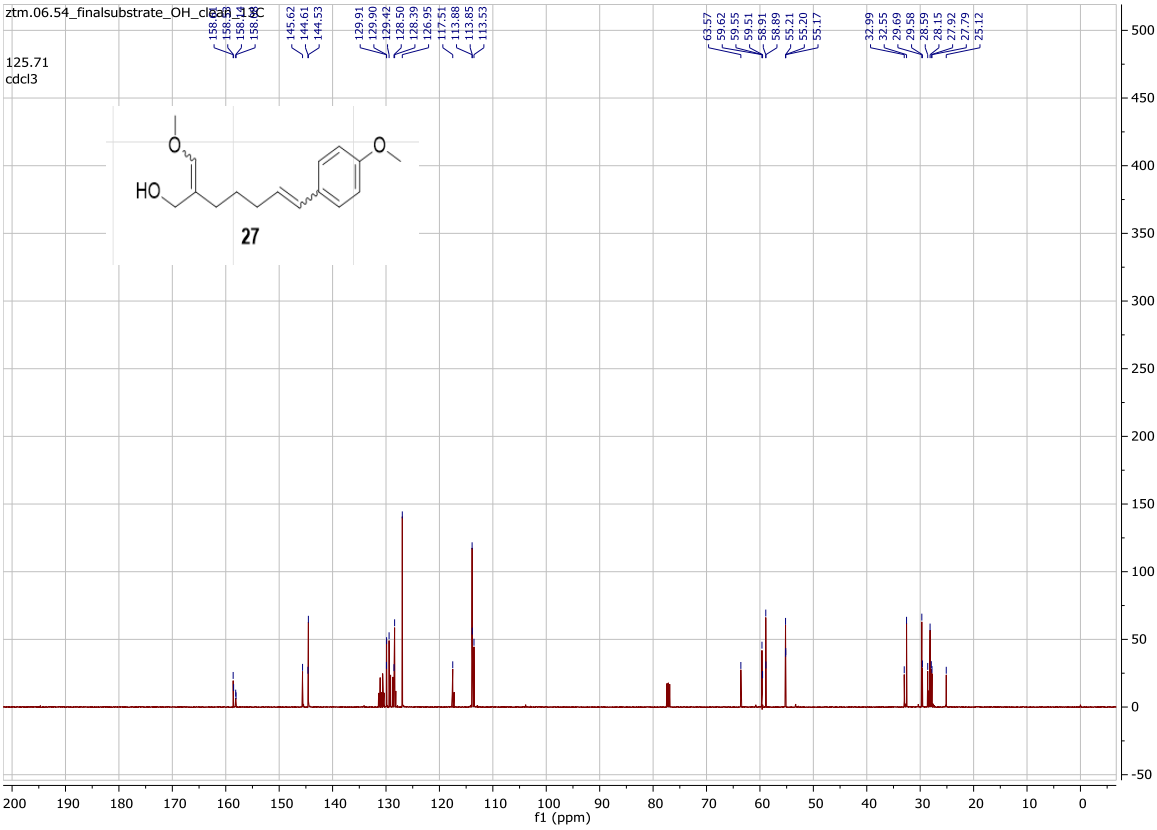
125.71
cdcl3
HO
O
O
27
f1 (ppm)

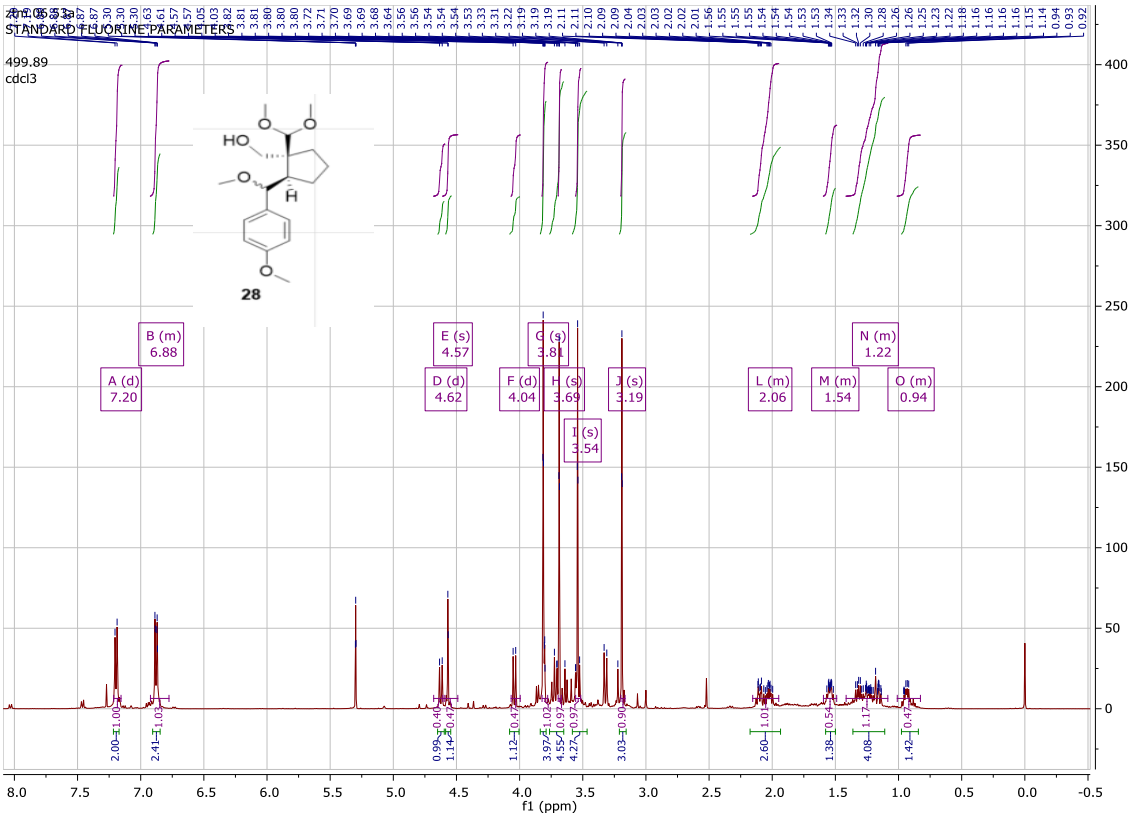
STANDARD FLUORINE PARAMETERS
499.89
cdcl3
28
B (m) 6.88
A (d) 7.20
E (s) 4.57
D (d) 4.62
G (s) 3.81
F (d) 4.04
H (s) 3.69
I (s) 3.54
J (s) 3.19
L (m) 2.06
N (m) 1.22
M (m) 1.54
O (m) 0.94
f1 (ppm)

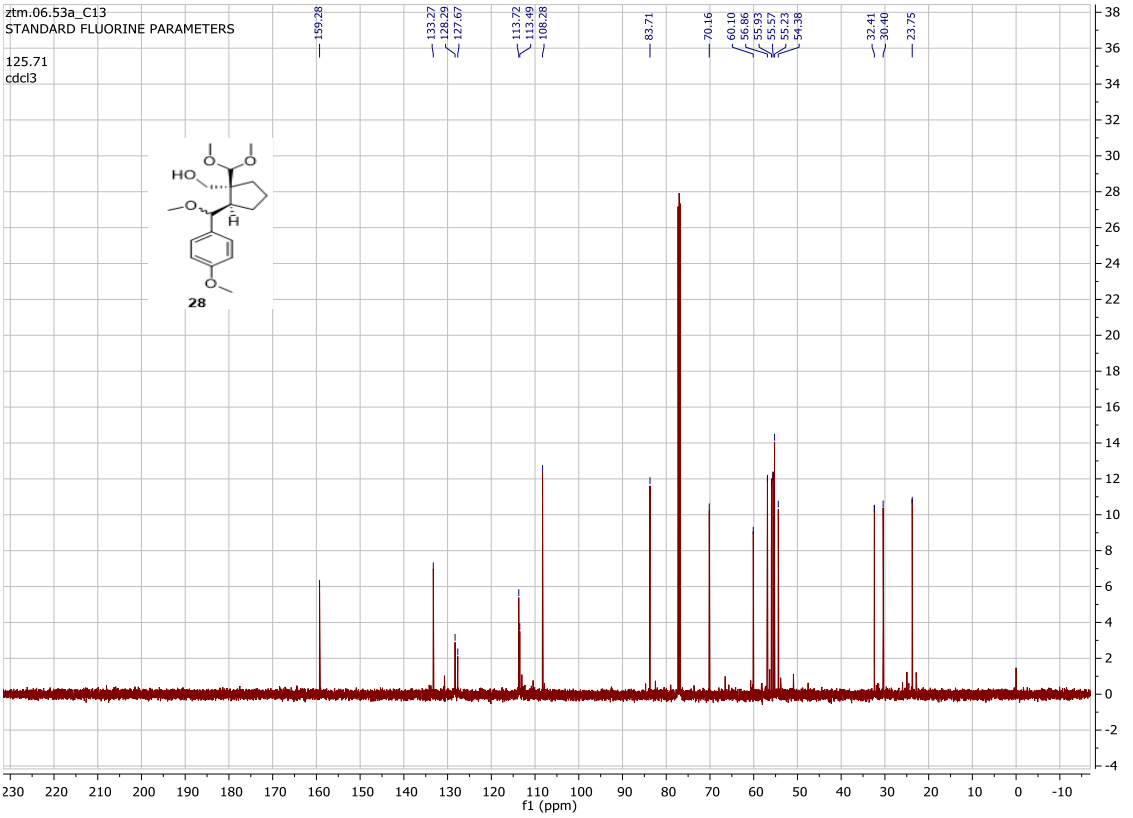
ztm.06.53a_C13
STANDARD FLUORINE PARAMETERS
125.71
cdcl3
28
159.28
133.27
128.29
127.67
113.72
113.49
108.28
83.71
70.16
60.10
56.86
55.93
55.57
55.23
54.38
32.41
30.40
23.75
f1 (ppm)

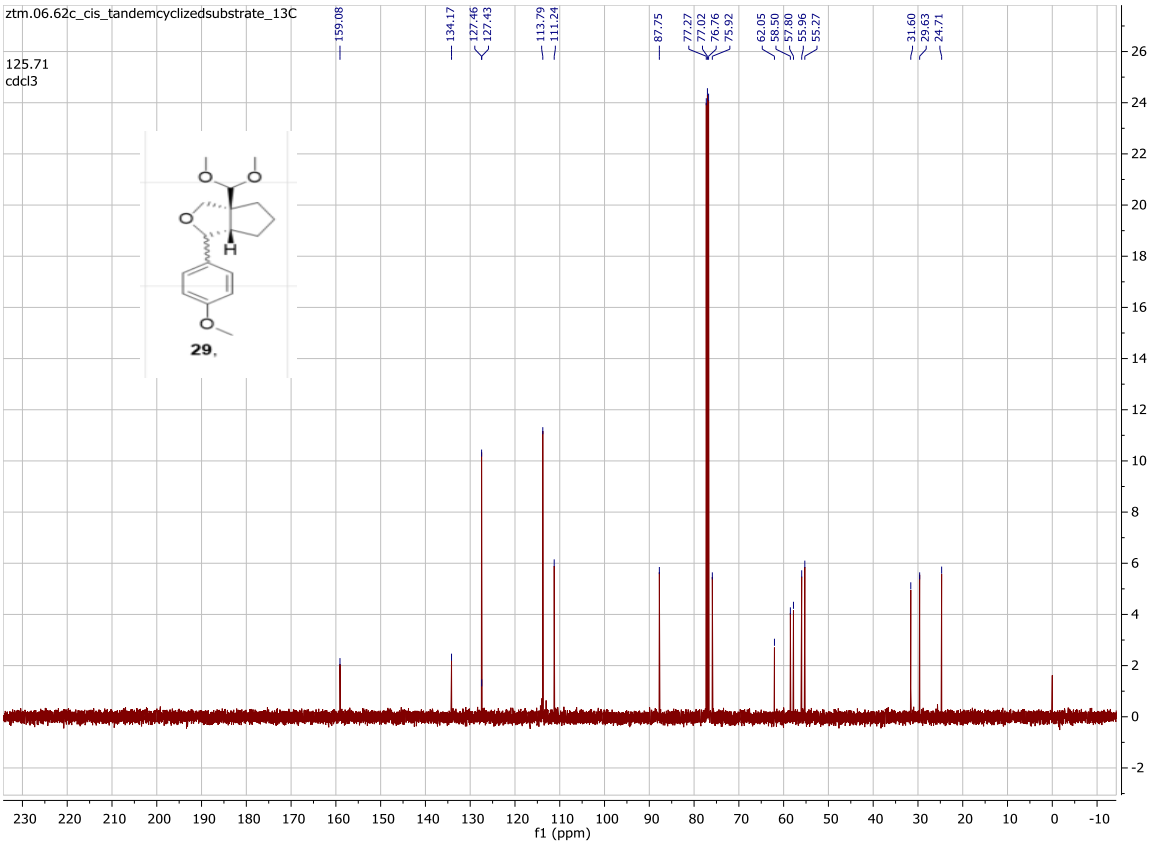
ztm.06.62c_cis_tandemcyclizedsubstrate_13C
125.71
cdcl3
159.08
134.17
127.46
127.43
113.79
111.24
87.75
77.27
77.02
76.76
75.92
62.05
58.50
57.80
55.96
55.27
31.60
29.63
24.71
29.
f1 (ppm)

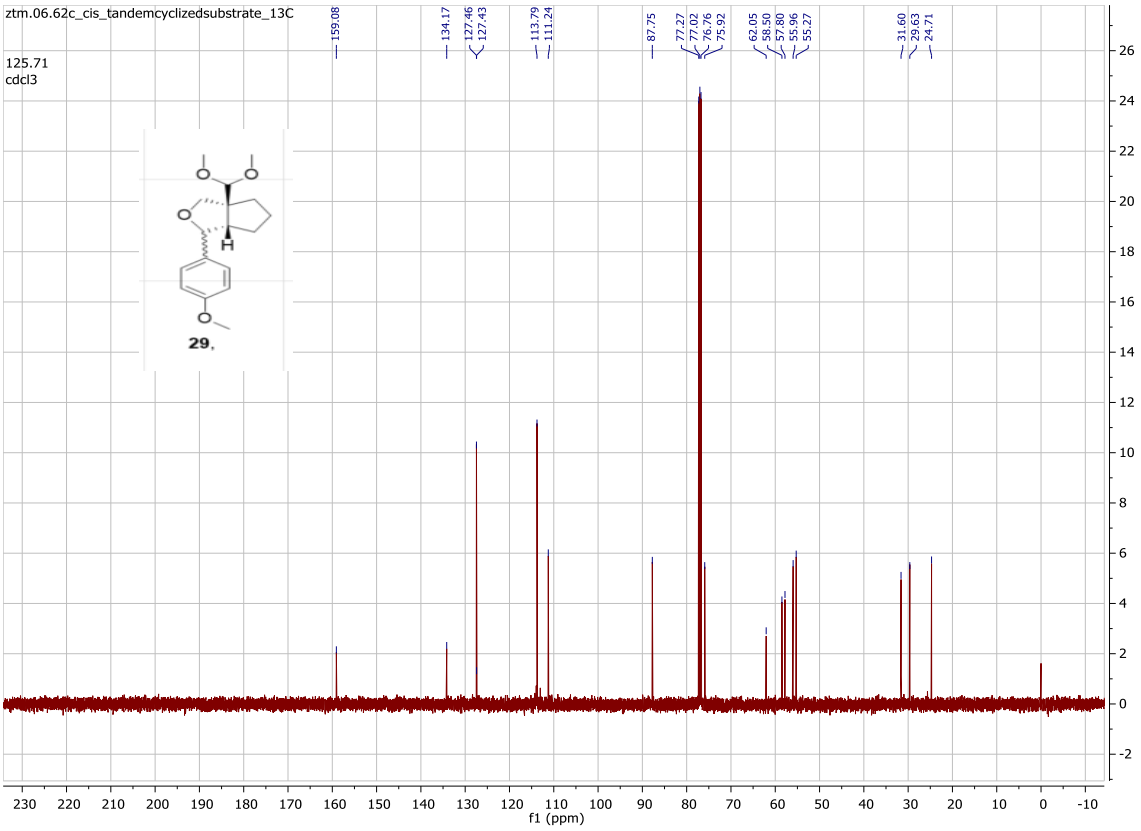
ztm.06.62c_cis_tandemcyclizedsubstrate_13C
125.71
cdcl3
159.08
134.17
127.46
127.43
113.79
111.24
87.75
77.27
77.02
76.76
75.92
62.05
58.50
57.80
55.96
55.27
31.60
29.63
24.71
29.
f1 (ppm)

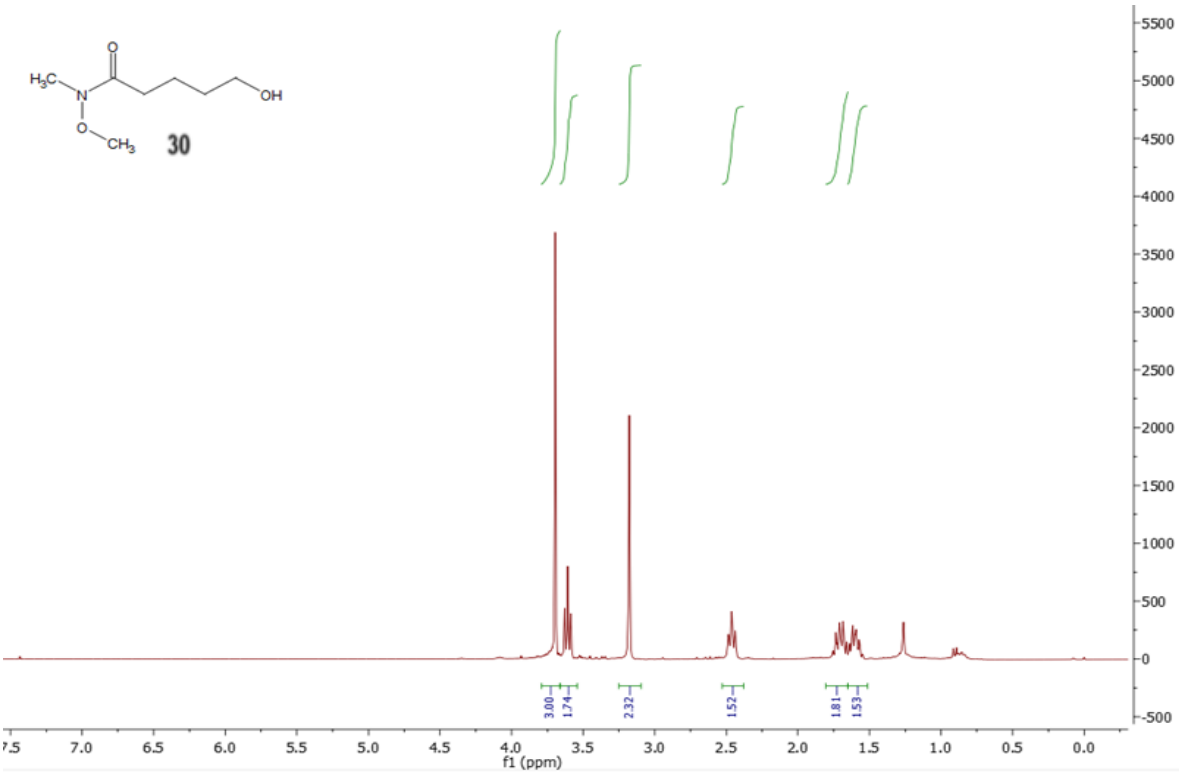
30
3.00
1.74
2.32
1.52
1.81
1.53
f1 (ppm)

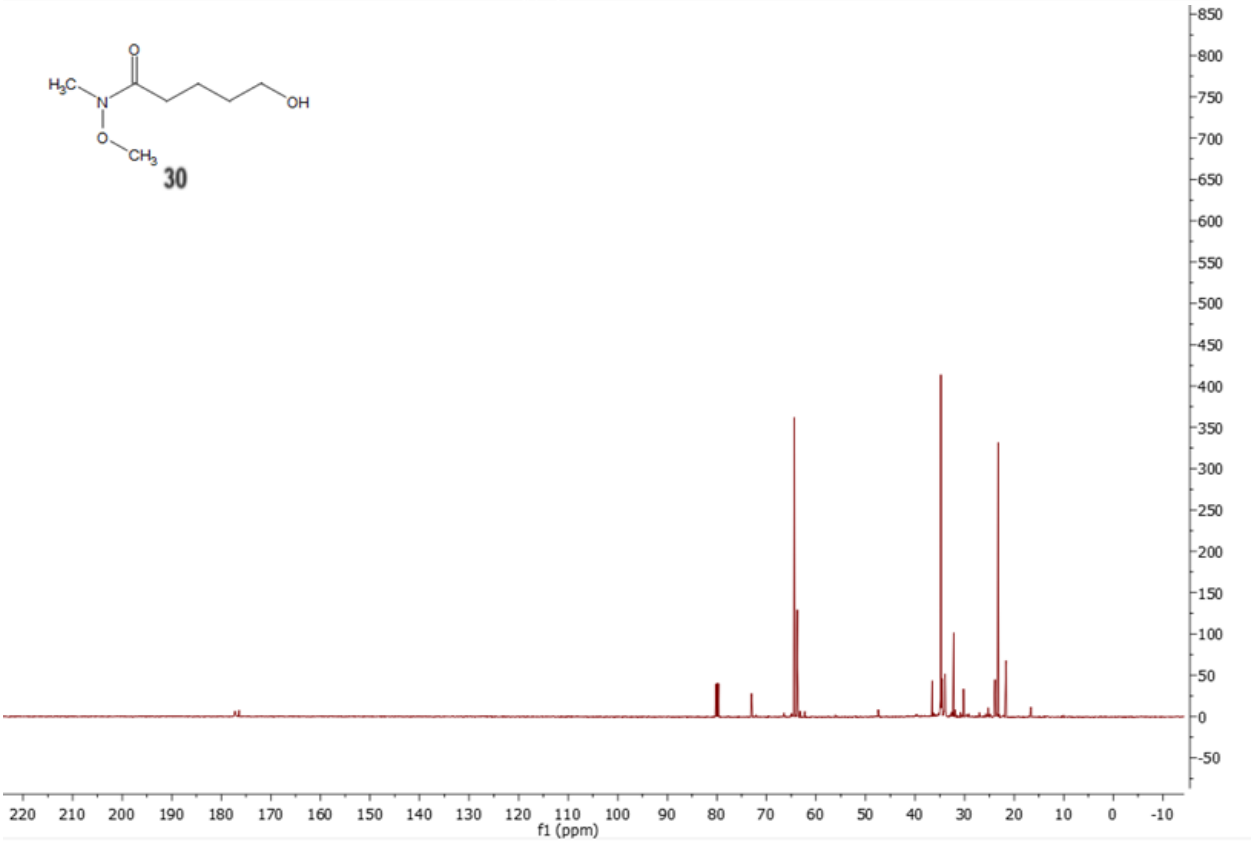
30
f1 (ppm)

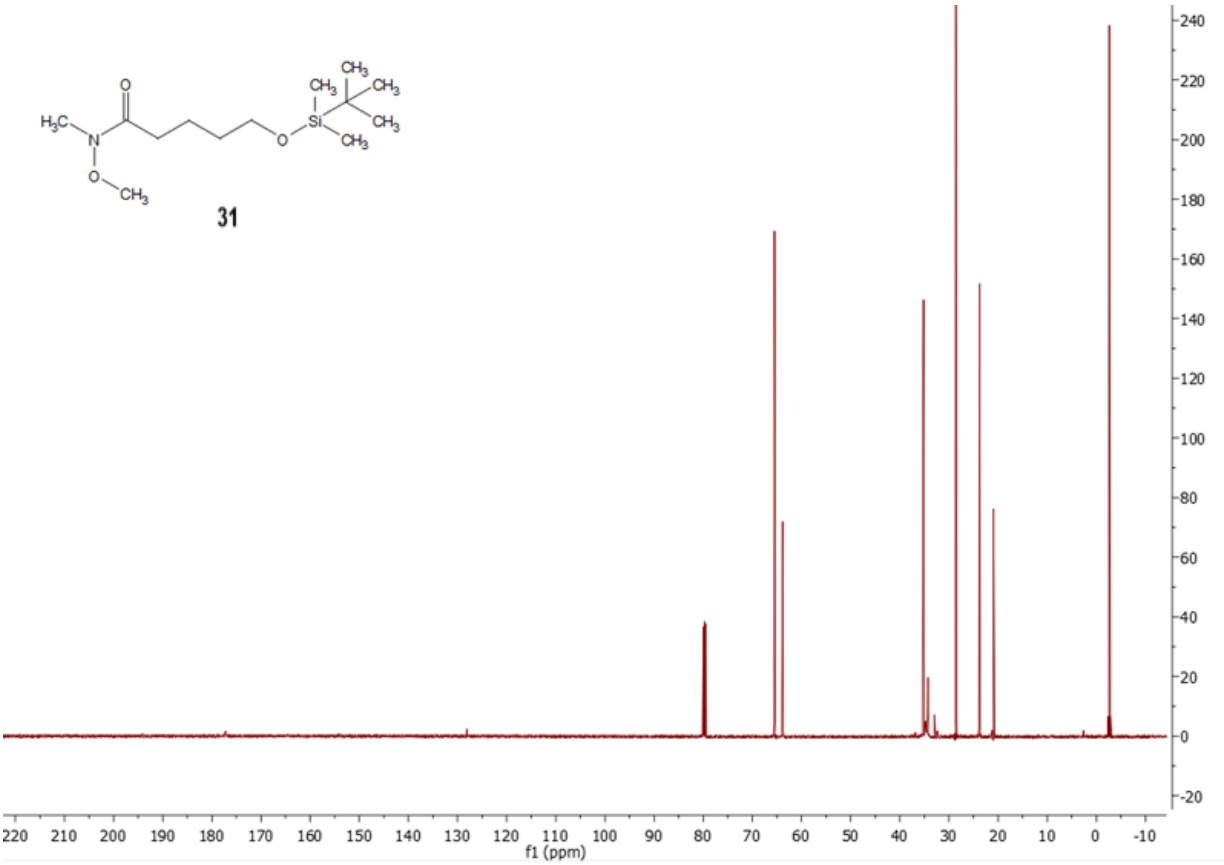
31
f1 (ppm)

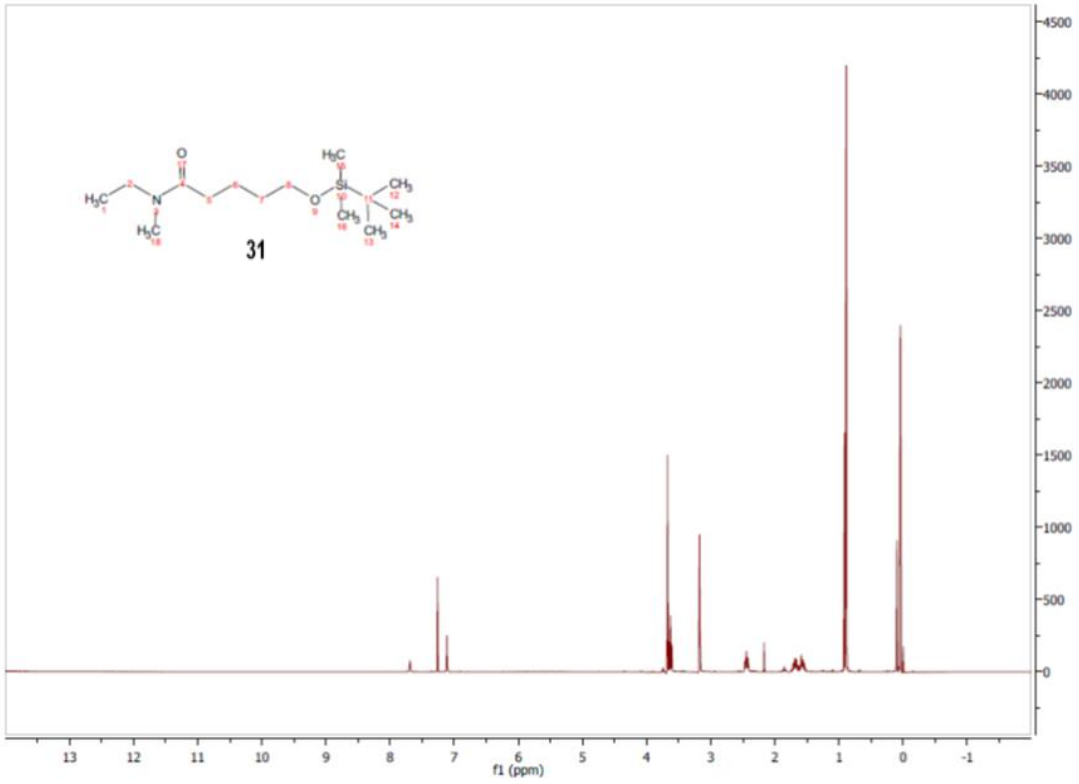
31
f1 (ppm)

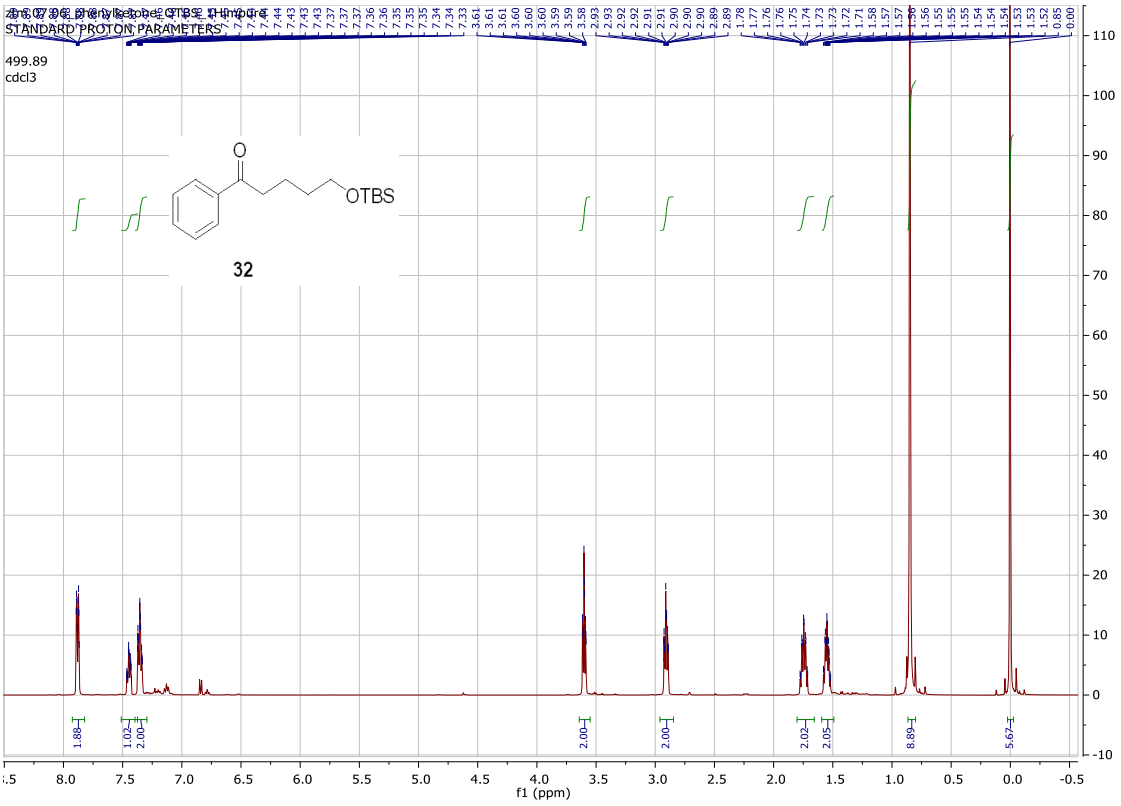
STANDARD PROTON PARAMETERS
499.89
cdcl3
O
OTBS
32
1.88
1.02
2.00
2.00
2.00
2.02
2.05
8.89
5.67
f1 (ppm)

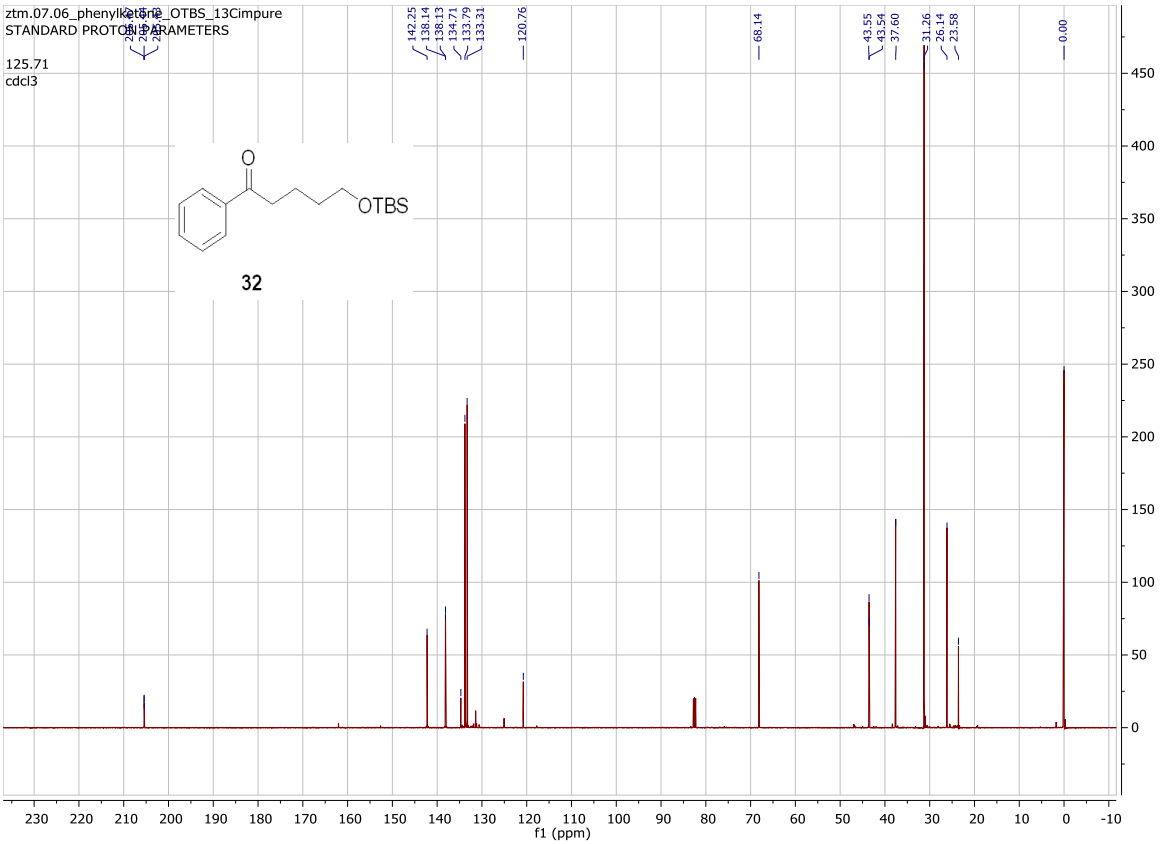
ztm.07.06_phenylketone_OTBS_13Cimpure
STANDARD PROTON PARAMETERS
125.71
cdcl3
O
OTBS
32
f1 (ppm)

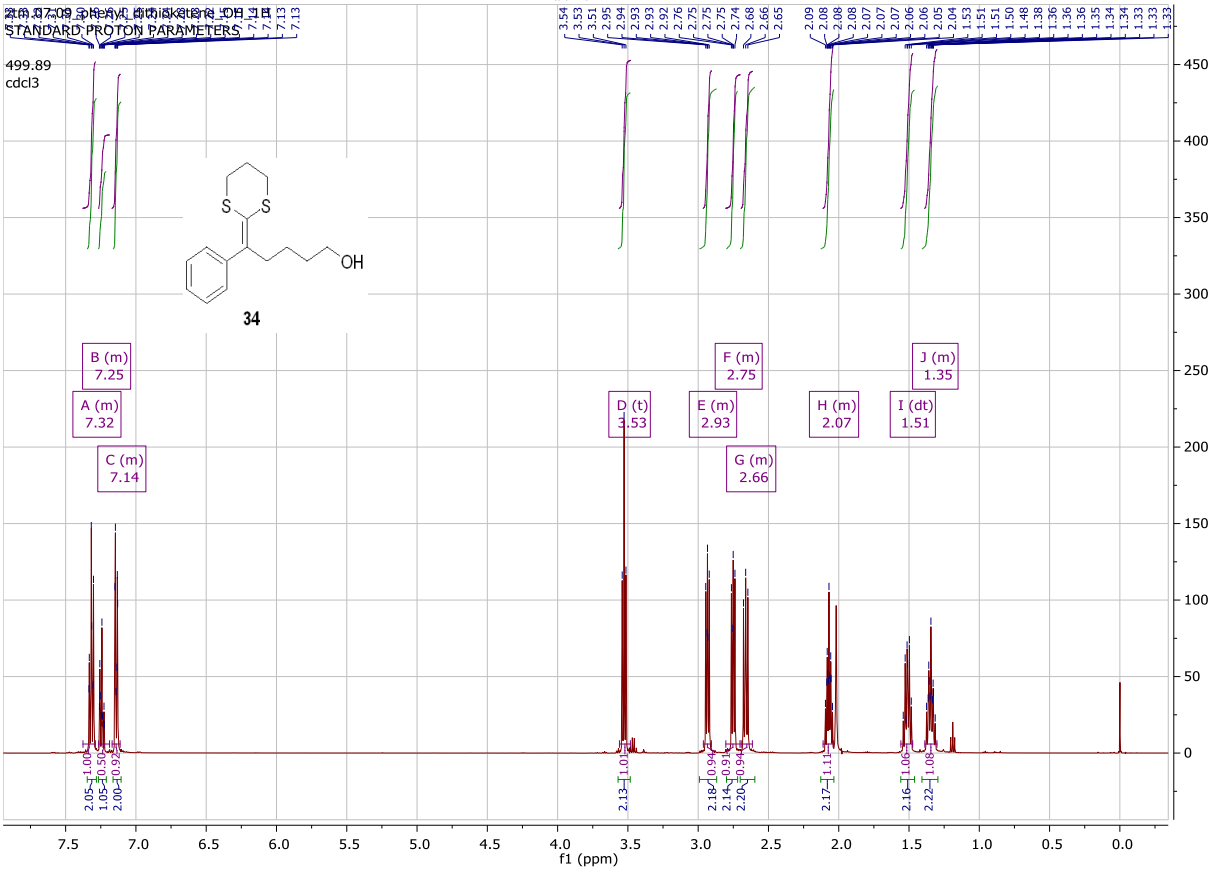
STANDARD PROTON PARAMETERS
499.89
cdcl3
S
S
OH
34
B (m) 7.25
A (m) 7.32
C (m) 7.14
D (t) 3.53
F (m) 2.75
E (m) 2.93
G (m) 2.66
H (m) 2.07
J (m) 1.35
I (dt) 1.51
f1 (ppm)

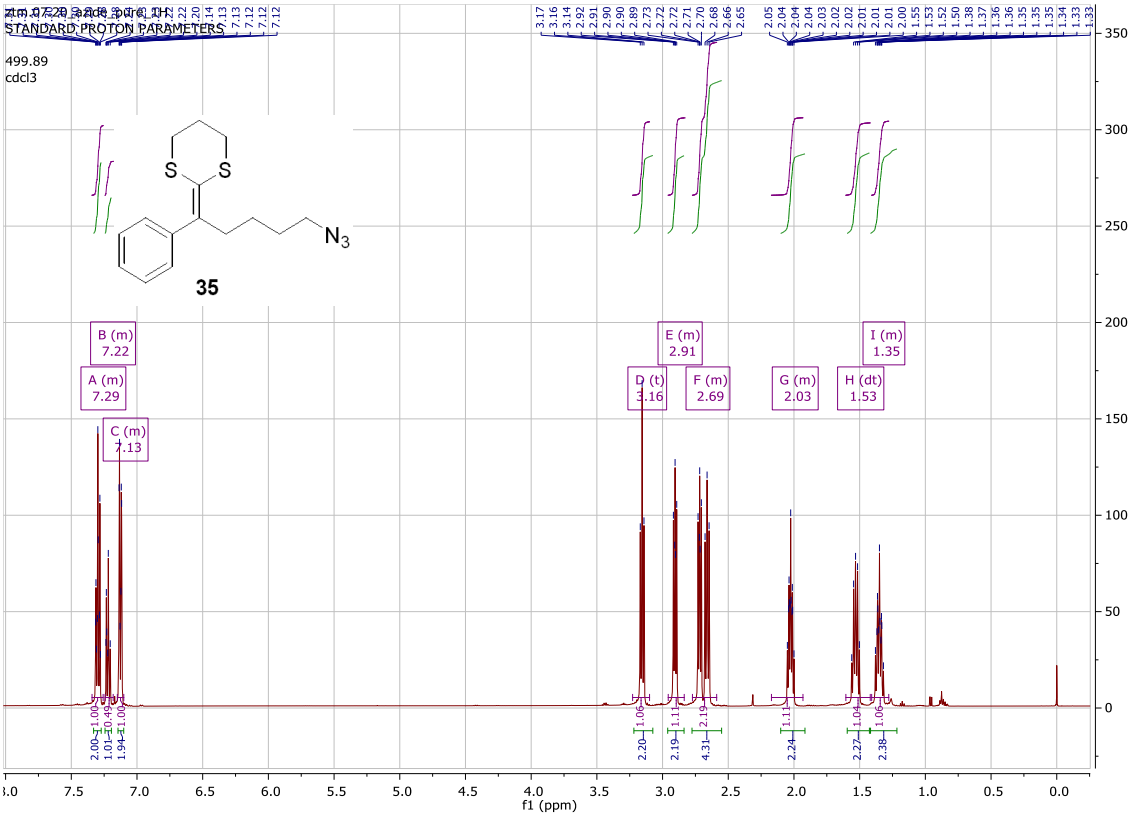
STANDARD PROTON PARAMETERS
499.89
cdcl3
35
B (m) 7.22
A (m) 7.29
C (m) 7.13
E (m) 2.91
D (t) 3.16
F (m) 2.69
G (m) 2.03
I (m) 1.35
H (dt) 1.53
f1 (ppm)

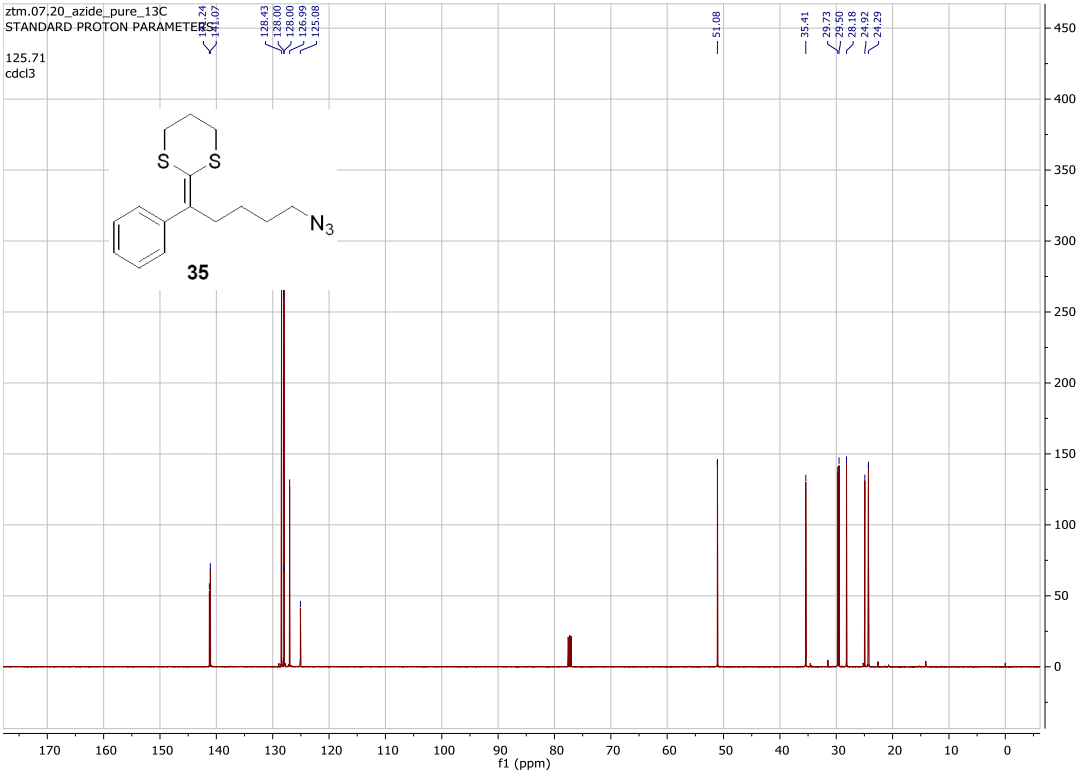
ztm.07.20_azide_pure_13C
STANDARD PROTON PARAMETERS
125.71
cdcl3
35
f1 (ppm)

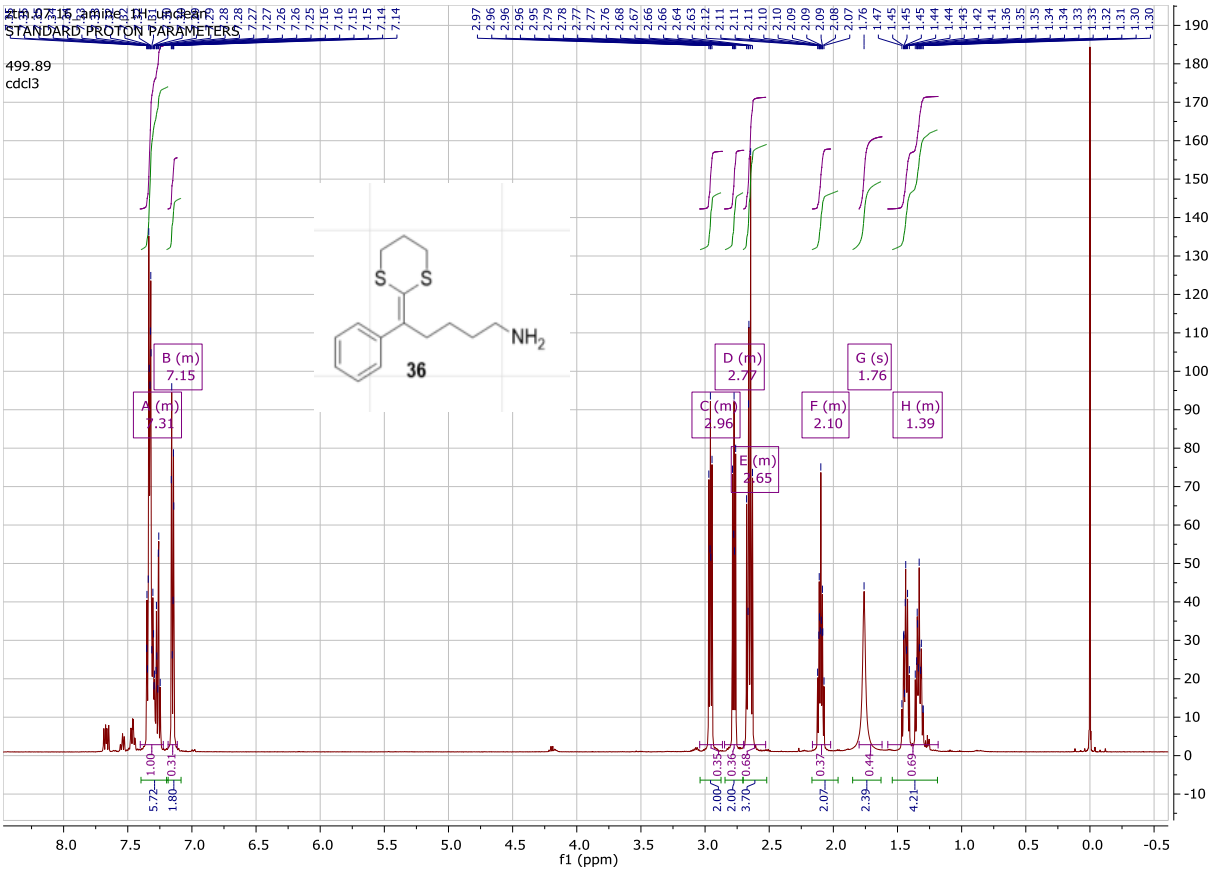
ztm.07.16_amine_1H_cdcl3
STANDARD PROTON PARAMETERS
499.89
cdcl3
36
B (m) 7.15
A (m) 7.31
D (m) 2.77
C (m) 2.96
E (m) 2.65
F (m) 2.10
G (s) 1.76
H (m) 1.39
f1 (ppm)

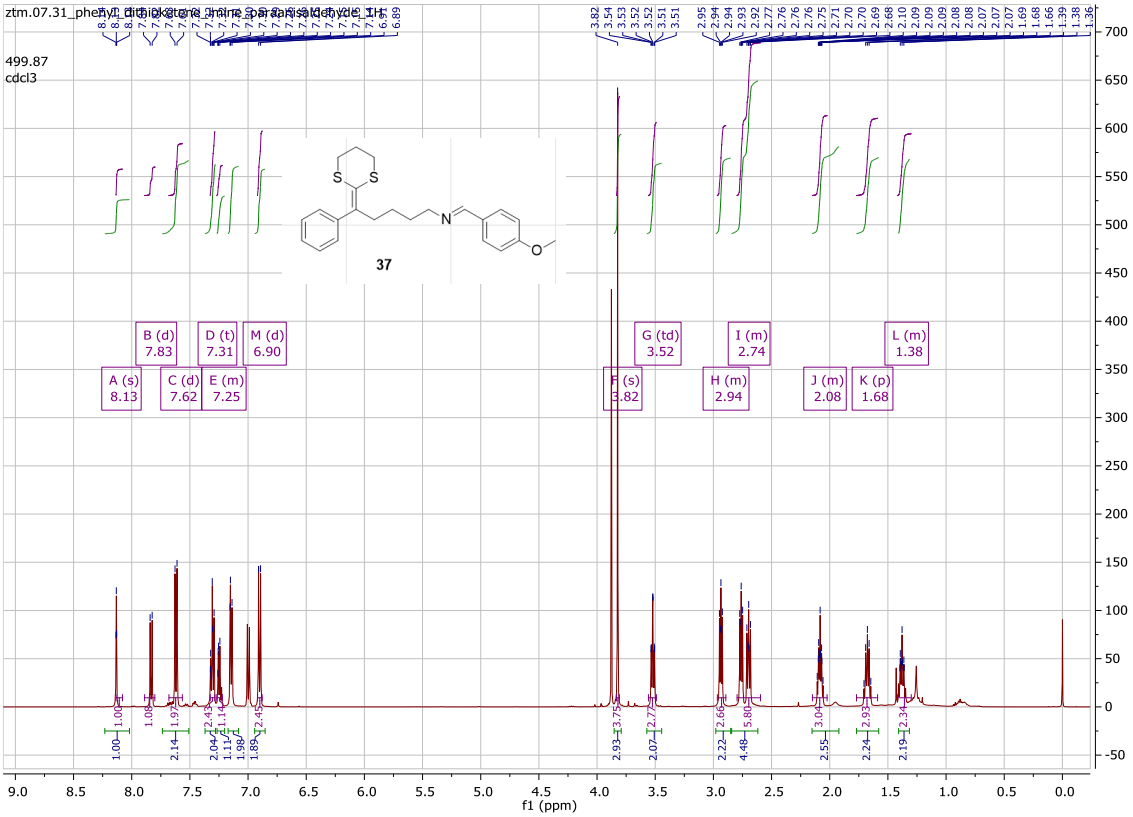
ztm.07.31_phenyl_dithiolketone_imine_paraanisaldehyde_1H
499.87
cdcl3
37
B (d) 7.83
D (t) 7.31
M (d) 6.90
A (s) 8.13
C (d) 7.62
E (m) 7.25
G (td) 3.52
I (m) 2.74
L (m) 1.38
F (s) 3.82
H (m) 2.94
J (m) 2.08
K (p) 1.68
f1 (ppm)

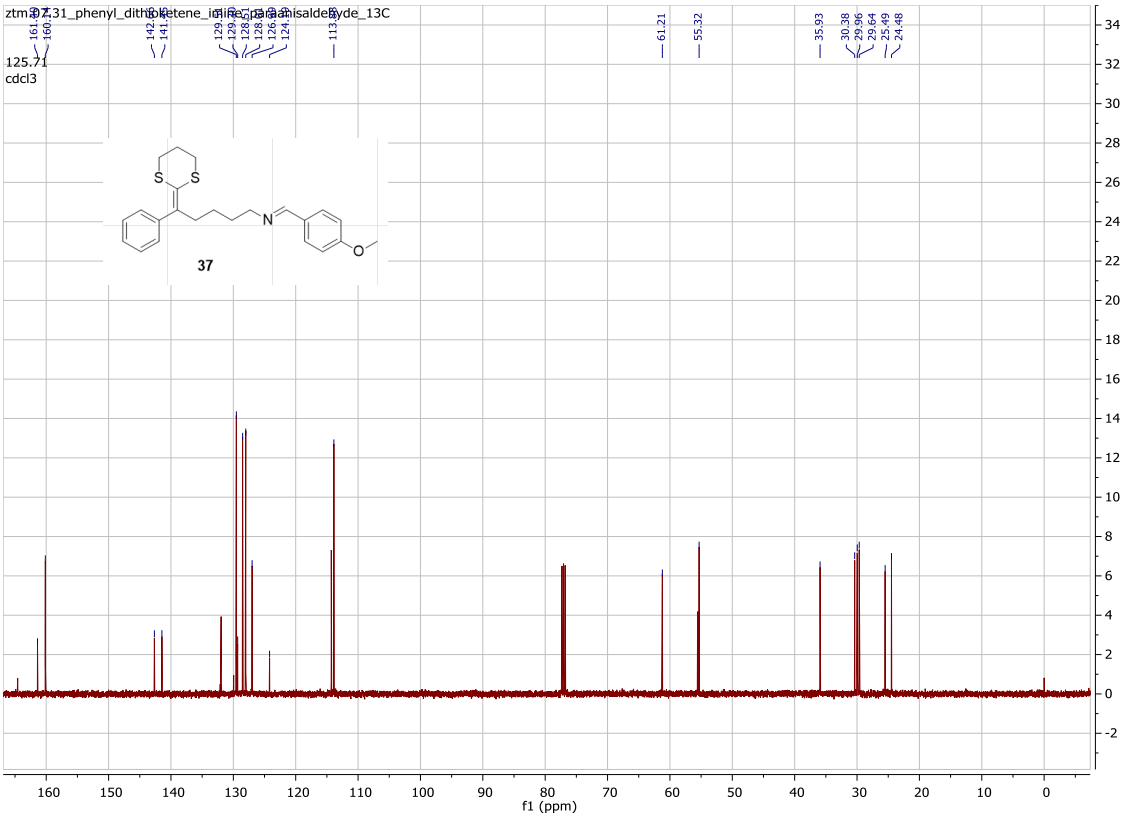
ztm.07.31_phenyl_dithioketene_imine_paraanisaldehyde_13C
125.71
cdcl3
37
f1 (ppm)

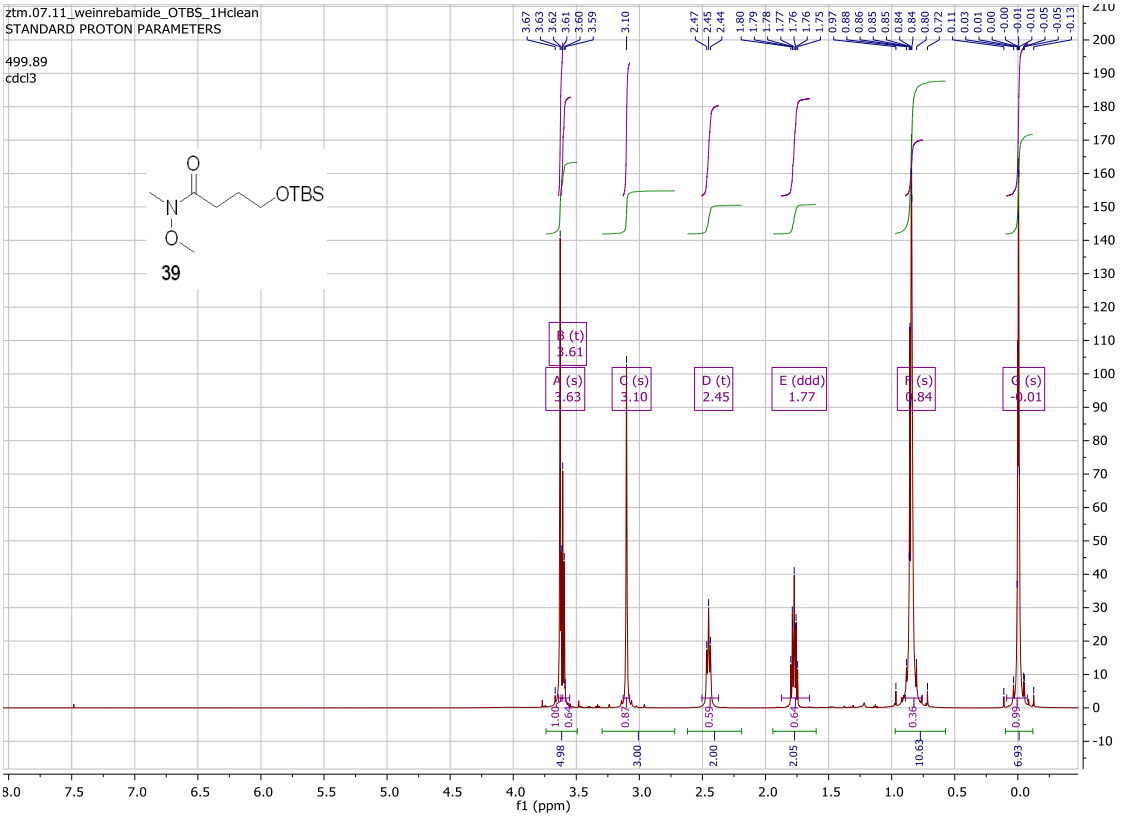
ztm.07.11_weinrebamide_OTBS_1Hclean
STANDARD PROTON PARAMETERS
499.89
cdcl3
OTBS
39
B (t) 3.61
A (s) 3.63
C (s) 3.10
D (t) 2.45
E (ddd) 1.77
F (s) 0.84
G (s) -0.01
f1 (ppm)

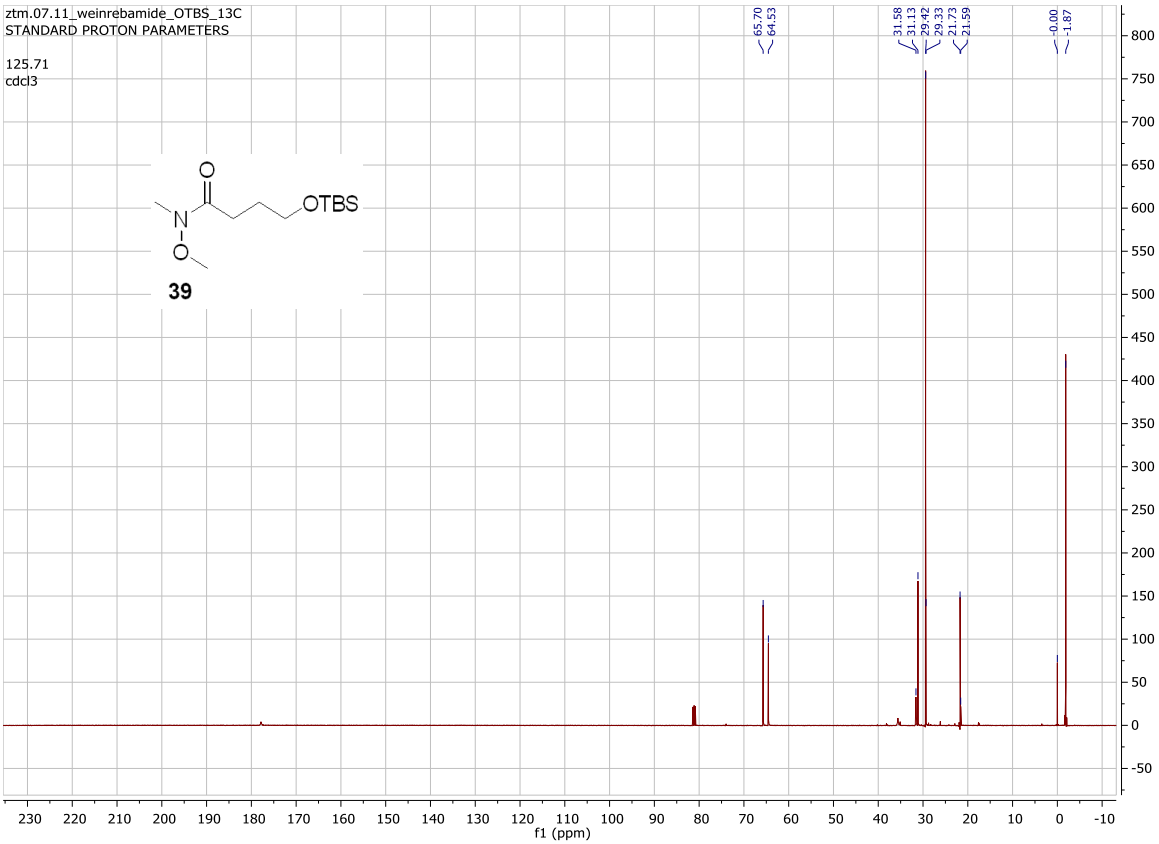
ztm.07.11_weinrebamide_OTBS_13C
STANDARD PROTON PARAMETERS
125.71
cdcl3
OTBS
39
f1 (ppm)

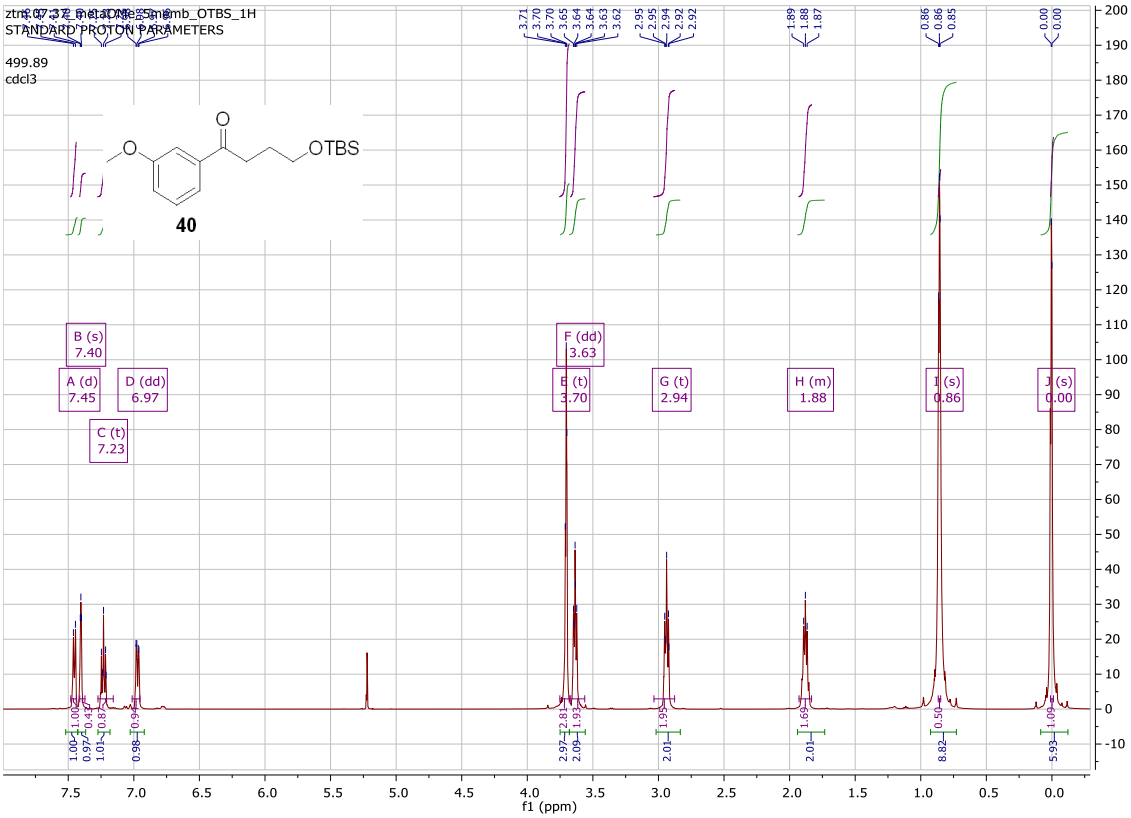
STANDARD PROTON PARAMETERS
499.89
cdcl3
OTBS
40
B (s) 7.40
A (d) 7.45
D (dd) 6.97
C (t) 7.23
F (dd) 3.63
E (t) 3.70
G (t) 2.94
H (m) 1.88
I (s) 0.86
J (s) 0.00
f1 (ppm)

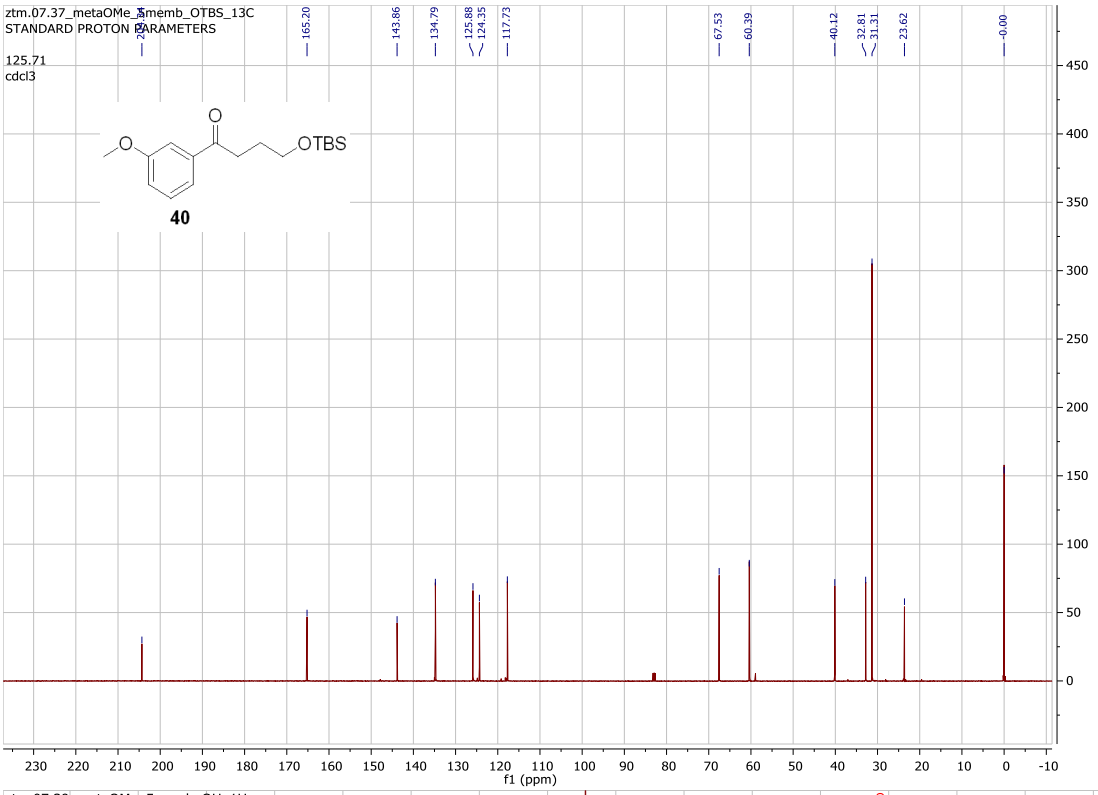
ztm.07.37_metaOMe_5memb_OTBS_13C
STANDARD PROTON PARAMETERS
125.71
cdcl3
OTBS
40
f1 (ppm)

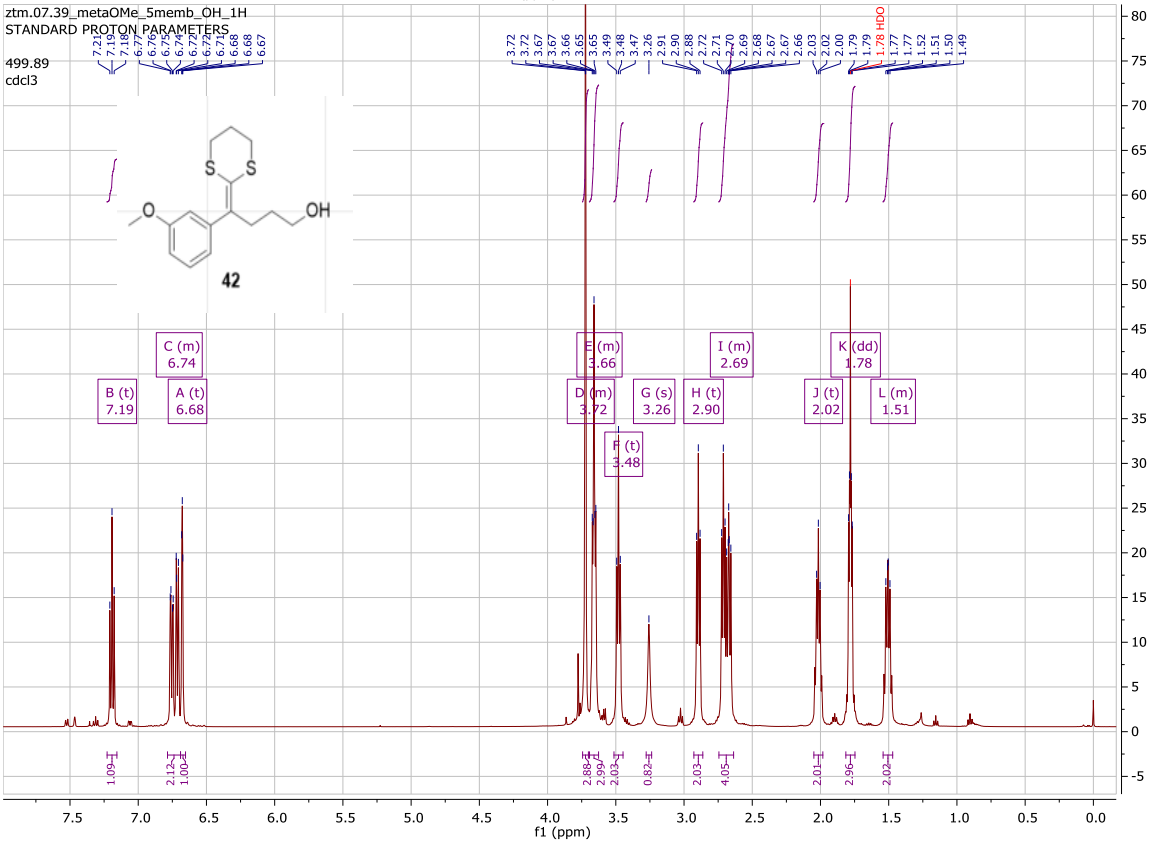
ztm.07.39_metaOMe_5memb_OH_1H
STANDARD PROTON PARAMETERS
499.89
cdcl3
OH
42
C (m) 6.74
B (t) 7.19
A (t) 6.68
I (m) 2.69
K (dd) 1.78
H (t) 2.90
G (s) 3.26
J (t) 2.02
L (m) 1.51
F (t) 3.48
f1 (ppm)

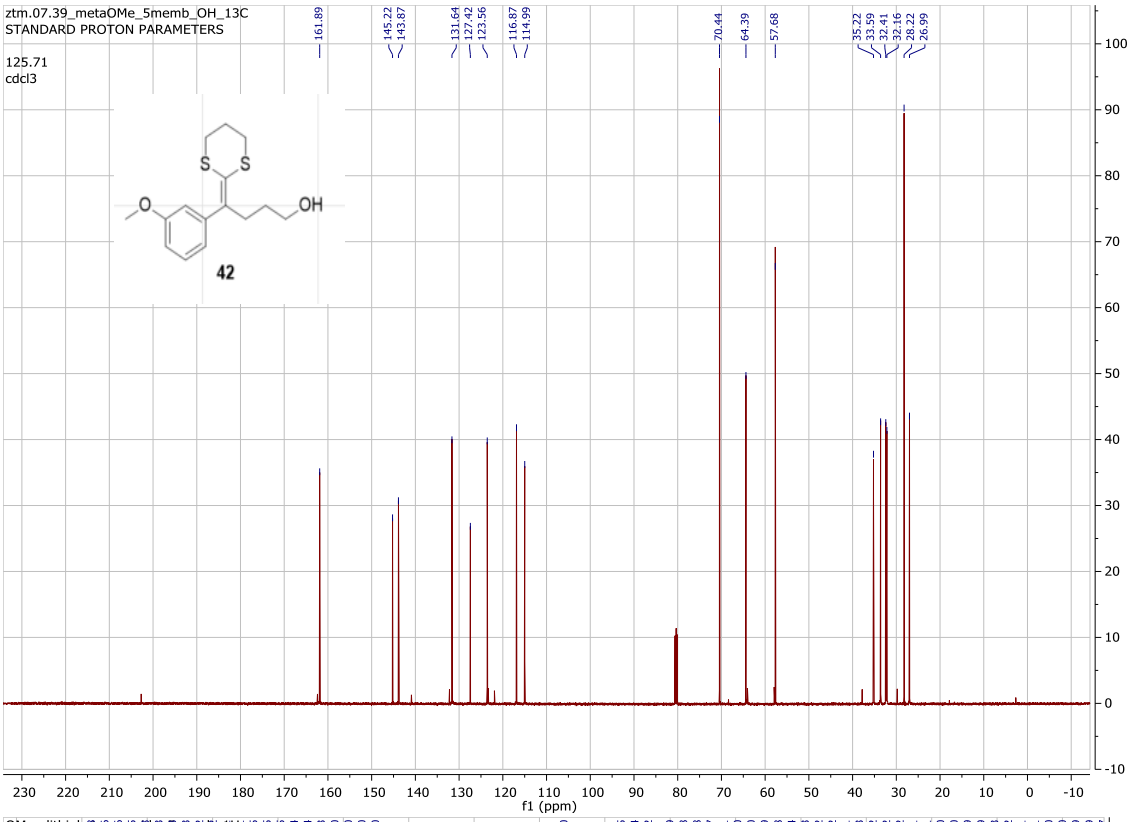
ztm.07.39_metaOMe_5memb_OH_13C
STANDARD PROTON PARAMETERS
125.71
cdcl3
161.89
145.22
143.87
131.64
127.42
123.56
116.87
114.99
70.44
64.39
57.68
35.22
33.59
32.41
32.16
28.22
26.99
S
S
O
OH
42
f1 (ppm)

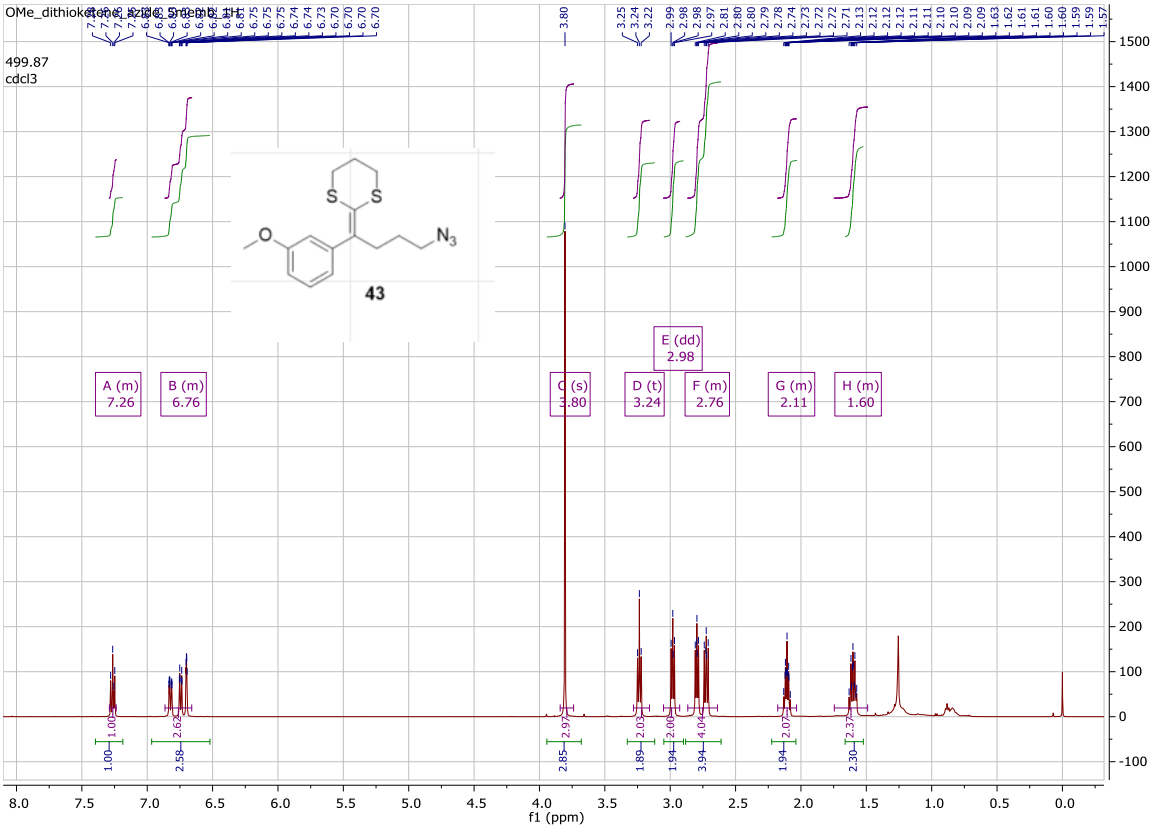
499.87
cdcl3
3.80
3.25
3.24
3.22
2.99
2.98
2.98
2.97
2.81
2.80
2.80
2.79
2.78
2.74
2.73
2.72
2.71
S
S
O
N3
43
E (dd)
2.98
A (m)
7.26
B (m)
6.76
C (s)
3.80
D (t)
3.24
F (m)
2.76
G (m)
2.11
H (m)
1.60
f1 (ppm)

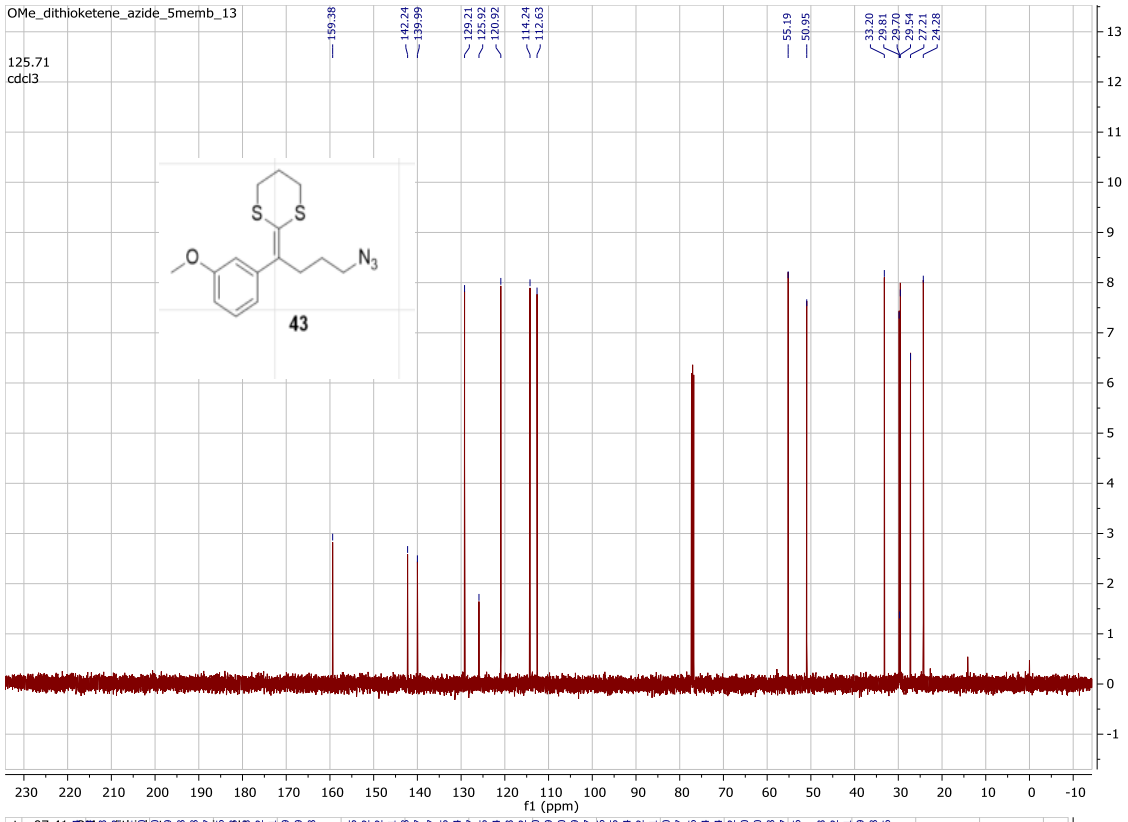
OMe_dithioketene_azide_5memb_13
125.71
cdcl3
159.38
142.24
139.99
129.21
125.92
120.92
114.24
112.63
55.19
50.95
33.20
29.81
29.70
29.54
27.21
24.28
S
S
O
N3
43
f1 (ppm)

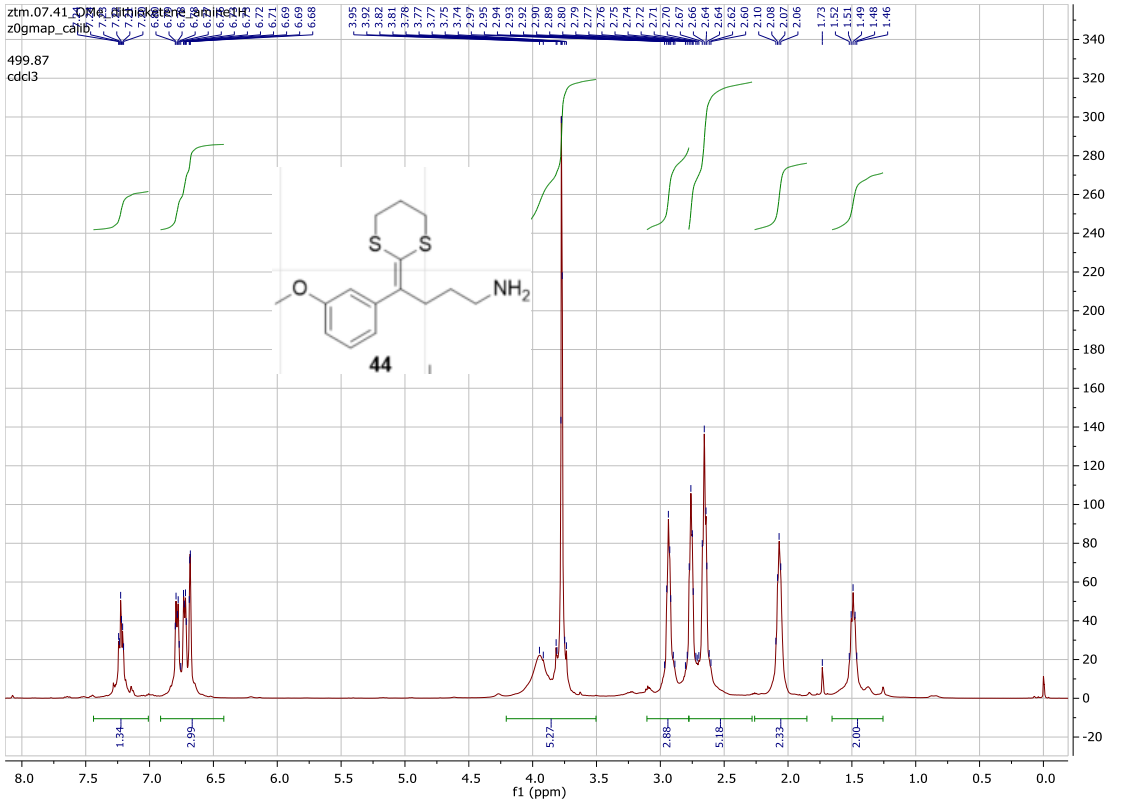
499.87
cdcl3
S
S
O
NH2
44
1.34
2.99
5.27
2.68
5.18
2.33
2.00
f1 (ppm)

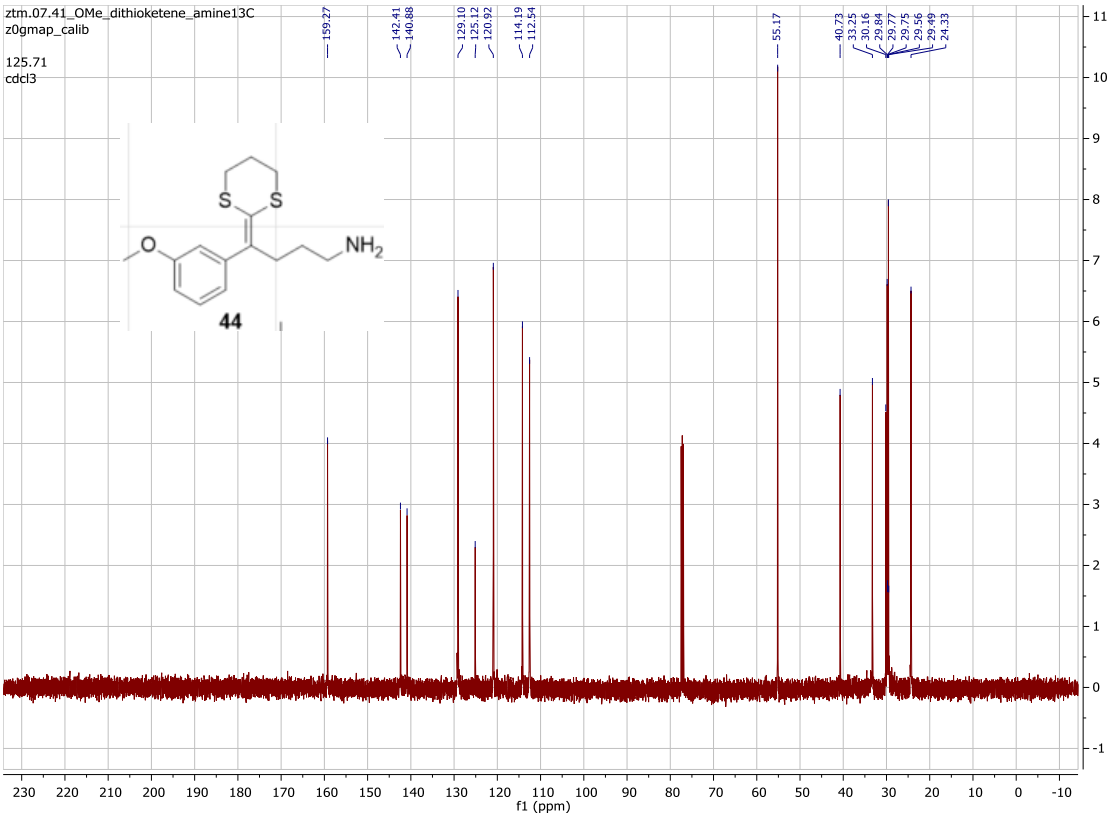
ztm.07.41_OMe_dithioketene_amine13C
z0gmap_calib
125.71
cdcl3
159.27
142.41
140.88
129.10
125.12
120.92
114.19
112.54
55.17
40.73
33.25
30.16
29.84
29.77
29.75
29.56
29.49
24.33
NH2
44
f1 (ppm)

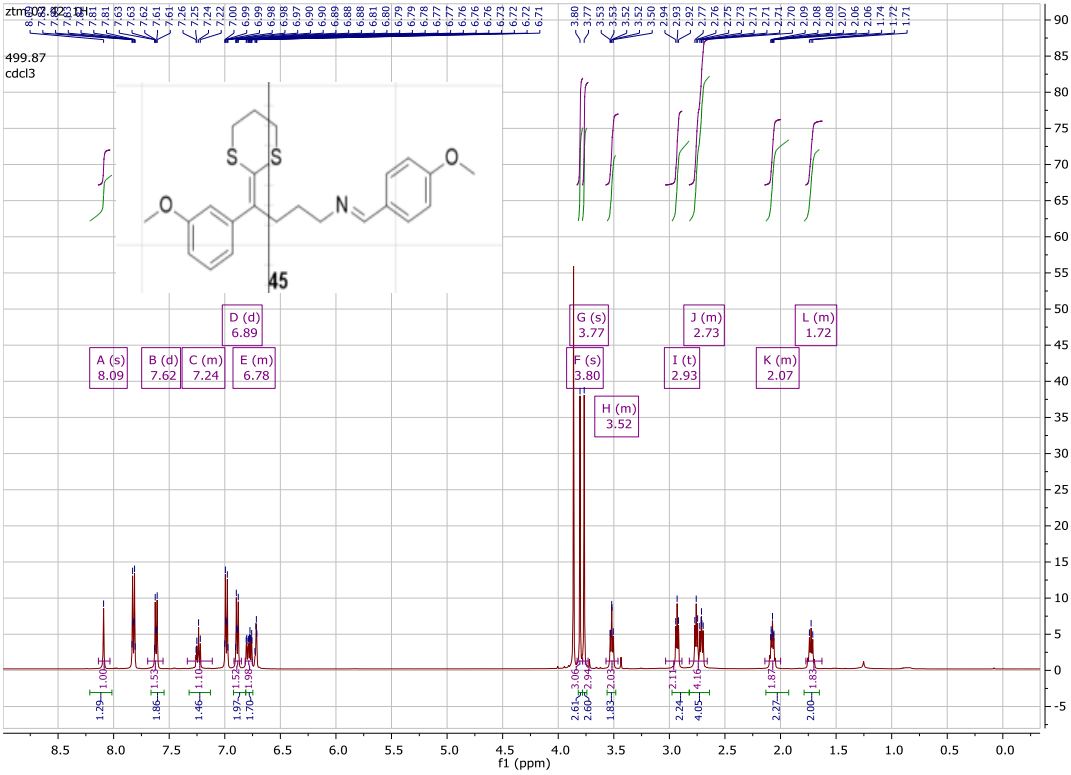
499.87
cdcl3
45
A (s) 8.09
B (d) 7.62
C (m) 7.24
D (d) 6.89
E (m) 6.78
F (s) 3.80
G (s) 3.77
H (m) 3.52
I (t) 2.93
J (m) 2.73
K (m) 2.07
L (m) 1.72
f1 (ppm)

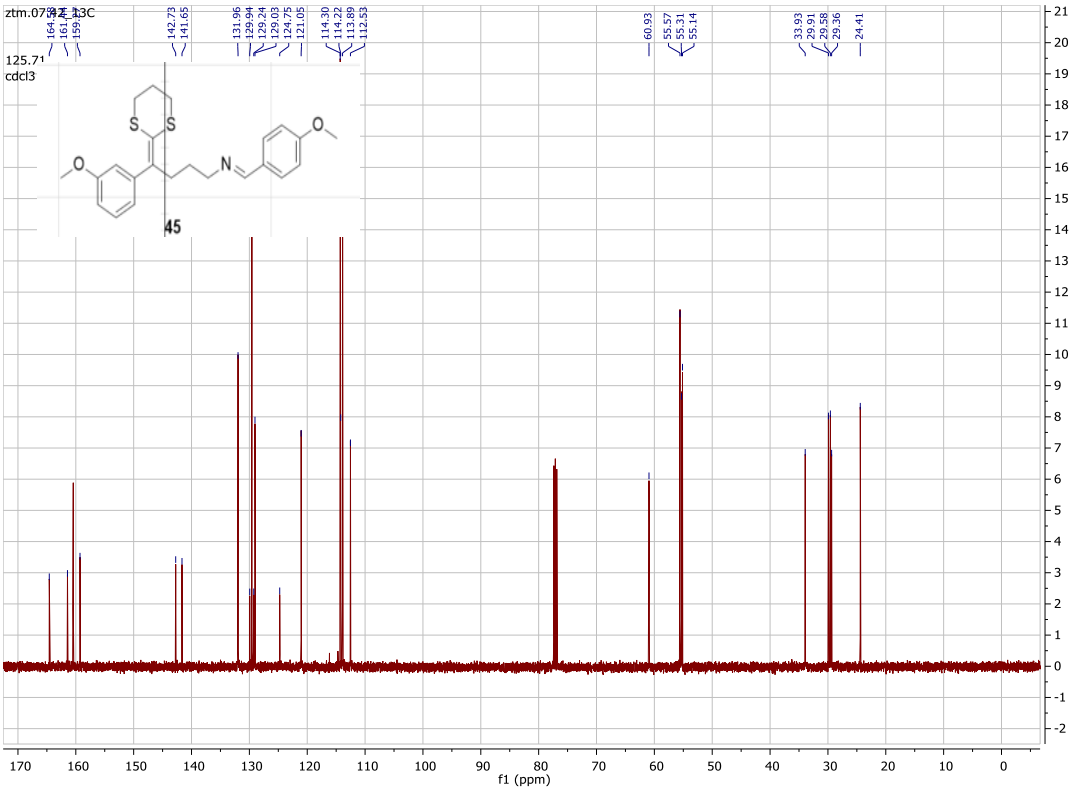
ztm.07142_13C
125.71
cdcl3
45
f1 (ppm)

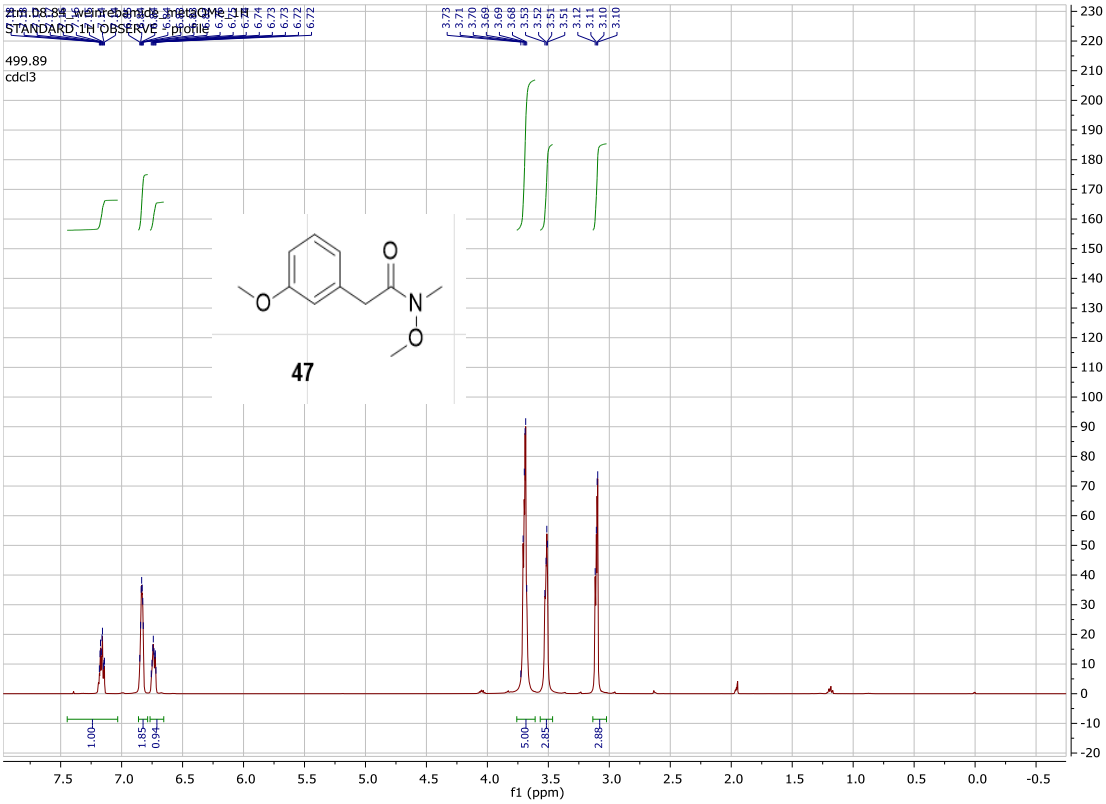
STANDARD 1H OBSERVE - proton
499.89
cdcl3
47
f1 (ppm)

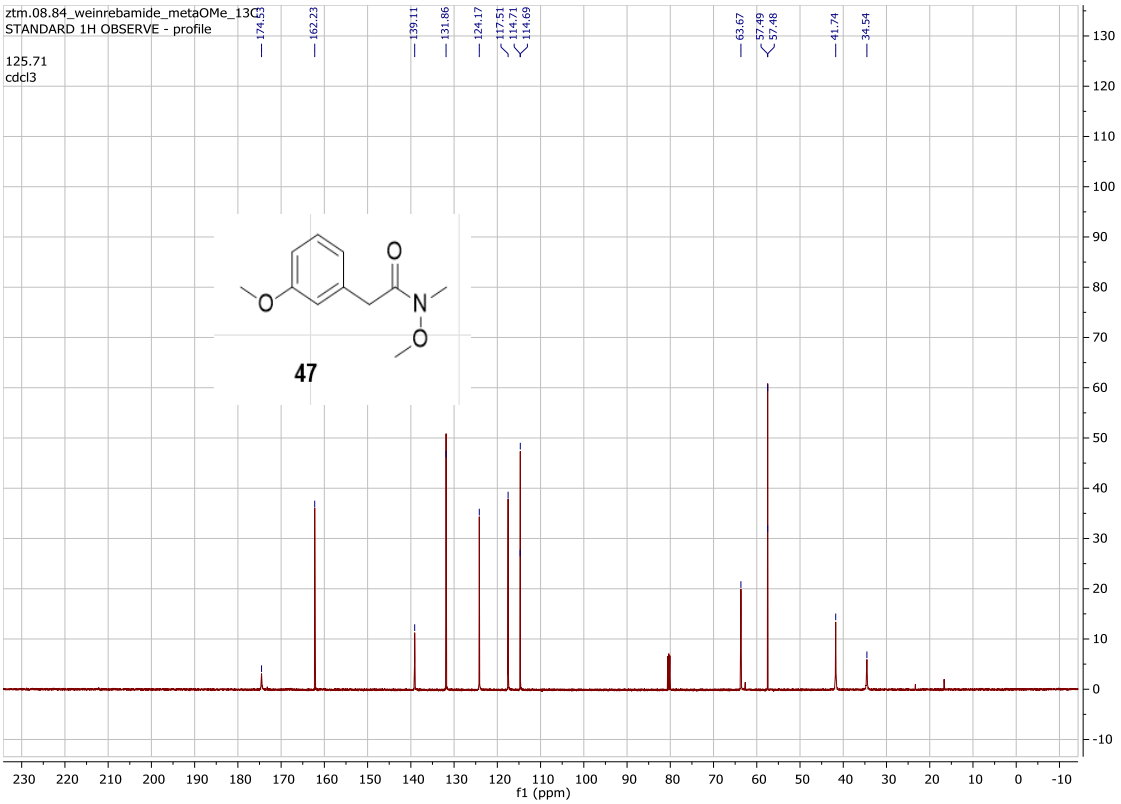
ztm.08.84_weinrebamide_metaOMe_13C
STANDARD 1H OBSERVE - profile
125.71
cdcl3
174.53
162.23
139.11
131.86
124.17
117.51
114.71
114.69
63.67
57.49
57.48
41.74
34.54
O
O
N
O
47
f1 (ppm)

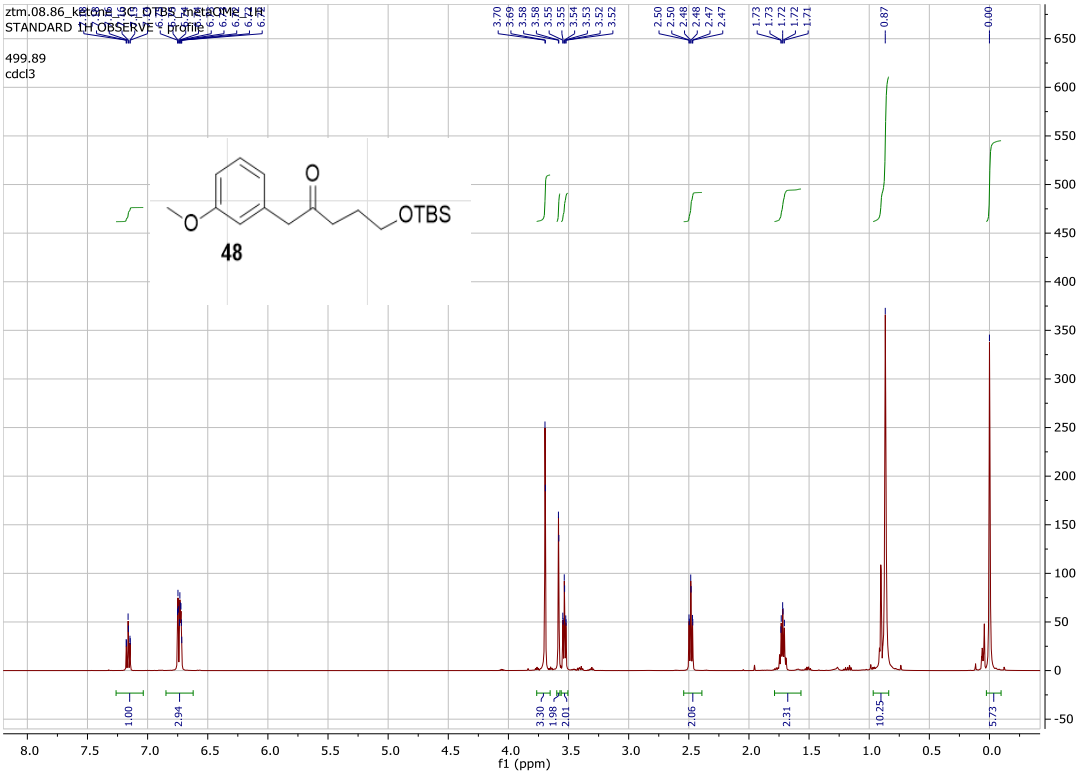
STANDARD 1H OBSERVE - profile
499.89
cdcl3
3.70
3.69
3.58
3.58
3.55
3.55
3.54
3.53
3.52
3.52
2.50
2.50
2.48
2.48
2.47
2.47
1.73
1.73
1.72
1.72
1.71
0.87
0.00
O
OTBS
48
1.00
2.94
3.30
3.08
2.01
2.06
2.31
10.25
5.73
f1 (ppm)

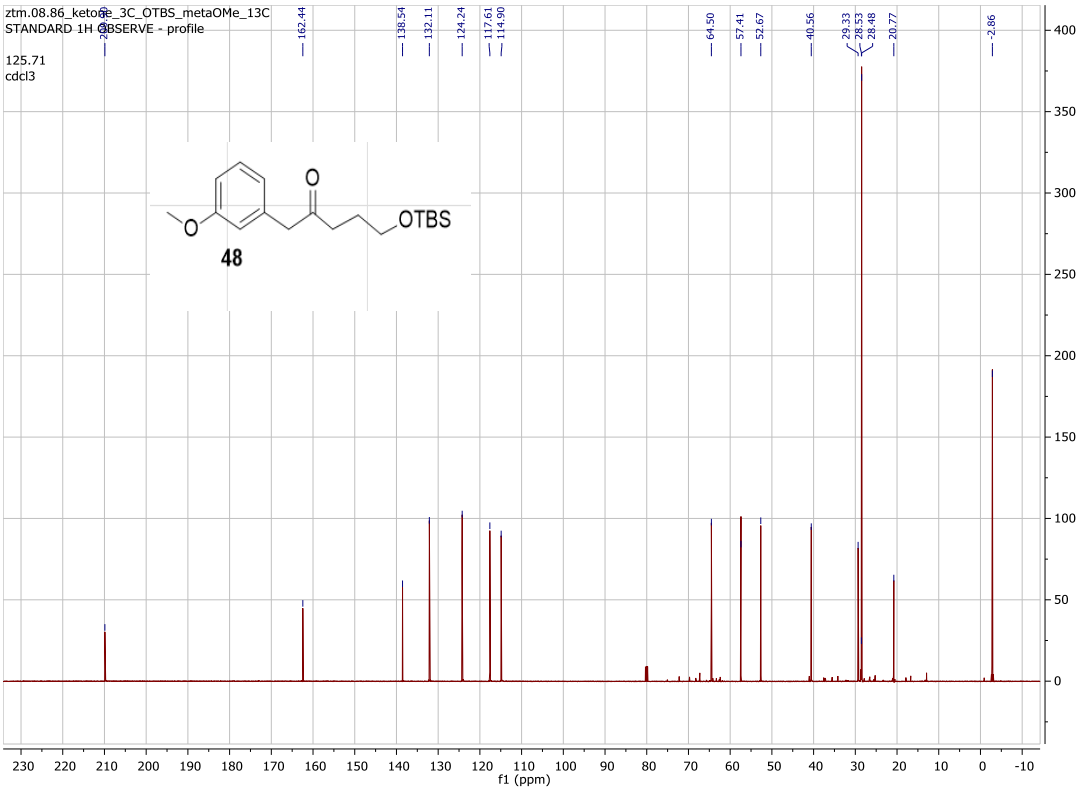
ztm.08.86_ketone_3C_OTBS_metaOMe_13C
STANDARD 1H OBSERVE - profile
125.71
cdcl3
O
O
OTBS
48
f1 (ppm)

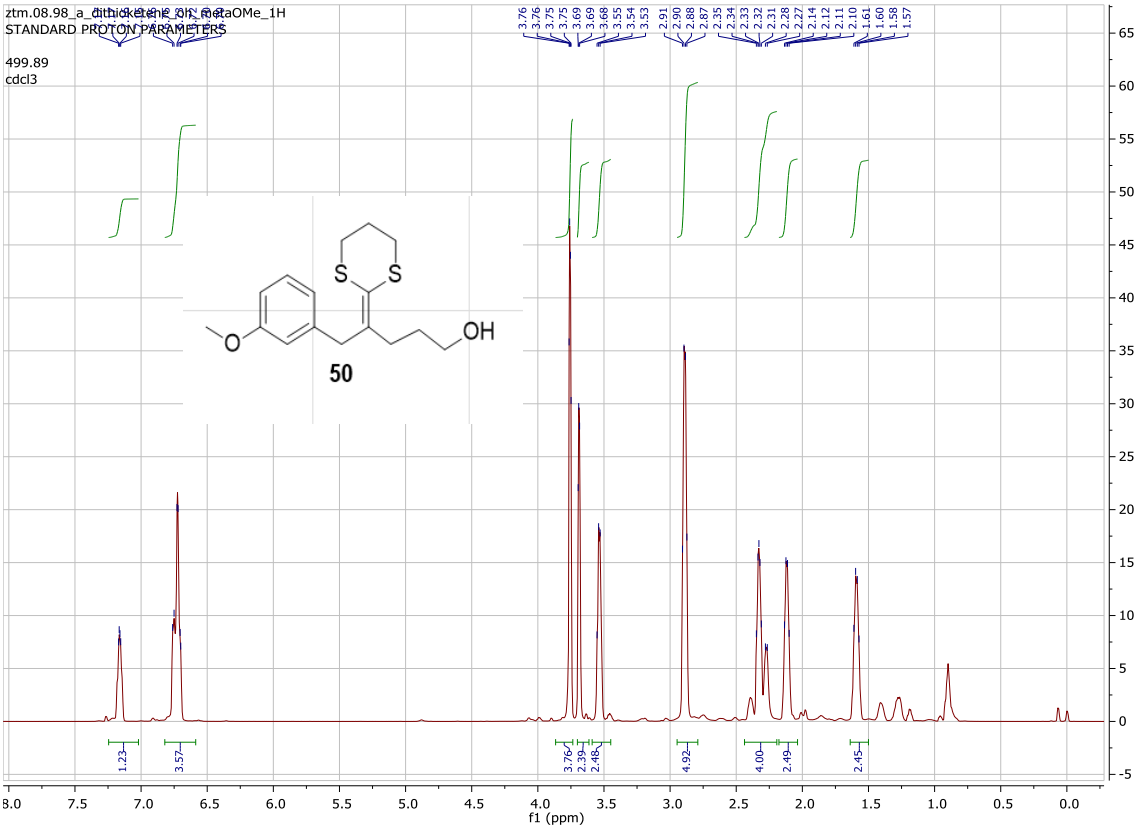
STANDARD PROTON PARAMETERS
499.89
cdcl3
S
S
O
OH
50
f1 (ppm)

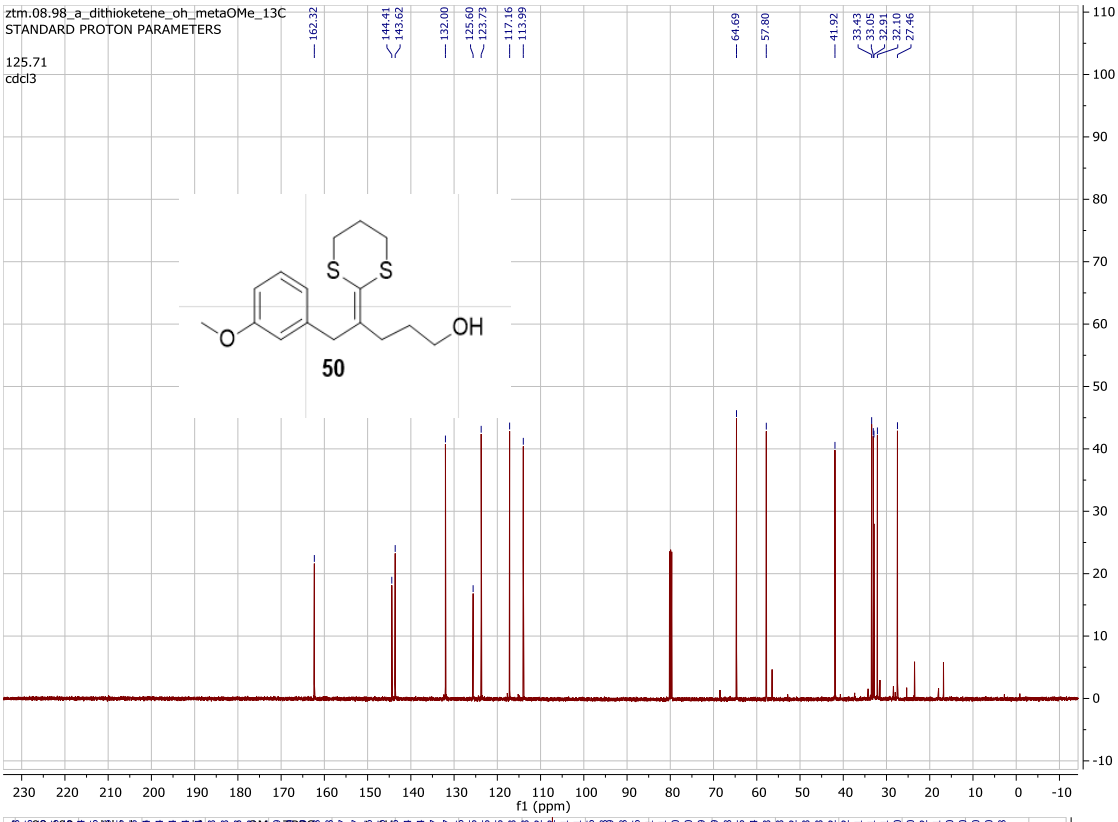
ztm.08.98_a_dithioketene_oh_metaOMe_13C
STANDARD PROTON PARAMETERS
125.71
cdcl3
162.32
144.41
143.62
132.00
125.60
123.73
117.16
113.99
64.69
57.80
41.92
33.43
33.05
32.91
32.10
27.46
S
S
O
OH
50
f1 (ppm)

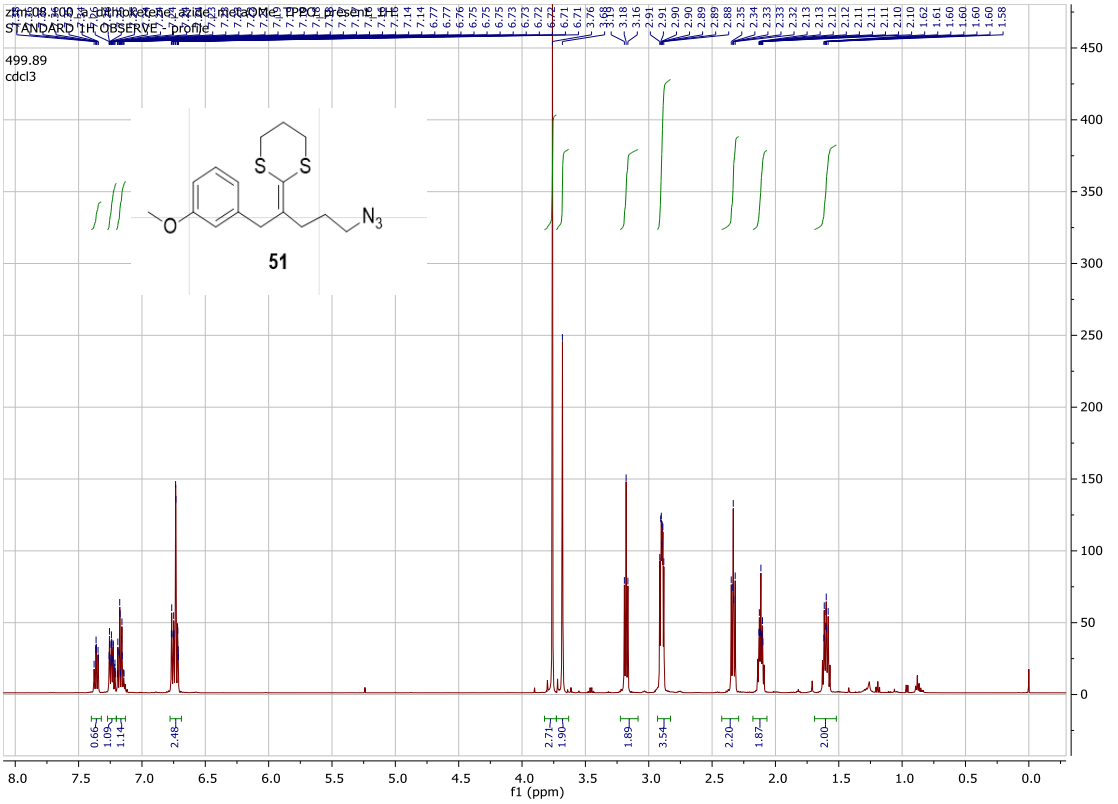
STANDARD 1H OBSERVE - profile
499.89
cdcl3
S
S
O
N3
51
0.66
1.09
1.14
2.48
2.71
1.90
1.89
3.54
2.20
1.87
2.00
f1 (ppm)

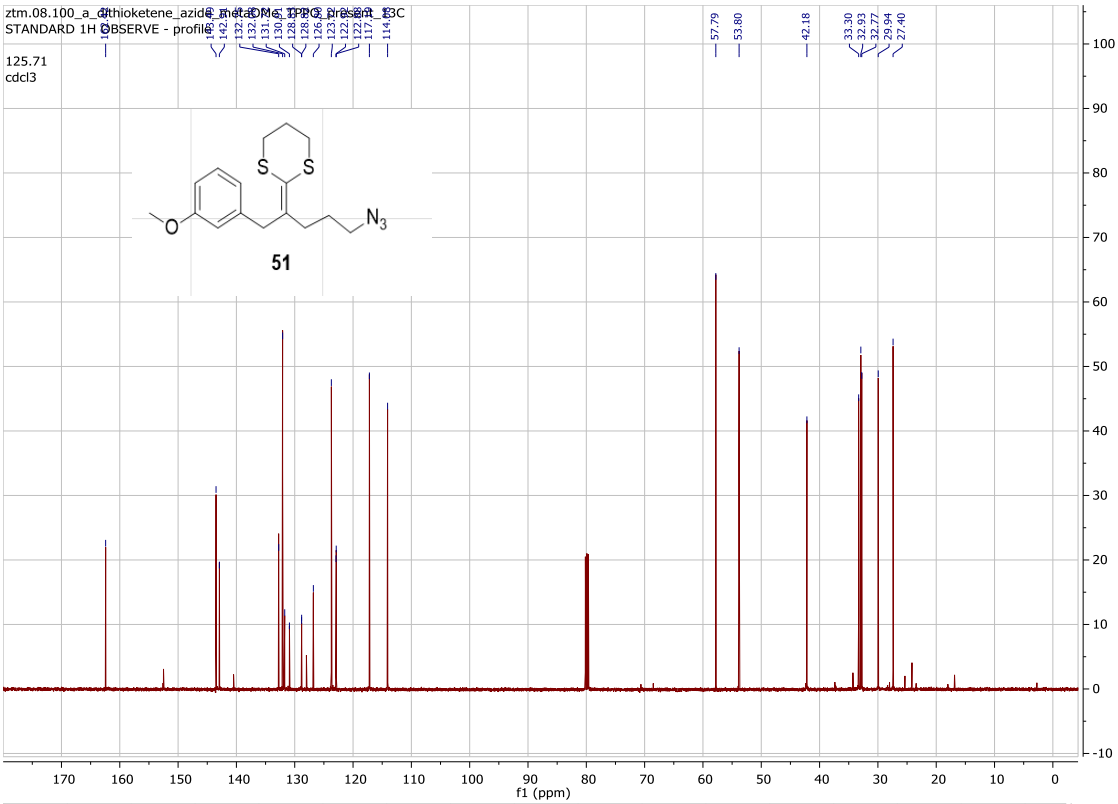
ztm.08.100_a_dithioketene_azide_metaOMe_tppo_present_13C
STANDARD 1H OBSERVE - profile
125.71
cdcl3
57.79
53.80
42.18
33.30
32.93
32.77
29.94
27.40
S
S
O
N3
51
f1 (ppm)

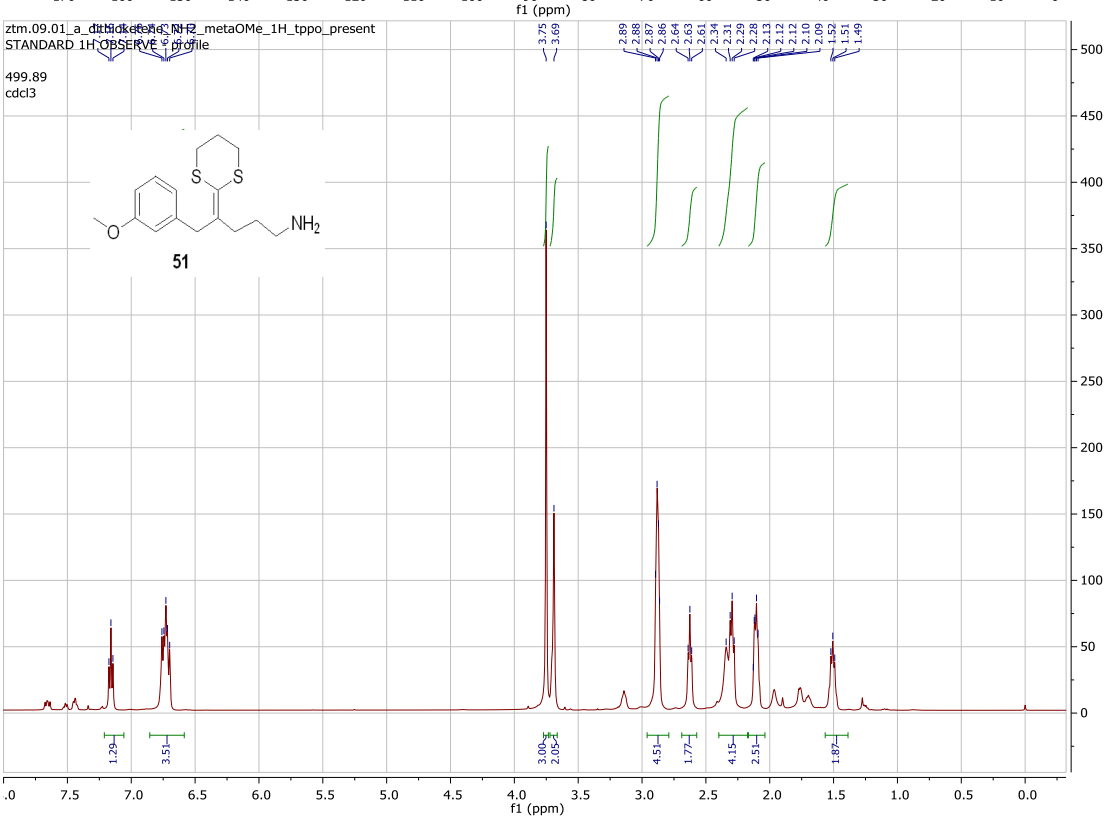
ztm.09.01_a_dithioketene_NH2_metaOMe_1H_tppo_present
STANDARD 1H OBSERVE - profile
499.89
cdcl3
3.75
3.69
2.89
2.88
2.87
2.86
2.64
2.63
2.61
2.34
2.31
2.29
2.28
2.13
2.12
2.12
2.10
2.09
1.52
1.51
1.49
S
S
O
NH2
51
1.29
3.51
3.00
2.05
4.51
1.77
4.15
2.51
1.87
f1 (ppm)

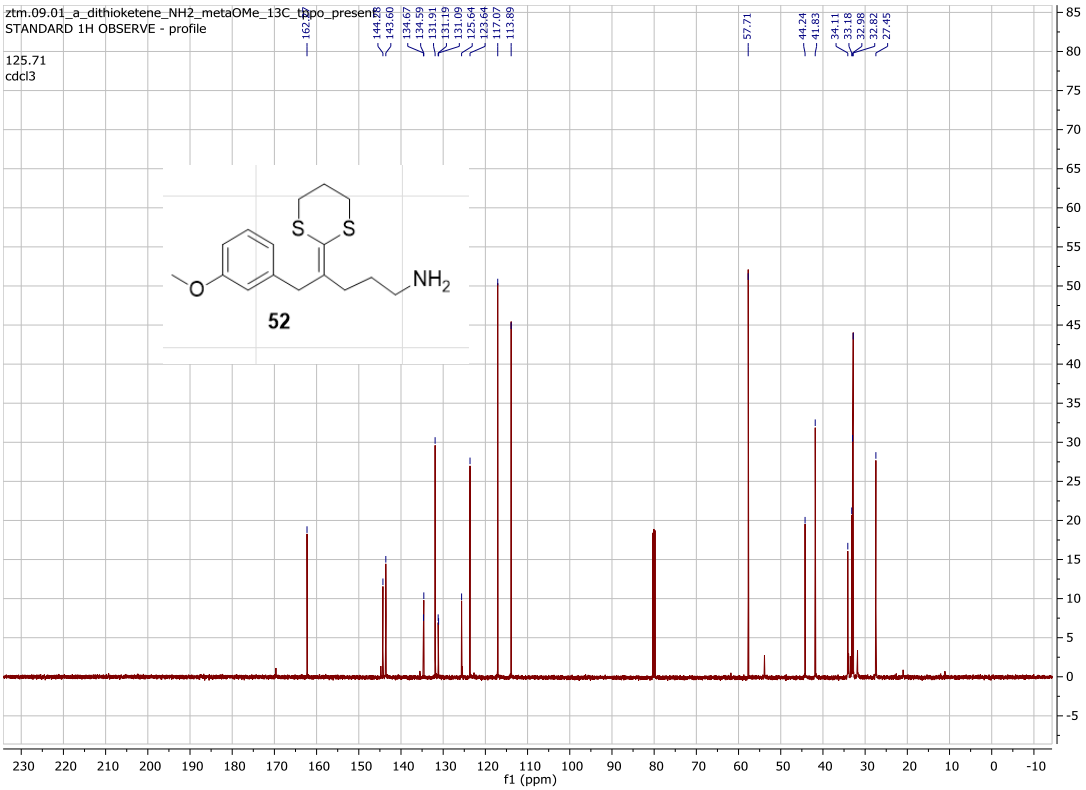
ztm.09.01_a_dithioketene_NH2_metaOMe_13C_tapo_present
STANDARD 1H OBSERVE - profile
125.71
cdcl3
S
S
O
NH2
52
f1 (ppm)

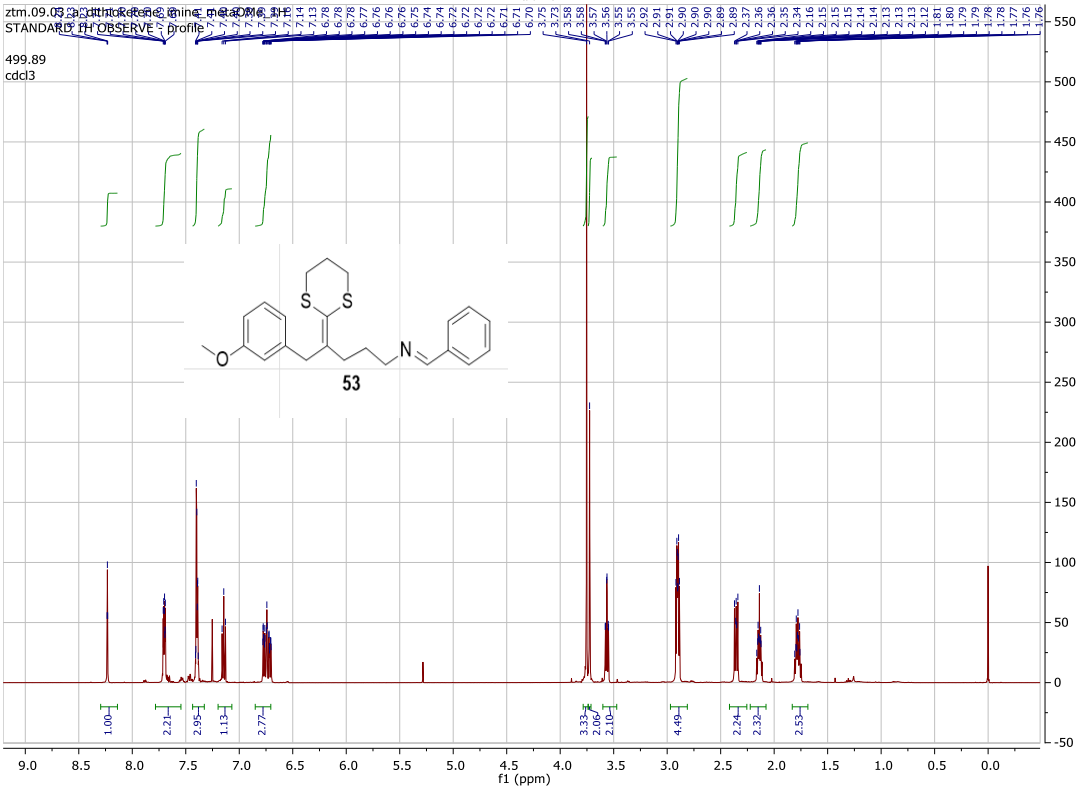
STANDARD 1H OBSERVE - profile
499.89
cdcl3
S
S
O
N
53
f1 (ppm)

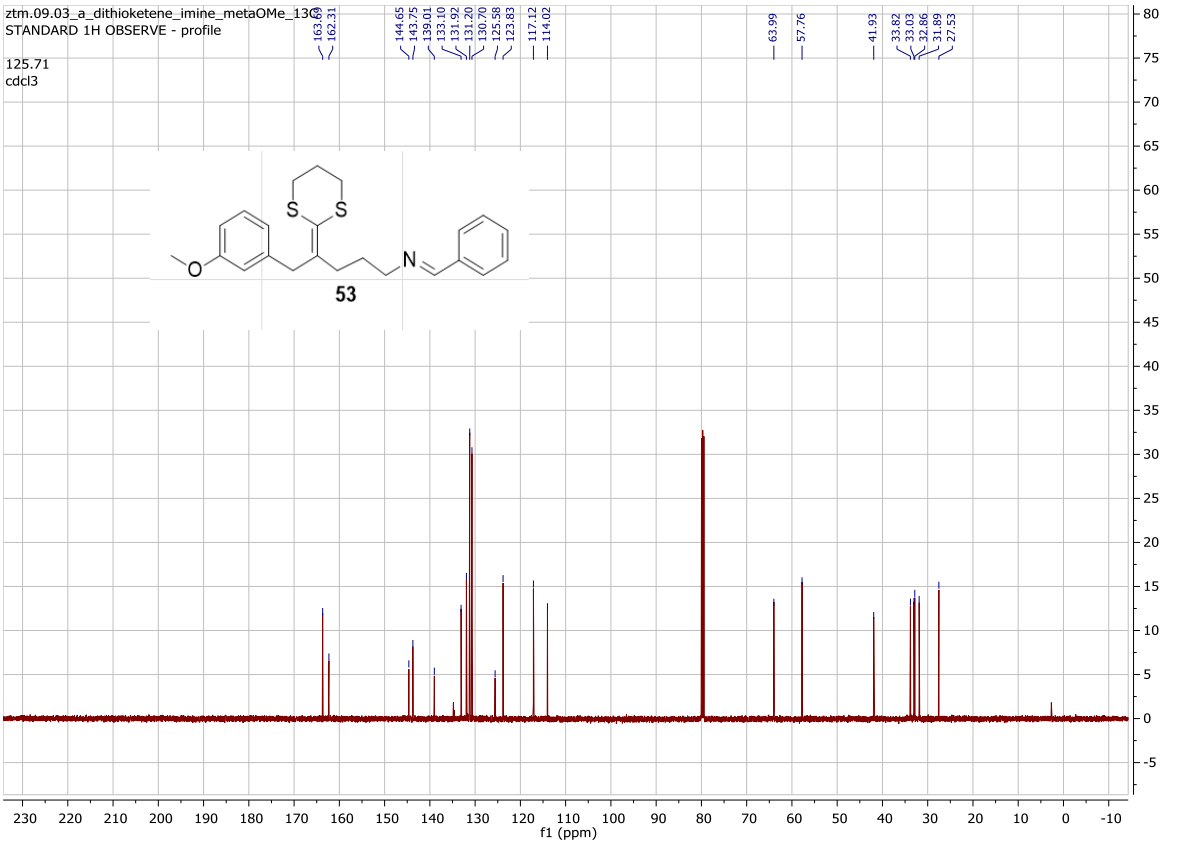
ztm.09.03_a_dithioketene_imine_metaOMe_13C
STANDARD 1H OBSERVE - profile
125.71
cdcl3
163.69
162.31
144.65
143.75
139.01
133.10
131.92
131.20
130.70
125.58
123.83
117.12
114.02
63.99
57.76
41.93
33.82
33.03
32.86
31.89
27.53
S
S
O
N
53
f1 (ppm)

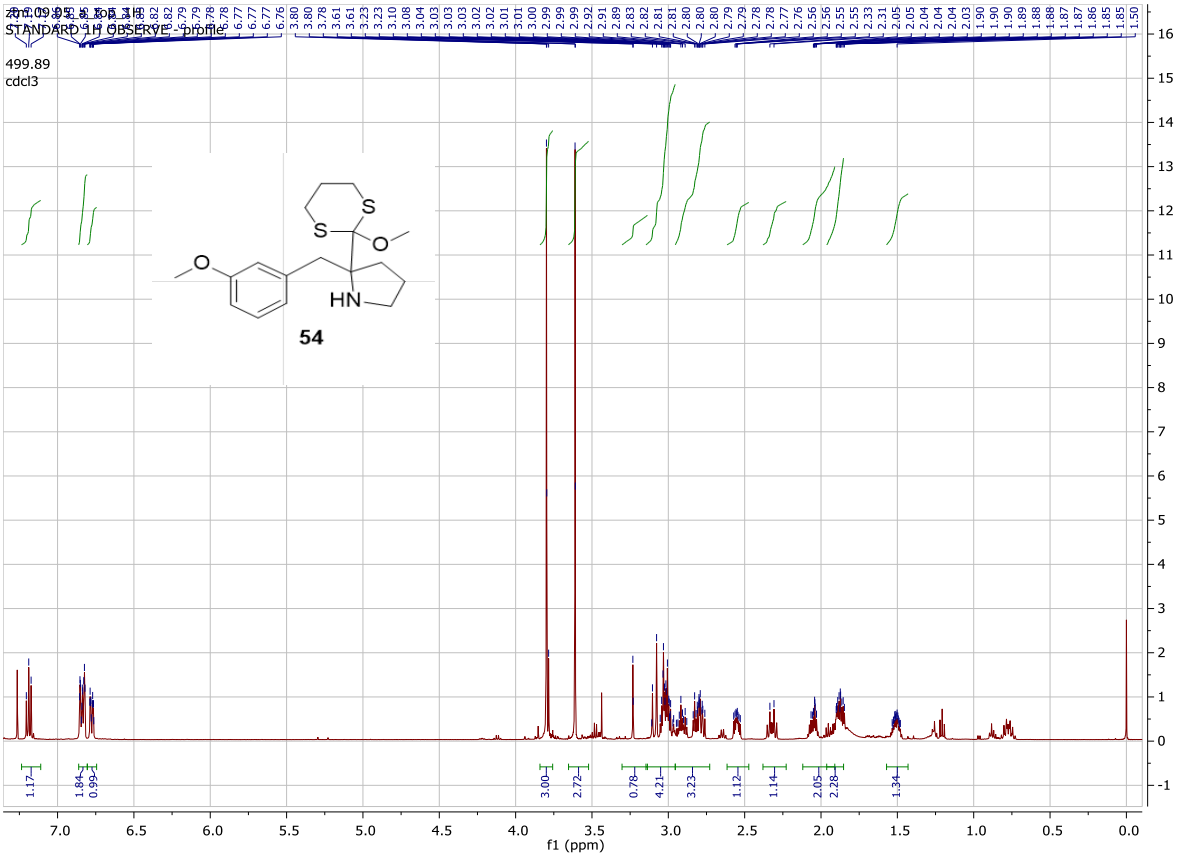
STANDARD 1H OBSERVE - profile
499.89
cdcl3
S
S
O
O
HN
54
1.17
1.84
0.99
3.00
2.72
0.78
4.21
3.23
1.12
1.14
2.05
2.28
1.34
f1 (ppm)

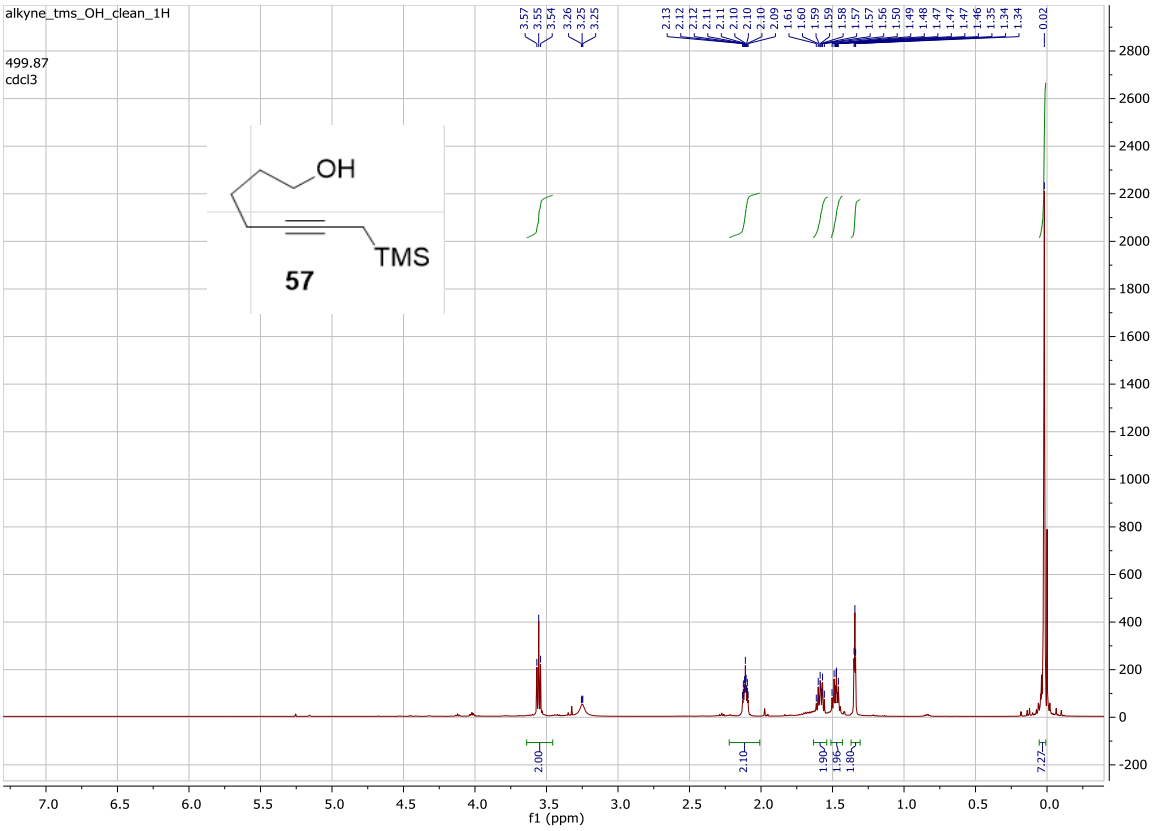
alkyne_tms_OH_clean_1H
499.87
cdcl3
OH
TMS
57
f1 (ppm)

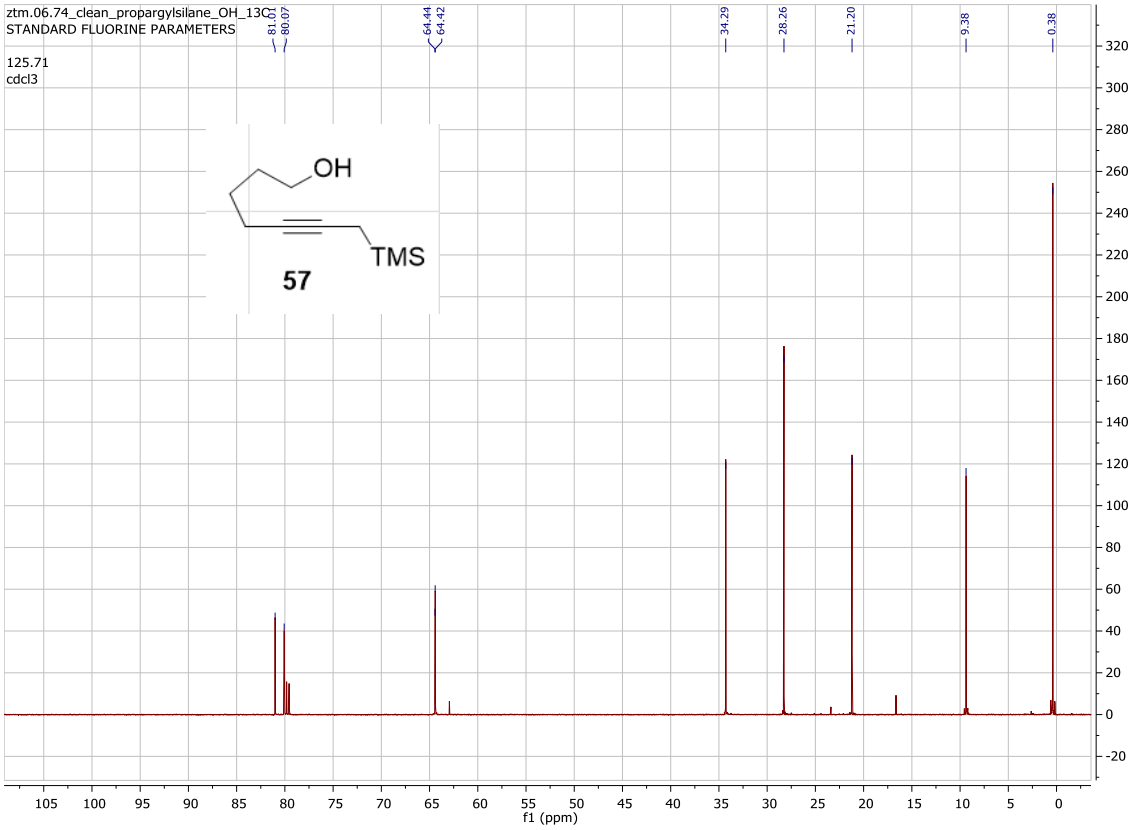
ztm.06.74_clean_propargylsilane_OH_13C
STANDARD FLUORINE PARAMETERS
125.71
cdcl3
OH
TMS
57
f1 (ppm)

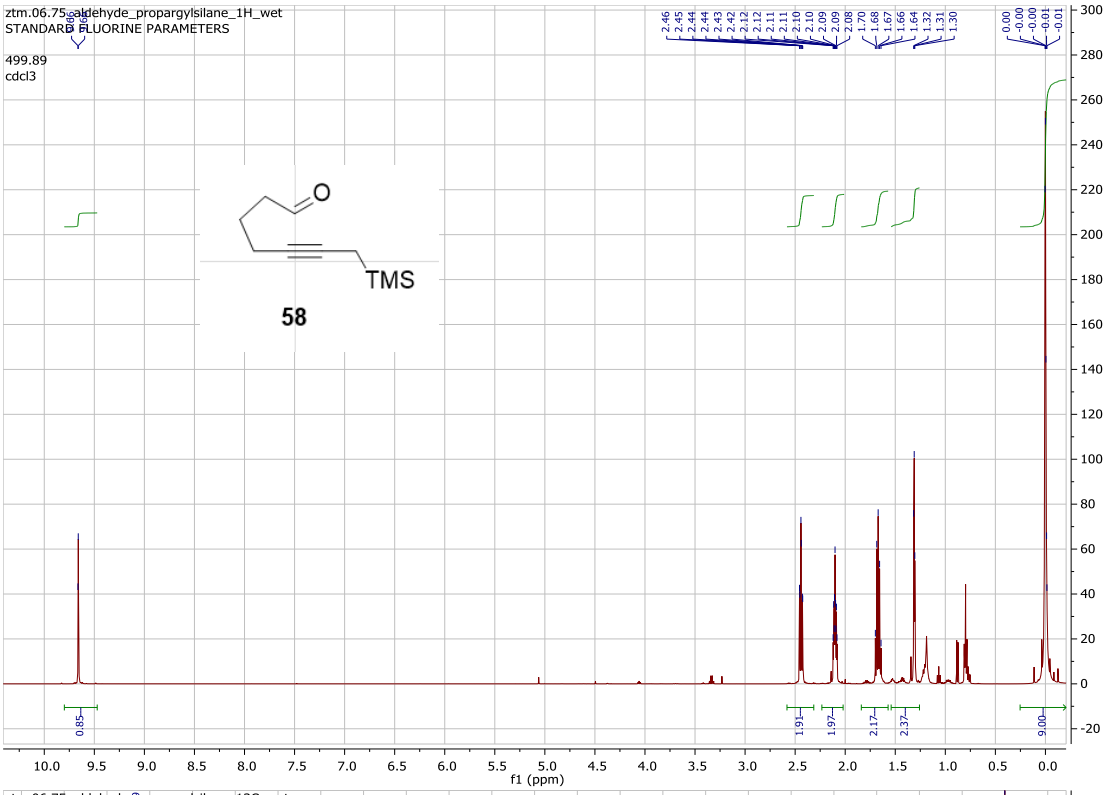
ztm.06.75_aldehyde_propargylsilane_1H_wet
STANDARD FLUORINE PARAMETERS
499.89
cdcl3
TMS
58
f1 (ppm)

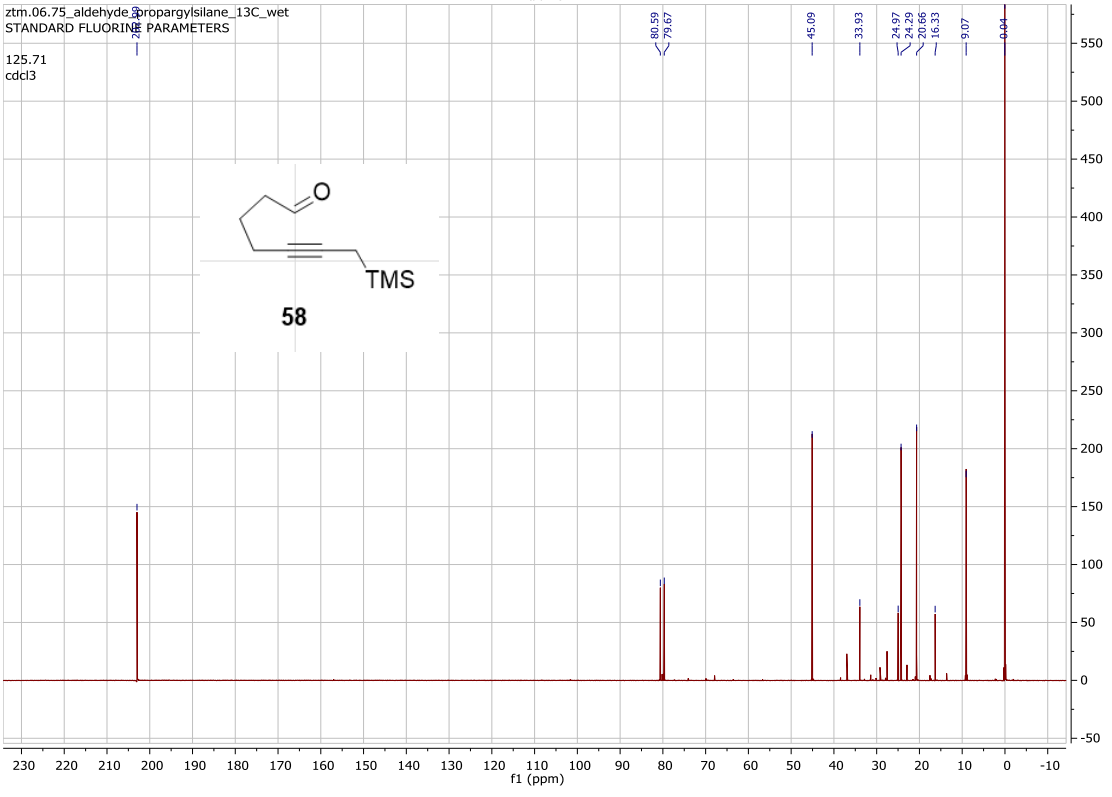
ztm.06.75_aldehyde_propargylsilane_13C_wet
STANDARD FLUORINE PARAMETERS
125.71
cdcl3
TMS
58
f1 (ppm)

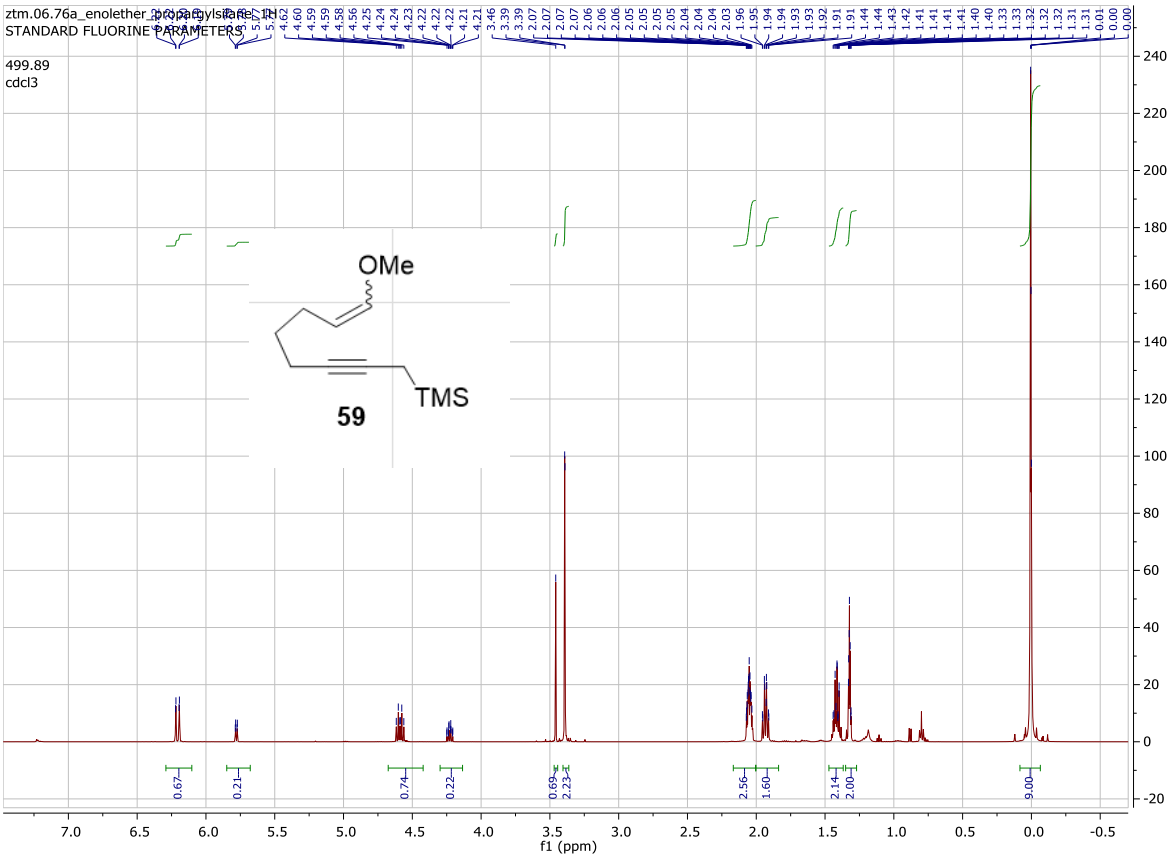
ztm.06.76a_enolether_propargylsilane_1H
STANDARD FLUORINE PARAMETERS
499.89
cdcl3
OMe
TMS
59
f1 (ppm)

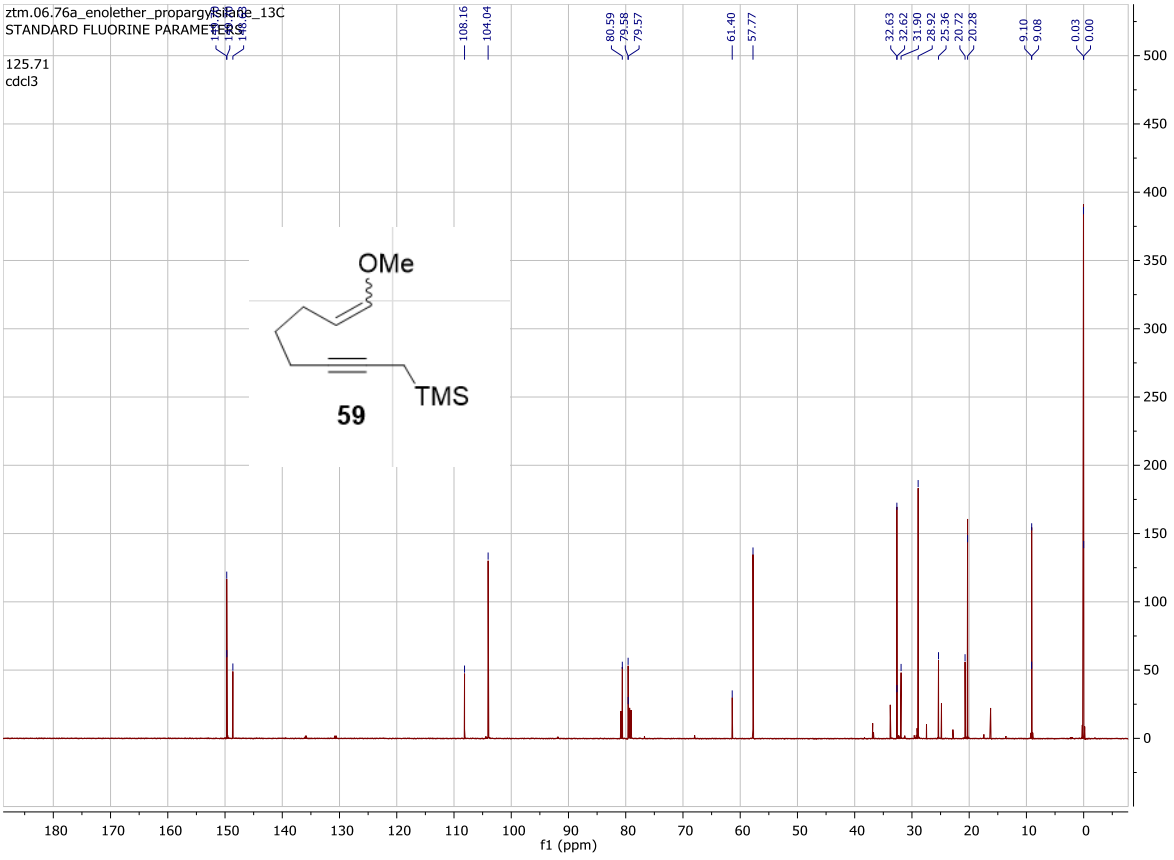
ztm.06.76a_enolether_propargylsilane_13C
STANDARD FLUORINE PARAMETERS
125.71
cdcl3
OMe
TMS
59
f1 (ppm)

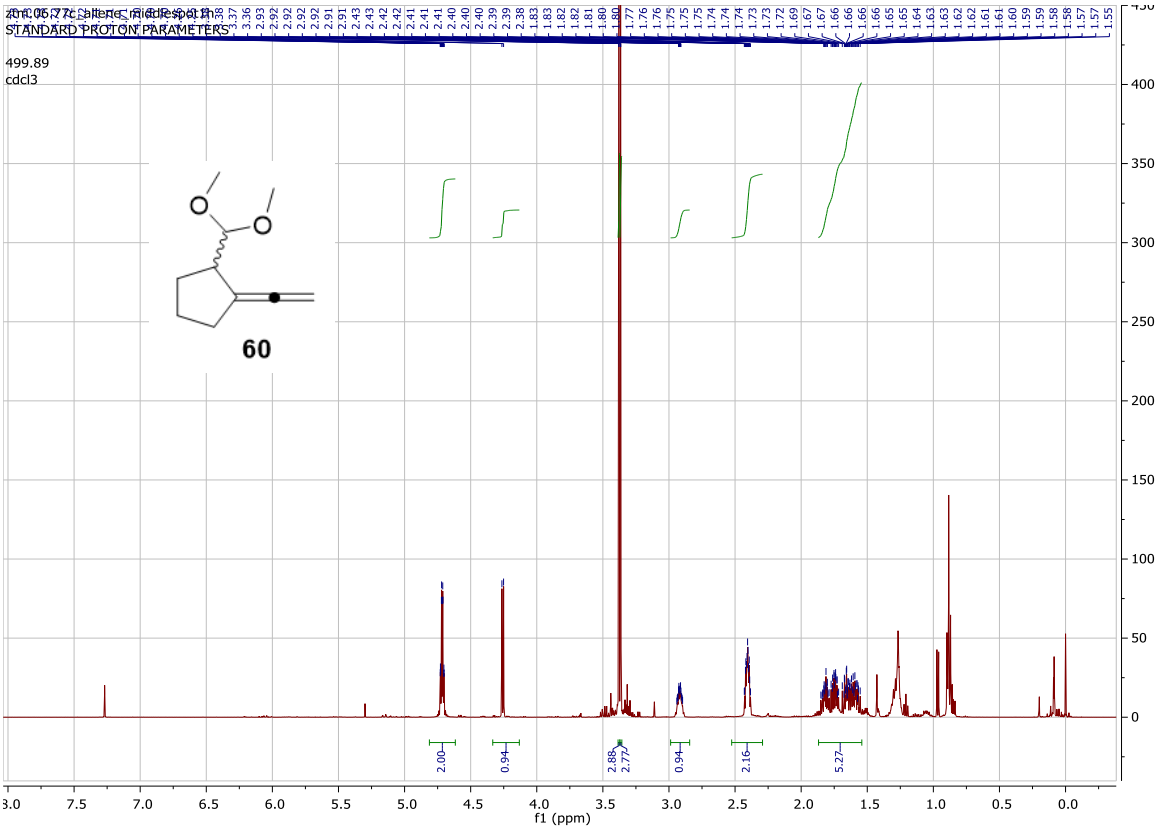
STANDARD PROTON PARAMETERS
499.89
cdcl3
60
f1 (ppm)

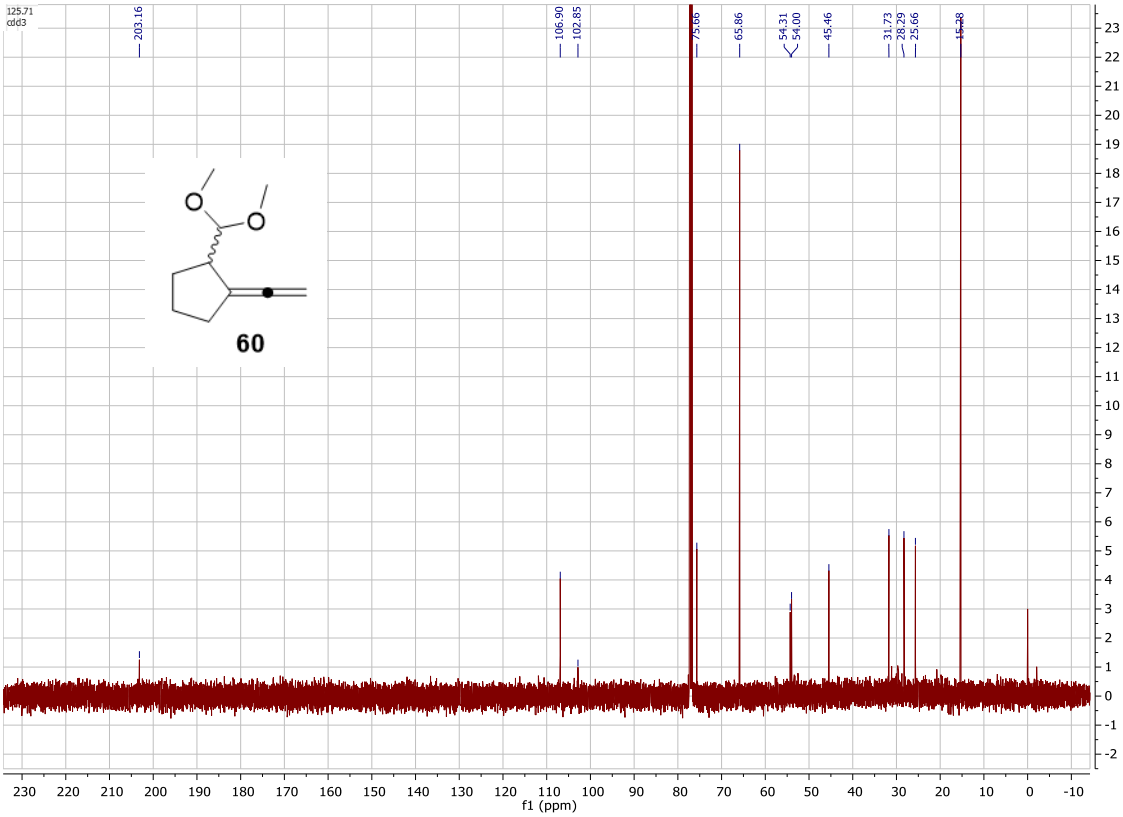
125.71
cdd3
203.16
106.90
102.85
75.66
65.86
54.31
54.00
45.46
31.73
28.29
25.66
15.28
60
f1 (ppm)

## References


(1) Medcalf, Z.; Moeller, K. D. Anodic Olefin Coupling Reactions: Elucidating Radical Cation Mechanisms and the Interplay between Cyclization and Second Oxidation Steps. *Chem. Rec.* **2021**, *21* (9), 2442–2452. https://doi.org/10.1002/tcr.202100118.

(2) Feng, R.; Smith, J. A.; Moeller, K. D. Anodic Cyclization Reactions and the Mechanistic Strategies That Enable Optimization. *Acc. Chem. Res.* **2017**, *50* (9), 2346–2352. https://doi.org/10.1021/acs.accounts.7b00287.

(3) Parsons, P. J.; Penkett, C. S.; Shell, A. J. Tandem Reactions in Organic Synthesis: Novel Strategies for Natural Product Elaboration and the Development of New Synthetic Methodology. *Chem. Rev.* **1996**, *96* (1), 195–206. https://doi.org/10.1021/cr950023+.

(4) Tzvetkov, N. T.; Arndt, T.; Mattay, J. Synthesis of Angularly Fused Cyclopentanoids and Analogous Tricycles via Photoinduced Ketyl Radical/Radical Anion Fragmentation–Cyclization Reactions. *Tetrahedron* **2007**, *63* (42), 10497–10510. https://doi.org/10.1016/j.tet.2007.07.092.

(5) Malacria, M. Selective Preparation of Complex Polycyclic Molecules from Acyclic Precursors via Radical Mediated- or Transition Metal-Catalyzed Cascade Reactions. *Chem. Rev.* **1996**, *96* (1), 289–306. https://doi.org/10.1021/cr9500186.

(6) Ryu, I.; Sonoda, N.; Curran, D. P. Tandem Radical Reactions of Carbon Monoxide, Isonitriles, and Other Reagent Equivalents of the Geminal Radical Acceptor/Radical Precursor Synthon. *Chem. Rev.* **1996**, *96* (1), 177–194. https://doi.org/10.1021/cr9400626.

(7) Taniguchi, T.; Tamura, O.; Uchiyama, M.; Muraoka, O.; Tanabe, G.; Ishibashi, H. Concise Synthesis of the Tricyclic Skeleton of Cylindricines Using a Radical Cascade Involving 6-Endo Selective Cyclization. *Synlett* **2005**, *2005* (7), 1179–1181. https://doi.org/10.1055/s-2005-865236.

(8) Curran, D. P. The Design and Application of Free Radical Chain Reactions in Organic Synthesis. Part 2. *Synthesis* **1988**, *1988* (7), 489–513. https://doi.org/10.1055/s-1988-27620.

(9) Studer, A. The Persistent Radical Effect in Organic Synthesis. *Chem. – Eur. J.* **2001**, *7* (6), 1159–1164. https://doi.org/10.1002/1521-3765(20010316)7:6<1159::AID-CHEM1159>3.0.CO;2-I.

(10) Studer, A. Tin-Free Radical Cyclization Reactions Using the Persistent Radical Effect. *Angew. Chem. Int. Ed.* **2000**, *39* (6), 1108–1111. https://doi.org/10.1002/(SICI)1521-3773(20000317)39:6<1108::AID-ANIE1108>3.0.CO;2-A.

(11) Wetter, C.; Studer, A. Microwave-Assisted Free Radical Chemistry Using the Persistent Radical Effect. *Chem. Commun.* **2004**, *0* (2), 174–175. https://doi.org/10.1039/B313139D.

(12) Helm, M. D.; Da Silva, M.; Sucunza, D.; Helliwell, M.; Procter, D. J. SmI2-Mediated Dialdehyde 'Radical Then Aldol' Cyclization Cascades: A Feasibility Study. *Tetrahedron* **2009**, *65* (52), 10816–10829. https://doi.org/10.1016/j.tet.2009.09.035.

(13) Kimura, T.; Hagiwara, M.; Nakata, T. SmI2-Induced Cyclization of Optically Active (*E*)- and (*Z*)-β-Alkoxyvinyl Sulfoxides with Aldehydes. *Tetrahedron* **2009**, *65* (52), 10893–10900. https://doi.org/10.1016/j.tet.2009.10.082.

(14) Park, S. R.; Findlay, N. J.; Garnier, J.; Zhou, S.; Spicer, M. D.; Murphy, J. A. Electron Transfer Activity of a Cobalt Crown Carbene Complex. *Tetrahedron* **2009**, *65* (52), 10756–10761. https://doi.org/10.1016/j.tet.2009.10.090.

(15) Gansäuer, A.; Greb, A.; Huth, I.; Worgull, D.; Knebel, K. Formal Total Synthesis of (±)-Fragranol via Template Catalyzed 4-*Exo* Cyclization. *Tetrahedron* **2009**, *65* (52), 10791–10796. https://doi.org/10.1016/j.tet.2009.09.033.
(16) Snider, B. B. Manganese(III)-Based Oxidative Free-Radical Cyclizations. *Chem. Rev.* **1996**, *96* (1), 339–364. https://doi.org/10.1021/cr950026m.
(17) Snider, B. B. Mechanisms of Mn(OAc)3-Based Oxidative Free-Radical Additions and Cyclizations. *Tetrahedron* **2009**, *65* (52), 10738–10744. https://doi.org/10.1016/j.tet.2009.09.025.
(18) Snyder, S. A.; Breazzano, S. P.; Ross, A. G.; Lin, Y.; Zografos, A. L. Total Synthesis of Diverse Carbogenic Complexity within the Resveratrol Class from a Common Building Block. *J. Am. Chem. Soc.* **2009**, *131* (5), 1753–1765. https://doi.org/10.1021/ja806183r.
(19) Curti, C.; Crozet, M. D.; Vanelle, P. Microwave-Assisted Manganese(III) Acetate Based Oxidative Cyclizations of Alkenes with β-Ketosulfones. *Tetrahedron* **2009**, *65* (1), 200–205. https://doi.org/10.1016/j.tet.2008.10.080.
(20) Mitasev, B.; Porco, J. A. Jr. Manganese(III)-Mediated Transformations of Phloroglucinols: A Formal Oxidative [4 + 2] Cycloaddition Leading to Bicyclo[2.2.2]Octadiones. *Org. Lett.* **2009**, *11* (11), 2285–2288. https://doi.org/10.1021/ol900590t.
(21) Yılmaz, M.; Uzunalioglu, N.; Tarık Pekel, A. Manganese(III) Acetate Based Oxidative Cyclizations of 3-Oxopropanenitriles with Conjugated Alkenes and Synthesis of 4,5-Dihydrofuran-3-Carbonitriles Containing Heterocycles. *Tetrahedron* **2005**, *61* (37), 8860–8867. https://doi.org/10.1016/j.tet.2005.07.019.
(22) Curry, L.; Hallside, M. S.; Powell, L. H.; Sprague, S. J.; Burton, J. W. Manganese(III)-Mediated Oxidative Free-Radical Cyclisations of Allenyl Malonates. *Tetrahedron* **2009**, *65* (52), 10882–10892. https://doi.org/10.1016/j.tet.2009.09.112.
(23) Nair, V.; Deepthi, A. Cerium(IV) Ammonium NitrateA Versatile Single-Electron Oxidant. *Chem. Rev.* **2007**, *107* (5), 1862–1891. https://doi.org/10.1021/cr068408n.
(24) Nair, V.; Deepthi, A. Recent Advances in CAN Mediated Reactions in Organic Synthesis. *Tetrahedron* **2009**, *65* (52), 10745–10755. https://doi.org/10.1016/j.tet.2009.10.083.
(25) Jung, H. H.; Floreancig, P. E. Mechanistic Analysis of Oxidative C–H Cleavages Using Inter- and Intramolecular Kinetic Isotope Effects. *Tetrahedron* **2009**, *65* (52), 10830–10836. https://doi.org/10.1016/j.tet.2009.10.088.
(26) Jevric, M.; Taylor, D. K.; Greatrex, B. W.; Tiekink, E. R. T. DDQ Induced Oxidative Cyclisations of 1,2-Dihydronaptho[2,1-*b*]Furans. *Tetrahedron* **2005**, *61* (7), 1885–1891. https://doi.org/10.1016/j.tet.2004.12.010.
(27) Snider, B. B.; Zhang, Q. Synthesis of (.+-.)-Okicenone and (.+-.)-Aloesaponol III. *J. Org. Chem.* **1993**, *58* (11), 3185–3187. https://doi.org/10.1021/jo00063a049.
(28) Zoretic, P. A.; Shen, Z.; Wang, M.; Ribeiro, A. A. A Biomimetic-like Radical Approach to Furanoditerpenes. *Tetrahedron Lett.* **1995**, *36* (17), 2925–2928. https://doi.org/10.1016/0040-4039(95)00433-D.
(29) Citterio, A.; Cerati, A.; Sebastiano, R.; Finzi, C.; Santi, R. Oxidative Deprotonation of Carbonyl Compounds by Fe(III) Salts. *Tetrahedron Lett.* **1989**, *30* (10), 1289–1292. https://doi.org/10.1016/S0040-4039(00)72739-0.
(30) Sha, C.-K.; Lee, F.-K.; Chang, C.-J. Tandem Radical Cyclizations Initiated with α-Carbonyl Radicals: First Total Synthesis of (+)-Paniculatine. *J. Am. Chem. Soc.* **1999**, *121* (42), 9875–9876. https://doi.org/10.1021/ja992315o.

(31) Amagata, T.; Doi, M.; Tohgo, M.; Minoura, K.; Numata, A. Dankasterone, a New Class of Cytotoxic Steroid Produced by a Gymnascella Species from a Marine Sponge. *Chem. Commun.* **1999**, No. 14, 1321–1322. https://doi.org/10.1039/A903840J.
(32) Hirst, G. C.; Johnson, T. O.; Overman, L. E. First Total Synthesis of Lycopodium Alkaloids of the Magellanane Group. Enantioselective Total Syntheses of (-)-Magellanine and (+)-Magellaninone. *J. Am. Chem. Soc.* **1993**, *115* (7), 2992–2993. https://doi.org/10.1021/ja00060a064.
(33) Baraldi, P. G.; Achille, B.; Simoneta, B.; Gian Piero, P.; Vinicio, Z. 2,3a,5,6,7,7a-Hexahydro-3h,4h-Benzothiophene-3,4-Dione and Cyclopenta [b]-Tetrahydrothiophene-3,4-Dione Enolate Anions as Synthetic Equivalents to Cyclohex-2-Enone and Cyclopent-2-Enone c-2-Carbanions. *Tetrahedron Lett.* **1984**, *25* (38), 4291–4294. https://doi.org/10.1016/S0040-4039(01)81420-9.
(34) Smith, J. A.; Moeller, K. D. Oxidative Cyclizations, the Synthesis of Aryl-Substituted C-Glycosides, and the Role of the Second Electron Transfer Step. *Org. Lett.* **2013**, *15* (22), 5818–5821. https://doi.org/10.1021/ol402826z.
(35) Sperry, J. B.; Wright, D. L. The Gem-Dialkyl Effect in Electron Transfer Reactions: Rapid Synthesis of Seven-Membered Rings through an Electrochemical Annulation. *J. Am. Chem. Soc.* **2005**, *127* (22), 8034–8035. https://doi.org/10.1021/ja051826+.
(36) Redden, A.; Perkins, R. J.; Moeller, K. D. Oxidative Cyclization Reactions: Controlling the Course of a Radical Cation-Derived Reaction with the Use of a Second Nucleophile. *Angew. Chem.* **2013**, *125* (49), 13103–13106. https://doi.org/10.1002/ange.201308739.
(37) Hudson, C. M.; Moeller, K. D. Intramolecular Anodic Olefin Coupling Reactions and the Use of Vinylsilanes. *J. Am. Chem. Soc.* **1994**, *116* (8), 3347–3356. https://doi.org/10.1021/ja00087a021.
(38) Campbell, J. M.; Xu, H.-C.; Moeller, K. D. Investigating the Reactivity of Radical Cations: Experimental and Computational Insights into the Reactions of Radical Cations with Alcohol and p-Toluene Sulfonamide Nucleophiles. *J. Am. Chem. Soc.* **2012**, *134* (44), 18338–18344. https://doi.org/10.1021/ja307046j.
(39) Torok, D. S.; Figueroa, J. J.; Scott, W. J. 1,3-Dioxolane Formation via Lewis Acid-Catalyzed Reaction of Ketones with Oxiranes. *J. Org. Chem.* **1993**, *58* (25), 7274–7276. https://doi.org/10.1021/jo00077a060.
(40) Hudson, C. M.; Marzabadi, M. R.; Moeller, K. D.; New, D. G. Intramolecular Anodic Olefin Coupling Reactions: A Useful Method for Carbon-Carbon Bond Formation. *J. Am. Chem. Soc.* **1991**, *113* (19), 7372–7385. https://doi.org/10.1021/ja00019a038.
(41) Tang, F.; Moeller, K. D. Intramolecular Anodic Olefin Coupling Reactions: The Effect of Polarization on Carbon−Carbon Bond Formation. *J. Am. Chem. Soc.* **2007**, *129* (41), 12414–12415. https://doi.org/10.1021/ja076172e.
(42) Tang, F.; Moeller, K. D. Anodic Oxidations and Polarity: Exploring the Chemistry of Olefinic Radical Cations. *Tetrahedron* **2009**, *65* (52), 10863–10875. https://doi.org/10.1016/j.tet.2009.09.028.
(43) Perkins, R. J.; Xu, H.-C.; Campbell, J. M.; Moeller, K. D. Anodic Coupling of Carboxylic Acids to Electron-Rich Double Bonds: A Surprising Non-Kolbe Pathway to Lactones. *Beilstein J. Org. Chem.* **2013**, *9* (1), 1630–1636. https://doi.org/10.3762/bjoc.9.186.
(44) Medcalf, Z.; Redd, E. G.; Oh, J.; Ji, C.; Moeller, K. D. Anodic Cyclizations and Umpolung Reactions Involving Imines. *Org. Lett.* **2023**, *25* (22), 4135–4139. https://doi.org/10.1021/acs.orglett.3c01399.

(45) Xu, H.-C.; Moeller, K. D. Intramolecular Anodic Olefin Coupling Reactions: The Use of a Nitrogen Trapping Group. *J. Am. Chem. Soc.* **2008**, *130* (41), 13542–13543. https://doi.org/10.1021/ja806259z.
(46) Wierschke, S. G.; Chandrasekhar, J.; Jorgensen, W. L. Magnitude and Origin of the .Beta.-Silicon Effect on Carbenium Ions. *J. Am. Chem. Soc.* **1985**, *107* (6), 1496–1500. https://doi.org/10.1021/ja00292a008.

# Chapter 5: Using Anodic Cyclizations to Target the Chrysosporazine Family of Natural Products

## 5.1 Introduction

The presence of polycyclic ring structures containing heteroatoms like nitrogen is a common feature in many biologically active molecules.[1] The increasing demand for synthesizing such molecules has led researchers to explore innovative and increasingly efficient methodologies to complement existing routes, enabling the construction of numerous analogs of the original target. One approach to open new synthetic possibilities is by leveraging umpolung reactions, which reverse the polarity of functional groups and in so doing enable them to be used in novel ways. Anodic olefin coupling reactions are particularly intriguing in this regard, as they can join electron-rich olefins to amine nucleophiles, facilitating the construction of alkaloid-type ring skeletons. For instance, consider the natural products outlined in Scheme 5.1, along with a potential anodic cyclization to produce these compounds. In the proposed reaction, an oxidation reaction would be employed to trigger the key nitrogen-carbon bond, shown in red, of the alkaloid ring skeleton. This bond is a core feature of the chrysosporazine family of natural products, and it would be formed here by coupling two nucleophiles. Interest in the chrysosporazing family of natural product stems from the observation that these pyrazinoisoquinolinone analogs act as inhibitors of P-glycoproteins, effectively reversing doxorubicin resistance.[2] While methods for partially constructing similar molecules have been documented,[3,4] the family of compounds themselves remain an attractive yet challenging target. Therefore, a potential new route to the ring skeleton, utilizing umpolung chemistry, presents an opportunity to change the synthetic approach—a

prospect too enticing to ignore. This was particularly compelling as we recognized that this effort could not only demonstrate the efficacy of anodic electrochemistry but also compel us to broaden the scope of the reactions.

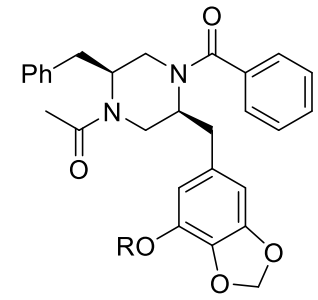


Chrysosporazine D, R = Me
Chrysosporazine E, R = H

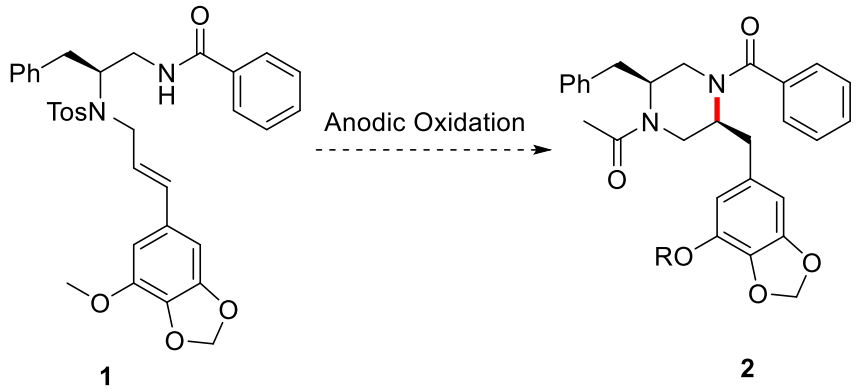


**Scheme 5.1: Anodic Cyclization to Afford Chrysosporazine Family Of Natural Products**

Previous studies have demonstrated that nitrogen amidyl radicals can be generated by an anodic oxidation, and that these reactive intermediates can be trapped by olefins to afford a variety of cyclic systems.[5] The positive outcomes from investigations into transition metal-mediated radical-phenyl coupling processes suggested that the formation of this key nitrogen-carbon bond can be accomplished with the use of a metal mediator (see section 5.2 for more details). Both of these

factors encouraged us to explore whether the two-electron oxidative cyclization can be accomplished as outlined in Scheme 5.1.

## 5.2 Anodic Cyclizations Mediated by Transition Metals and TEMPO

Nitrogen-centered radicals serve as useful intermediates in the synthesis of nitrogen-containing molecules. In the electrochemical oxidations we will be examining, these nitrogen radicals are generated through the oxidation of the respective nitrogen anions derived from amides. One can then trap these radical intermediates by using transition metals or TEMPO and channel the reaction down a productive pathway.[6]

### 5.2.1 Transition Metal-Mediated Electrochemical Nitrogen Cyclizations

#### Iron

Anodic cyclization reactions have been employed for the synthesis of polycyclic ring systems, particularly ring skeletons that contain a nitrogen atom. The Xu group demonstrated the generation of an amidyl radical using a ferrocene mediator (ferrocene undergoes oxidation at the anode to form a ferrocenium ion, which then oxidizes an amidyl anion), initiating a cascade process (Scheme 5.2).[5] In this reaction, the amidyl radical initially adds to an olefin, forming a cyclic radical that subsequently undergoes addition to the aromatic ring. Next, a second oxidation step occurs followed by the loss of a proton to return aromaticity and afford the tricyclic product **4**. We aimed to demonstrate the generality of this overall approach, showcasing its applicability even when the amide nitrogen is not functionalized with an aryl ring, as depicted in Scheme 5.1.

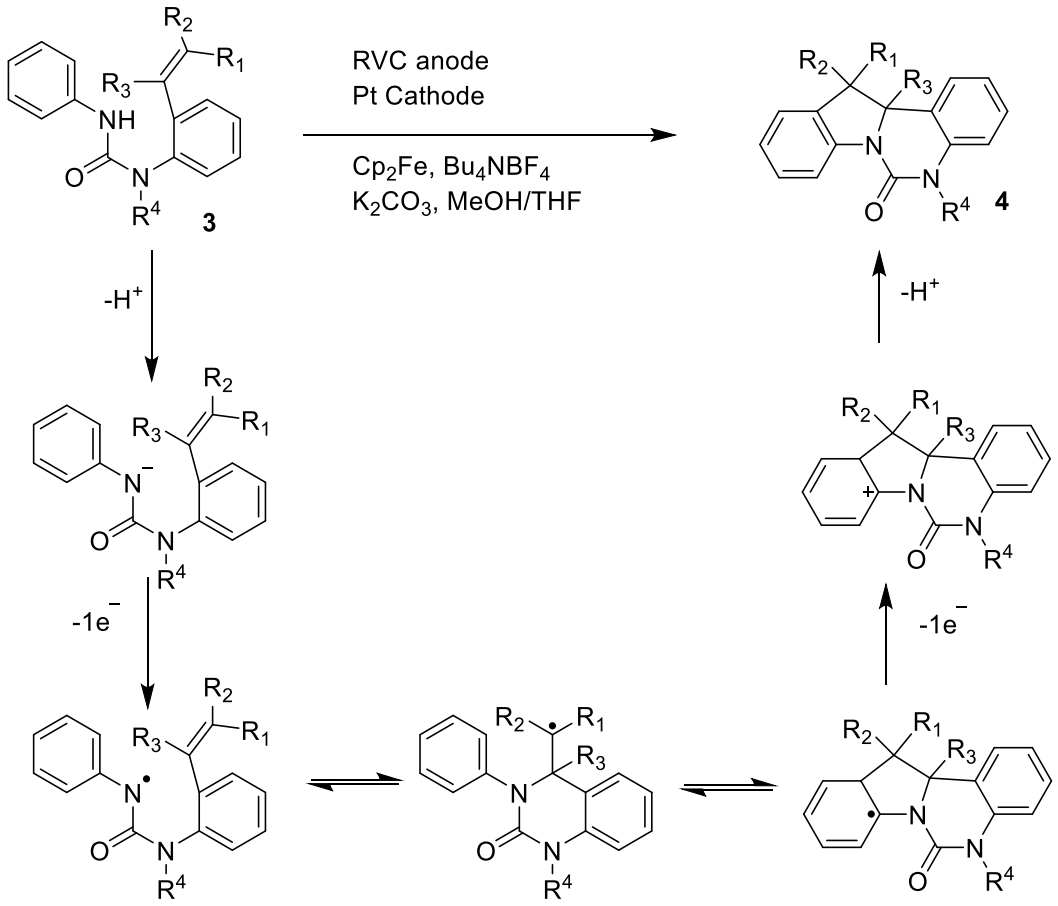


**Scheme 5.2: Amidyl Radical Induced Anodic Cascade Cyclization Mediated By Ferrocene**

In the chemistry forwarded by the Xu group, the presence of the phenyl ring on the amidyl nitrogen was crucial for the success of the reaction. First, its presence reduces the pKa of the amidyl proton, facilitating the formation of the anion that undergoes oxidation to yield the initial radical. Second, the second cyclization step involves the addition of a radical to the aromatic ring, placing a radical adjacent to the electron-donating nitrogen. This stabilization aids in the second oxidation step crucial for completing the overall transformation.

## Copper

Copper is another metal that can be employed for oxidative electrochemical reactions. Illustrated in Scheme 5.3 by the Hu group is a formal aza-Wacker cyclization of secondary and tertiary olefins

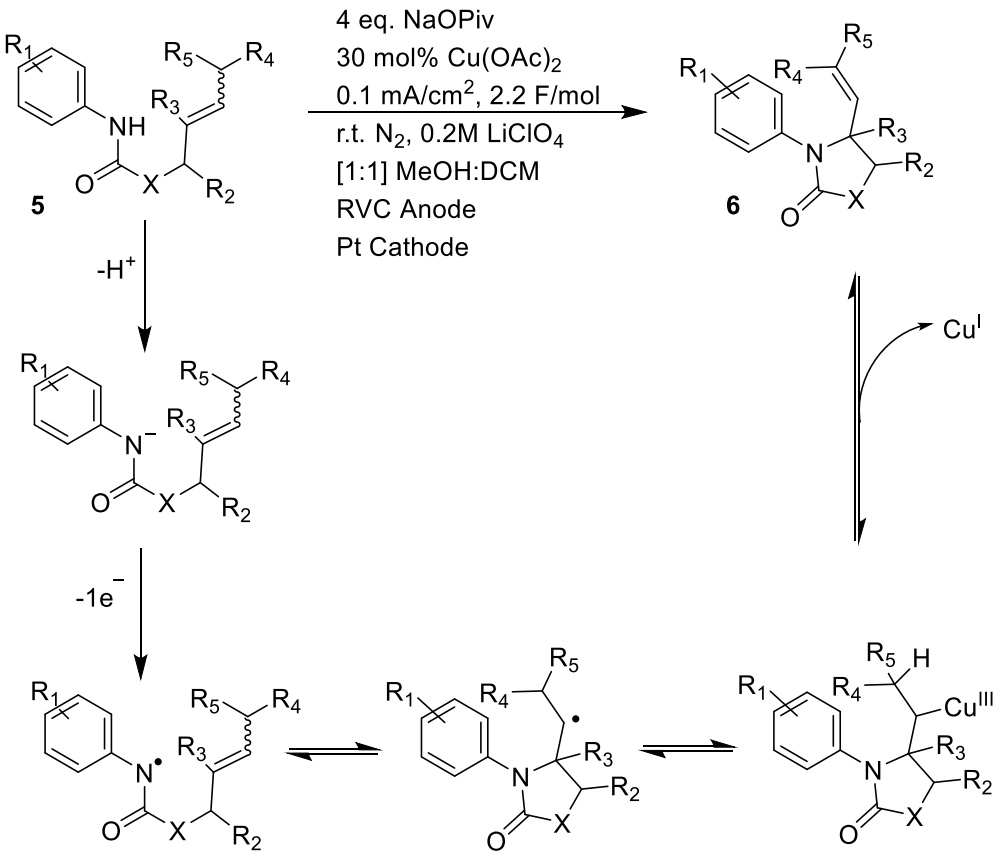


**Scheme 5.3: Electrochemical aza-Wacker Cyclization Using Copper Catalysis**

utilizing a copper catalyst, namely $Cu(OAc)_2$.[7] The mechanism of the reaction is as follows: first, sodium pivalate deprotonates substrate **5** giving an amidyl anion. Second, this anion is oxidized at the anode, resulting in the formation of an amidyl radical. Next, this radical engages in a 5-exo-trig cyclization with the olefin, producing an alkyl radical. From here, copper(II), generated through the oxidation of copper(I) at the anode, traps the allylic radical, giving rise to a copper(III) intermediate.[8] A base-assisted elimination reaction follows, leading to the formation of alkene **6** and copper(I). The latter is then oxidized at the anode to copper(II), allowing it to re-enter the catalytic cycle.

In the chemistry conducted by the Hu group, the success of the reaction was once again reliant on the presence of the phenyl ring attached to the amidyl nitrogen. The presence of the phenyl ring

lowers the pKa of the amidyl proton which allows for the formation of the anion. This anion undergoes oxidation to generate the initial radical which then undergoes the cyclization.

## 5.2.2 Tempo-Mediated Electrochemical Nitrogen Cyclizations

Shown in Scheme 5.4, is an electrochemical strategy by the Xu group for intramolecular aminooxygenation of unactivated alkenes, utilizing nitrogen-centered radicals generated through electrochemical oxidation by $TEMPO^+$ under basic conditions. The role of TEMPO in this reaction

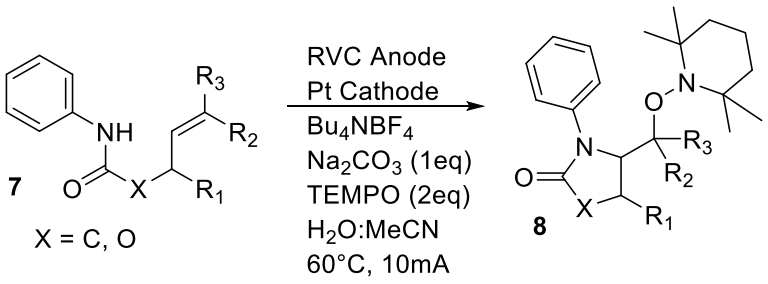


**Scheme 5.4: Electrochemical Amino-Oxygenation of Alkenes Mediated by TEMPO**

is twofold. First, TEMPO is used stoichiometrically as a radical trap to capture the cyclized radical intermediate. Second, TEMPO acts as a redox mediator to generate an amidyl radical.[9]

Once again, the chemistry shown in Scheme 5.4 was able to be carried out because of the presence of the phenyl ring on the amidyl nitrogen. This lowered the pKa of the amidyl proton so it could be deprotonated to give an anion. This anion was then oxidized to an amidyl radical by $TEMPO^+$, which was generated by the anode. Then the radical was trapped by the olefin giving an allyl radical which was then trapped by TEMPO to give product **8**.[9]

## 5.3 Anodic Cyclizations Applied to the Synthesis of Chrysosporazine

As described in section 5.2, we examined three cases of anodic cyclizations of nitrogen radicals that utilized a transition metal or $TEMPO^+$ to mediate. The success of all three reactions was

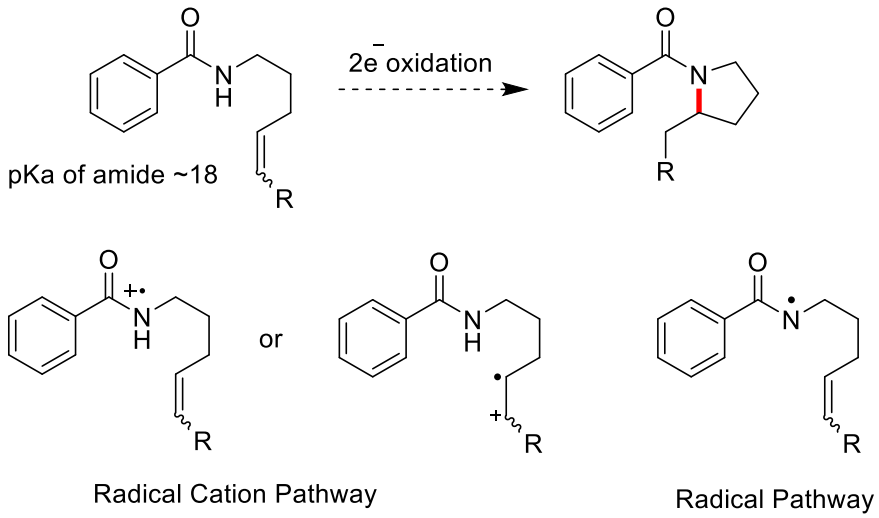


**Scheme 5.5: A New Model For A Nitrogen Based Anodic Cyclization**

contingent on a phenyl ring being attached to the amidyl nitrogen. The presence of this phenyl ring lowered the pKa of the amidyl proton, so it could be easily deprotonated and then the resulting anion oxidized to form a radical that initiated the cyclization reaction.

However, in our proposed cyclization, the nature of the product desired meant that this critical feature was not possible (Scheme 5.5). So, the question arose: how can such a transformation be achieved? There were two possibilities. The first, would be to push the reaction down a radical cation pathway. If this pathway was taken, then the cyclization would be controlled by the relative oxidation potentials of the amide and the styrene moiety. The success of this reaction is dependent

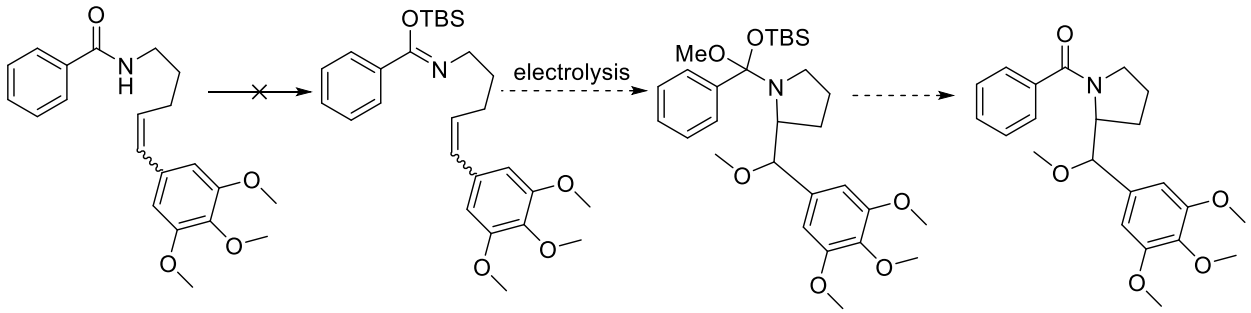


**Scheme 5.8: Failed Attempt to Generate Silyl-Based Imidate**

on lowering the oxidation potential of the starting material below that of the tertiary amine product to avoid overoxidation of the cyclized product. The second way would be to push this reaction down a radical pathway akin to the chemistry shown in section 5.2. If this method was employed we would need to either use a stronger base to make the amidyl anion or somehow lower the pKa of the amidyl proton so it could be easily deprotonated by a weaker base in solution.

## 5.3.1 Radical Cation Pathway

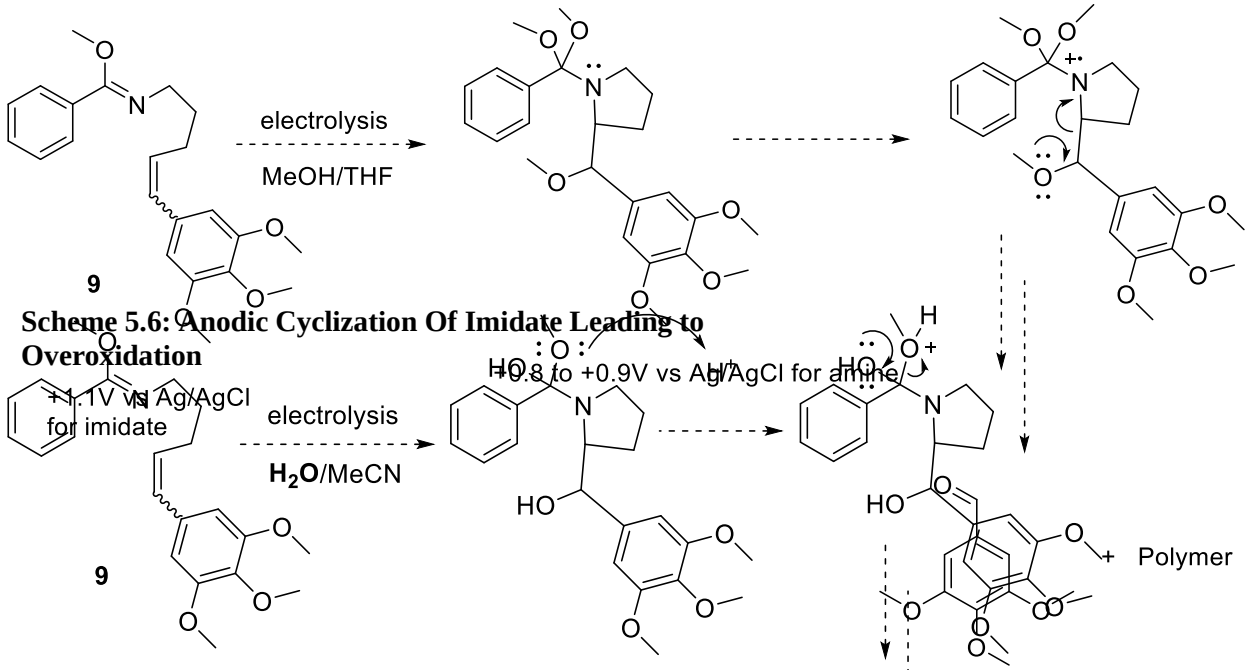


**Scheme 5.6: Anodic Cyclization Of Imidate Leading to Overoxidation**

**Scheme 5.7: Oxidation Potential of Cyclic Secondary Amine**

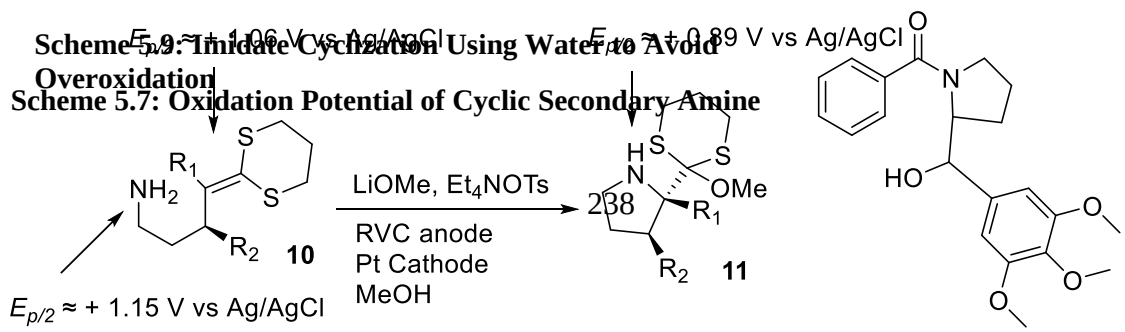


**Scheme 5.9: Imidate Cyclization Using Water to Avoid Overoxidation**

In summary, every reaction pushed down the radical cation pathway led to the formation of polymethoxylated polymer and aldehyde, arising from overoxidation of the cyclized tertiary amine intermediate. Scheme 5.6 provides a select example, along with the proposed mechanism for aldehyde formation. In the proposed mechanism, starting material **9** once oxidized would cyclize to a tertiary amine intermediate which would then be oxidized preferentially to the starting material. The resulting radical cation would then fragment to afford the aldehyde and a paraquinone methide cation that was presumably the origin of the polymer. The overoxidation of a secondary amine in an anodic cyclization was observed and discussed by Hai-Chao Xu when he was part of our group (Scheme 5.7 and Scheme 5.15).[10] As shown, the reaction would utilize a dithioketene acetal functional group as the electron-rich olefin undergoing oxidation. The isolated dithioketene acetal moiety has an oxidation potential of $E_{p/2}$ = +1.06 V vs Ag/AgCl, and the primary amine in **10** has an $E_{p/2}$ = +1.15 V vs Ag/AgCl. While the cyclic secondary amine **11** has an oxidation potential of $E_{p/2}$ = + 0.89 V vs Ag/AgCl, significantly lower than either of the two functional groups in the starting material. This situation would suggest the reaction would lead to an overoxidation of the product **11**. This analysis, however, overlooked the cyclization reaction and its potential impact on the oxidation potential of the substrate since fast cyclizations lower the oxidation potential of the substrate.[11–13] In actuality, the oxidation potential of **11** is $E_{p/2}$ = +0.60 V vs Ag/AgCl.[10] This drop in potential can be explained using the Nernst equation and steady-state kinetics (see chapter 1 for a more detailed discussion). Due to this drop in potential, overoxidation was avoided, leading to the formation of cyclic product. Unfortunately, in our case (Scheme 5.6) the cyclization was not fast enough to drop the oxidation potential of **9** below that of the cyclic amine intermediate.

Clearly, we need to avoid this amine intermediate and there are two ways we can accomplish this. The first way would be to use a silyl-based imidate as depicted in Scheme 5.8. Once oxidized, the styrene group would trap the radical cation. Next, we envisioned the silyl group being cleaved *in situ* during the anodic oxidation by methoxide generated at the cathode, resulting in the cyclic

**Scheme 5.11: Electrolysis of Imidate with Water as the Cosolvent**

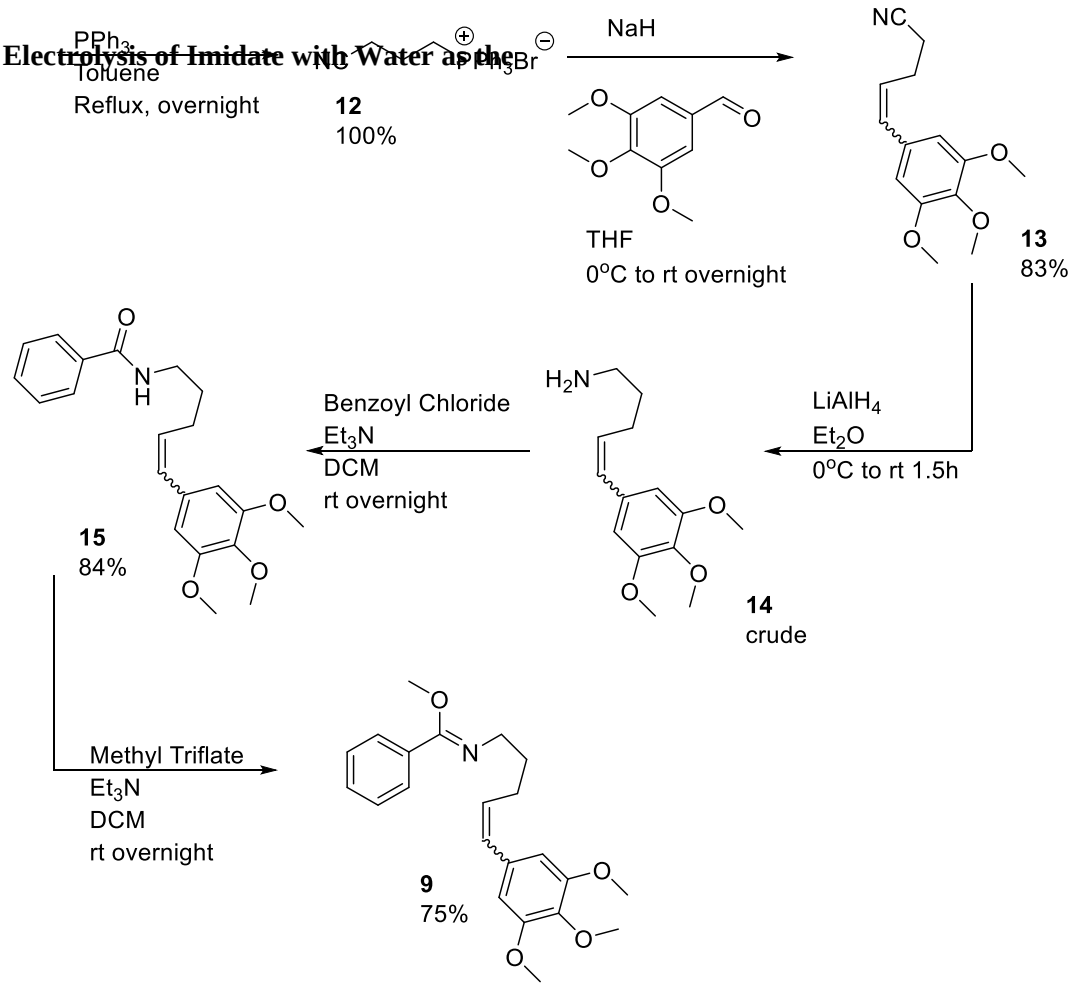


**Scheme 5.10: Synthesis of Imidate 9**

amide product. The presence of this carbonyl reduces the electron density on the nitrogen in the product, thereby increasing the oxidation potential of the product above that of the starting material, thus preventing over oxidation. Unfortunately, efforts to form a silyl-based imidate by treating the amide with a silylating agent in the presence of a base all proved unsuccessful. In the majority of cases, only the initial amide was successfully recovered.

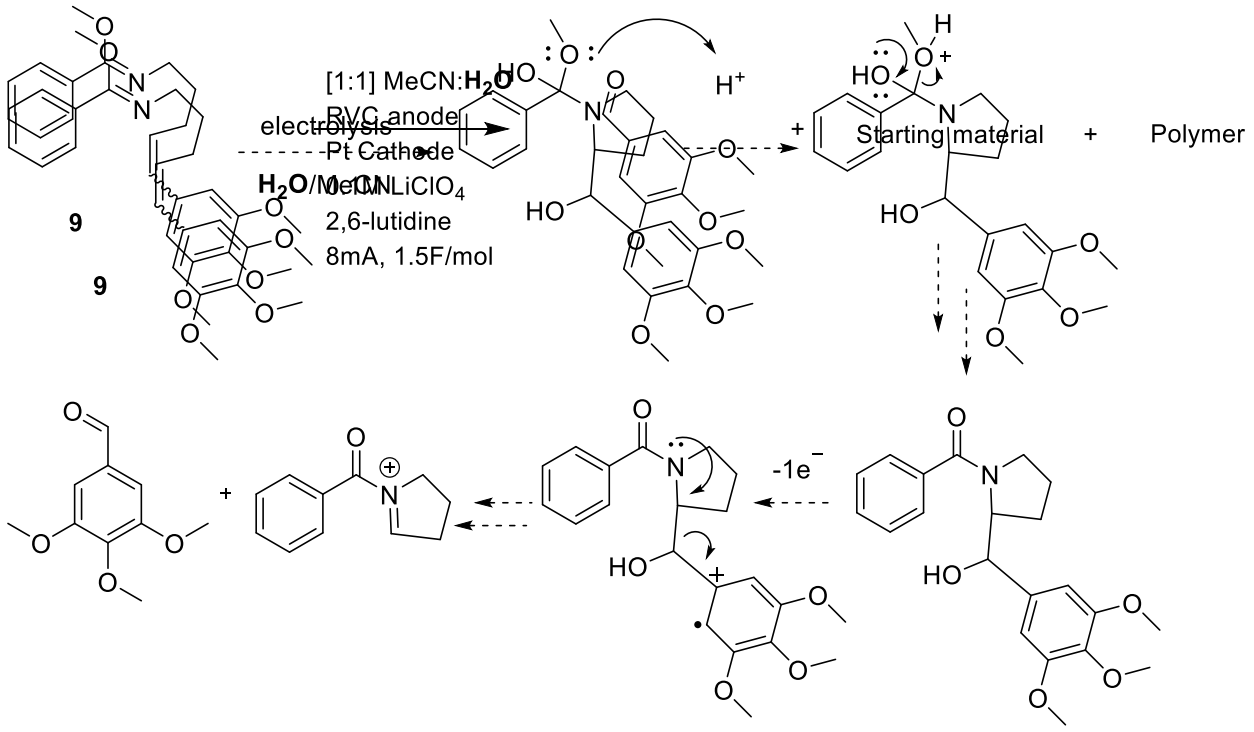


The second strategy to avoid this overoxidation would be to perform the reactions in water instead of methanol, a change that had been used in a previous oxidation reactions involving an amide substrate.[14] In this case, the hemi-ortho amide formed after cyclization would fall apart to an amide, an electron-deficient group that would not over oxidize (Scheme 5.9).

The construction of substrate **9** is shown in Scheme 5.10. It utilized a Wittig reaction on syringaldehyde to install the nitrile group in 83% yield. From here, the nitrile was reduced with $LiAlH_4$ to afford amine **14** which was used crude in the following step. Next, the amine is benzoylated to afford benzamide **15** in 84% yield. Finally, the amide is converted to imidate **9** in 75% yield with methyl triflate and triethylamine stirring overnight.

We took the following imidate with a trimethoxy styrene trapping group (Scheme 5.12) and performed the electrolysis with water as the cosolvent. Again, what we saw was syringaldehyde stemming from overoxidation of the tertiary amine intermediate along with polymer. How might this occur even if we are trapping the amine with water leading to the formation of the amide product? Scheme 5.12 provides a suggested answer to this question. Once the amide product was formed, the electron-rich trimethoxy aryl ring would be oxidized to generate a radical cation. Next, the nitrogen lone pairs would donate electron density, triggering fragmentation to afford an iminium cation that would polymerize along with syringaldehyde.

**Scheme 5.13: Synthesis of Imidate 19**

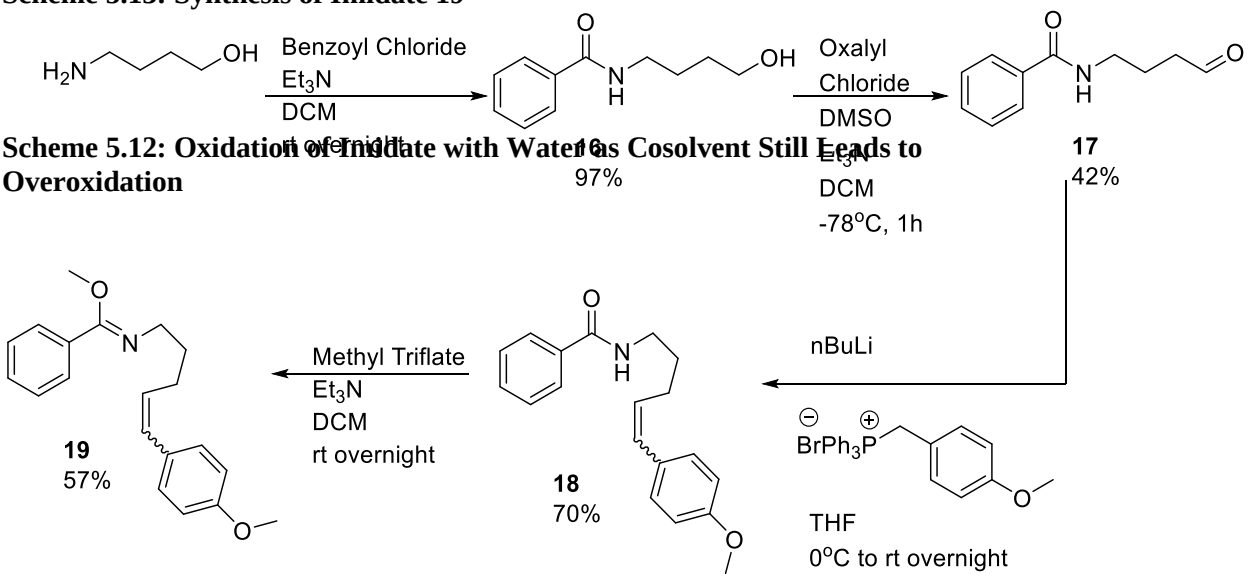


**Scheme 5.12: Oxidation of Imidate with Water as Cosolvent Still Leads to Overoxidation**

We then turned our attention towards a cyclization that would use a paramethoxy styrene trapping group (Scheme 5.13). The synthesis originated with 1-amino-butanol which was converted into the desired electrolysis substrate by benzoyl protecting the amine in 97% yield. The alcohol was then oxidized to an aldehyde in 42% using Swern conditions. The aldehyde was converted into

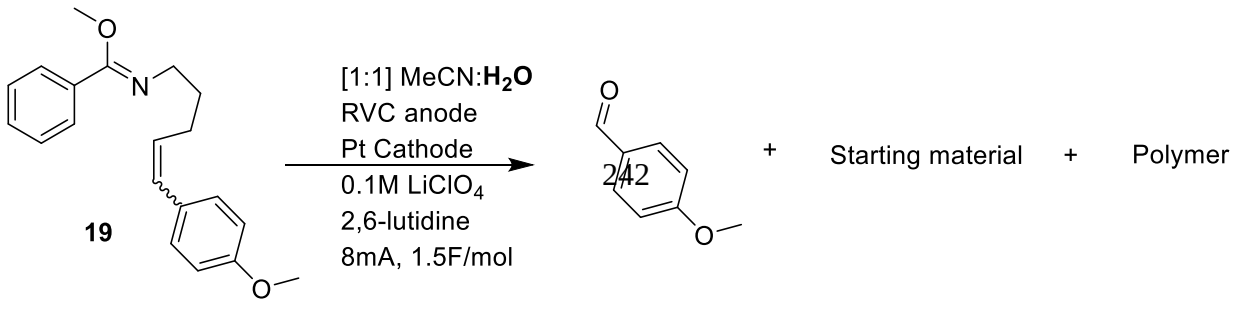

olefin **18** in 70% yield with a Wittig reaction. Finally, the amide is converted to imidate **19** in 57% yield with methyl triflate and triethylamine stirring overnight.

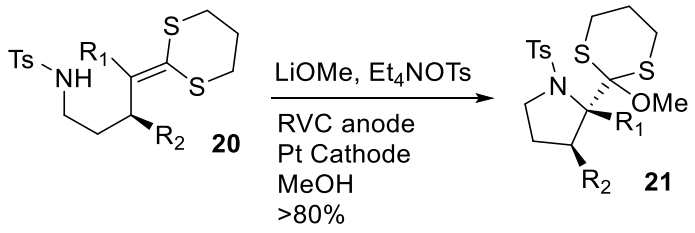


**Scheme 5.15: Previous Studies on Amine Cyclization and Overoxidation**

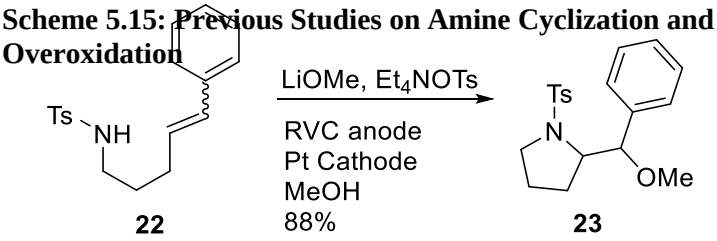


It was our hope that this less electron-rich aryl ring would prevent the overoxidation that occurred with the previous substrate in water. However, when the electrolysis was conducted using water as the cosolvent, what we observed was again the p-anisaldehyde and polymer resulting from overoxidation. At this point, it became evident that the radical-cation pathway needed to be avoided. This brought us to the next option, which was to push the cyclization reaction down the radical pathway, similar to the chemistry shown in section 5.2. To accomplish this, we have two options. The first is to use a stronger base than methoxide to pull the amidyl proton (pKa~18). The second option involves somehow lowering the pKa of the amidyl proton, allowing it to be

**Scheme 5.14: Electrolysis with Paramethoxy Styrene Trapping Group Still Leads to Overoxidation**

deprotonated by methoxide generated in solution.

## 5.3.2 Radical Pathway

With the difficulties observed, we wondered if the styrene group itself was compatible with trapping of a nitrogen radical. To test this idea, we took inspiration from the work of Xu and

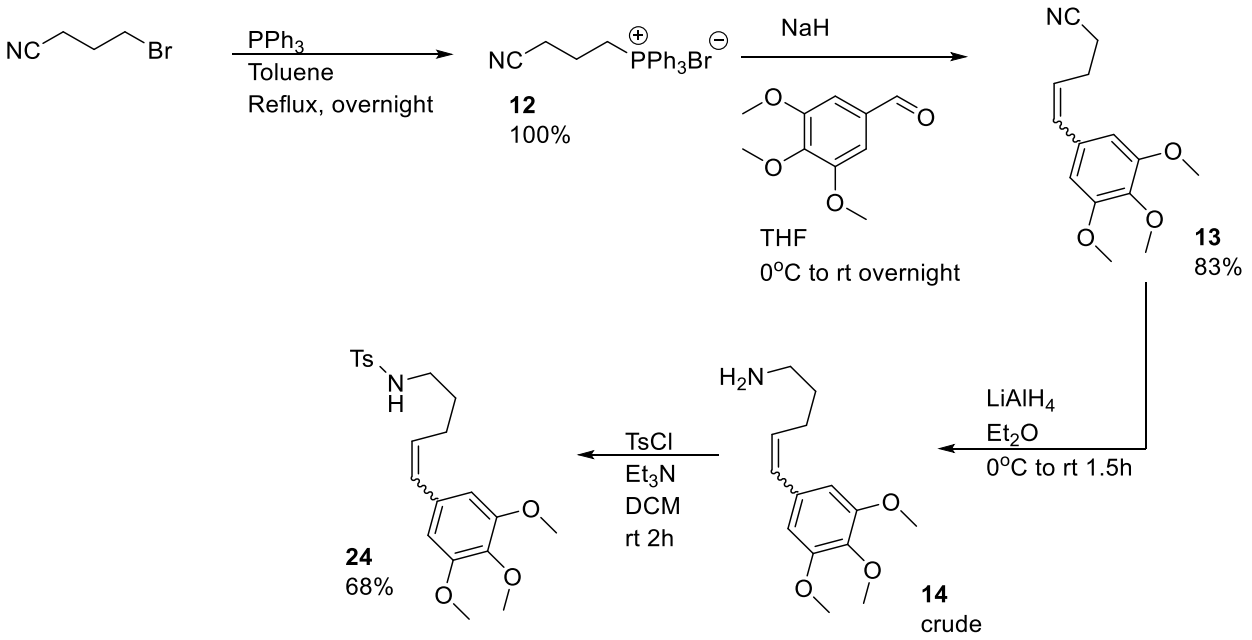


**Scheme 5.16: Synthesis of Tosyl Protected Amine 23**

Moeller in 2010 (Scheme 5.7 and Scheme 5.15).[10] In their research, they demonstrated that the amine cyclization worked because of a Nernstian shift that lowered the oxidation potential of the substrate below that of the product. Before this observation was made, initial calculations predicted an overoxidation issue, which they addressed by employing a sulfonyl protecting group on the amine. The rationale behind this strategy was to lower the acidity of the N-H in the substrate leading to a substrate following deprotonation with a lower oxidation potential than the cyclic amine product. Additionally, they were aware that if the oxidation occurred at the dithioketene acetal group, sulfonamides are better nucleophiles than amides. The cyclization of nitrogen-radicals was also shown to be compatible with a simple styrene trapping group, a reaction that proceeded in a high yield.

Inspired by this work, we sought to test the generality of this reaction using a more electron-rich styrene trapping group. Along this line, substrate **24**, with a sulfonamide and a trimethoxy styrene trapping group, was synthesized (Scheme 5.16) and oxidized employing similar conditions to those employed by Xu and Moeller to afford the desired cyclized product in a 74% isolated yield (Scheme 5.17). Our hypothesis was that the reaction proceeded as follows: First, methoxide deprotonated the N-H of the sulfonamide to afford the corresponding anion. Second, the anion was oxidized at the anode to form a radical that then added to the trimethoxy styrene group. A rapid second oxidation step took place producing a benzylic cation, that was promptly trapped by methanol to afford the final product. Clearly, an electron-rich styrene trapping group could trap a nitrogen radical. We now turned our attention back towards the model system shown in Scheme 5.5 with a plan in mind. To prevent overoxidation, it is necessary to push this reaction down a

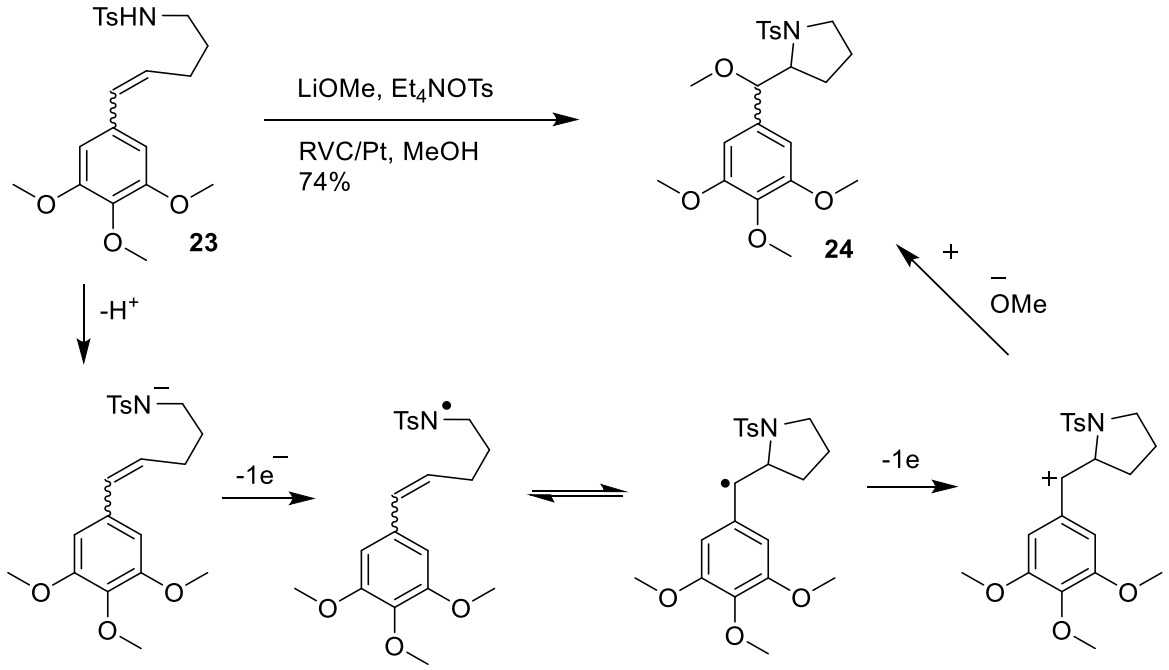


**Scheme 5.17: Successful Cyclization with the Use of a Toluenesulfonyl Group**

radical pathway. To achieve this, a method to decrease of the pKa of the N-H of the amide must

be employed. At that same time, we hoped to avoid the use of the sulfonamide since it would require deprotection of the product followed by a coupling reaction to build the chyrsosporazine ring skeleton. We hoped to avoid these extra steps.

**Using a Thioamide to Lower the Pka**

One approach to reduce the pKa of an amide N-H involved converting it into a thioamide. This modification would make the N-H proton more acidic (ΔpKa = -6).[15,16] The transformation, as depicted in Scheme 5.18, can be achieved by using Lawesson's Reagent in refluxing THF for 2.5 hours. When the amide with the trimethoxy styrene group was transformed into the corresponding thioamide, the yield was 88%. Similarly, the amide with the paramethoxy styrene trapping group resulted in a 74% yield of the thioamide product. Having the two substrates in hand, compound **27a** was initially oxidized using similar conditions to those employed by the Xu group, as seen in Table 5.1. The outcome was cyclic product **28a** in 38% yield (Table 5.1 entry 1). With the initial cyclization proving successful, we directed our efforts toward improving the

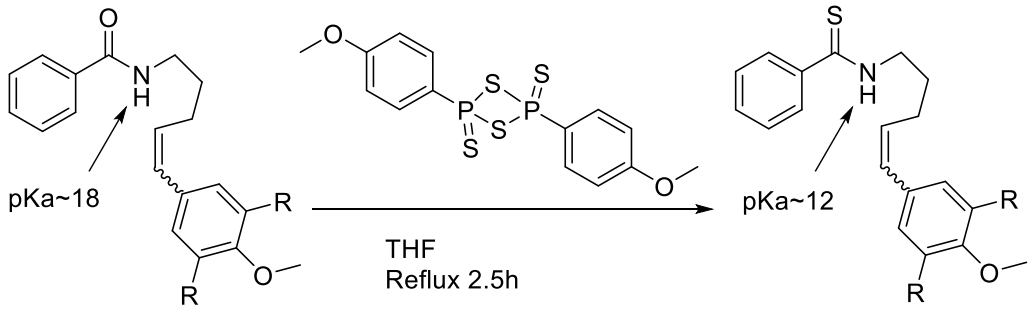


**Scheme 5.18: Converting Amide into Thioamide with Lawesson's Reagent**

reaction yield by altering the base. This idea stemmed from the observation that previous sulfonamide cyclizations all utilized n-butyllithium, a stronger base, to generate methoxide, a

**Table 5.1: Electrolysis of Thioamide Leading to Cyclic Product**

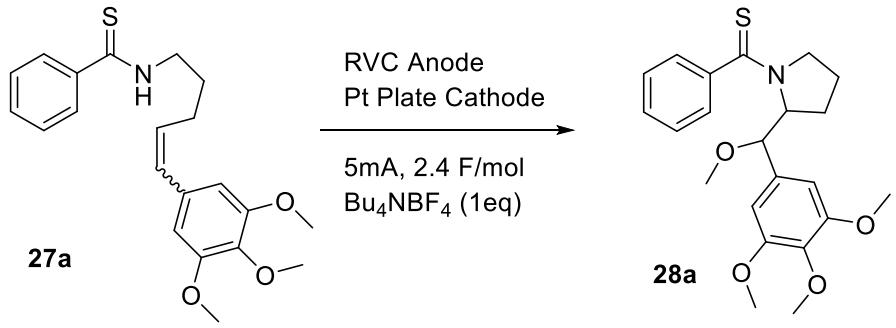


| Entry | Solvent | Base | Ferrocene (5 mol%) | Yield |
|---|---|---|---|---|
| 1 | 1:1 THF:MeOH | $K_2CO_3$ (1.0 eq) | Yes | 38% |
| 2 | 1:1 THF:MeOH | nBuLi (0.5 eq) | Yes | 66% |
| 3 | 1:1 THF:MeOH | nBuLI (0.5 eq) | No | 35% |

strategy that increased the pH of the overall reaction. As seen in entry 2 of Table 5.1, the modification towards using a stronger base (LiOMe) led to a yield of 66% for the product. Next, we questioned whether ferrocene was mediating the reaction and if its presence was crucial for the success of the reaction. As depicted in entry 3 Table 5.1, it indeed played a critical role. When ferrocene was not included, the yield sharply decreased to 35%, and the reaction appeared notably messier.

**Table 5.2: Electrolysis of Thioamide with a Paramethoxy Styrene Trapping Group**

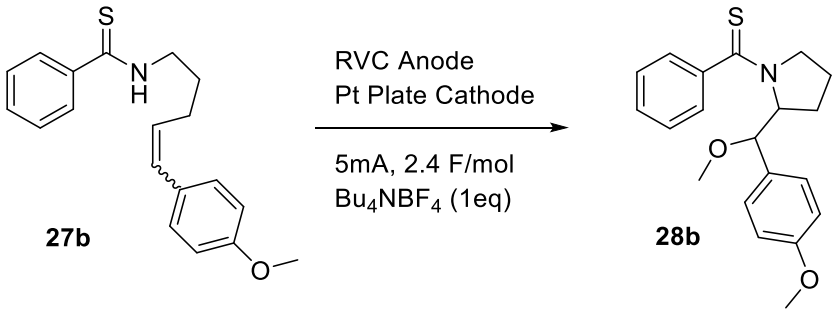


| Entry | Solvent | Base | Ferrocene (5 mol%) | Yield |
|---|---|---|---|---|
| 1 | 1:1 THF:MeOH | nBuLi (0.5 eq) | Yes | 68% |
| 2 | 1:9 THF:MeOH | nBuLi (0.5 eq) | Yes | 31% |

With the success of thioamide using a trimethoxy styrene trapping group, we sought to test the generality of the reaction and see if the less electron-rich paramethoxy styrene trapping group would give comparable yields of cyclic product. As shown in Table 5.2, when **27b** was oxidized using the using nBuLi as the base and ferrocene as the mediator, **28b** was formed in a 68% yield. Next, the concentration of methanol was increased from a 1:1 mixture of THF:Methanol to a 1:9 ratio. When this was done the yield dropped significantly to 31%.

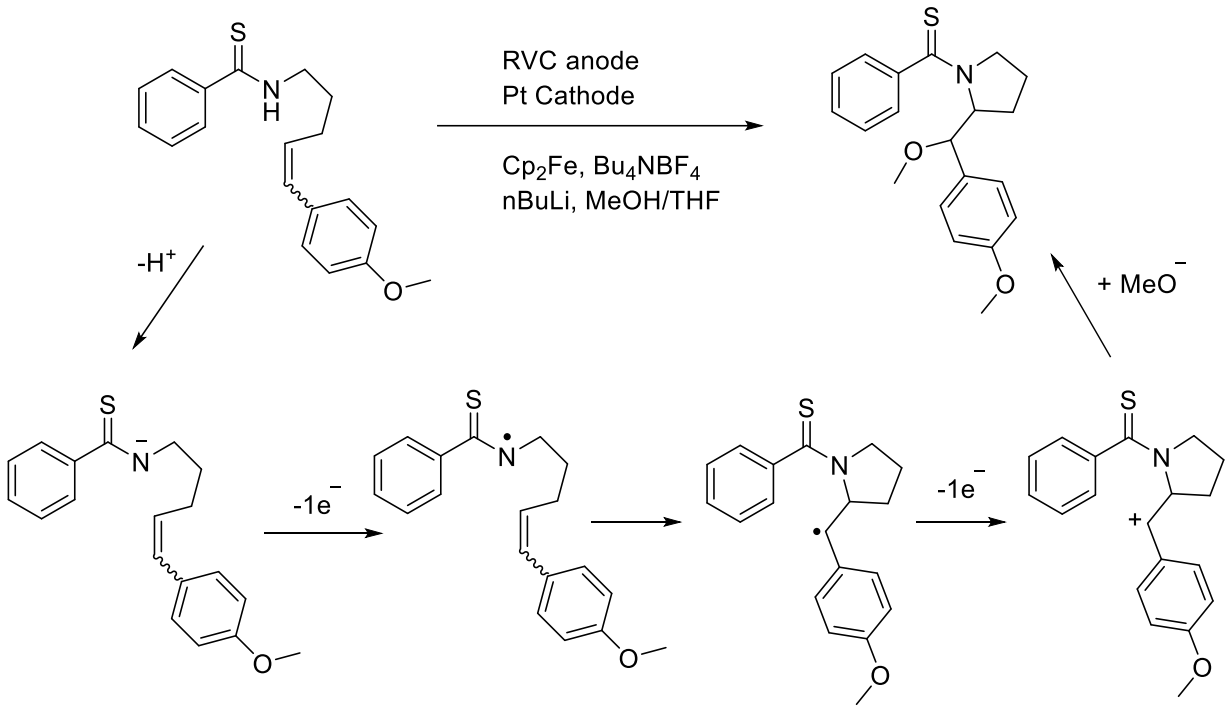


**Scheme 5.19: Proposed Mechanism of Cyclization**

We envision the reaction proceeding as illustrated in Scheme 5.19. First, the acidic N-H of the thioamide will be deprotonated resulting in an anion. Second, a ferrocenium ion will oxidize the anion into the corresponding nitrogen radical, which will then be trapped by the styrene group. The newly formed benzylic radical will undergo a fast second oxidation step to give a benzylic cation. This intermediate will then be trapped by methanol to afford the cyclized thioamide product.

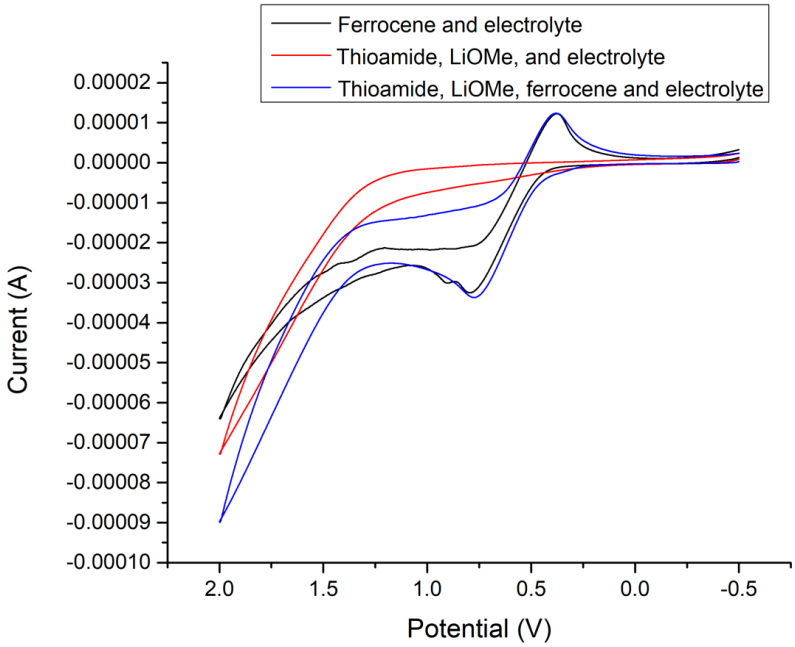


**Figure 5.1 Cyclic Voltammetry of Thioamide (27b)**

The cyclic voltammetry data (Figure 5.1) helped to explain the experimental significance of ferrocene in the reaction. The red curve represents the CV for the reaction when the ferrocene is excluded from the thioamide, lithium methoxide, and electrolyte, focusing solely on the oxidation of the thioamide. The lack of almost any wave suggests very slow reaction kinetics at the electrode until the background oxidation of methoxide. The black curve shows a reversible wave for the oxidation of ferrocene. The blue curve, which includes ferrocene and the substrate, reveals that the

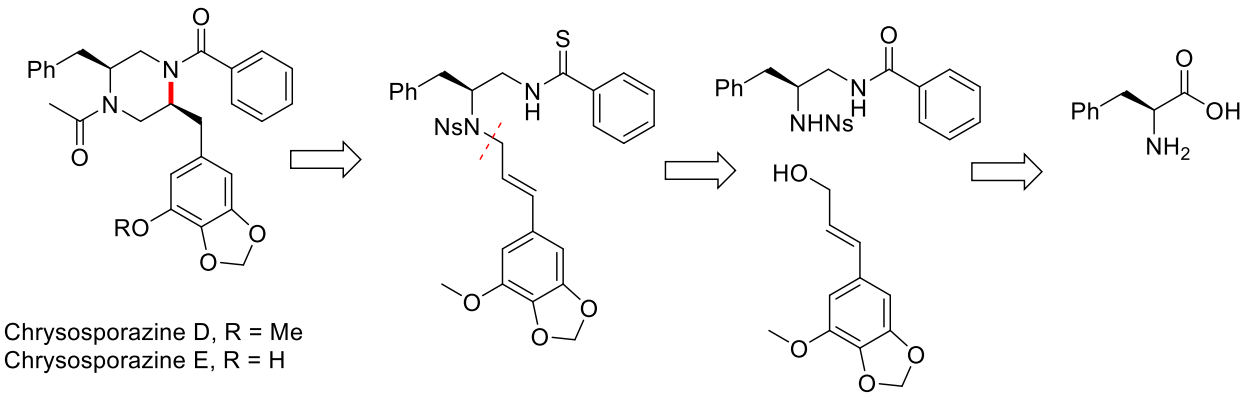


**Scheme 5.20: Retrosynthetic Analysis of Chrysosporazine D/E**

oxidation of ferrocene occurs initially. The ferrocenium ion then goes on to oxidize the thioamide

anion and mediates the reaction. While the kinetics of the reaction between the substrate and the ferrocenium ion is slow enough to prevent the appearance of a significant catalytic current, one can see a decrease in the current associated with the reduction wave for the ferrocenium ion at the cathode. The change in the reverse wave for the ferrocene does indicate a chemical reaction with the ferrocenium ion in solution that is slowing diffusing to the electrode surface.

**Failed Route to Synthesize Chrysosporazine Family of Natural Products**

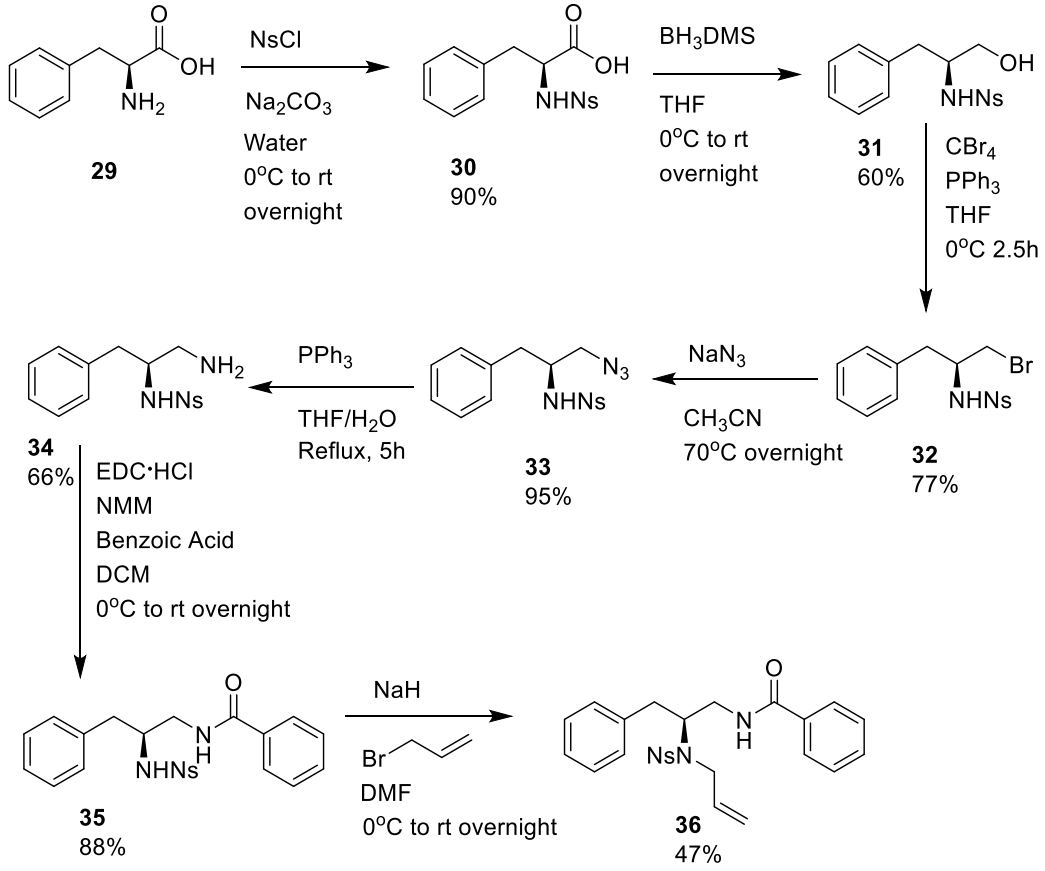


**Scheme 5.21: Forward Synthesis of Chrysosporazine**

As depicted in Scheme 5.1, the ultimate goal is the synthesis of the chrysosporazine family of natural products, with the key bond shown in red being made electrochemically. The retrosynthetic analysis for the synthesis of chrysosporazine D and E can be seen in Scheme 5.20. First, the key bond shown in red would be formed with an anodic cyclization between a thioamide and an

electron-rich styrene. This acyclic compound would be synthesized through a coupling reaction between the top bridge derived from phenylalanine and the bottom bridge, ultimately being derived from lignin.

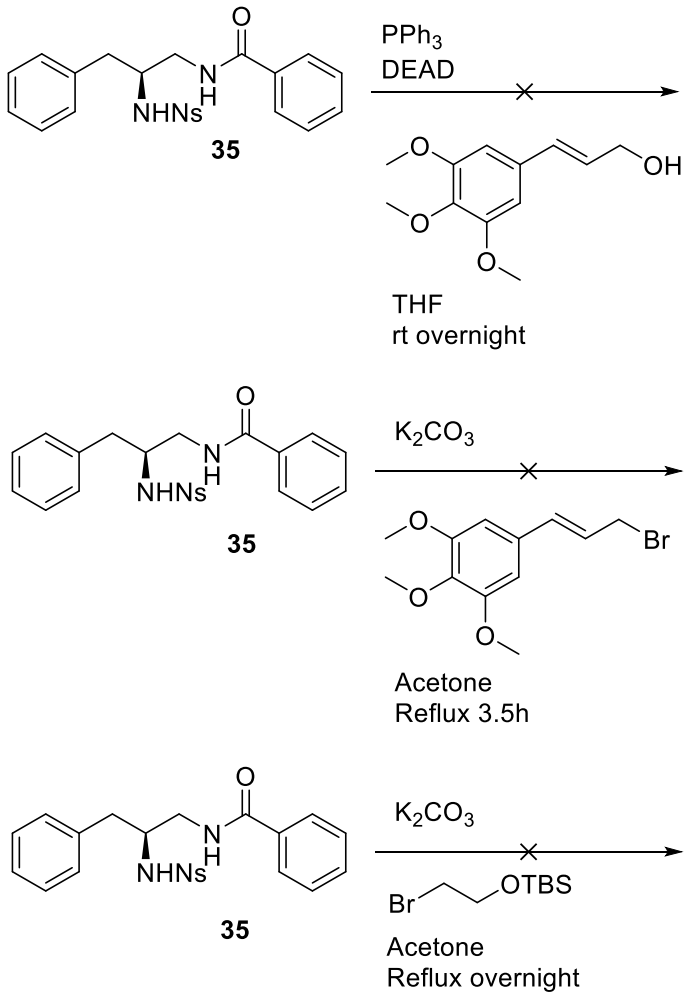


The forward synthesis of chrysosporazine D and E (Scheme 5.21) started with the nosyl-protection

**Scheme 5.22: Failed Reactions to Couple Top Bridge**

of phenylalanine overnight, using sodium carbonate as the base and 4-nitrobenzenesulfonyl chloride as the electrophile. Having the protected amine in hand, the carboxylic acid was then reduced overnight using borane dimethyl sulfide to yield an alcohol which was subsequently

converted into an alkyl bromide using the Appel reaction. The bromide was then displaced with sodium azide, and the resulting alkyl azide was reduced with Staudinger reduction conditions to give the primary amine. This amine was coupled to benzoic acid with the use of the peptide coupling agent EDC to yield the benzamide. Efforts to directly couple the bottom bridge to the top bridge proved unsuccessful (Scheme 5.22). Which prompted a more indirect approach to be taken. This process involved allylating the top bridge using sodium hydride as the base and allyl bromide as the electrophile. The allylated top bridge was then coupled to the electron-rich styrene through a cross metathesis catalyzed by Grubb's Gen II catalyst (Scheme 5.23). The amide was then transformed into the corresponding thioamide using Lawesson's Reagent in refluxing THF for 2.5 hours.

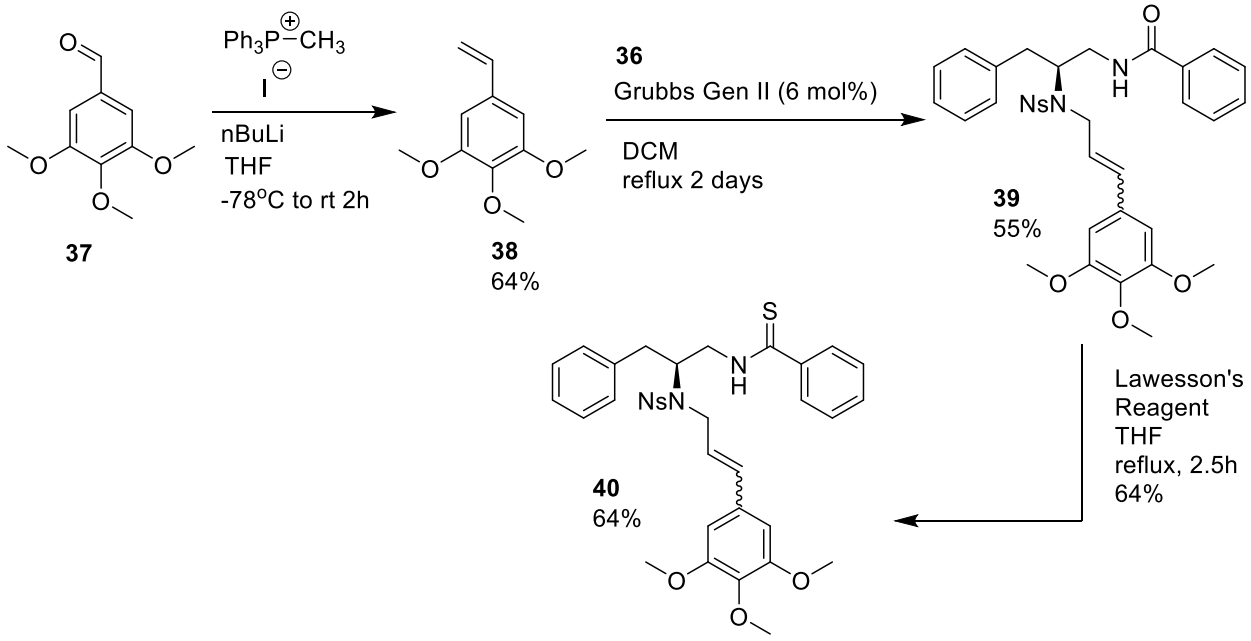


**Scheme 5.23: Installation of Bottom Bridge to Top Bridge**

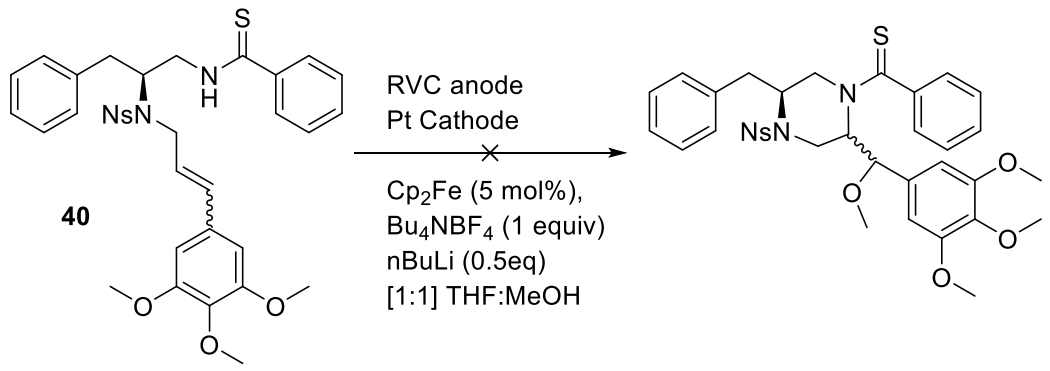


**Scheme 5.24: Failed Six-Membered Ring Cyclization**

When the electrolysis was performed on **40** (Scheme 5.24), using the same conditions utilized in the successful five-membered ring cyclizations, no product was observed. There were two possible explanations for this: first, the six-membered ring cyclization might have been too slow compared

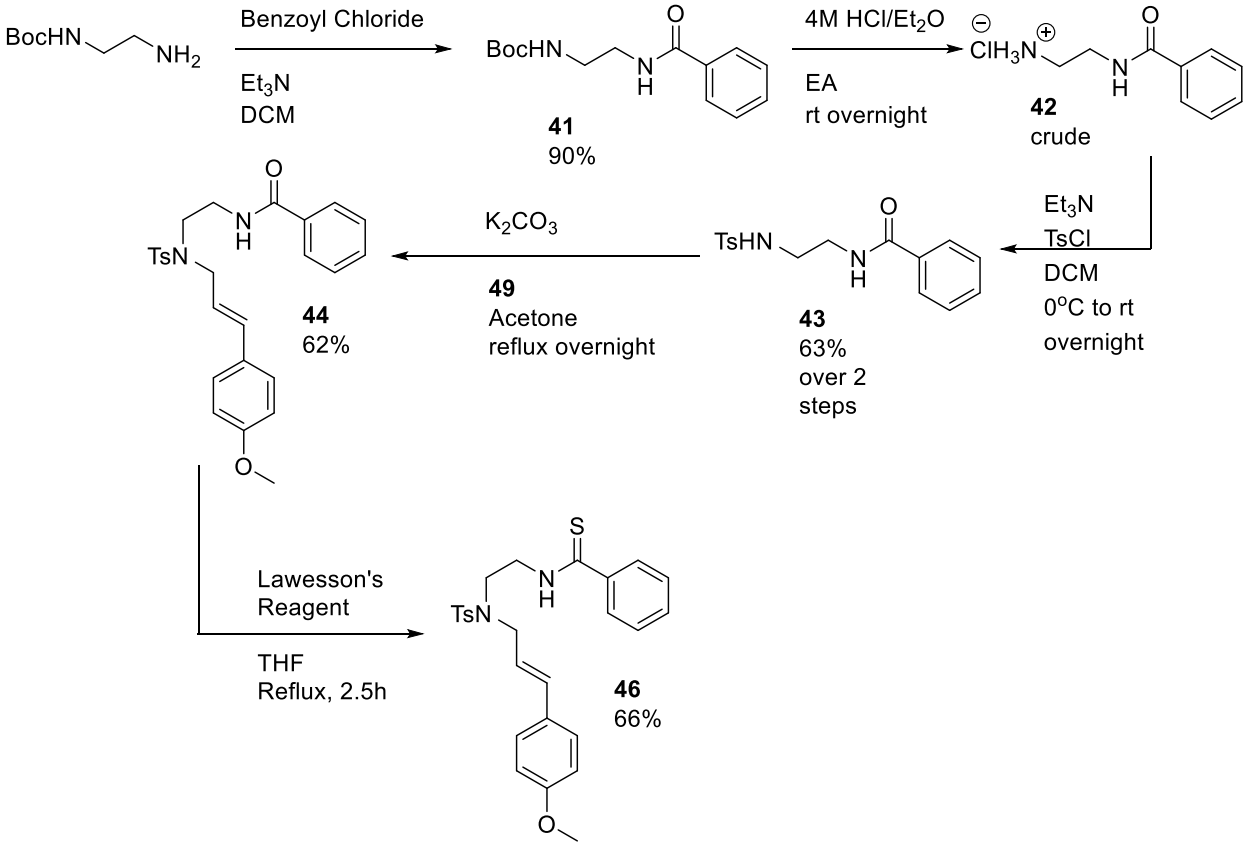


**Scheme 5.25: Synthesis of Model Substrate with a Tosyl Protecting Group**

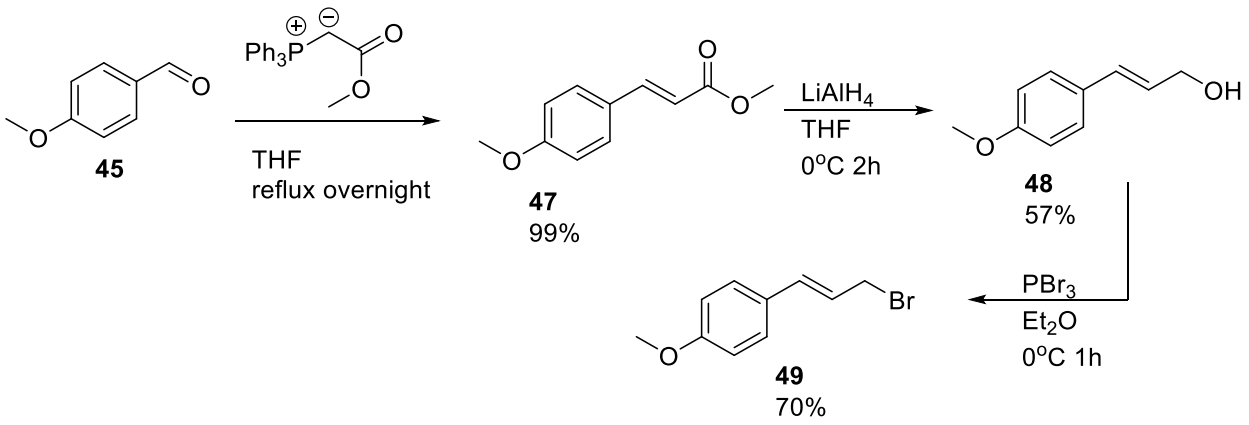


**Scheme 5.26: Synthesis of 49**

to other competing reactions. Second, the nosyl group is not electrochemically stable.[18] It can undergo reduction at the cathode, a fact that was not taken into consideration at the time. After failure of the cyclization, worries formed around a potential reduction of the nitro-group Efforts were then directed toward a model substrate using a tosyl-protected amine to test if the six-membered ring cyclization is possible in the absence of such a reducable protecting group.

**Cyclizations to give 6-membered Ring Using a Tosyl Protecting Group**

The substrate for the cyclization with the tosyl-protected amine started by benzoylating n-boc-ethylenediamine (Scheme 5.25). The BOC group was then removed by stirring it overnight in 4M HCl. This amine salt was carried forward crude to the next step. From here, the amine was Tosyl protected. The tosyl amine was then coupled to styrene **49**. Finally, the amide was converted into thioamide **46** with the use of Lawesson's reagent. With this thioamide in hand, we conducted the electrolysis using the same conditions that were used in the five-membered ring case (Table 5.3 entry 1). While the cyclic product was generated, the yield was lower compared to the 5-membered ring cyclization, and the reaction was notably messier. This is not surprising, as six-membered rings cyclize more slowly than their five-membered ring counterparts. The delayed cyclization would result in both a lower yield of the product and more potential side reactions which would

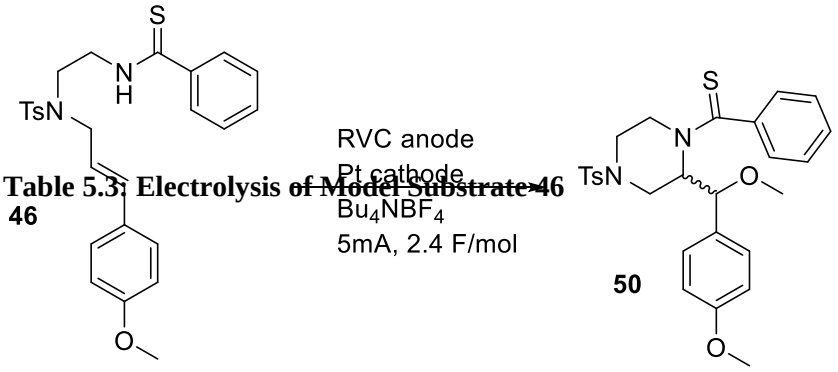


**46** **50**

**Table 5.3: Electrolysis of Model Substrate 46**

lead to a messier reaction. We then aimed to alter the additive in the cyclization. This involved changing the mediator to copper acetate, with the hope that this modification would enhance the yield of the cyclization by stabilizing the radical and helping with the addition to the olefin. When this change was made (Table 5.3 entry 2) the yield of the reaction rose to 58% of cyclic product **50**.

| Entry | Solvent | Base | Additive (5 mol%) | Yield |
|---|---|---|---|---|
| 1 | 1:1 THF:MeOH | nBuLi (0.5 eq) | Ferrocene | 20%(messy) |
| 2 | 1:1 THF:MeOH | nBuli (0.5 eq) | $Cu(OAc)_2$ | 58% |

It is important to note that the cyclic intermediates formed (**28a**, **28b**, and **50**) are all still the thioamide, as evidenced by mass spectrometry. The initial speculation that they were amides was based on the C-13 NMR spectra (schemes 5.27 – 5.29). In Scheme 5.27, the C-13 NMR of amide **18** is depicted, which shows three labeled peaks. The first peak corresponds to the amide carbonyl at 167.51 ppm. The second peak corresponds to the ipso carbon at 158.76 ppm. Finally, the third peak corresponds to carbon 3 at 158.29 ppm, which is ipso to the carbonyl. In Scheme 5.28, the C-13 NMR of thioamide **27b** is depicted, which shows three labeled peaks. The first peak corresponds to the thioamide carbonyl shifted downfield to 201.70 ppm, a shift that is known to

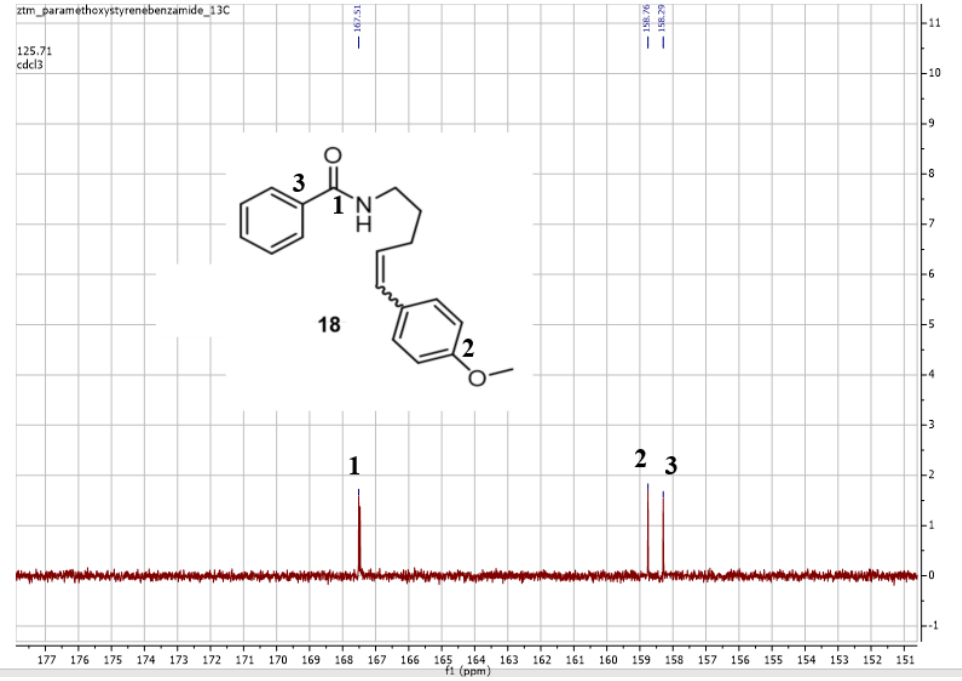


**Scheme 5.27: Carbon NMR of Amide 18**

occur to thioamides.[15] The second peak corresponds to the ipso carbon at 161.58 ppm. Finally, the third peak corresponds to carbon 3 at 144.58 ppm, which is ipso to the thiocarbonyl. In Scheme 5.29, the C-13 NMR of cyclic thioamide **28b** is depicted with four labeled peaks highlighted. The first peak corresponds to the thiocarbonyl at 165.54 ppm. We attribute this peak shifting upfield due to π–π stacking of the aromatic rings, which results in anisotropy and shields the thiocarbonyl, shifting it upfield. Mass spectrometry and IR spectroscopy confirms that it is the thioamide, not the amide, in the final product. This was true for all three cyclic thioamide compounds (**28a**, **28b**, and **50**). The second corresponds to the ipso carbon at 162.26. The

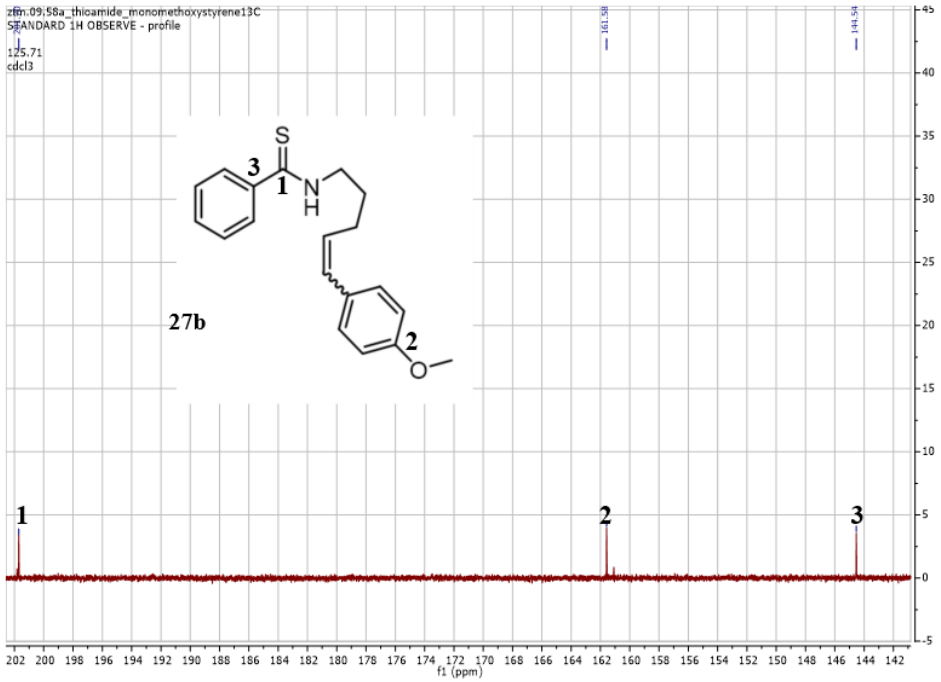


**Scheme 5.28: Carbon NMR of Thioamide 27b**

third carbon appears at 142.48 ppm, which is ipso to the thiocarbonyl. Finally, carbon 4 is observed at 88.64 ppm, located at the benzylic position with a methoxy group attached to the carbon. Anodic cyclizations which employ a styrene trapping group exhibit a C-13 peak in the range of 80-90 ppm for the benzylic position bearing a methoxy group.[17]

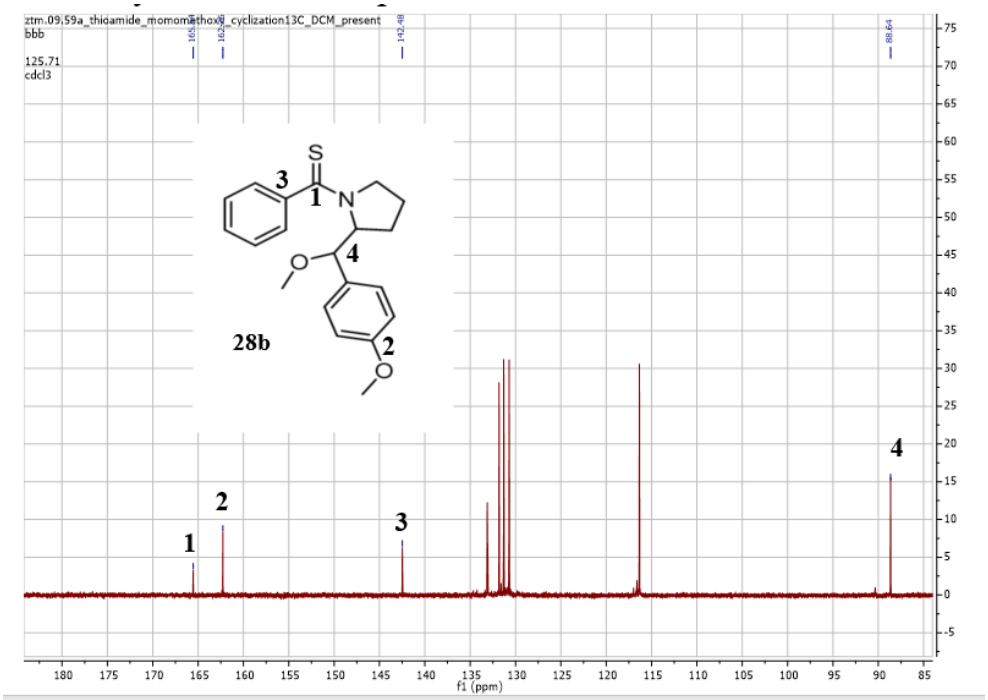


**Scheme 5.29: Carbon NMR of Cyclic Thioamide Product**

Current efforts to convert cyclic thioamide **28b** to its cyclic amide counterparts have proven unsuccessful (Table 5.4). The first set of conditions employed silver carbonate stirring for two days in DCM which resulted in recovered starting material. The second conditions tried used hydrogen peroxide and $TiCl_4$ which resulted in recovered starting material and polymer. The third set of conditions utilized were stirring the thioamide overnight with methyl iodide in DCM and then performing an aqueous workup to hydrolyze the thioamide into an amide. This resulted in recovered starting material. Once conditions to accomplish this transformation are found the resulting amide will undergo mass spectrometry analysis to confirm it is in fact the amide.

**Table 5.4: Failed Attempts to Convert Thioamide into Amide**

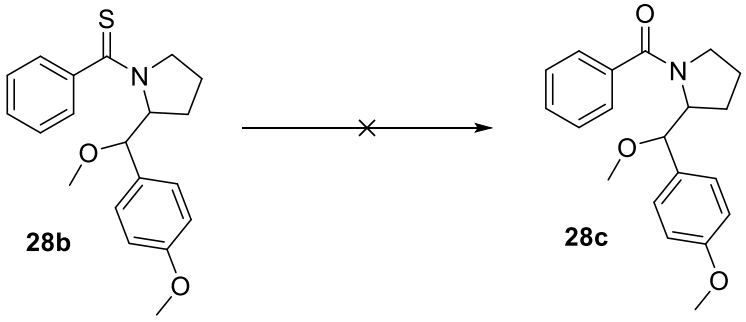


| Entry | Conditions | Solvent | Time | Result |
|---|---|---|---|---|
| 1 | $Ag_2CO_3$ | DCM | 2 days | sm |
| 2 | 30% $H_2O_2$/$TiCl_4$ | $CH_3CN$ | 2 min | sm + polymer |
| 3 | MeI (aqueous workup) | DCM | Overnight | sm |

## 5.4 Conclusions and Future Directions

In this study, we have developed an efficient oxidative route for the synthesis of cyclic amines from the coupling of an amide to a styrene group. This effort targeting the chrysosporazine family of natural products first addressed the limitations for state-of-the-art cyclization of this nature by specifically overcoming the requirement for an aryl substituent on the N-atom involved in the cyclization. While efforts to circumvent the issue with the use of a radical cation intermediate could not overcome issues with overoxidation of the amine product, lowering the pKa of N-H of the amide by converting it into a thioamide did provide a successful solution, at least for five-membered ring cyclizations. The change to a thioamide allowed for deprotonation of this coupling partner so that it could be selectively oxidized to a radical that then triggered the subsequent cyclizations. The cyclizations leading to five-membered rings used ferrocene as the oxidative

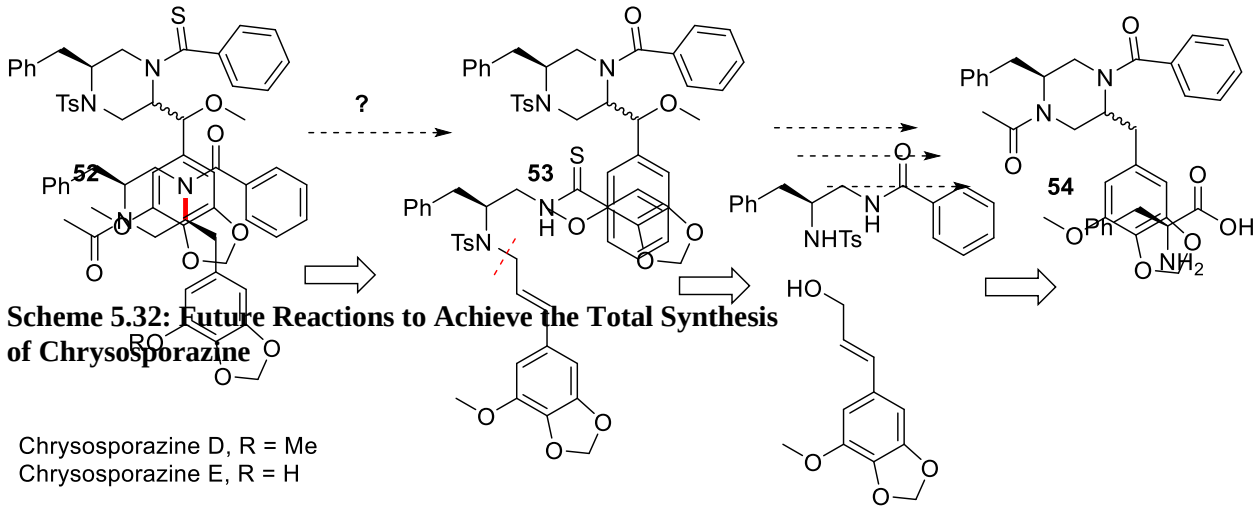


**Scheme 5.32: Future Reactions to Achieve the Total Synthesis of Chrysosporazine**

**Scheme 5.30: Updated Retrosynthetic Analysis of Chrysosporazine**

mediator. However, in the six-membered ring example that directly targeted the chrysosporazine ring skeleton the oxidative mediator was changed to copper acetate. This modification enabled the six-membered ring cyclization to occur with yields comparable to those of the five-membered ring cyclizations. In all three successful cyclizations, they gave a cyclic thioamide as determined by mass spectrometry and IR spectroscopy. Additionally, the use of a tosyl protecting group on the amine proved critical for this cyclization. The nosyl group is electrochemically unstable and it can be reduced at the cathode. The change to the tosyl group prevented this cathodic cleavage from

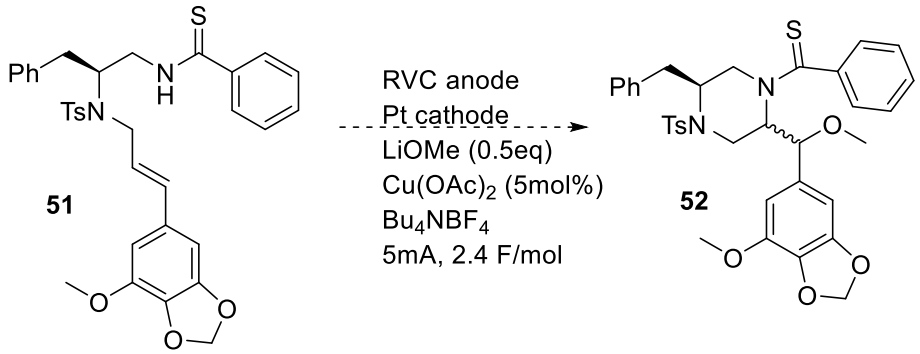


**Scheme 5.31: Anodic Cyclization to Make Chrysosporazine Ring System**

occurring which allowed the cyclization to happen.

The future directions of this project are twofold. First, find successful reaction conditions to convert the cyclic thioamides into their corresponding cyclic amide counterpart. Conditions attempted to accomplish this transformation are shown in Table 5.4. Conditions that could accomplish this transformation include: silver(I) acetate, p,p-dichlorophenylphosphine oxide and superoxide, dinitrogen tetraoxide, or mercury(II) oxide. Second, with the successful formation of a six-membered ring in the model system, as seen in Table 5.3. we will return to the total synthesis of the chrysosporazine family of natural products. The key bond shown in red would be made electrochemically. The updated retrosynthetic analysis for the synthesis of chrysosporazine D and E can be seen in Scheme 5.30. Two major distinctions will allow for the success of this total synthesis. First, the use of a tosyl protecting group on the amine will prevent decomposition of the protecting group at the cathode. An issue with the first synthesis was the use of a nosyl group which would be cleaved at the cathode. Second, the key bond shown in red would be formed with an anodic cyclization between a thioamide and an electron-rich styrene. The conditions for this transformation include copper acetate as the mediator for the reaction. This additive will stabilize the radical and help with the addition to the olefin (Scheme 5.31). Once cyclized the thioamide will need to be converted to an amide with the conditions developed for its deprotection (Scheme 5.32). From here, the methoxy at the benzylic position needs to be removed. Selective conditions for this transformation could be $BF_3Et_2O$ and $Et_3SiH$. This group could also be removed by using Birch reduction conditions. If this latter is chosen, the tosyl protecting group will be removed in the same synthetic step. Finally, the secondary amine needs to be acylated. Conditions that could accomplish this transformation include acyl chloride or acetic anhydride with triethylamine or another amine base such as diisopropyl ethyl amine. This synthetic sequence will afford Chrysoporazine D/E.

## 5.5 Experimental Section

### 5.5.1 General Experimental

NMR spectra were acquired on either a Varian Mercury 300 or Agilent DD2 500 MHz, spectrometer at either 300, or 500 MHz for 1H or 75 or 126 MHz for 13C{1H} unless otherwise noted. Chemical shifts (δ) are reported in ppm relative to tetramethylsilane (0 ppm) for 1H and 13C{1H}. Mass spectra were recorded on either a Thermo LTQ-Orbitrap spectrometer under positive ion mode or a Maxis 4G ESI-QTOF spectrometer with flow rate of 3 μL/min. Reactions were run under either an argon or nitrogen atmosphere unless otherwise noted. Flasks were flame-dried under vacuum unless otherwise noted. Tetrahydrofuran was purchased from Sigma-Aldrich Corporation and distilled from sodium benzophenone ketyl under argon atmosphere prior to use. Triethylamine and dichloromethane reaction solvent were purchased from Sigma-Aldrich Corporation and distilled from calcium hydride under argon atmosphere prior to use. Flash column chromatography was performed on 60 Å silica gel purchased from Sorbent Technologies. Thin layer chromatography was performed on Analtec UNIPLATE™ and visualized by ultraviolet irradiation, ceric ammonium molybdate, phosphomolybdic acid, or 2,4-dinitrophenylhydrazine.. All other starting materials and reagents were purchased from Sigma-Aldrich Corporation and used as received. Electrolysis reactions were conducted using a model 630 coulometer, a model 410 potentiostatic controller, and a model 420A power supply purchased from the Electrosynthesis Company, Inc. (now Electroytica). Carbon rods were also purchased from the Electrolytica Company. Reticulated vitreous carbon (RVC) electrodes were purchased from ERG Aerospace Corp. CV studies were conducting using a 3-mm-diameter glassy carbon working electrode with a scan rate of 400 mV s−1 in 50% MeOH/50% THF containing 1 equivalent of $nBu_4BF_4$. A platinum wire was employed as the auxiliary electrode. The reference electrode was Ag/AgCl.

## 5.5.2 Synthesis and Electrolysis of Compounds

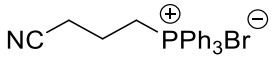


**12**

4-bromobutyronitrile (7.40 g, 50 mmol) and triphenylphosphine (13.11 g, 50 mmol) were dissolved in 125 mL of toluene. The reaction was refluxed at 130 ℃ for 24 hours, and then the mixture cooled to room temperature. A white precipitate 12 was removed by filtration and washed with hexanes to yield 20.500 grams of **12** in 100% yield. The salt was used in the subsequent Wittig reaction without further purification.

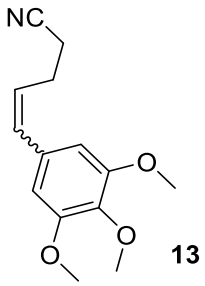


**13**

Phosphonium salt **12** (2.050 g, 5 mmol) and syringaldehyde (0.981g, 5 mmol) were placed in a flask with 40 mL THF at 0 ℃. Then an access amount of sodium hydride (60 % in oil, 600 mg, 15 mmol) was added to the reaction and the mixture was stirred at room temperature for 16 hours. The reaction was then quenched with ice and water respectively, the layers were separated, and the aqueous layer was washed with diethyl ether for three times. The combined organic layer was dried with $MgSO_4$ and solvent was removed in vacuo. And target product **13** was isolated by column chromatography using a gradient eluent starting from 1:10 to 1:4 ethyl acetate: hexanes. 1.026g of **13** (83 %) of desired product was able to be isolated.

1H NMR ($CDCl_3$, 300 MHz): δ 6.56 (d, J = 11.5 Hz, 1H), 6.46 (s, 2H), 5.61 (dt, J = 11.4 Hz, 7.2 Hz, 1H), 3.86 (s, 6H), 3.86 (s, 3H), 2.68 (m, 2H), 2,46 (m, 2H).

13C NMR ($CDCl_3$, 125 MHz): δ 153.25, 137.51, 132.49, 132.27, 127.42, 119.31, 105.98, 61.06, 56.33, 24.65, 17.74.

ESI HRMS m/z $(M+Na)^+$: 270.1105

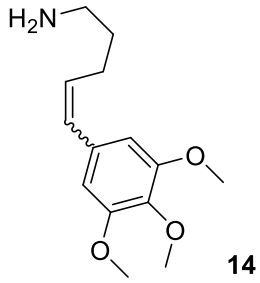


**14**

Lithium aluminum hydride (50 mg, 1.33 mol) and 3 mL of diethyl ether were placed in a flask under argon at 0 °C. A solution of **13** (100 mg, 0.53 mmol) in 2 mL of diethyl ether was added then added to the flask, and the reaction was stirred for 15 minutes before it was warmed to room temperature. The reaction was allowed to stir for another 90 minutes at room temperature before it was quenched by the addition of wet diethyl ether and 1 M NaOH aqueous solution respectively. This mixture was stirred for 20 minutes. Then anhydrous MgSO4 was added. The resulting mixture was stirred for another 20 minutes and then filtered through a celite plug. Evaporation under vacuum obtained the primary amine.**14** which was used directly for the next step without further purification and was fully characterized after the next step.

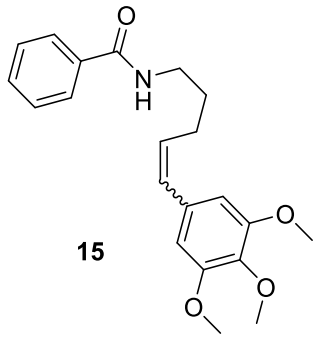


**15**

To a round bottom flask under an argon atmosphere, amine **14** (342 mg, 1.36 mmol) in 10 mL of DCM was added along with triethylamine (0.54 mL,3.87 mmol). A solution of benzoyl chloride (0.16mL, 1.36 mmol) in 5 mL of DCM was injected into the solution. The reaction was stirred overnight and then quenched with water. The layers were separated, and then the aqueous layer was extracted with DCM 2x. The combined organic layer was dried by $MgSO_4$ and solvent was removed by rotary evaporator. The residue was purified through column chromatography (eluent: 1:4 ethyl acetate: hexanes) to obtain 0.4060g of amide **15** in 84% yield.

$^1$H NMR ($CDCl_3$, 500 MHz): δ 7.63 (m, 2H), 7.47 (m, 1H), 7.40 (m, 2H), 6.49 (s, 2H), 6.43 (d, J = 11.7 Hz, 1H), 5.65 (dt, J = 11.5 Hz, 7.3 Hz, 1H), 3.84 (s, 3H), 3.82 (s, 6H), 3.48 (m, 2H), 2.47 (m, 2H), 1.78 (m, 2H).

$^{13}$C NMR ($CDCl_3$, 125 MHz): δ 167.43, 153.00, 136.99, 134.55, 133.00, 131.38, 131.27, 129.90, 128.53, 126.72, 105.91, 60.90, 56.10, 39.33, 29.51, 25.83.

ESI HRMS m/z $(M+Na)^+$: 378.1680

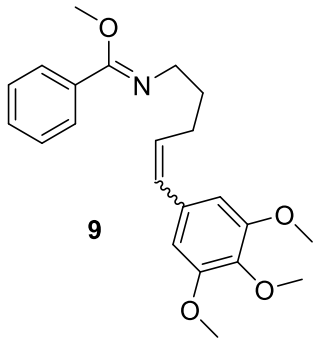


**9**

Imidate **9** was prepared by placing **15** (0.1018g, 0.29 mmol) in a round bottom flask under argon. 1.45 mL of dichloromethane and trifluoromethanesulfonate (0.04mL, 0.44 mmol) was injected into the flask respectively. The mixture was stirred at room temperature overnight. Then triethylamine (0.08mL, 0.58 mmol) was added and was let to stir for 30 minutes. The reaction was

concentrated in vacuo. Residue was purified by column chromatography 1:19:0.6 to 1:9:0.3 EA:Hexane:$Et_3N$ to afford 0.0790g (75%) of compound **9**.

$^1$H NMR ($CDCl_3$, 500 MHz): δ 7.39 (m, 3H), 7.30 (m, 2H), 6.47 (s, 2H), 6.31 (d, J = 11.6 Hz, 1H), 5.60 (dt, J = 11.6 Hz, 7.3 Hz, 1H), 3.84 (s, 3H), 3.82 (s, 6H), 3.76 (s, 3H), 3.32 (t, J = 7.0 Hz, 2H), 2.36 (m, 2H), 1.72 (m, 2H).

$^{13}$C NMR ($CDCl_3$, 125 MHz): δ 153.00, 136.97, 133.50, 132.57, 132.50, 129.49, 129.09, 128.42, 127.96, 106.10, 61.03, 56.21, 53.01, 49.67, 32.33, 26.61

ESI HRMS m/z $(M+H)^+$: 370.2018

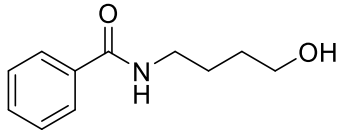


**16**

4-Amino-1-butanol (2.07mL, 22.44 mmol), dichloromethane (100 mL), and triethylamine (8.5 mL, 115.7 mmol) were added in a round bottom flask. Benzoyl chloride (2.6 mL, 22.44 mmol) was dissolved in 20 mL DCM and the solution was injected dropwise into the reaction flask. The mixture was stirred overnight and then quenched by adding a saturated sodium bicarbonate aqueous solution. The layers were separated, and the organic layer was extracted with DCM for three times. The combined organic layer was dried over MgSO4, the solvent removed using a rotary evaporator, and the product **16** carried on without further purification (4.206g, 97 %). The proton NMR of the crude product matched the previously reported data.[19]

$^1$H NMR ($CDCl_3$, 500 MHz): δ 7.75 (d, J = 8.0 Hz, 2H), 7.45 (t, J = 7.0 Hz, 1H), 7.37 (t, J = 7.5 Hz, 2H), 6.93 (br, 1H), 3.66 (t, J = 6.0 Hz, 2H), 3.44 (m, 2H), 2.87 (br, 1H), 1.65 (tt, J = 6.0, 6.5 Hz, 4H)

ESI HRMS m/z $(M+Na)^+$: 216.0997

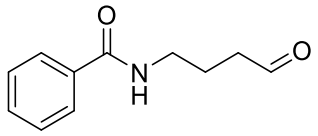

**17**

Oxalyl chloride (2.57mL, 30 mmol) was placed in a protected round bottom flask under argon along with 80 mL of dichloromethane at -78 ℃. DMSO (5 mL, 70 mmol) in 16 mL of DCM was then carefully injected over 20 minutes. Five minutes after injection, a solution of **16** (3.10 g, 16 mmol) in 20 mL DCM was added over a period of 20 minutes. The mixture was stirred at -78℃ for another one hour before (14 mL, 100mmol) of triethylamine was added. The reaction was warmed to room temperature and quenched by brine solution. The layers were separated and the aqueous phase was extracted with DCM three times. The organic layers were then dried over $MgSO_4$ and concentrated *in vacuo*. The aldehyde product **17** was chromatographed through silica gel using 1:2 ethyl acetate: hexanes as eluent to afford product (5.734g, 42 %).

$^1H$ NMR ($CDCl_3$, 500 MHz): δ 9.83 (s, 1H), 7.77 (d, J = 7.8 Hz, 2H), 7.50 (m, 1H), 7.42 (m, 2H), 3.49 (m, 6.5 Hz, 2H), 2.63 (t, J = 6.8 Hz, 2H), 1.97 (m, 2H).

$^{13}C$ NMR ($CDCl_3$, 125 MHz): δ 202.26, 167.73, 134.13, 131.64, 128.74, 126.98, 41.95, 39.77, 21.99.

ESI HRMS m/z $(M+Na)^+$: 214.0839

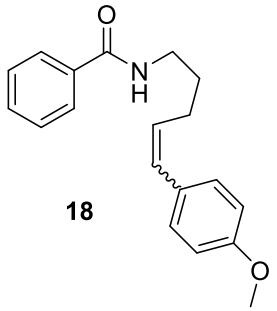

**18**

4-methoxy benzyltriphenylphosphonium bromide (4.63 g, 10 mmol) was placed in a round bottom flask under argon along with 20 mL of THF at 0 ℃. Next, 2.5 M *n*-Butyllithium (4 mL, 10 mmol) was added dropwise, and the mixture was stirred for 30 minutes. Then **17** (0.98 g, 5.13 mmol) in 8 mL of THF was added over 15 minutes before the reaction was raised to room temperature and stirred overnight. The reaction was quenched with aqueous saturated sodium chloride solution, the layers were separated, and the aqueous phase was extracted with ethyl acetate for three times. The combined organic layer was dried over MgSO4, concentrated *in vacuo*, and the crude product chromatographed through silica gel using 1:4 ethyl acetate:hexanes as eluent to afford 2.067g (70%) of product **18**.

$^{1}$H NMR ($CDCl_3$, 500 MHz): δ 7.77 – 7.69 (m, 1.28H), 7.66 – 7.57 (m, 1.06H), 7.47 – 7.39 (m, 1.29H), 7.37 – 7.31 (m, 2.43H), 7.24 (d, $J$ = 8.6 Hz, 1H) 7.19 (d, $J$ = 8.5 Hz, 1H), 6.87 – 6.77 (m, 2.29H), 6.61 (br, 0.58), 6.45 – 6.28 (m, 1.62H), 6.06 (dt, $J$ = 15.8, 7.0 Hz, 0.57H), 5.55 (dt, $J$ = 11.5, 7.4 Hz, 0.55H), 3.77 (s, 1.55H), 3.76 (s, 1.50H), 3.59 – 3.31 (m, 2.41H), 2.58 – 2.33 (m, 1.13H), 2.33 – 2.20 (m, 1.17H), 1.86 – 1.65 (m, 2.38H).

$^{13}$C NMR ($CDCl_3$, 125 MHz): δ 167.51, 167.47, 158.76, 158.29, 134.67, 134.60, 131.23, 131.21, 130.29, 130.10, 129.94, 129.89, 129.27, 128.43, 128.38, 127.57, 127.06, 126.87, 126.86, 126.83, 113.91, 113.67, 55.25, 55.18, 39.81, 39.27, 30.63, 29.36, 29.32, 25.56.

HRMS m/z $(M+H)^+$: 296.1658

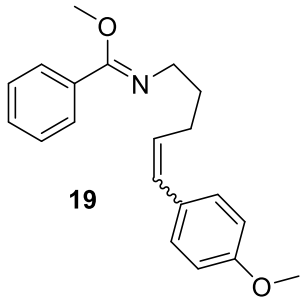

**19**

Imidate **19** was prepared by placing **18** (0.0960g, 0.325 mmol) in a round bottom flask under argon. 1.45 mL of dichloromethane and trifluoromethanesulfonate (0.04mL, 0.44 mmol) was injected into the flask respectively. The mixture was stirred at room temperature overnight. Then triethylamine (0.09mL, 0.65 mmol) was added and was let to stir for 30 minutes. The reaction was concentrated in vacuo. Residue was purified by column chromatography 1:9:0.3 to 1:4:0.15 EA:Hexane:$Et_3N$ to afford 0.0575g (57%) of compound **19**.

$^1H$ NMR ($CDCl_3$, 500 MHz): δ 7.38 (m, 2.81H), 7.34 – 7.27 (m, 1.90H), 7.20 (m, 1.90H), 6.82 (m, 2.10H), 6.35 – 6.19 (m, 1.14H), 6.01 (m, 0.79H), 5.53 (m, 0.76H), 3.81 (s, 1.54H), 3.79 (s, 1.47H), 3.78 (s, 2.77H), 3.31 (m, 2.11H), 2.40 – 2.28 (m, 1.09H), 2.19 (m, 1.18H), 1.70 (m, 2.30H).

$^{13}C$ NMR ($CDCl_3$, 125 MHz): δ 163.59, 163.56, 161.28, 160.83, 135.20, 135.18, 133.70, 133.38, 133.08, 132.59, 132.58, 131.96, 131.14, 131.05, 130.94, 130.93, 130.56, 130.53, 129.62, 129.61, 116.53, 116.19, 57.93, 57.90, 55.56, 55.54, 52.14, 51.98, 34.89, 34.39, 33.19, 29.00.

ESI HRMS m/z $(M+H)^+$: 310.1818

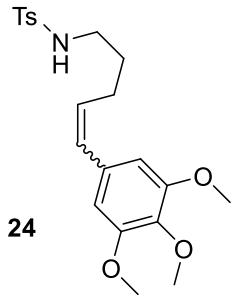


**24**

To a round bottom flask under argon, a solution of amine **14** (0.142g, 0.56 mmol) in 10 mL of DCM was added along with (0.3 mL, 2.1 mmol) of triethylamine. To this mixture was added a solution of p-toluenesulfonyl chloride (114 mg, 0.6 mmol, dissolved in 2 mL DCM) and the reaction allowed to stir at room temperature for 2 hours. The solvent was removed, and the crude residue was placed chromatographed through silica gel using 1:2 ethyl acetate: hexanes with 1% triethylamine as eluent to afford 0.1543g pure tosyl amine **24** in 68 % yield

$^{1}$H NMR ($CDCl_3$, 500 MHz): δ 7.70 (d, J = 8.3 Hz, 2H), 7.27 (d, J = 7.7 Hz, 2H), 6.43 (s, 2H), 6.36 (d, J = 11.6 Hz, 1H), 5.51 (J = 11.6 Hz, 7.2 Hz, 1H), 3.85(s, 3H), 3.83 (s, 6H), 2.95 (m, 2H), 2.41 (s, 3H), 2.34 (m, 2H), 1.62 (m, 2H).

$^{13}$C NMR ($CDCl_3$, 125 MHz): δ 153.08, 143.50, 137.13, 137.08, 133.00, 130.83, 130.11, 129.81, 127.12, 106.02, 61.02, 56.25, 42.91, 29.95, 25.77, 21.62.

HRMS m/z $(M+Na)^+$: 428.1501

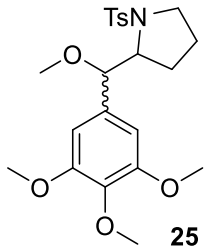


**25**

RVC anode and platinum cathode were prepared and fixed into thermometer adaptor and placed into a three-neck flask. Tosyl protected amine **24** (61 mg, 0.15 mmol) and tetraethylammonium *p*-toluenesulfonate (150 mg, 0.5 mmol) was placed in flask under Argon protection. 5 mL of methanol and n-butyllithium (2.5 M, 0.1 mmol, 0.04 mL) was injected respectively. 2.2 F/mol of charge was allowed to pass through the cell in 6 mA. 0.0483 of product **25** was isolated in 74 % yield through column chromatography with the aid of 30% ethyl acetate in hexanes with 1% of triethylamine.

$^{1}$H NMR (CDCl3, 500 MHz): δ 7.77 (d, J = 8.3 Hz, 0.65H), 7.73 (d, J = 8.3 Hz, 1.35H), 7.33 (d, J = 8.6 Hz, 0.65H), 7.30 (d, J = 8.0 Hz, 1.65H), 6.70 (s, 0.65H), 6.56 (s, 1.35H), 4.74 ( d, J = 2.3 Hz, 0.67H), 4.72 (d, J = 4.6 Hz, 0.33H), 4.03~3.98 (s, 0.35H), 3.88 (s, 4H), 3.87 (s, 2H) 3.86 (s, 1H), 3.85 (s, 2H), 3.74 (m, 0.65H), 3.49 ~3.44 (m, 0.9H), 3.41 (s, 1H), 3.37 (s, 2H), 3.31~3.27 (m, 0.9H), 2.95~2.93 (dd, J = 7.8 Hz, 5.7 Hz, 0.7H), 2.44 (s, 1H), 2.42 (s, 2H), 2.05~1.79 (m, 1.70H), 1.47~1.12 (m, 2.00H), 0.77~0.68 (m, 0.30H)

$^{13}$C NMR ($CDCl_3$, 125 MHz): δ 153.53, 153.12, 143.61, 143.50, 137.45, 137.24, 135.60, 135.24, 134.52, 132.89, 129.83, 129.80, 127.62, 127.53, 104.74, 103.22, 85.73, 84.21, 65.90, 62.88, 61.05, 60.96, 58.31, 57.73, 56.36, 56.33, 49.88, 49.30, 25.93, 25.22, 25.10, 23.93, 21.66, 21.63.

ESI HRMS m/z $(M+Na)^{+}$: 458.1611

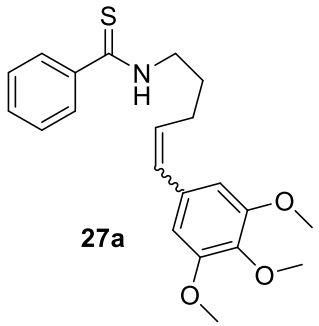


**27a**

Thioamide **27a** was prepared by placing Lawesson's Reagent (0.1198g, 0.296 mmol) in a round bottom flask. Reflux Condenser was attached. Next, the flask was placed under argon and 3 mL of THF was added. Now, **15** (0.1035g, 0.296 mmol) in 1 mL of THF was added. The reaction was refluxed for 2.5 hours. The reaction was brought to rt and washed with sat aq $NaHCO_3$ solution. Aqueous layer was extracted 3x with diethyl ether. Organic layers were combined, dried over $MgSO_4$ and concentrated in vacuo. Residue was purified by column chromatography with 1:9:0.6 to 1:4:0.3 EA:Hexane:$Et_3N$ to afford 0.0968g (88%) of compound **27a**.

$^1H$ NMR ($CDCl_3$, 500 MHz): δ 7.70 (m, 1.12H), 7.61 (m, 0.93H), 7.43 (m, 1.01H), 7.37 – 7.25 (m, 2.02H), 6.56 (s, 0.93H), 6.47 (s, 0.98H), 6.46 – 6.35 (m, 0.86H), 6.17 (dt, *J* = 15.7, 7.0 Hz, 0.54H), 5.70 – 5.59 (m, .41H) 3.95 – 3.78 (m, 11.39H), 2.53 – 2.47 (m, 0.82H), 2.42 – 2.33 (m, 1.02H), 1.95 (m, 2H).

$^{13}C$ NMR ($CDCl_3$, 125 MHz): δ 199.28, 199.13, 153.31, 153.04, 141.87, 137.53, 137.08, 133.05, 132.81, 131.07, 131.06, 131.02, 130.79, 130.38, 128.80, 128.50, 128.47, 126.55, 126.45, 105.89, 103.11, 60.92, 60.90, 56.16, 56.07, 46.52, 45.97, 30.68, 27.93, 27.77, 25.88.

IR (neat, $cm^{-1}$) 2936, 1581, 1507, 1449, 1417, 1328, 1264, 1236, 1183, 1126, 1000, 963, 842, 731, 671

ESI HRMS m/z $(M+H)^+$: 372.1630

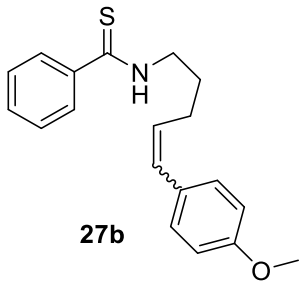


**27b**

Thioamide **27b** was prepared by placing Lawesson's Reagent (0.1376g, 0.340 mmol) in a round bottom flask. Reflux Condenser was attached. Next, the flask was placed under argon and 3 mL of THF was added. Now, **18** (0.1005g, 0.340 mmol) in 1 mL of THF was added. The reaction was refluxed for 2.5 hours. The reaction was brought to rt and washed with sat aq $NaHCO_3$ solution. Aqueous layer was extracted 3x with diethyl ether. Organic layers were combined, dried over $MgSO_4$ and concentrated in vacuo. Residue was purified by column chromatography with 1:9:0.6 to 1:4:0.3 EA:Hexane:$Et_3N$ to afford 0.0784g (74%) of compound **27b**.

$^1$H NMR ($CDCl_3$, 500 MHz): δ 7.71 – 7.65 (m, 2.07H), 7.57 – 7.55(m, 0.39H), 7.45 – 7.37 (m, 1.06H), 7.35 – 7.23 (m, 3.69H), 7.21 – 7.15 (m, 0.38H), 6.84 – 6.81 (m, 1.94H), 6.46 (d, *J* = 11.5 Hz, 0.18H), 6.40 (d, *J* = 15.8 Hz, 0.75H), 6.09 (dt, *J* = 15.8, 7.0 Hz, 0.79H), 5.59 (dt, *J* = 11.5, 7.3 Hz, 0.17H) 3.88 (m, 1.63H), 3.79 (s, 2.3H), 3.77 (s, 0.66H), 2.46 (m, 0.38H), 2.34 (m, 1.63H), 2.01 – 1.81 (m, 2H).

$^{13}$C NMR ($CDCl_3$, 125 MHz): δ 201.70, 161.58, 144.54, 133.62, 133.58, 133.18, 132.77, 132.59, 132.47, 132.31, 131.12, 131.07, 129.82, 129.72, 129.24, 129.20, 116.66, 116.43, 57.98, 57.90, 49.28, 48.62, 33.43, 30.49, 30.41, 28.32.δ

IR (neat, $cm^{-1}$) 3262, 1606, 1510, 1487, 1448, 1388, 1303, 1250, 1175, 1030, 966, 835, 802, 768, 735, 694

ESI HRMS m/z $(M+H)^+$: 312.1420

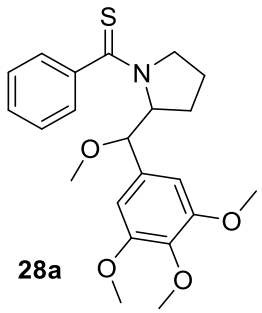

**28a**

First, (0.0858g, 0.261 mmol) of $Bu_4NBF_4$, (0.0024g, 0.013 mmol) of ferrocene was added to a three-neck flask. Now 4mL of methanol (dried overnight with molecular sieves) is added. The RVC anode and platinum plate cathode were prepared and fixed into thermometer adaptor and placed into a three-neck flask. The flask was placed under an Argon atmosphere. Next, (0.0968g, 0.261mmol) of thioamide **27a** in 4 mL of THF was added along with (0.08mL,0.13mmol) of nBuLi was added. The reaction was set at 5mA of current and the electrolysis was run until 58.3C of charge had passed (2.4F/mol). Once complete, reaction was concentrated in vacuo. Residue was purified by column chromatography with 1:9:0.1 to 1:4:0.05 to 1:1:0.2 EA:Hexane:$Et_3N$ to afford 0.0686g (66%) of compound **28a**.

$^1$H NMR (500 MHz, Chloroform-*d*) δ 7.91 – 7.83 (m, 1.54H), 7.44 – 7.37 (m, 1.32H), 7.37 – 7.30 (m, 1.94H), 6.57 (s, 2H), 4.13 (d, *J* = 6.8 Hz, 0.89H), 3.86 (s, 8.99H), 3.51 (ddd, *J* = 10.1, 6.8, 1.9 Hz, 1.06H), 3.29 (s, 2.61H), 2.26 – 2.16 (m, 0.93H), 2.13 – 2.01 (m, 1.21H), 1.94 – 1.84 (m, 1.19H), 1.82 – 1.72 (m, 1.23H).

$^{13}$C NMR (126 MHz, $cdcl_3$) δ 162.76, 153.15, 139.83, 137.77, 134.12, 130.54, 128.61, 128.51, 128.46, 128.07, 126.70, 104.69, 86.49, 60.89, 57.33, 56.15, 53.87, 49.96, 28.47, 24.42.

IR (neat, $cm^{-1}$) 2926, 1591, 1504, 1459, 1418, 1326, 1264, 1223, 1180, 1125, 1031, 1003, 946, 907, 833, 733, 694

ESI HRMS m/z $(M+H)^+$: 402.1777

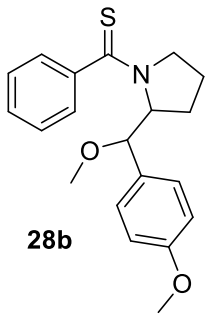


**28b**

First, (0.0830g, 0.252 mmol) of $Bu_4NBF_4$, (0.0023g, 0.013 mmol) of ferrocene was added to a three-neck flask. Now 4mL of methanol (dried overnight with molecular sieves) is added. The RVC anode and platinum plate cathode were prepared and fixed into thermometer adaptor and placed into a three-neck flask. The flask was placed under an Argon atmosphere. Next, (0.0784g, 0.252mmol) of thioamide **27a** in 4 mL of THF was added along with (0.08mL,0.13mmol) of nBuLi was added. The reaction was set at 5mA of current and the electrolysis was run until 58.3C of charge had passed (2.4F/mol). Once complete, reaction was concentrated in vacuo. Residue was purified by column chromatography with 1:9:0.1 to 1:4:0.05 EA:Hexane:$Et_3N$ to afford 0.0576g (68%) of compound **28b**.

$^1$H NMR (500 MHz, Chloroform-*d*) δ 7.85 (d, *J* = 7.0 Hz, 1.79H), 7.42 – 7.27 (m, 5.5H), 6.91 (d, *J* = 8.7 Hz, 1.89H), 4.20 – 4.09 (m, 1.13H), 4.08 – 3.92 (m, 2.18H), 3.81 (s, 3H), 3.56 (ddd, *J* = 10.1, 7.2, 1.7 Hz, 0.99H), 3.22 (s, 2.76H), 2.32 – 2.23 (m, 1.02H), 2.12 – 2.00 (m, 1.05H), 1.89 – 1.68 (m, 2.53H).

$^{13}$C NMR (126 MHz, $cdcl_3$) δ 165.54, 162.26, 142.48, 133.11, 133.05, 131.81, 131.31, 130.70, 116.33, 88.64, 59.55, 57.91, 56.33, 52.65, 30.97, 27.27.

IR (neat, $cm^{-1}$) 2929, 1608, 1594, 1573, 1509, 1444, 1302, 1245, 1203, 1172, 1082, 1030, 966, 933, 903, 733, 694, 662, 628, 573

ESI HRMS m/z $(M+H)^+$: 342.1567

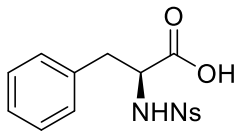


**30**

First, (3.300g, 20 mmol) of phenylalanine was added to a round-bottom flask. Next, 50 mL of di$H_2O$ was added and the flask was placed in an ice-bath. Now, (2.544g, 24 mmol) of sodium carbonate was added to the stirring flask. Finally, (5.319g, 24 mmol) of 4-NsCl was added portionwise over 1 hour. The reaction was left to stir to rt overnight. The reaction was acidified to pH=2 and extracted 3x with EA. The organic layers were combined, dried over $MgSO_4$ and concentrated in vacuo to yield 6.274g of **30** (90%) which was used without further purification.

$^1$H NMR (500 MHz, DMSO-$d_6$) δ 12.89 (s, 1.00H), 8.74 (d, $J$ = 9.0 Hz, 0.99H), 8.21 (d, $J$ = 8.9 Hz, 1.71H), 7.76 (d, $J$ = 8.9 Hz, 1.73H), 7.12 (m, 4.19H), 3.98 (td, $J$ = 9.3, 4.8 Hz, 1.17H), 3.00 (dd, $J$ = 13.8, 4.9 Hz, 1.07H), 2.73 (dd, $J$ = 13.8, 9.9 Hz, 1.02H).

$^{13}$C NMR (126 MHz, dmso) δ 172.04, 149.01, 146.55, 136.58, 129.10, 128.01, 127.55, 126.29, 124.03, 57.56, 37.49.

ESI HRMS m/z $(M+H)^+$: 351.0630

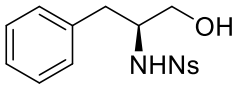


**31**

First, the reaction was placed under an Argon atmosphere. Next, (6.756g, 19.3 mmol) of **30** was added to a round-bottom flask. Next, 70mL of THF was added and the flask was placed in an ice-bath. Now, (4.5mL, 48.3 mmol) of borane dimethylsulfide was added to the stirring flask dropwise. The reaction was left to stir to rt overnight. The reaction was quenched at 0°C with a sat aq $K_2CO_3$ solution and extracted 3x with EA. The organic layers were combined, dried over $MgSO_4$ and concentrated in vacuo. The crude mixture was purified via column chromatography eluting with 1:2 to 1:1 EA:Hexanes to yield 3.921g of **31** (60%).

$^1$H NMR (500 MHz, Acetone-$d_6$) δ 8.20 (d, $J$ = 8.8 Hz, 2H), 7.86 (d, $J$ = 8.8 Hz, 1.97H), 7.17 – 7.02 (m, 4.84H), 6.86 (d, $J$ = 7.7 Hz, 1.09H), 3.68 – 3.44 (m, 2.80H), 2.98 (dd, $J$ = 13.8, 5.2 Hz, 1.13H), 2.67 (dd, $J$ = 13.8, 8.3 Hz, 1.0H).

$^{13}$C NMR (126 MHz, acetone) δ 152.22, 150.01, 140.93, 131.95, 130.82, 130.50, 128.70, 126.77, 126.68, 66.90, 60.74, 40.21.

ESI HRMS m/z $(M+H)^+$: 337.0843

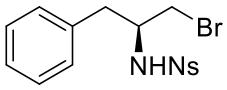


**32**

First, (1.158g, 4.4 mmol) of triphenylphosphine was added to a round-bottom flask. The reaction was placed under Argon. Next, (0.9896g, 2.94 mmol) of **31** in 15 mL of THF was added and the flask was placed in an ice-bath. Now, (1.464g, 4.4 mmol) of carbon tetrabromide in 6 mL of THF

was added dropwise in 3 portions over 15 minutes. The reaction was left to stir at 0ºC for 2.5h. The reaction was concentrated in vacuo. A plug column was used eluting with THF which was then concentrated in vacuo. The crude mixture was purified via column chromatography eluting with 1:19 to 1:9 to 1:4 to 1:1 EA:Hexanes to yield 0.9149g of **32** (77%).

$^{1}$H NMR (500 MHz, Acetone-$d_6$) δ 8.18 (d, $J$ = 8.8 Hz, 2.0H), 7.82 (d, $J$ = 8.9 Hz, 2.07H), 7.25 (d, $J$ = 8.0 Hz, 1.11H), 7.17 – 6.81 (m, 5.39H), 3.86 – 3.81 (m, 1.14H), 3.63 (d, $J$ = 4.6 Hz, 2.46H), 3.00 (dd, $J$ = 13.9, 5.2 Hz, 1.19H), 2.76 (dd, $J$ = 13.9, 8.9 Hz, 1.17H).

$^{13}$C NMR (126 MHz, acetone) δ 152.32, 149.28, 139.72, 131.92, 131.90, 131.02, 130.99, 130.50, 130.48, 129.13, 126.83, 59.05, 41.48, 40.80.

ESI HRMS m/z $(M+H)^+$: 400.9975

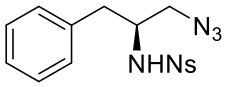


**33**

First, (0.8503g, 13.1 mmol) of sodium azide was added to a round-bottom flask. The reaction was placed under Argon. Next, (1.305g, 3.27 mmol) of **32** in 33mL of acetonitrile was added and the flask was heated to 70ºC in an oil bath overnight. After stirring overnight, the reaction was brought to room temperature and diluted with EA which was then washed with di$H_2O$ (2x) and brine (1x). The organic layers were combined, dried over $MgSO_4$ and concentrated in vacuo to yield 1.120g **33** (95%) which was used without further purification.

$^{1}$H NMR (500 MHz, Acetone-$d_6$) δ 8.19 (d, $J$ = 8.9 Hz, 2.0H), 7.85 (d, $J$ = 8.9 Hz, 1.7H), 7.08 (m, 5.50H), 3.76 – 3.71 (bs, 0.95H), 3.55 (dd, $J$ = 12.5, 4.8 Hz, 0..77H), 3.46 (dd, $J$ = 12.5, 5.1 Hz, 0.82H), 2.88 (dd, $J$ = 13.9, 5.6 Hz, 0.84H), 2.73 (dd, $J$ = 13.8, 8.8 Hz, 0.81H).

$^{13}$C NMR (126 MHz, acetone) δ 152.31, 149.58, 139.93, 131.93, 130.99, 130.48, 129.07, 129.06, 126.81, 58.59, 58.00, 40.92.

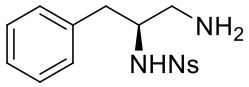


**34**

Compound **34** was prepared by placing triphenylphosphine (2.032g, 7.75 mmol) in a round bottom flask. Reflux Condenser was attached. Next, the flask was placed under argon and (1.120g, 3.10 mmol) of **33** in 21 mL of THF was added. Now, (0.28 mL, 15.5 mmol) of water was added. The reaction was refluxed for 5 hours. The reaction was brought to rt concentrated in vacuo. solution. Residue was purified by column chromatography with 1:19:0.2 to 1:9:0.1 MeOH:DCM:$Et_3N$ to afford 0.6853g (66%) of compound **34**.

$^1$H NMR (500 MHz, Acetone-$d_6$) δ 8.24 (d, $J$ = 8.9 Hz, 2.0H), 7.92 (d, $J$ = 8.9 Hz, 2.03H), 7.12 (m, 5.38H), 3.74 (m, 1.13H), 3.29 (dd, $J$ = 14.5, 4.5 Hz, 1.14H), 3.20 (dd, $J$ = 14.4, 6.0 Hz, 1.19H), 2.96 (dd, $J$ = 13.6, 6.3 Hz, 1.74H), 2.90 (bs, 1.49H), 2.76 (dd, $J$ = 13.7, 8.0 Hz, 1.25H).

$^{13}$C NMR (126 MHz, $cdcl_3$) δ 155.43, 146.38, 137.19, 136.00, 135.82, 133.87, 131.91, 64.91, 62.45, 47.00.

ESI HRMS m/z $(M+H)^+$: 336.0991

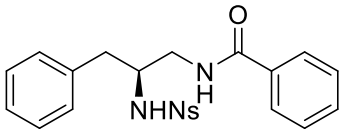


**35**

First, (0.1343g, 1.10 mmol) of benzoic acid was added to a round-bottom flask along with (0.2300g, 1.20 mmol) of EDC. The reaction was placed under Argon and 5 mL of DCM was added.

The flask was placed in an ice-bath. Next, (0.12mL, 1.10 mmol) of NMM was added. Finally, (0.3350g, 0.999 mmol) of **34** in 5mL of DCM was added and the flask was allowed to stir to rt overnight. After stirring overnight, the reaction was diluted with DCM and washed with sat aq $NaHCO_3$ solution. The aqueous layer was extracted 2x with DCM. The organic layers were combined, dried over $MgSO_4$ and concentrated in vacuo. The crude mixture was purified with column chromatography using 1:2 EA:Hexanes as eluent to yield 0.3874g (88%) **35**.

$^1$H NMR (500 MHz, Acetone-$d_6$) δ 8.02 (d, $J$ = 8.9 Hz, 2.0H), 7.85 (d, $J$ = 8.8 Hz, 2.29H), 7.82 (s, 1.38H), 7.78 – 7.68 (m, 2.11H), 7.49 (t, $J$ = 7.4 Hz, 1.14H), 7.42 – 7.38 (m, 2.25H), 7.22 – 7.09 (m, 6.32H), 3.88 – 3.73 (m, 1.31H), 3.62 – 3.50 (m, 1.38H), 3.47 – 3.40 (m, 1.42H), 3.01 – 2.85 (m, 2.86H).

$^{13}$C NMR (126 MHz, acetone) δ 167.27, 167.24, 167.24, 149.36, 146.75, 137.75, 134.16, 133.65, 131.44, 129.41, 128.29, 128.20, 128.17, 127.81, 127.07, 127.05, 126.31, 124.05, 57.06, 43.43, 39.98.

ESI HRMS m/z $(M+2H)^+$:441.1294

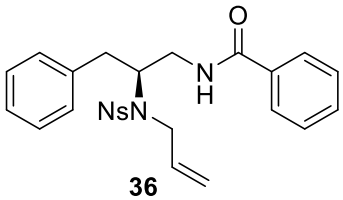


**36**

First, (0.0128g, 0.532 mmol) of NaH (60% dispersion) was added to a round-bottom flask. The reaction was placed under Argon. Next, 2mL of DMF was added. Now, (0.1170g, 0.266 mmol) of **35** in 2.5 mL of DMF was added and the flask was placed in an ice-bath and stirred for 30 minutes. Finally, allyl bromide (0.035mL, 0.399 mmol) was added dropwise. Reaction was left to stir to rt

overnight. After stirring overnight, the reaction was quenched with water. The aqueous layer was extracted 2x with EA. The organic layers were combined, dried over $MgSO_4$ and concentrated in vacuo. The crude mixture was purified with column chromatography using 1:9 to 1:6 1:4 to 1:2 EA:Hexanes as eluent to yield 0.0594g (47%) **36**.

$^1$H NMR (500 MHz, Chloroform-*d*) δ 8.05 (d, *J* = 8.8 Hz, 2.0H), 7.81 – 7.73 (m, 2.08H), 7.65 (d, *J* = 8.9 Hz, 2.05H), 7.53 – 7.46 (m, 1.08H), 7.45 – 7.38 (m, 2.12H), 7.23 – 7.14 (m, 3.12H), 7.05 – 6.98 (m, 2.18H), 6.69 (bs, 1.07H), 5.84 (dddd, *J* = 17.4, 10.1, 7.6, 5.6 Hz, 1.04H), 5.36 (dd, *J* = 17.1, 1.3 Hz, 1.11H), 5.22 (dd, *J* = 10.0, 1.2 Hz, 1.15H), 4.44 – 4.37 (m, 1.08H), 4.09 – 4.03 (m, 1.13H), 4.02 – 3.92 (m, 1.12H), 3.81 – 3.67 (m, 1.12H), 3.65 – 3.46 (m, 1.11H), 2.96 – 2.71 (m, 2.25H).

$^{13}$C NMR (126 MHz, cdcl$_3$) δ 169.99, 169.96, 152.26, 148.80, 139.59, 137.10, 134.38, 131.64, 131.53, 131.28, 131.25, 130.75, 129.71, 129.59, 129.57, 126.75, 62.83, 49.51, 44.33, 40.44.

ESI HRMS m/z $(M+2H)^+$: 481.1592

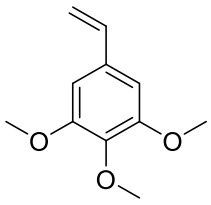


**38**

First, (3.254 g, 8.0 mmol) of methyl triphenylphosphonium iodide was added to a round-bottom flask. The reaction was placed under Argon. Next, 60mL of THF of was added. The flask was placed in a dry ice-acetone bath. Now, (5mL, 8.0 mmol) of nBuLi was added dropwise over 5 minutes. Reaction was allowed to stir at rt for 30 minutes. Flask was placed back in dry ice-acetone

bath. Finally, syringaldehyde (1.432g, 7.3mmol) in 15 mL of THF was added dropwise in 3 portions over 15 minutes. The reaction was allowed to stir to rt over 2 hours. After 2h, the reaction was quenched with sat aq $NH_4Cl$ and extracted 3x with diethyl ether. The organic layers were combined, dried over $MgSO_4$ and concentrated in vacuo. The crude mixture was purified with column chromatography using 1:9 to 1:4 to 1:2 EA:Hexanes as eluent to yield 0.9132g (64%) of **38**.

$^1H$ NMR ($CDCl_3$, 500 MHz): δ δ 6.63 (t, J = 12.0 Hz, 3H), 5.65 (d, J = 20.0 Hz, 1H), 5.20 (d, J = 12.0 Hz, 1H), 3.87 (2s, 9H

$^{13}C$ NMR (126 MHz, cdcl$_3$) δ 155.87, 139.38, 135.87, 115.60, 105.89, 63.25, 58.48.

ESI HRMS m/z $(M+H)^+$: 195.1009

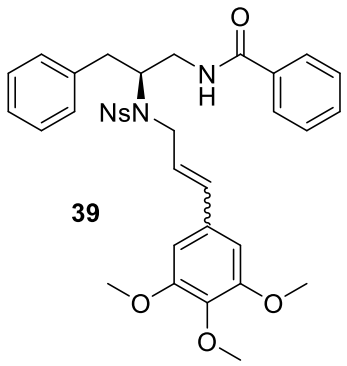


**39**

First, (0.0339g, 0.0707 mmol) of **36** in 1mL of DCM was added to a round-bottom flask. The reflux condenser was attached to the flask and the reaction was placed under Argon. Next, (0.0412g, 0.212 mmol) of **38** in 1mL of DCM was added. Finally, (0.0036g, 0.00434mmol) of Grubbs Gen 2 in 0.5mL of DCM was added. The reaction was refluxed for 2 days. After stirring for two days, the reaction was brought to room temperature and concentrated in vacuo. Residue

was purified by column chromatography using 1:9:0.06 to 1:4:0.03 to 1:2:0.018 to 1:1:0.012 EA:Hexanes:$Et_3N$ to yield 0.0252g (55%) of **39**.

$^1$H NMR (500 MHz, Chloroform-*d*) δ 8.00 (d, *J* = 8.8 Hz, 1.01H), 7.76 – 7.65 (m, 1.52H), 7.64 (d, *J* = 8.8 Hz, 1.05H), 7.48 (t, *J* = 7.4 Hz, 0.52H), 7.39 (t, *J* = 7.6 Hz, 1.04H), 7.19 (d, *J* = 7.2 Hz, 1.52H), 7.11 – 7.05 (m, 1.06H), 6.94 (s, 0.46H), 6.74 (m, 1.36H), 6.54 (d, *J* = 15.8 Hz, 0.52H), 6.48 (s, 0.98H), 5.99 (m, 0.49H), 4.52 – 4.44 (m, 0.52H), 4.28 – 4.19 (m, 1H), 3.93 – 3.78 (4s, 9H), 3.57 – 3.49 (m, 1H), 2.95 – 2.83 (m, 2H).

$^{13}$C NMR (126 MHz, cdcl$_3$) δ 169.93, 169.90, 156.08, 156.03, 152.16, 148.95, 139.62, 136.81, 135.60, 134.38, 134.02, 131.71, 131.52, 131.25, 131.21, 130.79, 130.77, 129.75, 129.55, 129.53, 127.00, 126.68, 106.28, 106.19, 63.63, 63.56, 63.04, 62.70, 58.79, 58.72, 48.97, 44.46, 40.51, 23.70, 16.86.

ESI HRMS m/z $(M+2H)^+$: 647.2230

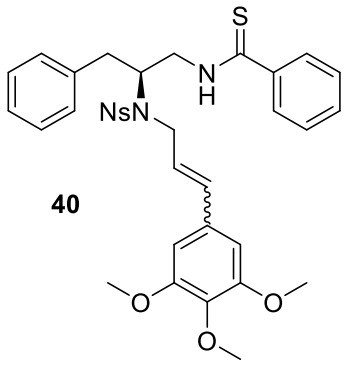


**40**

Thioamide **40** was prepared by placing Lawesson's Reagent (0.0127g, 0.0313 mmol) in a round bottom flask. Reflux Condenser was attached. Next, the flask was placed under argon. Now, **39** (0.0202g, 0.0313 mmol) in 3 mL of THF was added. The reaction was refluxed for 2.5 hours. The reaction was brought to rt and washed with sat aq $NaHCO_3$ solution. Aqueous layer was extracted

3x with diethyl ether. Organic layers were combined, dried over $MgSO_4$ and concentrated in vacuo. Residue was purified by column chromatography with 1:9:0.01 to 1:4:0.05 to 1:2:0.03 to 1:1:0.02 EA:Hexane:$Et_3N$ to afford 0.0132g (64%) of compound **40**.

$^1H$ NMR (500 MHz, Chloroform-*d*) δ 8.39 (bs, 0.85H), 8.08 (d, *J* = 8.8 Hz, 2.10H), 7.85 – 7.77 (m, 2.15H), 7.70 (d, *J* = 8.8 Hz, 2.20H), 7.45 (t, *J* = 7.4 Hz, 1.11H), 7.35 (t, *J* = 7.6 Hz, 2.18H), 7.23 – 7.10 (m, 3.43H), 7.06 – 6.95 (m, 2.25H), 6.58 (d, *J* = 15.7 Hz, 1.06H), 6.47 (s, 2.28H), 5.99 (ddd, *J* = 15.6, 7.8, 5.8 Hz, 1.11H), 4.62 – 4.52 (m, 1.08H), 4.39 – 4.20 (m, 2.24H), 4.16 – 4.06 (m, 1.57H), 3.83 (s, 3H), 3.77 (s, 6H), 2.94 (dd, *J* = 14.2, 6.3 Hz, 1.09H), 2.85 (dd, *J* = 14.2, 8.4 Hz, 1.16H).

$^{13}C$ NMR (126 MHz, cdcl$_3$) δ 201.81, 155.98, 152.42, 148.37, 146.85, 139.02, 137.39, 134.05, 133.86, 131.61, 131.57, 131.16, 131.12, 130.74, 129.89, 129.46, 129.43, 126.87, 126.42, 106.43, 63.56, 61.52, 58.76, 51.57, 40.14.

ESI HRMS m/z $(M+H)^+$:

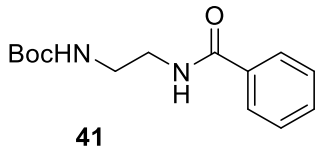


**41**

The reaction was placed under Argon. Then *N*-Boc-ethylenediamine (0.95mL, 6.0 mmol) in 15 mL DCM was added. The reaction was stirred at rt. Now, (1.25mL, 9.0 mmol) triethylamine was added. Finally, benzoyl chloride (0.84mL, 7.2 mmol) in 12mL DCM was added slowly. The reaction stirred at room temperature overnight. Then the organic mixture was washed with water, extracted 3x with DCM. The organic layers were combined, dried with $MgSO_4$ and concentrated

in vacuo. Crude product was chromatographed through silica gel using 1:1 EA:Hexanes as eluent to afford benzoylated product **41** in 90 % yield.

$^{1}$H NMR (500 MHz, Acetone-$d_6$) δ 7.89 (d, $J$ = 7.4 Hz, 2.64H), 7.53 – 7.48 (m, 0.85H), 7.44 (m, 1.76H), 6.26 (bs, 0.80H) 3.49 (q, $J$ = 5.8 Hz, 2.0H), 3.32 (q, $J$ = 6.0 Hz, 2.0H), 1.40 (s, 9H).

$^{13}$C NMR (126 MHz, acetone) δ 166.67, 156.46, 134.95, 130.98, 128.19, 127.06, 77.96, 40.52, 40.11, 27.71.

ESI HRMS m/z $(M+H)^+$: 265.1539

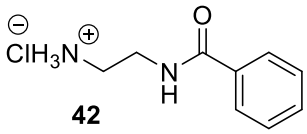


**42**

The reaction was placed under Argon. Then **41** (1.386g, 5.25 mmol) in 29 mL EA was added and the reaction was stirred at room temperature. 4N HCl was prepared by adding 13.2 mL concentrated HCl to 26.8 mL diethyl ether which was then added to the stirring solution of **41**. The reaction was allowed to stir at room temperature overnight. The reaction was then concentrated in vacuo until ~80% of the solvent was removed. Benzene was added and the solvent was removed in vacuo to yield 1.054 g of **42** which was carried forward to the next step crude.

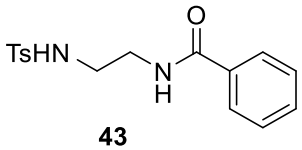


**43**

First, (1.054g, 5.25 mmol) of **42** was added to a round-bottom flask. The reaction was placed under Argon. Next, 18 mL DCM was added. Now, (5.1mL, 36.8 mmol) of triethylamine was added. The flask was placed in an ice-bath. Finally, (1.502g, 7.9 mmol) of TsCl was added to the stirring

solution at 0ºC. The reaction was stirred for 15 min at 0ºC before removing the ice-bath and stirring at room temperature overnight. The reaction was quenched with sat aq $NaHCO_3$ solution. Aqueous layer was extracted 2x with DCM. The organic layers were combined, dried with $MgSO_4$ and concentrated in vacuo. Crude product was chromatographed through silica gel using 1:3 to 1:2 to 1:1 EA:Hexanes as eluent to afford tosylated product **43** in 63 % yield over two steps.

$^1$H NMR (500 MHz, Methanol-$d_4$) δ 7.80 – 7.74 (m, 2H), 7.72 – 7.68 (m, 2H), 7.52 – 7.45 (m, 1H), 7.44 – 7.37 (m, 2H), 7.31 – 7.23 (m, 2H), 3.44 (t, $J$ = 6.3 Hz, 2H), 3.08 (t, $J$ = 6.3 Hz, 2H), 2.33 (s, 3H).

$^{13}$C NMR (126 MHz, $cd_3od$) δ 168.97, 143.27, 137.34, 133.92, 131.34, 129.38, 128.13, 126.91, 126.60, 41.96, 39.65, 20.12.

ESI HRMS m/z $(M+H)^+$: 319.1103

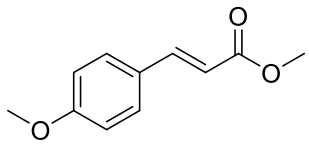

**47**

First, (5.015g, 15.0 mmol) of Methyl (triphenylphosphoranylidene)acetate was added to a round-bottom flask. The reflux condenser was attached to the flask and the reaction was placed under Argon. Next, 10 mL of THF was added. Now para-anisaldehyde (1.2mL, 10.0 mmol) was added and the reaction was refluxed overnight. The reaction was brought to room temperature and the reaction was concentrated in vacuo. The crude product was purified via column chromatography using 1:9 EA:Hexanes as the eluent to afford 1.903g of **47** (99%).

$^{1}$H NMR (500 MHz, Chloroform-*d*) δ 7.65 (d, *J* = 16.0 Hz, 1H), 7.46 (d, *J* = 8.6 Hz, 2H), 6.89 (d, *J* = 8.8 Hz, 2H), 6.31 (d, *J* = 16.0 Hz, 1H), 3.82 (s, 3H), 3.79 (s, 3H).

$^{13}$C NMR (126 MHz, cdcl$_3$) δ 167.71, 161.36, 144.49, 129.69, 127.08, 115.24, 114.29, 55.33, 51.53.

ESI HRMS m/z $(M+H)^+$: 193.0850

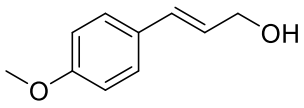


**48**

First, (0.1123g, 2.96 mmol) of solid $LiAlH_4$ was added to a round-bottom flask. The reaction was placed under Argon. Now, 10 mL of THF was added. The flask was placed in an ice-bath. Next, (0.4556g, 2.37 mmol) of **47** in 8 mL of THF was added. The reaction was stirred for 2h at 0ºC. The reaction was quenched with sat aq $NH_4Cl$ and extracted 2x with EA. The organic layers were combined, dried with $MgSO_4$ and concentrated in vacuo. The crude product was purified via column chromatography using 1:4 EA:Hexanes as the eluent to afford 0.2235g of **48** (57%). Data consistent with the literature.[20]

$^{1}$H NMR (500 MHz, Chloroform-*d*) δ 7.29 (d, *J* = 8.7 Hz, 2H), 6.84 (d, *J* = 8.8 Hz, 2H), 6.52 (d, *J* = 15.9 Hz, 1H), 6.20 (dt, *J* = 15.8, 5.9 Hz, 1H), 4.26 (dd, *J* = 5.9, 1.5 Hz, 1H), 3.78 (s, 3H).

$^{13}$C NMR (126 MHz, cdcl$_3$) δ 159.22, 130.72, 129.48, 127.63, 126.35, 113.98, 63.71, 55.25.

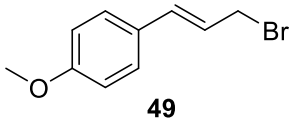


**49**

The reaction was placed under Argon. Then **48** (0.2146g, 1.31 mmol) in 6.6 mL diethyl ether was added and the flask was placed in an ice-bath. Now, (0.12mL, 1.31 mmol) of $PBr_3$ was added and the reaction was stirred at 0ºC for 1h. The reaction was quenched with sat aq $NaHCO_3$ solution and extracted 2x with diethyl ether. The organic layers were combined, dried with $MgSO_4$ and concentrated in vacuo to yield 0.2071 g of product **49** (70% crude yield). Chromatography of this product risks bromide decomposition. So it was avoided. The proton NMR of the crude product matched the previously reported data.[21]

$^1$H NMR (500 MHz, Chloroform-*d*) δ 7.33 (d, *J* = 8.7 Hz, 2H), 6.87 (d, *J* = 8.8 Hz, 2H), 6.60 (d, *J* = 15.5 Hz, 1H), 6.27 (dt, *J* = 15.6, 7.9 Hz, 1H), 4.19 – 4.14 (m, 2H), 3.81 (s, 3H).

$^{13}$C NMR (126 MHz, cdcl$_3$) δ 159.82, 134.22, 128.54, 128.07, 122.98, 114.09, 55.31, 34.24.

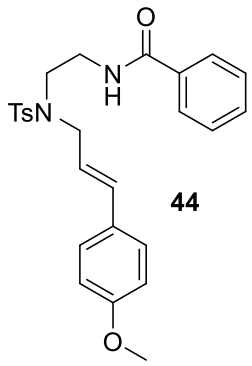


**44**

First, (0.1313g, 0.95 mmol) of potassium carbonate was added to a round-bottom flask. The reflux condenser was attached to the flask and the reaction was placed under Argon. Now (0.2006g, 0.63 mmol) of **43** in 3 mL acetone (dried overnight with molecular sieves) was added to the flask. Next, (0.2163g, 0.95 mmol) of **49** in 3 mL acetone was added. The reaction was refluxed overnight. After refluxing overnight, the reaction was brought to room temperature and concentrated in vacuo. The crude product was purified via column chromatography using 1:4 to 1:2 EA:Hexanes with 1% $Et_3N$ as the eluent to afford 0.1812g of **44** (62%).

$^{1}$H NMR (500 MHz, Chloroform-*d*) δ 7.82 (d, *J* = 1.5 Hz, 2.11H), 7.70 (d, *J* = 8.3 Hz, 2.36H), 7.45 – 7.29 (m, 4.5H), 7.23 (d, *J* = 8.0 Hz, 2.68H), 7.12 (d, *J* = 8.8 Hz, 2.60H), 6.76 (d, *J* = 8.7 Hz, 2.37H), 6.39 (d, *J* = 15.8 Hz, 1H), 5.80 (dt, *J* = 15.8, 6.9 Hz, 1H), 4.00 - 3.96 (m, 1.91H), 3.73 (s, 3.54H), 3.62 – 3.56 (m, 1.92H), 3.42 – 3.34 (m, 2.20H), 2.35 (s, 3.08H).

$^{13}$C NMR (126 MHz, cdcl$_3$) δ 167.64, 159.49, 143.65, 136.32, 134.10, 131.37, 129.85, 129.62, 129.42, 128.68, 128.45, 128.41, 128.32, 127.73, 127.42, 127.21, 127.12, 127.10, 127.03, 126.91, 120.92, 114.03, 113.96, 113.93, 55.23, 51.35, 46.45, 39.02, 21.46.

ESI HRMS m/z $(M+H)^+$: 465.1826

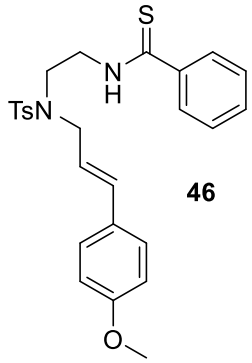


**46**

Thioamide **46** was prepared by placing Lawesson's Reagent (0.1578, 0.39 mmol) in a round bottom flask. Reflux Condenser was attached. Next, the flask was placed under argon. Now, 1.5 mL THF was added to the flask. Next, **39** (0.1812g, 0.39 mmol) in 1.5 mL of THF was added. The reaction was refluxed for 2.5 hours. The reaction was brought to rt and washed with sat aq $NaHCO_3$ solution. Aqueous layer was extracted 3x with diethyl ether. Organic layers were combined, dried over $MgSO_4$ and concentrated in vacuo. Residue was purified by column chromatography with 1:4 to 1:2 EA:Hexanes with 1% $Et_3N$ to yield 0.1238g (66%) of compound **46**.

$^{1}$H NMR (500 MHz, Chloroform-*d*) δ 8.75 (bs, 0.76H), 7.92 – 7.86 (m, 1.58H), 7.72 (d, *J* = 8.3 Hz, 1.80H), 7.48 – 7.41 (m, 0.92H), 7.40 – 7.27 (m, 3.46H), 7.16 (d, *J* = 8.8 Hz, 1.70H), 6.80 (d, *J* = 8.8 Hz, 1.70H), 6.43 (d, *J* = 15.8 Hz, 0.71H), 5.78 (dt, *J* = 15.7, 7.0 Hz, 0.70H), 4.03 – 3.97 (m, 1.39H), 3.98 – 3.90 (m, 1.43H), 3.78 (s, 2.68H), 3.52 – 3.46 (m, 1.57H), 2.42 (s, 2.68H).

$^{13}$C NMR (126 MHz, cdcl$_3$) δ 199.06, 159.64, 144.01, 140.79, 135.94, 134.70, 131.20, 131.18, 129.99, 129.88, 128.51, 128.43, 128.37, 127.83, 127.25, 127.00, 126.96, 126.94, 126.92, 120.31, 114.03, 55.31, 51.63, 45.80, 45.17, 21.55.

IR (neat, cm$^{-1}$) 2950, 1509, 1329, 1303, 1246, 1152, 1088, 1030, 952, 812, 730, 693, 651, 545

ESI HRMS m/z (M+H)$^{+}$: 481.1590

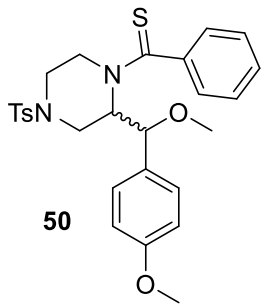


**50**

First, (0.0428g, 0.13 mmol) of $Bu_4NBF_4$, (0.00118g, 0.0065 mmol) of $Cu(OAc)_2$ was added to a three-neck flask. Now 4mL of methanol (dried overnight with molecular sieves) is added. The RVC anode and platinum plate cathode were prepared and fixed into thermometer adaptor and placed into a three-neck flask. The flask was placed under an Argon atmosphere. Next, (0.0619g, 0.13mmol) of thioamide **46** in 4 mL of THF was added along with (0.04mL,0.065mmol) of nBuLi was added. The reaction was set at 5mA of current and the electrolysis was run until 58.3C of charge had passed (2.4F/mol). Once complete, reaction was concentrated in vacuo. Residue was

purified by column chromatography with 1:4 to 1:2 EA:Hexane with 1%$Et_3N$ to afford 0.0381g (58%) of compound **50**.

$^1$H NMR (500 MHz, Chloroform-*d*) δ 7.98 (d, *J* = 7.1 Hz, 1.18H), 7.80 (d, *J* = 7.2 Hz, 0.55H), 7.47 – 7.34 (m, 3.64H), 7.31 – 7.16 (m, 4.91H) 7.11 – 7.05 (m, 1.94H), 6.95 (d, *J* = 8.7 Hz, 1.94H), 4.58 – 4.43 (m, 0.93H), 4.41 (d, *J* = 5.1 Hz, 0.62H), 4.26 (d, *J* = 5.0 Hz, 0..30H), 4.21 – 4.15 (m, 0.98H), 4.09 – 4.01 (m, 1.27H), 3.86 (s, 0.81H), 3.86 (s, 1.81H), 3.84 – 3.71 (m, 2.30H), 3.57 – 3.40 (m, 1.40H), 3.28 (s, 1.06H), 3.19 (s, 2.20H), 3.04 – 2.82 (m, 1.89H), 2.35 (s, 1.78H), 2.33 (s, 0.81H).

$^{13}$C NMR (126 MHz, cdcl$_3$) δ 162.09, 159.49, 143.23, 143.10, 139.87, 135.65, 131.20, 130.59, 130.49, 130.42, 129.99, 129.55, 129.46, 128.96, 128.87, 128.46, 128.43, 128.40, 128.24, 128.11, 128.05, 127.82, 127.50, 127.27, 127.13, 127.07, 126.95, 120.27, 114.05, 113.84, 113.73, 84.55, 84.30, 60.39, 57.41, 57.28, 57.20, 55.90, 55.38, 55.35, 55.31, 54.31, 53.57, 50.34, 49.34, 48.97, 30.32, 29.70, 21.48, 14.20.

IR (neat, cm$^{-1}$) 2953, 1510, 1337, 1247, 1153, 1089, 1030, 1006, 894, 811, 733, 655, 547

ESI HRMS m/z $(M+H)^+$: 511.1690

## 5.5.3 $^{1}H$ and $^{13}C$ NMR Spectra

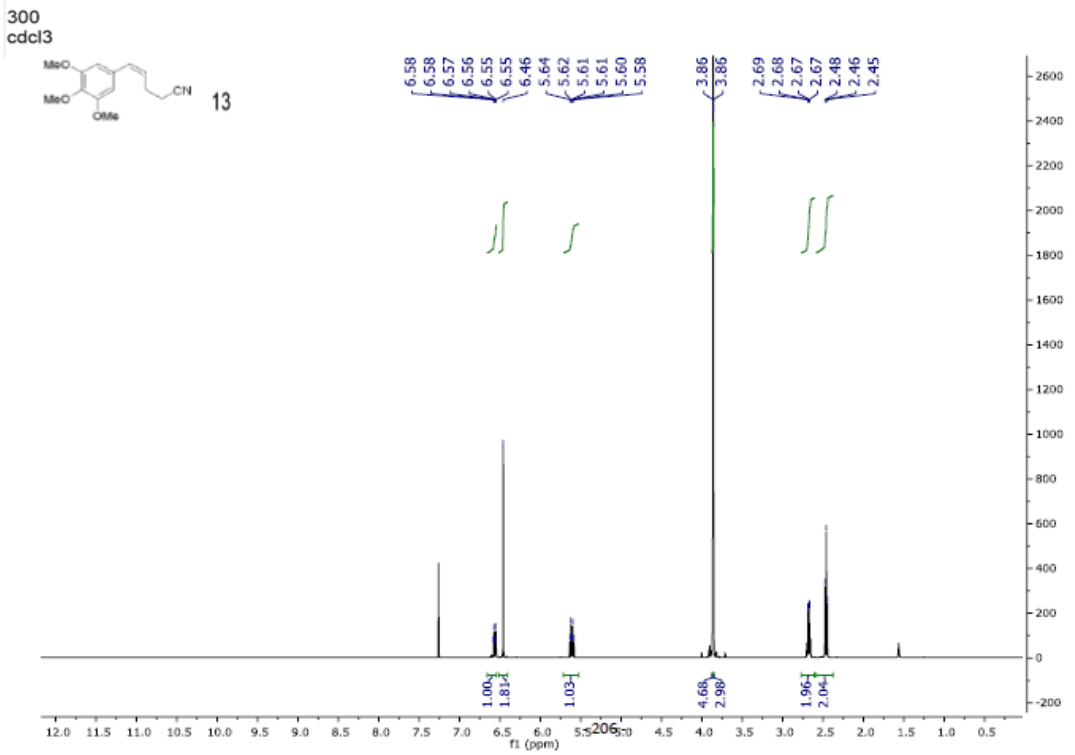


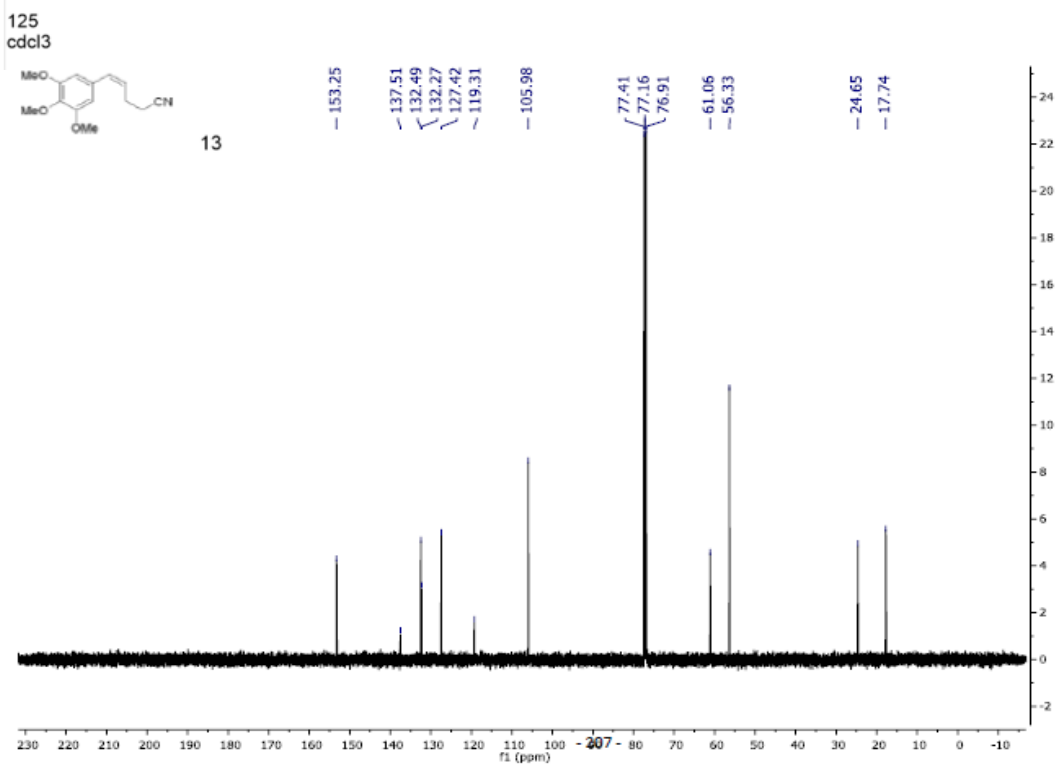

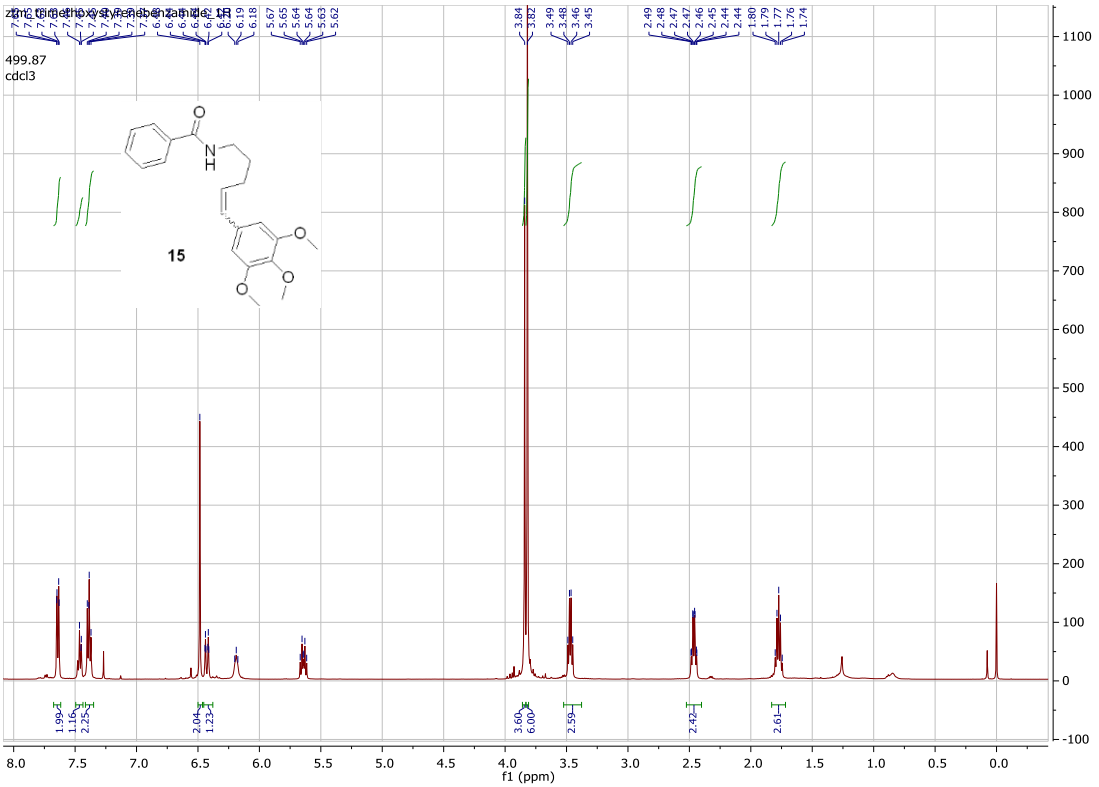
499.87
cdcl3
15
f1 (ppm)

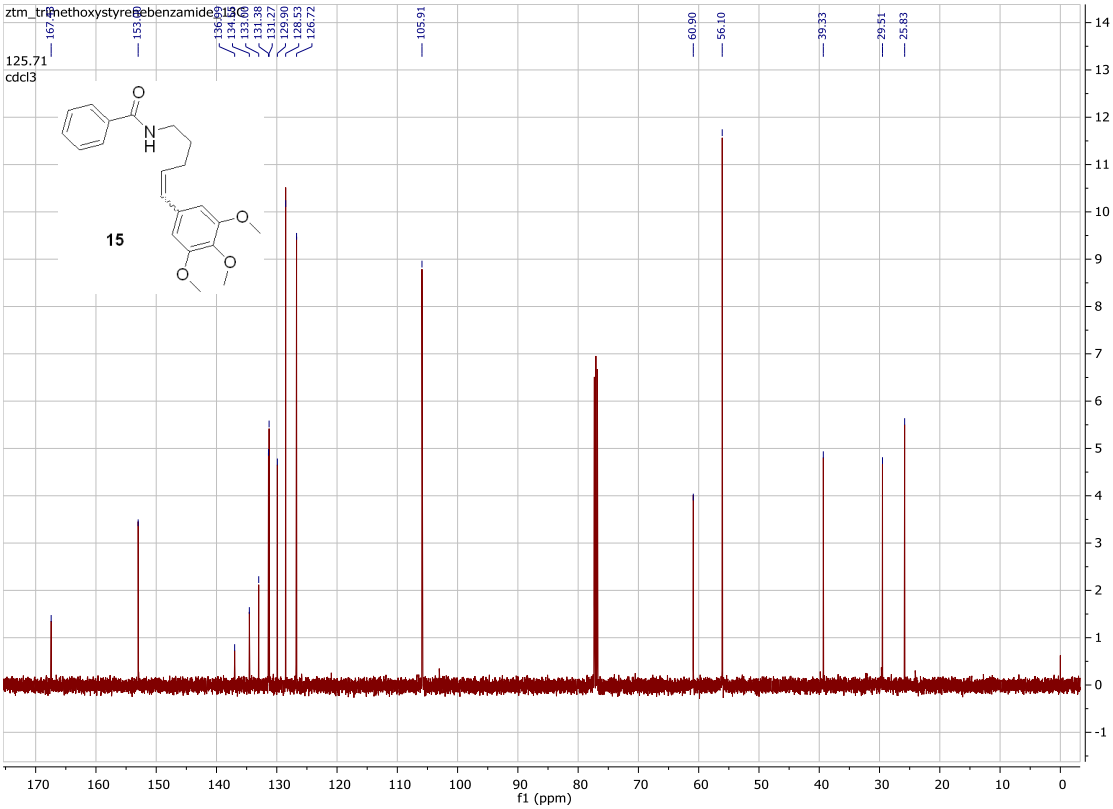
125.71
cdcl3
15
f1 (ppm)

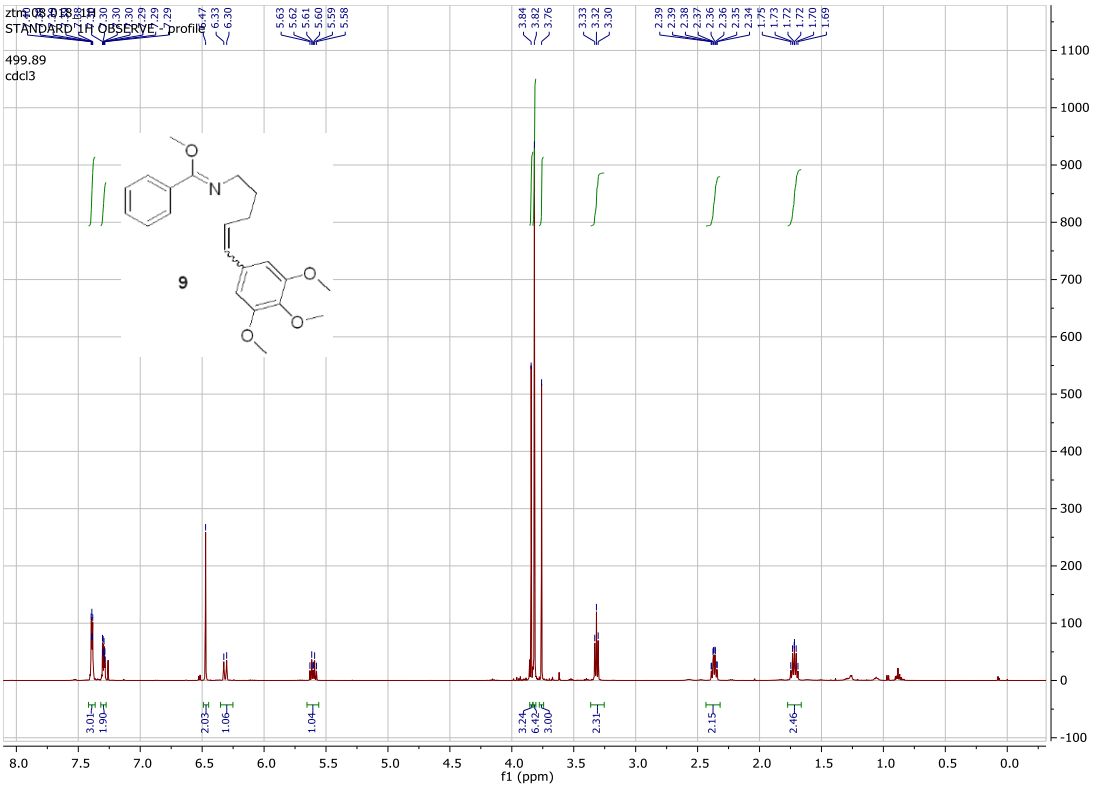
499.89
cdcl3
9
f1 (ppm)

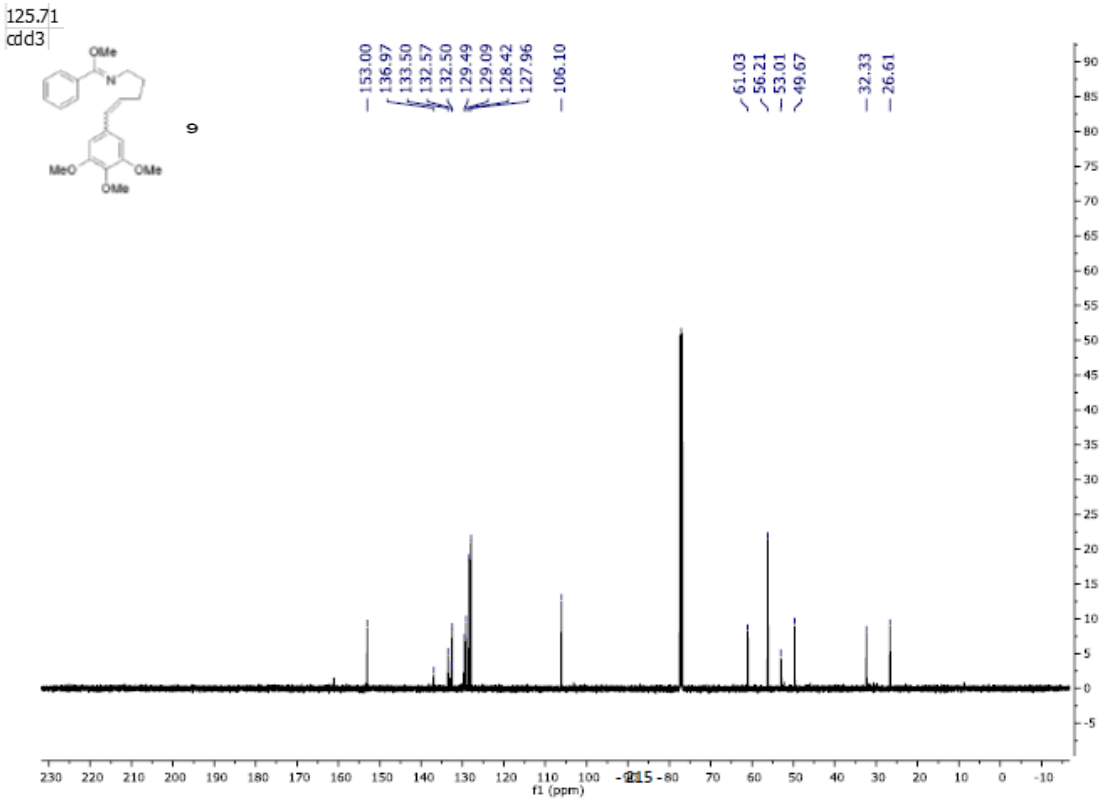
125.71
cdd3
9
153.00
136.97
133.50
132.57
132.50
129.49
129.09
128.42
127.96
106.10
61.03
56.21
53.01
49.67
32.33
26.61
f1 (ppm)

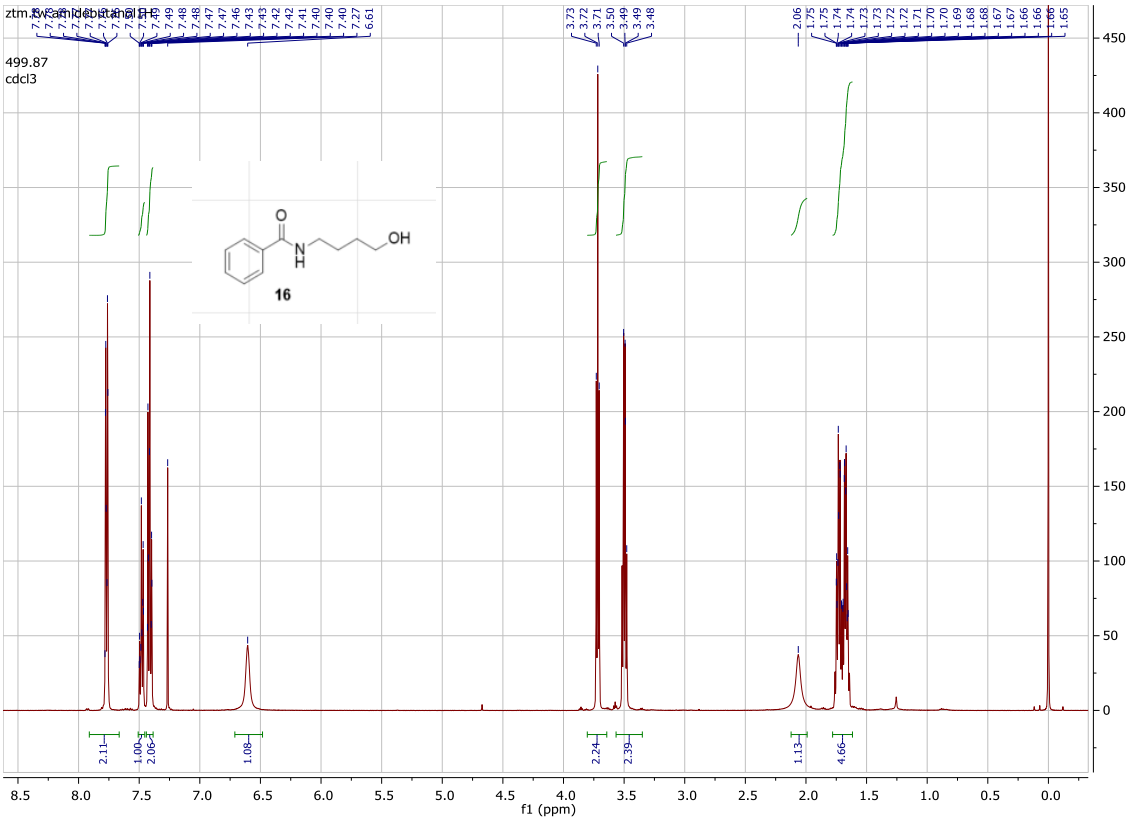
499.87
cdcl3
16
f1 (ppm)

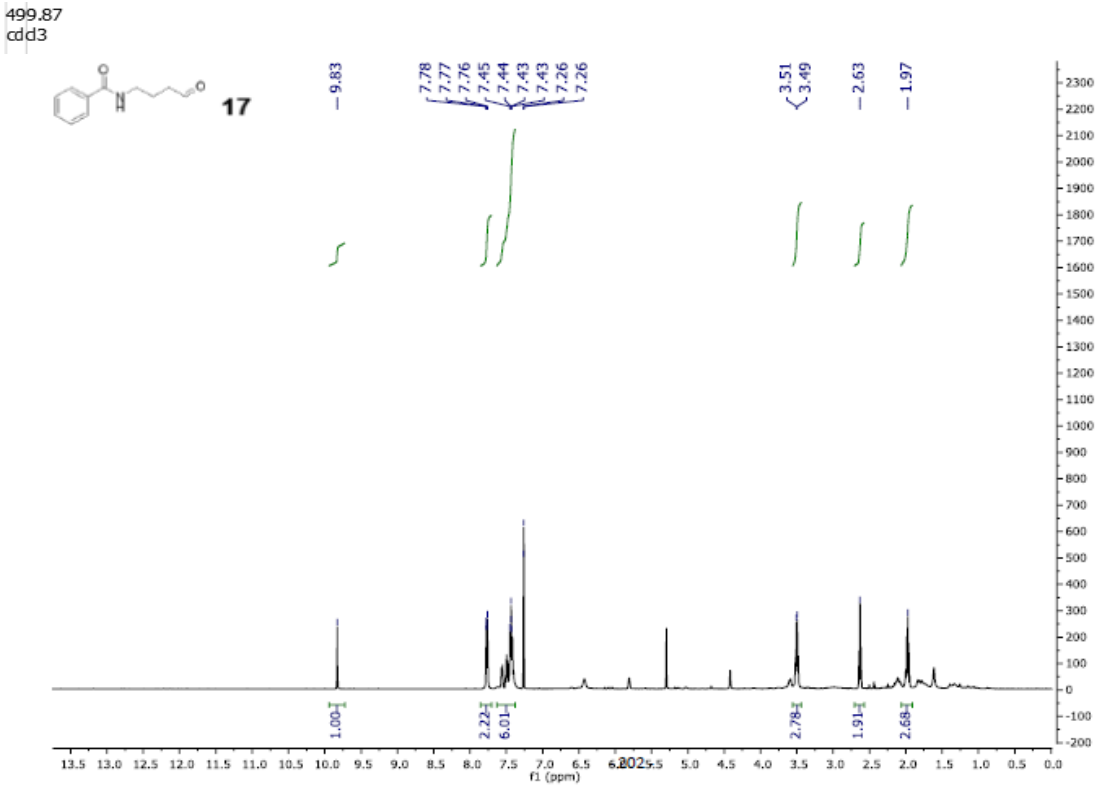
499.87
cdcl3
17
f1 (ppm)

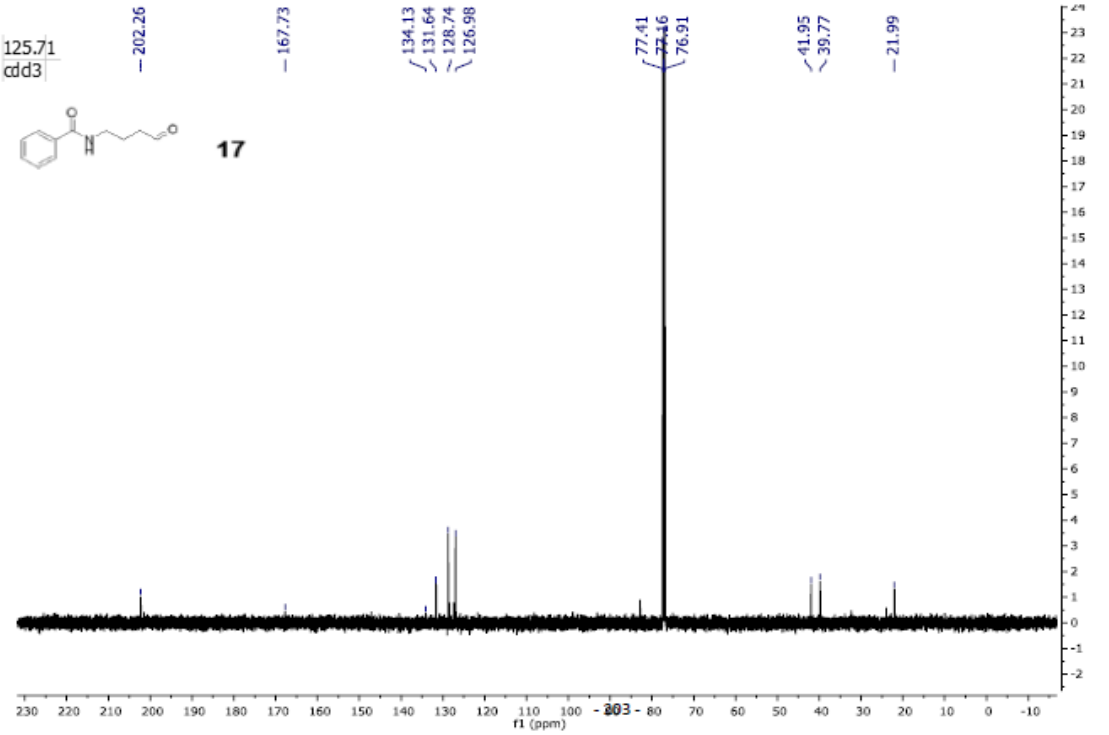
125.71
cdd3
202.26
167.73
134.13
131.64
128.74
126.98
77.41
77.16
76.91
41.95
39.77
21.99
17
f1 (ppm)

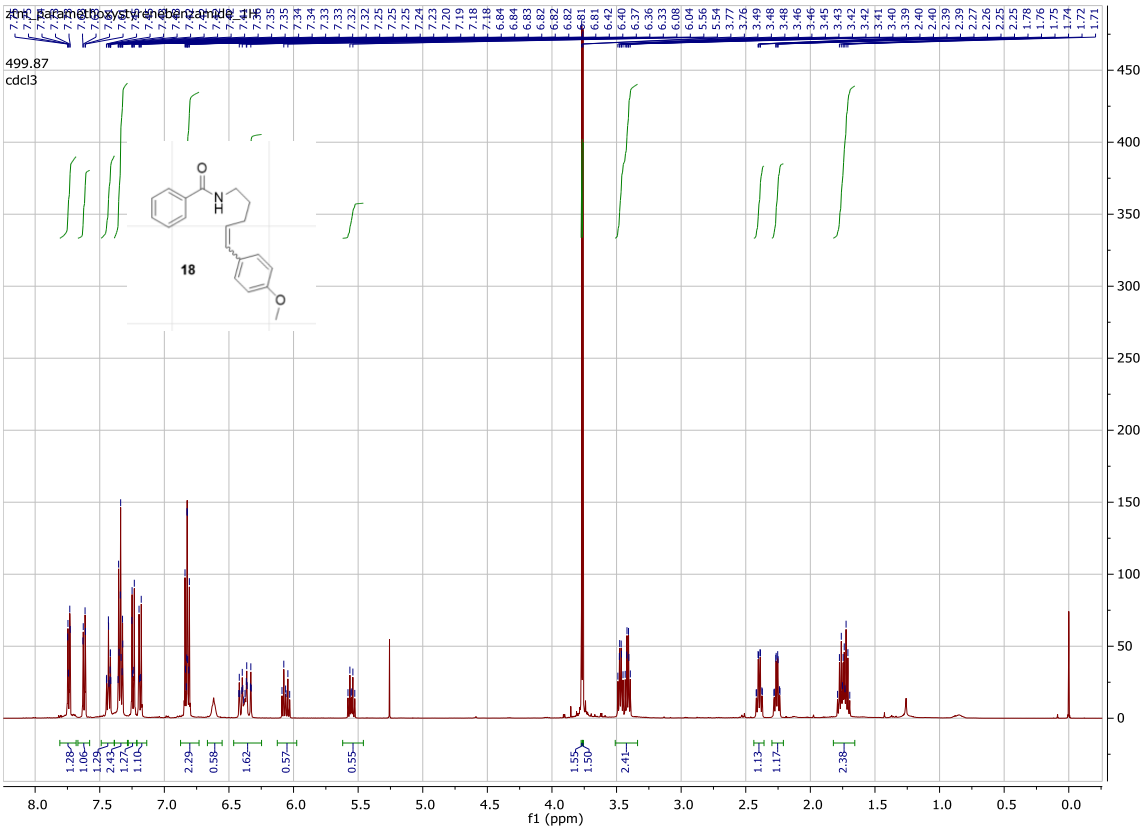
499.87
cdcl3
18
f1 (ppm)

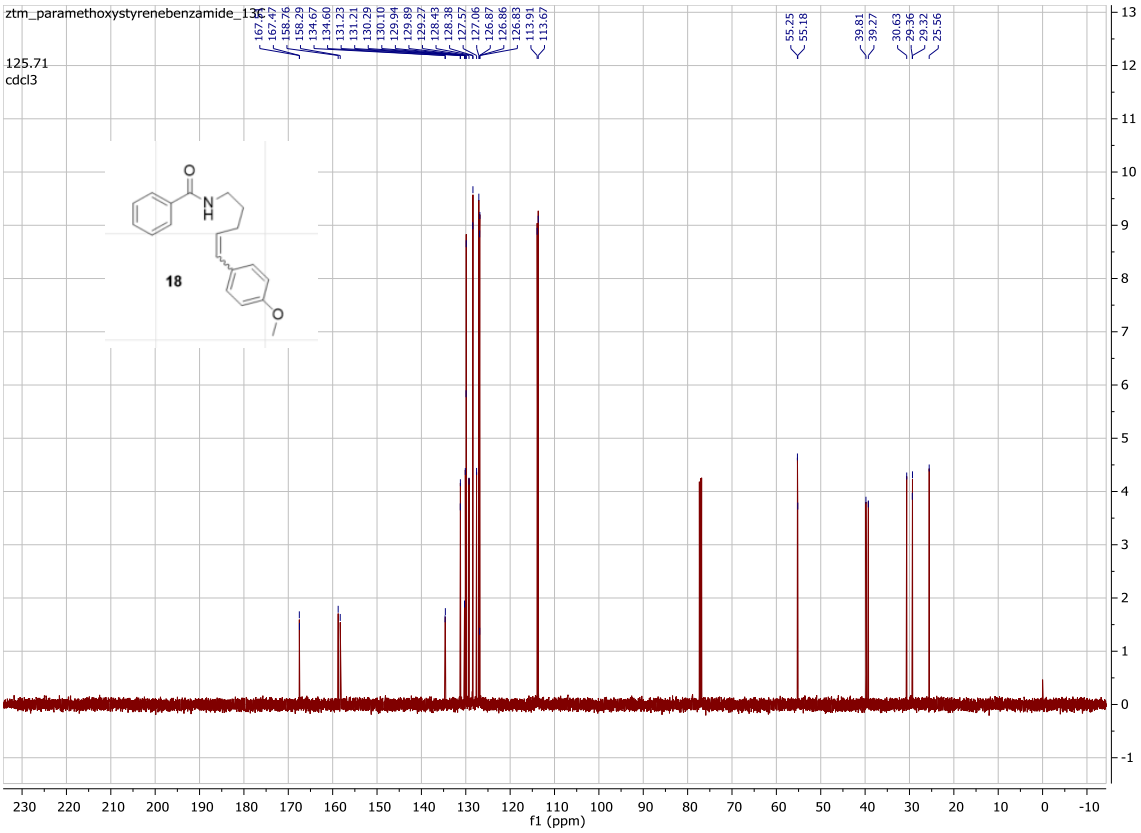
ztm_paramethoxystyrenebenzamide_13C
125.71
cdcl3
18
f1 (ppm)

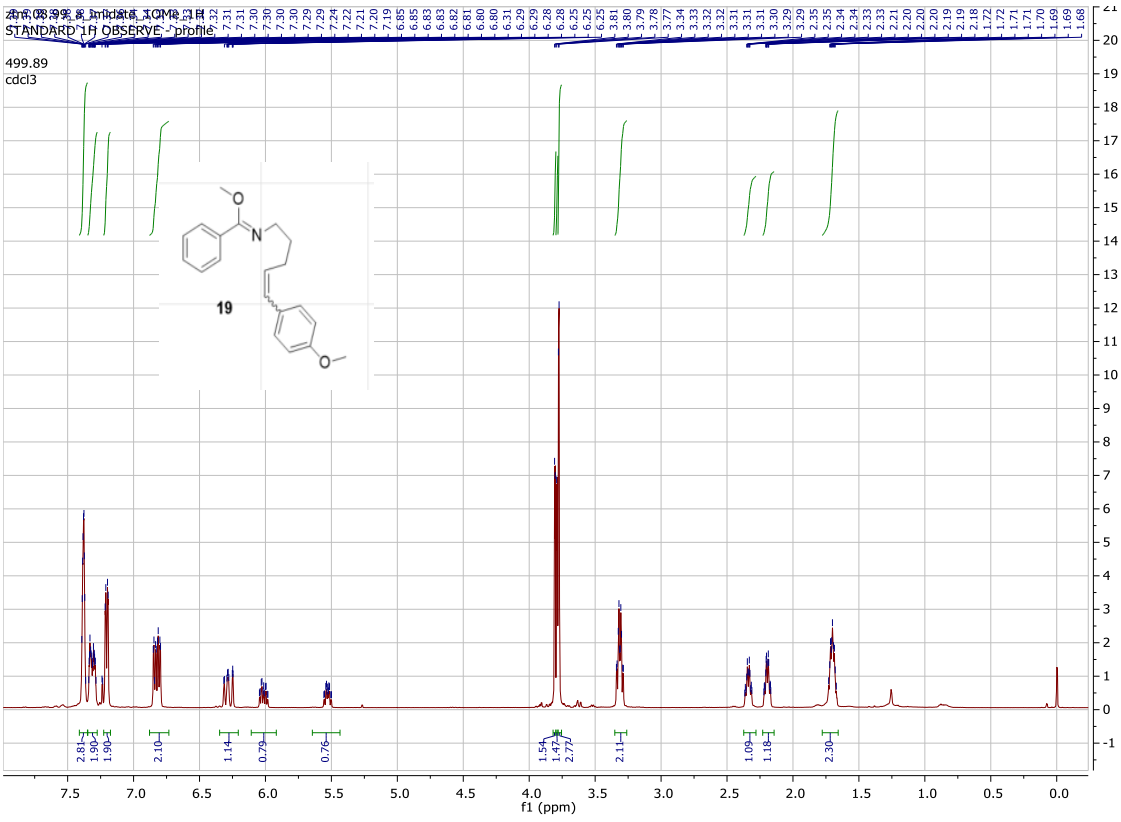
STANDARD 1H OBSERVE_ profile
499.89
cdcl3
19
f1 (ppm)

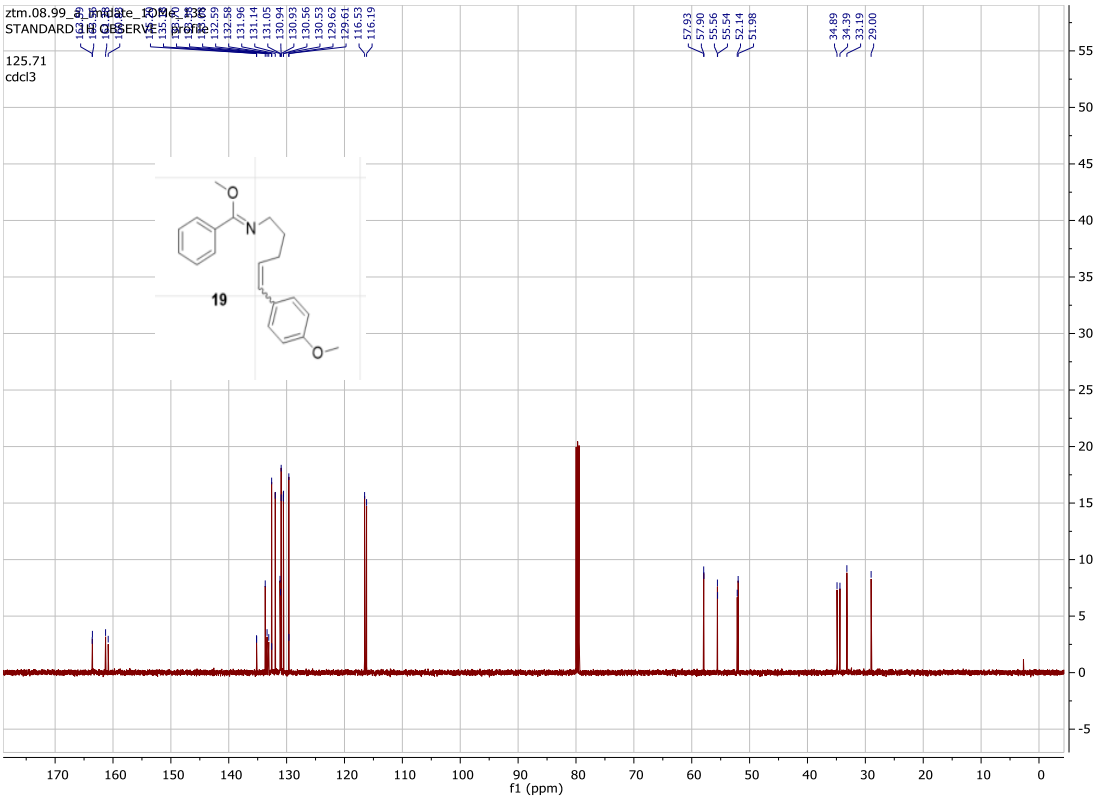
125.71
cdcl3
19
f1 (ppm)

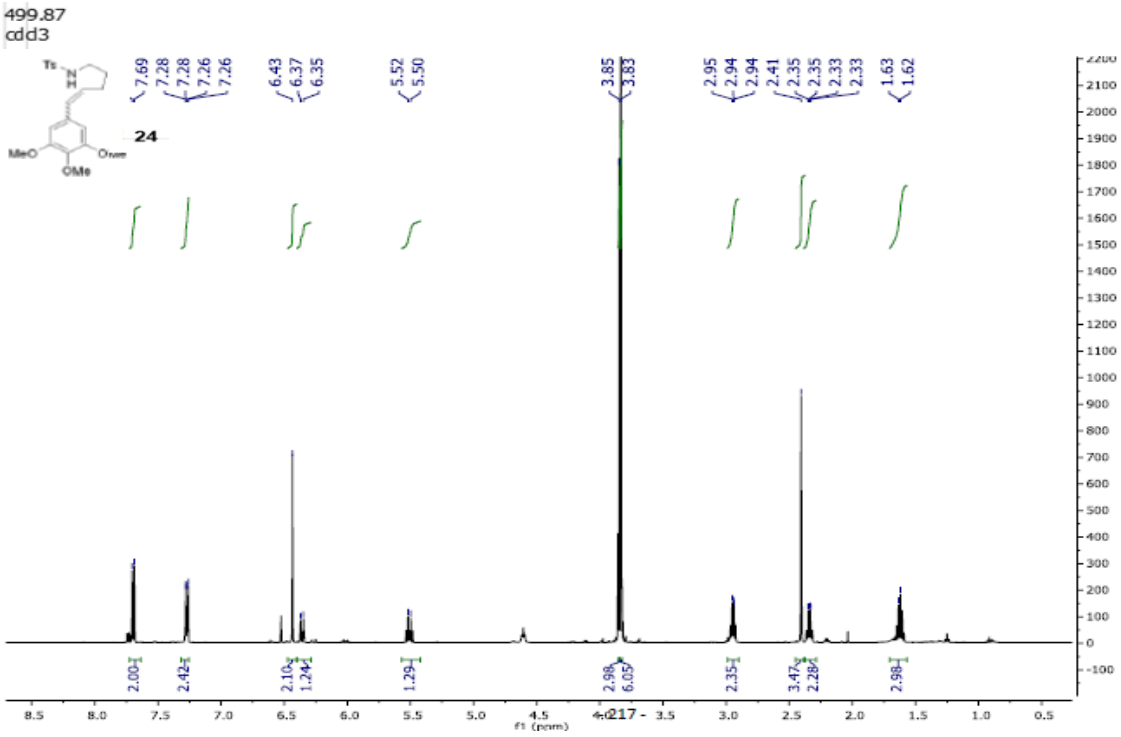
499.87
cdd3
24
f1 (ppm)

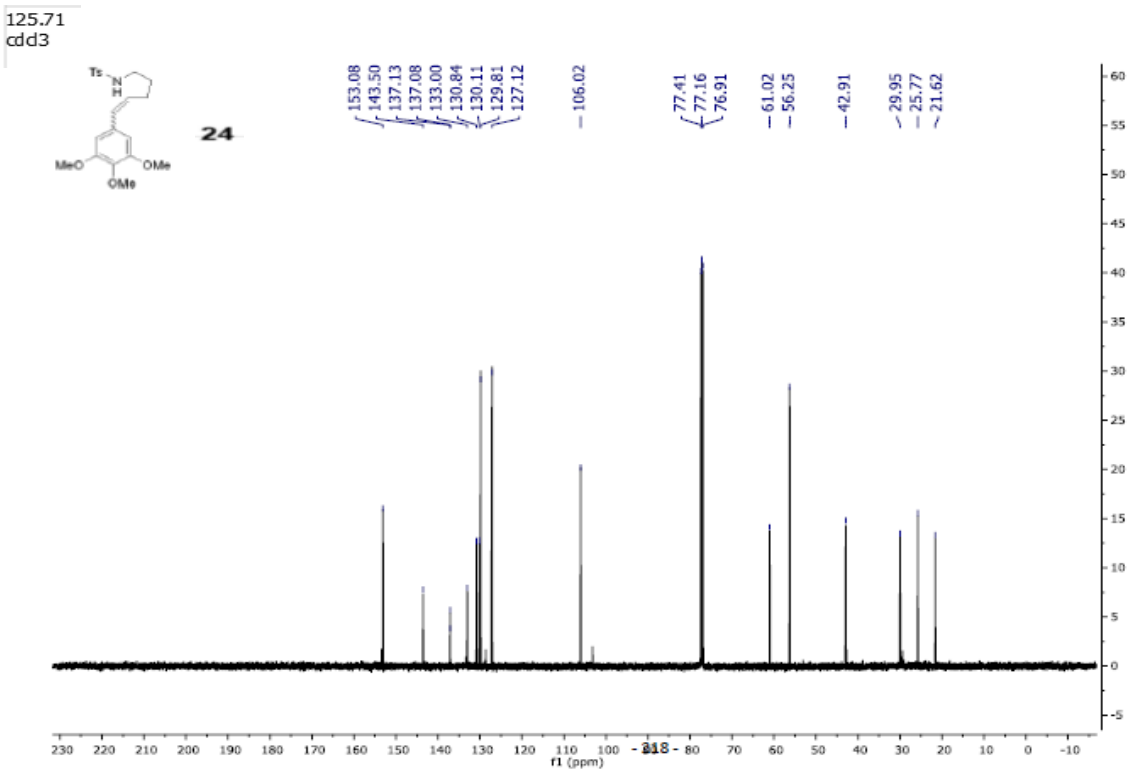
125.71
cdd3
24
153.08
143.50
137.13
137.08
133.00
130.84
130.11
129.81
127.12
106.02
77.41
77.16
76.91
61.02
56.25
42.91
29.95
25.77
21.62
f1 (ppm)

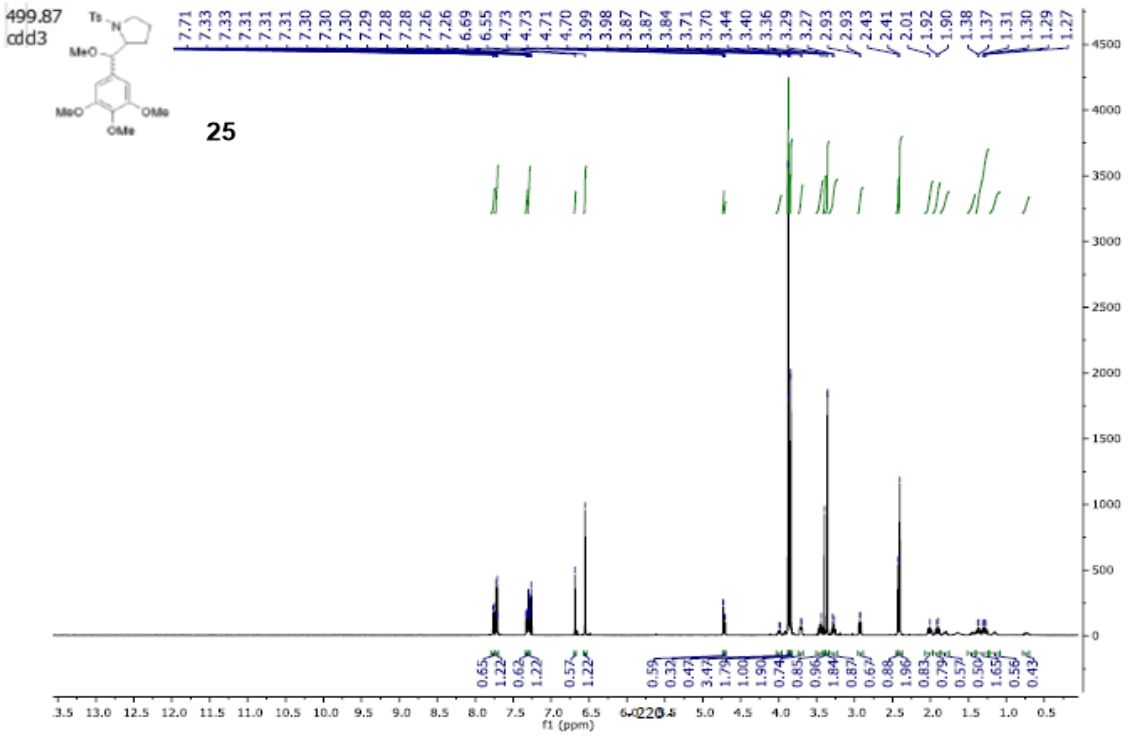
499.87
cdd3
25
7.71
7.33
7.33
7.31
7.31
7.31
7.30
7.30
7.30
7.29
7.28
7.28
7.26
7.26
6.69
6.55
4.73
4.73
4.71
4.70
3.99
3.98
3.87
3.87
3.84
3.71
3.70
3.44
3.40
3.36
3.29
3.27
2.93
2.93
2.43
2.41
2.01
1.92
1.90
1.38
1.37
1.31
1.30
1.29
1.27
f1 (ppm)

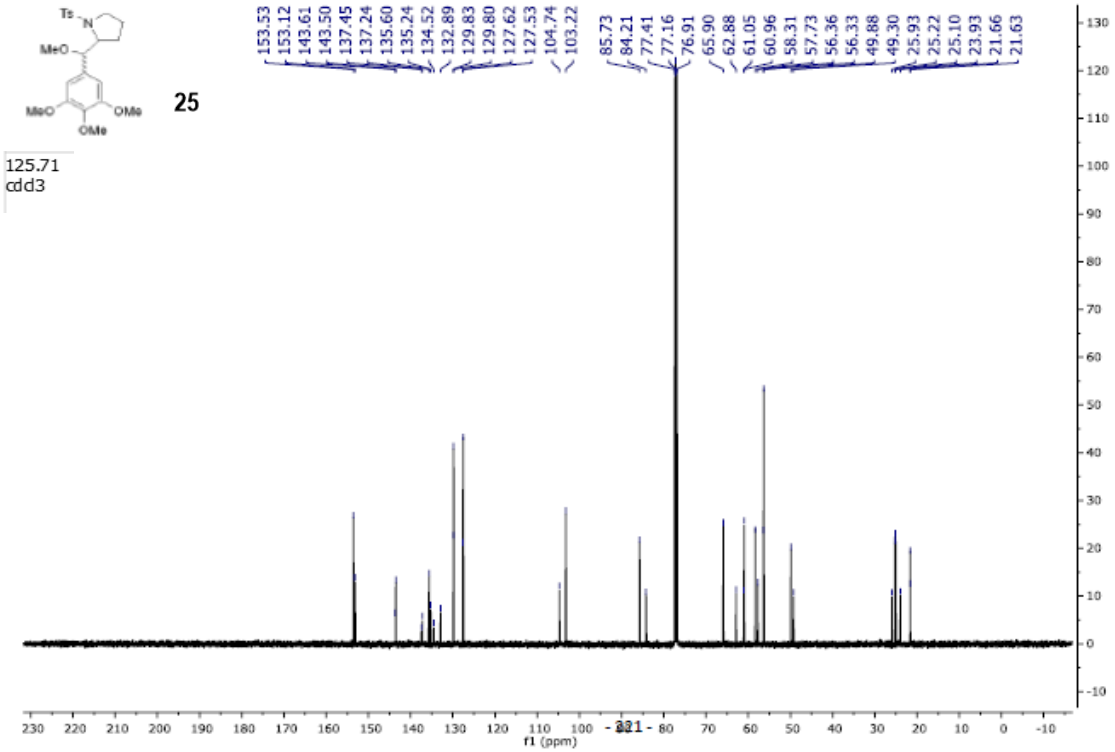
25
125.71
cdd3
153.53
153.12
143.61
143.50
137.45
137.24
135.60
135.24
134.52
132.89
129.83
129.80
127.62
127.53
104.74
103.22
85.73
84.21
77.41
77.16
76.91
65.90
62.88
61.05
60.96
58.31
57.73
56.36
56.33
49.88
49.30
25.93
25.22
25.10
23.93
21.66
21.63
f1 (ppm)

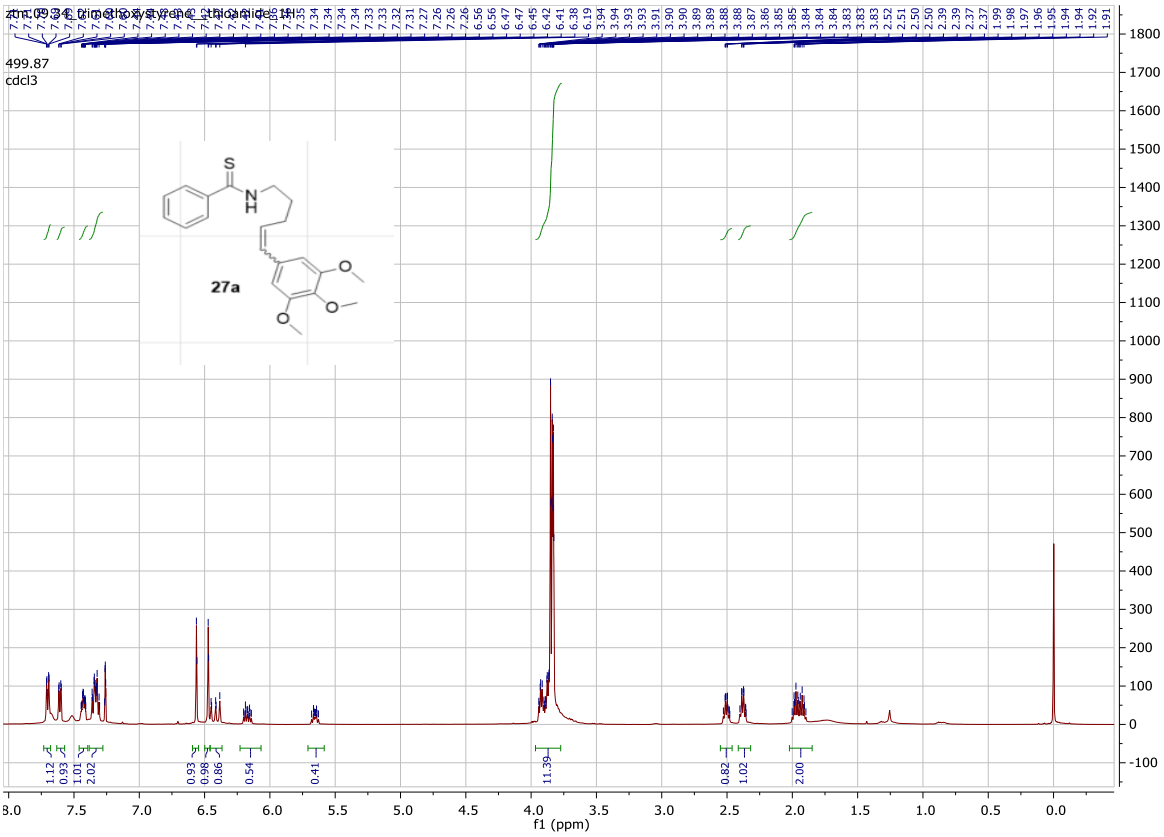
499.87
cdcl3
27a
1.12
0.93
1.01
2.02
0.93
0.98
0.86
0.54
0.41
11.39
0.82
1.02
2.00
f1 (ppm)

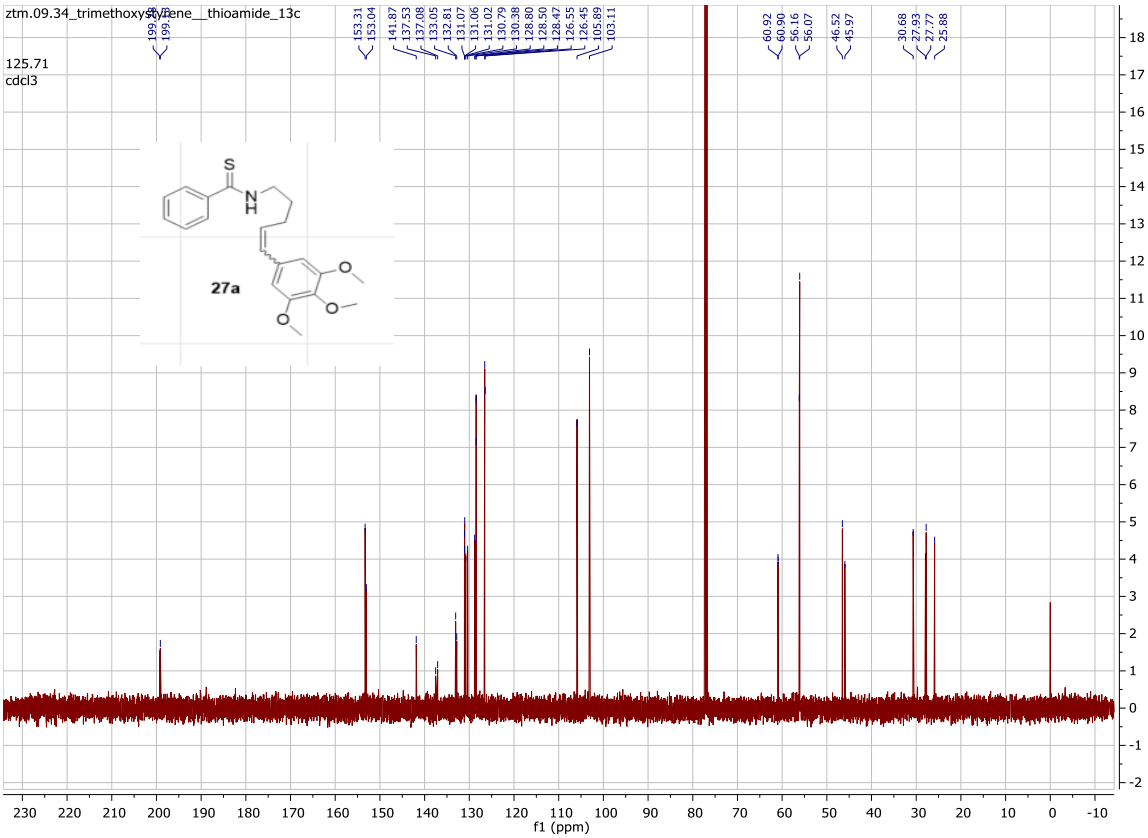
ztm.09.34_trimethoxystyrene__thioamide_13c
125.71
cdcl3
27a
f1 (ppm)

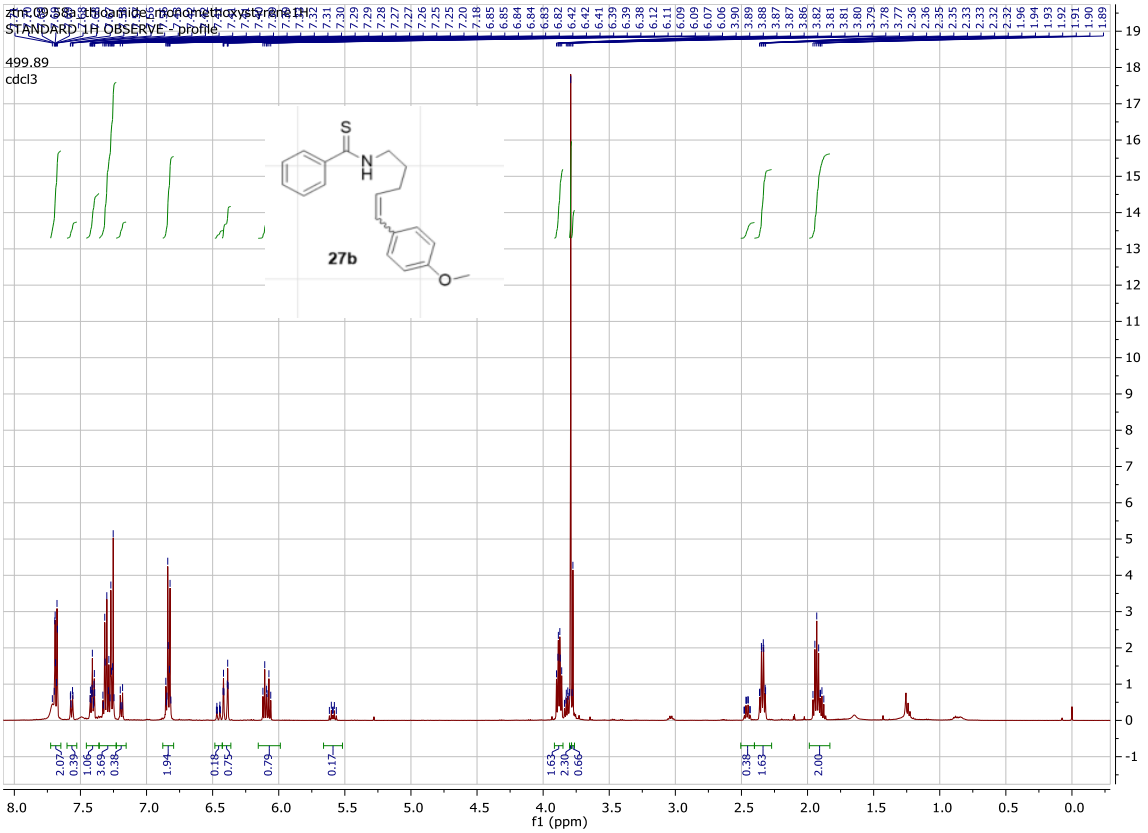
STANDARD 1H OBSERVE - profile
499.89
cdcl3
27b
f1 (ppm)

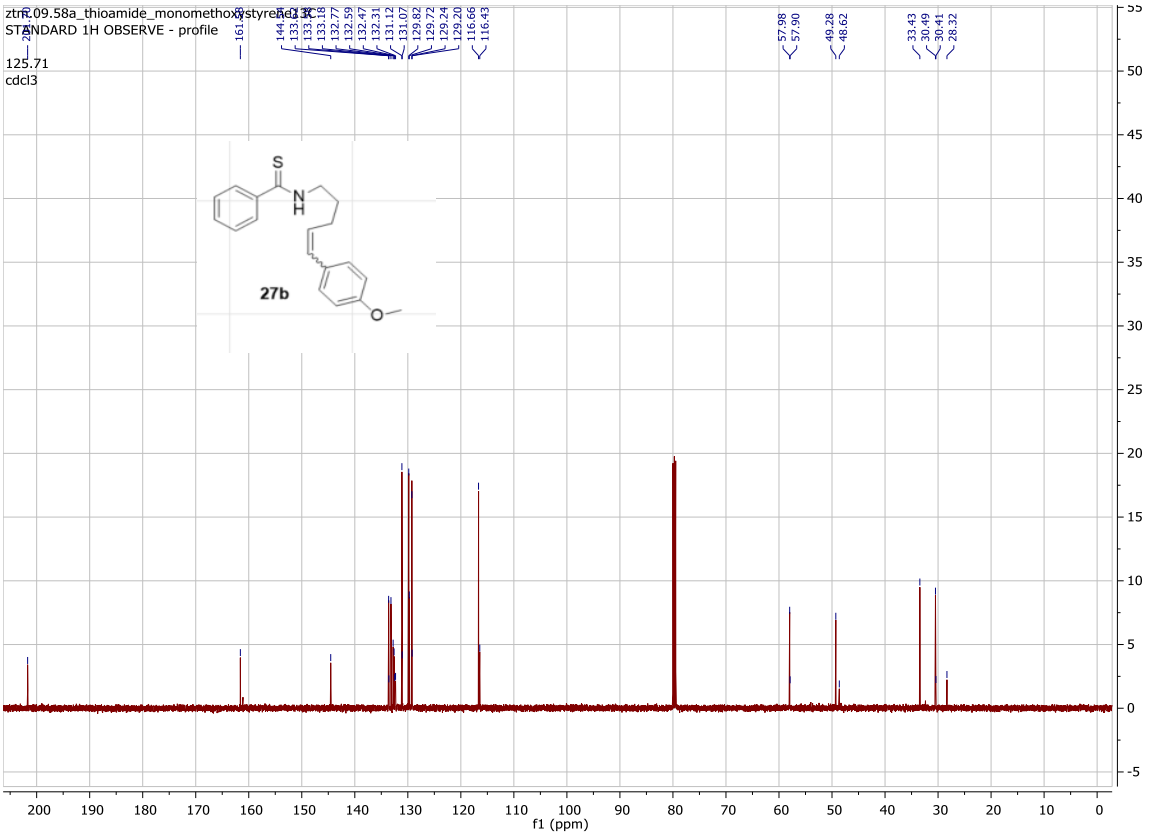
ztm.09.58a_thioamide_monomethoxystyrene_13C
STANDARD 1H OBSERVE - profile
125.71
cdcl3
27b
f1 (ppm)

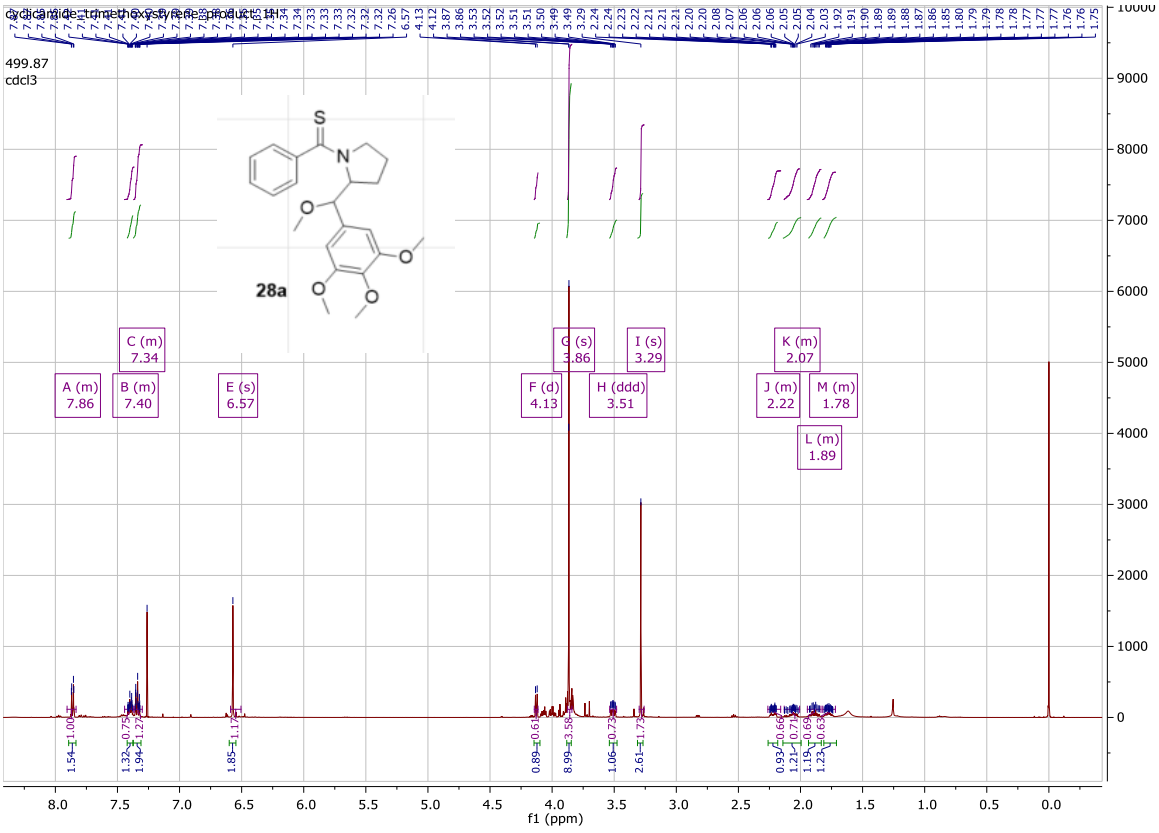
499.87
cdcl3
28a
A (m) 7.86
B (m) 7.40
C (m) 7.34
E (s) 6.57
F (d) 4.13
G (s) 3.86
H (ddd) 3.51
I (s) 3.29
J (m) 2.22
K (m) 2.07
L (m) 1.89
M (m) 1.78
f1 (ppm)

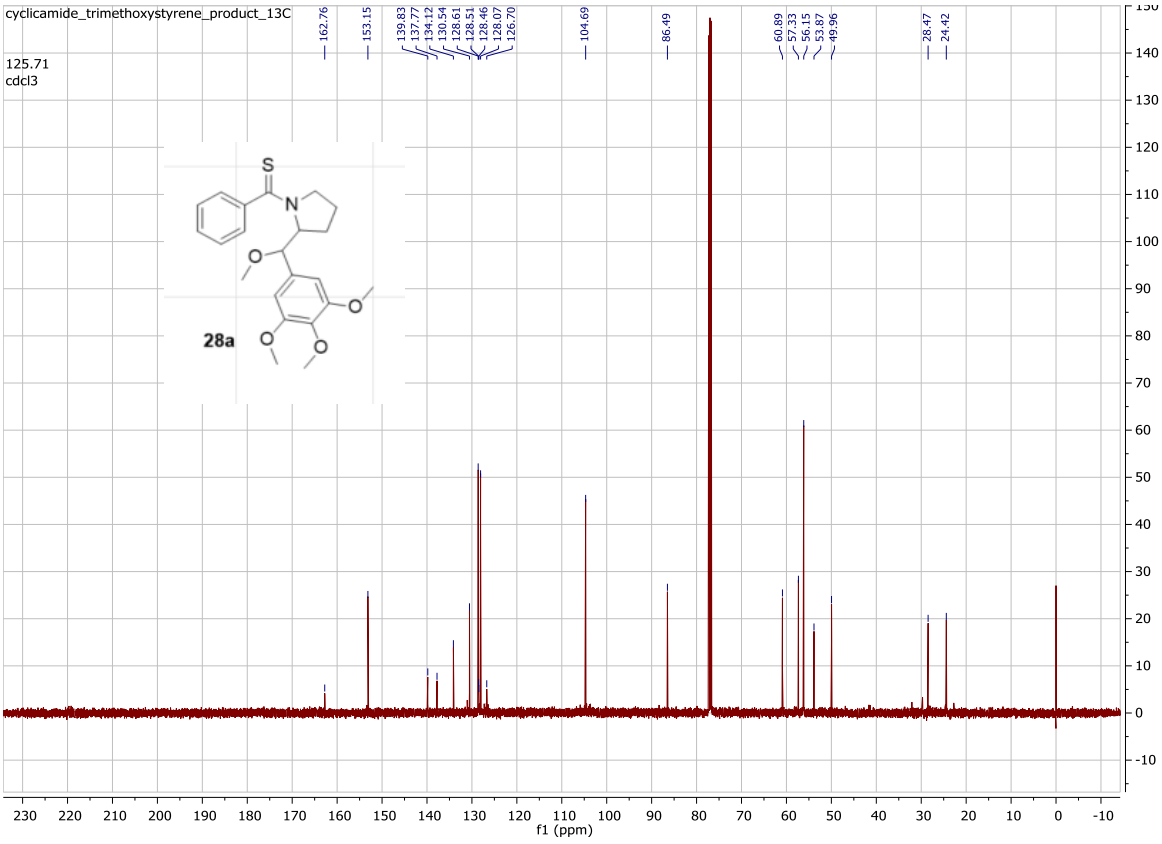
cyclicamide_trimethoxystyrene_product_13C
125.71
cdcl3
162.76
153.15
139.83
137.77
134.12
130.54
128.61
128.51
128.46
128.07
126.70
104.69
86.49
60.89
57.33
56.15
53.87
49.96
28.47
24.42
28a
f1 (ppm)

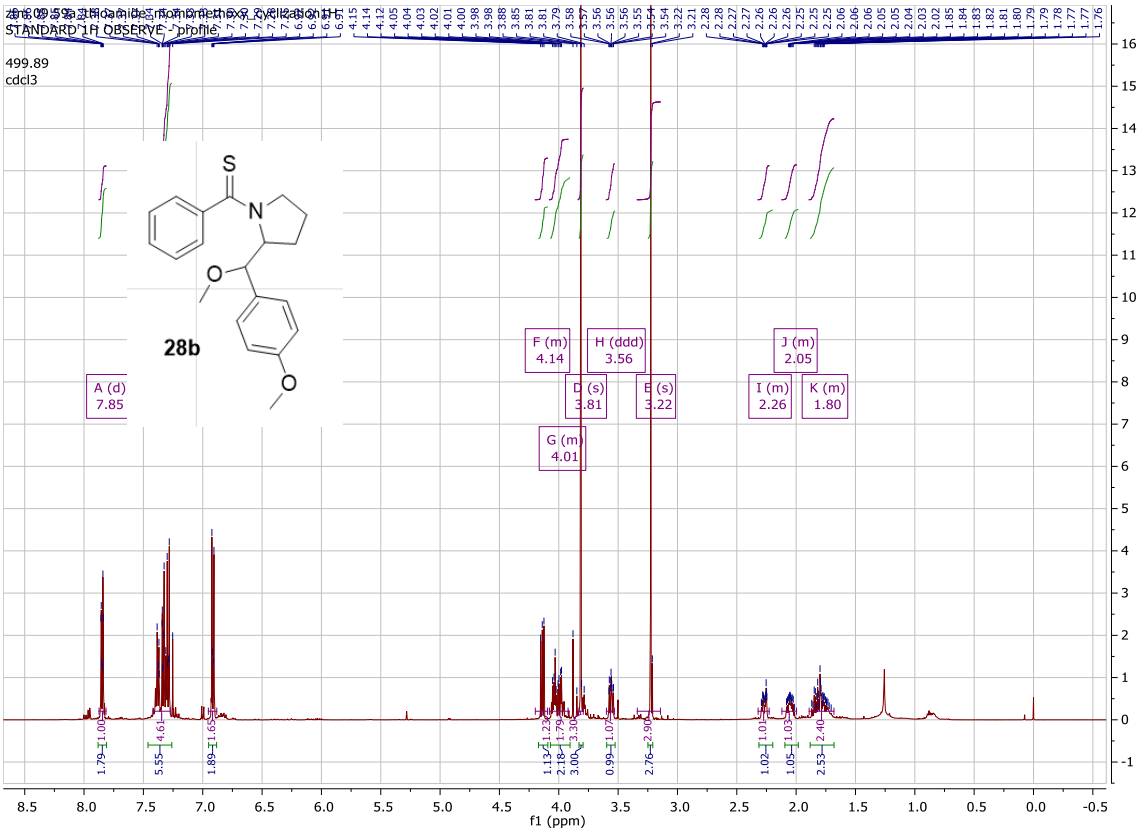
STANDARD 1H OBSERVE - profile
499.89
cdcl3
28b
A (d)
7.85
F (m)
4.14
H (ddd)
3.56
D (s)
3.81
E (s)
3.22
G (m)
4.01
J (m)
2.05
I (m)
2.26
K (m)
1.80
f1 (ppm)

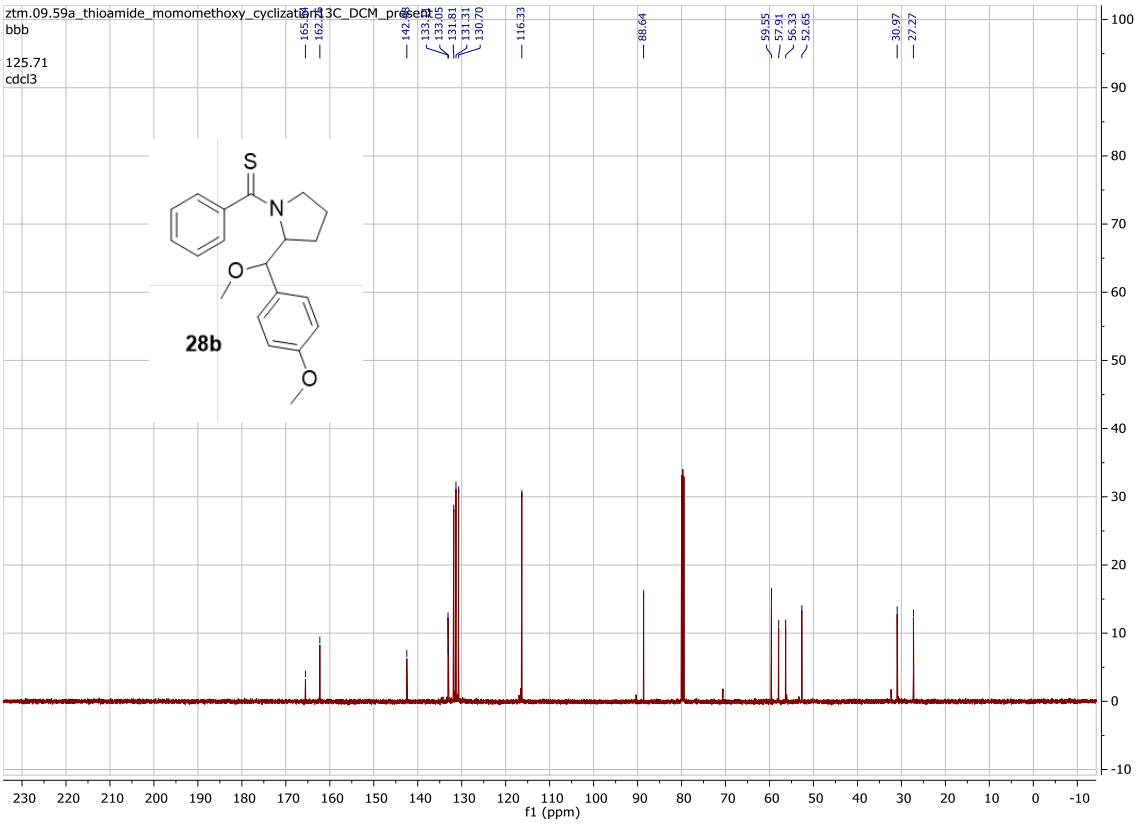
ztm.09.59a_thioamide_momomethoxy_cyclization_13C_DCM_present
bbb
125.71
cdcl3
28b
f1 (ppm)

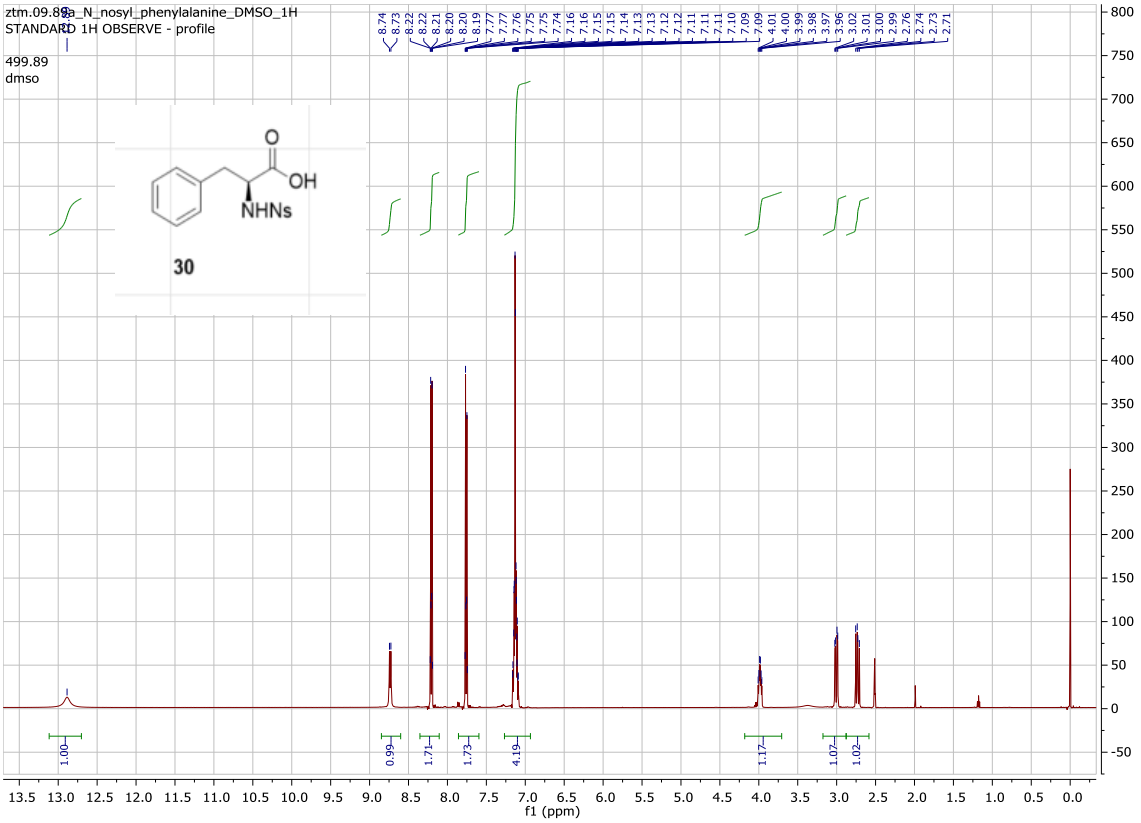
ztm.09.89a_N_nosyl_phenylalanine_DMSO_1H
STANDARD 1H OBSERVE - profile
499.89
dmso
30
f1 (ppm)

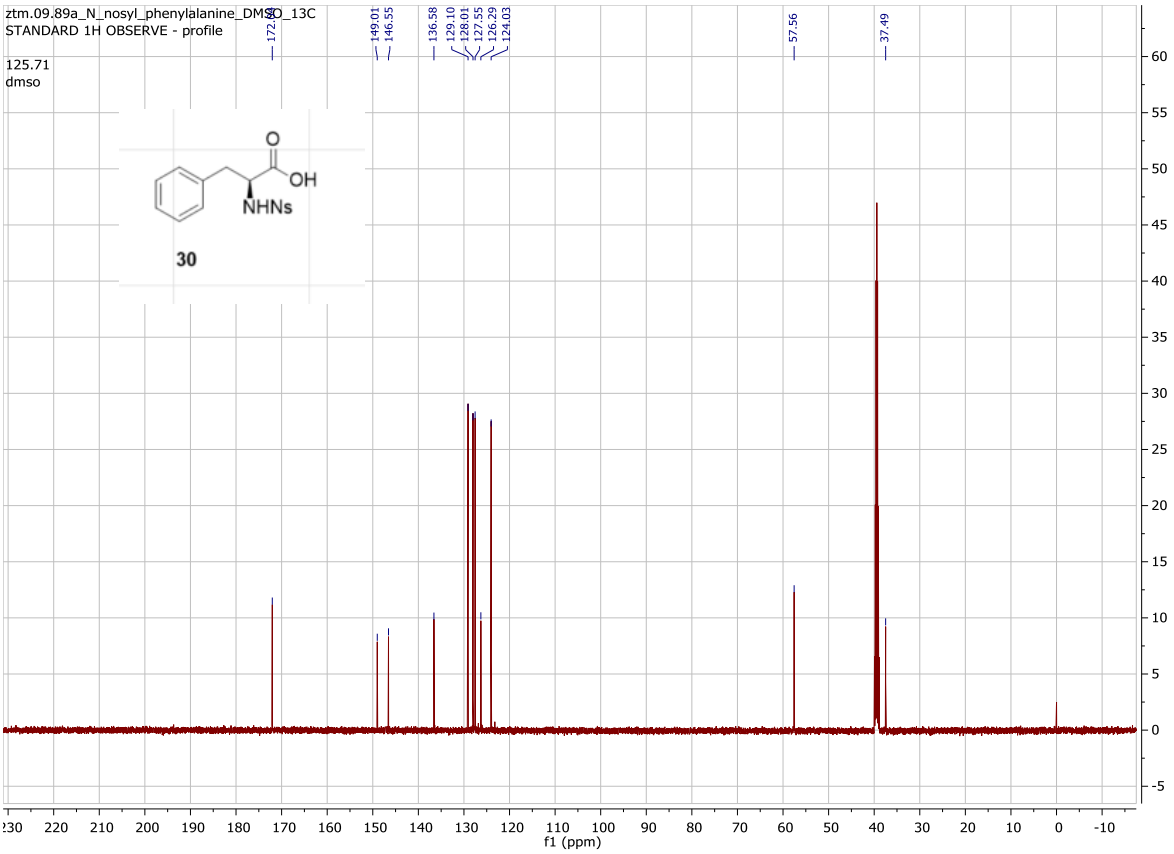
ztm.09.89a_N_nosyl_phenylalanine_DMSO_13C
STANDARD 1H OBSERVE - profile
125.71
dmso
172.
149.01
146.55
136.58
129.10
128.01
127.55
126.29
124.03
57.56
37.49
O
OH
NHNs
30
f1 (ppm)

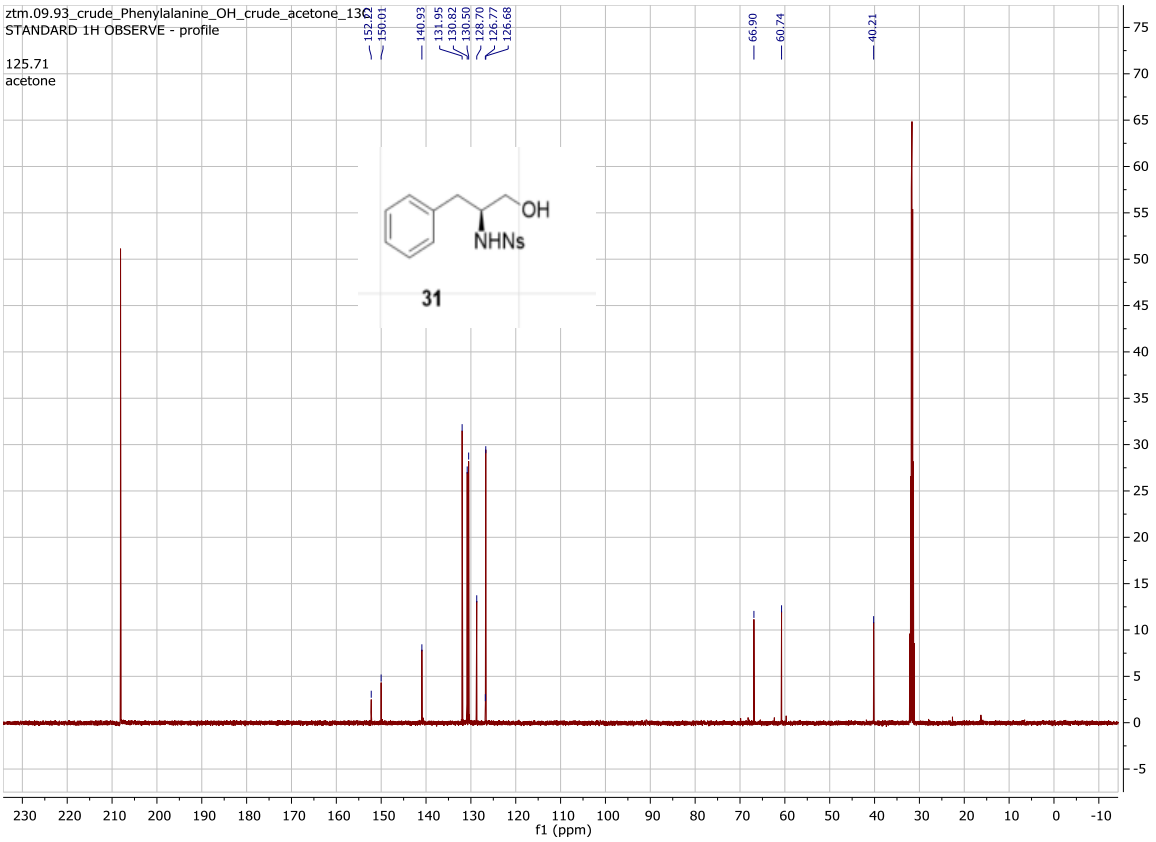
ztm.09.93_crude_Phenylalanine_OH_crude_acetone_13C
STANDARD 1H OBSERVE - profile
125.71
acetone
152.42
150.01
140.93
131.95
130.82
130.50
128.70
126.77
126.68
66.90
60.74
40.21
OH
NHNs
31
f1 (ppm)

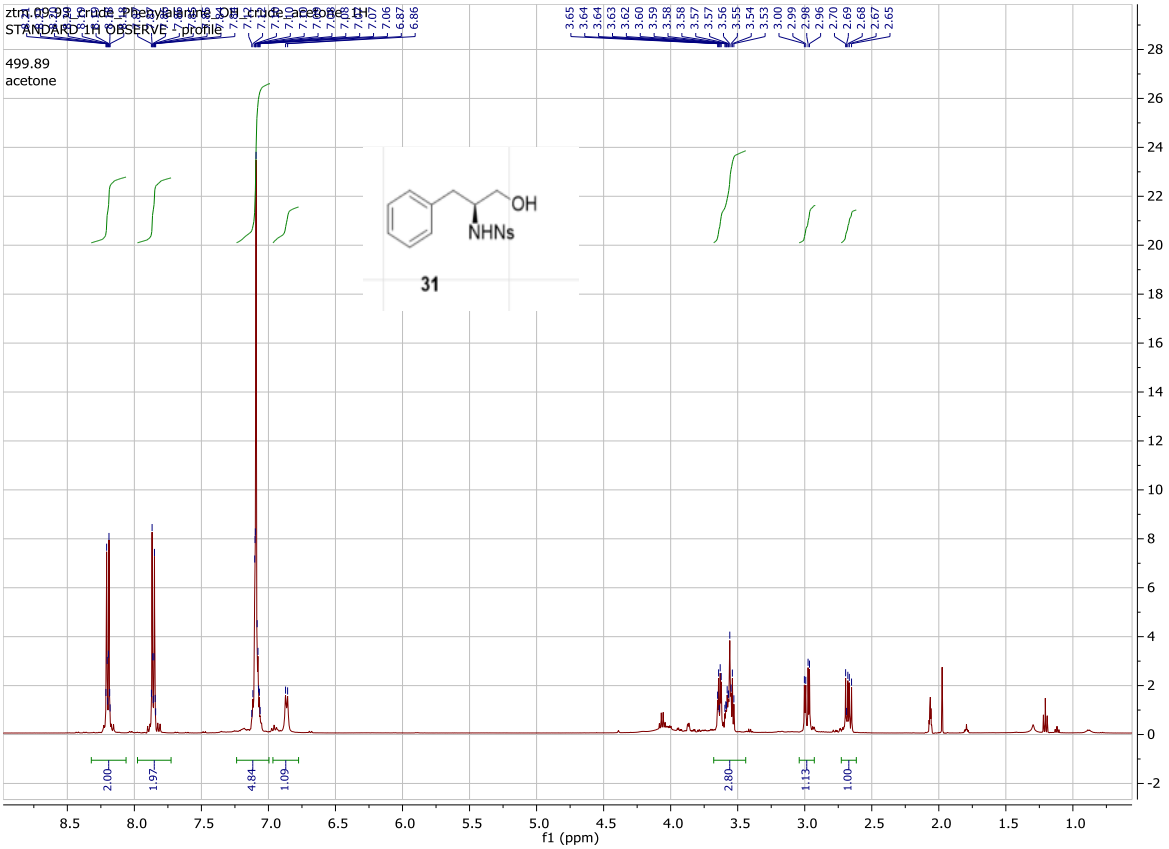
STANDARD 1H OBSERVE - profile
499.89
acetone
OH
NHNs
31
2.00
1.97
4.84
1.09
2.80
1.13
1.00
f1 (ppm)

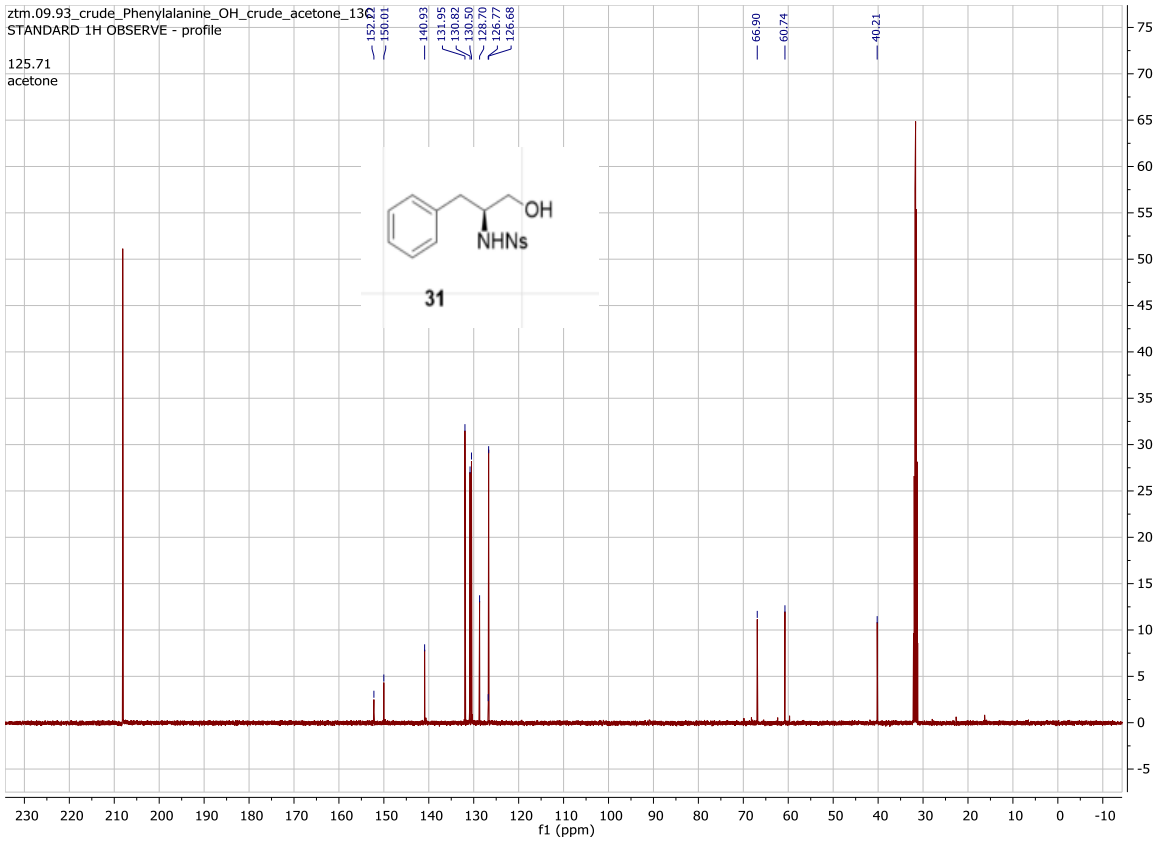
ztm.09.93_crude_Phenylalanine_OH_crude_acetone_13C
STANDARD 1H OBSERVE - profile
125.71
acetone
152.21
150.01
140.93
131.95
130.82
130.50
128.70
126.77
126.68
66.90
60.74
40.21
OH
NHNs
31
f1 (ppm)

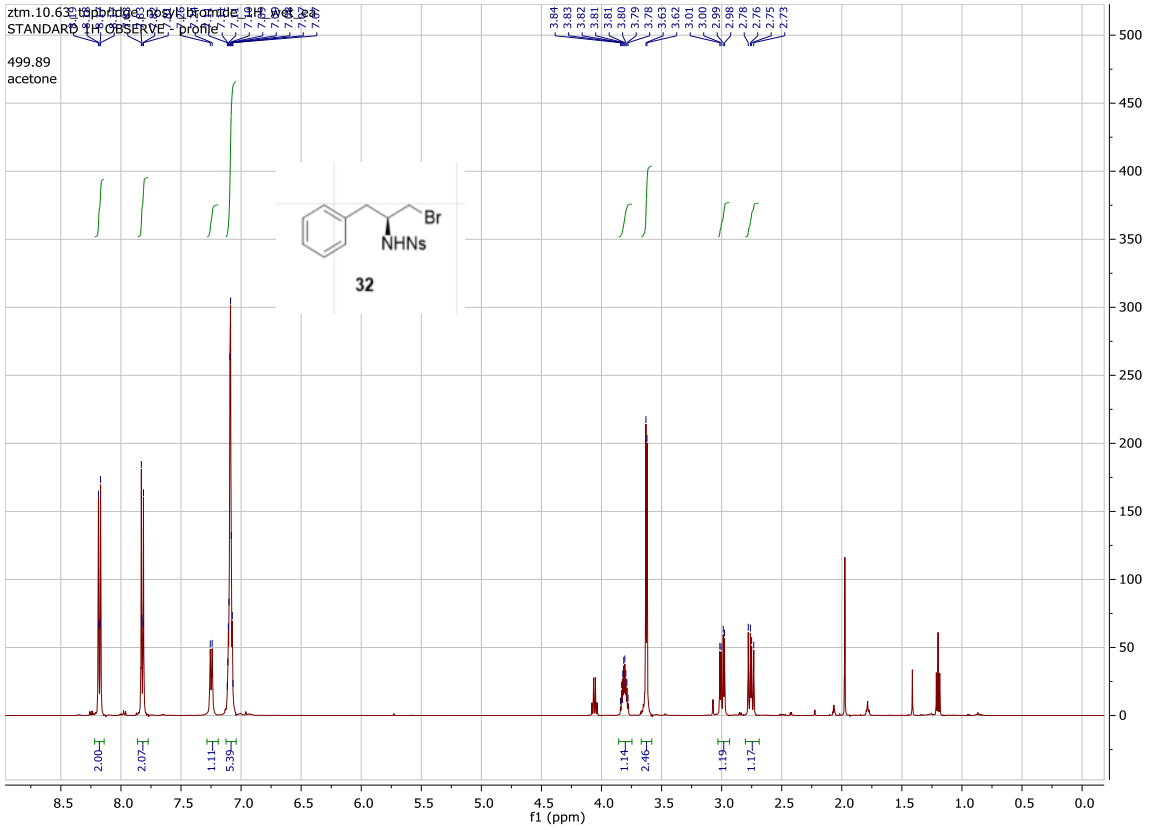
STANDARD 1H OBSERVE - profile
499.89
acetone
3.84
3.83
3.82
3.81
3.81
3.80
3.79
3.78
3.63
3.62
3.01
3.00
2.99
2.98
2.78
2.76
2.75
2.73
Br
NHNs
32
2.00
2.07
1.11
5.39
1.14
2.46
1.19
1.17
f1 (ppm)

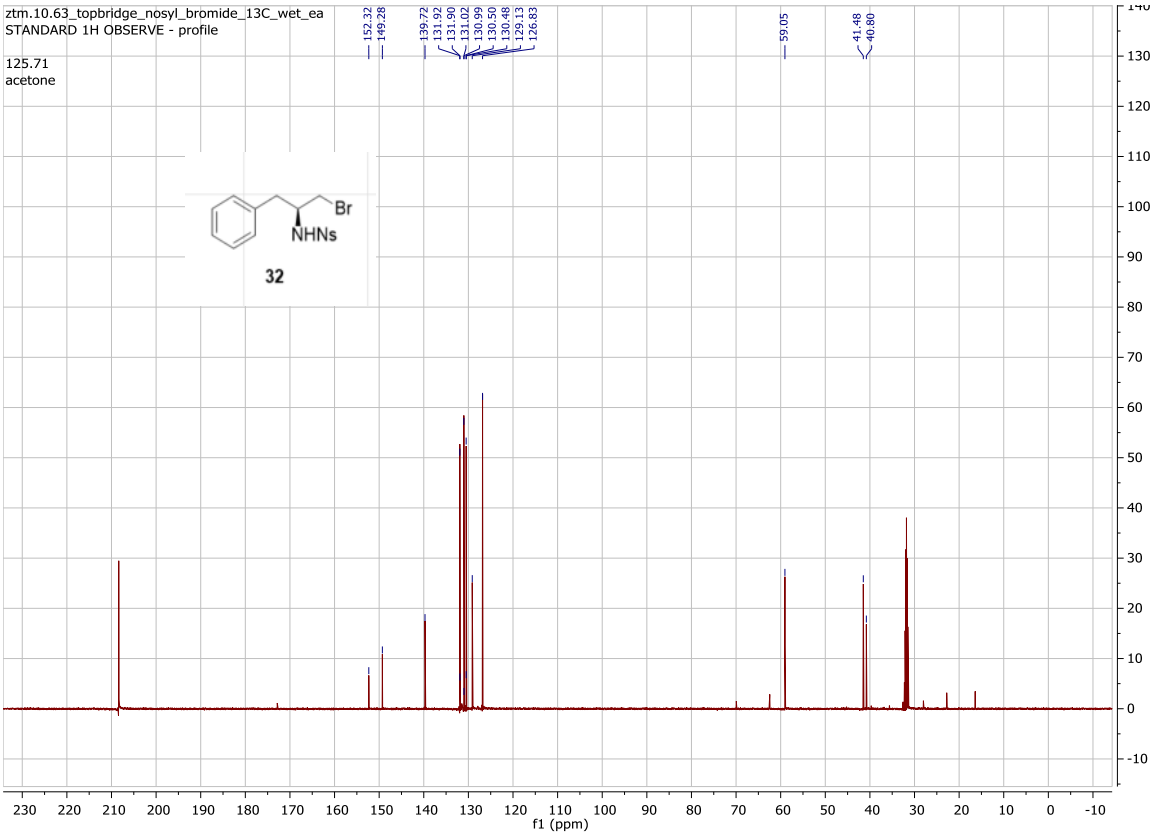
ztm.10.63_topbridge_nosyl_bromide_13C_wet_ea
STANDARD 1H OBSERVE - profile
125.71
acetone
152.32
149.28
139.72
131.92
131.90
131.02
130.99
130.50
130.48
129.13
126.83
59.05
41.48
40.80
Br
NHNs
32
f1 (ppm)

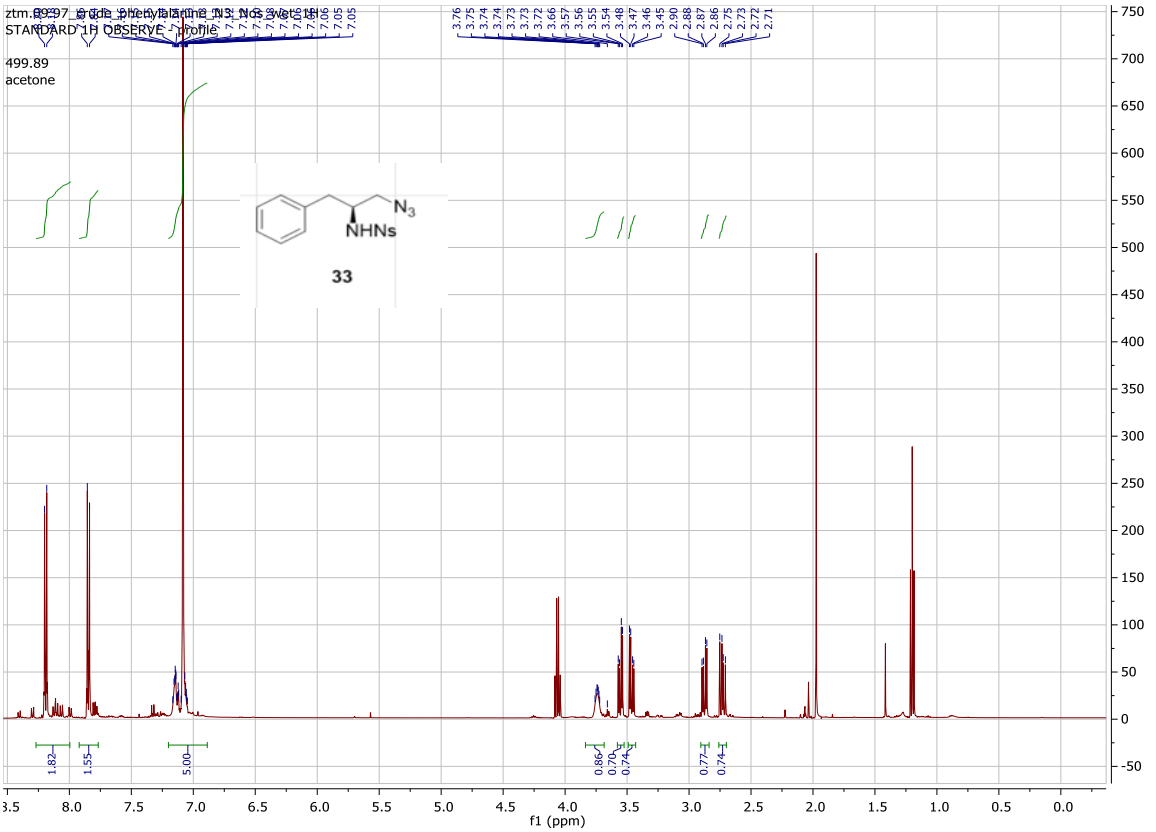
STANDARD 1H OBSERVE - profile
499.89
acetone
N3
NHNs
33
1.82
1.55
5.00
0.86
0.70
0.74
0.77
0.74
f1 (ppm)

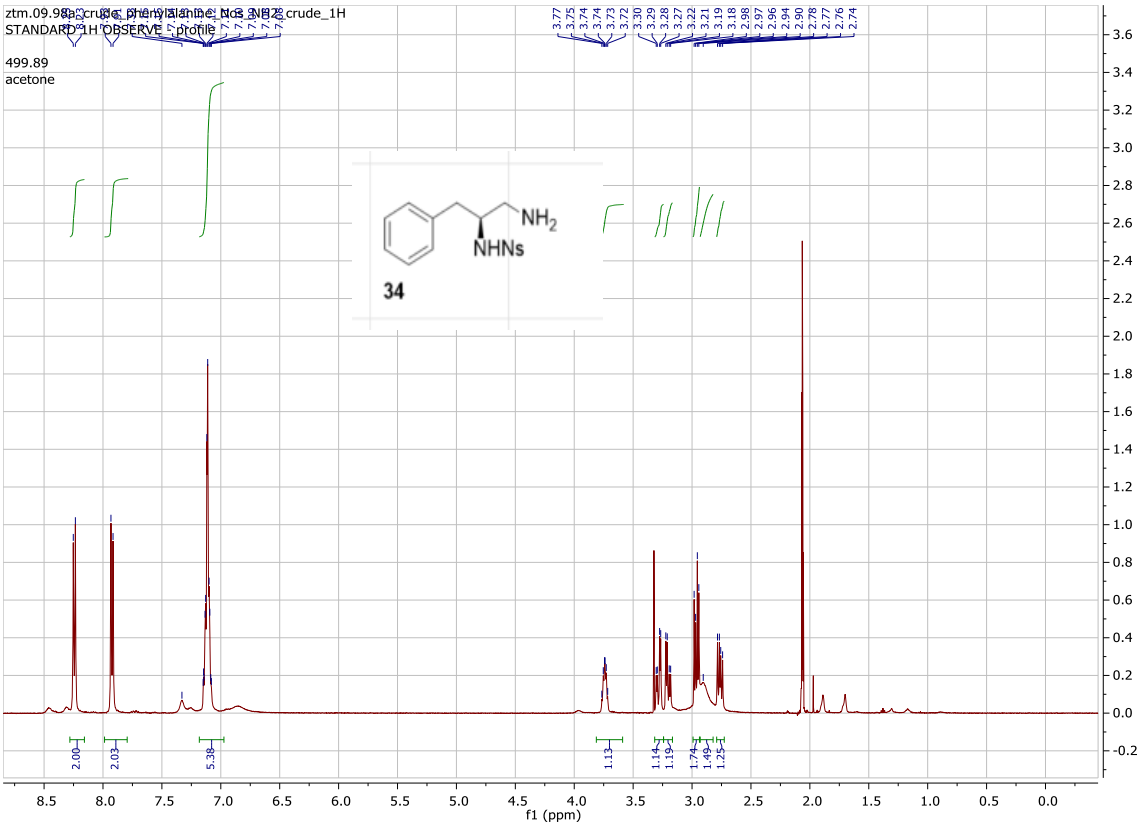
ztm.09.98a_crude_phenylalanine_Nos_NH2_crude_1H
STANDARD 1H OBSERVE - profile
499.89
acetone
NH2
NHNs
34
f1 (ppm)

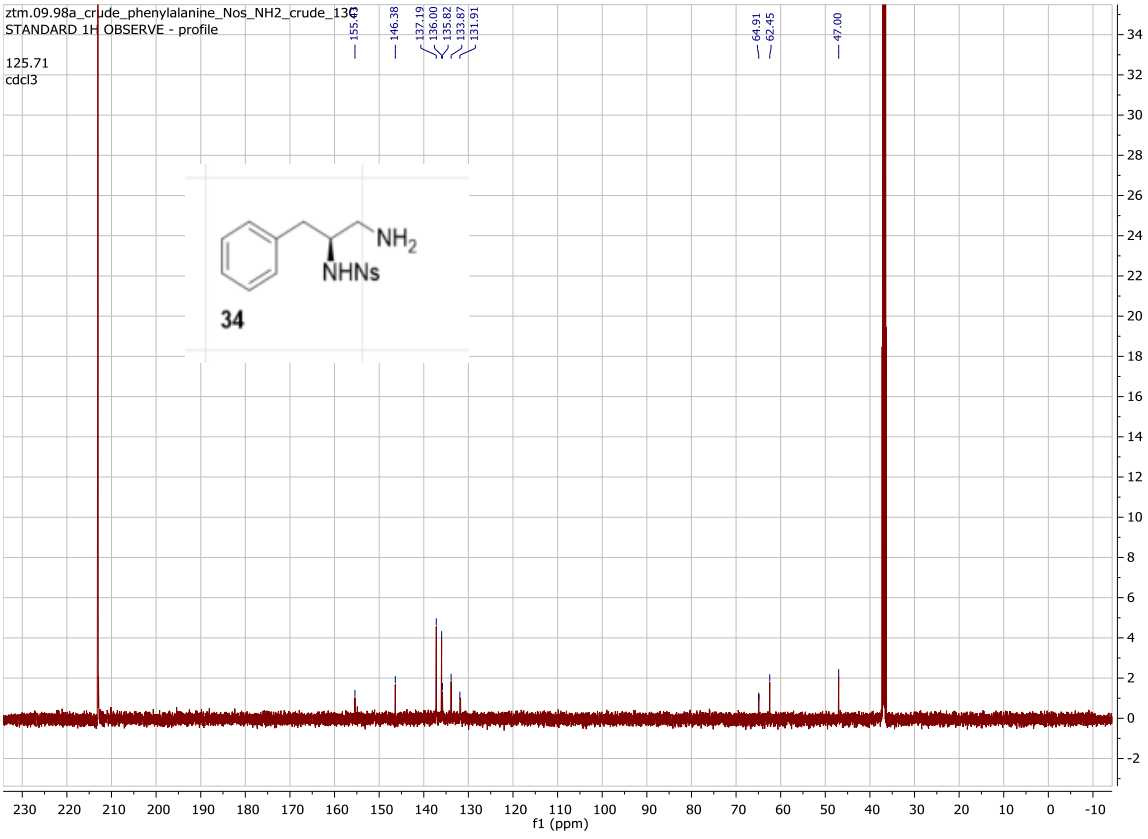
ztm.09.98a_crude_phenylalanine_Nos_NH2_crude_13C
STANDARD 1H OBSERVE - profile
125.71
cdcl3
155.43
146.38
137.19
136.00
135.82
133.87
131.91
64.91
62.45
47.00
NH2
NHNs
34
f1 (ppm)

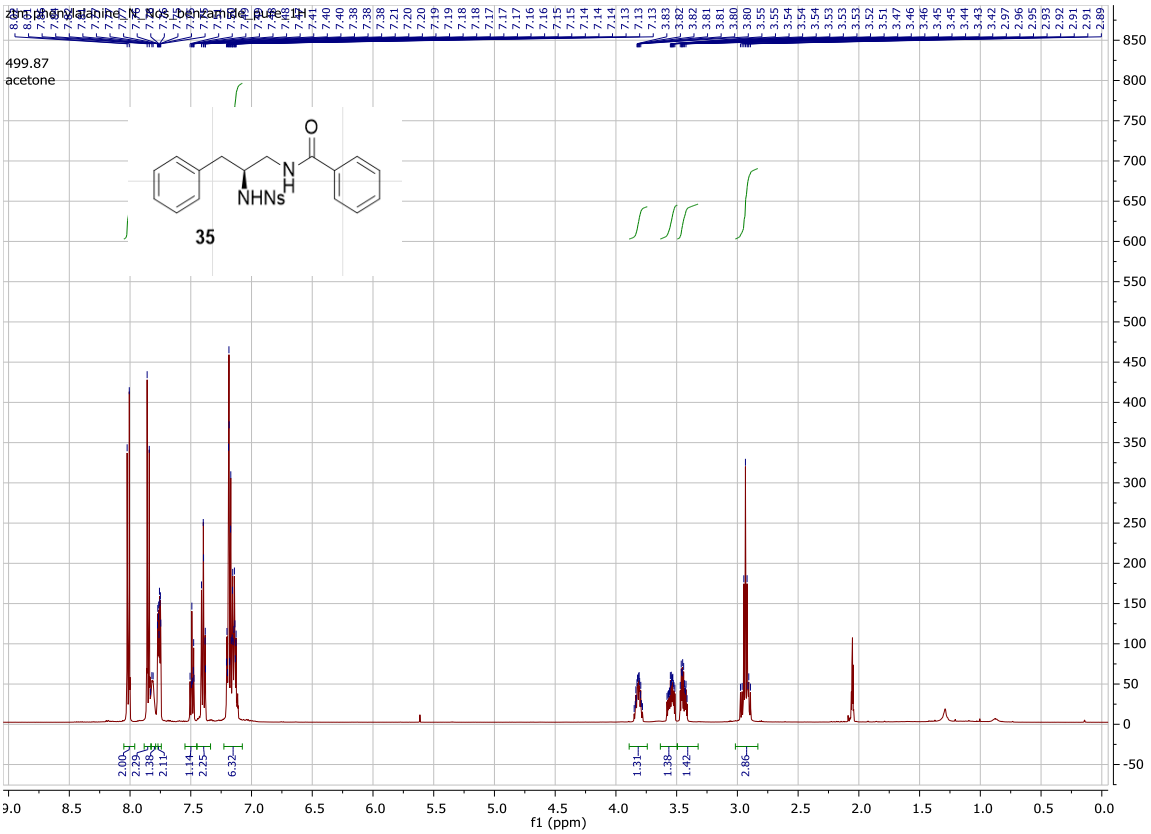
499.87
acetone
NHNs
35
f1 (ppm)

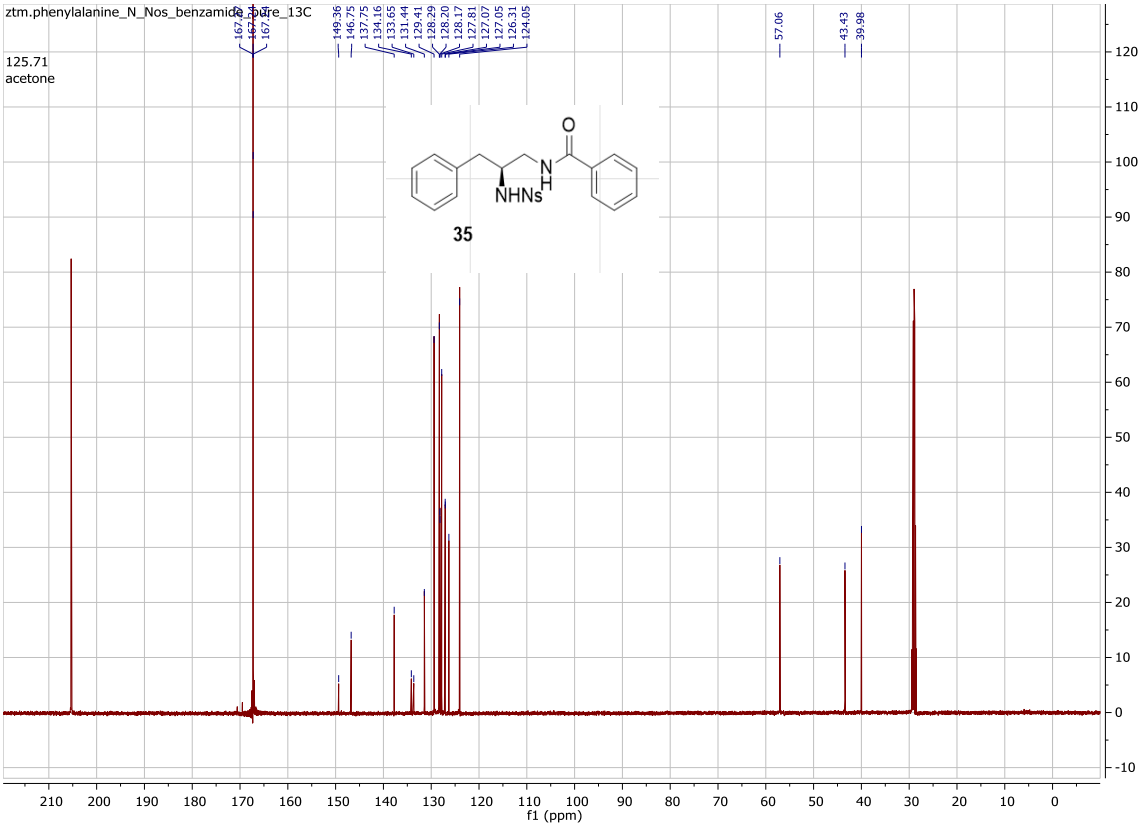
125.71
acetone
NHNs
35
f1 (ppm)

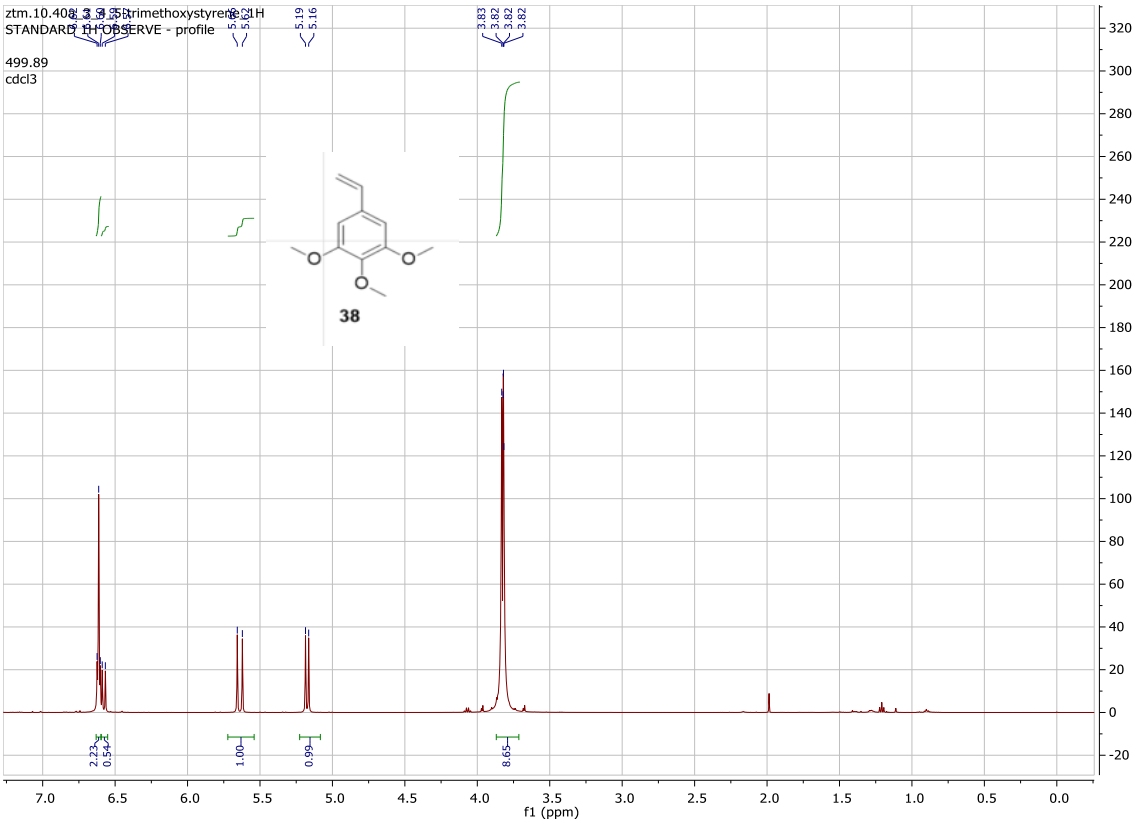
ztm.10.40a_3_4_5-trimethoxystyrene_1H
STANDARD 1H OBSERVE - profile
499.89
cdcl3
38
f1 (ppm)

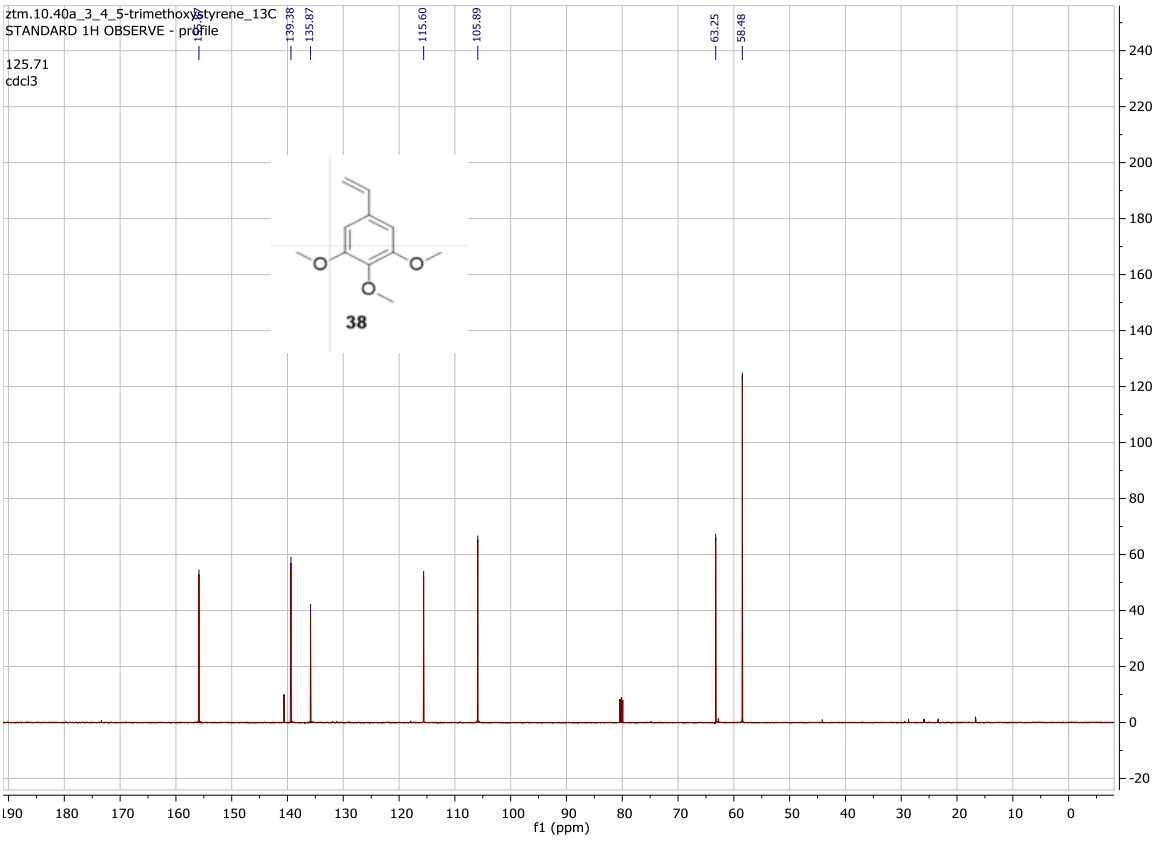
ztm.10.40a_3_4_5-trimethoxystyrene_13C
STANDARD 1H OBSERVE - profile
125.71
cdcl3
139.38
135.87
115.60
105.89
63.25
58.48
38
f1 (ppm)

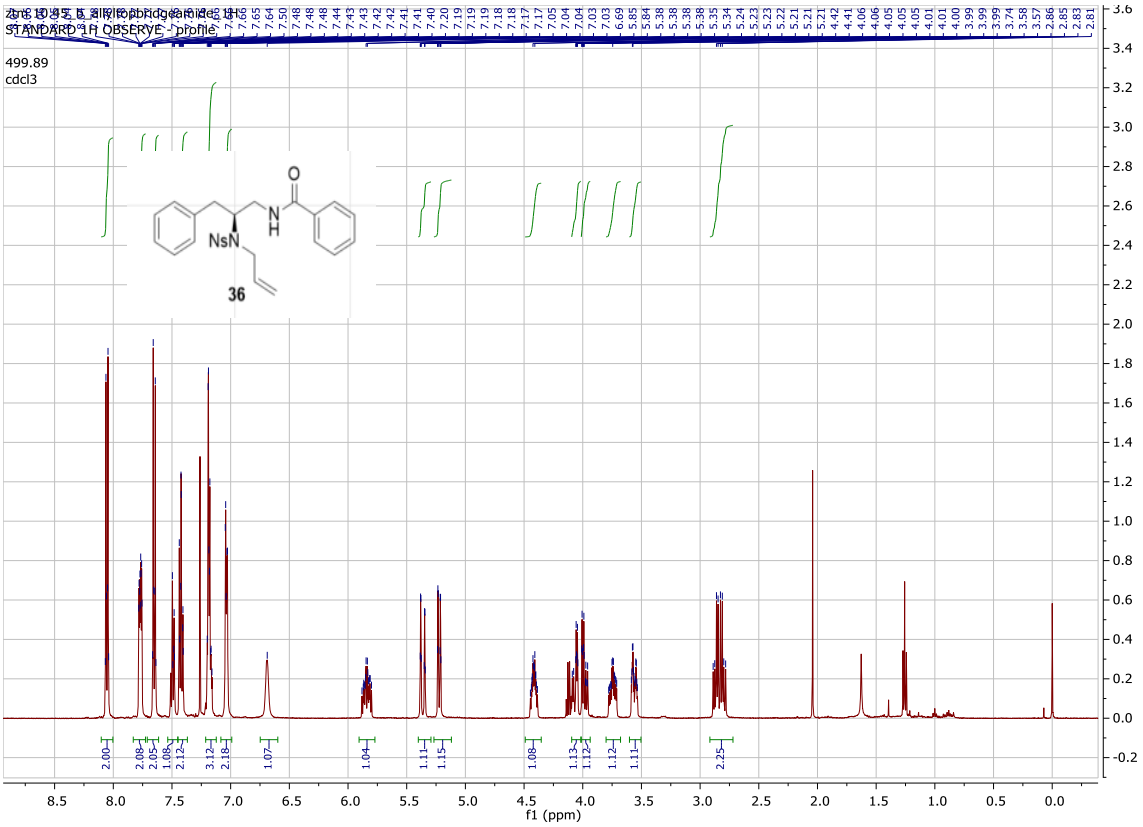
STANDARD 1H OBSERVE - profile
499.89
cdcl3
NsN
N
H
O
36
f1 (ppm)

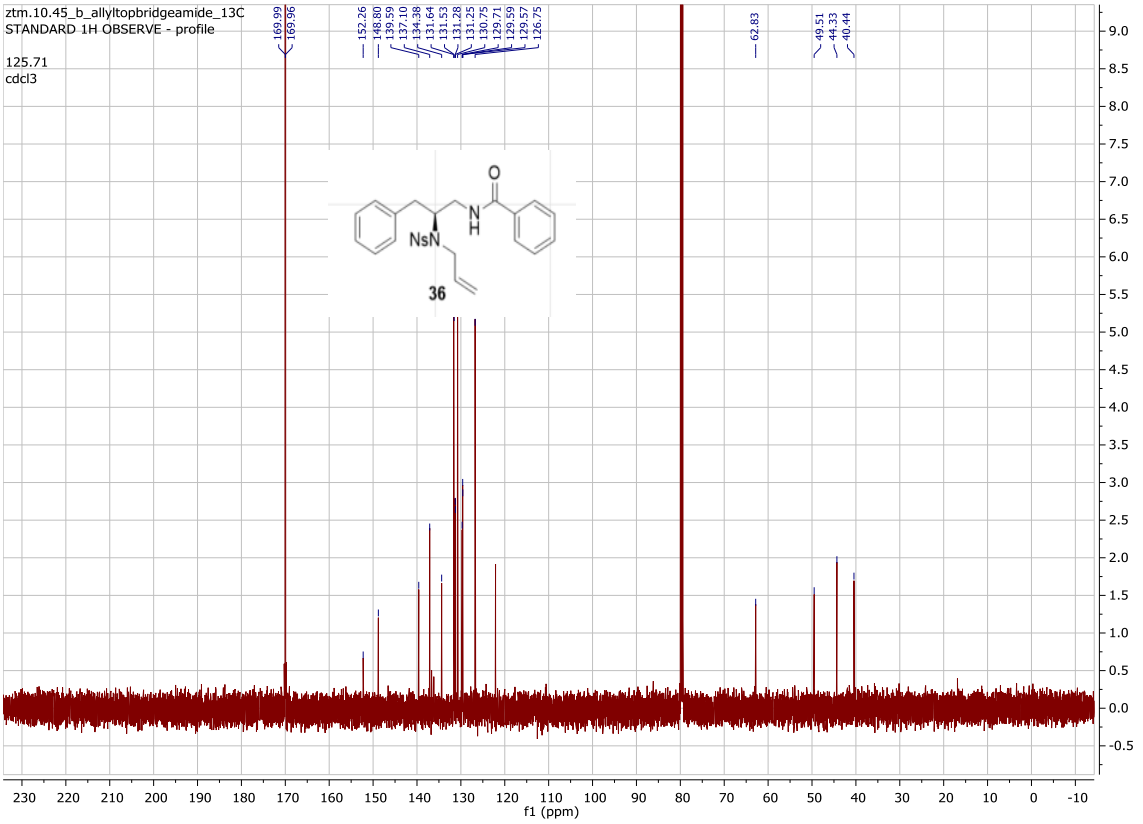
ztm.10.45_b_allyltopbridgeamide_13C
STANDARD 1H OBSERVE - profile
125.71
cdcl3
169.99
169.96
152.26
148.80
139.59
137.10
134.38
131.64
131.53
131.28
131.25
130.75
129.71
129.59
129.57
126.75
62.83
49.51
44.33
40.44
NsN
N
H
O
36
f1 (ppm)

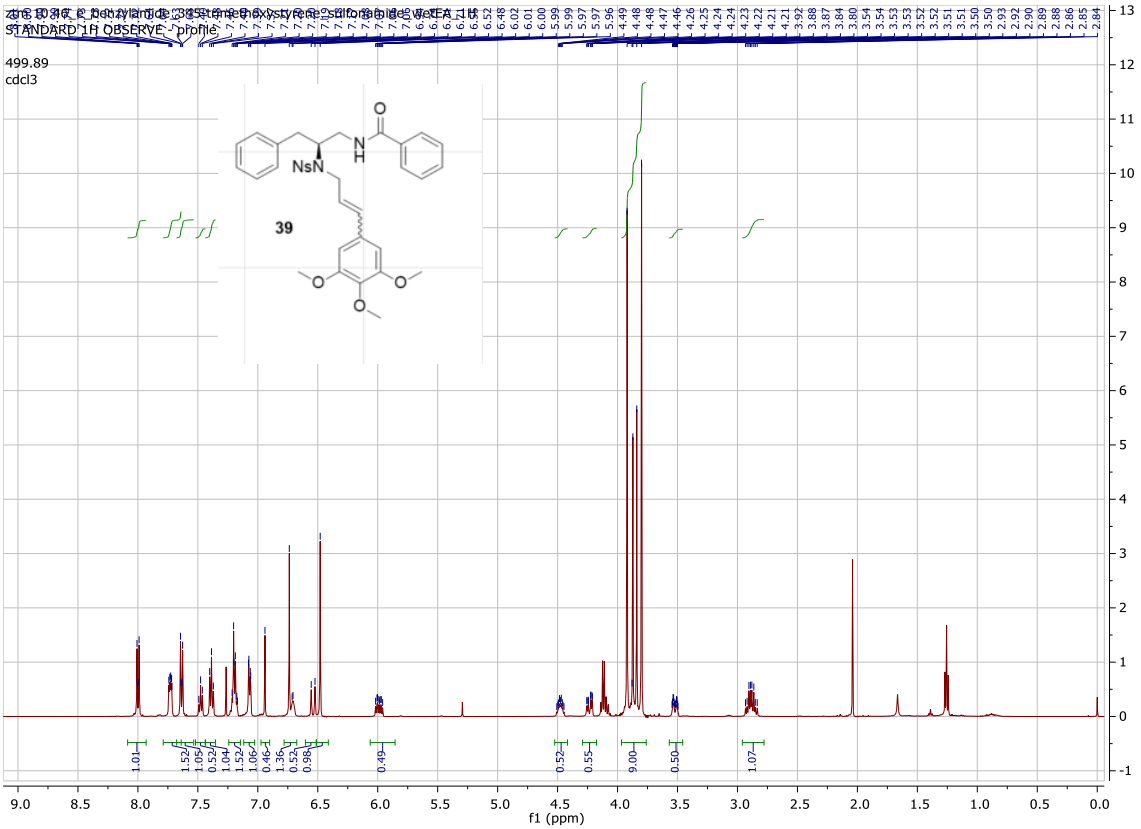
STANDARD 1H OBSERVE_1 profile
499.89
cdcl3
NsN
39
f1 (ppm)

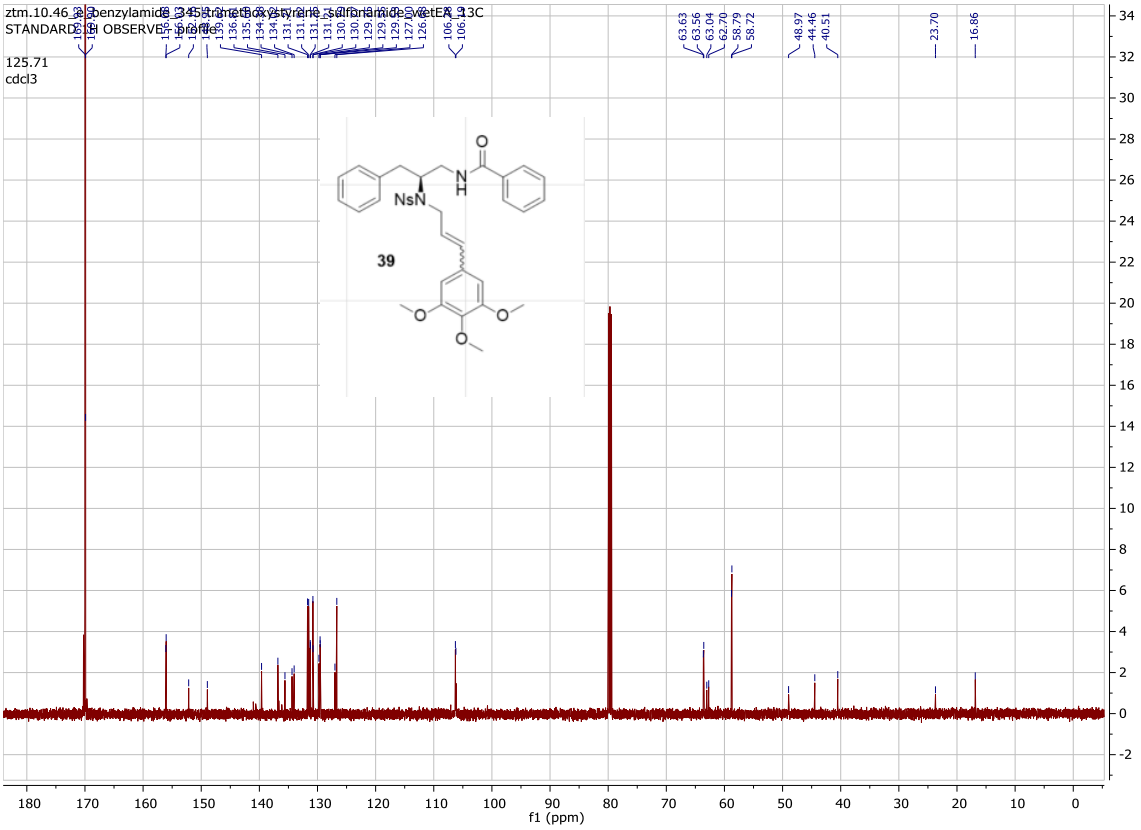
STANDARD 13C OBSERVE_1 profile
125.71
cdcl3
NsN
39
f1 (ppm)

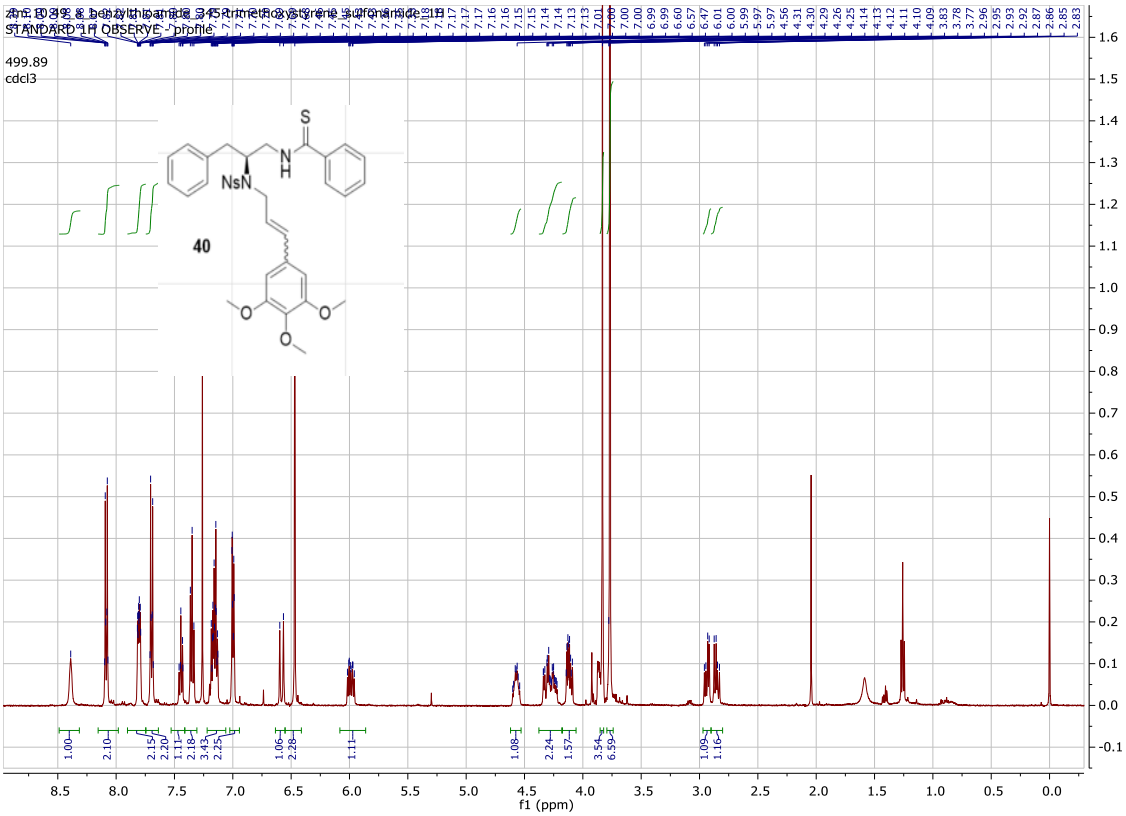
STANDARD 1H OBSERVE - profile
499.89
cdcl3
40
f1 (ppm)

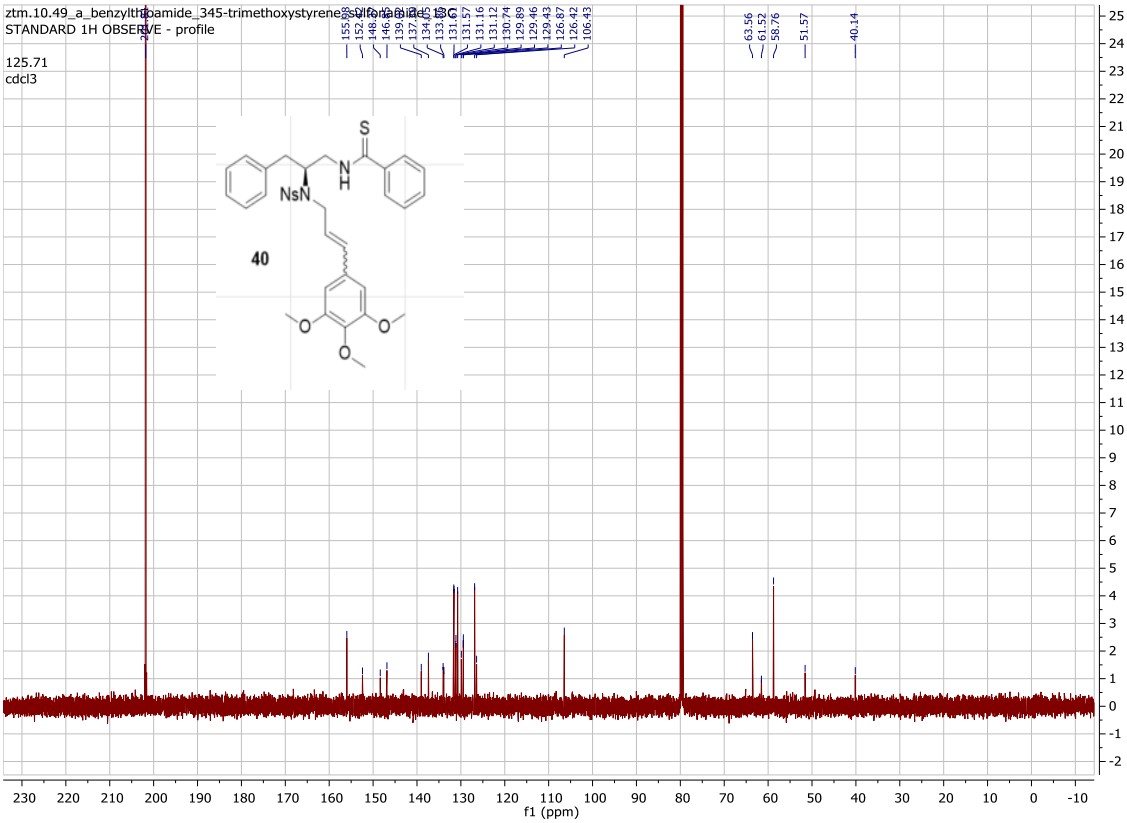
STANDARD 1H OBSERVE - profile
125.71
cdcl3
40
f1 (ppm)

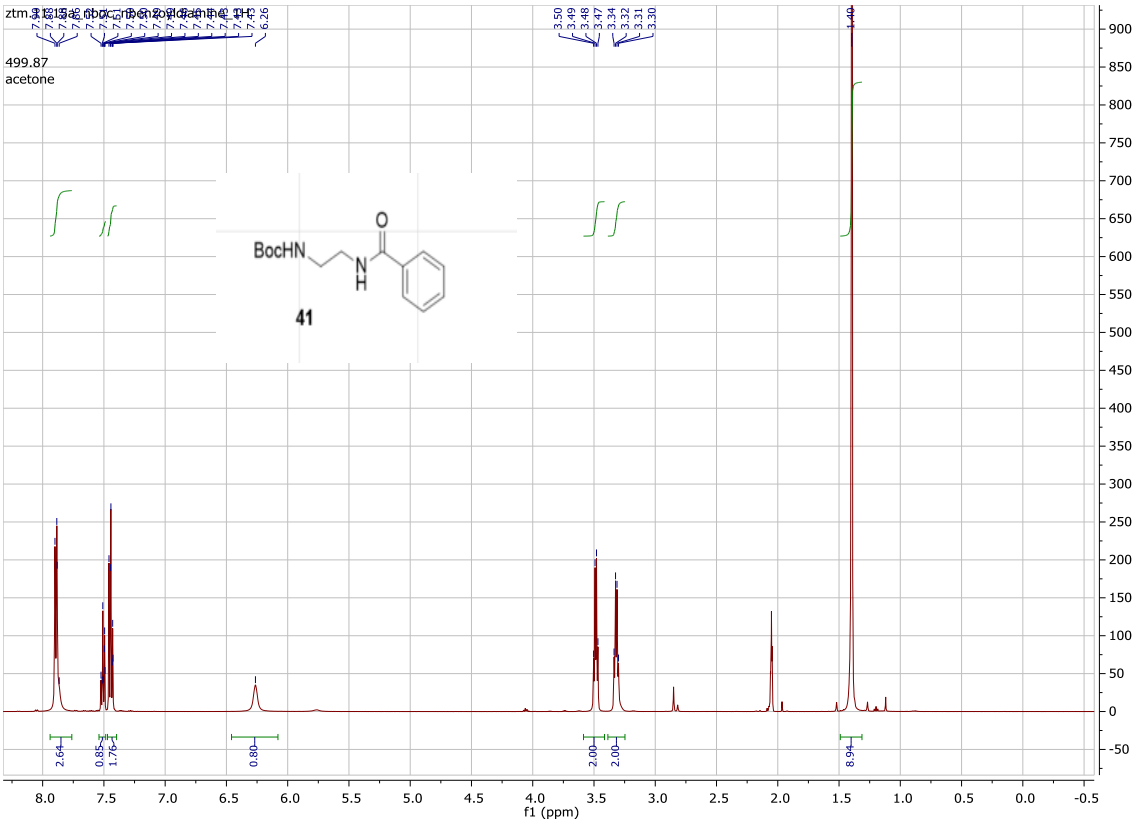
499.87
acetone
BocHN
N
H
O
41
f1 (ppm)

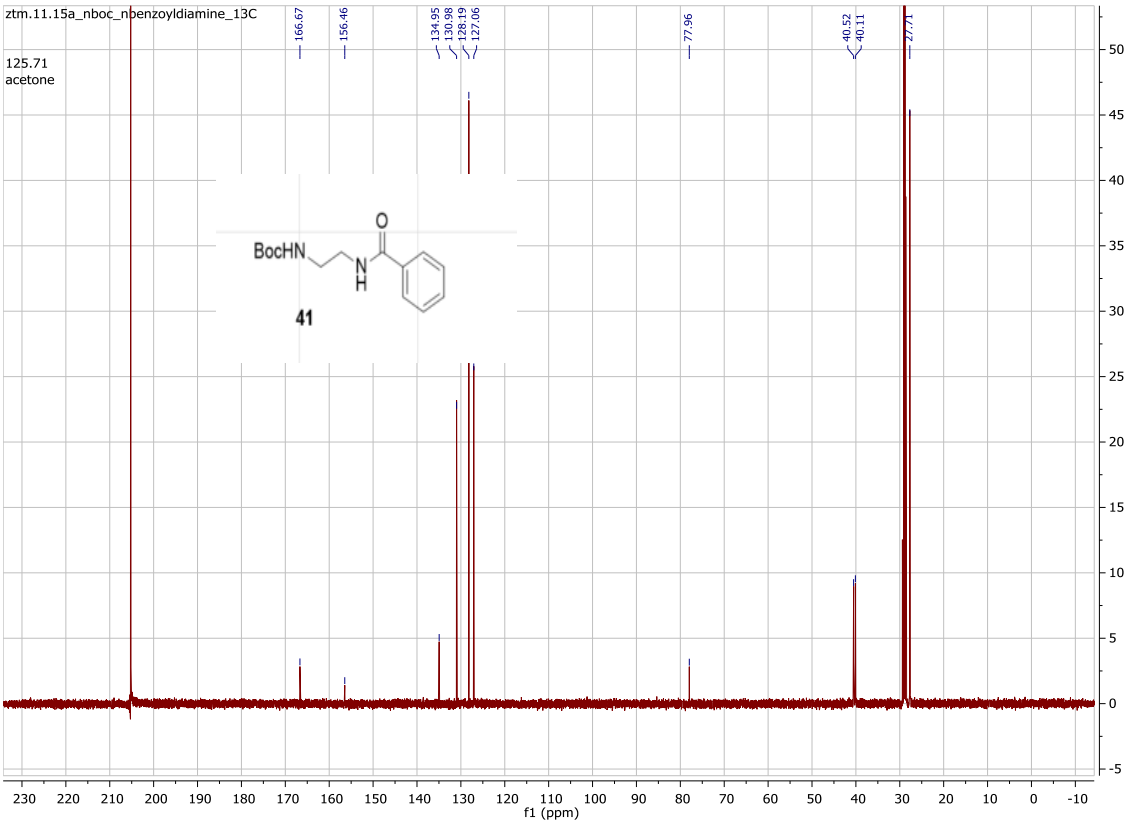
ztm.11.15a_nboc_nbenzoyldiamine_13C
125.71
acetone
166.67
156.46
134.95
130.98
128.19
127.06
77.96
40.52
40.11
27.71
BocHN
N
H
O
41
f1 (ppm)

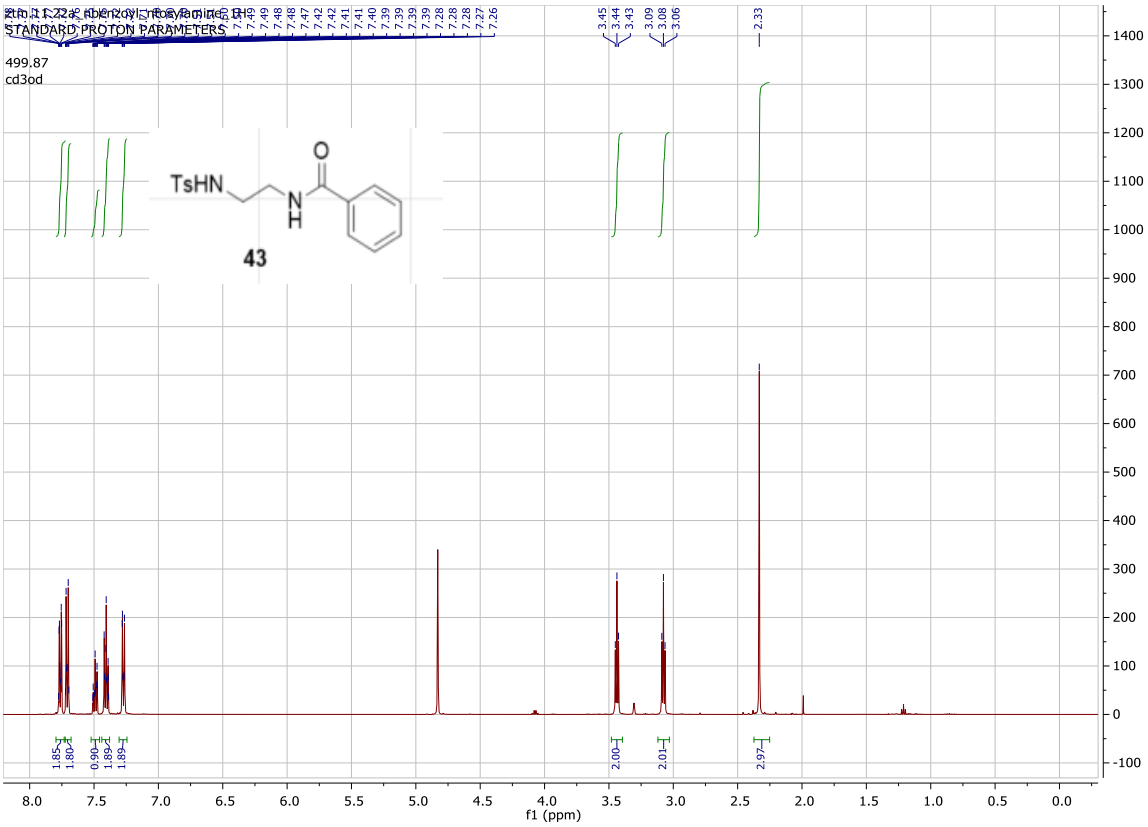
ztm.11.22a_nbenzoyl_ntosylamine_1H
STANDARD PROTON PARAMETERS
499.87
cd3od
TsHN
O
N
H
43
f1 (ppm)

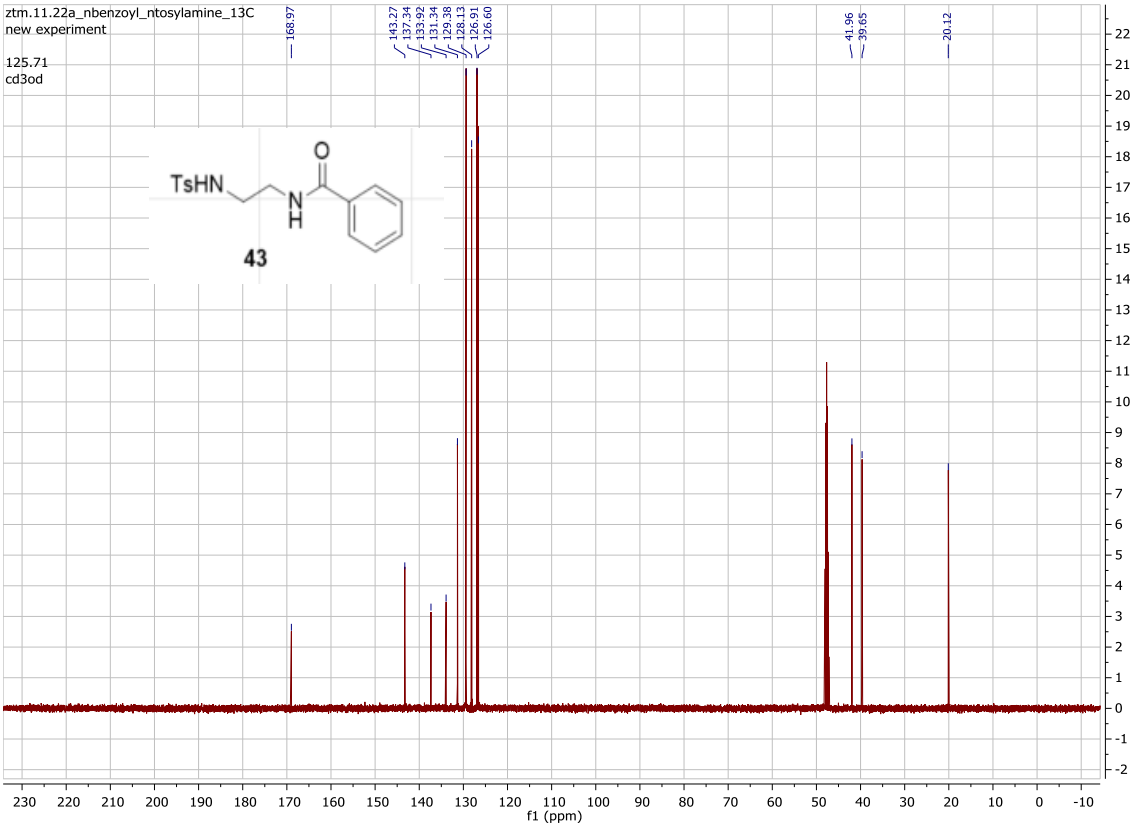
ztm.11.22a_nbenzoyl_ntosylamine_13C
new experiment
125.71
cd3od
168.97
143.27
137.34
133.92
131.34
129.38
128.13
126.91
126.60
41.96
39.65
20.12
TsHN
O
N
H
43
f1 (ppm)

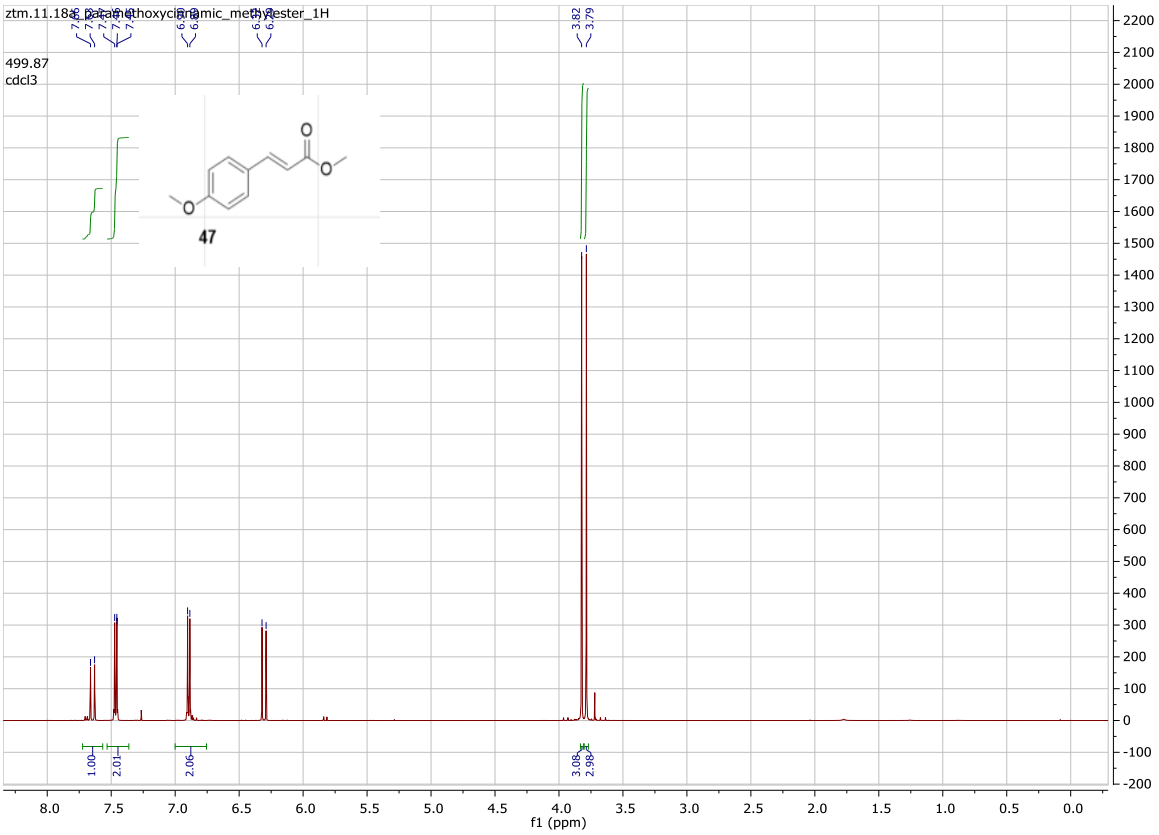
ztm.11.18a_paramethoxycinnamic_methylester_1H
499.87
cdcl3
47
f1 (ppm)

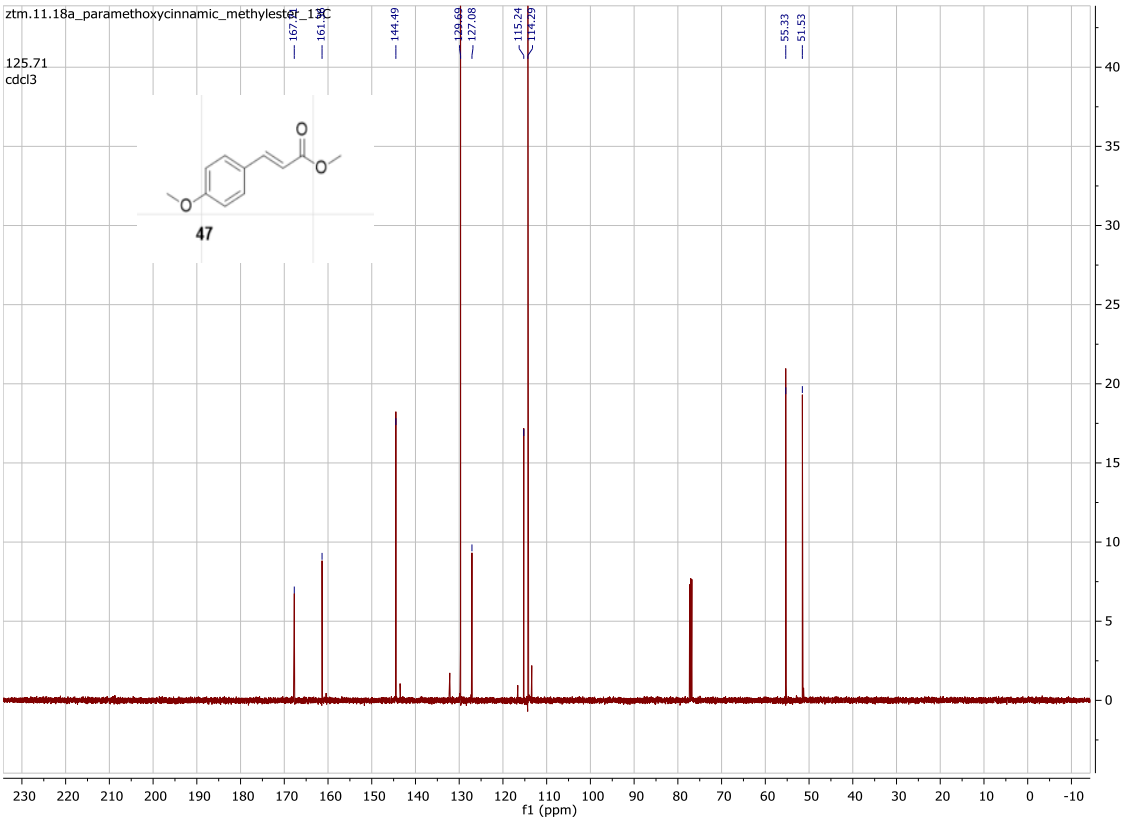
ztm.11.18a_paramethoxycinnamic_methylester_13C
125.71
cdcl3
47
f1 (ppm)

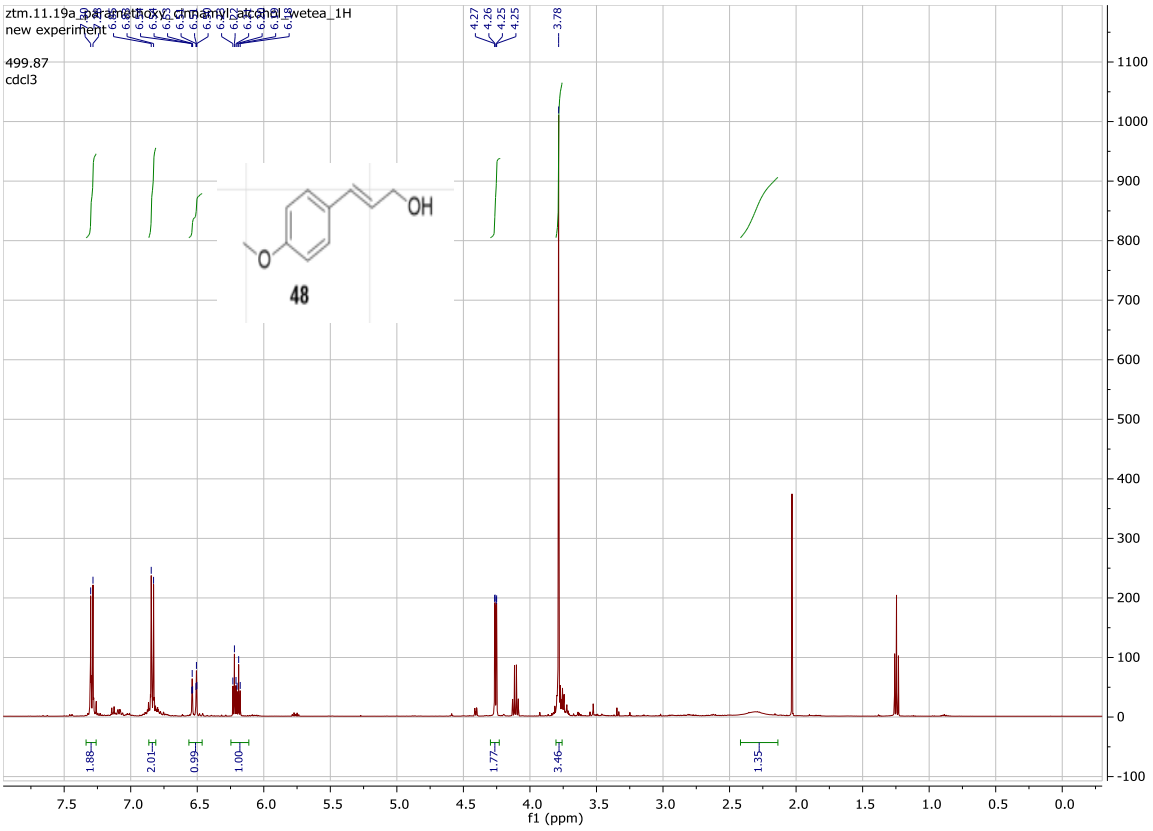
ztm.11.19a_paramethoxy_cinnamyl_alcohol_wetea_1H
new experiment
499.87
cdcl3
OH
O
48
f1 (ppm)

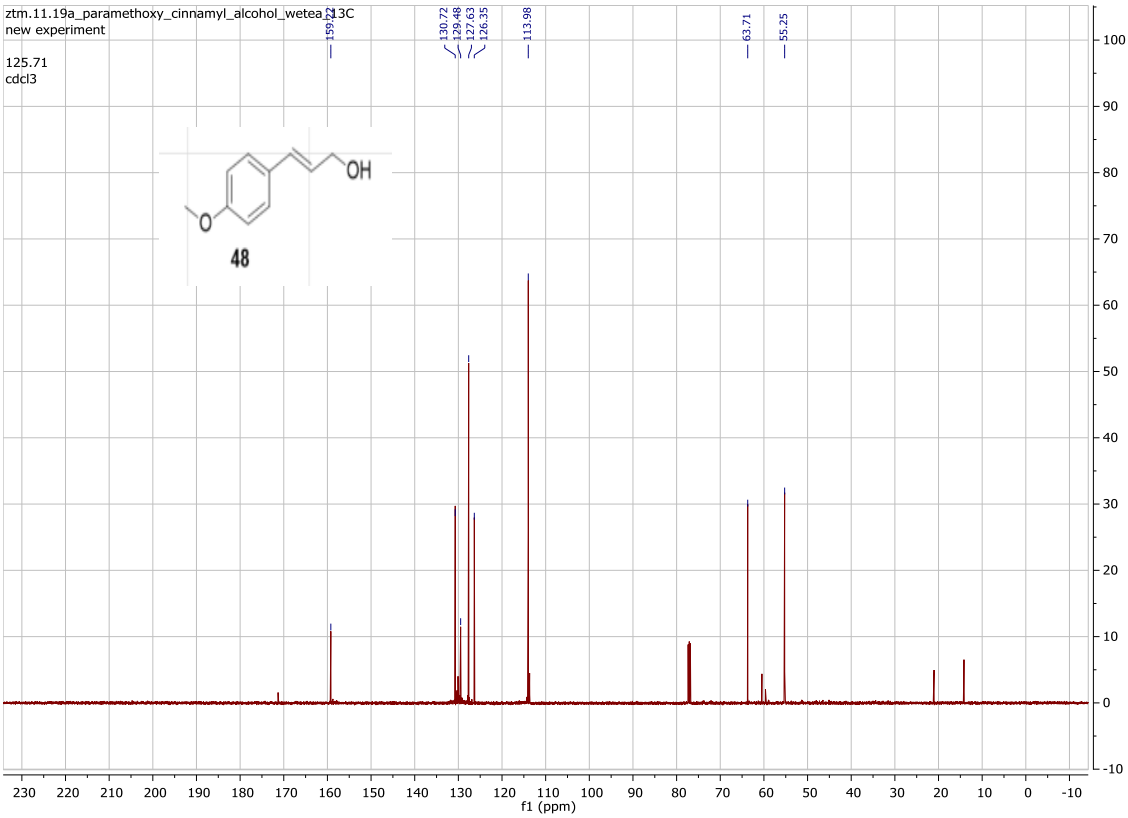
ztm.11.19a_paramethoxy_cinnamyl_alcohol_wetea_13C
new experiment
125.71
cdcl3
159.51
130.72
129.48
127.63
126.35
113.98
63.71
55.25
OH
O
48
f1 (ppm)

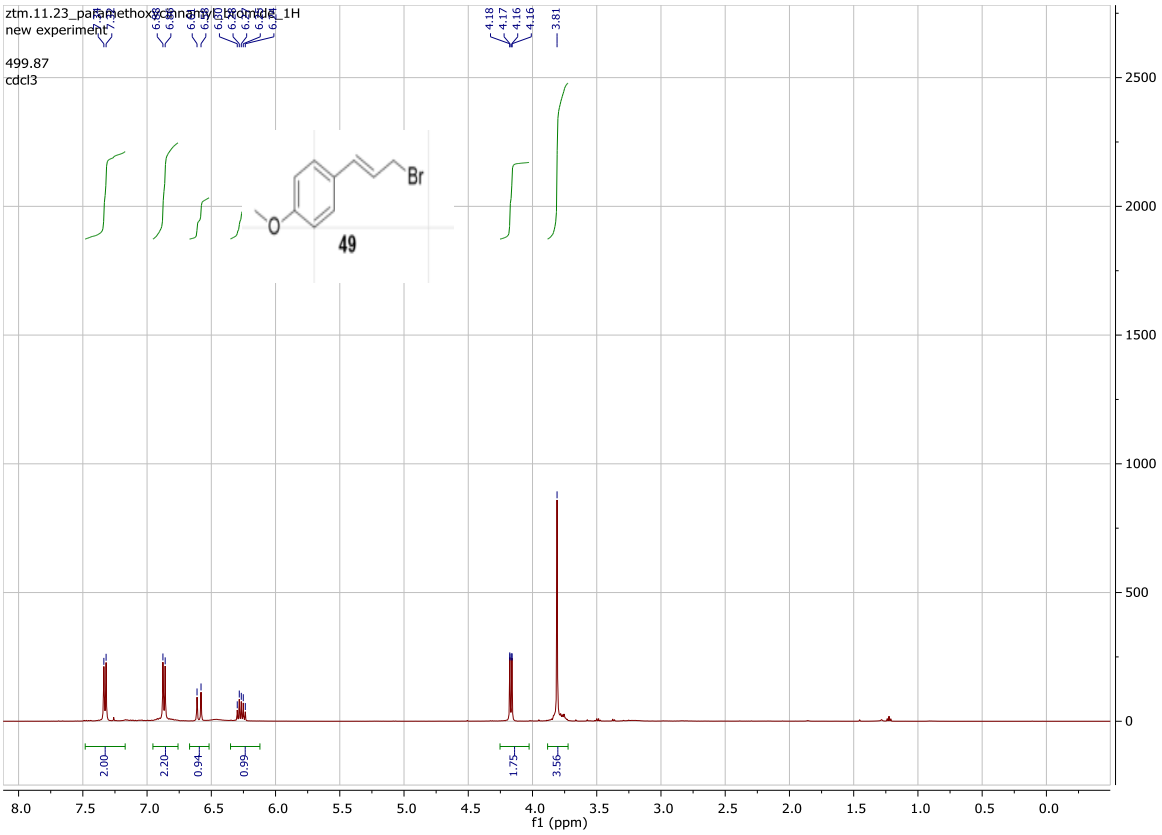
ztm.11.23_parametho
new experiment
499.87
cdcl3
Br
O
49
4.18
4.17
4.16
3.81
2.00
2.20
0.94
0.99
1.75
3.56
f1 (ppm)

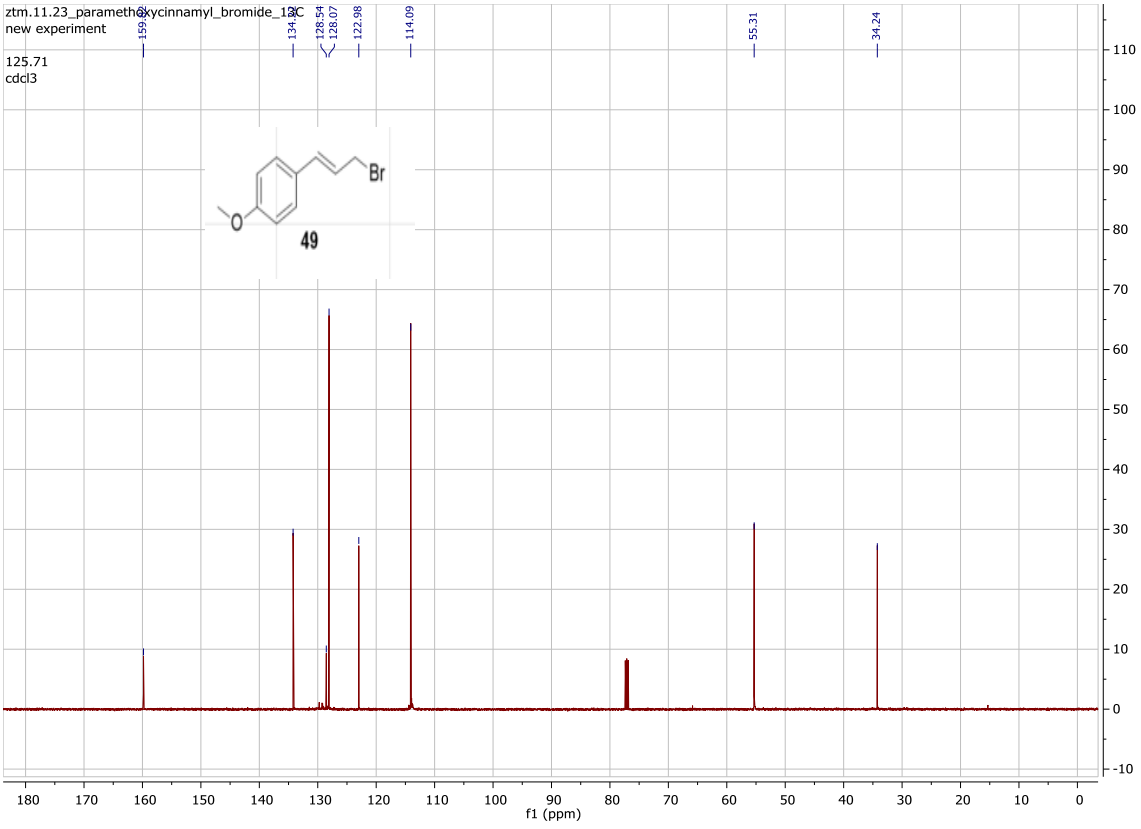
ztm.11.23_parametho
new experiment
125.71
cdcl3
159.
134.
128.54
128.07
122.98
114.09
55.31
34.24
Br
O
49
f1 (ppm)

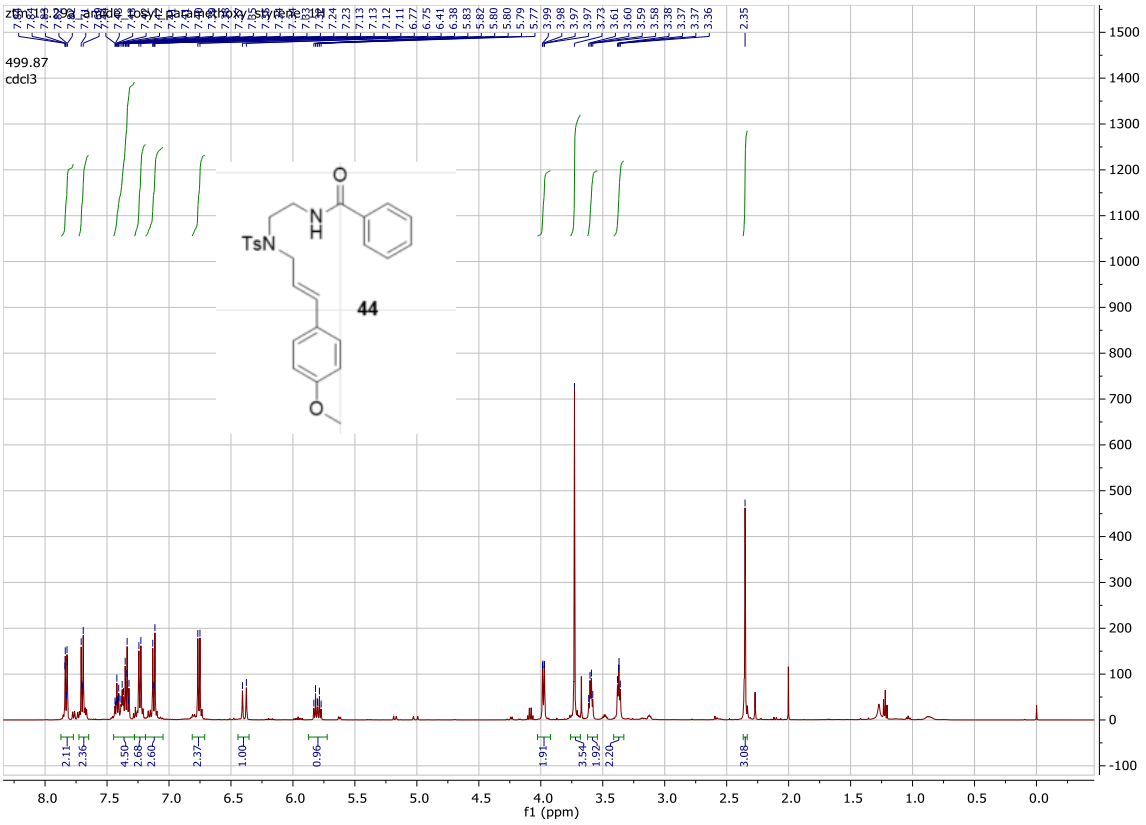
499.87
cdcl3
TsN
44
f1 (ppm)

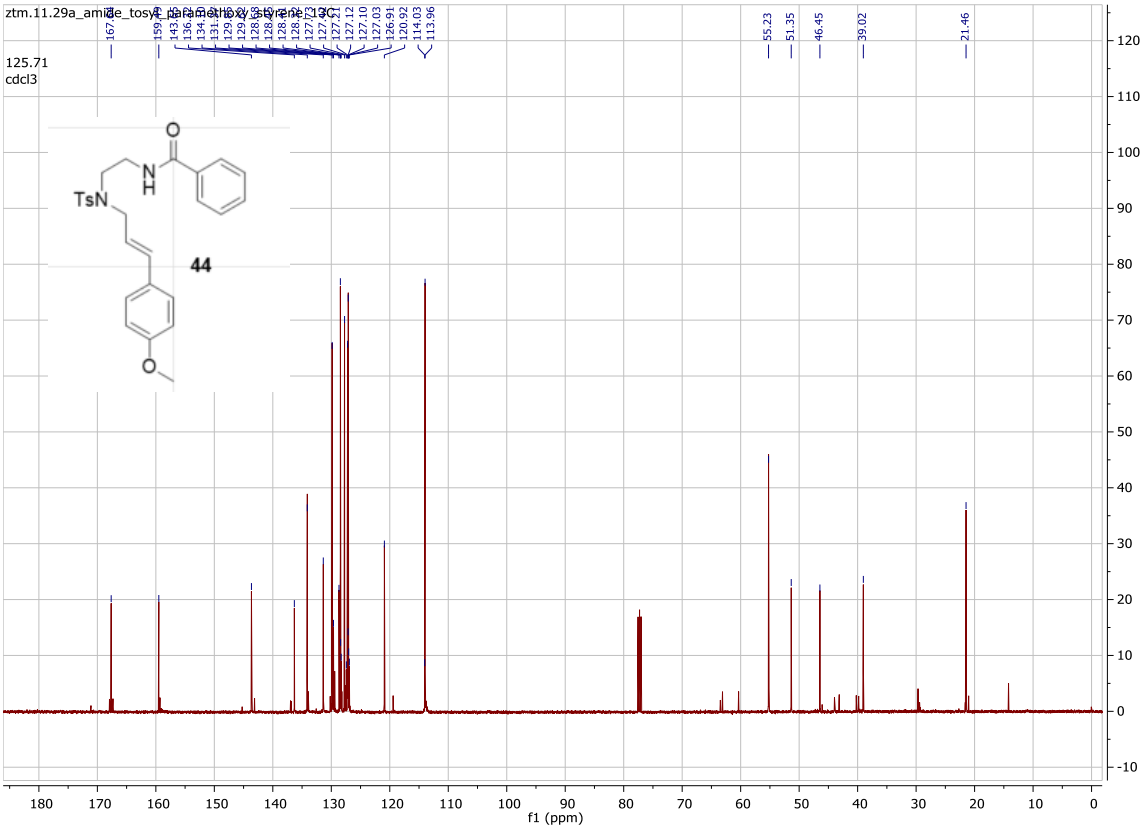
125.71
cdcl3
TsN
44
f1 (ppm)

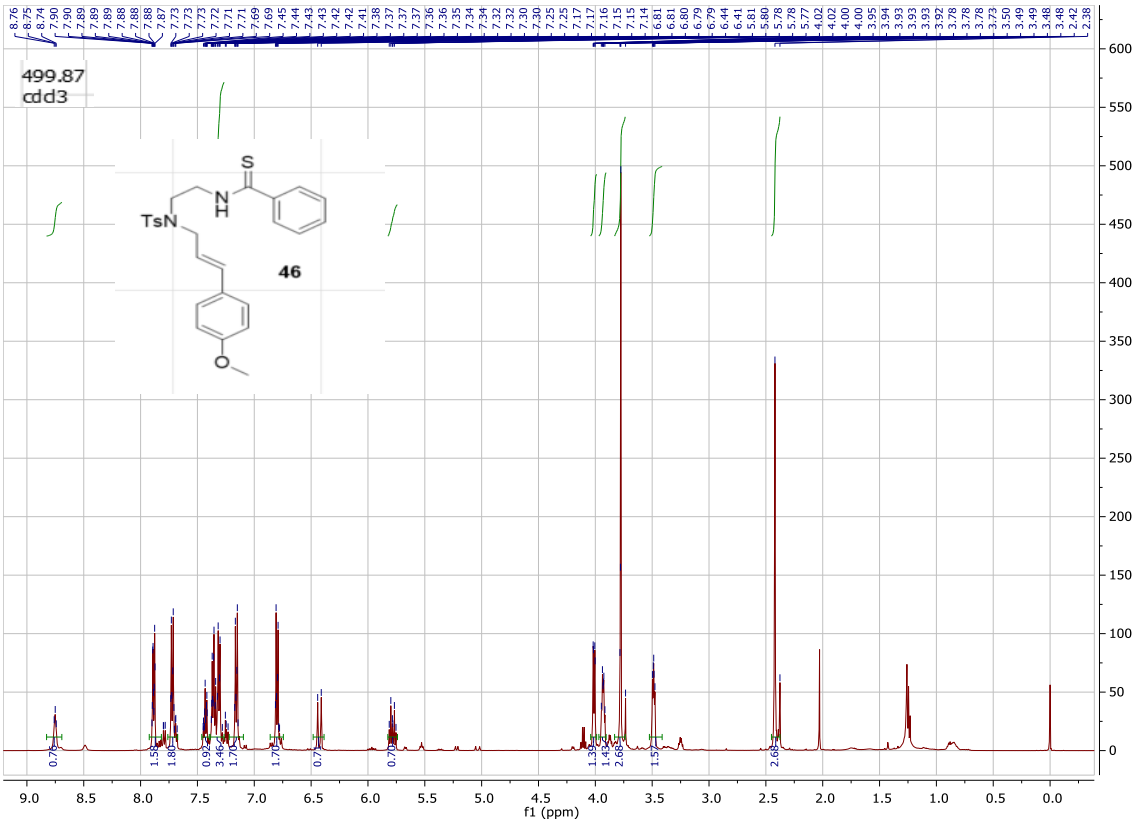
499.87
cdd3
S
N
H
TsN
46
O
f1 (ppm)

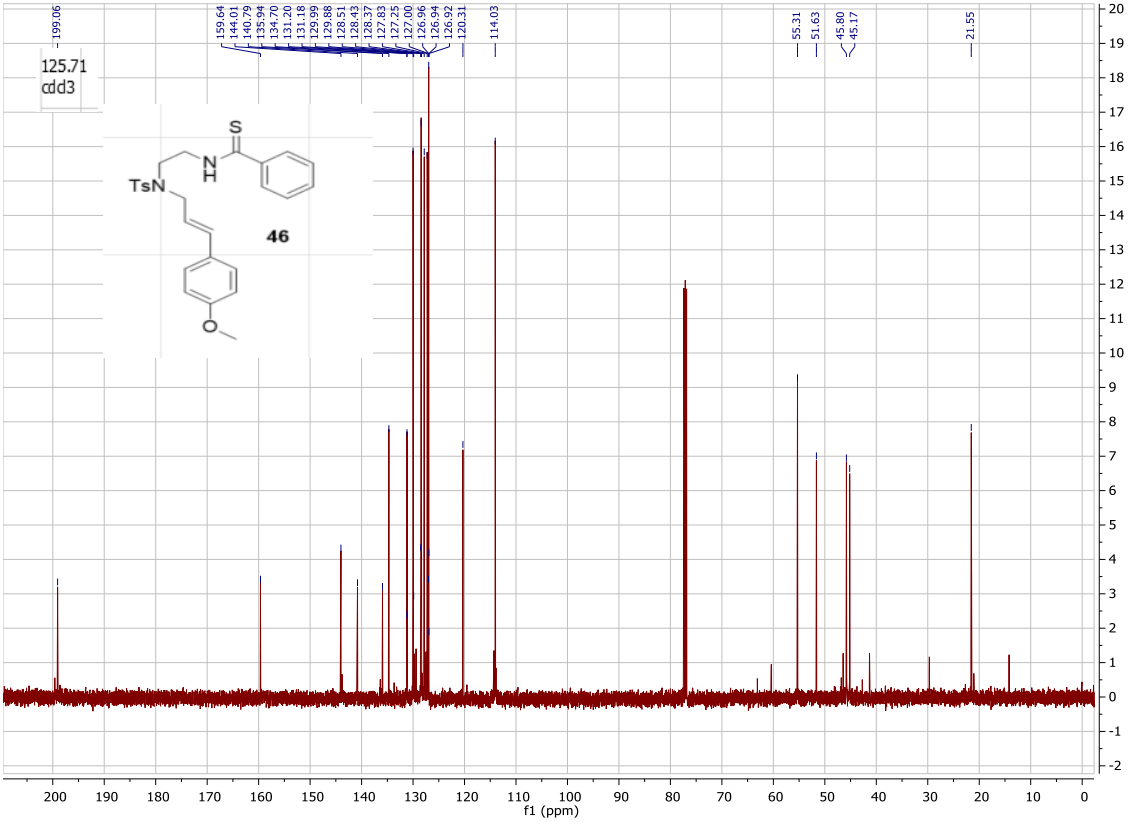
125.71
cdd3
S
N
H
TsN
46
O
f1 (ppm)

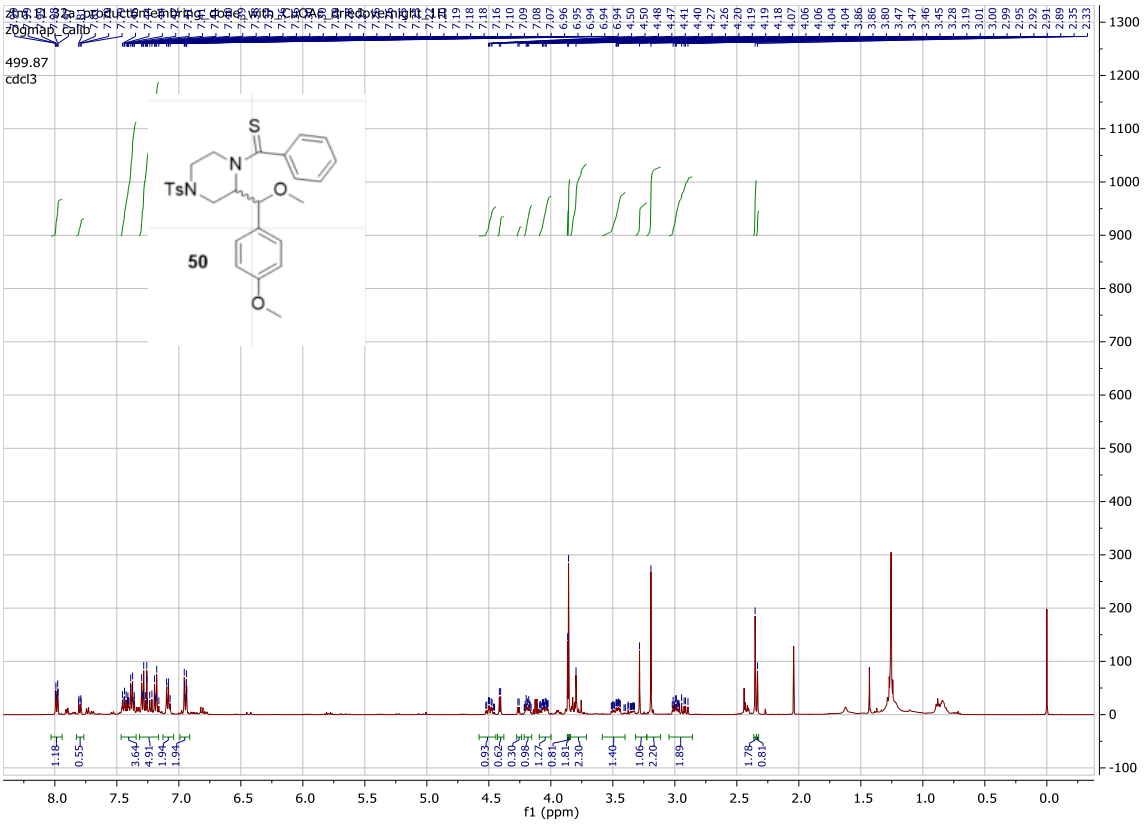
499.87
cdcl3
50
f1 (ppm)

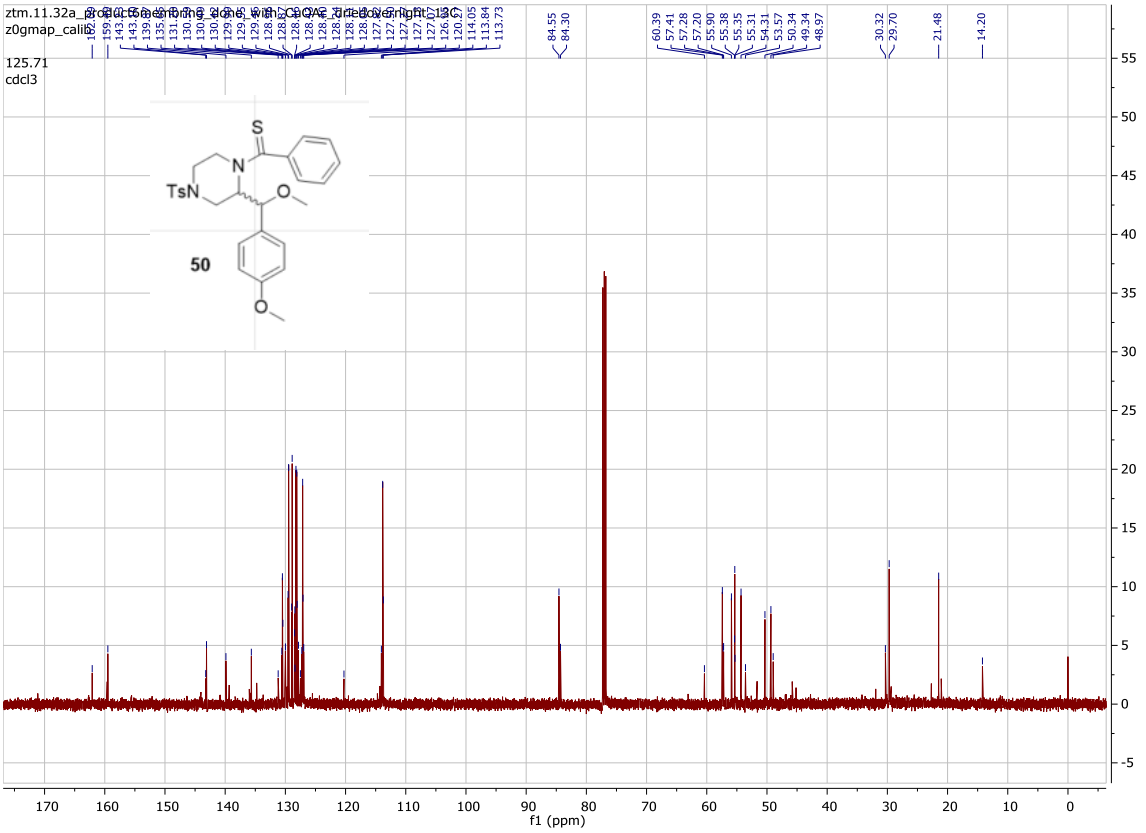
125.71
cdcl3
50
f1 (ppm)

**References**

(1) Pozharskii, A. F.; Soldatenkov, A. T.; Katritzky, A. R. *Heterocycles in Life and Society: An Introduction to Heterocyclic Chemistry, Biochemistry and Applications*; Wiley, 2011.

(2) Elbanna, A. H.; Khalil, Z. G.; Bernhardt, P. V.; Capon, R. J. Chrysosporazines A–E: P-Glycoprotein Inhibitory Piperazines from an Australian Marine Fish Gastrointestinal Tract-Derived Fungus, Chrysosporium Sp. CMB-F214. *Org. Lett.* **2019**, *21* (19), 8097–8100. https://doi.org/10.1021/acs.orglett.9b03094.

(3) Conner, E. S.; Crocker, K. E.; Fernando, R. G.; Fronczek, F. R.; Stanley, G. G.; Ragains, J. R. Visible-Light-Promoted Selenofunctionalization of Alkenes. *Org. Lett.* **2013**, *15* (21), 5558–5561. https://doi.org/10.1021/ol402753u.

(4) Zhao, G.; Kwon, C.; Bisaha, S. N.; Stein, P. D.; Rossi, K. A.; Cao, X.; Ung, T.; Wu, G.; Hung, C.-P.; Malmstrom, S. E.; Zhang, G.; Qu, Q.; Gan, J.; Keim, W. J.; Cullen, M. J.; Rohrbach, K. W.; Devenny, J.; Pelleymounter, M. A.; Miller, K. J.; Robl, J. A. Synthesis and SAR of Potent and Selective Tetrahydropyrazinoisoquinolinone 5-HT2C Receptor Agonists. *Bioorg. Med. Chem. Lett.* **2013**, *23* (13), 3914–3919. https://doi.org/10.1016/j.bmcl.2013.04.061.

(5) Xiong, P.; Xu, H.-C. Chemistry with Electrochemically Generated N-Centered Radicals. *Acc. Chem. Res.* **2019**, *52* (12), 3339–3350. https://doi.org/10.1021/acs.accounts.9b00472.

(6) Novaes, L. F. T.; Liu, J.; Shen, Y.; Lu, L.; Meinhardt, J. M.; Lin, S. Electrocatalysis as an Enabling Technology for Organic Synthesis. *Chem. Soc. Rev.* **2021**, *50* (14), 7941–8002. https://doi.org/10.1039/D1CS00223F.

(7) Yi, X.; Hu, X. Formal Aza-Wacker Cyclization by Tandem Electrochemical Oxidation and Copper Catalysis. *Angew. Chem. Int. Ed.* **2019**, *58* (14), 4700–4704. https://doi.org/10.1002/anie.201814509.

(8) Kochi, J. K.; Bemis, A.; Jenkins, C. L. Mechanism of Electron Transfer Oxidation of Alkyl Radicals by Copper(II) Complexes. *J. Am. Chem. Soc.* **1968**, *90* (17), 4616–4625. https://doi.org/10.1021/ja01019a018.

(9) Xu, F.; Zhu, L.; Zhu, S.; Yan, X.; Xu, H.-C. Electrochemical Intramolecular Aminooxygenation of Unactivated Alkenes. *Chem. – Eur. J.* **2014**, *20* (40), 12740–12744. https://doi.org/10.1002/chem.201404078.

(10) Xu, H.-C.; Moeller, K. D. Intramolecular Anodic Olefin Coupling Reactions: Use of the Reaction Rate To Control Substrate/Product Selectivity. *Angew. Chem.* **2010**, *122* (43), 8176–8179. https://doi.org/10.1002/ange.201003924.

(11) Moeller, K. D.; Tinao, L. V. Intramolecular Anodic Olefin Coupling Reactions: The Use of Bis Enol Ether Substrates. *J. Am. Chem. Soc.* **1992**, *114* (3), 1033–1041. https://doi.org/10.1021/ja00029a036.

(12) Reddy, S. H. K.; Chiba, K.; Sun, Y.; Moeller, K. D. Anodic Oxidations of Electron-Rich Olefins: Radical Cation Based Approaches to the Synthesis of Bridged Bicyclic Ring Skeletons. *Tetrahedron* **2001**, *57* (24), 5183–5197. https://doi.org/10.1016/S0040-4020(01)00358-1.

(13) Huang, Y.; Moeller, K. D. Anodic Cyclization Reactions: Probing the Chemistry of N,O-Ketene Acetal Derived Radical Cations. *Tetrahedron* **2006**, *62* (27), 6536–6550. https://doi.org/10.1016/j.tet.2006.04.009.

(14) Brandt, J. D.; Moeller, K. D. Oxidative Cyclization Reactions: Amide Trapping Groups and the Synthesis of Furanones. *Org. Lett.* **2005**, *7* (16), 3553–3556. https://doi.org/10.1021/ol051296m.

(15) Mahanta, N.; Szantai-Kis, D. M.; Petersson, E. J.; Mitchell, D. A. Biosynthesis and Chemical Applications of Thioamides. *ACS Chem. Biol.* **2019**, *14* (2), 142–163. https://doi.org/10.1021/acschembio.8b01022.

(16) Bordwell, F. G. Equilibrium Acidities in Dimethyl Sulfoxide Solution. *Acc. Chem. Res.* **1988**, *21* (12), 456–463. https://doi.org/10.1021/ar00156a004.

(17) Hudson, C. M.; Marzabadi, M. R.; Moeller, K. D.; New, D. G. Intramolecular Anodic Olefin Coupling Reactions: A Useful Method for Carbon-Carbon Bond Formation. *J. Am. Chem. Soc.* **1991**, *113* (19), 7372–7385. https://doi.org/10.1021/ja00019a038.

(18) Wuts, P. G. M. Protection for the Amino Group. In *Greene's Protective Groups in Organic Synthesis*; John Wiley & Sons, Ltd, 2014; pp 895–1193. https://doi.org/10.1002/9781118905074.ch07.

(19) Zhang, X.; Cao, B.; Yu, S.; Zhang, X. Rhodium-Catalyzed Asymmetric Hydroformylation of *N*-Allylamides: Highly Enantioselective Approach to $\beta^2$-Amino Aldehydes<a/>. *Angew. Chem. Int. Ed.* **2010**, *24* (49), 4047–4050. https://doi.org/10.1002/anie.201000955.

(20) West, T. H.; Daniels, D. S. B.; Slawin, A. M. Z.; Smith, A. D. An Isothiourea-Catalyzed Asymmetric [2,3]-Rearrangement of Allylic Ammonium Ylides. *J. Am. Chem. Soc.* **2014**, *136* (12), 4476–4479. https://doi.org/10.1021/ja500758n.

(21) Zhu, Y.; Colomer, I.; Donohoe, T. J. Hypervalent Iodine Initiated Intramolecular Alkene Dimerisation: A Stereodivergent Entry to Cyclobutanes. *Chem. Commun.* **2019**, *55* (69), 10316–10319. https://doi.org/10.1039/C9CC04383G.